# A Curvature-Corrected Rough Surface Scattering Theory Through The Single-Scatter Subtraction Method

Kevin P. Diomedi II

Dissertation submitted to the Faculty of the
Virginia Polytechnic Institute and State University
in partial fulfillment of the requirements for the degree of

Doctor of Philosophy
in
Electrical Engineering

Gary S. Brown, Chair
Majid Manteghi
Ahmad Safaai-Jazi
Gregory D. Earle
Werner E. Kohler

Feb 14, 2019
Blacksburg, Virginia

Keywords: electromagnetics, rough surface scattering, single-scatter,integral equations

Copyright 2019, Kevin P. Diomedi II

# A Curvature-Corrected Rough Surface Scattering Theory Through The Single-Scatter Subtraction Method

Kevin P. Diomedi II

(ABSTRACT)

A new technique is presented to study radio propagation and rough surface scattering problems based on a reformulation of the Magnetic Field Integration Equation (MFIE) called the Single-Scatter Subtraction ($S^3$) method. This technique amounts to a physical preconditioning by separating the single- and multiple-scatter currents and removing the single-scattering contribution from the integral term that is present in the MFIE. This requires the calculation of a new quantity that is the kernel of the MFIE integral call the kernel integral or $\overline{G}$. In this work, 1-dimensional deterministically rough surfaces are simulated by surfaces consisting of single and multiple cosines. In order to truncate the problem domain, a beam illumination is used as the source term and it is shown that this also causes the kernel integral to have a finite support. Using the Single Scatter Subtraction method on these surfaces, closed-form expressions are found for the kernel integral and thus the single-scatter current for a well defined region of validity of surface parameters which may then be efficiently radiated into the far field numerically. Both the closed-form expressions, and the computed radiated fields are studied for their physical significance. This provides a clear physical intuition for the technique as an augmentation to existing ones as a bent-plane approximation as shown analytically and also validated by numeric results. Further analysis resolves a controversy on the nature of Bragg scatter which is found to be a multiple-scatter phenomenon. Error terms present in the kernel integral also raise new questions on the effect of truncation for any MFIE-based solution. Additionally, a dramatic enhancement of backscatter predicted by this new approach versus the Kirchhoff method is observed as the angle of incidence increases due to the error terms.

# A Curvature-Corrected Rough Surface Scattering Theory Through The Single-Scatter Subtraction Method

Kevin P. Diomedi II

(GENERAL AUDIENCE ABSTRACT)

A new technique is presented to study the interaction of electromagnetic waves with rough surfaces. Building on the technique called the Magnetic Field Integral Equation (MFIE) which allows the solution for the electromagnetic fields scattered from the surface by considering only the induced electric and magnetic currents on the surface, the Single-Scatter Substraction ($S^3$) method separates the surface currents into those that interact with the surface only once or single-scatter, and those that interact multiple times called multiple-scatter. Since this is the introduction of this technique, only the former is investigated. In this study, a new quantity which is an integral of one of the components of the standard MFIE is studied and closed-form approximations are presented along with bounds of validity. This provides closed form solutions for the single-scattering currents, from which the radiated fields may be efficiently found numerically. Since they are closed form, the expressions provide insight into the nature of the physical scattering process. Numerical results of these expressions are compared to the standard approximate technique as well as the "exact" solution found by numerically solving the MFIE. Compared to the standard approximate technique which approximates the surface by a tangent plane at each point on the surface, the single-scatter currents approximate the surface with a bent-plane at each point. This shifts the scattered fields from certain directions to others, and highlights where single- and multiple-scattering have an effect.

# Dedication

*To Judith.*

*The best thing that ever happened and the source of all my wisdom.*

*And Ruby.*

# Acknowledgments

To Professor Gary S. Brown, I extend my most sincere thanks and gratitude for his support, mentorship and the opportunity he afforded me during this phase of my life. I've learned so much from him and couldn't have asked for a better adviser. Our discussions on electromagnetics, career and life are always illuminating and I cherish each one. It's unfortunate that they don't make them like him anymore and we all suffer as a result. I hope I can live up to his example.

I am grateful for all the advanced electromagnetics Dr. Majid Manteghi passed to me in courses and discussions in his office. For that knowledge and general discussions on life, thank you.

I wouldn't be the engineer I am today without Dr. Ahmad Safaai-Jazi who in addition to serving on my committee was almost single-handedly responsible for my entire undergraduate electrical engineering education at Tech. Whether or not you wish to take that blame, I was fortunate to have taken so many of your classes and am sincerely grateful.

Thank you to Dr. Gregory Earle for serving on my committee, offering advice, encouragement, and interesting discussions on electromagnetics, as well as space and plasma science.

I and a large number of current and former EMIL students are deeply indebted to Dr. Werner Kohler for providing mathematical grounding to our researches. Thank you for your shrewd comments and observations

Thank you also to all the faculty and staff that have supported me during my time at Virginia Tech, those seen and those working quietly in the background.

I would also like to thank Dr. Rick Clark and all the instructors at Virginia Western Community College for the excellent Engineering Associate's degree program and the opportunities they provided there. I heartily recommend anyone interested in engineering to begin their education there for a leg up on their peers. Special thanks also to Mr. Hammer, who like Dr. Jazi for my electrical engineering, is responsible for nearly all of my undergraduate mathematics education.

Thank you also to Dr. Steven Russell and the Office of Naval Research (ONR) for supporting this research.

Great thanks to all current and past members of the Electromagnetics Interactions Lab (EMIL). While I wouldn't flatter myself by saying I ever saw far, it was a great honor to stand on the shoulders of each of you. Though Bob and I may be the last of the Mohicans, we carry the torch you all lit onward. Special thanks to Dan Davis for everything you taught me, from electromagnetics to architecting code to solve practical problems and for introducing me to vim, my daily companion. To Bob Stockland for everything I've learned from you and our stimulating conversations. Good luck to you in your defense as well. I extend great appreciation to Thaddeus Black for his superb teaching and for introducing me to Dr. Brown, one day I hope to work through your Derivations of Applied Mathematics. And to Ben Westin who I only met in passing but whose reputation and great work affected me. I wish you all the best.

I wish to also thank Torc Robotics for providing additional support to me for this research. Thank you to Mike Avitable for approving this and providing the appropriate blend of support and taunting, the other team leads and the ASIF team.

Thank you to everyone in the Bushnell family who all immediately took me in as one of their own. Your constant love, support and encouragement means the world.

Special thanks to my entire family, parents, step-parents, grandparents, step-grandparents and everyone. I could not have done anything without the warm, loving support from all of you and I am forever indebted to each one of you. Thank you for everything. You truly built a solid foundation in me and I love you all. I have greater luck than I could ever deserve, in part because of you, so a big thanks to you all and to Whom provides it.

And finally, Judith. Words completely fail to express what they need to. Thank you so much for your constant love and support and endless patience. Your strength and will astound me daily and your style and grace inspire to carry me effortlessly to the end of this task. I wouldn't have wished to share all of this with anyone else and am so grateful for our life together. I love you.

# Contents

**List of Figures** xv

**List of Tables** xxvi

**1 Introduction** 1

1.1 Introduction . . . 1

1.1.1 Research Goals . . . 2

1.1.2 Accomplishments . . . 2

1.1.3 Questions Answered . . . 3

1.2 Motivation . . . 4

1.3 Research Outline . . . 5

**2 Review of Literature** 8

2.1 Existing Literature Reviews . . . 8

2.2 Perturbation Approaches . . . 9

2.2.1 Classical Development . . . 9

2.3 Kirchhoff Solutions . . . 9

2.3.1 Classic Development . . . 9

2.3.2 Non-local Corrections . . . 10

2.3.3 Curvature Corrections . . . 11

2.4 Composite Models . . . 11

2.5 Applications . . . 12

**3 Single Scatter Subtraction** **13**

3.1 Introduction . . . 13

3.2 Problem Formulation . . . 13

3.2.1 Problem Geometry . . . 13

3.2.2 Surface Characterization . . . 14

3.2.2.1 Sinusoidal Surfaces . . . 15

3.2.3 Magnetic Field Integral equation . . . 16

3.2.3.1 Kirchhoff Solution . . . 18

3.2.4 Beam illumination . . . 18

3.2.4.1 Thorsos Taper . . . 19

3.2.5 Scattered Fields . . . 20

3.3 Single Scatter Subtraction Method . . . 22

3.3.1 Motivation . . . 22

3.3.2 Formulation . . . 23

3.3.3 Discussion on Convergence . . . 25

3.3.4 Discussion on Truncation . . . 25

3.3.5 Iteration . . . 28

3.4 Summary . . . 29

**4 Kernel (Green Function) Integral** **30**

4.1 Introduction . . . 30

4.2 Calculation of the Kernel Integral . . . 30

4.2.1 Example Integrands . . . 32

4.3 Numeric Results . . . 32

4.3.1 Confirmation of numeric results . . . 35

4.3.2 Infinite Support . . . 45

4.3.2.1 Near the singular portion . . . 45

4.3.3 Finite Support . . . 63

4.3.4 Conclusion . . . 66

4.4 Extend Rough Surface Analytical Approximations . . . 66

4.4.1 Introduction . . . 66

4.4.2 Infinite Support . . . 71

4.4.3 Finite Support . . . 81

4.4.3.1 TE Integration Tails . . . 86

4.4.3.2 TM Integration Tails . . . 88

4.4.3.3 TM Small Argument Integral Single/Spectral Surface . . . 90

4.4.3.4 TM Higher Order Approximation . . . 95
4.4.3.5 TE Polarization Empiric formula . . . 104
4.4.3.6 Empiric Analytic Formula . . . 105
4.4.4 Spectral Surfaces . . . 171
4.4.4.1 Predicted Singularities . . . 188
4.4.4.2 Singular Single Frequency . . . 201
4.4.4.3 TM Linearity . . . 201
4.4.4.4 Characterization vs RMS slope . . . 201
4.4.4.5 RMS curvatures . . . 225
4.5 Summary . . . 234

**5 Physical Significance and Scattering Results 236**

5.1 Introduction . . . 236
5.2 Physical Based Approximations . . . 237
5.2.1 Interpretation of $\overline{G}$ results . . . 237
5.2.1.1 Bent Tangent Plane Approximation . . . 237
5.2.1.2 Bragg Scattering . . . 238
5.2.2 Affect of finite truncation . . . 239
5.3 Scattering Results . . . 239
5.3.1 Short Surface Wavelengths . . . 240

5.3.2 Multiple frequency surfaces . . . 255

5.4 Summary . . . 261

**6 Conclusion** **266**

6.1 Summary . . . 266

6.2 Accomplishments . . . 268

6.3 Future Research . . . 271

**Bibliography** **273**

**Appendices** **280**

**Appendix A Fresnel-Based Finite Analytic Tail Approximations** **281**

A.1 TE Finite Analytic Tail Integration . . . 281

A.1.1 Squared Slope Terms . . . 284

A.1.2 Lower Tail Integral . . . 286

A.1.2.1 Unity Term of Lower Integral . . . 286

A.1.2.2 Squared Slope Term of Lower Integral . . . 287

A.1.3 Upper Tail Integral . . . 288

A.1.3.1 Unity term of Upper Integral . . . 289

A.1.3.2 Squared Slope Term of Upper Integral . . . 290

A.1.4 Conclusion . . . 291

A.2 TM Finite Analytic Tail Integration . . . 292
A.2.1 Starting with the lower Integral . . . 296
A.2.2 Now for the upper integral: . . . 297
A.3 Analytic Tail Integrals Extension to Spectral Surfaces . . . 298
A.3.1 Squared Slope . . . 299
A.3.2 TM Polarization . . . 302
A.3.3 TE Polarization . . . 303
A.3.3.1 Lower Squared Slope Term . . . 305
A.3.3.2 Upper Squared Slope Term . . . 307
A.3.4 Conclusion . . . 310
A.3.4.1 TM . . . 310
A.3.4.2 TE . . . 310
A.4 TM Higher-Order Integral Tails Approximation . . . 311
A.4.1 Conclusion . . . 323

**Appendix B $\overline{\overline{G}}$ Empiric Analytic Formula** **324**

B.1 $\overline{\overline{G}}$ TM Derived Formula . . . 324
B.2 $\overline{\overline{G}}$ TE Derived Formula . . . 327
B.2.1 Introduction . . . 327
B.2.2 Full expression from infinite. . . . 328

**Appendix C A Note on Fresnel Integrals** **334**

C.1 Fresnel Integrals . . . . . 334

C.2 Imaginary Argument . . . . . 336

**Appendix D Convergence of $\overline{G}$** **337**

D.1 Introduction . . . . . 337

D.2 TE . . . . . 338

D.2.1 Heuristic argument . . . . . 338

D.2.2 Rigorous argument . . . . . 338

D.3 TM . . . . . 340

D.3.1 Heuristic argument . . . . . 340

D.3.2 Rigorous argument . . . . . 341

# List of Figures


3.1 Rough Surface Problem Geometry . . . . . 14

3.2 Incident Beam illumination and $S^3$ truncation . . . . . 28

4.1 TE Plot of $\overline{G}$ Integrand . . . . . 33

4.2 TM Plot of $\overline{G}$ Integrand . . . . . 34

4.3 TE $\lambda_s = 20\lambda_0$ Surface . . . . . 37

4.4 TM $\lambda_s = 20\lambda_0$ Surface . . . . . 38

4.5 TE $\lambda_s = 7\lambda_0$ Surface . . . . . 39

4.6 TM $\lambda_s = 7\lambda_0$ Surface . . . . . 40

4.7 TE $\lambda_s = 5\lambda_0$ Surface . . . . . 41

4.8 TM $\lambda_s = 5\lambda_0$ Surface . . . . . 42

4.9 TE $\lambda_s = 3\lambda_0$ Surface . . . . . 43

4.10 TM $\lambda_s = 3\lambda_0$ Surface . . . . . 44

4.11 TE Long Numerical Integration 0.5 Amplitude $\mp 1M$ $\lambda_0$ integration window . 46

4.12 TE Long Numerical Integration Amplitude Comparison $\mp 1M$ $\lambda_0$ integration window . . . . . 47

4.13 TM Long Numerical Integration 0.5 Amplitude $\mp 1M$ $\lambda_0$ integration window 48

4.14 TE Long Numerical Integration Amplitude Comparison $\mp 1M$ $\lambda_0$ integration window . . . . . 49

4.15 TE $1\lambda$ period Comparison . . . . . 51

4.16 TM $1\lambda$ period Comparison . . . . . 52

4.17 TE $1.05\lambda$ period Comparison . . . . . 53

4.18 TM $1.05\lambda$ period Comparison . . . . . 54

4.19 TE $0.9\lambda$ period Comparison . . . . . 55

4.20 TM $0.9\lambda$ period Comparison . . . . . 56

4.21 TE $2\lambda$ period Comparison . . . . . 57

4.22 TM $2\lambda$ period Comparison . . . . . 58

4.23 TE $1.5\lambda$ period Comparison . . . . . 59

4.24 TM $1.5\lambda$ period Comparison . . . . . 60

4.25 TE $1.2\lambda$ period Comparison . . . . . 61

4.26 TM $1.2\lambda$ period Comparison . . . . . 62

4.27 TE Periodicity of Finite integration . . . . . 64

4.28 TM Periodicity of Finite integration . . . . . 65

4.29 TE Sensitivity to Integration Support to $80 \leq \alpha \leq 85$ . . . . . 67

4.30 TE Sensitivity to Integration Support to $86 \leq \alpha \leq 90$ . . . . . 68

4.31 TM Sensitivity to Integration Support to $80 \leq \alpha \leq 85$ . . . . . 69

4.32 TM Sensitivity to Integration Support to $86 \leq \alpha \leq 90$ . . . . . 70

4.33 Comparison of $\overline{G}$ and $\overline{\Gamma}$ for $\frac{\lambda_s}{\lambda_0} = 20$ . . . . . 73

4.34 Comparison of $\overline{G}$ and $\overline{\Gamma}$ for $\frac{\lambda_s}{\lambda_0} = 10$ . . . . . 74

4.35 Comparison of $\overline{G}$ and $\overline{\Gamma}$ for $\frac{\lambda_s}{\lambda_0} = 8$ . . . . . 75

4.36 Comparison of $\overline{G}$ and $\overline{\Gamma}$ for $\frac{\lambda_s}{\lambda_0} = 7$ . . . . . 76

4.37 Comparison of $\overline{G}$ and $\overline{\Gamma}$ for $\frac{\lambda_s}{\lambda_0} = 5$ . . . . . 77

4.38 Comparison of $\overline{G}$ and $\overline{\Gamma}$ for $\frac{\lambda_s}{\lambda_0} = 4$ . . . . . 78

4.39 Comparison of $\overline{G}$ and $\overline{\Gamma}$ for $\frac{\lambda_s}{\lambda_0} = 2$ . . . . . 79

4.40 Comparison of $\overline{G}$ and $\overline{\Gamma}$ for $\frac{\lambda_s}{\lambda_0} = 1$ . . . . . 80

4.41 TE Peak Amplitude Ratio $\frac{b}{\lambda_0} = 0.5$ . . . . . 82

4.42 TM Peak Amplitude Ratio $\frac{b}{\lambda_0} = 0.5$ . . . . . 83

4.43 TE Peak Amplitude Ratio $\frac{b}{\lambda_0} = 0.05$ . . . . . 84

4.44 TM Peak Amplitude Ratio $\frac{b}{\lambda_0} = 0.05$ . . . . . 85

4.45 Combinations of Numeric and Analytic Computations . . . . . 87

4.46 Analytic Only Fresnel ApproximationTE Comparison of Integration Support 91

4.47 Analytic Only Fresnel Approximation TM Comparison of Integration Support 92

4.48 Struve Approximation of $\overline{\overline{G}}$ $\frac{\lambda_s}{\lambda_0} = 20$ small support . . . . . 96

4.49 Struve Approximation of $\overline{\overline{G}}$ $\frac{\lambda_s}{\lambda_0} = 20$ slightly larger support . . . . . 96

4.50 Struve Approximation of $\overline{\overline{G}}$ $\frac{\lambda_s}{\lambda_0} = 11$ small support . . . . . 97

4.51 Struve Approximation of $\overline{\overline{G}}$ $\frac{\lambda_s}{\lambda_0} = 8$ small support . . . . . 97

4.52 TM $\overline{\overline{G}}$ Variation with $\frac{\alpha}{\lambda_0}$ Explained by Fresnel Approximation -$\frac{j\zeta_{xx}}{2k_0}$ . . . . . 100

4.53 TM $\overline{\overline{G}}$ Variation with $\frac{\alpha}{\lambda_0}$ Explained by Fresnel Approximation -$\frac{j\zeta_{xx}}{2k_0}$ . . . . . 100

4.54 Simplified New Empiric $\frac{b}{\lambda_0} = 0.75$ . . . . . 105

4.55 Simplified New Empiric $\frac{b}{\lambda_0} = 0.05$ . . . . . 106

4.56 TM Empiric Analytic . . . . . 109

4.57 TM Empiric Analytic . . . . . 110

4.58 TM Empiric Analytic . . . . . 111

4.59 TM Empiric Analytic . . . . . 112

4.60 TM Empiric Analytic . . . . . 113

4.61 TM Empiric Analytic . . . . . 114

4.62 TM Empiric Analytic . . . . . 115

4.63 TM Empiric Analytic . . . . . 116

4.64 TM Empiric Analytic . . . . . 117

4.65 TM Empiric Analytic . . . . . 118

4.66 TM Empiric Analytic . . . . . 119

4.67 TM Empiric Analytic . . . . . 120

4.68 TM Empiric Analytic . . . . . 121

4.69 TM Empiric Analytic . . . . . 122

4.70 TM Empiric Analytic . . . . . 123

4.71 TM Empiric Analytic . . . . . 124

4.72 TM Empiric Analytic . . . . . 125

4.73 TM Empiric Analytic . . . . . 126
4.74 TM Empiric Analytic . . . . . 127
4.75 TM Empiric Analytic . . . . . 128
4.76 TM Empiric Analytic . . . . . 129
4.77 TM Empiric Analytic . . . . . 130
4.78 TM Empiric Analytic . . . . . 131
4.79 TM Empiric Analytic . . . . . 132
4.80 TM Empiric Analytic . . . . . 133
4.81 TM Empiric Analytic . . . . . 134
4.82 TM Empiric Analytic . . . . . 135
4.83 TM Empiric Analytic . . . . . 136
4.84 TM Empiric Analytic . . . . . 137
4.85 TM Empiric Analytic . . . . . 138
4.86 TE Empiric Analytic . . . . . 140
4.87 TE Empiric Analytic . . . . . 141
4.88 TE Empiric Analytic . . . . . 142
4.89 TE Empiric Analytic . . . . . 143
4.90 TE Empiric Analytic . . . . . 144
4.91 TE Empiric Analytic . . . . . 145
4.92 TE Empiric Analytic . . . . . 146

4.93 TE Empiric Analytic . . . . . 147
4.94 TE Empiric Analytic . . . . . 148
4.95 TE Empiric Analytic . . . . . 149
4.96 TE Empiric Analytic . . . . . 150
4.97 TE Empiric Analytic . . . . . 151
4.98 TE Empiric Analytic . . . . . 152
4.99 TE Empiric Analytic . . . . . 153
4.100TE Empiric Analytic . . . . . 154
4.101TE Empiric Analytic . . . . . 155
4.102TE Empiric Analytic . . . . . 156
4.103TE Empiric Analytic . . . . . 157
4.104TE Empiric Analytic . . . . . 158
4.105TE Empiric Analytic . . . . . 159
4.106TE Empiric Analytic . . . . . 160
4.107TE Empiric Analytic . . . . . 161
4.108TE Empiric Analytic . . . . . 162
4.109TE Empiric Analytic . . . . . 163
4.110TE Empiric Analytic . . . . . 164
4.111TE Empiric Analytic . . . . . 165
4.112TE Empiric Analytic . . . . . 166

4.113TE Empiric Analytic . . . . . 167

4.114TE Empiric Analytic . . . . . 168

4.115TE Empiric Analytic . . . . . 169

4.116Range of Validity of Analytic Formula . . . . . 170

4.117TE $\frac{\lambda_s}{\lambda_0} = \{20, 8\}$ $\frac{b}{\lambda_0} = \{0.5, 0.05\}$ All Numeric Calculations . . . . . 174

4.118TE $\frac{\lambda_s}{\lambda_0} = \{20, 8\}$ $\frac{b}{\lambda_0} = \{0.5, 0.1\}$ All Numeric Calculations . . . . . 175

4.119TE $\frac{\lambda_s}{\lambda_0} = \{20, 8\}$ $\frac{b}{\lambda_0} = \{0.5, 0.5\}$ All Numeric Calculations . . . . . 176

4.120TE $\frac{\lambda_s}{\lambda_0} = \{20, 10\}$ $\frac{b}{\lambda_0} = \{0.5, 0.05\}$ All Numeric Calculations . . . . . 177

4.121TE $\frac{\lambda_s}{\lambda_0} = \{20, 10\}$ $\frac{b}{\lambda_0} = \{0.5, 0.1\}$ All Numeric Calculations . . . . . 178

4.122TE $\frac{\lambda_s}{\lambda_0} = \{20, 10\}$ $\frac{b}{\lambda_0} = \{0.5, 0.5\}$ All Numeric Calculations . . . . . 179

4.123TE $\frac{\lambda_s}{\lambda_0} = \{20, 15\}$ $\frac{b}{\lambda_0} = \{0.5, 0.05\}$ All Numeric Calculations . . . . . 180

4.124TM $\frac{\lambda_s}{\lambda_0} = \{20, 8\}$ $\frac{b}{\lambda_0} = \{0.5, 0.05\}$ All Numeric Calculations . . . . . 181

4.125TM $\frac{\lambda_s}{\lambda_0} = \{20, 8\}$ $\frac{b}{\lambda_0} = \{0.5, 0.1\}$ All Numeric Calculations . . . . . 182

4.126TM $\frac{\lambda_s}{\lambda_0} = \{20, 8\}$ $\frac{b}{\lambda_0} = \{0.5, 0.5\}$ All Numeric Calculations . . . . . 183

4.127TM $\frac{\lambda_s}{\lambda_0} = \{20, 10\}$ $\frac{b}{\lambda_0} = \{0.5, 0.05\}$ All Numeric Calculations . . . . . 184

4.128TM $\frac{\lambda_s}{\lambda_0} = \{20, 10\}$ $\frac{b}{\lambda_0} = \{0.5, 0.1\}$ All Numeric Calculations . . . . . 185

4.129TM $\frac{\lambda_s}{\lambda_0} = \{20, 10\}$ $\frac{b}{\lambda_0} = \{0.5, 0.5\}$ All Numeric Calculations . . . . . 186

4.130TM $\frac{\lambda_s}{\lambda_0} = \{20, 15\}$ $\frac{b}{\lambda_0} = \{0.5, 0.05\}$ All Numeric Calculations . . . . . 187

4.131TE $\frac{b}{\lambda_0} = 0.05$ $\frac{\alpha}{\lambda_0} = 50$ . . . . . 189

4.132TE $\frac{b}{\lambda_0} = 0.05$ $\frac{\alpha}{\lambda_0} = 50$ . . . . . 190

4.133TE $\frac{b}{\lambda_0} = 0.05$ $\frac{\alpha}{\lambda_0} = 400$ . . . . . 191

4.134TE $\frac{b}{\lambda_0} = 0.05$ $\frac{\alpha}{\lambda_0} = 400$ . . . . . 192

4.135TE $\frac{b}{\lambda_0} = 0.5$ $\frac{\alpha}{\lambda_0} = 50$ . . . . . 193

4.136TE $\frac{b}{\lambda_0} = 0.5$ $\frac{\alpha}{\lambda_0} = 50$ . . . . . 194

4.137TE $\frac{b}{\lambda_0} = 0.5$ $\frac{\alpha}{\lambda_0} = 400$ . . . . . 195

4.138TE $\frac{b}{\lambda_0} = 0.5$ $\frac{\alpha}{\lambda_0} = 400$ . . . . . 196

4.139TE $\frac{b}{\lambda_0} = 1.0$ $\frac{\alpha}{\lambda_0} = 50$ . . . . . 197

4.140TE $\frac{b}{\lambda_0} = 1.0$ $\frac{\alpha}{\lambda_0} = 50$ . . . . . 198

4.141TE $\frac{b}{\lambda_0} = 1.0$ $\frac{\alpha}{\lambda_0} = 400$ . . . . . 199

4.142TE $\frac{b}{\lambda_0} = 1.0$ $\frac{\alpha}{\lambda_0} = 400$ . . . . . 200

4.143TM $\frac{\lambda_s}{\lambda_0} = \{20, 1\}$ $\frac{\alpha}{\lambda_0} = 50$ . . . . . 202

4.144TM $\frac{\lambda_s}{\lambda_0} = \{20, 1\}$ $\frac{\alpha}{\lambda_0} = 100$ . . . . . 203

4.145TM $\frac{\lambda_s}{\lambda_0} = \{20, 1\}$ $\frac{\alpha}{\lambda_0} = 200$ . . . . . 204

4.146TM $\overline{\overline{G}}$ $\frac{\lambda_s}{\lambda_0} = \{8, 7\}$ $\frac{b}{\lambda_0} = \{1, 1\}$ . . . . . 205

4.147TM $\overline{\overline{G}}$ $\frac{\lambda_s}{\lambda_0} = \{8, 7\}$ $\frac{b}{\lambda_0} = \{2, 2\}$ . . . . . 206

4.148TE $\overline{\overline{G}}$ $\frac{\lambda_s}{\lambda_0} = \{20, 40\}$ $\frac{b_{rms}}{\lambda_0} = 30$ (Enlarged) . . . . . 209

4.149TE $\overline{\overline{G}}$ $\frac{\lambda_s}{\lambda_0} = \{20, 40\}$ $\frac{b_{rms}}{\lambda_0} = 45$ (Enlarged) . . . . . 210

4.150TM $\overline{\overline{G}}$ $\frac{\lambda_s}{\lambda_0} = \{20, 40\}$ $\frac{b_{rms}}{\lambda_0} = 30$ (Enlarged) . . . . . 211

4.151TM $\overline{\overline{G}}$ $\frac{\lambda_s}{\lambda_0} = \{20, 40\}$ $\frac{b_{rms}}{\lambda_0} = 45$ (Enlarged) . . . . . 212

4.152TE $\overline{\overline{G}}$ $\frac{\lambda_s}{\lambda_0} = \{19, 20\}$ $\frac{b_{rms}}{\lambda_0} = 30$ (Enlarged) . . . . . 213

4.153TE $\overline{\overline{G}}$ $\frac{\lambda_s}{\lambda_0} = \{19, 20\}$ $\frac{b_{rms}}{\lambda_0} = 45$ (Enlarged) . . . . . 214

4.154TM $\overline{\overline{G}}$ $\frac{\lambda_s}{\lambda_0} = \{19, 20\}$ $\frac{b_{rms}}{\lambda_0} = 30$ (Enlarged) . . . . . 215

4.155TM $\overline{\overline{G}}$ $\frac{\lambda_s}{\lambda_0} = \{19, 20\}$ $\frac{b_{rms}}{\lambda_0} = 45$ (Enlarged) . . . . . 216

4.156TE $\overline{\overline{G}}$ $\frac{\lambda_s}{\lambda_0} = \{7, 20\}$ $\frac{b_{rms}}{\lambda_0} = 30$ (Enlarged) . . . . . 217

4.157TE $\overline{\overline{G}}$ $\frac{\lambda_s}{\lambda_0} = \{7, 20\}$ $\frac{b_{rms}}{\lambda_0} = 45$ (Enlarged) . . . . . 218

4.158TM $\overline{\overline{G}}$ $\frac{\lambda_s}{\lambda_0} = \{7, 20\}$ $\frac{b_{rms}}{\lambda_0} = 30$ (Enlarged) . . . . . 219

4.159TM $\overline{\overline{G}}$ $\frac{\lambda_s}{\lambda_0} = \{7, 20\}$ $\frac{b_{rms}}{\lambda_0} = 45$ (Enlarged) . . . . . 220

4.160TE $\overline{\overline{G}}$ $\frac{\lambda_s}{\lambda_0} = \{7, 8\}$ $\frac{b_{rms}}{\lambda_0} = 30$ (Enlarged) . . . . . 221

4.161TE $\overline{\overline{G}}$ $\frac{\lambda_s}{\lambda_0} = \{7, 8\}$ $\frac{b_{rms}}{\lambda_0} = 45$ (Enlarged) . . . . . 222

4.162TM $\overline{\overline{G}}$ $\frac{\lambda_s}{\lambda_0} = \{7, 8\}$ $\frac{b_{rms}}{\lambda_0} = 30$ (Enlarged) . . . . . 223

4.163TM $\overline{\overline{G}}$ $\frac{\lambda_s}{\lambda_0} = \{7, 8\}$ $\frac{b_{rms}}{\lambda_0} = 45$ (Enlarged) . . . . . 224

4.164TE $\overline{\overline{G}}$ $\frac{\lambda_s}{\lambda_0} = \{10, 15, 20\}$ $\frac{b_{rms}}{\lambda_0} = 30$ (Enlarged) . . . . . 226

4.165TE $\overline{\overline{G}}$ $\frac{\lambda_s}{\lambda_0} = \{10, 15, 20\}$ $\frac{b_{rms}}{\lambda_0} = 45$ (Enlarged) . . . . . 227

4.166TM $\overline{\overline{G}}$ $\frac{\lambda_s}{\lambda_0} = \{10, 15, 20\}$ $\frac{b_{rms}}{\lambda_0} = 30$ (Enlarged) . . . . . 228

4.167TM $\overline{\overline{G}}$ $\frac{\lambda_s}{\lambda_0} = \{10, 15, 20\}$ $\frac{b_{rms}}{\lambda_0} = 45$ (Enlarged) . . . . . 229

4.168TE $\overline{\overline{G}}$ $\frac{\lambda_s}{\lambda_0} = \{7, 8, 9\}$ $\frac{b_{rms}}{\lambda_0} = 30$ (Enlarged) . . . . . 230

4.169TE $\overline{\overline{G}}$ $\frac{\lambda_s}{\lambda_0} = \{7, 8, 9\}$ $\frac{b_{rms}}{\lambda_0} = 45$ (Enlarged) . . . . . 231

4.170TM $\overline{\overline{G}}$ $\frac{\lambda_s}{\lambda_0} = \{7, 8, 9\}$ $\frac{b_{rms}}{\lambda_0} = 30$ (Enlarged) . . . . . 232

4.171TM $\overline{\overline{G}}$ $\frac{\lambda_s}{\lambda_0} = \{7, 8, 9\}$ $\frac{b_{rms}}{\lambda_0} = 45$ (Enlarged) . . . . . 233

5.1 TM Scattered Fields from $\lambda_s = 2\lambda_0$ Surface Normal Incidence . . . . . 242

5.2 TM Scattered Fields from $\lambda_s = 2\lambda_0$ Surface $\theta_i = 15°$ Incidence . . . . . 242

5.3 TM Scattered Fields from $\lambda_s = 2\lambda_0$ Surface $\theta_i = 15°$ Incidence . . . . . 243

5.4 Scattered Fields from $\lambda_s = 3\lambda_0$ Surface Normal Incidence . . . . . 244

5.5 Scattered Fields from $\lambda_s = 3\lambda_0$ Surface $\theta_0 = 15°$ Incidence . . . . . 245

5.6 Scattered Fields from $\lambda_s = 3\lambda_0$ Surface $\theta_0 = 45°$ Incidence . . . . . 246

5.7 Scattered Fields from $\lambda_s = 4\lambda_0$ Surface Normal Incidence . . . . . 247

5.8 Scattered Fields from $\lambda_s = 4\lambda_0$ Surface $\theta_0 = 15°$ Incidence . . . . . 248

5.9 TM Scattered Fields from $\lambda_s = 4\lambda_0$ Surface $\theta_0 = 45$ Incidence . . . . . 249

5.10 Scattered Fields from $\lambda_s = 5\lambda_0$ Surface Normal Incidence . . . . . 250

5.11 Scattered Fields from $\lambda_s = 5\lambda_0$ Surface $\theta_0 = 15°$ Incidence . . . . . 251

5.12 Scattered Fields from $\lambda_s = 5\lambda_0$ Surface $\theta_0 = 45°$ Incidence . . . . . 252

5.13 $\frac{\lambda_s}{\lambda_0} = 5$ Backscatter $\theta_i = -\theta_s$ . . . . . 253

5.14 $\frac{\lambda_s}{\lambda_0} = 2$ Backscatter $\theta_i = -\theta_s$ . . . . . 254

5.15 Gentle Two Frequency Surface Normal Incidence . . . . . 256

5.16 Gentle Two Frequency Surface Mild Incident Angle . . . . . 257

5.17 Gentle Two Frequency Surface Moderate Incident Angle . . . . . 258

5.18 Moderate Two Frequency Surface Normal Incidence . . . . . 259

5.19 Moderate Two Frequency Surface Mild Incident Angle . . . . . 260

5.20 Moderate Two Frequency Surface Moderate Incident Angle . . . . . 261

5.21 Three Frequency Surface Normal Incidence . . . . . 262

5.22 Three frequency Surface Mild Incident Angle . . . . . 263

5.23 Three Frequency Surface Moderate Incident Angle . . . . . 264

# List of Tables

4.4.1 Term by Term Maximum Value Analysis Struve Based Approximation . . . . 94

4.4.2 Surface Parameters for Simulation . . . . . 207

4.4.3 RMS surface curvatures . . . . . 234

# List of Abbreviations

| | |
|---|---|
| $\alpha$ | Limit of integration support of $\overline{\overline{G}}$, aka the half-width of the surface $L = 2 * \alpha$ |
| $\psi_s$ | Scattered Field |
| $\overline{G}(x)$ | Infinite integration of integral equation kernel |
| $\overline{\Gamma}$ | Empiric Formula for $\overline{G}$ |
| $\overline{\overline{G}}(x)$ | Finite integration of integral equation kernel |
| $J_0$ | Incident Current (Kirchhoff Current) |
| $J_{00}$ | Mutiple Scatter Source Current |
| $J_{ms}$ | Mutiple Scatter Current |
| $J_{ss}$ | Single Scatter Current |
| $S^3$ | Single Scatter Subtraction Method |
| $b$ | Sinusoidal Surface Amplitude |
| $\zeta_{xx}(x)$ | Surface Curvature (Second Derivative of height) |
| $L$ | Length of Surface |
| $\zeta_x(x)$ | Surface Slope (First Derivative of height) |
| $\lambda_s$ | Surface Wavelength |
| $S$ | Surface |

$\theta_i$ Angle of Incidence

$\theta_{sc}$ Scattering Angle

# Chapter 1

# Introduction

## 1.1 Introduction

The study of electromagnetic scattering from rough surfaces continues to interest researchers of communication and remote sensing systems. The typical approach to solving this class of problem is to set up a boundary value problem where the entire scattering system can be described in terms of currents on the surface of the interface between different media.

Herein a new technique is presented to study rough surface scattering based on a reformulation of the Magnetic Field Integration Equation. This technique performs a physics-based preconditioning of the integral equation by separating the single- and multiple-scattering currents and removing the single scattering portion from the integral. Using this method requires the definition of a new quantity which is the integral of the kernel of the original MFIE integral. Closed form expressions are found for this quantity and thus directly the single-scatter current for a well-defined region of validity of surface parameters that are then efficiently radiated into the far field. Both the closed form expressions, and the computed radiated fields are studied for their physical significance. This provides a clear physical intuition for the technique as an augmentation to existing ones, resolves an old dispute of scattering physics, and raises new questions on the effect of truncation. In this work for the first time polarization sensitivity is predicted and demonstrated for single-scattering.

A general overview of the simulation model used is as follows. First a deterministic corduroy rough surface is generated which is assumed to be infinite in extent. Then the currents generated by an prescribed incident field are found by the physical optics or Kirchhoff method. This incident field has a finite beamwidth that truncates the problem to a finite one which can be solved numerically. From the incident field the Kirchhoff, single-scatter or total currents are found. Finally, these currents are allowed to radiate and are examined in the far-field. Additionally, the multiple-scattered currents may be found by the new technique presented but such an investigation is left to future work.

### 1.1.1 Research Goals

The goals of this work are simply stated:

1. Derive a novel method of studying electromagnetic rough surface scattering based on a decomposition of the current into single and multiple scattering ($S^3$ method)
2. Use this method to provide analytic approximate theories for rough surface scattering.
3. Deepen the understanding of scattering physics through the use of these new techniques.

### 1.1.2 Accomplishments

- Introduced Single-Scatter Subtraction Method
- "Empiric-analytic" formulas for finite and infinite kernel integral
  - Closed-form expression for single-scatter currents
  - Clearly defined, and wide range of surface parameters

  - Bent tangent-plane

- First time a single-scattering result has shown a polarization dependence

- Closed-form improvement of Kirchhoff currents with "bent" tangent plane

### 1.1.3 Questions Answered

- What is the single scattering doing physically?

  - Bent-tangent plane

- Is Bragg scattering single or multiple scattering?

  - Empiric-analytic formulas tell us no $k_0$ dependent terms in single-scattering thus is multiple-scatter

- Is single scattering polarization sensitive?

  - Yes, demonstrated herein for the first time

- What is the affect of truncating the problem?

  - Anomalous enhanced backscatter observed with truncated empiric-analytic single-scatter results

  - Further terms in $S^3$ should cancel this out

## 1.2 Motivation

A number of forces coalesce to motivate this work: from the computational complexity of solving fully 3-dimensional rough surface scattering to the lack of insight provided by numerical techniques versus analytic ones, which themselves have limited and ambiguous ranges of validity.

The computational complexity of realistic environmental scattering cases of interest continue to outpace computation capacity improvements. For the simulation of large surface scattering problems, the use of methods such as Finite Difference Time Domain do not apply as they must discretize the entire space around the extended scatterer leading to a prohibitively large simulation domain [29]. Instead, surface integral equations discretized by the Method of Moments (MOM) are used to reduce the computational requirements [26]. Still, there is a continuous need to solve bigger and more realistic complex rough surface scattering problems which are too big to be fully simulated despite advancements in preconditioning techniques and iterative methods. One such iterative method that has shown promise in studying 2-dimensional scattering problems is the Method of Ordered Multiple Interactions (MOMI), a technique based on a mathematical preconditioning of the Method of Moments [30]. Unfortunately, due to its complex nature there is no clear path to extend the technique to 3D. This motivates a new technique based on a physical preconditioning that offers a clear path to studying 3-dimensional scattering problems.

Additionally, all strictly numerical techniques suffer from a lack of insight in comparison to analytical methods. Candidate analytical theories include the physical and geometric diffraction theories [32, 56] but these are only applicable to scattering from finite and deterministic objects as they require the use of canonical geometries so cannot be applied to extended statistically rough surfaces. The analytical approximations which may be applied, discussed

further in the literature review, suffer from known failures and ambiguous ranges of validity. Therefore there is a pressing need for analytical approximations to rough surface scattering that are an improvement over the Kirchhoff approximation to provide the understanding required to drive novel applications and interpret existing results.

## 1.3 Research Outline

This work begins with a literature review in Chapter 2 which begins with an overview of the field, followed by a development of the existing analytical approaches to the rough surface scattering problem and finally ending with applications.

Chapter 3 defines the problem addressed. First, the geometry and surface description is provided in Section 3.2 while defining some of the nomenclature used throughout. Next, the Magnetic Field Integral Equation (MFIE) for a 1-dimensionally rough surface (2-D scattering) is introduced which is a standard full-wave numerical approach in the literature that provides the total current on surface given a description of the surface and the incident currents. Then the beam illumination used to allow the problem to be solved numerically by reducing the infinite surface to a finite one is detailed in Section 3.2.4. This is followed by the method to compute the scattered fields from the total current on a surface and a convenient figure of merit of these fields called the Normalized Scattering Cross Section (NSCS). The use of the NSCS removes the dependence on distance and incident power and additionally reduces a vector quantity to a scalar one. Finally, the Single Scatter Subtraction method ($S^3$), a novel current decomposition based on the MFIE, that forms the basis of this thesis is introduced in Section 3.3. The $S^3$ section introduces a new quantity, the kernel integral $\overline{G}$ in the finite case and $\overline{\overline{G}}$ for the finite, and defines expressions describing the single- and multiple-scattered surface currents.

The kernel integral introduced by the $S^3$ method is the focus of Chapter 4 which begins with a discussion of the difficulty of its calculation and demonstrates some example integrands. Following this, numeric results for the kernel integral are presented, first for the infinite case which is approximated by a surface two million electromagnetic wavelengths long. Next, a study of finite surfaces finds the result to mirror that of the infinite results with an additional small scale perturbation. Section 4.4 gives analytic and empirically derived approximations to the integral of the Green function kernel of the MFIE, which is shown in this work as sufficient and necessary for identifying the single scattering currents.

The goal achieved in this section is to produce closed form expressions for the single scattering current. From the series of simulation experiments a formula is "empirically" derived describing $\overline{G}$ on an infinite surface to excellent agreement for a wide range of surface parameters before attention is given to the finite case. First, an approximation based on a large argument expansion of the Hankel function is derived for both linear polarizations, providing the integral in the regions of large separation between source and observation point for a single frequency surface. Then another approximation is given for the small argument region, where the source is close to the observation point for a general spectral surface and clear, simple bounds on validity are provided. Based on comparisons to numerical results, it is shown that the previously derived large argument approximations may not fully describe the behavior of TM polarization and a higher-order approximation given. Unfortunately, the bounds of validity of the small argument approximation fail to reach even the higher order approximation bounds so their combination cannot be used to describe the full solution. Next an approximate empirical formula is given for the entire finite kernel integral for TE polarization from numerical computations. Consistent with the failure of the first order approximation to describe the TM results, a purely empirically derived formula remained

elusive been found[1] for this case. This instead prompted a combination empiric analytic formula to be found by subtracting the analytic integration tail approximation, derived above, from the infinite case empiric formula which for both polarizations finds excellent agreement and is, with hard bounds on its validity, the crowning technical achievement of this work. Finally, despite the fact that TE appears analytically to require a special formula, the single frequency approximations are generalized to the spectral surface case by a simple linear superposition for both TM and TE polarizations.

Finally, Chapter 5 begins by discussing the ramifications of the proposed method in furthering the understanding of rough surface scattering physics. First, the augmentation provided by this method to the Kirchhoff solution is discussed, which was not apparent in the initial formulation of this method, but matches the next step anticipated by the literature. Then the classification of Bragg scattering as a multiple scattering phenomenon is discussed, despite its representation based only on local parameters, which has been argued by other authors. Next, the effect of truncation on the physics of the rough surface scattering problem is examined as elucidated by the approximations developed in section 4.4.3.6. The chapter closes with section 5.3 where results of the scattered fields predicted by the empiric analytic approximation of the single scattering current are compared against the Kirchhoff current for single sinusoid surfaces with wavelengths approaching but not reaching the electromagnetic wavelength, as well as combinations of two and three sinusoids for which good agreement for $\overline{\overline{G}}$ was previously found.

A summary of the work, accomplishments and suggestions for further research follow in Chapter 6. Additionally, the Appendix contains detailed derivations of the analytic approximations discussed in Chapter 4.

[1] In other words, TM polarization is complicated with a functional dependence on surface parameters and integration support not easily recognized by intuition and experience.

# Chapter 2

# Review of Literature

## 2.1 Existing Literature Reviews

The classic comprehensive reviews of the literature are provided in [7, 8, 44]. They generally trace the beginnings of the study of rough surface scattering to Rayleigh in the late 19th century [46]. Each of these reviews builds successively on the last with [8] covering the scalar Kirchhoff method for a single scale of roughness, [7] adding the perturbation approach, shadowing and multiple scales of roughness and finally [44] adding multiple scattering and numerical techniques.

Despite over a century of study, no generally applicable analytical method has been developed. This is evidenced in a modern review of analytic theories in which most of the over 30 theories listed fail to meet half of the author's criteria [20] for a comprehensive, successful rough surface theory. Analytical theories can be divided into three broad classes: those applicable to small-scale roughness derived through perturbation techniques, those for large-scale roughness through the tangent plane or Kirchhoff method and composite methods derived through a variety of means which attempt to account for multiple scales of roughness.

A modern review [50] shows numerical methods apply to a wide array of simulation parameters, but fail to give the physical insight given by analytic approaches. Further, the numerical complexity of realistic cases still outpaces computational improvements and an-

alytic approximations are needed to verify their accuracy as many methods are difficult to physically reason about.

The standard diffraction theories [32, 35, 56, 57] view diffraction as a local phenomenon but require the subdivision of the scattering surface into canonical geometries [3] which cannot be applied to rough surfaces where the geometry is only "known" in a statistical sense [13].

## 2.2 Perturbation Approaches

### 2.2.1 Classical Development

The perturbation method is based on a small-height expansion of the scattered fields and finds validity in the low-frequency regime [47, 58]. One technique which aims to improve the theory is known as the method of smoothing and is based on a decomposition of the current into a coherent and incoherent part before substitution in the surface current integral equation [10].

## 2.3 Kirchhoff Solutions

### 2.3.1 Classic Development

Kirchhoff theory uses the current of the zeroth order iteration of the second kind integral equation as the basis of solution [41]. Arising in the mid 20th century originally by Russian authors, it was soon thereafter published in English [7, 16]. This amounts to assuming the current at each point on the surface is equivalent to that produced on an infinite tangent plane centered on that point and for this reason is often also called the tangent plane method

[7]. It thus requires the local surface curvature be small, making this method suited only to large scale roughness. Depending on the approximations made and in the high frequency limit, it also encompasses the physical optics and geometrical optics methods which are successively rougher approximations to the Kirchhoff integrals [20, 25, 45].

In [25] Fung rebukes the position [5] that the high frequency limit, or stationary phase approximation for fields and deep phase modulation approximation for power, is a requirement of the Kirchhoff method despite a fundamental change in the character of the resultant equations. This is achieved by a comparison with Monte Carlo moment method calculations for a Gaussian surface with large radii of curvature. Thus a frequency dependance correctly appears in the more general Kirchhoff and physical optics solutions, separating them from the more approximate geometrical optics solution that is frequency independent.

It is important to note that by definition, classical Kirchhoff theory is a purely local theory which means multiple scattering and surface self-shadowing are not accounted for. Additionally, as a tangent plane approximation, local curvature effects are not included. These limitations signal two avenues to augment the theory.

### 2.3.2 Non-local Corrections

Attempts at non-local corrections to Kirchhoff theory include considering iterations of the boundary integral equations for surface currents for multiple scattering as well as shadowing functions. Attempts of considering multiple iterations of integral equations have had some success but run into issues with evaluation of difficult integrals and convergence properties [28, 36, 40].

While they have been shown to provide some improvement [52, 60], shadowing functions have a number of issues. Most glaring is that they result in surface currents dependent on

observation angle as shown by Brown [12], thereby eliminating any rigorous basis. Ogilvy also notes that shadowing functions are only applicable in cases where the assumptions of Kirchhoff theory are violated with either large slopes and curvatures or near grazing angles [44].

### 2.3.3 Curvature Corrections

Improvements to the Kirchhoff solutions have come as curvature and diffraction corrections [39, 48, 49, 61]. A series of papers [23, 24] by Fuks develops a diffraction correction to the geometric optics (GO) solution up to order $\frac{1}{k_0^2}$ by considering the first two iterations of an integral equation of the first kind for scattering from a Gaussian rough surface at normal incidence. In this work, Fuks observes cross-polarized backscattering from the surface curvature not predicted by the standard GO formulations and an apparent smoothing of the surface roughness. Bringer et al. show the Fuks diffraction corrected GO model has deficiencies predicting near nadir backscattering from the sea surface compared to a simple physical optics (PO) model including kurtosis which they found consistent with observed NSCS [9].

## 2.4 Composite Models

To overcome the limitations of the perturbation and Kirchhoff methods which apply to opposite regimes by taking approximations that conflict with each other, a large number of composite models have been introduced to varying degrees of success [11, 19, 20, 44]. Most methods suffer problems with difficult integrations, unknown convergence properties, or poor extension to statistical surfaces.

## 2.5 Applications

Random rough surface theory finds applications to radar systems observing oceans for both determination of sea state [4, 6, 53] and target detection [33, 34]. A review specific to ocean rough surface models can be found in [59]. Further applications can be found in remote sensing of terrestrial and extraterrestrial land and ice[8, 43, 52].

An interesting physical result comes from surface waves half of the incident field's wavelength called Bragg scattering and first described by [15] for ocean surfaces but also finding important applications in atmospheric hazard detection [42]. Bragg scattering dominates ocean clutter with returns often exceeding signal levels of targets, prohibiting their detection. A thorough understanding of the mechanism of this and other physical phenomenon have advanced clutter suppression techniques [33].

# Chapter 3

# Single Scatter Subtraction

## 3.1 Introduction

In this section, the general class of problems addressed is described and nomenclature defined. First, the problem is formulated by describing the geometry and mathematical description of the surface. Then the Magnetic Field Integral Equation (MFIE) is presented, followed by the incident illumination and the computation of the scattered fields. Finally, upon this foundation a new solution technique is presented. The general method of solution is to describe a surface, generate the incident illuminating surface current, solve for the resultant current either exactly with the MFIE or through approximate methods, then compute the scattered fields from these currents.

## 3.2 Problem Formulation

### 3.2.1 Problem Geometry

All cases considered in this work consist of the illumination of mean planar surfaces along $z = 0$ that are infinite in extent with no variation in the $\hat{y}$ direction. Figure 3.1 shows the two-dimensional problem geometry. The plane of incidence is the xz-plane with the incidence angle $\theta_i$ the angle between the incident wave vector and the z-axis. Likewise the scattering

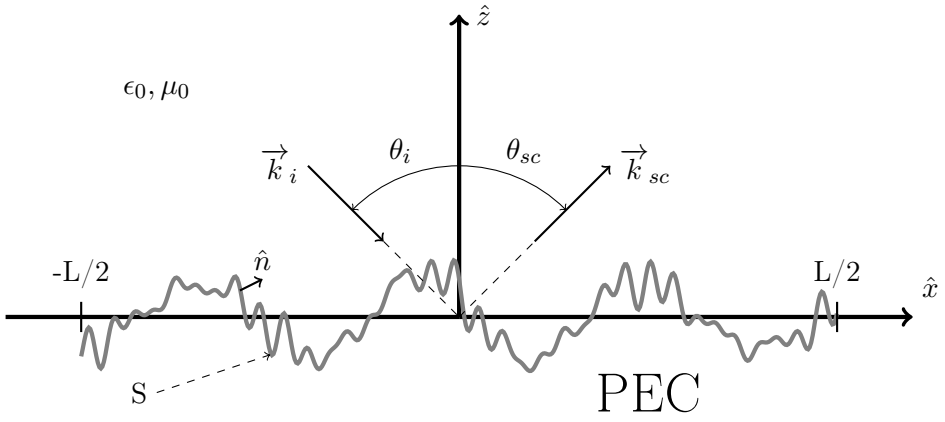


Figure 3.1: Rough Surface Problem Geometry

angle $\theta_s$ is between the scattered wave vector and the z-axis. The upper half-space will be assumed to be homogenous free space, while the lower half-space is a homogenous perfectly electrical conducting (PEC) medium.

### 3.2.2 Surface Characterization

All surfaces considered are deterministically rough with no re-entrant features, that is the surface height $\zeta(x)$ is a (proper single-valued) function of x as described below. Randomly rough surfaces are saved for future research. Since the approach proposed in this work is to the best of the author's knowledge quite novel, it is important to be able to confirm the results obtained by careful mathematical and physical reasoning by examining simplified models before more complicated, realistic cases. To do so, the deterministically rough surfaces will consist of sinusoids and simple products of sinusoids to simplify the problem for initial

validation as well as to isolate and highlight physical scattering phenomenon. After obtaining an understanding of the technique and scattering from singly sinusoid surfaces attention will be turned to the confounding effects of multiple surface frequencies from the superposition of sinusoids. With this understanding it will be possible to apply intuition to the results of scattering from realistic rough surfaces known only by their statistical properties in future work.

#### 3.2.2.1 Sinusoidal Surfaces

The simplest case of rough surface to be examined will be the singly sinusoid surface which will be normalized to the free space electromagnetic wavelength $\lambda_0$ in order to generalize the results. Thus the height profile will given by:

$$\frac{\zeta\left(\frac{x}{\lambda_0}\right)}{\lambda_0} = \frac{b}{\lambda_0}\cos\left(2\pi K_s \frac{x}{\lambda_0}\right) \tag{3.2.1}$$

with $K_s = \frac{k_s}{k_0} = \frac{\lambda_0}{\lambda_s}$ the normalized surface wavenumber and $\frac{\lambda_s}{\lambda_0}$ the normalized surface wavelength. $k_0$ is the free space electromagnetic wavenumber. No phase shift will be considered so two parameters fully describe the surface: the surface amplitude and surface period.

Additionally, some cases of the superposition of sinusoids will be examined where

$$\frac{\zeta\left(\frac{x}{\lambda_0}\right)}{\lambda_0} = \sum_{n}^{N} \frac{b_n}{\lambda_0}\cos\left(2\pi K_{sn} \frac{x}{\lambda_0}\right) \tag{3.2.2}$$

for some small finite $N \in \mathbb{Z}$ . This surface has N frequency components, each with their own normalized amplitude $\frac{b_n}{\lambda_0}$ and normalized surface wavenumber $K_{sn}$.

### 3.2.3 Magnetic Field Integral equation

The Magnetic Field Integral Equation, hence forth the MFIE, provides the solution of scattered electromagnetic fields from a set of sources and a closed surface. Since it has the unknown solution both within and outside of the integral it is a second kind integral equation. In contrast the Electric Field Integral Equation or EFIE is a first kind integral equation so the unknown current is only inside the integral. Both can be derived from Maxwell's equations and allow finding the entire electromagnetic fields in a region by only considering the currents on the boundaries between media. While both may be discretized for numerical solution, the MFIE generally has better convergence properties and will be used to form the basis of the new approach proposed in this work.

The MFIE has been studied extensively for this class of 2D problem so only the final equations are presented here and the interested reader is directed to [2, 17, 30, 55, 63] for more detail. For a PEC surface the MFIE can be written as follows:

$$J(x) = J_0(x) + 2\int G(x,x')\,J(x')\,ds' \tag{3.2.3}$$

Where $J(x)$ is the unknown surface current, and in terms of the fields is for TE polarization $J(x) = \frac{\partial E}{\partial n}$, the normal derivative of the electric field, or for TM $J = H$, the magnetic field. $J_0$ is the known incident current discussed further in section 3.2.4 which for this work will be represented by either Eq. 3.2.9 or 3.2.10 depeding on polarization. The differential element contains the surface projection onto the mean zero plane:

$$ds' = \sqrt{1+\zeta_{x'}^2(x')}dx'$$

The kernel $G(x,x')$ is a derivative of the 2D free space Green function $G_0(x,x')$. Notice

lack of a subscript for the kernel and the subscript naught for the 2D Green function. For TE, the kernel will be equal to the negative of the derivative of the Green function with respect to the surface normal at the point of observation, while for TM it is the derivative with respect to the surface normal at the source point which is the point of integration.

Thus, since the 2D free-space Green function is given by Eq. 3.2.4 [2],

$$G_0(x,x') = \frac{-j}{4} H_0^{(2)}\left(k_0\sqrt{(x-x')^2 + \left(\zeta(x) - \zeta(x)'\right)^2}\right) \tag{3.2.4}$$

where $H_0^{(2)}(x)$ is the zeroth-order Hankel function of the second kind that represents a 2D outward travelling wave, the TE polarization kernel specifically is $G(x,x') = -\frac{\partial G_0(x,x')}{\partial n}$ as shown in Eq. 3.2.5.

$$\frac{\partial G_0(x,x')}{\partial n} = \frac{-k_0}{4j} \frac{\{-\zeta_x(x)(x-x') + (\zeta(x) - \zeta(x'))\}}{\sqrt{1+\zeta_x^2(x)}\sqrt{(x-x')^2 + (\zeta(x) - \zeta(x'))^2}} \cdot H_1^{(2)}\left(k_0\sqrt{(x-x')^2 + \left(\zeta(x) - \zeta(x)'\right)^2}\right) \tag{3.2.5}$$

Likewise, for TM the kernel is $G(x,x') = \frac{\partial G_0(x,x')}{\partial n'}$ as shown in Eq. 3.2.6.

$$\frac{\partial G_0(x,x')}{\partial n'} = \frac{k_0}{4j} \frac{\{-\zeta_x'(x')(x-x') + (\zeta(x) - \zeta(x'))\}}{\sqrt{1+\zeta_{x'}^2(x')}\sqrt{(x-x')^2 + (\zeta(x) - \zeta(x'))^2}} \cdot H_1^{(2)}\left(k_0\sqrt{(x-x')^2 + \left(\zeta(x) - \zeta(x)'\right)^2}\right) \tag{3.2.6}$$

Note the principle value of the integral has already been incorporated in Eq. 3.2.3.

In these equations $n$ is the surface normal at the point of observation $x$ and $n'$ is the surface

normal at the source or integration point $x'$. $\zeta(x)$ is the surface height at the point $x$, and $\zeta_x(x)$ represents the first derivative of the height or the surface slope.

#### 3.2.3.1 Kirchhoff Solution

A simple approximate method discussed in Section 2.3, the Kirchhoff solution, uses the first term on the right hand side of Eq. 3.2.3 as an approximation for the current. Note that it is the exact solution for a perfectly flat surface as can be seen by equations 3.2.5 and 3.2.6 which go to zero for zero slope and zero height difference[1]. The chief advantage of this technique is its computational simplicity as each point on the surface may be calculated independently and no difficult integrals are required to be solved. The disadvantages and non-physical nature of this solution outside of the electromagnetic high-frequency limit were discussed in the literature review. Nonetheless, it will be used as a basis of comparison for the new approximate methods developed in this thesis due to its prominence in use. Kirchhoff currents will be described as $J_{Kir} = J_0$ when used as a solution current, and either the full name or the abbreviation "Kirch" used to describe field or scattered quantities obtained by this method.

### 3.2.4 Beam illumination

As mentioned previously, the MFIE only applies to closed surfaces, so the surfaces described in Section 3.2.2 must closed at infinity. To allow numerical calculations, some form of truncation must be imposed on the simulation boundaries. One method of achieving this is to impose a finite support to the current by the use of a tapered illumination which describe a beam of illumination.

[1]Even for non-zero slope or a slanted plane, we may redefine the coordinate system to give a level plane and modified incident angle

Tapered illuminations are given in the general form:

$$\psi_0(x,z) = T(x,z)\, e^{-j\vec{k_i}\bullet\vec{r}} \tag{3.2.7}$$

with $\vec{k_i}\bullet\vec{r} = k_0(x\sin\theta_i - z\cos\theta_i)$ for 2D and $\psi_0(x,z)$ a general scalar[2] field quantity at the point $(x,z)$. Note the exponential represents the incoming electromagnetic wave with angle of incidence $\theta_i$ , and $T(x,z)$ represents the taper converting the plane wave to a beam-limited illumination.

Since the edges of the beam approach zero, the surface in these regions may be neglected and the simulation domain truncated.

#### 3.2.4.1 Thorsos Taper

One such taper that has been extensively used in the study of acoustic and electromagnetic scattering from rough surfaces is that introduced by Thorsos [54]. The Thorsos taper applied to the 2D electromagnetic problem is given by [63]:

$$T(x,z) = \exp\left\{\frac{-\xi^2}{g^2} - j\frac{\vec{k_i}\bullet\vec{r}}{(k_0 g\cos\theta_i)^2}\left[\frac{2\xi^2}{g^2} - 1\right]\right\} \tag{3.2.8}$$

with $\xi = x + z\tan\theta_i$. Here the parameter $g$ is the spot-size of the illumination on the surface. and $k_0$is the electromagnetic wavelength

Note that in the MFIE for TM, the current is simply given by

$$J_0(x) = 2H_i(x) = 2\psi_0 \tag{3.2.9}$$

[2]Scalar because of the considered 1D rough surface or 2D scattered field considered in this work.

while for TE it is

$$J_0(x) = 2\frac{\partial E_i}{\partial n}(x)\frac{1}{k_0\eta} = 2\hat{n} \bullet \nabla\psi_0\frac{1}{k_0\eta} \tag{3.2.10}$$

Before using the Thorsos taper, it is important to understand the assumptions taken in its derivation so that it may be properly used to simulate real physics.

This illumination is an approximation using Laplace's method to evaluate the following integral [2]:

$$\psi_i = \frac{1}{\sqrt{\pi}\Delta\theta}\int_{-\pi/2}^{\pi/2}\exp\left[(\theta-\theta_i)^2/\Delta\theta^2\right]\exp\left[-j\overrightarrow{k_i}\bullet\overrightarrow{r}\right]d\theta \tag{3.2.11}$$

Adwadallah notes the following 3 assumptions are taken:

1. Slow variation in exponential $\exp\left(-j\overrightarrow{k}\bullet\overrightarrow{r}\right)$
2. $kg\cos\theta_i \gg 1$ which means the majority of the integral comes from angles near the incident angle
3. $g > \frac{2\sqrt{C}}{k\left(\frac{\pi}{2}-\theta_i\right)\cos\theta_i}$ with C a problem specific constant

The Thorsos taper breaks down as the incident angle approaches grazing as it begins to describe waves incident from below the surface. Further difficulties lie in the fact that the Thorsos taper is not an exact solution to Maxwell's equations, although has been found to be a better solution than a standard Gaussian beam [55].

### 3.2.5 Scattered Fields

Ultimately we are interested in the field scattered from the rough surface so the bistatic normalized scattering cross section(NSCS) will be considered. The NSCS is defined as the ratio of scattered power in at specific angle with the distance-dependence multiplied out and

normalized by the total incident power [31] and is typically given in decibels:

$$\text{NSCS} = \frac{r \left\langle \psi_s \cdot \psi_s^* \right\rangle}{g \cos\left(\theta_i\right) \sqrt{\frac{\pi}{2}}} \tag{3.2.12}$$

with $\psi_s$ the scattered field calculated by the radiation integral:

$$\psi_s = \int_{-\infty}^{\infty} J \tilde{P} dS \tag{3.2.13}$$

Where $J$ is the solution current to be radiated. $r$ is the distance from the surface after taking the far field approximation[3] to remove the distance dependence from the scattered results. Note the denominator of Eq. 3.2.12 is the total incident power on the surface for the Thorsos tapered illumination. For the two polarizations, the other quantities are

1. TE
   (a) $\psi_s = E_s$
   (b) $\tilde{P} = -G_0\left(x, x'\right)$
2. TM
   (a) $\psi_s = H_s$
   (b) $\tilde{P} = \frac{\partial G_0(x,x')}{\partial n'}$

In cases of interest, we are in the far field so the following approximation may be made for the 2D freespace Green function (Eq. 3.2.4) and its normal derivative (Eq. 3.2.6)

$$G_0\left(x, x'\right) \approx \frac{1}{4j} \sqrt{\frac{2}{k_0 r \pi}} \exp\left\{j\left(k_{sx} x' + k_{sz} \zeta\left(x'\right)\right)\right\} \exp\left\{-j\left(k_0 r - \frac{\pi}{4}\right)\right\}$$

[3] $|r - r'| \approx r$ for $r \gg r'$

$$\frac{\partial G_0(x,x')}{\partial n'} \approx \frac{1}{4j}\sqrt{\frac{2}{k_0 r\pi}}\frac{\left[-\zeta_x(x')\,k_{sx}+k_{sz}\right]}{\sqrt{1+\zeta_x^2(x')}}\exp\left\{j\left(k_{sx}x'+k_{sz}\zeta(x')\right)\right\}\exp\left\{-j\left(k_0 r-\frac{3\pi}{4}\right)\right\}$$

In these expressions, the following shorthand is used:

$$k_{sx} = k_0 \sin\theta_s$$

$$k_{sz} = k_0 \cos\theta_s$$

$$dS = \sqrt{1+\zeta_{x'}^2(x')}dx'$$

## 3.3 Single Scatter Subtraction Method

### 3.3.1 Motivation

Despite advances in computing power, the direct solution of the MFIE through the Method of Moments (MoM) [26] technique remains computationally expensive for modern problems of interest. This has led to the development of fast iterative solvers such as the Method of Ordered Multiple Interactions (MOMI) [30, 31] which is suited 2-dimensional problems. Unfortunately, MOMI has difficult path to 3-D and like all numerical based techniques, does not give the depth of insight into scattering physics as analytic techniques. Noticing that there must be some local or single scattering contribution coming from the integral in the MFIE suggests that physical preconditioning, as opposed to MOMI's mathematical preconditioning, can be performed by pulling this local contribution out of the integral term. From this, extended analytical approximations may be found.

### 3.3.2 Formulation

The Single Scatter Subtraction method ($S^3$) is based on the hypothesis that the Kirchhoff (or physical optics) current $J_0(x)$ does not comprise the entire single scattering current because there must be some contribution from the integral term. The method consists of subtracting the local portion of the current from the integral term and rearranging, then decomposing the total current into single and multiple scattering current.

Beginning with the MFIE (Eq. 3.2.3) for PEC rough surface scattering with the surface projection and factor of 2 pulled into $G(x, x')$:

$$J(x) = J_0(x) + \int_{-\infty}^{\infty} G(x, x') J(x') \, dx'$$

Now extract the single scattering from the interaction integral,

$$J(x) = J_0(x) + \int_{-\infty}^{\infty} G(x, x') [J(x') - J(x)] \, dx' + J(x) \int_{-\infty}^{\infty} G(x, x') \, dx' \tag{3.3.1}$$

giving:

$$J(x) = \frac{J_0(x)}{1 - \overline{G}(x)} + \int_{-\infty}^{\infty} \frac{G(x, x')}{1 - \overline{G}(x)} \Delta J(x, x') \, dx' \tag{3.3.2}$$

with

$$\overline{G}(x) = \int_{-\infty}^{\infty} G(x, x') \, dx' \tag{3.3.3}$$

and

$$\Delta J(x, x') = J(x') - J(x)$$

which equals zero when $x' = x$ such that the integral for $J(x)$ contains no contribution from $J(x)$.

Now that the single scattering has been removed from the interaction integral, define the single scattering current as the non-integral term:

$$J_{ss}(x) = \frac{J_0(x)}{1 - \overline{G}(x)} \tag{3.3.4}$$

By decomposing the total current into the single and multiple scattering parts, that is $J(x) = J_{ss}(x) + J_{ms}(x)$, it can be shown that the multiple scatter part must satisfy:

$$J_{ms}(x) = J_{00}(x) + \int_{-\infty}^{\infty} \left[ G'(x, x') - \frac{\overline{G}(x)}{1 - \overline{G}(x)} \delta(x' - x) \right] J_{ms}(x')\, dx' \tag{3.3.5}$$

The source term of the multiple scattering defined by:

$$J_{00}(x) = \int_{-\infty}^{\infty} G'(x, x') \left[ J_{ss}(x') - J_{ss}(x) \right] dx' \tag{3.3.6}$$

and the short hand

$$G'(x, x') = \frac{G(x, x')}{1 - \overline{G}(x)}$$

Identifying and separating the local and non-local parts in this manner provides an improved definition of the single and multiple scattering portions of the total current induced on a PEC rough surface by an incident field. In this process no assumption has been made about the problem dimensionality, surface roughness or incident illumination[4]. The main focus of this work is the solution the kernel integral Eq. 3.3.3 and its effect on the single scattering predicted by Eq. 3.3.4.

[4]Though no assumption is mentioned here, care must be taken to ensure the kernel integral $\overline{G}$ actually exists for the problem at hand. See Appendix **??** for the 1-dimensionally rough surface considered in this work.

### 3.3.3 Discussion on Convergence

It is important at this point to consider whether Equation 3.3.3 exists. For a 2D surface (3D scattering) the matter is relatively simple as the Green's function has a $\frac{1}{r^2}$ dependence allowing the integral to converge, but further care must be considered for a 1D surface (2D scattering) because of the $\frac{1}{\sqrt{|r|}}$ dependence which on its own diverges for an infinite support. This matter is discussed further in Section 3.3.4 and Appendix 4 which builds on results presented in Section 4.4, but essentially the oscillating surface components allow conditional convergence. Specific surface frequencies cause oscillations that exactly cancel the electromagnetic oscillations from the Hankel term for which this integral diverges. For TE, the surface frequency is $\frac{\lambda_s}{\lambda_0} = 2$ while for TM it is $\frac{\lambda_s}{\lambda_0} = 1$ that causes divergence of the integral.

### 3.3.4 Discussion on Truncation

In order to numerically compute the MFIE a beam incident illumination is used to truncate the simulation domain by imposing a finite support to the integral term. When integrating the product $J(x')\,G(x,x')$ the integral limits are essentially set by $J_0(x)$ while allowing for diffraction effects outside of the support of the incident illumination. In practice the surface used for computation is some multiple of the spot size of the incident illumination which can be considered the support of the integral.

For the Single-Scatter Subtraction method two additional integrals appear, both amounting to integrating $G(x,x')$ by itself. With a decay of $\frac{1}{\sqrt{\Delta x}}$, the support of these integrals are very large and also highly oscillatory. As an additional complication, for both polarizations

specific surface frequencies[5], as well as combinations of surface frequencies for TE[6], the value of these integrals is infinite as the surface oscillations cancel the electromagnetic oscillations resulting in the integral $\int_{-\infty}^{\infty} \frac{1}{\sqrt{|x|}} dx$.

Fortunately, it can be shown that an infinite support[7] corresponds to plane wave illumination and for a finite beam, the integrals should be truncated to match the beam truncation. Consider once more Equation 3.3.1:

$$J(x) = J_0(x) + \int_{-\infty}^{\infty} G(x, x') [J(x') - J(x)] dx' + J(x) \int_{-\infty}^{\infty} G(x, x') dx'$$

Begin by assuming the support of the total current is $(-\alpha, \alpha)$, that is $J(x) \equiv 0$ for $|x| > \alpha$. Thus $J(x')$ goes to zero in the tails of the first integral. Splitting the integral at these points:

$$\begin{aligned} J(x) &= J_0(x) \\ &+ \int_{-\infty}^{-\alpha} G(x, x') [J(x') - J(x)] dx' + \int_{-\alpha}^{\alpha} G(x, x') [J(x') - J(x)] dx' + \int_{\alpha}^{\infty} G(x, x') [J(x') - J(x)] dx' \\ &\quad + J(x) \int_{-\infty}^{\infty} G(x, x') dx' \end{aligned}$$

But $J(x')$ is zero in the first and third integrals,

[5] $\frac{\lambda_s}{\lambda_0} = 2$ and $\frac{\lambda_s}{\lambda_0} = 1$ for TE and TM respectively

[6] pairs of frequencies with normalized periods separated by 2

[7] Where $G(x, x')$ would guide the support of the integral.

$$J(x) = J_0(x) - J(x)\int_{-\infty}^{-\alpha} G(x,x')\,dx' + \int_{-\alpha}^{\alpha} G(x,x')\left[J(x') - J(x)\right]dx' - J(x)\int_{\alpha}^{\infty} G(x,x')\,dx' + J(x)\int_{-\infty}^{\infty} G(x,x')\,dx'$$

whose combination can now be seen to cancel with the final integral:

$$J(x) = J_0(x) + \int_{-\alpha}^{\alpha} G(x,x')\left[J(x') - J(x)\right]dx' + J(x)\int_{-\alpha}^{\alpha} G(x,x')\,dx'$$

Now define the truncated kernel integral as

$$\overline{\overline{G}}(x,\alpha) = \int_{-\alpha}^{\alpha} G(x,x')\,dx' \tag{3.3.7}$$

Note that the shorthand $\overline{\overline{G}}(x)$ will be used from now on for the finite-limit kernel integral, while $\overline{G}(x)$ will continue to represent the infinite-limit kernel integral. With the finite $\overline{\overline{G}}(x)$, the rest of the derivation of $S^3$ method is exactly the same but with $\overline{G}(x) \to \overline{\overline{G}}(x)$ and the infinite limits replaced with $(-\alpha, \alpha)$ to match those of $\overline{\overline{G}}(x)$.

Thus the limits of integration in $S^3$ should be finite with beam illumination, and set by the truncation of $J(x)$. This truncation is the same as that used in previous scattering problems with MoM or MOMI [17, 30, 63] techniques and must account for surface current diffracted outside of the incident beam. It is important to note that no additional support function is imposed on $\overline{\overline{G}}$ and the finite support of the integration of $\overline{\overline{G}}$ comes from recognizing that $J(x')$ goes to zero in the tails of the integral which then cancels with the tails of $\overline{G}$. Therefore if $J(x')$ has infinite support, as in the case of a plane wave, $\overline{\overline{G}}$ must also have infinite support.

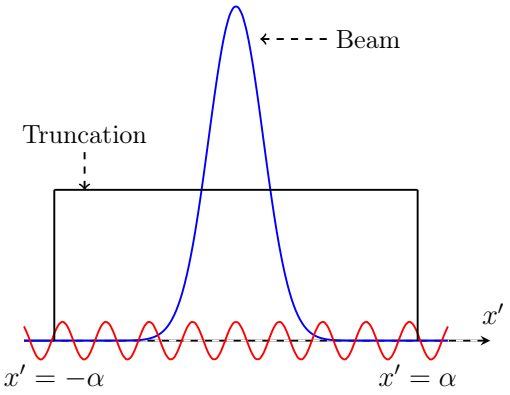


Figure 3.2: Incident Beam illumination and $S^3$ truncation

Note if asymmetrical limits of integration are used, this result still holds provided the upper and lower limits of integration match on all integral terms. This formulation has the benefit of removing the singularities present in $\overline{G}$ with infinite support, as the integration of $\frac{1}{\sqrt{\Delta x}}$ will now be on a finite support which will no longer be infinite. Further, as with other MFIE solution techniques and as demonstrated in Figure 3.2, it is not necessary to know a priori the exact current support (beam) as long as the integral support (truncation) is larger as any excess support will result in cancellation.

Interestingly, there has also been no limitation placed on considering x outside of the integral support. While the current has been assumed zero here, in principle there is no violation to consider $\overline{G}$ here, and it will be seen that this term has interesting physics in such a case.

### 3.3.5 Iteration

While both the full solution of the single scatter subtraction method, and the multiple scatter current term are left for future work, equation 3.3.2 may be cast in a form suitable

for solution by iteration by the Method of Moments [26]:

$$J(x) = \frac{J_0(x)}{1 - \overline{G}(x)} + \int_{-\infty}^{\infty} \left[ G'(x, x') - \frac{G(x, x')}{1 - \overline{G}(x)} \delta(x' - x) \right] J(x')\, dx'$$

Where we have modified the integral kernel and source term.

Results discussed in Chapter 4 show $\overline{G}(x)$ to be pure imaginary for plane wave illumination and proportional to the surface curvature for a range of long surface wavelengths, preventing the kernel from becoming singular. The finite support $\overline{\overline{G}}(x)$ contains a real component, but for the range of surface parameters studied here no combinations of parameters would lead to a singular kernel. Initial tests show promise in achieving convergence in a similar number of iterations as the MFIE on sinusoidal surfaces where $\left|\overline{\overline{G}}(x)\right| \ll 1$, though no work has been done for surfaces which could be expected to appreciably change the integral kernel.

## 3.4 Summary

After describing the geometry and physics of the problems considered, this chapter introduced a new approach to solving the Magnetic Field Integral Equation derived without any assumptions on dimensionality, surface roughness or incident illumination. This technique, called the Single-Scatter Subtraction method separates the single- and multiple-scattering currents, providing a modified integral kernel and providing insight to the scattering physics.

# Chapter 4

# Kernel (Green Function) Integral

## 4.1 Introduction

The new method introduced in Section 3.3 defines and hinges on a new quantity which is the integral of the kernel of the MFIE and has never been investigated before. In this chapter, the character of this integral is examined and the difficulties in its computation discussed. Then results of numerical computation are presented for single and spectral surfaces. Finally, a series of analytic approximations to the single frequency surfaces are presented along with a method to extend these to multi-frequency surfaces. The ultimate result of this chapter is a set of analytic approximations for each electromagnetic polarization and hard bounds on their range of validity. Building on this development, a simple analytic extension to the Kirchhoff method is introduced in the following chapter.

## 4.2 Calculation of the Kernel Integral

In the new MFIE-based Single Scatter Subtraction method, the calculation of an Integral Green function integral is required. Before the cancellation in the integrals due to assumed beam-limited illumination was recognized (as demonstrated in Section 3.3.4), it was initially thought that these integrals should also extend to infinity since mathematically the extended surfaces are closed at infinity. This was found to be a perilous task due to its highly oscillatory

nature, the slow $\frac{1}{\sqrt{R}}$ decay of the Hankel function in 2D and the general difficulty of a double infinite exponential integral in 3D. While some traction could be found on simple periodic cosine surfaces numerically with some confirmation afforded by analysis, the cases of interest are rough surfaces which are inherently aperiodic. An initial analytic investigation of such integrals of simple cosine surfaces by complex analysis was, as expected, found to be difficult by the author. Since a pure analysis-based approach appears unworkable, attention was turned to numerical integration.

Unfortunately, oscillatory quadrature is itself a difficult problem, with most work focused on purely trigonometric oscillation [18, 21]. A review of mathematical literature focused on numerical integration of Bessel functions with infinite limits found such techniques only applied to relatively simple cosine or Bessel function products[1] [38, 51]. These methods all involve integrating over periods of the integrand then extrapolating and accelerating convergence of the integrals. While it seems possible to apply these methods to simple integrals of a composite function of a few periodic functions, they do not apply to the inherently aperiodic nature of rough surfaces [37]. Some newer research involving the creation of generalized numerical integration rules could be an avenue of further pursuit [22].

By taking bounds on the maximum amplitude and curvature of frequency components, it may be possible to consider the Green function integrals as a sum of sinusoidal components times the Bessel kernel. Therefore by splitting the integral into a sum of integrals and with an appropriate routine to calculate the resultant period of the new integrals, traction with these methods may be possible for limited cases. A naive implementation of the technique proposed by [51] was found to have poor convergence properties for this problem, vastly under-performing a simple Newton-Cotes rule discretized to a hundredth of a wavelength. Additionally, on rough surfaces of interest there may be thousands of component frequencies,

[1] As in, much simpler expressions than the integrals of interest to this work.

making such an approach unattractive as one difficult numerical integration could possibly be exchanged for thousands of highly expensive numerical integrations for each of thousands of observation points for a single realization; this further hinging on significant improvements of the oscillatory quadrature accelerator algorithms or the development of a new problem-specific quadrature rule. Since the purpose of this work is to develop physics-based approximations to the rough surface scattering problem, thereby improving physical intuition of electromagnetic interactions, this was not pursued.

### 4.2.1 Example Integrands

Figures 4.1 and 4.2 show the TE and TM integrand of $\overline{G}$ for three observation points of a single frequency, highlighting the difficulties of numerically integrating them. Note that for TE, observation points with zero surface slope appear to decay rapidly, while very slow decay is observed in regions of high slope. TM has a radically different shape than TE and all observation points feature slow decay due to the difference in source versus observation slope in the integrand for TM and TE. In addition to the slow decay, all cases are highly oscillatory with multiple frequencies present. For spectral or fully random surfaces, this integrand becomes even more complicated.

## 4.3 Numeric Results

Despite the fact that the $\overline{\overline{G}}$ integrals used in problems of interested using the $S^3$ method have finite support from the beam-limited illumination, the results of the infinite $\overline{G}$ will be discussed here since a simple "empiric" formula was found to have excellent agreement, the plane wave case may be of interest analytically and there are similarities between the

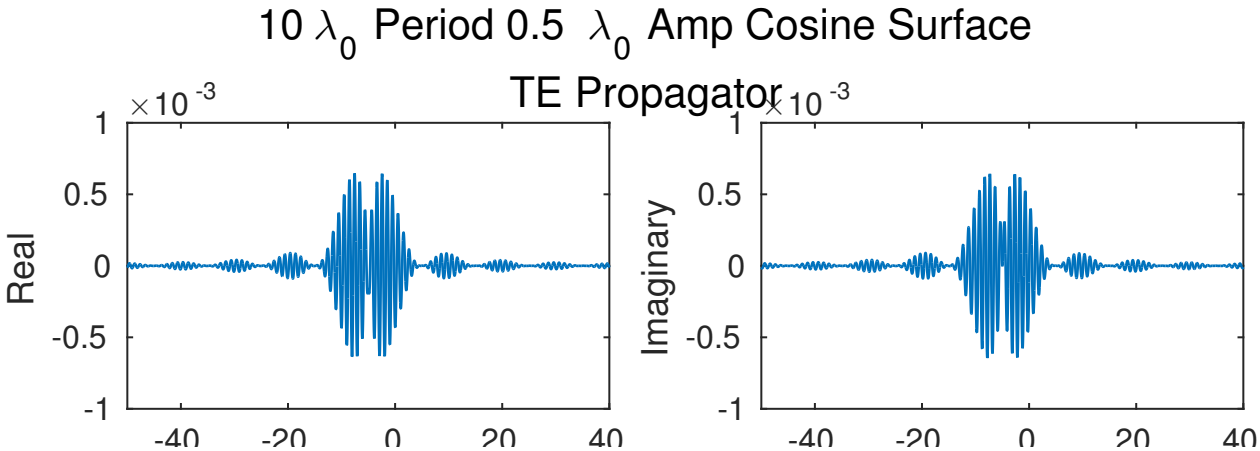


(a) x=5.005

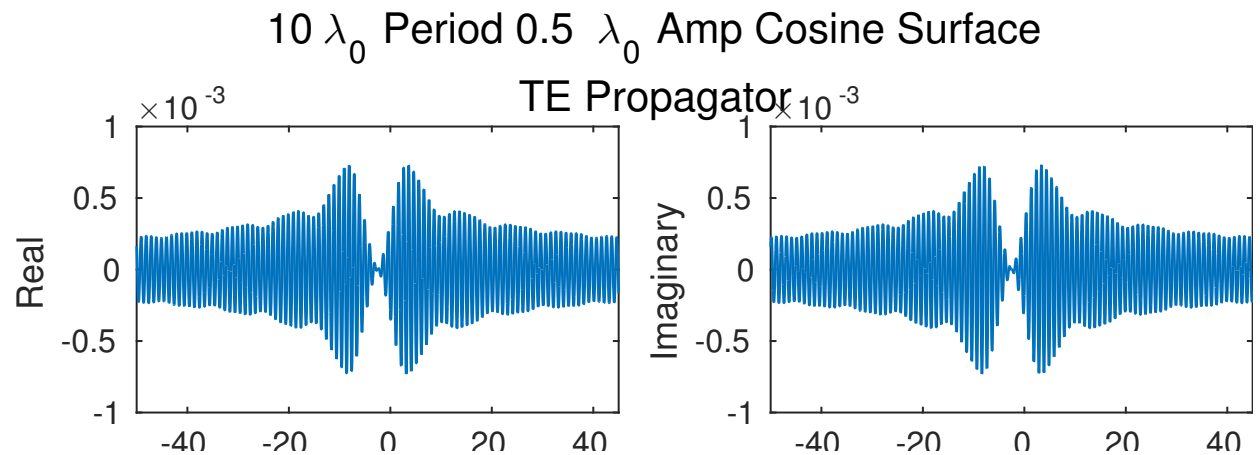


(b) x=-2.505

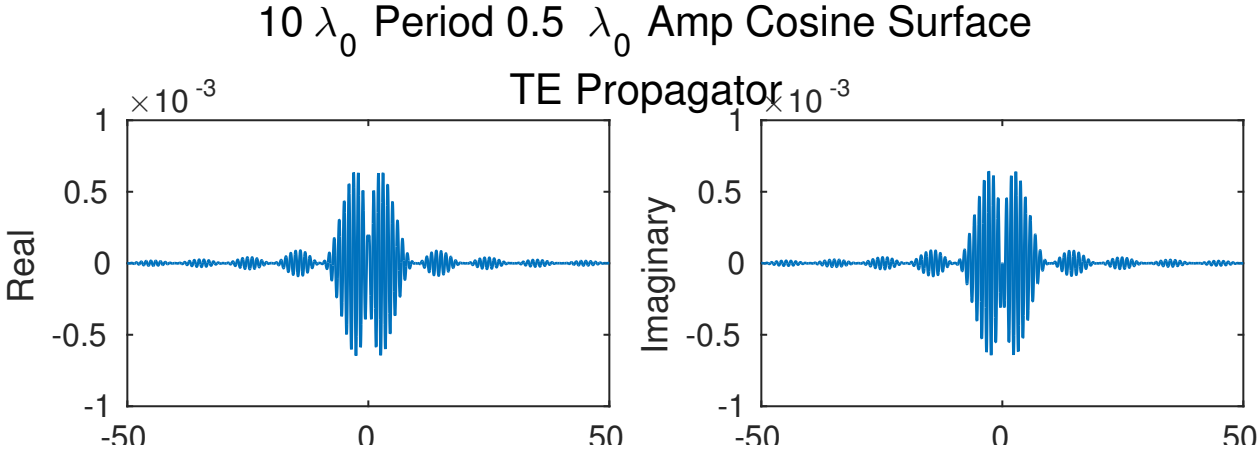


(c) x=0.005

Figure 4.1: TE Plot of $\overline{G}$ Integrand

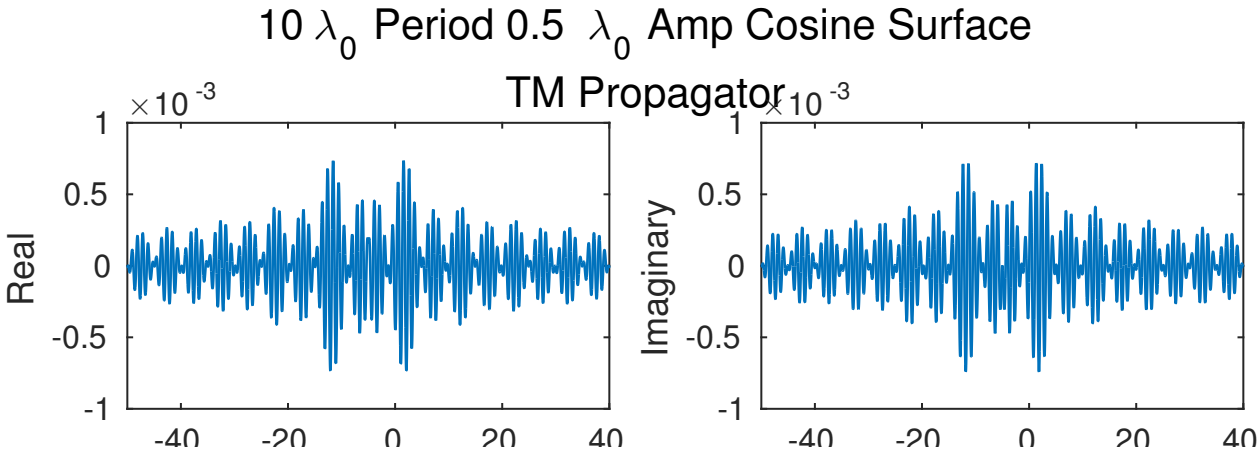


(a) x=5.005

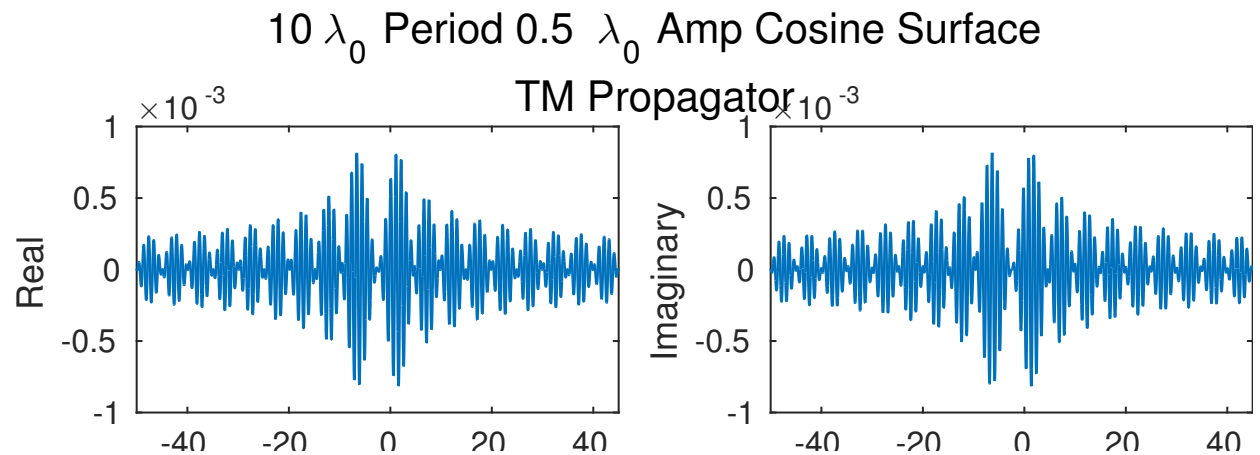


(b) x=-2.505

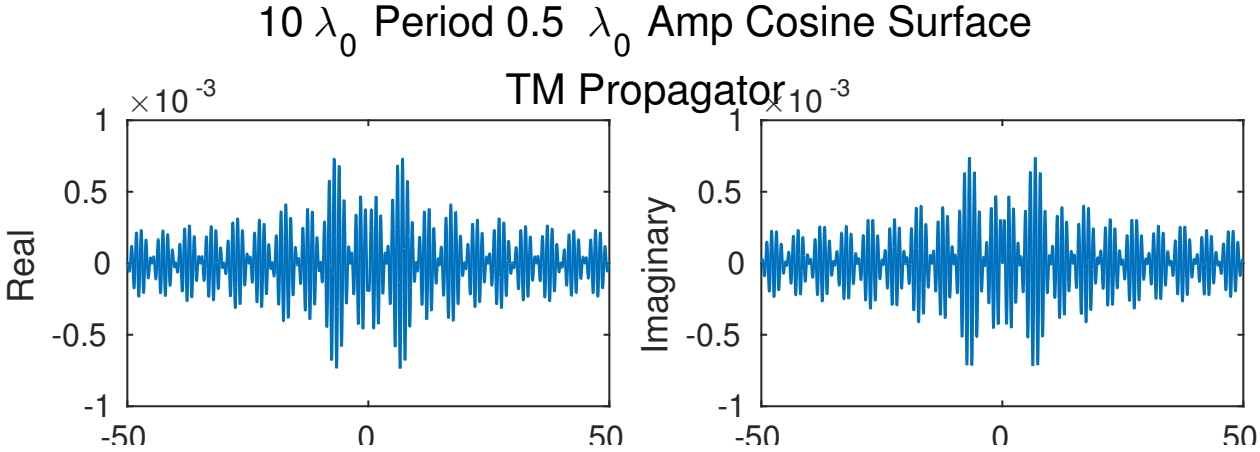


(c) x=0.005

Figure 4.2: TM Plot of $\overline{G}$ Integrand

imaginary components of the finite and infinite case. The term "empiric" is used here in a slightly different sense than in traditional parlance where it signals derivation from *physical* experiments. In this work it means derived from *simulation* experiments or computation, where intuition and hypothesis guided by experience produces analytic expressions that are then verified against computation and/or analysis. This is expanded upon in Section 4.4 where so called "empiric analytic" formulas are produced which find excellent agreement with numeric computation, derived from a combination of this new definition of empiric and, admittedly not fully justified, analysis.

For these infinite results, long integration supports were required to achieve numerical convergence, with symmetric supports of $\alpha = 10^6$ compared to derive an empiric formula, and validated with combinations of numeric and analytic approximations given in Section 4.4.

For surface wavelengths larger than the electromagnetic wavelength, $\overline{G}$ is almost entirely imaginary with negligible real component and a 180° phase difference between TM and TE. As $\frac{\lambda_s}{\lambda_0} \to 2$ for TE and $\frac{\lambda_s}{\lambda_0} \to 1$ for TM both the real and imaginary parts become very large, due to the electromagnetic oscillations[2] canceling the surface oscillations leaving a $\frac{1}{\sqrt{d}}$ in the integrals. The integral of $\frac{1}{\sqrt{d}}$ is of course unbounded on an infinite support, so numerical integration should be expected to fail in this case.

### 4.3.1 Confirmation of numeric results

As a check on the numerical integration of $\overline{G}$, Brown derived results for a small interval ($\Delta x = \mp\lambda_0/4$) of integration [14]:

$$\overline{G}_{TE}^{short}(x) \approx \left[\frac{-1}{4\pi\left(1+\zeta_x^2(x)\right)} + j\frac{(2\pi)^2}{768}\right]\zeta_{xx}(x)\,\lambda_0 \tag{4.3.1}$$

[2] Hankel Function oscillations

$$\overline{G}_{TM}^{short}(x) = -\overline{G}_{TE}^{short}(x)$$

with $\zeta_x(x)$ the surface slope and $\zeta_{xx}(x)$ the surface curvature.

This result was checked against a variety of surface slopes and amplitudes with $\lambda_s = 3, 5, 7$, and $20\lambda_0$ presented in Figures 4.3 through 4.10 below for both 0.5 and 0.05 surface amplitude.

As expected, the results are an order of magnitude higher for the 0.5 than the 0.05 amplitude surfaces. There appears to be about a 10% difference across the board between the analytic and short numeric. It should be noted that Equation 4.3.1 is approximate so exact agreement is not expected and instead the general character of the integral over this short interval is what is of interest for comparison.

Now that the numeric computation has been validated on a short interval, results will be presented on the full infinite range of $\overline{G}$.

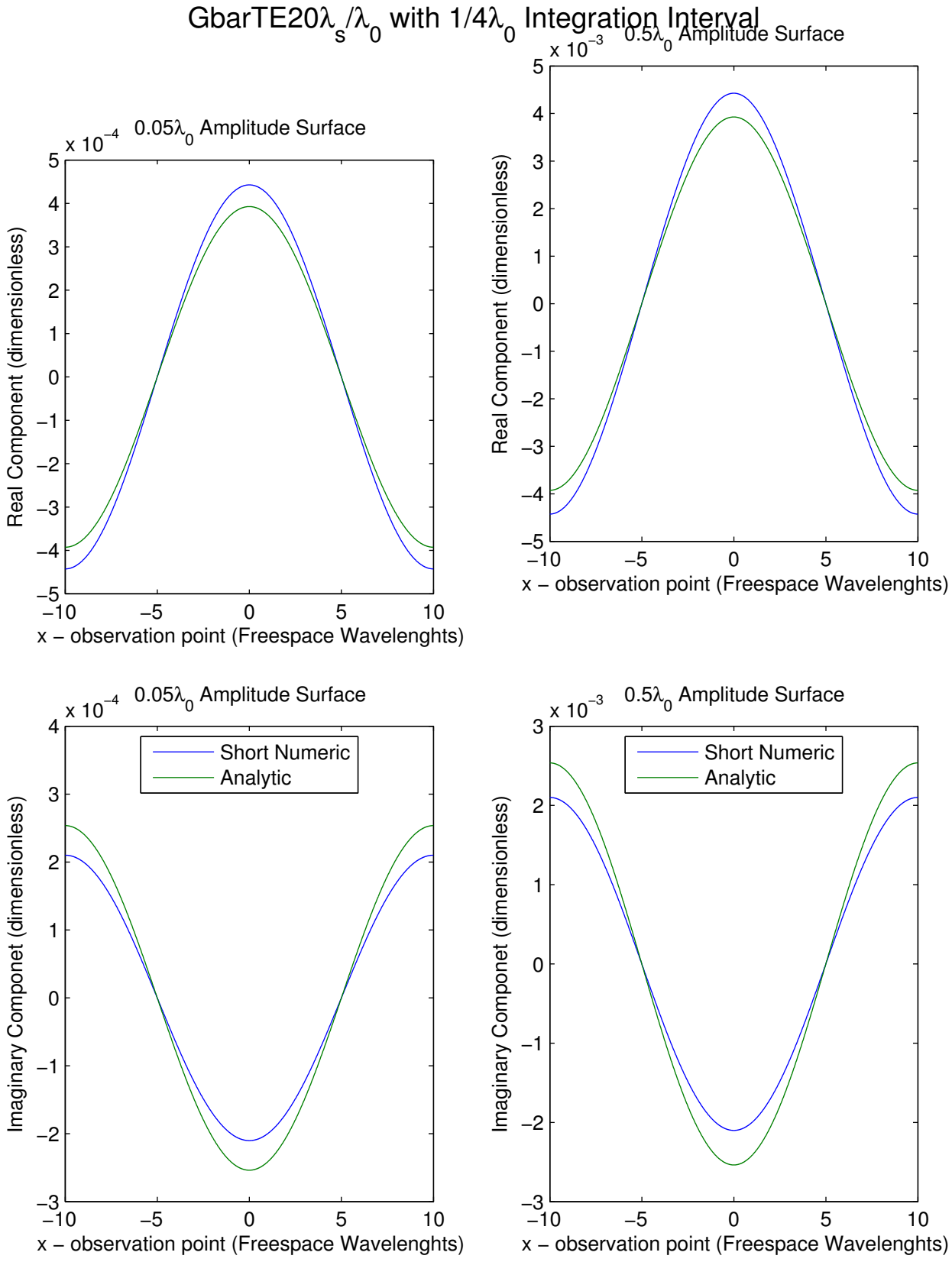


Figure 4.3: TE $\lambda_s = 20\lambda_0$ Surface

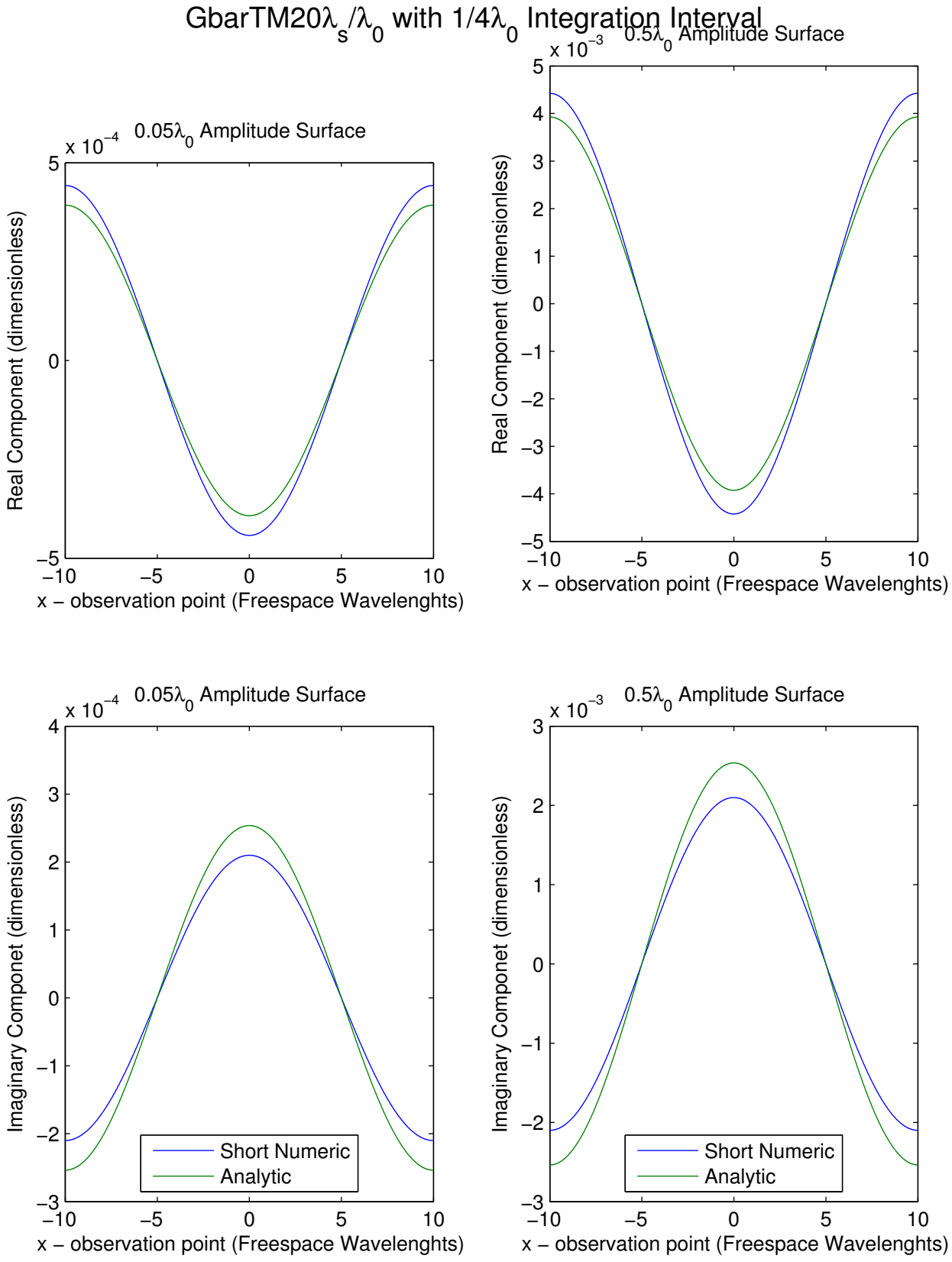


Figure 4.4: TM $\lambda_s = 20\lambda_0$ Surface

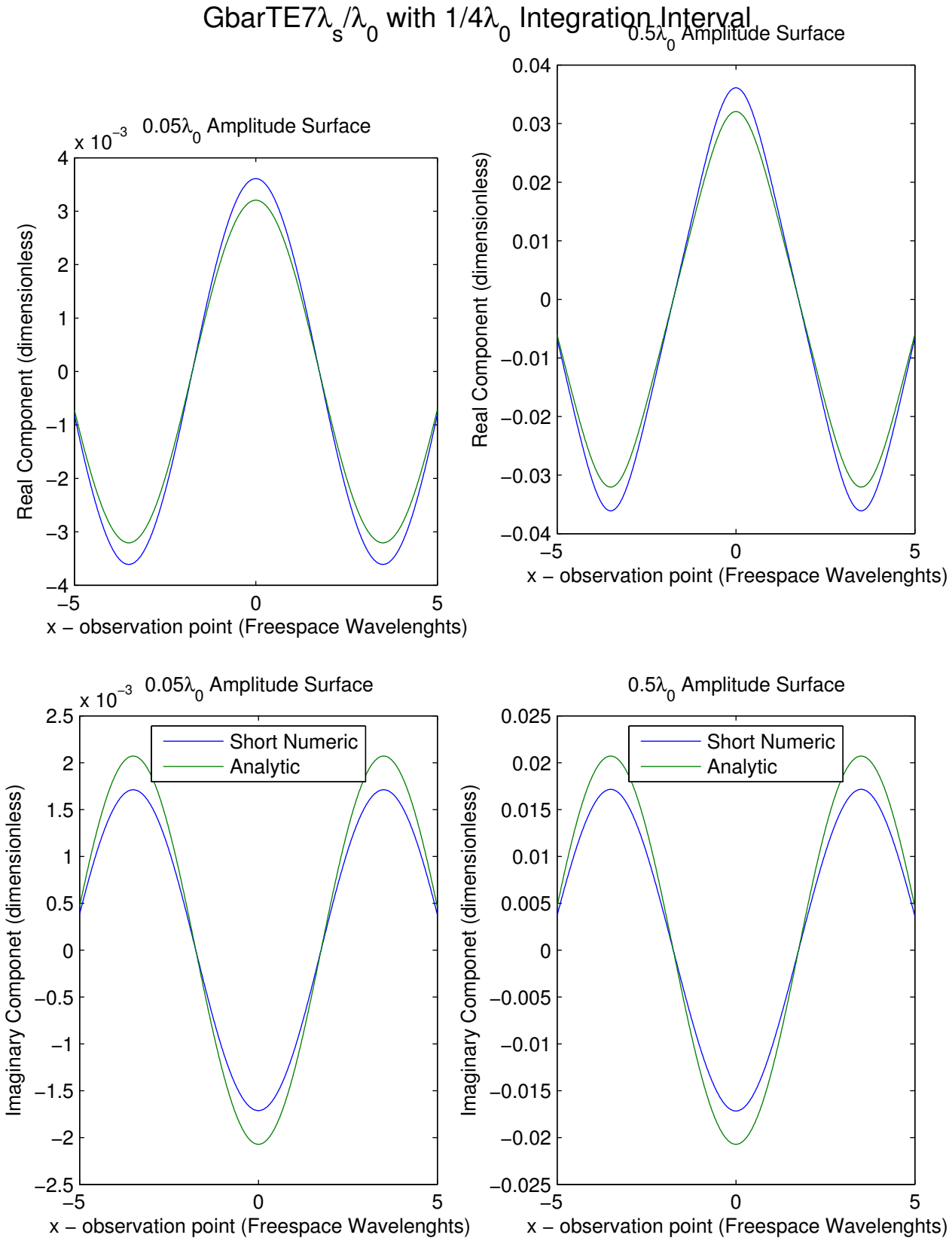


Figure 4.5: TE $\lambda_s = 7\lambda_0$ Surface

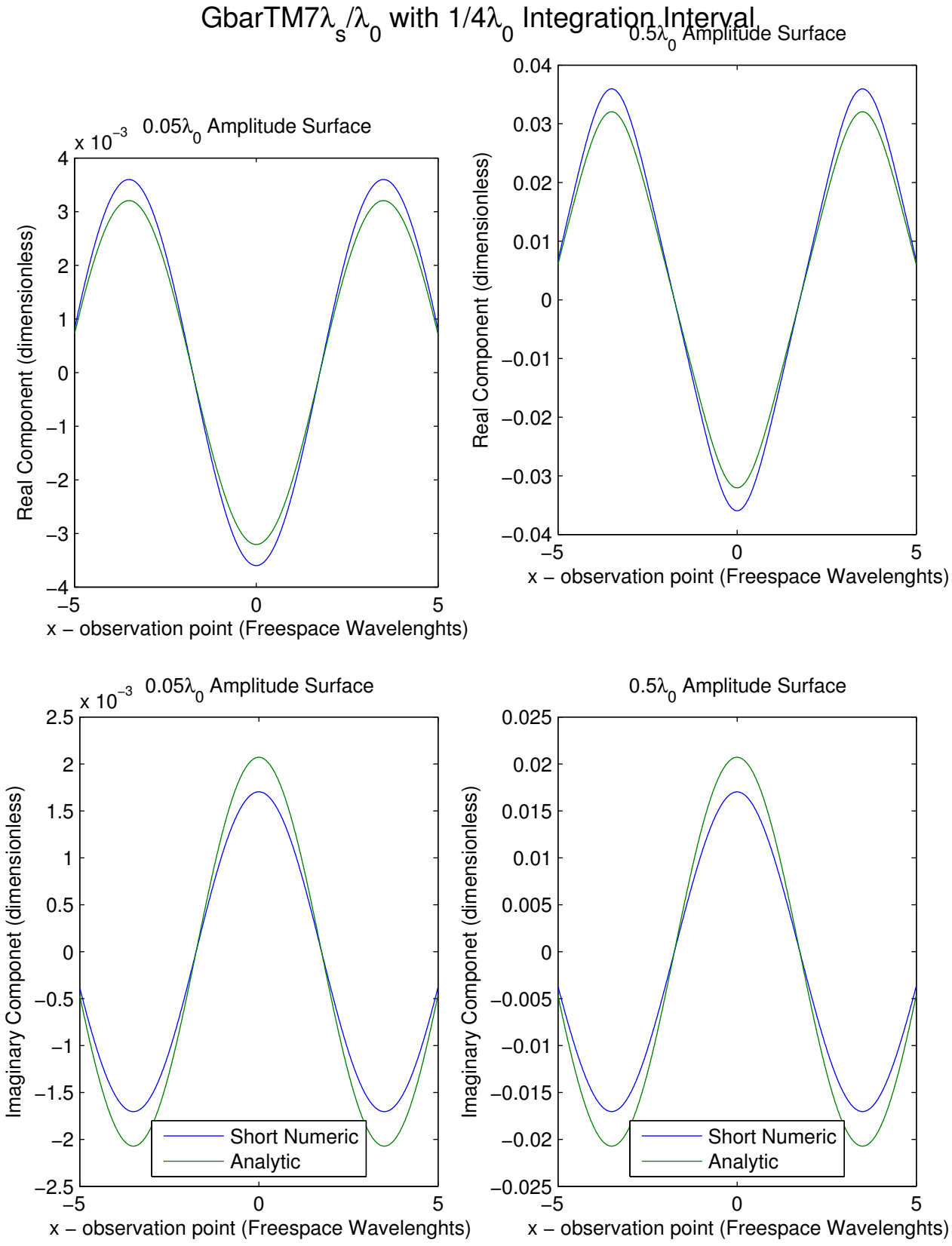


Figure 4.6: TM $\lambda_s = 7\lambda_0$ Surface

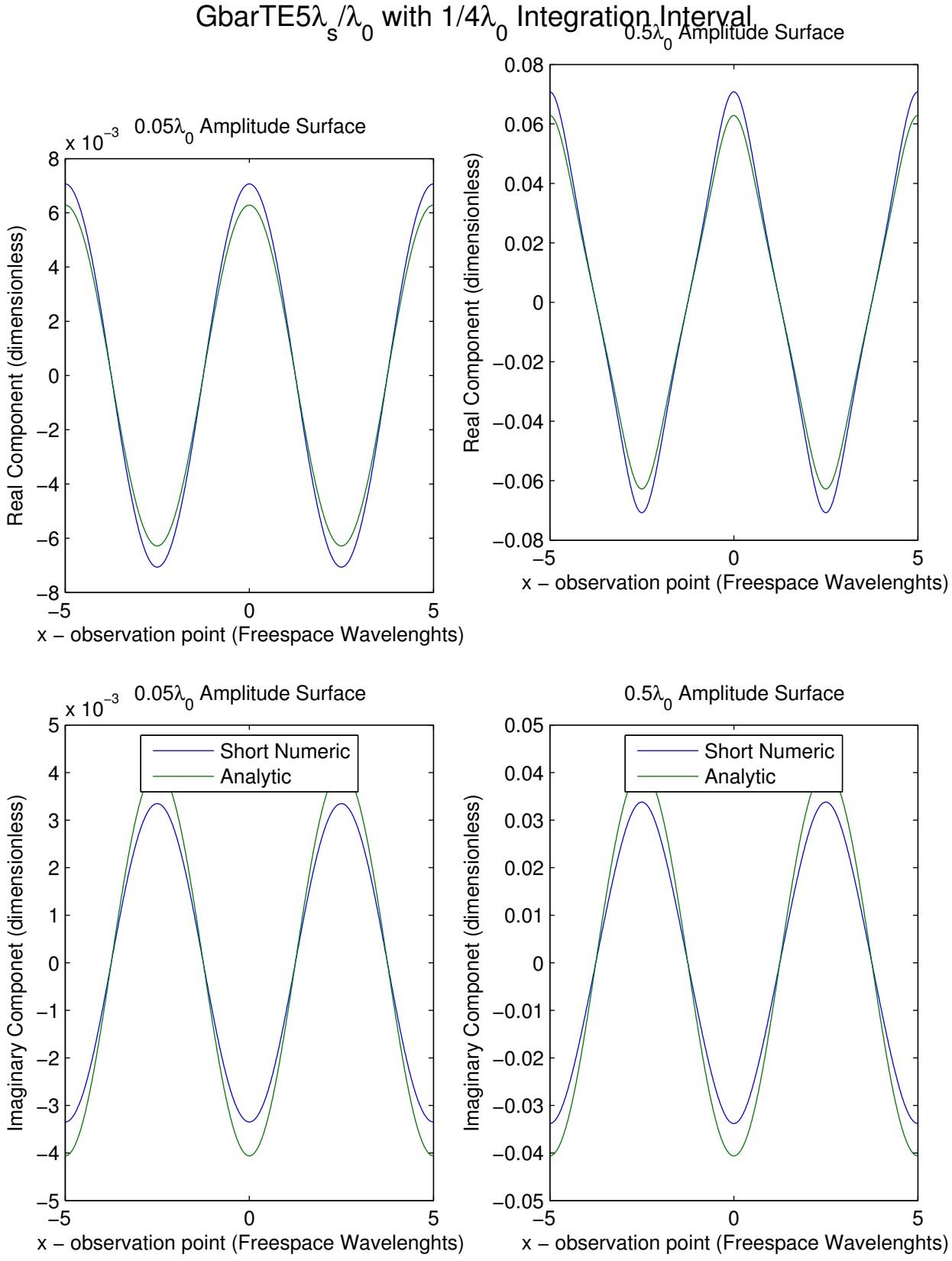


Figure 4.7: TE $\lambda_s = 5\lambda_0$ Surface

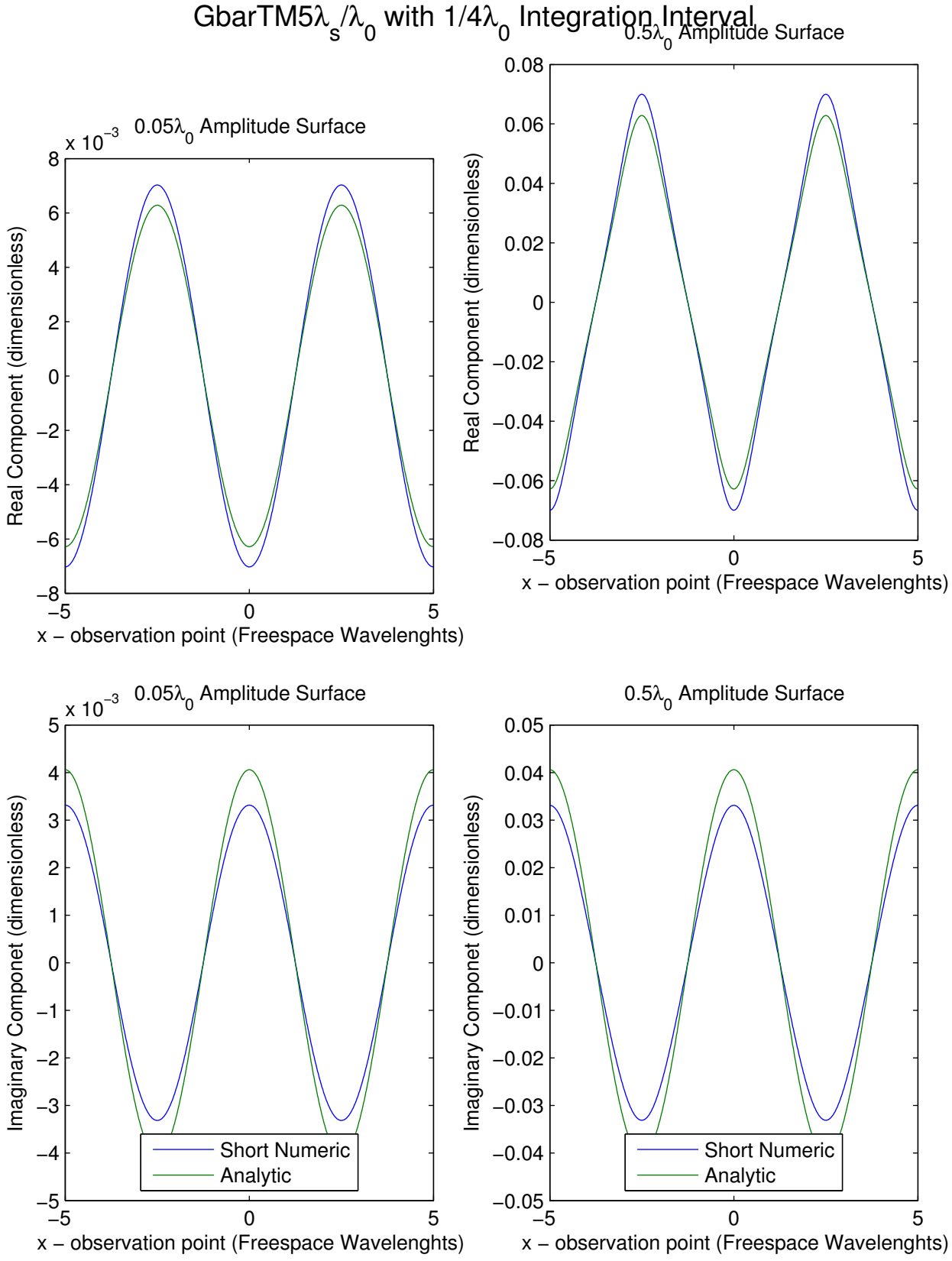


Figure 4.8: TM $\lambda_s = 5\lambda_0$ Surface

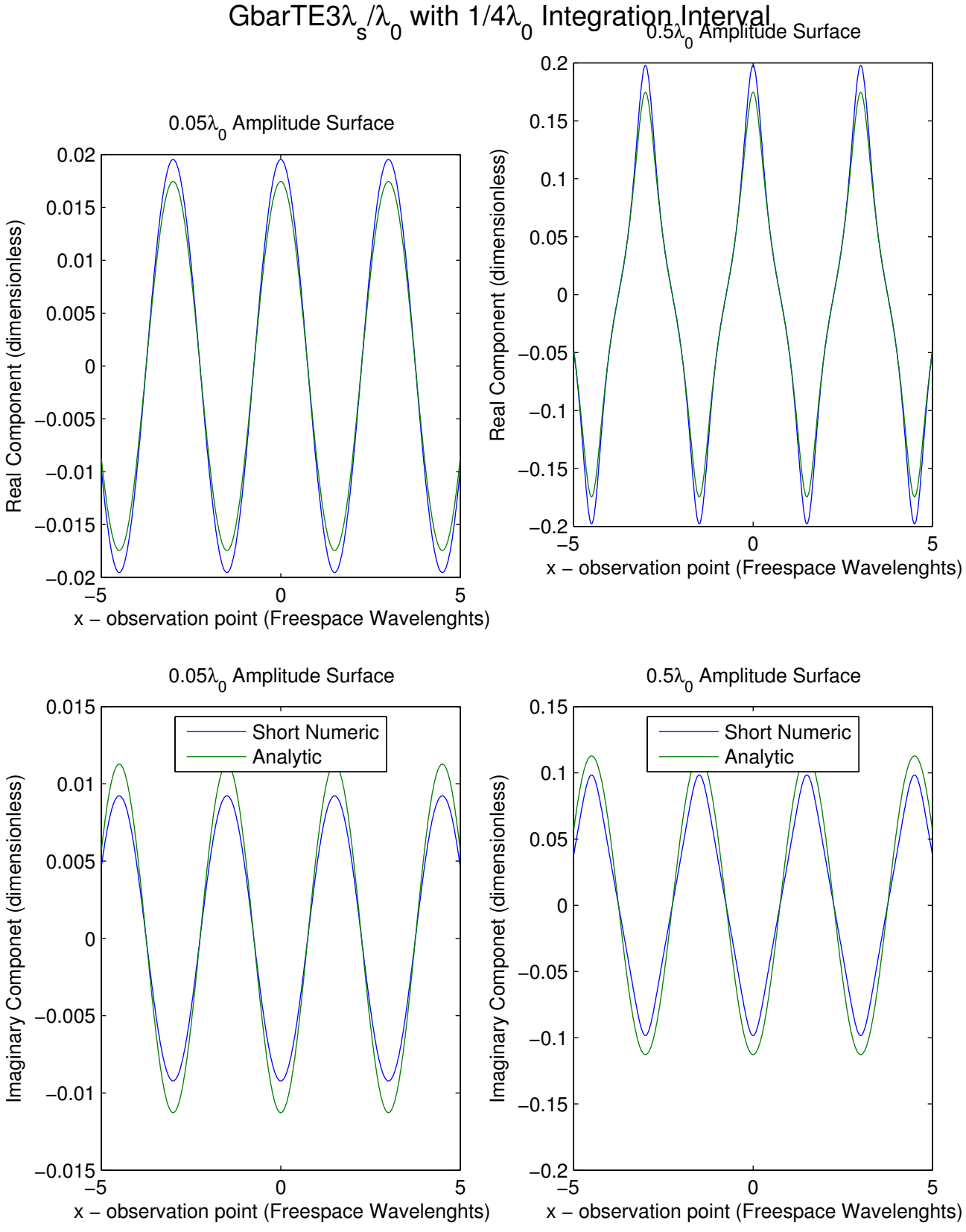


Figure 4.9: TE $\lambda_s = 3\lambda_0$ Surface

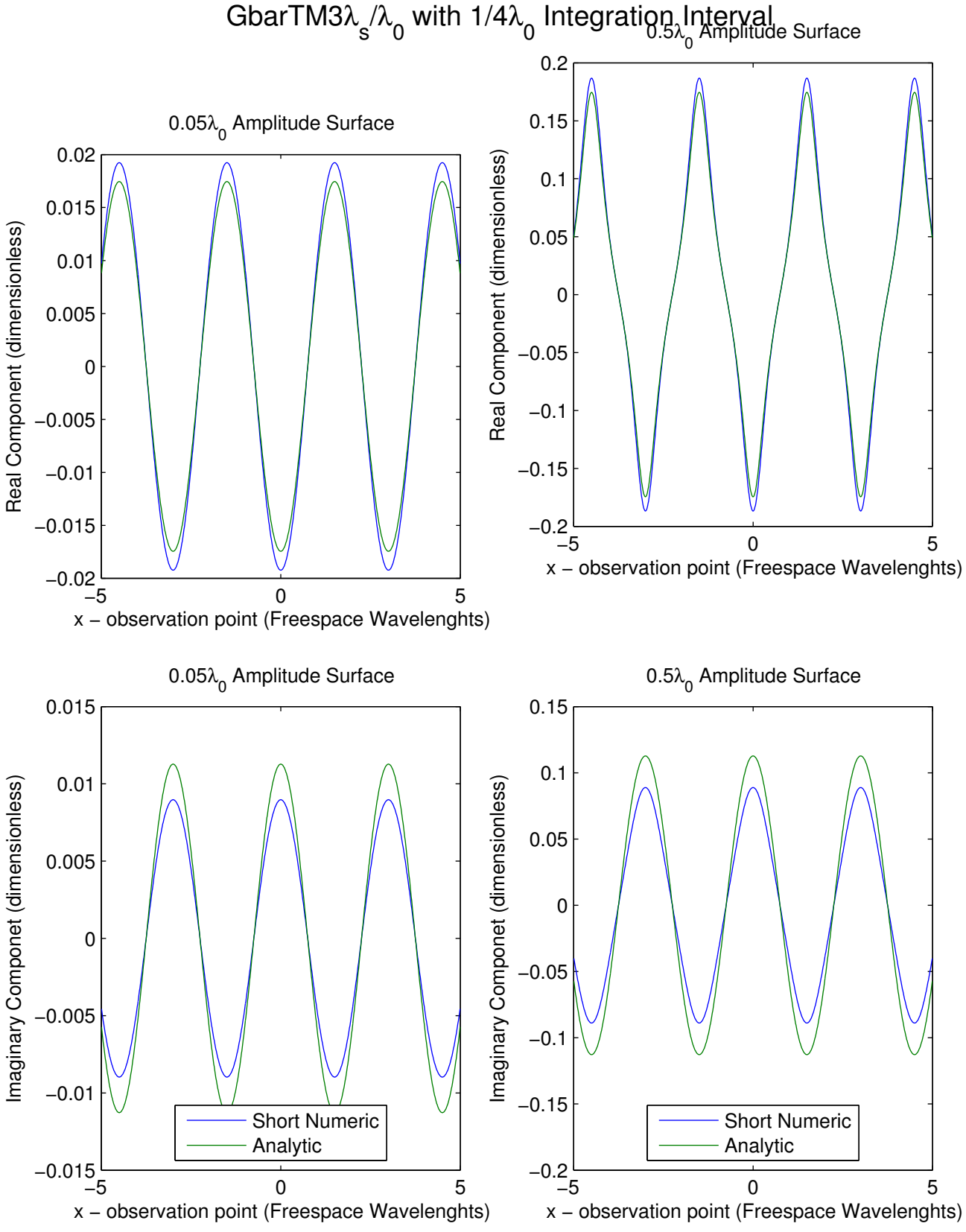


Figure 4.10: TM $\lambda_s = 3\lambda_0$ Surface

### 4.3.2 Infinite Support

To approximate an infinite integral, an integration support of 1 million wavelengths was used. Two gentle surfaces with wavelengths of $10\lambda_0$ and $20\lambda_0$ are presented below. Attention is focused on the center of the surface, showing a full surface period so the detail may be observed. TE is shown in Figures 4.11 for $20\lambda_0$ and 4.12 for $10\lambda_0$ which also shows the effect of a change in the order of magnitude of the surface amplitude from $0.5\lambda_0$ to $0.05\lambda_0$. Note the difference in the x-axis scale. The general structure is similar but the $10\lambda_0$ has additional oscillatory components not present on the longer wavelength. For both cases, the real component is significantly smaller than the imaginary. In contrast, TM polarization has no additional oscillatory components on the $10\lambda_0$ surface in Figure 4.14 compared to the $20\lambda_0$ in Figure 4.13. Similarly the real component is significantly smaller than the imaginary and both show a decrease in the amplitude causes a dramatic decrease in magnitude by more than a corresponding order of magnitude.

#### 4.3.2.1 Near the singular portion

Now attention will be turned to the character of the infinite kernel integral as the surface wavelength approaches the the singular region. Recall the kernel integral becomes singular because the integral becomes proportional to $\frac{1}{\sqrt{x}}$ which is infinite on an infinite support, but will be finite on a finite support. First, surface period around $\frac{\lambda_s}{\lambda_0} = 1$ where TM is expected to become singular are examined, followed by $\frac{\lambda_s}{\lambda_0} = 2$ for TE. As above, the infinite integration support is approximated by one million wavelengths. Figure 4.15 shows that TE has a larger amplitude that longer wavelength surfaces but appears to still be finite, while Figure 4.16 shows that TM is dramatically larger and continues to increase with longer integration supports even for small amplitudes. Also of interest, the TM imaginary component retains

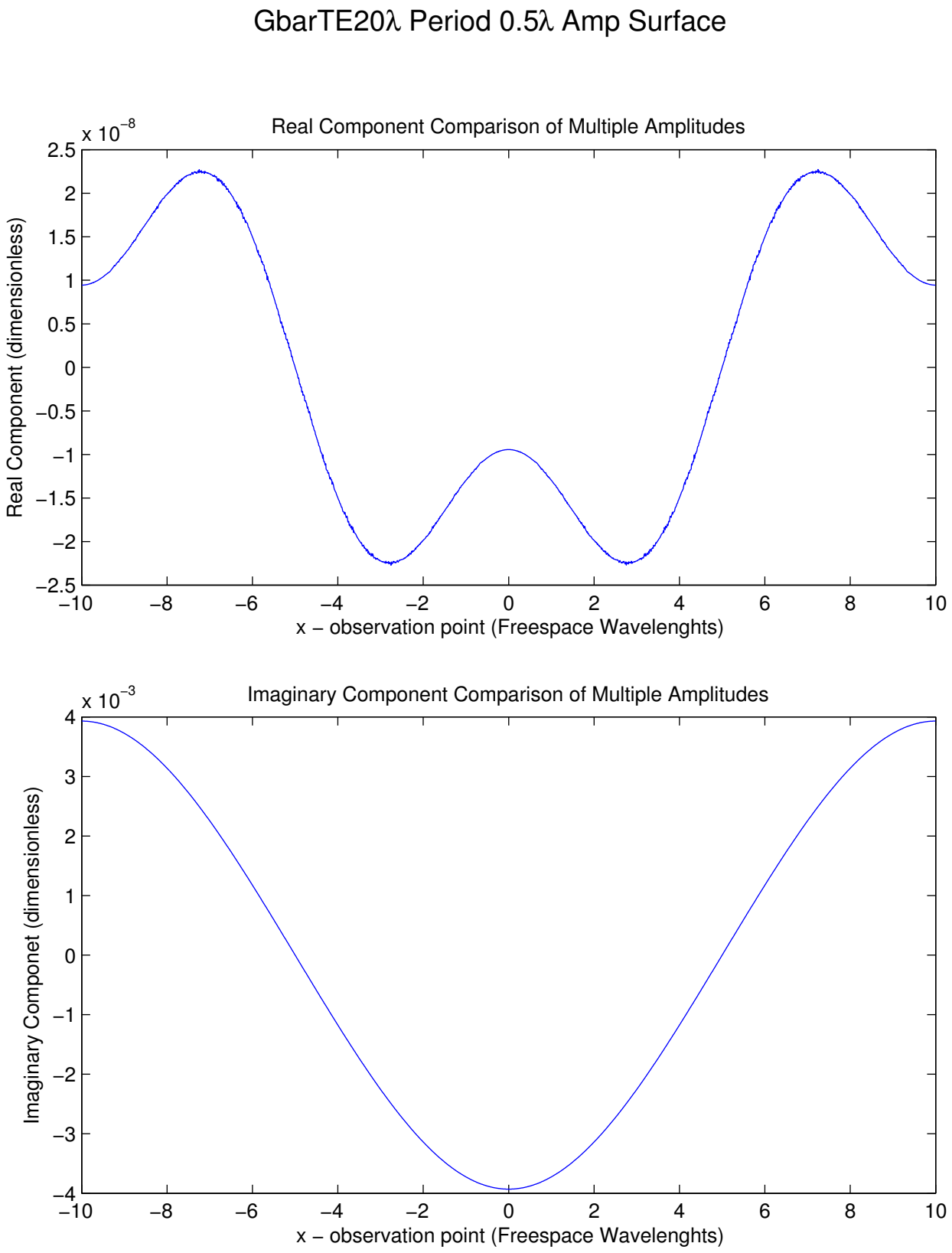


Figure 4.11: TE Long Numerical Integration 0.5 Amplitude $\mp 1M$ $\lambda_0$ integration window

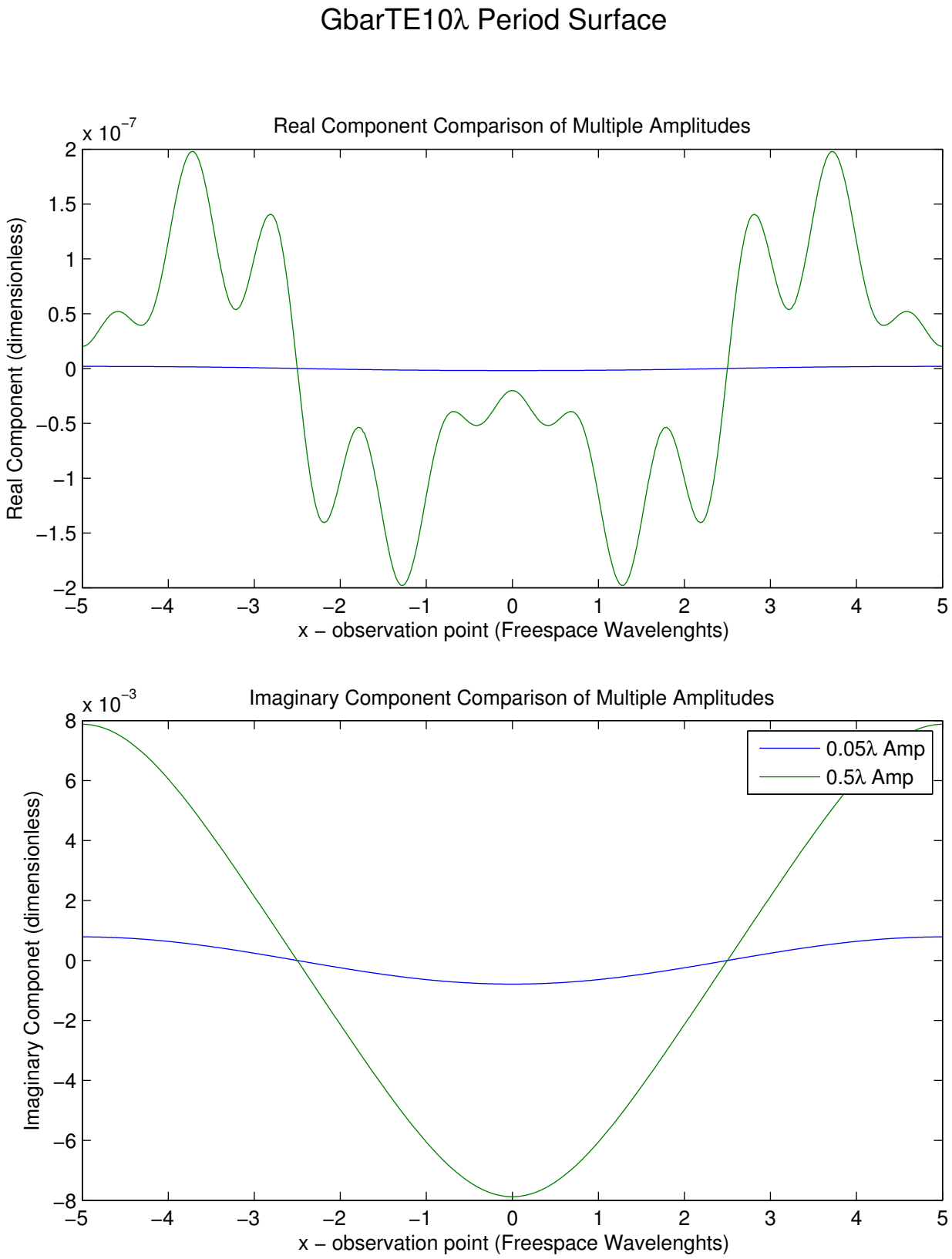


Figure 4.12: TE Long Numerical Integration Amplitude Comparison $\mp 1M$ $\lambda_0$ integration window

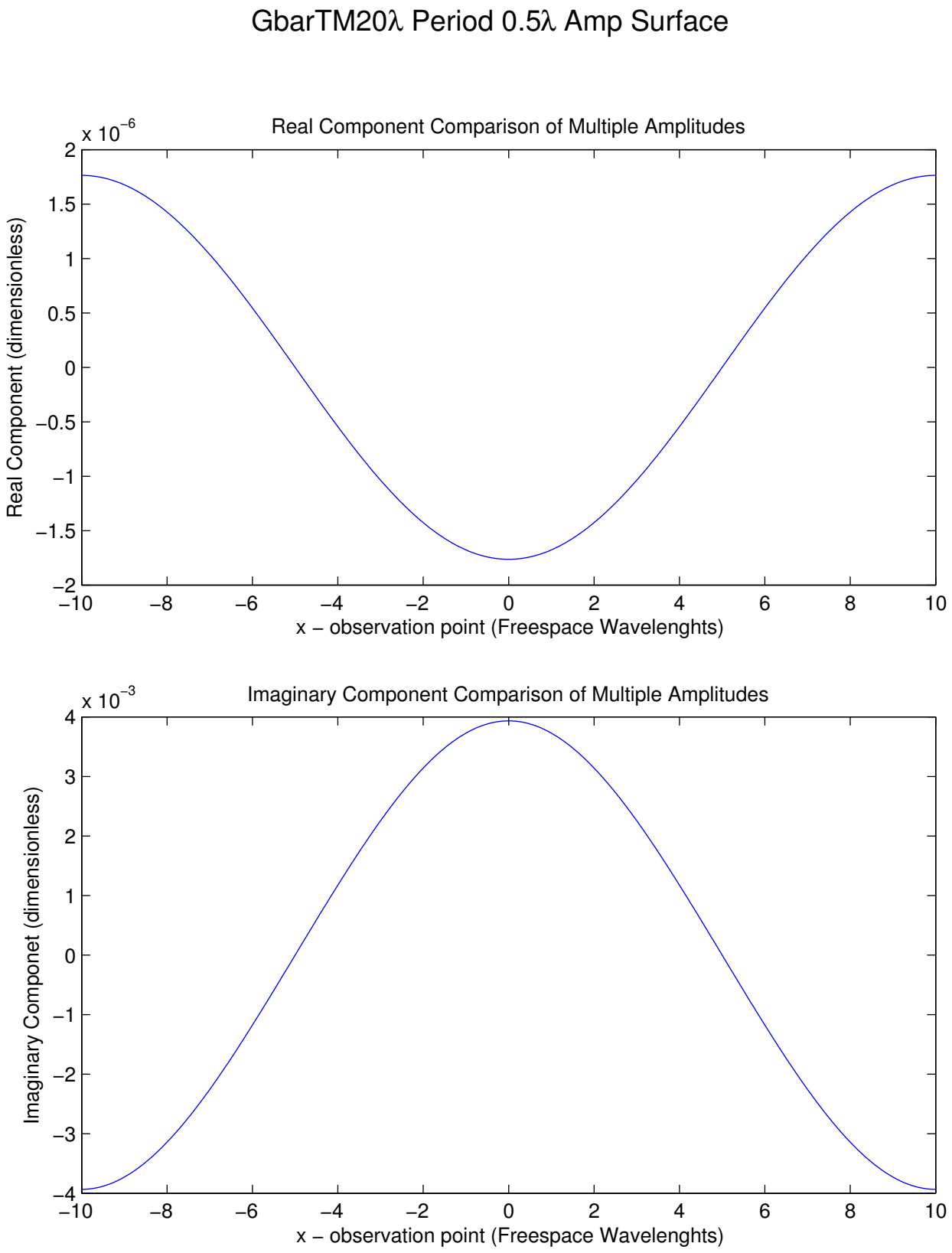


Figure 4.13: TM Long Numerical Integration 0.5 Amplitude $\mp 1M$ $\lambda_0$ integration window

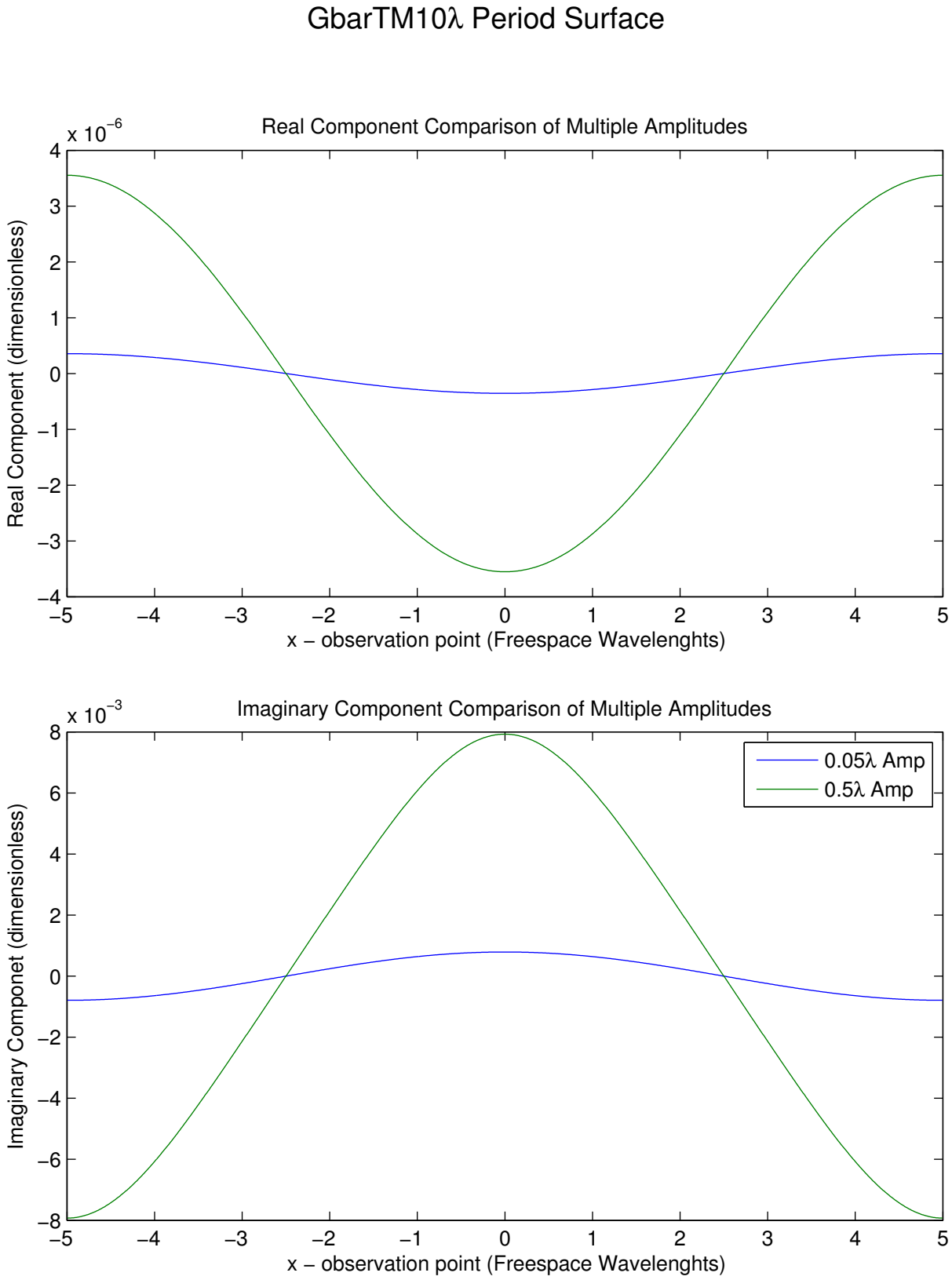


Figure 4.14: TE Long Numerical Integration Amplitude Comparison $\mp 1M$ $\lambda_0$ integration window

the same structure as higher wavelengths with a predominantly surface-wavelength period oscillation, but the amplitude of this oscillation takes off.

This is latter fact is further supported by Figures 4.18 and 4.20 which show a small perturbation to either side from the exactly singular surface wavelength have finite amplitudes. Interestingly, despite not being a symmetric distance in surface wavelength from the singular period, they have similar real component amplitudes, while the imaginary component shows a steep drop off the further away from the singular wavelength. At these same wavelengths the TE integral, shown in Figures 4.17 and 4.19, has decreasing amplitude with decreasing wavelength as it is moving farther away from the singular wavelength of 2 for this polarization.

At the singular wavelength for TE shown in Figure 4.21, the amplitude is less than TM at its singular wavelength, but the imaginary component has a dramatically different structure than non-singular surface periods. Figure 4.22 shows TM has a similar scale to TE in Figure 4.15 where it is off the singular surface period by one wavelength and also now has a modify imaginary component.

Examining further surface wavelengths between the two polarizations respective singular periods shows the switch happening, TM doubles in magnitude when going from 1.5 to $1.2\lambda_0$ in Figures 4.23 and4.26 respectively, as the surface wavelength moves towards singular. TE decreases as it moves away from the singular, but it is not quite halving for the same surface wavelengths shown in Figures 4.23 and 4.25. Interestingly, for both polarizations changing the surface amplitude completely changes the character of the imaginary component, highlighting different components of the kernel.

Near the singular surface wavelengths the character of $\overline{G}$ is complex, but only a small perturbation from the singular period is required to make the results finite once again.

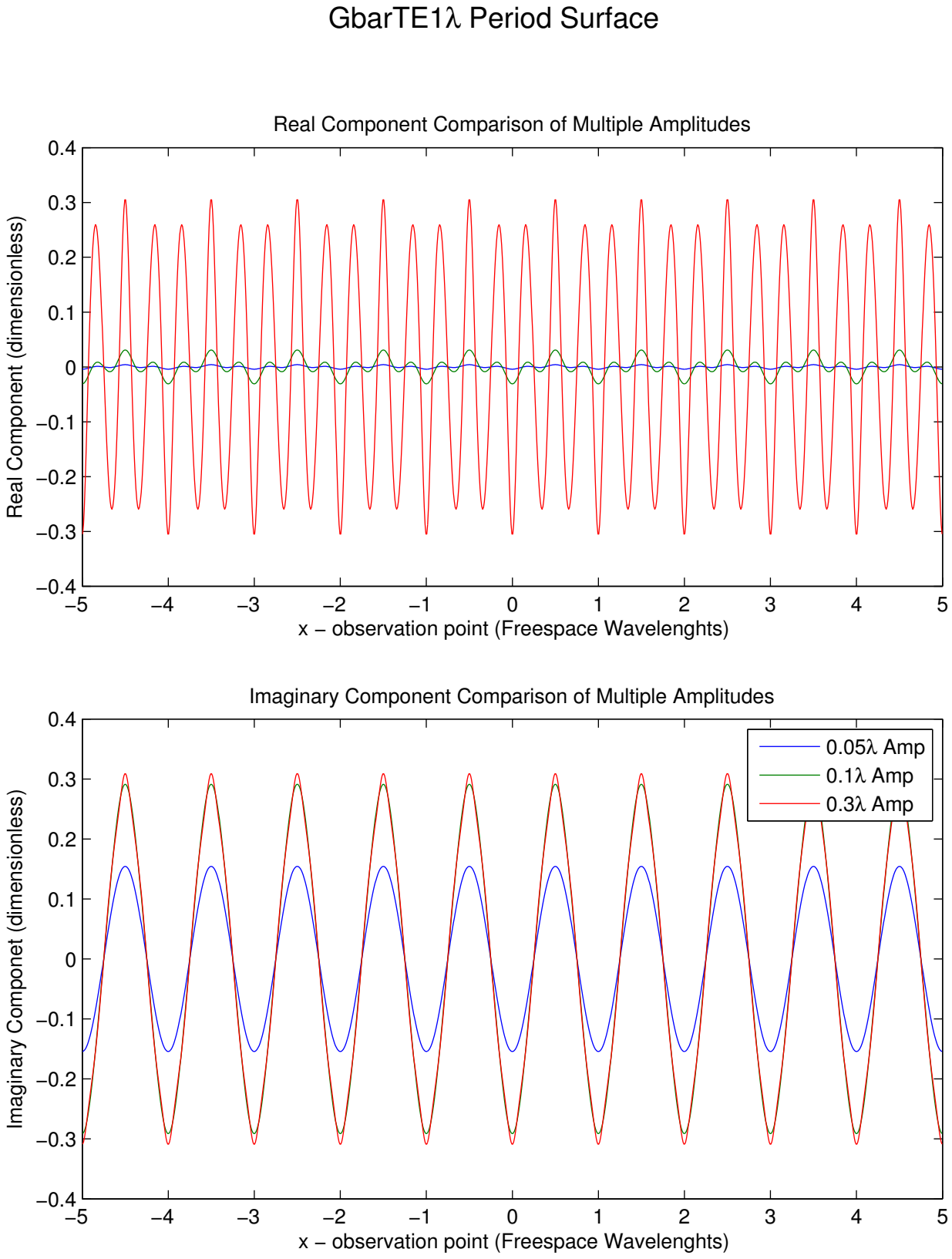


Figure 4.15: TE 1$\lambda$ period Comparison

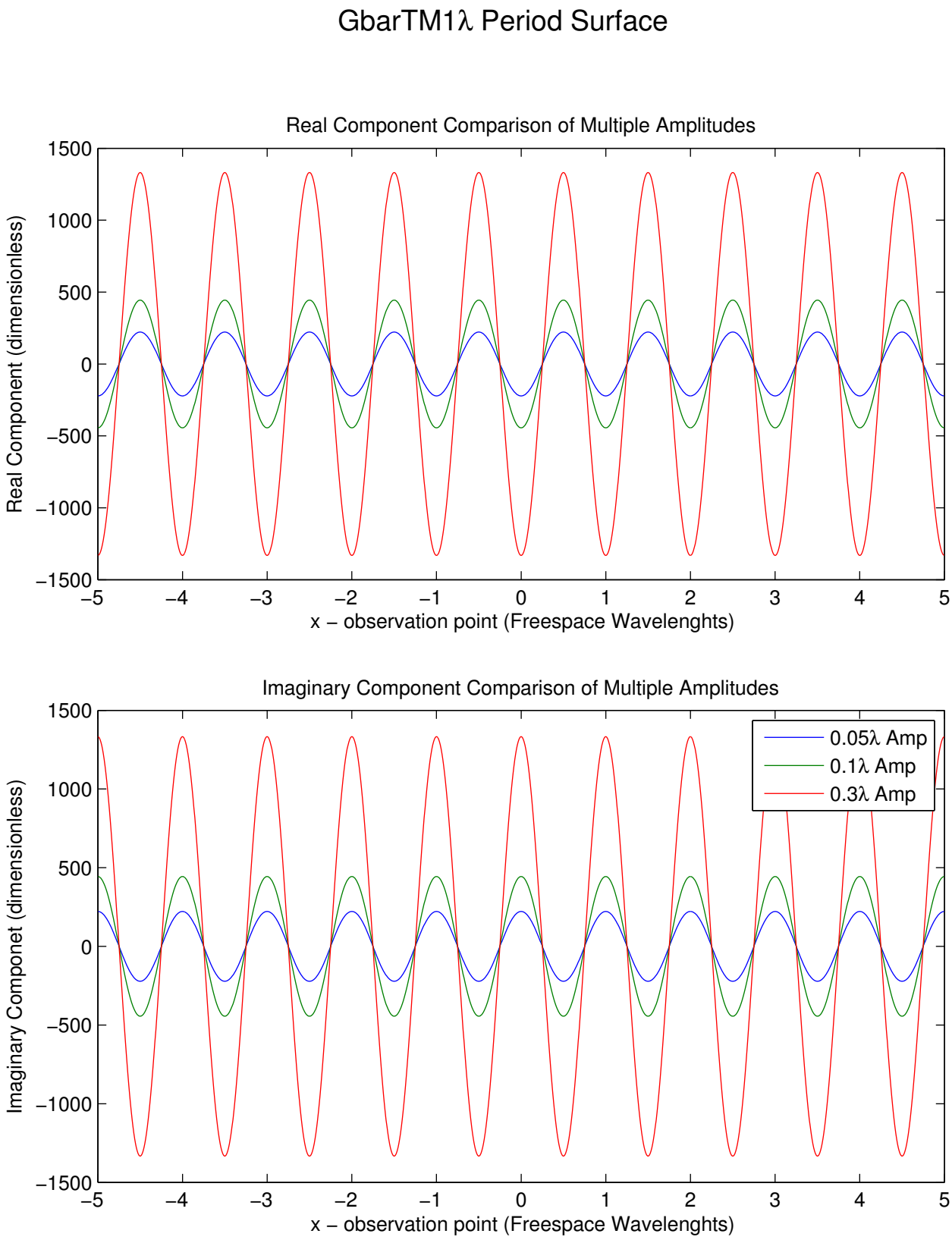


Figure 4.16: TM 1$\lambda$ period Comparison

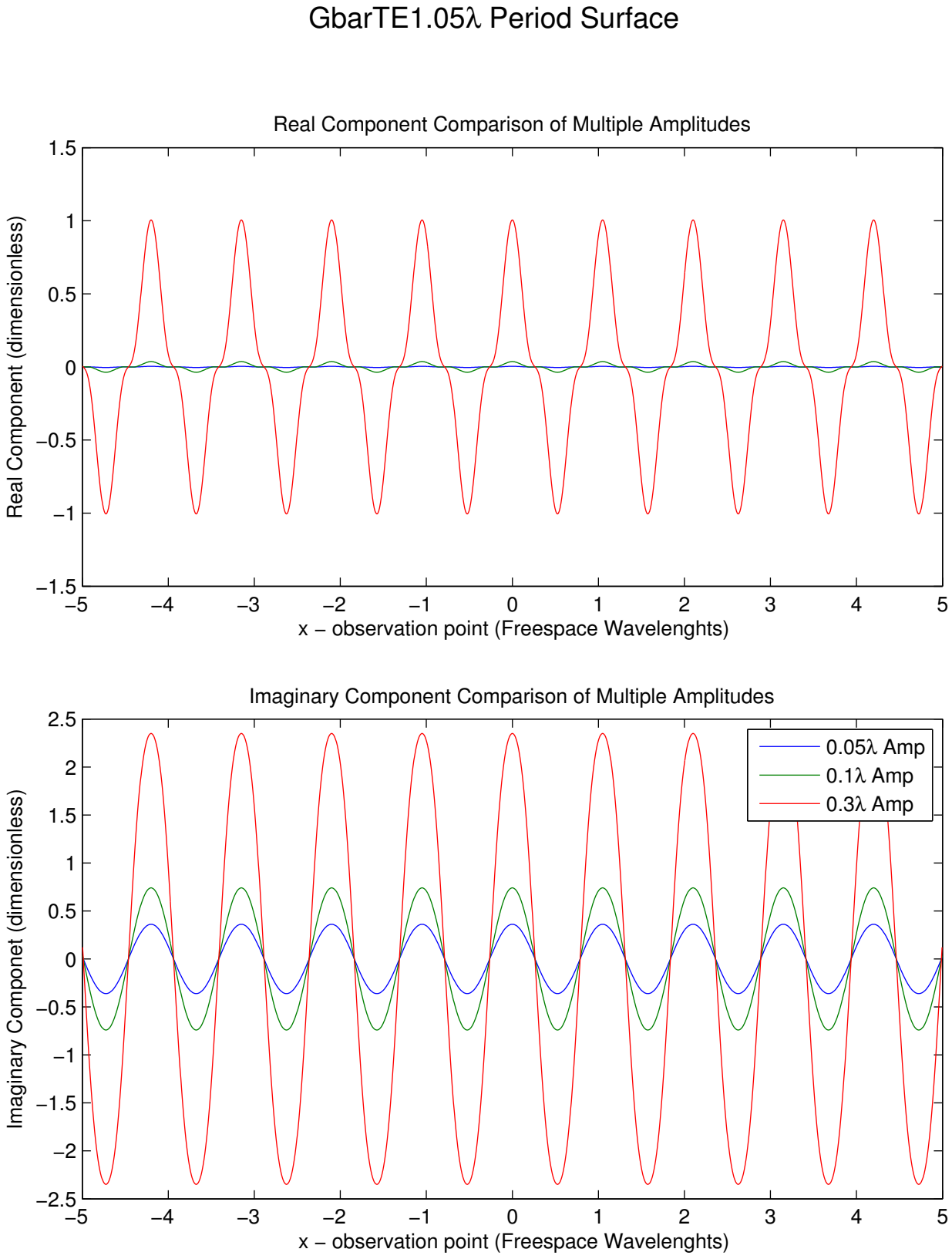


Figure 4.17: TE 1.05$\lambda$ period Comparison

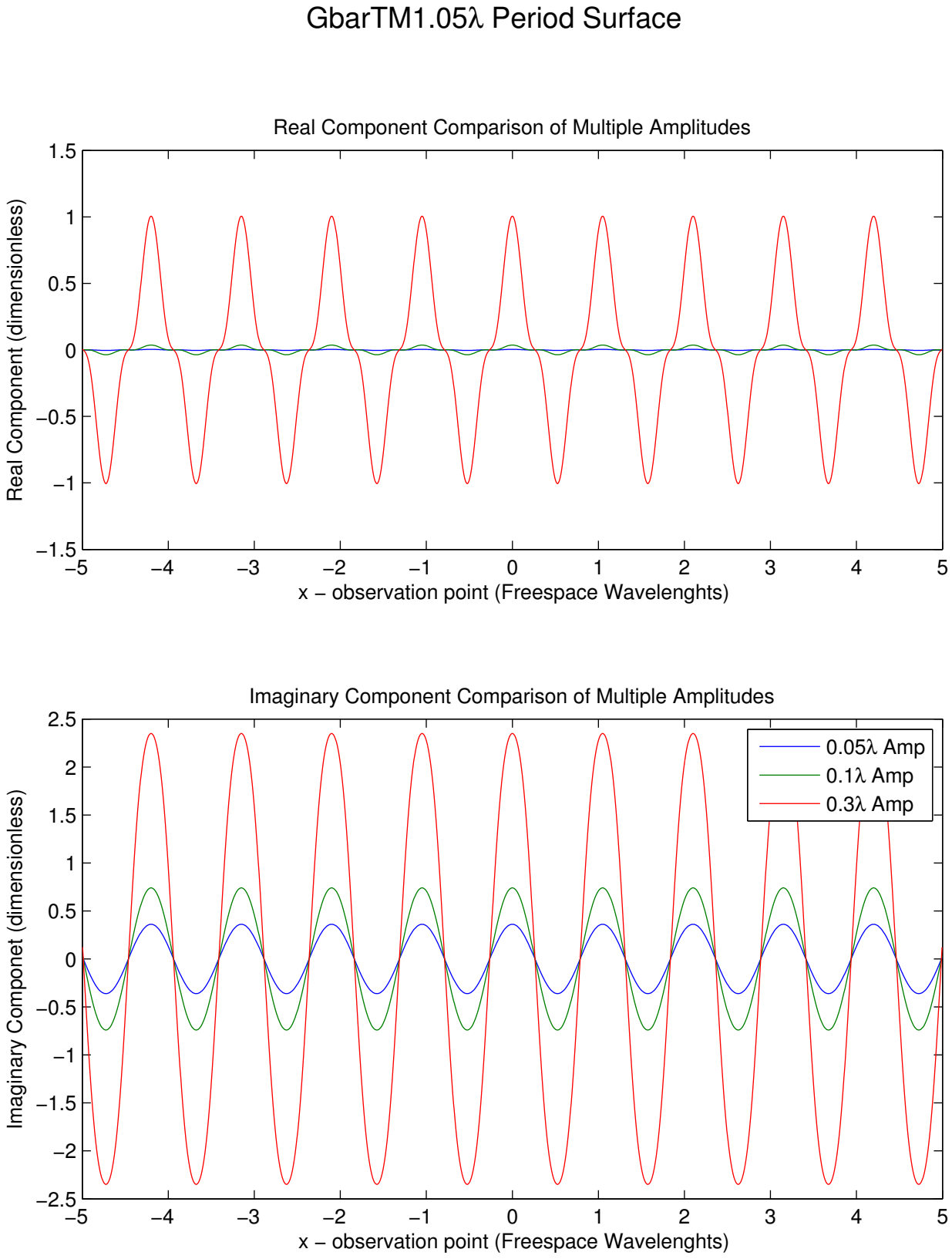


Figure 4.18: TM 1.05λ period Comparison

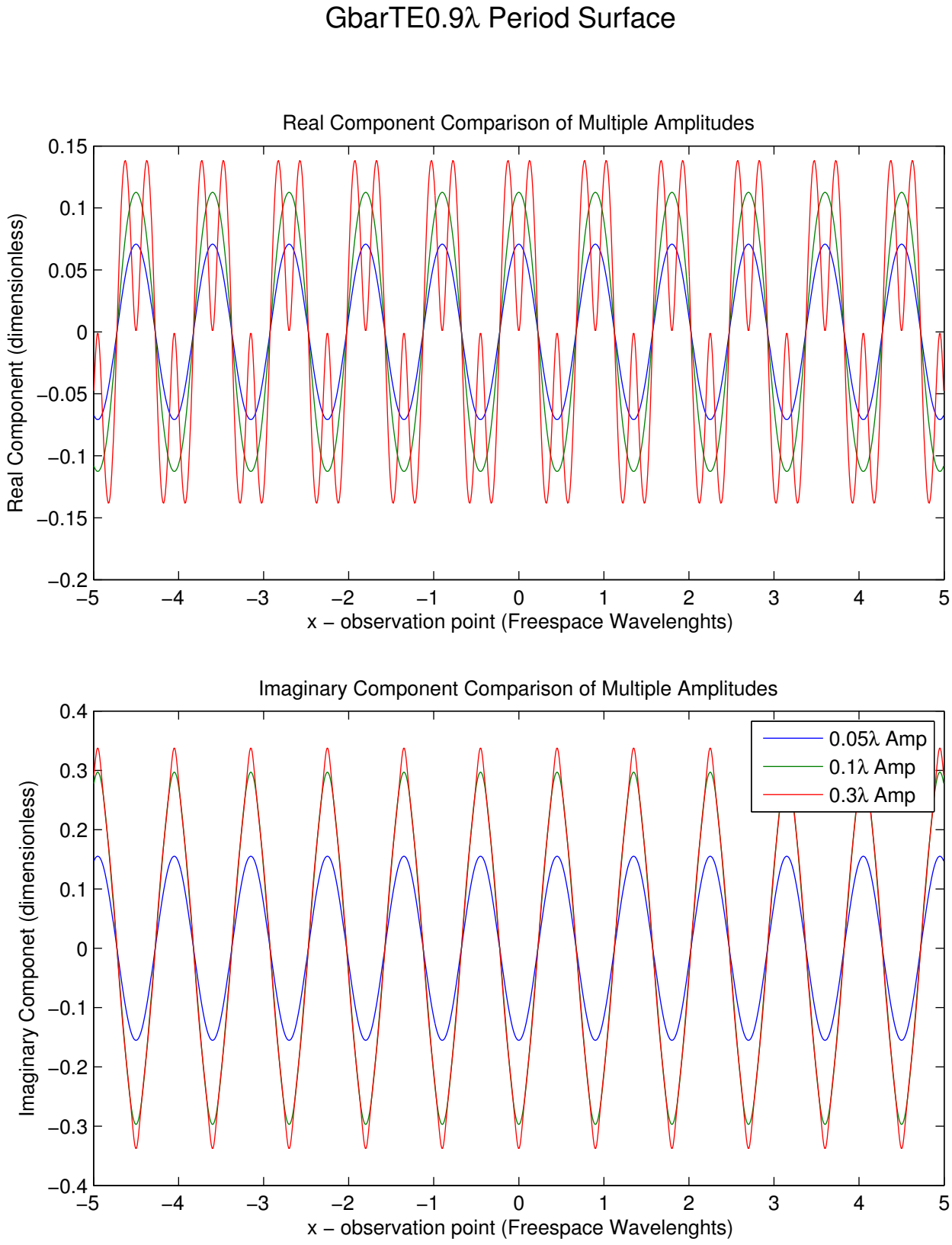


Figure 4.19: TE 0.9λ period Comparison

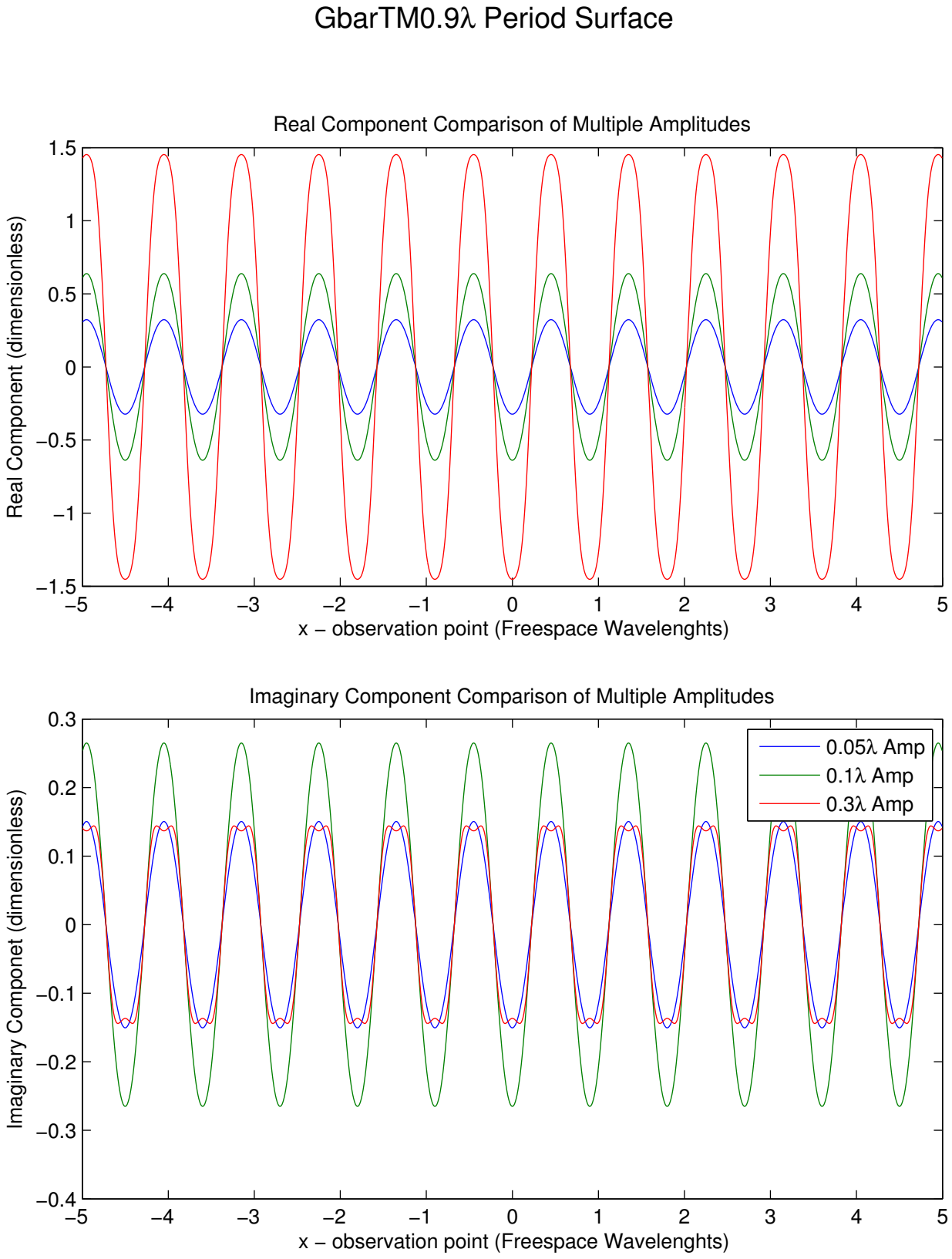


Figure 4.20: TM 0.9$\lambda$ period Comparison

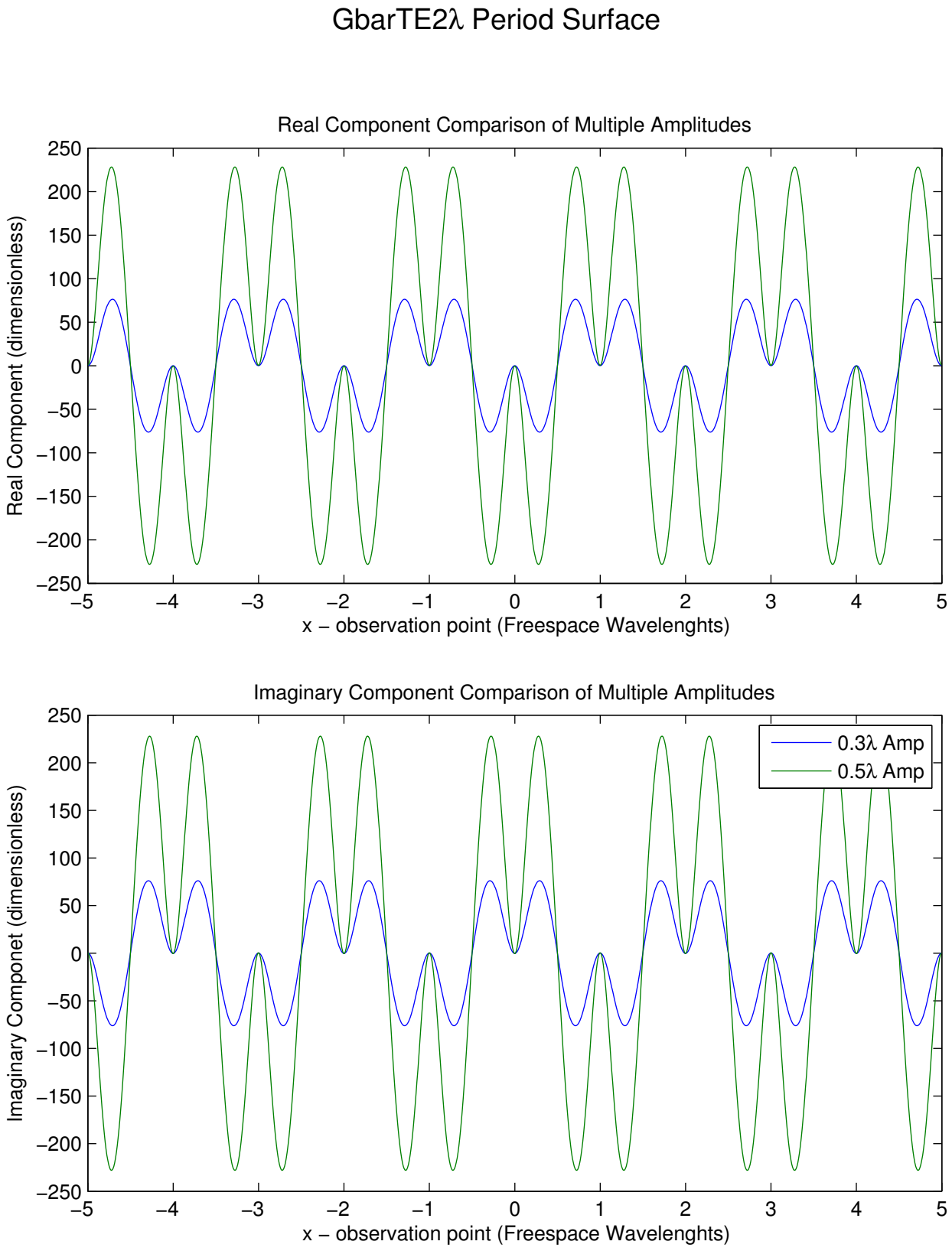


Figure 4.21: TE 2$\lambda$ period Comparison

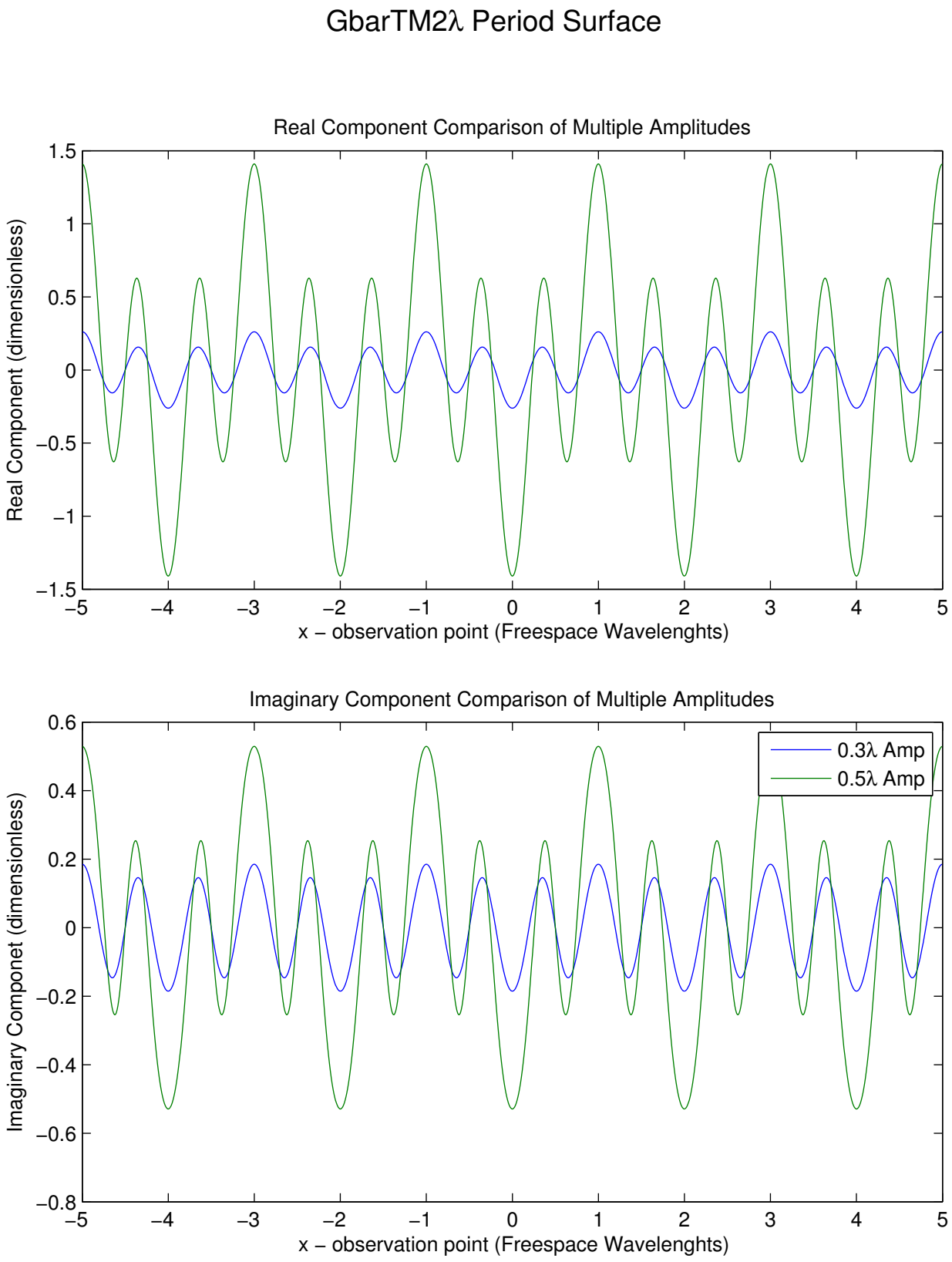


Figure 4.22: TM $2\lambda$ period Comparison

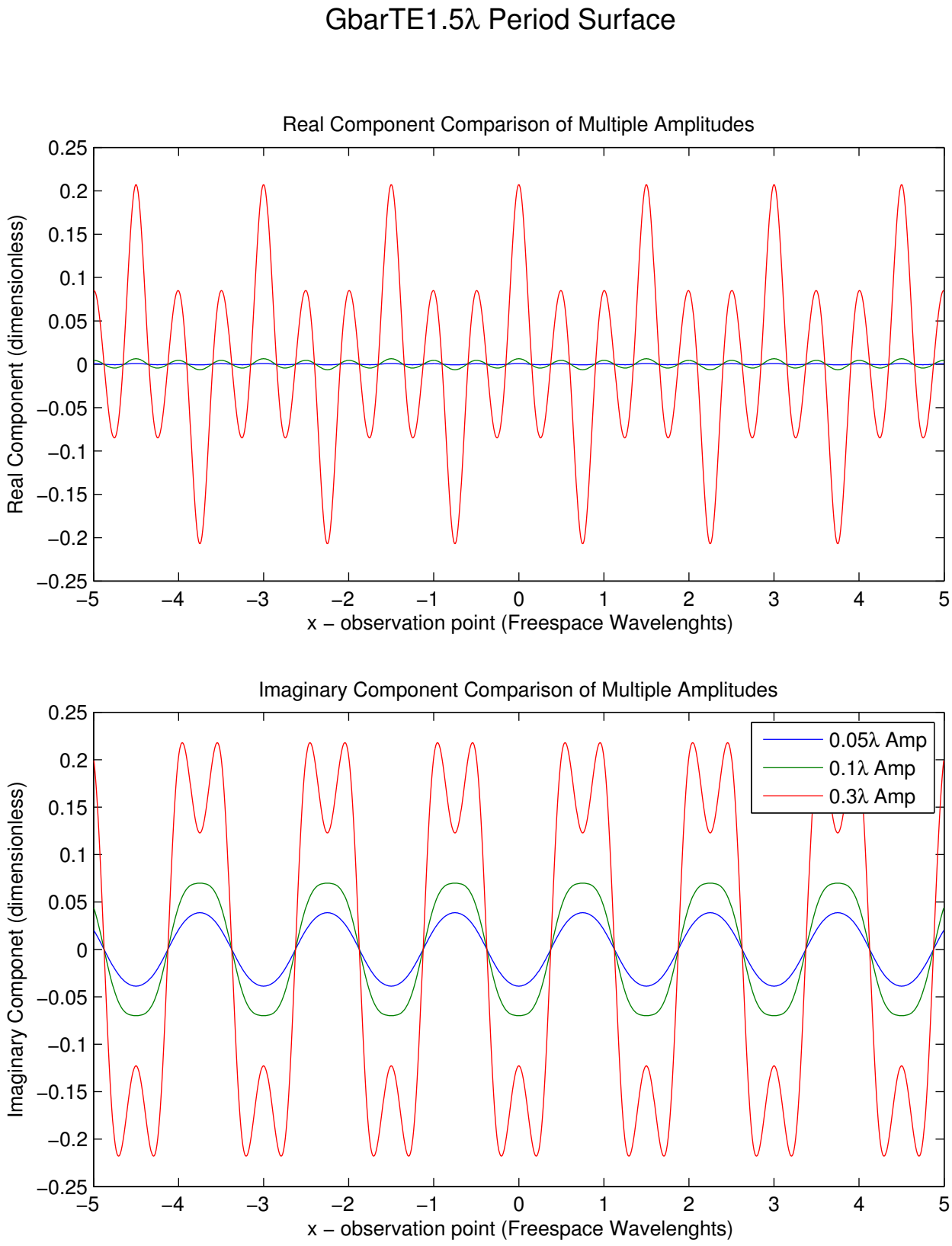


Figure 4.23: TE 1.5λ period Comparison

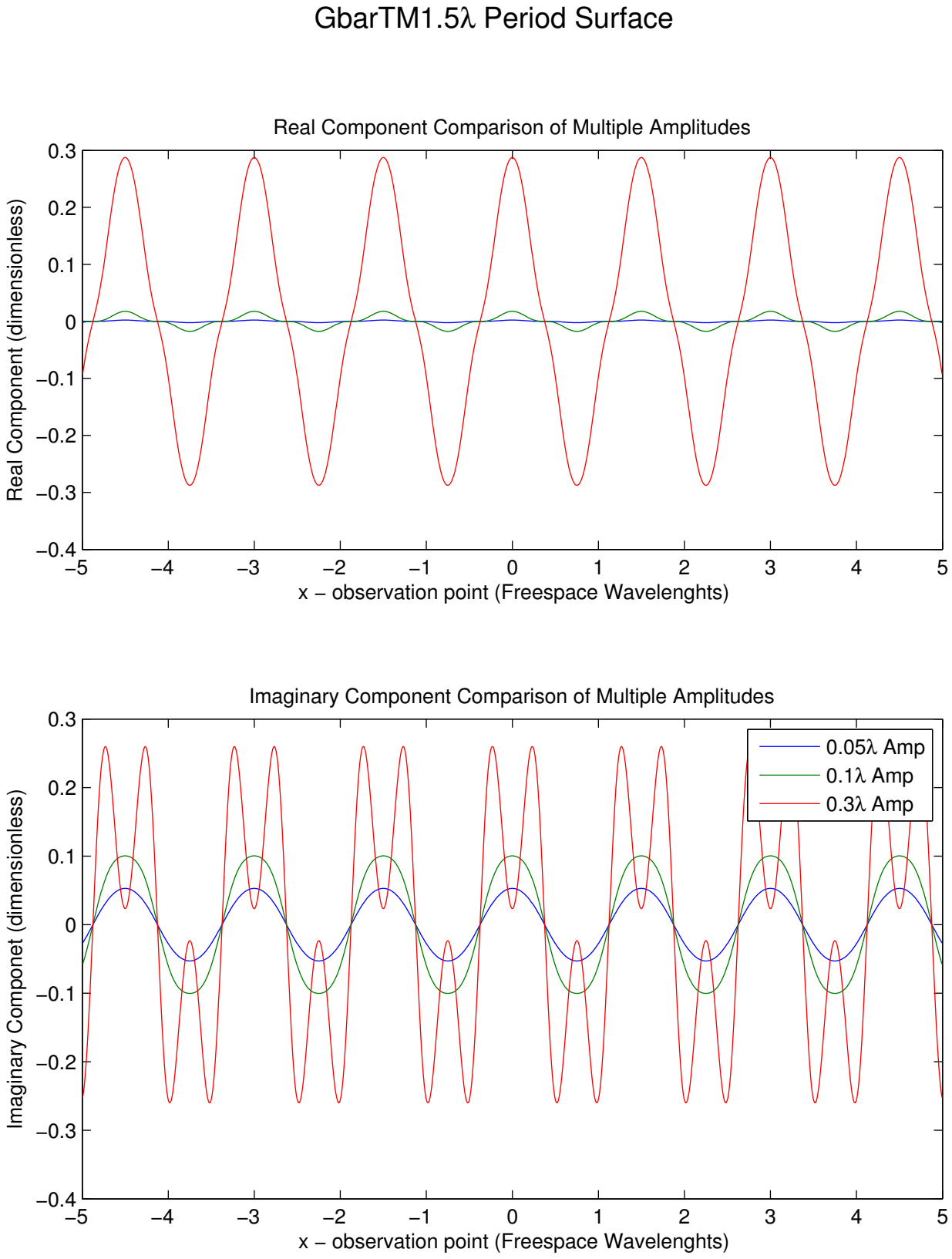


Figure 4.24: TM 1.5$\lambda$ period Comparison

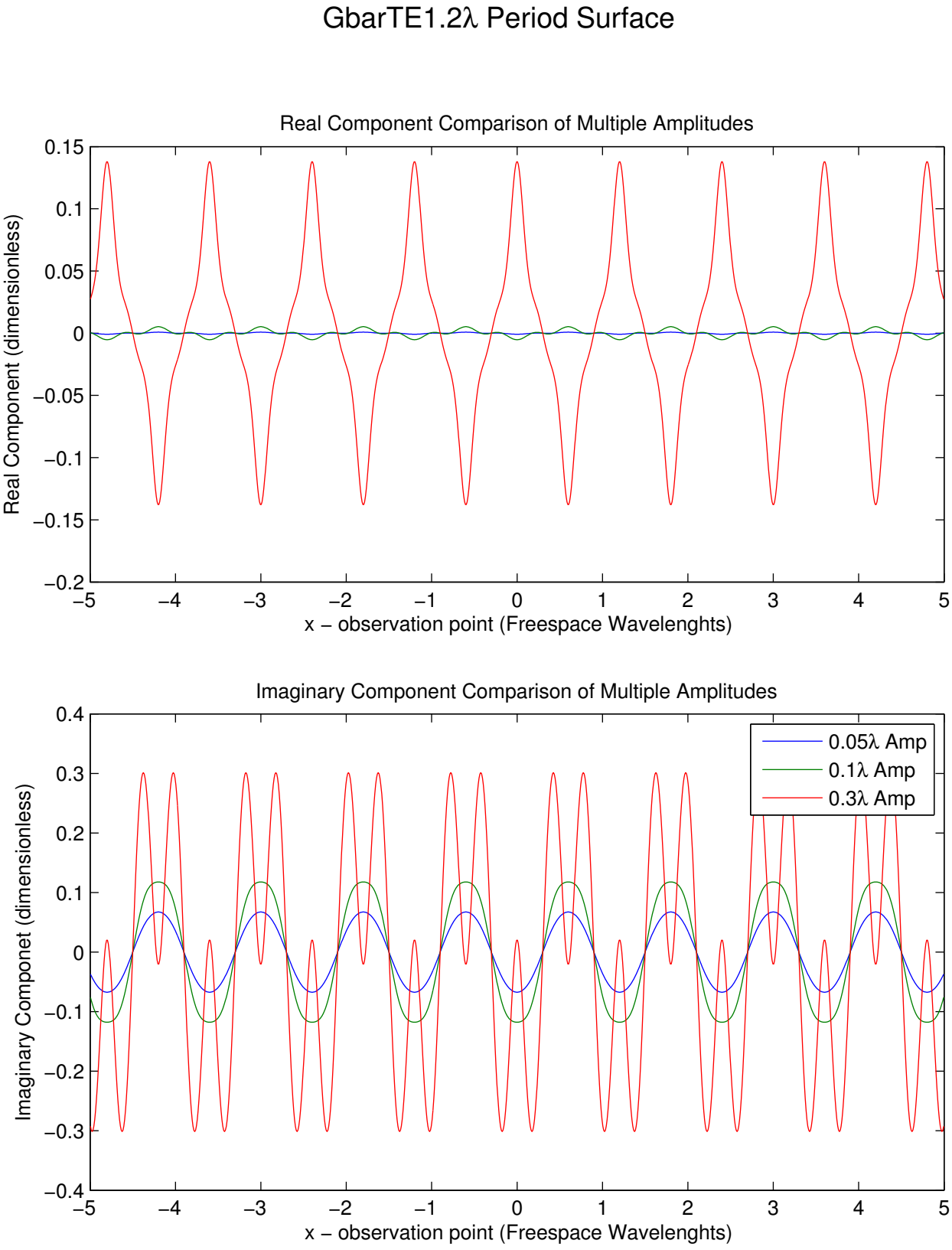


Figure 4.25: TE 1.2$\lambda$ period Comparison

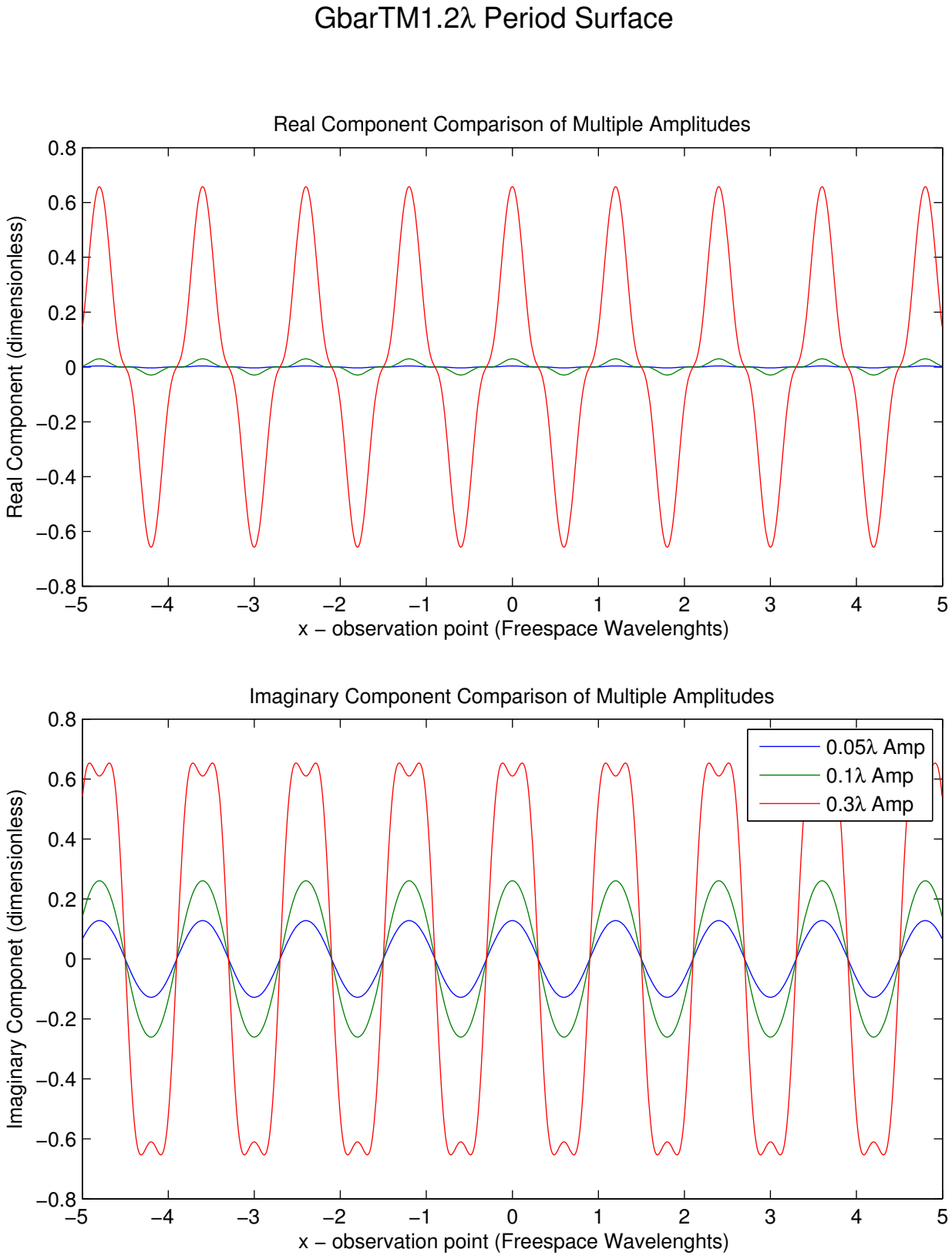


Figure 4.26: TM 1.2$\lambda$ period Comparison

### 4.3.3 Finite Support

Demonstrating how sensitive the result is to the integration support.

The results for a finite integration support are also extremely sensitive the exact length of that support. As in the previous section, results are focused on the center of the surface to show detail and capture the character of the periodic integral. The result is much larger and more chaotic at the extreme edges of the surface which correspond to the end of the integration support. When using this quantity in in the Single Scatter Subtraction method, the surface current will be zero in this region so it may be safely ignored. Both TE and TM have a surface-period dependent oscillation in the real component as shown in Figures 4.27 and 4.28 respectively. On this 10 wavelength period surface, the real component of integral multiples of the surface period are similar with some small attenuation for successively increasing multiples of 80 and 90 wavelength integration support $\alpha$, and dramatically different for $\alpha = 85\lambda_0$ which has a completely different phase and much larger amplitude. The real component for both polarization is two orders of magnitude less than imaginary for integer, and one order of magnitude less for the non-integer multiple of the surface period shown here. On the other hand, the imaginary component is nearly constant for the three integration supports, and the same amplitude but opposite phase for the two polarizations.

As the integration support is increased from $\frac{\alpha}{\lambda_0} = 80$ to 85, then 90 the imaginary component of TE remains constant, but the real component continuously changes as shown in Figures 4.29 and 4.30. Both the magnitude and phase of multiple oscillatory components, all of different frequencies, of the the real part change. In contrast, the real part of the TM polarization seems to be composed of a single oscillatory component but has a dramatically more pronounced increase in amplitude for non-integer or half-integer[3] integration supports. Also striking is the imaginary component of TM whose amplitude continuously changes with

[3]That is the 8, 8.5 and 9 times the surface period, with 8.5 being called the "half-integer" multiple.

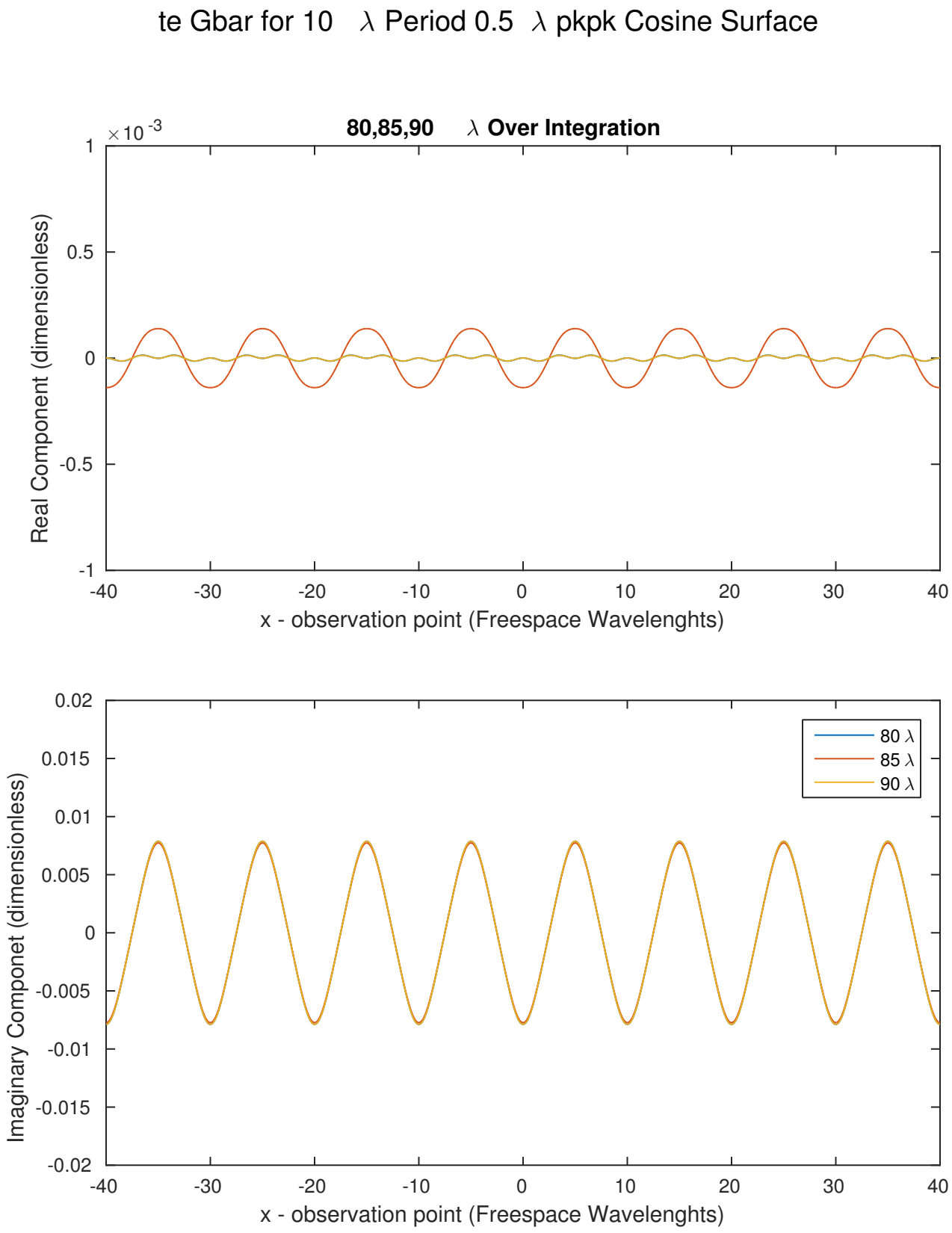


Figure 4.27: TE Periodicity of Finite integration

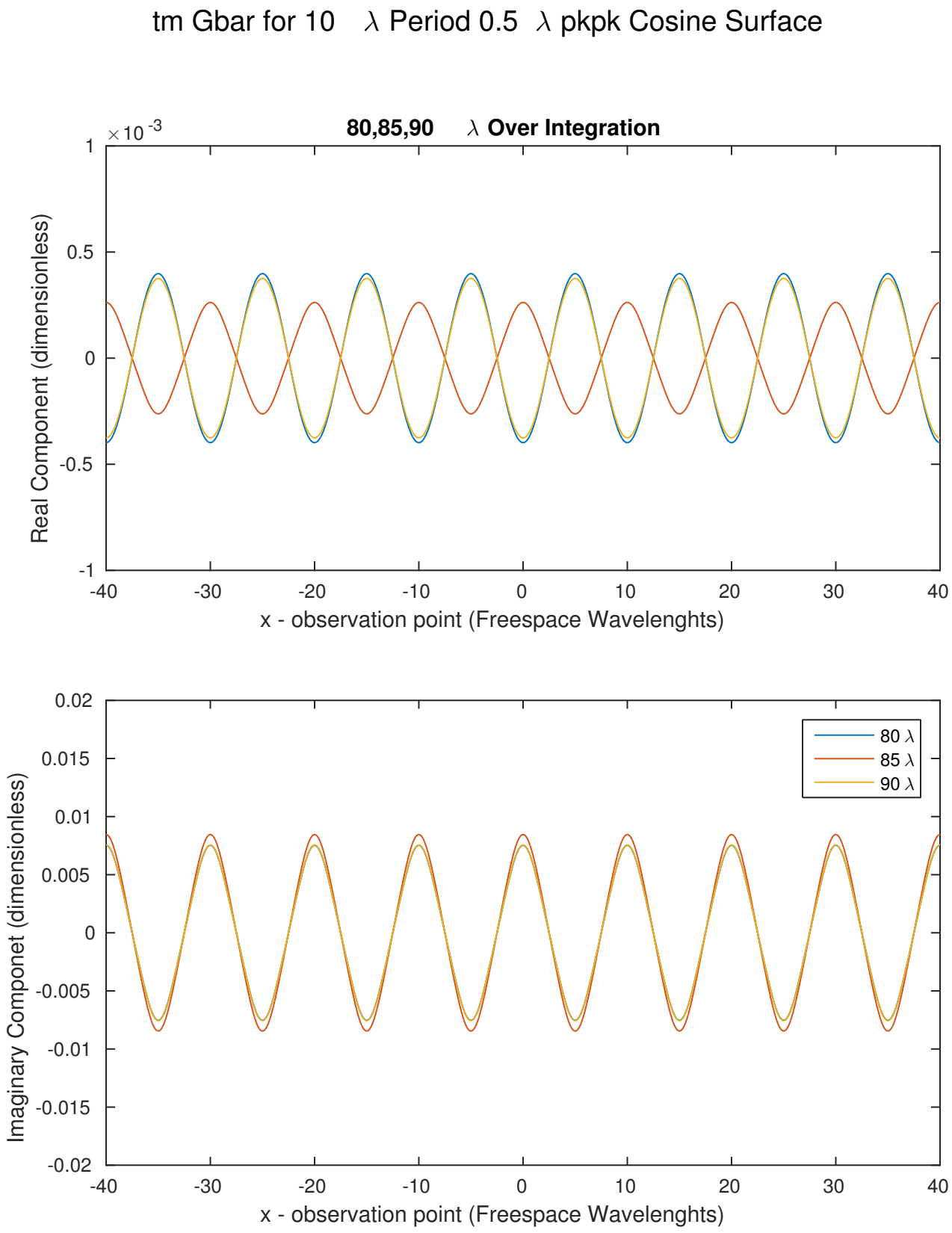


Figure 4.28: TM Periodicity of Finite integration

the change in integration support.

### 4.3.4 Conclusion

This section has shown that the kernel integral, $\overline{G}$ in the infinite case and $\overline{\overline{G}}$ in the finite case, is a complicated and difficult integral to evaluate. Numerical results were presented showing the complex relationship between polarization, amplitude, surface period and integration support. In the next section, a suite of powerful approximations will be presented that accuracy capture this character and enable the introduction of new approximate scattering theories.

## 4.4 Extend Rough Surface Analytical Approximations

### 4.4.1 Introduction

The goal of this research effort is to provide extensions to rough surface scattering analytical approximations. As noted in the literature review, the physical, uniform and geometrical diffraction theories are not applicable to rough surface scattering since they require canonical geometries and exact knowledge of the scattering object. This coupled with the fact that simulation complexity requirements still outpace computation capacity improvements, creates a strong need for simple analytic expressions which describe complex scattering physics.

Building on the numeric results above, approximations to the kernel integrals required in the $S^3$ method are analytically and empirically derived.

First, analytic approximations to the tails of the kernel integral of the finite $\overline{\overline{G}}$ are derived for both TE and TM for a single sinusoid surface. Next, an approximation is derived for the

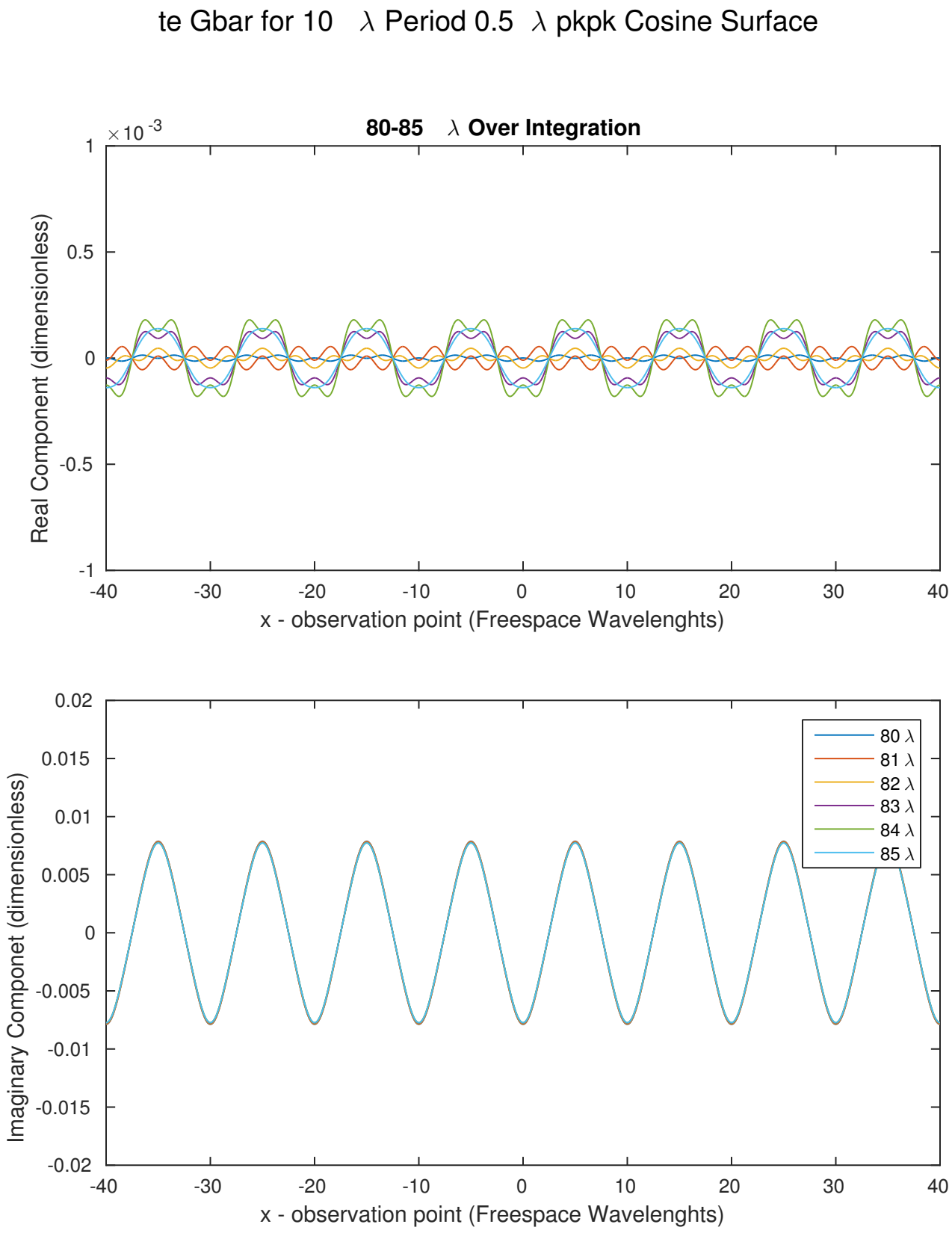


Figure 4.29: TE Sensitivity to Integration Support to $80 \leq \alpha \leq 85$

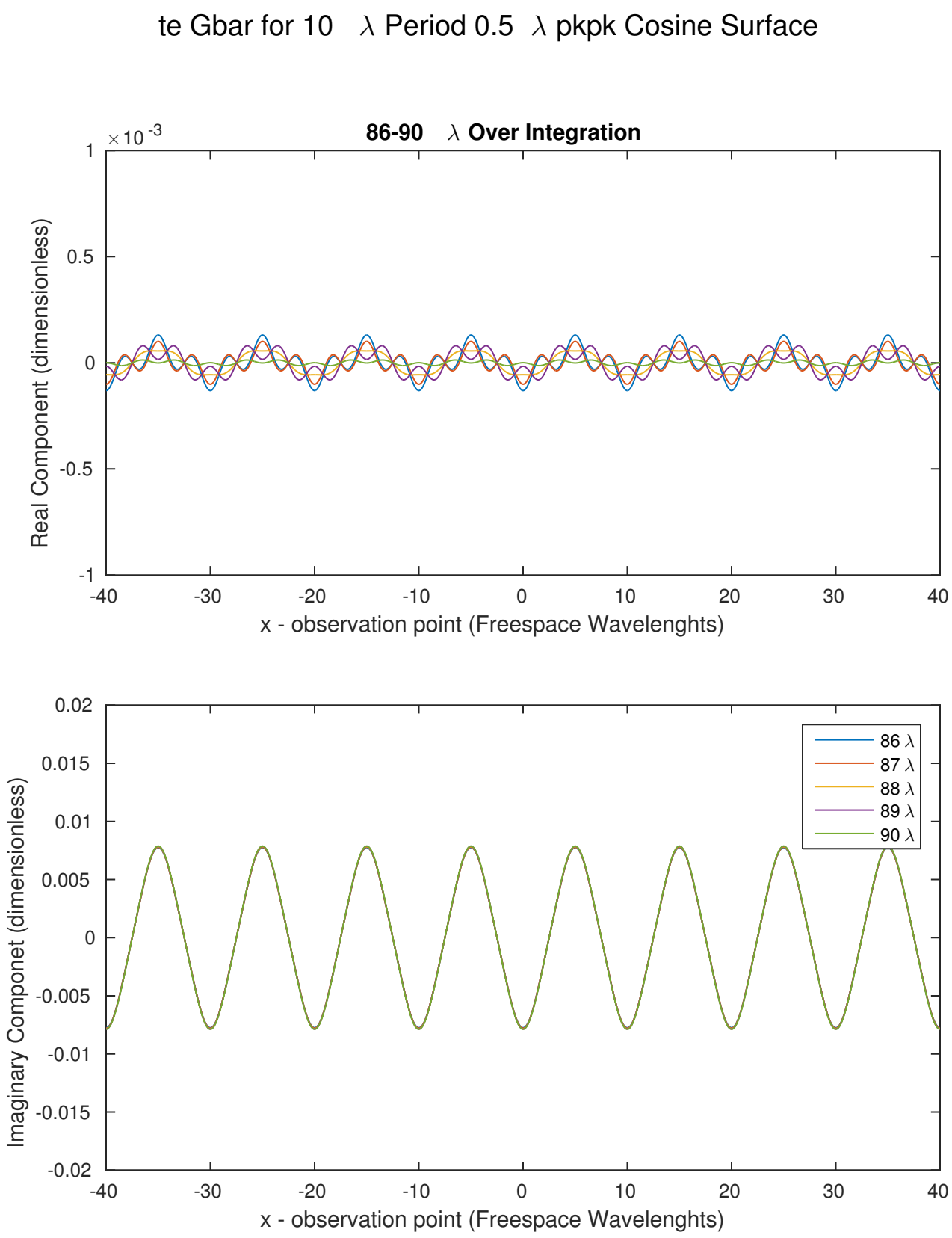


Figure 4.30: TE Sensitivity to Integration Support to $86 \leq \alpha \leq 90$

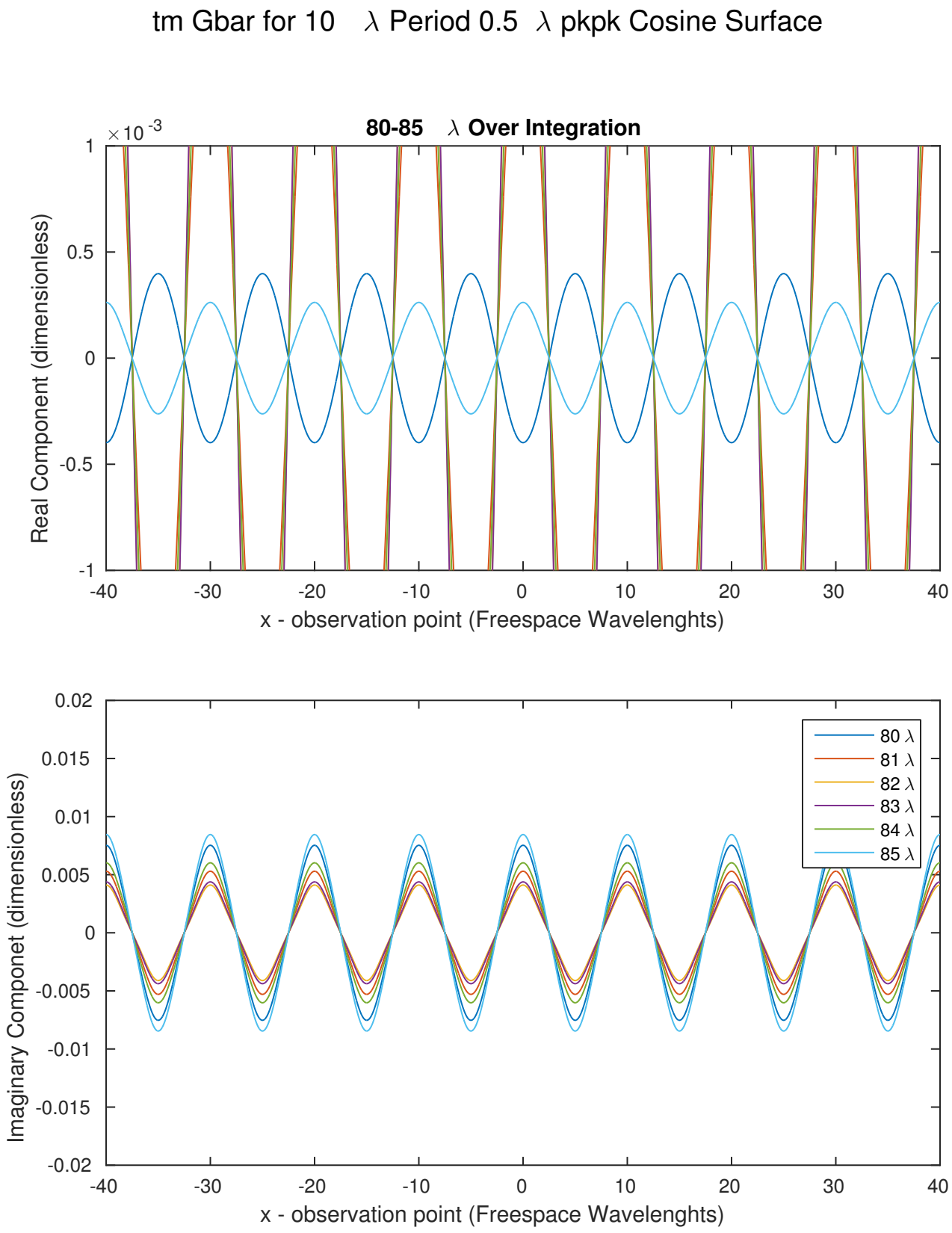


Figure 4.31: TM Sensitivity to Integration Support to $80 \leq \alpha \leq 85$

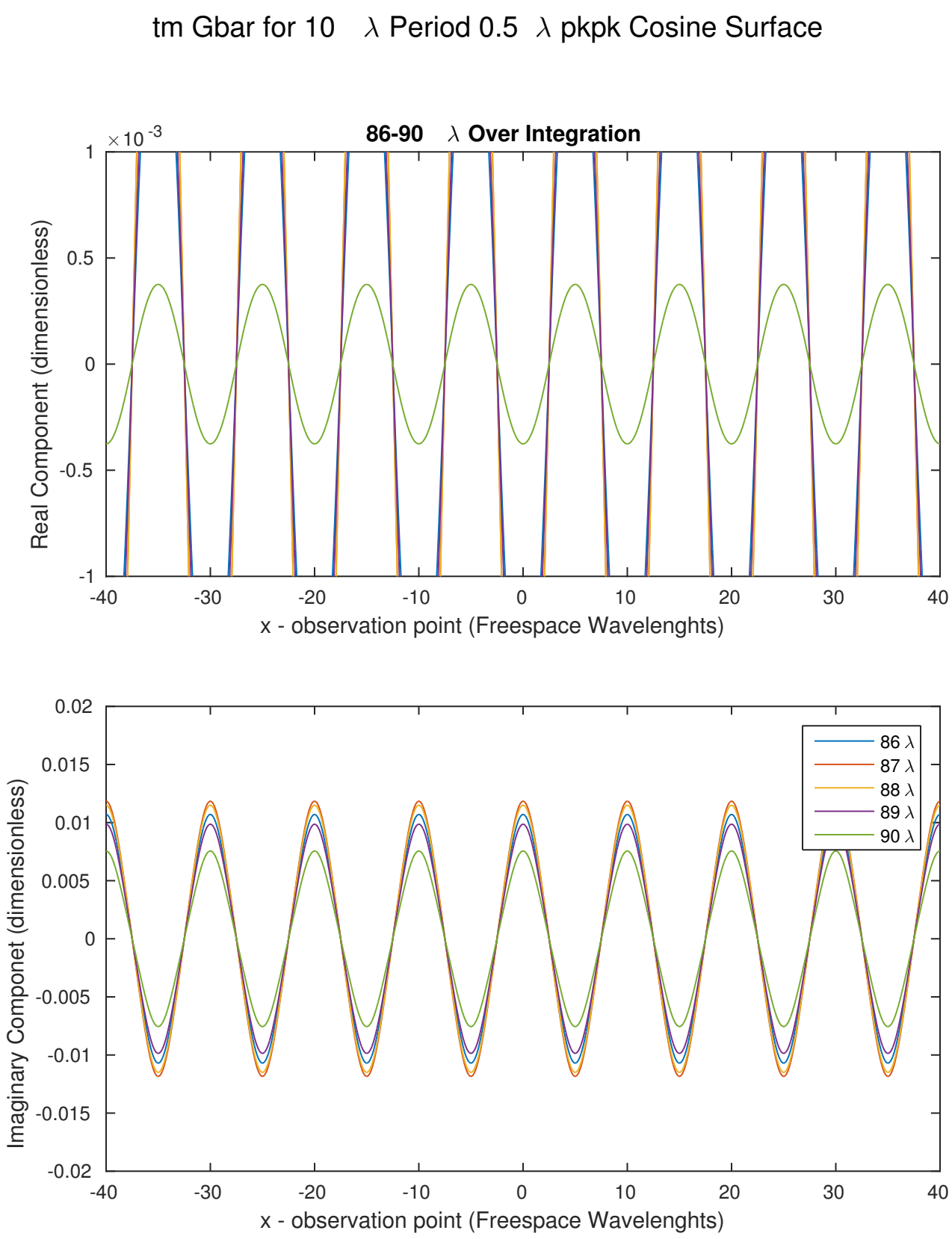


Figure 4.32: TM Sensitivity to Integration Support to $86 \leq \alpha \leq 90$

small argument[4] integral for TM polarization and bounds on its validity established which are found to prevent a complete analytic approximation for $\overline{\overline{G}}_{TM}$ when used in combination with the integral tails. Then results are presented showing that the first-order approximation to the integral tails may not be satisfactory for TM and in an attempt to bridge the gap between the tails and the small argument approximation, a higher order approximation is derived. Then an empiric formula is presented from TE which provides excellent agreement over a well-defined range of surface parameters for a sinusoid surface.

Finally, the tail integrals are extended to the infinite integration of $\overline{G}$, approximated, and combined with the infinite empiric formula producing a relatively simple empiric analytic formula for both polarizations for the finite case, and the single sinusoid approximations are applied to spectral surfaces.

These analytic and empiric approximations may help to reduce the numerical computation necessary for scattering research and provide insight into scattering physics.

### 4.4.2 Infinite Support

It was quickly recognized from computations with an integration support $\frac{\alpha}{\lambda_0} = 10^6$, that the real component was essentially negligible and the imaginary component was a simple sinusoid. By examining the dependence on surface period and amplitude, an empiric formula which has excellent agreement for $\frac{\lambda_s}{\lambda_0} \geq 5$ and $\frac{b}{\lambda_0} \leq 0.5$ was found as

$$\overline{G}_{pp'} = -\tau_{pp'} \frac{\zeta_{xx}(x)}{2k_0} \tag{4.4.1}$$

[4] $x'$ in the region of x.

where

$$\tau_{pp'} = \begin{cases} j & \text{TE} \\ -j & \text{TM} \end{cases}$$

The physical interpretation of this result will be discussed in Chapter 5. A comparison of this formula with numerically computed values with a 1 million wavelength integration support are shown in Figures 4.33 through 4.40. Figures 4.33 and 4.34 show a comparison of the numerically computed $\overline{G}$ vs empiric formula $\overline{G}$ for both TE and TM real and imaginary component ($\text{Re}\left\{\overline{G}\right\} \equiv 0$ ) for $\frac{\lambda_s}{\lambda_0} = 20$ and 10 respectively, showing excellent agreement. Figure 4.37 shows the edge of the empiric fit as a higher frequency component of the imaginary part of $\overline{G}$ appears and the real component starts to increase, with only an order of magnitude separating real and imaginary on TM. The very large value for TE on $\frac{\lambda_s}{\lambda_0} = 2$ is shown in Figure 4.39 where TM is also larger than the previous cases, but generally in line with larger wavelengths. Figure 4.40 shows the very large values for TM on $\frac{\lambda_s}{\lambda_0} = 1$, where TE has returned to a normal state.

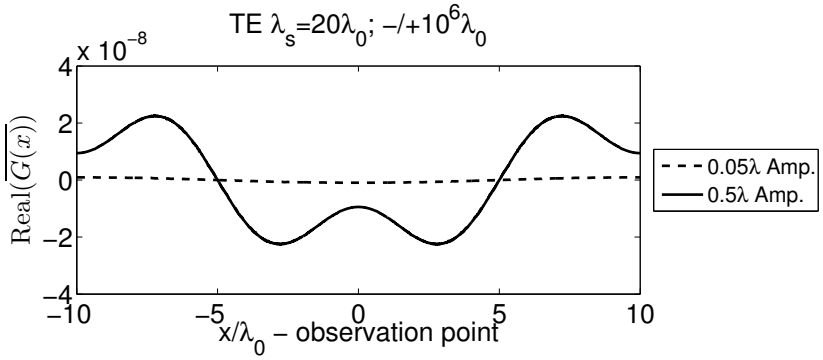


(a) Real TE

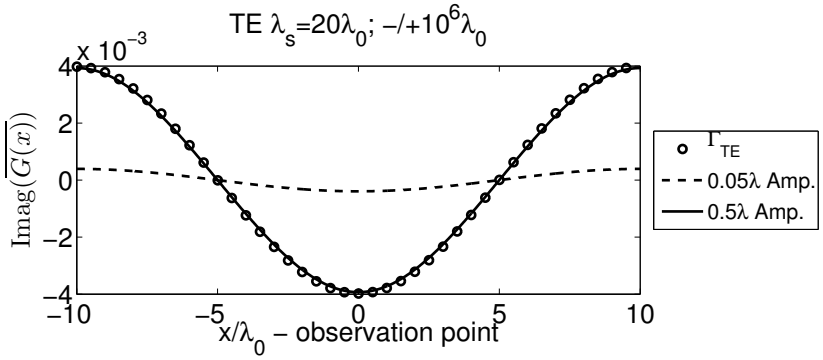


(b) Imag TE

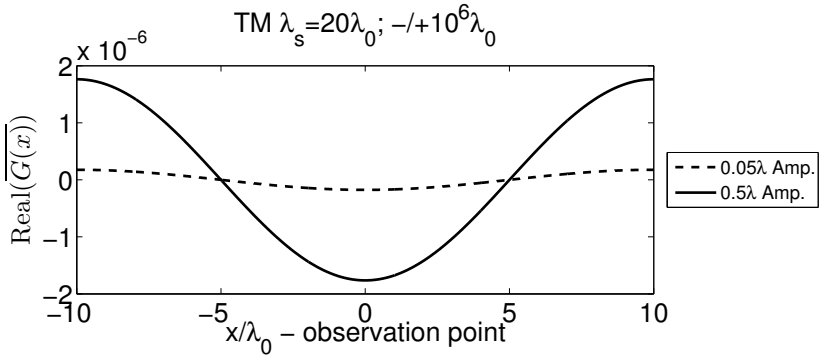


(c) Real TM

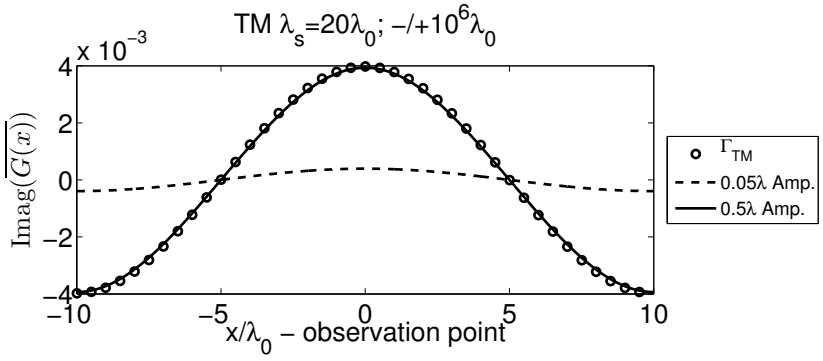


(d) Imag TM

Figure 4.33: Comparison of $\overline{G}$ and $\overline{\Gamma}$ for $\frac{\lambda_s}{\lambda_0} = 20$

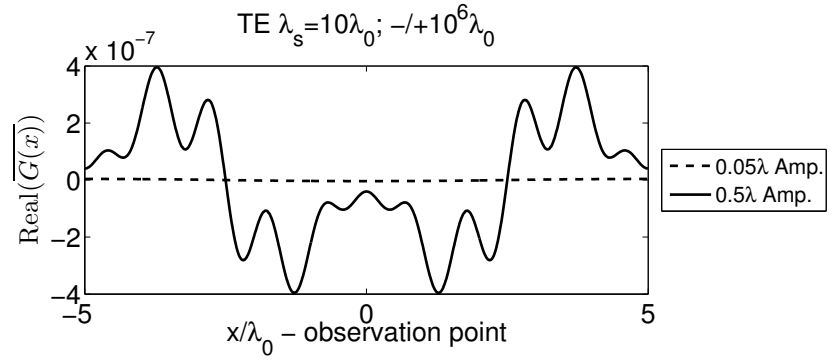


(a) Real TE

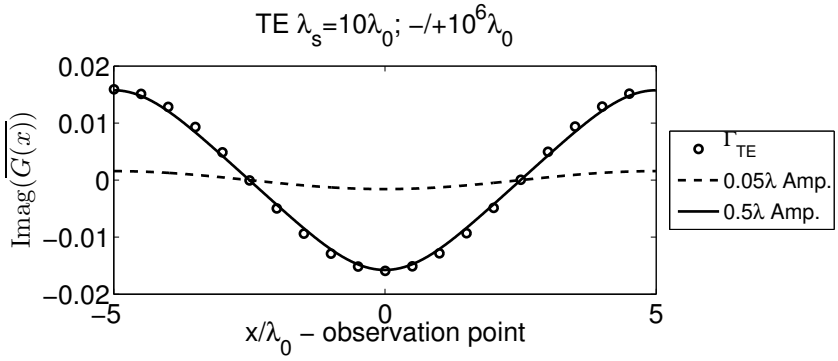


(b) Imag TE

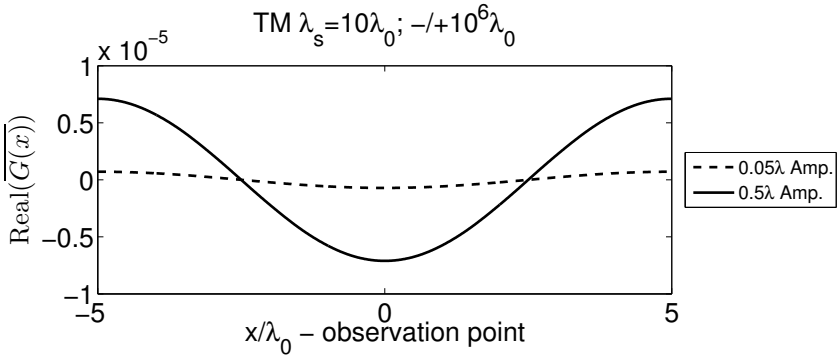


(c) Real TM

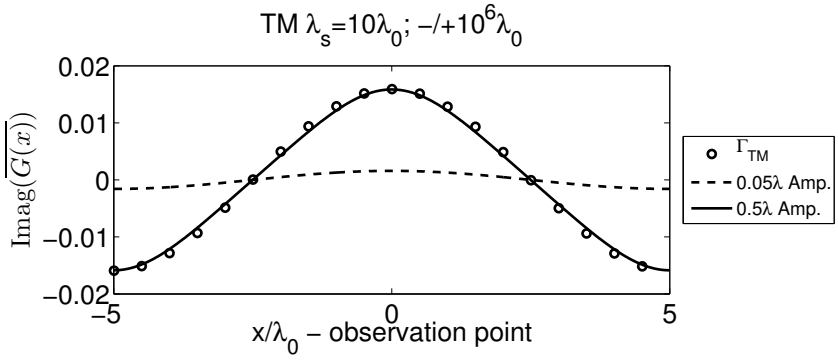


(d) Imag TM

Figure 4.34: Comparison of $\overline{G}$ and $\overline{\Gamma}$ for $\frac{\lambda_s}{\lambda_0} = 10$

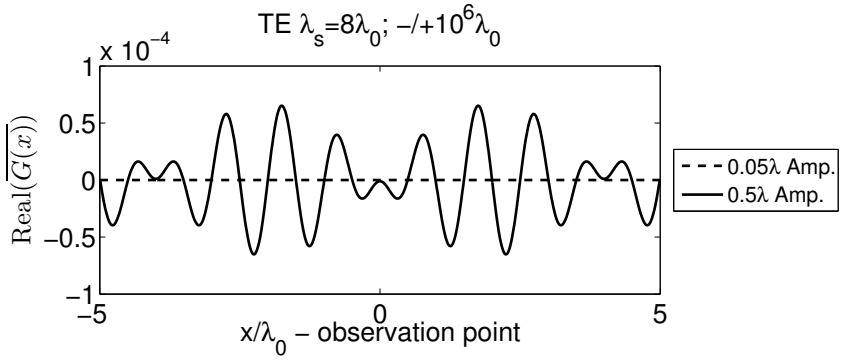


(a) Real TE

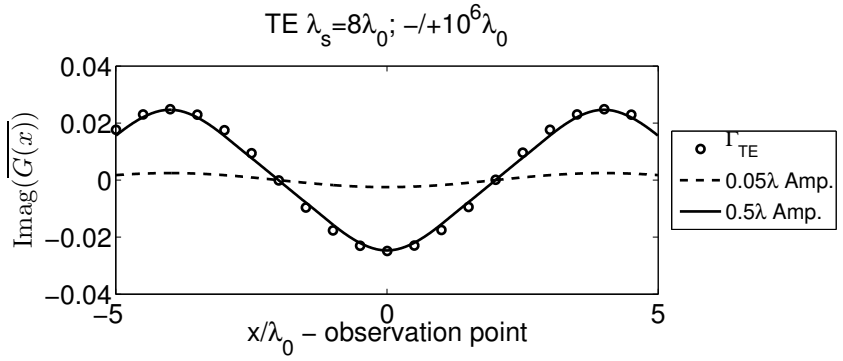


(b) Imag TE

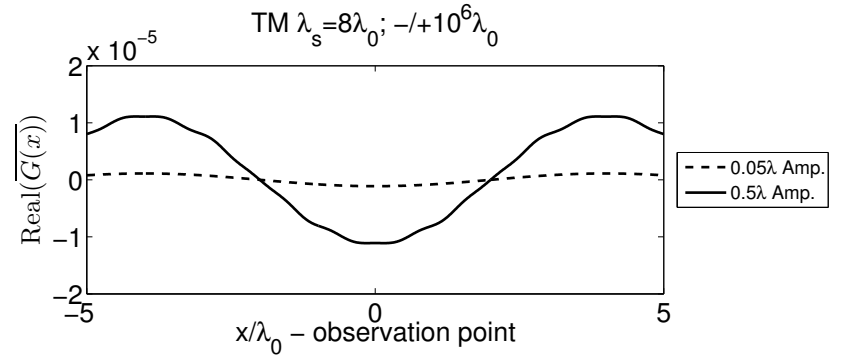


(c) Real TM

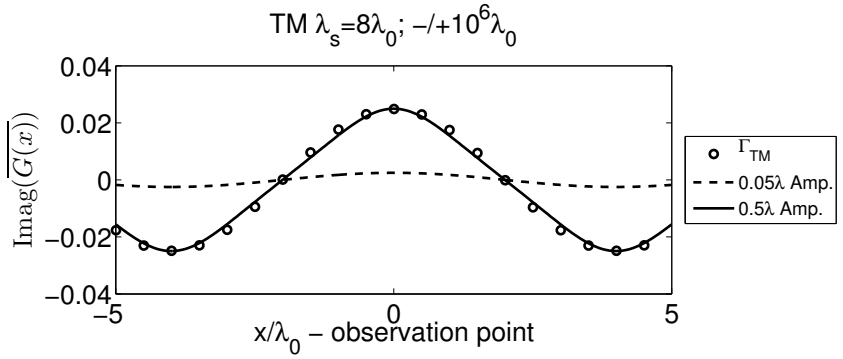


(d) Imag TM

Figure 4.35: Comparison of $\overline{G}$ and $\overline{\Gamma}$ for $\frac{\lambda_s}{\lambda_0} = 8$

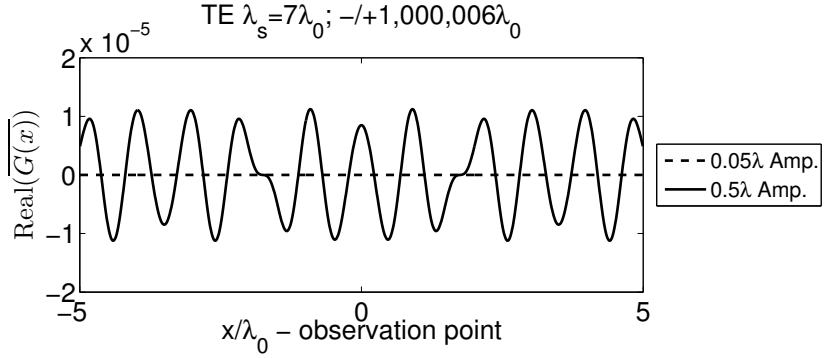


(a) Real TE

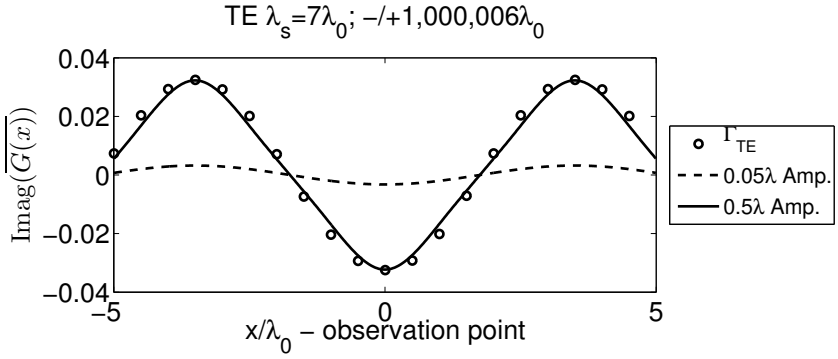


(b) Imag TE

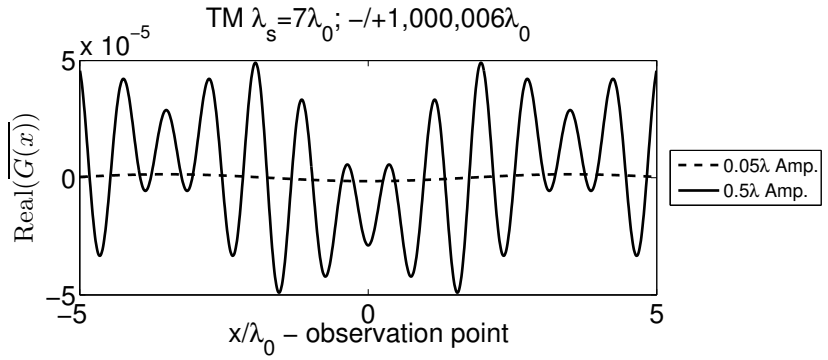


(c) Real TM

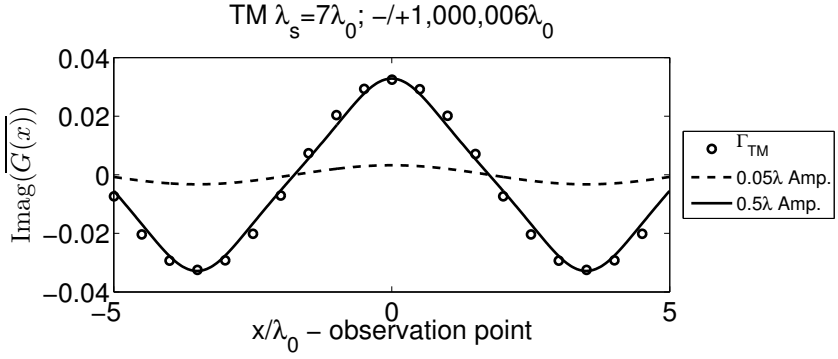


(d) Imag TM

Figure 4.36: Comparison of $\overline{G}$ and $\overline{\Gamma}$ for $\frac{\lambda_s}{\lambda_0} = 7$

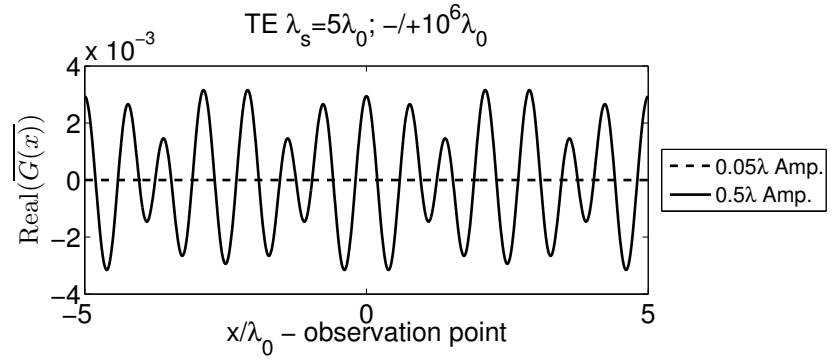


(a) Real TE

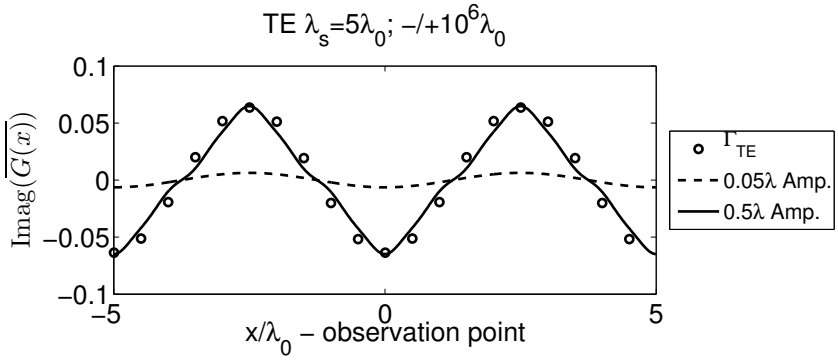


(b) Imag TE

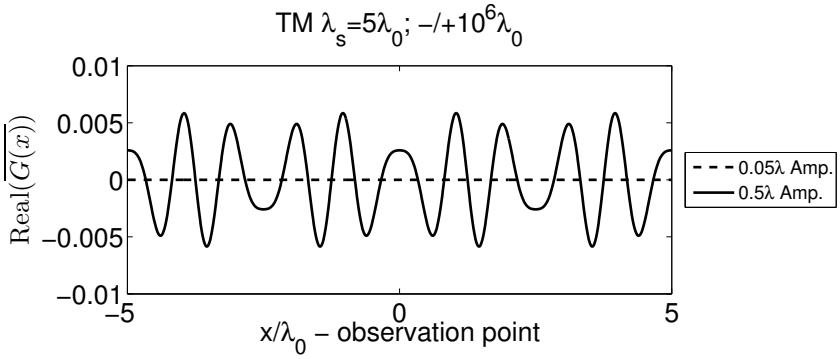


(c) Real TM

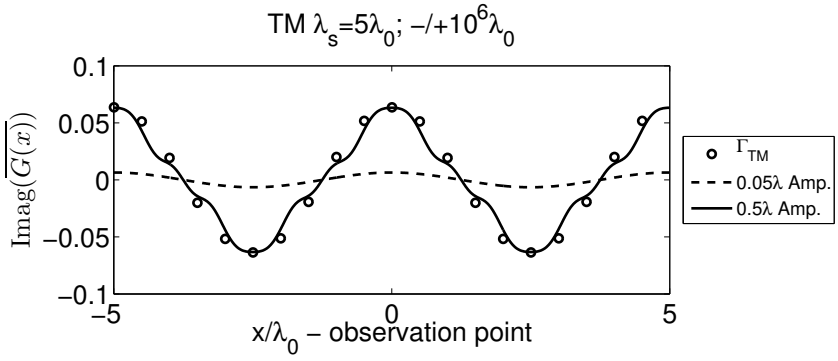


(d) Imag TM

Figure 4.37: Comparison of $\overline{G}$ and $\overline{\Gamma}$ for $\frac{\lambda_s}{\lambda_0} = 5$

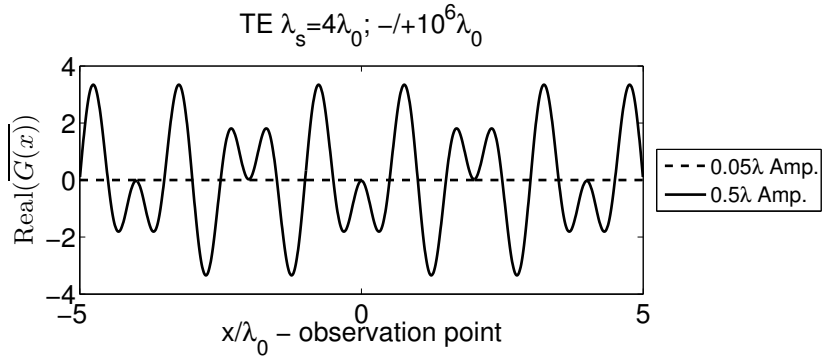


(a) Real TE

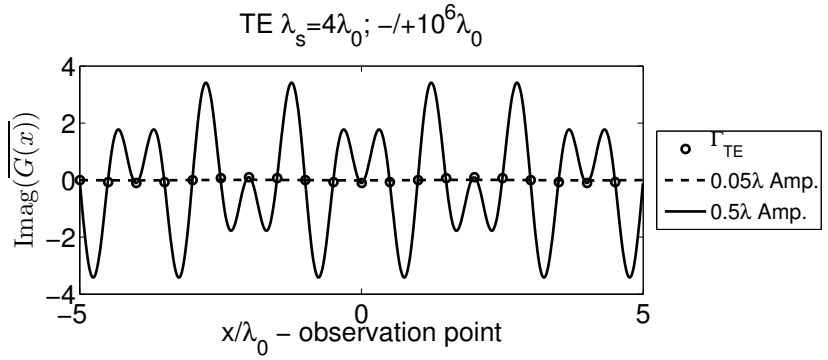


(b) Imag TE

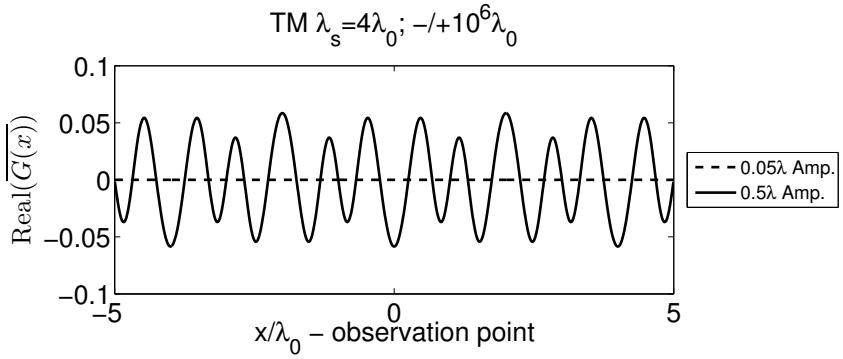


(c) Real TM

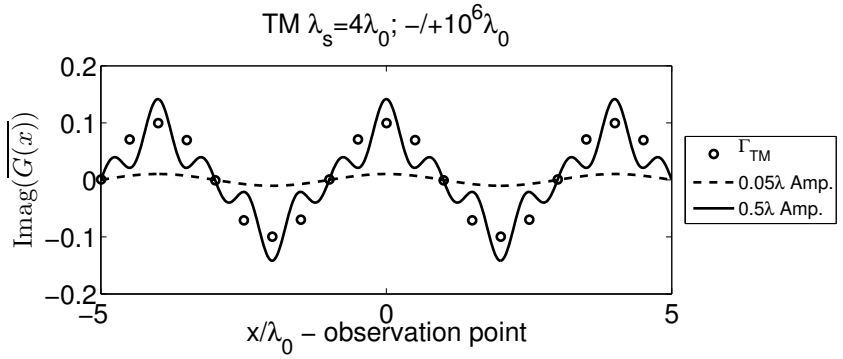


(d) Imag TM

Figure 4.38: Comparison of $\overline{G}$ and $\overline{\Gamma}$ for $\frac{\lambda_s}{\lambda_0} = 4$

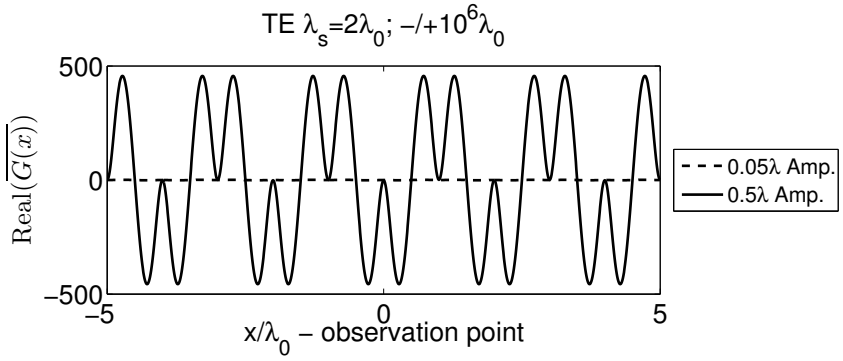


(a) Real TE

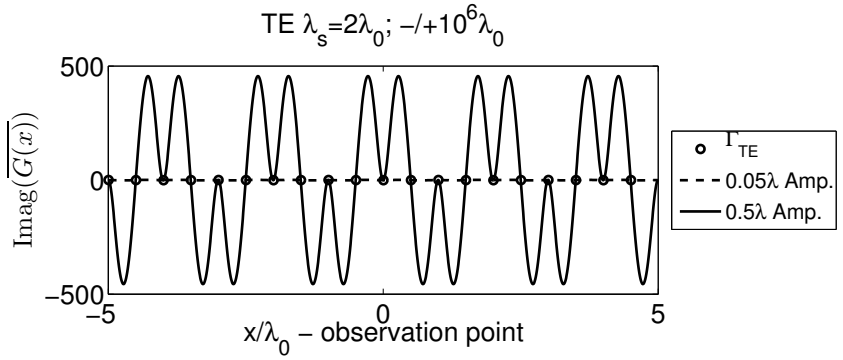


(b) Imag TE

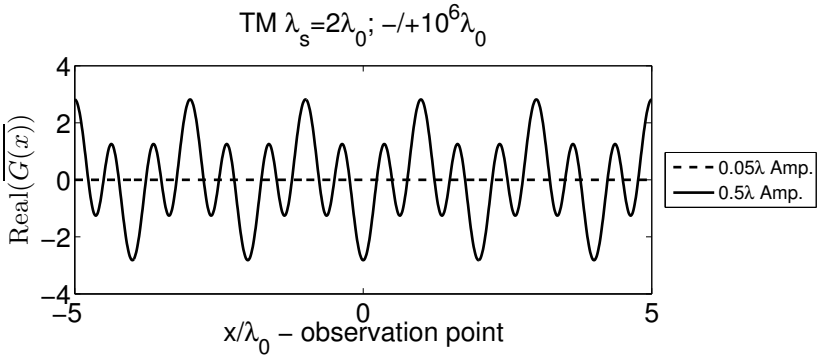


(c) Real TM

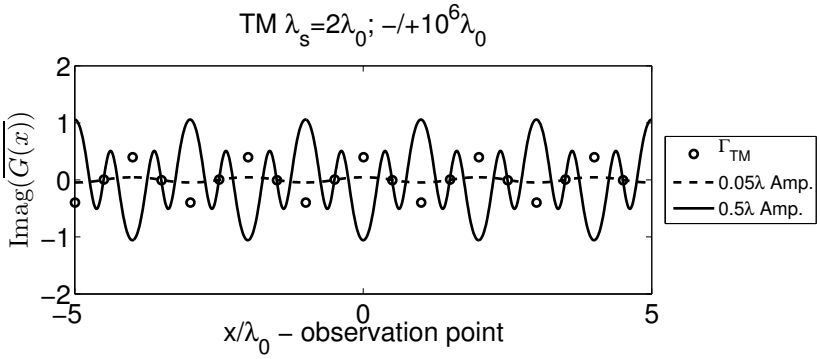


(d) Imag TM

Figure 4.39: Comparison of $\overline{G}$ and $\overline{\Gamma}$ for $\frac{\lambda_s}{\lambda_0} = 2$

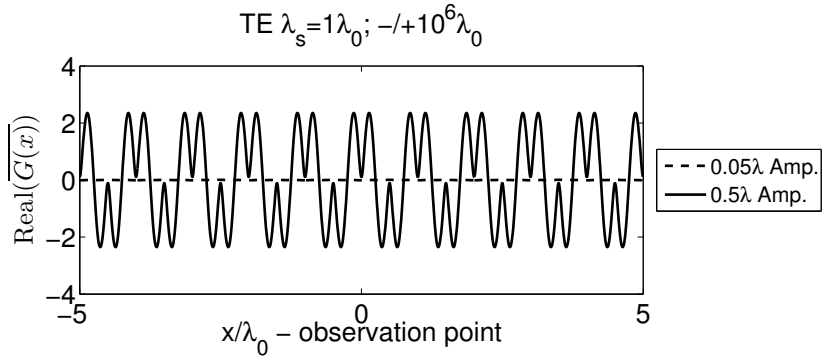


(a) Real TE

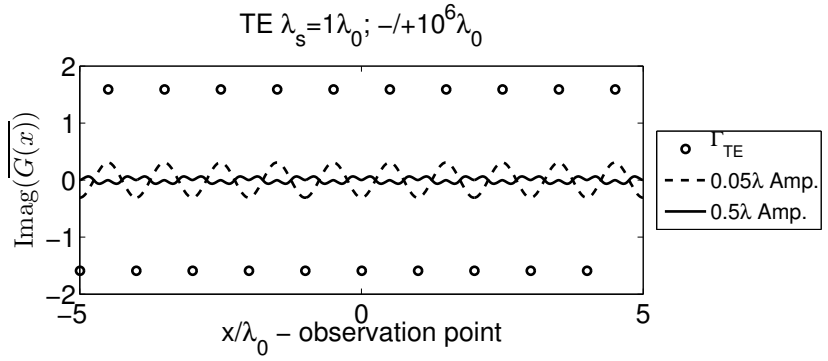


(b) Imag TE

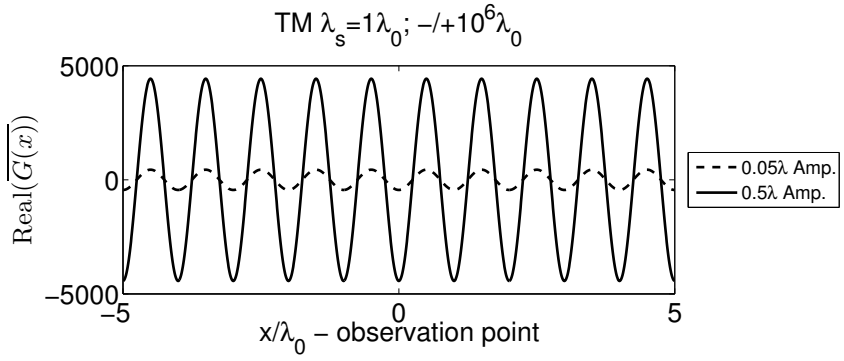


(c) Real TM

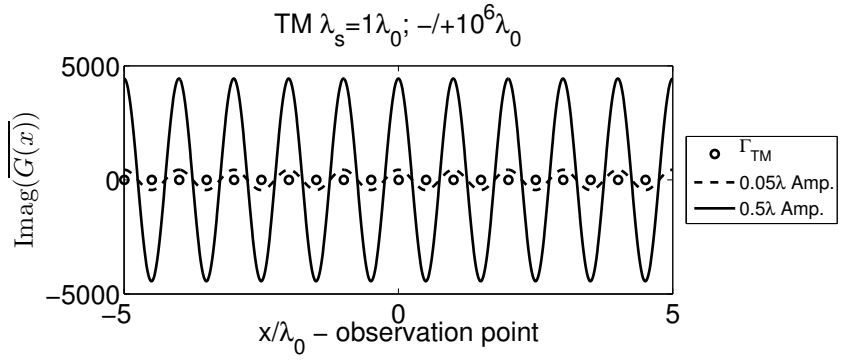


(d) Imag TM

Figure 4.40: Comparison of $\overline{G}$ and $\overline{\Gamma}$ for $\frac{\lambda_s}{\lambda_0} = 1$

It is important to note that the Empiric formula singularity is different from that of the true Green function Integral singularities at $\frac{\lambda_s}{\lambda_0}$ =2 or 1, instead being placed at $\frac{\lambda_s}{\lambda_0} = 0$. Despite this, excellent agreement was found for surface wavelengths from 5 to $108\lambda_0$. This trend is expected to continue for larger values of $\frac{\lambda_s}{\lambda_0}$ but fail for smaller values as there is a singularity at 2 and 1 for TE and TM respectively. By examining the relative peak amplitudes of $\overline{G}$ and the empiric formula, a large deviation from this empiric formula was found for $0.5\lambda_0$ amplitude surfaces for values of 2.5 to 4.5 in 0.5 $\frac{\lambda_s}{\lambda_0}$ spacings with errors increasing from 19.5% to 69.8% as $\frac{\lambda_s}{\lambda_0}$ decreases to 2.5 as shown in Figures 4.41 and 4.42. Lowering the surface amplitude by an order of magnitude to $0.05\lambda_0$ causes the errors to decrease to 2.6% and 10.4% as $\frac{\lambda_s}{\lambda_0}$ decreases from 4.6 to 2.5 ( Figures 4.43 and 4.44).

### 4.4.3 Finite Support

As discussed in Section 3.3.4, the Single Scatter Subtraction ($S^3$) method does not require the infinite integral of the green function kernel for the 2D MFIE on a PEC surface when used with a beam illumination, instead only a finite region of integration is required:

$$\overline{\overline{G}}(x,\alpha) = \int_{-\alpha}^{\alpha} G(x,x')\,dx' \tag{4.4.2}$$

Where $G(x,x')$ is the appropriate derivative of the green function for TE or TM polarization projected onto the z=0 plane. Since the integral is over a finite domain, the singularities from the surface oscillation exactly canceling the Hankel function oscillation should no longer exist. In these cases we are integrating $\int \frac{1}{\sqrt{x}} dx \propto \sqrt{x}$ which with finite intervals is finite. Further, integration supports of over a million wavelengths are not required for numerical convergence. Unfortunately, the real component is not negligible here so some extension to the empiric formula (Eq. 4.4.1) of the infinite case must be found.

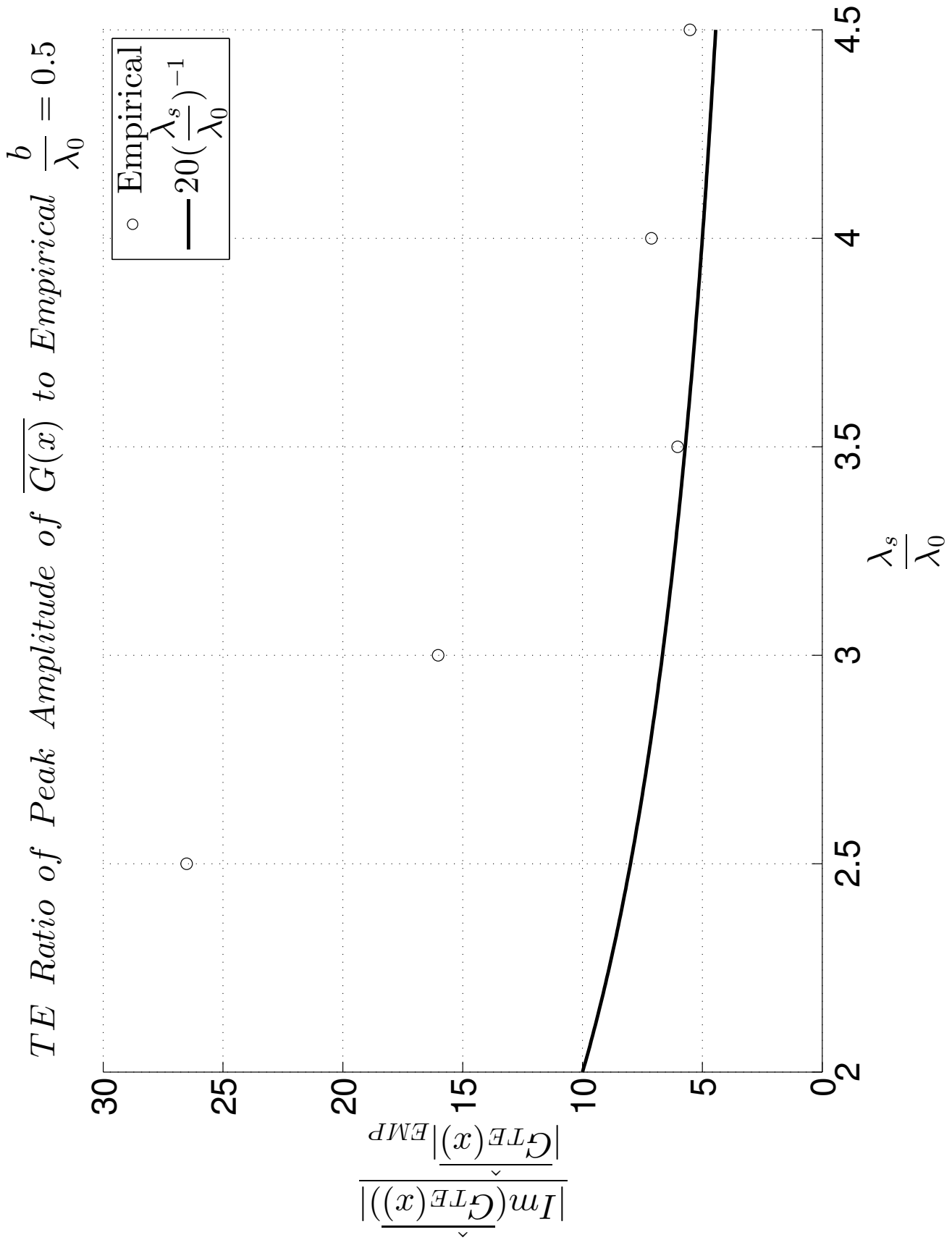


Figure 4.41: TE Peak Amplitude Ratio $\frac{b}{\lambda_0} = 0.5$

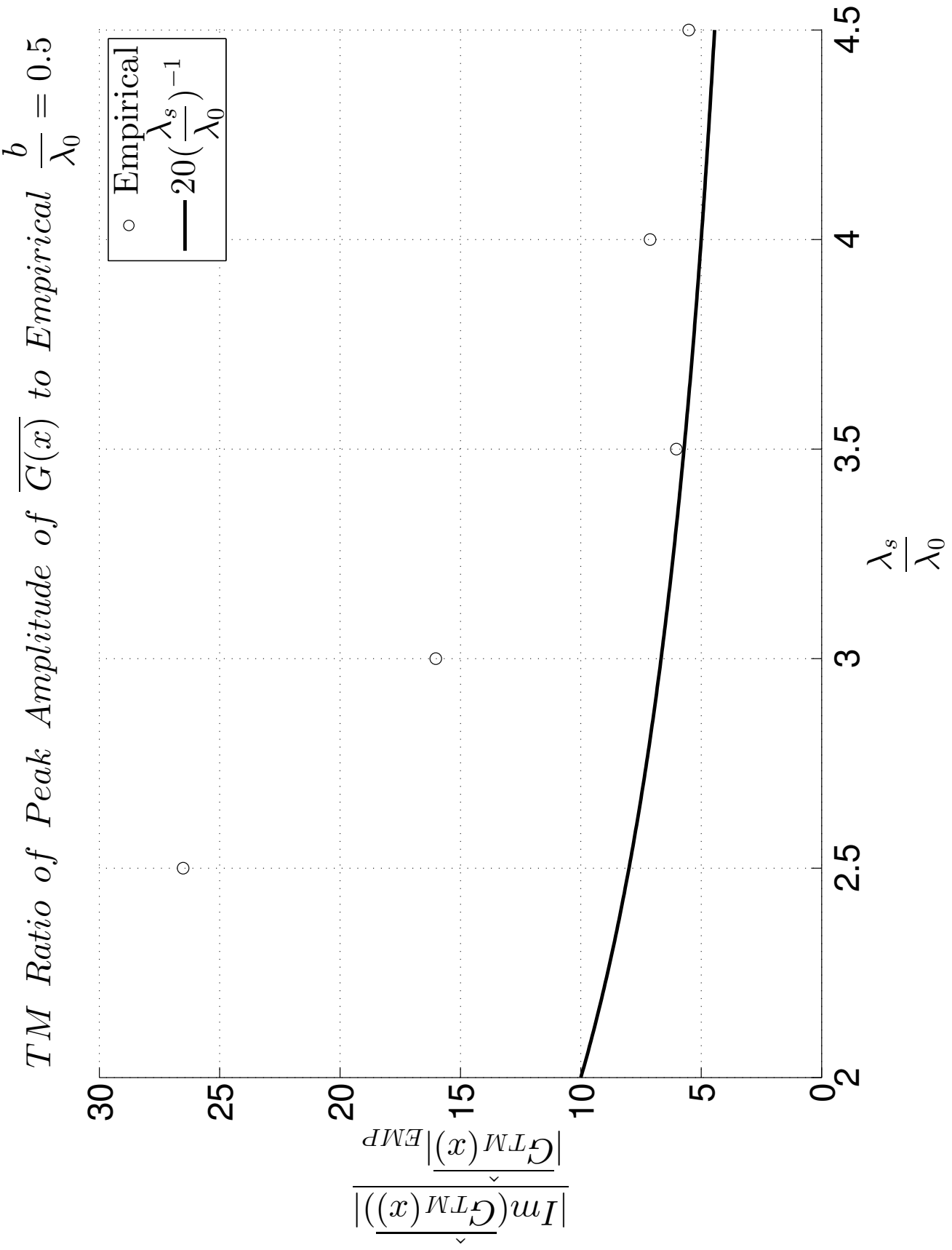


Figure 4.42: TM Peak Amplitude Ratio $\frac{b}{\lambda_0} = 0.5$

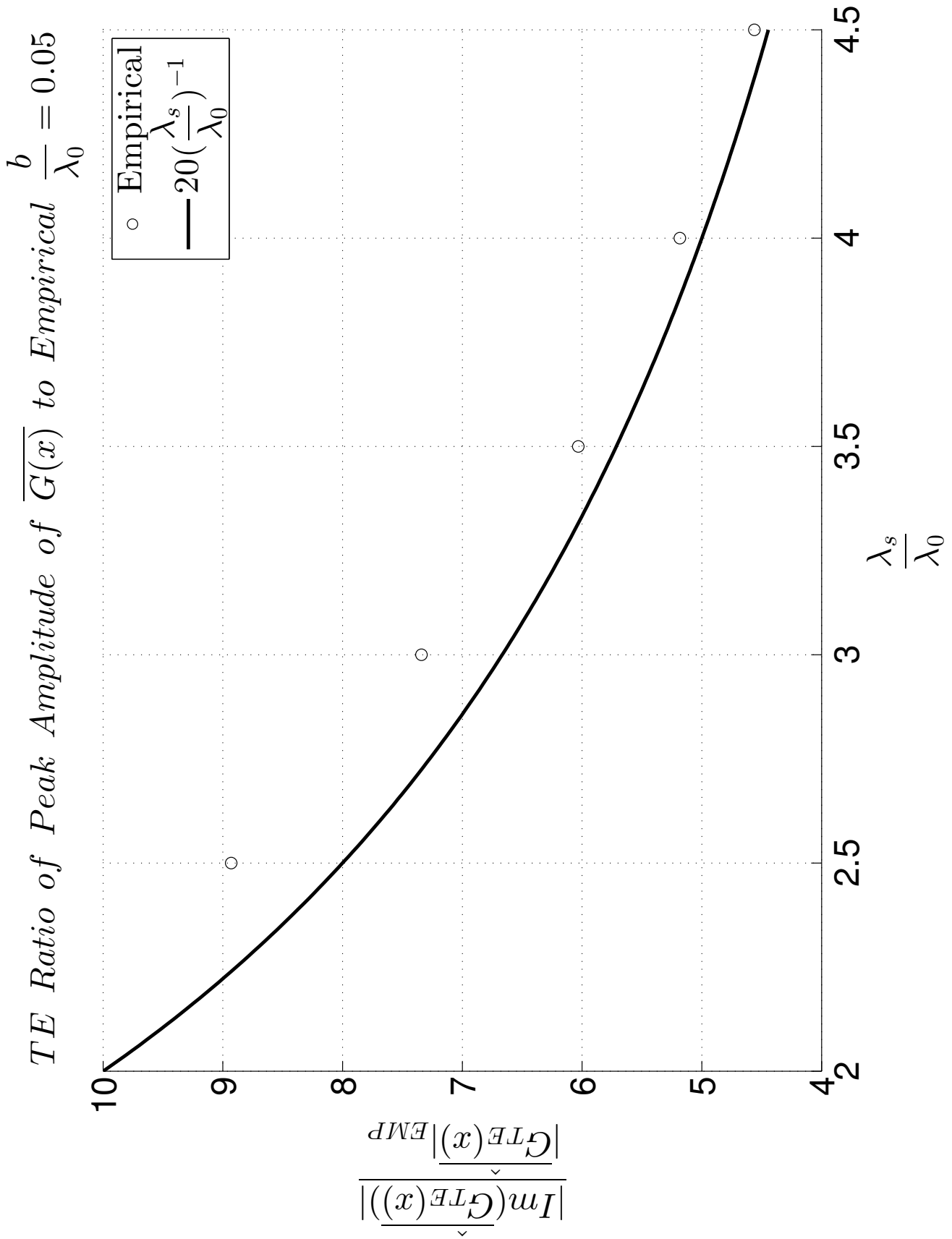


Figure 4.43: TE Peak Amplitude Ratio $\frac{b}{\lambda_0} = 0.05$

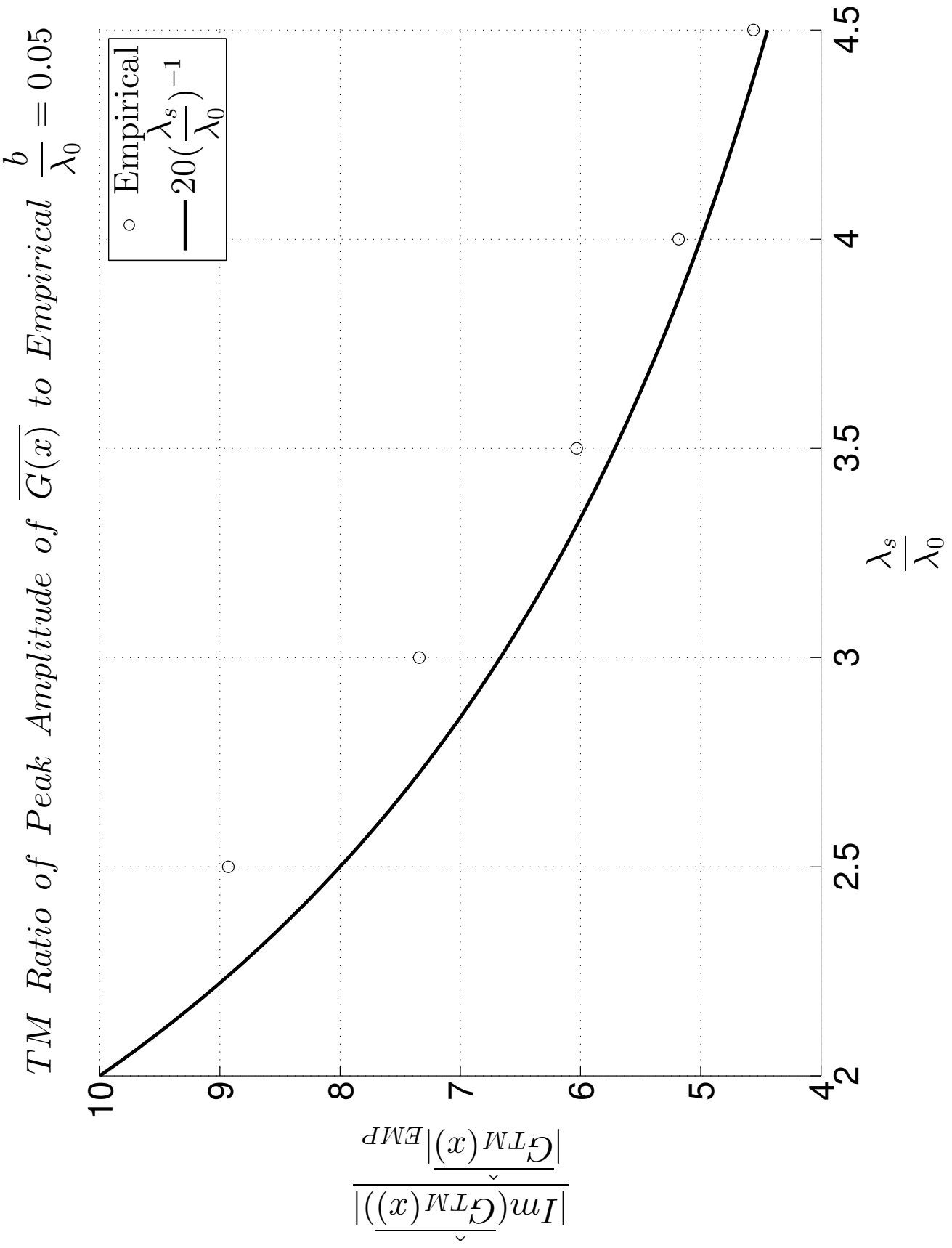


Figure 4.44: TM Peak Amplitude Ratio $\frac{b}{\lambda_0} = 0.05$

In this section a series of such extensions are presented. First, large argument approximations are used to analytically derive expressions describing the upper and lower tails of the kernel integral for both polarizations. Then in an attempt to fill the gap between these tail integrals, a small argument approximation based on Struve functions is derived for TM but in a parallel to the gap between the Kirchhoff and perturbation theories, unfortunately is found to have bounds of validity too short to meet the integral tails. In an attempt to overcome this deficiency, a higher order approximation to the integral tails is derived. This approximation has a single remaining infinite sum that could not be found in closed form. Then a purely empiric formula is presented for TE. Finally, by combining an approximate form of the analytic tail integrals with the infinite support integral empiric formula, an empiric analytic formula is found to have excellent agreement with numeric results, extending even beyond the range of the infinite empiric formula.

Figure 4.45 demonstrates the use of the analytic formulas discussed below. With them it is possible to confirm the accuracy of long numeric results, reduce numeric computation to some small fixed region for all integration supports required as well as extend numeric results to an infinite integration support. In this figure, the dashed line represents the analytic portion of integral approximated in the integral tails formulas below.

#### 4.4.3.1 TE Integration Tails

By splitting Equation 4.4.2 at some point above and below the observation point, where the Hankel function may be approximated to first order and the difference in surface heights is small compared to the separation of source and observation points, an analytic approximation to the integral may be made:

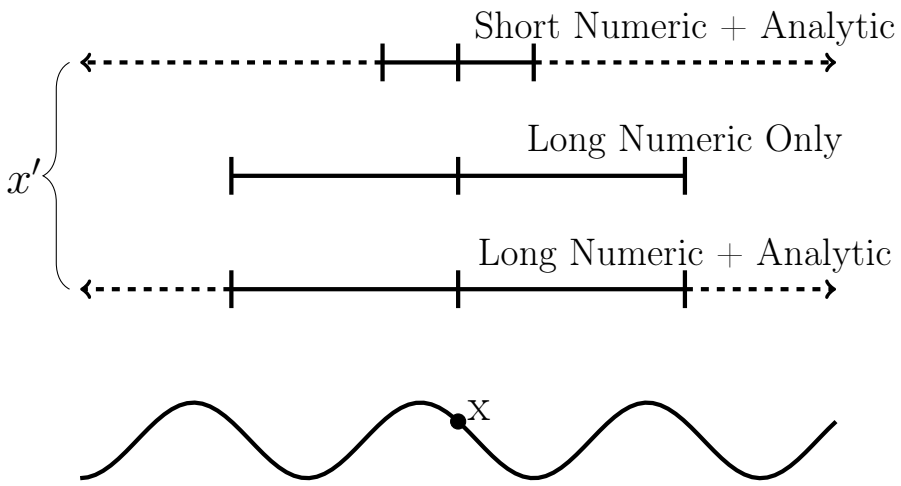


Figure 4.45: Combinations of Numeric and Analytic Computations

$$\overline{\overline{G}}(x,\alpha) = \int_{-\alpha}^{c} G(x,x')\,dx' + \int_{c}^{d} G(x,x')\,dx' + \int_{d}^{\alpha} G(x,x')\,dx' \tag{4.4.3}$$

with $-\alpha < c < x < d < \alpha$. Define

$$A^{FF_{te}}(x,\alpha,c,d) = \int_{-\alpha}^{c} G(x,x')\,dx' + \int_{d}^{\alpha} G(x,x')\,dx'$$

First split this into the upper and lower tail integrals:

$$A^{FF_{te}}(x,\alpha,c,d) = A_l^{FF_{te}}(x,\alpha,c) + A_u^{FF_{te}}(x,\alpha,d)$$

$$A_l^{FF_{te}}(x,\alpha,c) = \frac{\zeta_x(x)\sqrt{k_0}}{j\sqrt{1+\zeta_x^2(x)}} e^{j\frac{3\pi}{4}} \int_{x-c}^{x-\alpha} \left(1 + \frac{1}{2}\zeta_{\Delta x}^2(x-\Delta x)\right) \sqrt{\frac{1}{2\pi\Delta x}} \exp(-jk_0\Delta x)\,d\Delta x \tag{4.4.4}$$

$$A_u^{FF_{te}}(x,\alpha,d) = \frac{-\zeta_x(x)\sqrt{k_0}}{j\sqrt{1+\zeta_x^2(x)}} e^{j\frac{3\pi}{4}} \int_{d-x}^{\alpha-x} \left(1+\frac{1}{2}\zeta_{\Delta x}^2(x+\Delta x')\right) \sqrt{\frac{1}{2\pi\Delta x'}} \exp(-jk_0\Delta x')\, d\Delta x' \tag{4.4.5}$$

In these equations, the first-order large-argument approximation of the Hankel function and the first-order small-slope approximation have been made.

These integrals can both be split into two on the sum, giving a unity term and a squared slope term. Then by variable substitutions and simplifications the total tail integrals can be written as:

$$\begin{aligned} A^{TE_{ff}}(x,\alpha,c,d) = \frac{\zeta_x(x)(-1+j)}{j\sqrt{1+\zeta_x^2}\sqrt{2}} \Bigg\{ \left(1+\frac{b^2k_s^2}{4}\right) [\{F(r_{\alpha l}k_0) - F(r_c k_0)\} - \{F(r_{\alpha u}k_0) - F(r_d k_0)\}] \\ + \frac{b^2k_s^2}{8} \Bigg[ \exp(j2k_s x) \left( \frac{\{F(r_{\alpha u}k_-) - F(r_d k_-)\}}{\sqrt{(1-2K_s)}} - \frac{\{F(r_{\alpha l}k_+) - F(r_c k_+)\}}{\sqrt{(1+2K_s)}} \right) \\ + \exp(-j2k_s x) \left( \frac{\{F(r_{\alpha u}k_+) - F(r_d k_+)\}}{\sqrt{(1+2K_s)}} - \frac{\{F(r_{\alpha l}k_-) - F(r_c k_-)\}}{\sqrt{(1-2K_s)}} \right) \Bigg] \Bigg\} \end{aligned} \tag{4.4.6}$$

With $r_{\alpha u} = (\alpha - x)$ , $r_{\alpha l} = (x + \alpha)$ , $r_d = (d - x)$ , $r_c = (x - c)$ , $k_+ = (k_0 + 2k_s)$ and $k_- = (k_0 - 2k_s)$. $F(x) = C(x) + jS(x)$ is the Fresnel function [1]. A detailed derivation is given in Appendix A.1.

#### 4.4.3.2 TM Integration Tails

As with the TE integral, by splitting Equation 4.4.2 at some point above and below the observation point, where the Hankel function may be approximated to first order and the difference in surface heights is small compared to the separation of source and observation

points, an analytic approximation to the integral may be made:

$$\overline{\overline{G}}(x,\alpha) = \int_{-\alpha}^{c} G(x,x')\,dx' + \int_{c}^{d} G(x,x')\,dx' + \int_{d}^{\alpha} G(x,x')\,dx'$$

with $-\alpha < c < x < d < \alpha$. Since the $\sqrt{1+\zeta_x^2(x')}$ term from TE is not present, the resulting expression will be much simpler.

Define

$$A^{FF_{tm}}(x,\alpha,c,d) = \int_{-\alpha}^{c} G(x,x')\,dx' + \int_{d}^{\alpha} G(x,x')\,dx'$$

And identifying the upper and lower tail integrals:

$$A^{FF_{tm}}(x,\alpha,c,d) = A_l^{FF_{tm}}(x,\alpha,c) + A_u^{FF_{tm}}(x,\alpha,d) \tag{4.4.7}$$

It can be shown that

$$A_l^{FF_{tm}}(x,\alpha,c) = -\frac{bk_s}{2}\frac{(-1+j)}{\sqrt{2}}\left\{\frac{e^{jk_sx}}{\sqrt{1+K_s}}\left[F\left((k_0+k_s)(x+\alpha)\right) - F\left((k_0+k_s)(x-c)\right)\right]\right.$$
$$\left. -\frac{e^{-jk_sx}}{\sqrt{1-K_s}}\left[F\left((k_0-k_s)(x+\alpha)\right) - F\left((k_0-k_s)(x-c)\right)\right]\right\} \tag{4.4.8}$$

and

$$A_u^{FF_{tm}}(x,\alpha,d) = \frac{bk_s}{2}\frac{(-1+j)}{\sqrt{2}}\left\{\frac{e^{jk_sx}}{\sqrt{(1-K_s)}}\left[F\left((k_0-k_s)(\alpha-x)\right) - F\left((k_0-k_s)(d-x)\right)\right]\right.$$
$$\left. -\frac{e^{-jk_sx}}{\sqrt{(1+K_s)}}\left[F\left((k_0+k_s)(\alpha-x)\right) - F\left((k_0+k_s)(d-x)\right)\right]\right\} \tag{4.4.9}$$

Where $F(x) = C(x) + jS(x)$ is the Fresnel function [1]. A detailed derivation of this equation is given in Appendix A.2. While for both TM and TE equal outer limits were used, the results are easily generalizable to arbitrary limits. Additionally, an analytic formula for the integral tails of Eq. 3.3.3 can be found by letting $\alpha \to \infty$ in Eq. 4.4.6 for TE polarization and Eq. 4.4.7 for TM. This causes all Fresnel functions which contain $\alpha$ in the argument to go to $\frac{1}{2}(1-j)$ while everything else stays the same. Examples of different inner integration limits for this case with infinite outer limits are shown in Figures 4.46 and 4.47 for TE and TM respectively.

#### 4.4.3.3 TM Small Argument Integral Single/Spectral Surface

While analytic forms were derived above for $|x - x'|$ very large, and empiric formulas were found for the infinite support case and one for the TE finite case, it would be beneficial to have an analytic form for the intermediate case of $|x - x'|$ to either combine with the integral tails ($|x - x'|$ large) formulas found above or use alone with a small to medium beamwidth.

For TM polarization, an approximation to the kernel integral in this region is:

$$A^{NF_{tm}}(x) = -j\frac{\left(\frac{\zeta_{xx}(x)}{2k_0}\right)}{D(x)^{\frac{3}{2}}}\frac{\pi}{4}\Big\{y_1 H_1^{(2)}(y_1) H_0(y_1) - y_1 H_0^{(2)}(y_1) H_1(y_1) + y_2 H_1^{(2)}(y_2) H_0(y_2) - y_2 H_0^{(2)}(y_2) H_1(y_2)\Big\} \quad (4.4.10)$$

with

$$y_1 = k_0 D(x)(x + \beta_1) \quad (4.4.11)$$

$$y_2 = k_0 D(x)(\beta_2 - x) \quad (4.4.12)$$

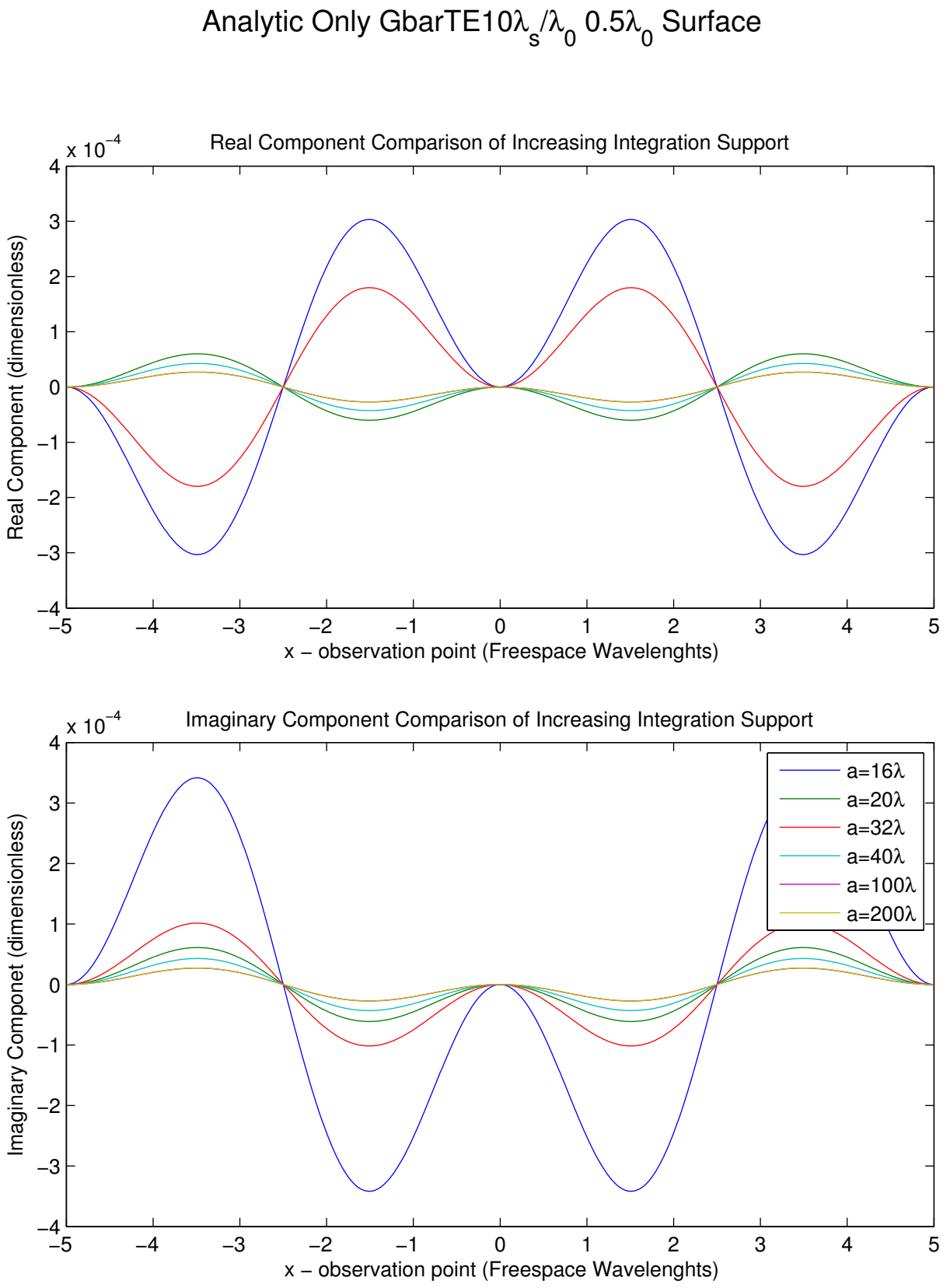


Figure 4.46: Analytic Only Fresnel ApproximationTE Comparison of Integration Support

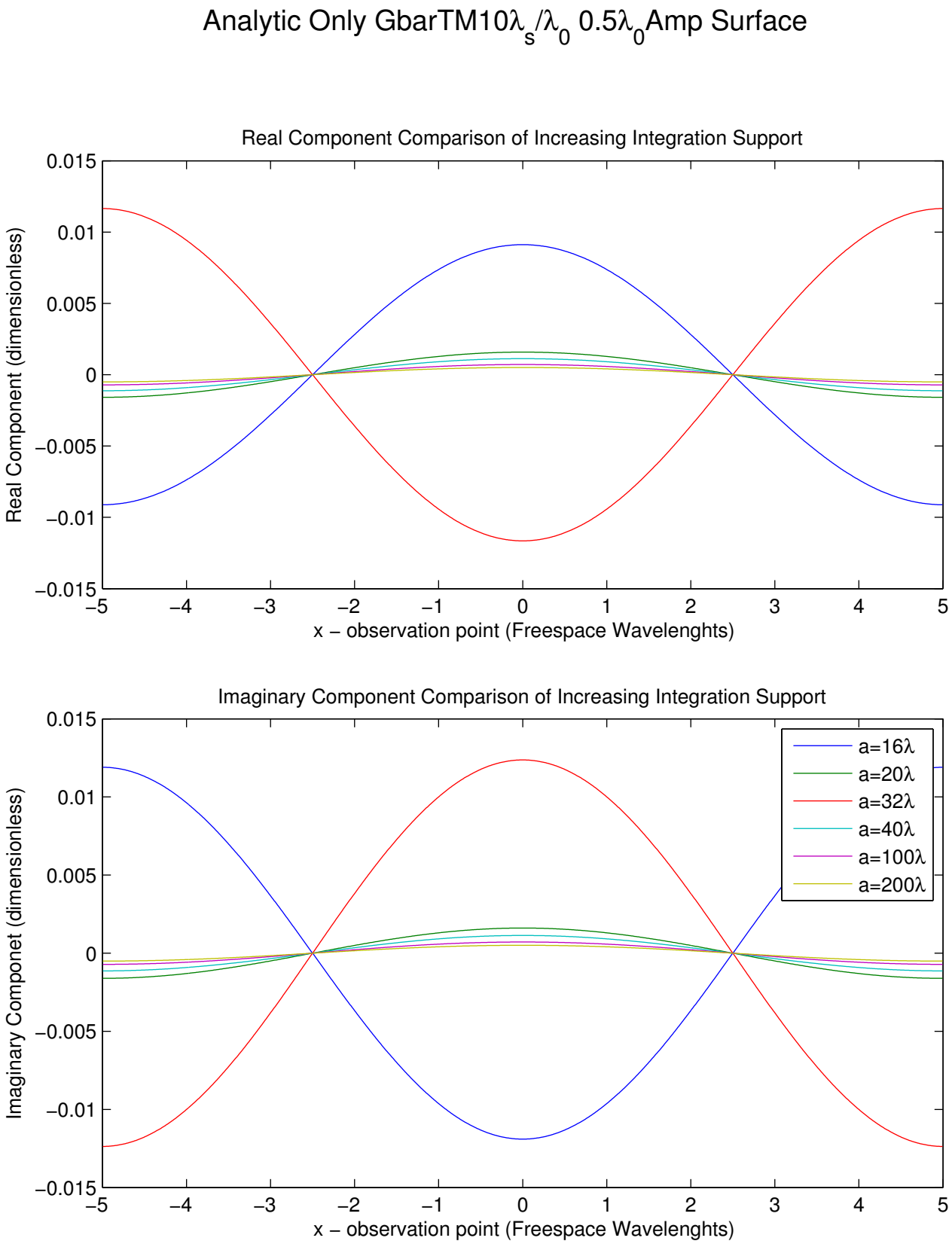


Figure 4.47: Analytic Only Fresnel Approximation TM Comparison of Integration Support

$$D(x) = \sqrt{1 + \zeta_x^2(x)} \tag{4.4.13}$$

and $-\alpha \leq c \leq \beta_1 \leq \beta_2 \leq d \leq \alpha$ so that

$$\overline{\overline{G}}(x) = \int_{-\alpha}^{c} G(x,x')\,dx' + \int_{c}^{\beta_1} G(x,x')\,dx' + \int_{\beta_1}^{\beta_2} G(x,x')\,dx' + \int_{\beta_2}^{d} G(x,x')\,dx' + \int_{d}^{\alpha} G(x,x')\,dx'$$

Where the ideal case would be $\beta_1 = -\alpha$ and $\beta_2 = \alpha$ or $\beta_1 = c$ and $\beta_2 = d$ so that for example with the latter case the kernel integral could be computed by:

$$\begin{aligned}\overline{\overline{G}}(x) &= \int_{-\alpha}^{\beta_1} G(x,x')\,dx' + \int_{\beta_1}^{\beta_2} G(x,x')\,dx' + \int_{\beta_2}^{\alpha} G(x,x')\,dx' \\ &= A^{NF_{pol}}(x) + A^{FF_{pol}}(x)\end{aligned}$$

so that no numerical integration is necessary.

Note that here an explicit general form was kept to allow a possible asymmetry in the integral support of $A^{NF_{pol}}$ to allow this approximation to be used at the edges of the $\overline{\overline{G}}$ integral. This was not necessary for $A^{FF_{pol}}$ as we have elected to center the coordinate axis on the middle of the beamwidth, thus making the required integration support symmetric.

**Bounds on validity** Care must be taken in choosing values of $\beta_1$ and $\beta_2$ so that $A^{NF_{pol}}$ is a good approximation to the integral over these bounds. In deriving the Struve function analytic formula for $\overline{\overline{G}}$, two approximations were taken: an expansion on the surface height was performed where only terms up to the first order were kept and an assumption that the slope was much larger than the curvature times the distance squared. The bound on validity produced by the former is much more restrictive than the latter for the surfaces previously analyzed.

Examining the approximation of the expansion of the surface height on a sinusoidal surfaces

| $\frac{\lvert x'-x\rvert}{\lambda_0}$ | n=1 | 2 | 3 | 4 |
|---|---|---|---|---|
| 2 | 7.9e-2 | 6.2e-2 | 3.2e-2 | 1.3e-2 |
| 3 | 1.2e-1 | 1.4e-1 | 1.1e-1 | 6.4e-2 |
| 4 | 1.6e-1 | 2.5e-1 | 2.6e-1 | 2.0e-1 |

(a) $\frac{\lambda_s}{\lambda_0} = 8$

Table 4.4.1: Term by Term Maximum Value Analysis Struve Based Approximation

gives a series of sinusoidal terms. The terms of this series have maximum value:

$$\frac{b\left[\frac{2\pi}{\lambda_s}\lvert x'-x\rvert\right]^n}{n!}$$

While these terms all vary cos- or sinusoidally, some idea of the error of neglecting the higher order terms may be found by examining the maximum values. Table 4.4.1 shows the maximum possible value for the first four terms, for surface wavelengths $\frac{\lambda_s}{\lambda_0} = 8$ with amplitude $\frac{b}{\lambda_0} = 0.05$ for a range of $\frac{\lvert x'-x\rvert}{\lambda_0}$. From this we see for $\frac{\lambda_s}{\lambda_0} = 8$ the second order term is larger than the first order for both $\frac{\lvert x'-x\rvert}{\lambda_0} = 3$ and 4 so $A^{NF_{pol}}$ should not be expected to perform well for these large values.

From this, a bound on the validity (on neglecting second and higher order terms) can be found by requiring the second order term to be half of the first:

$$\frac{1}{2}\frac{b\left[\frac{2\pi}{\lambda_s}\lvert x'-x\rvert\right]^1}{1!} \geq \frac{b\left[\frac{2\pi}{\lambda_s}\lvert x'-x\rvert\right]^2}{2!}$$

$$\frac{\lambda_s}{\lambda_0} \geq 2\pi\frac{\lvert x'-x\rvert}{\lambda_0} \tag{4.4.14}$$

or as an example for the $\frac{\lambda_s}{\lambda_0} = 20$ surface

$$\frac{\lvert x'-x\rvert}{\lambda_0} \leq 3$$

Which means $\beta_2 - \beta_1 \leq 3$. This bound depends only on the surface wavelength and does not relate to the amplitude. As the amplitude increases, the error may be effected and an alternative bound guided by the second approximation discussed above can be found by examining the peak values of the surface slope and curvature in the approximation for $D(x)$:

$$\frac{|x' - x|}{\lambda_0} \ll 0.0716 \frac{\left(\frac{\lambda_s}{\lambda_0}\right)^2}{\left(\frac{b}{\lambda_0}\right)} \tag{4.4.15}$$

Which relates the maximum integration bounds with both the surface curvature and height. Due to the square, the surface wavelength is still the dominant factor.

Supporting these bounds, Figure 4.48 shows good agreement for a $20\lambda_0$ surface and $\alpha = 2\lambda_0$, while the same surface period has poor agreement in Figure 4.49 for the only slightly larger integration support of $\alpha = 10\lambda_0$. On a $\lambda_s$=$11\lambda_0$ surface, the bound of Equation 4.4.14 is under $\alpha = 2\lambda_0$ supported by Figure 4.50 where significant error is starting to appear. Large error for this same integration support and $\lambda_s = 8\lambda_0$ is shown in Figure 4.51.

Even for the relatively mild surface wavelength of $20\lambda_0$, this approximation fails to reach near the large argument approximation of the integral tails presented in Section 4.4.3.2. Some method must be used to bridge the gap or numerical integration must be used between these two techniques. Due to this short coming, no attempt was made at a similar derivation for TE polarization.

#### 4.4.3.4 TM Higher Order Approximation

**Motivation** As an addition motivation beyond the failure of the Struve-based near region approximation to meet the integral tails region, anomalous behavior as the integration support $\frac{\alpha}{\lambda_0}$ increases is observed in numeric results, with the most pronounced on TM polar-

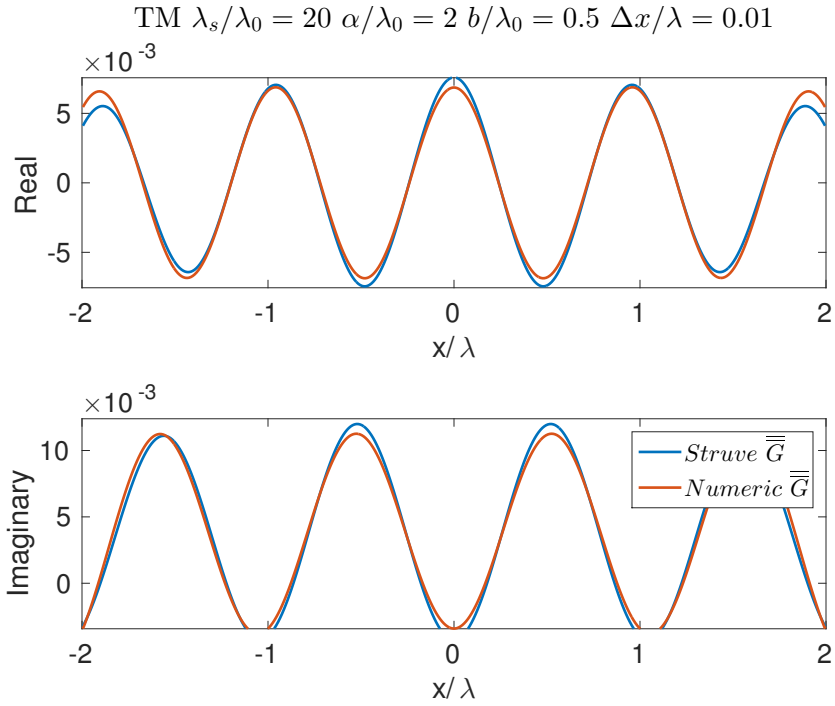


Figure 4.48: Struve Approximation of $\overline{\overline{G}}$ $\frac{\lambda_s}{\lambda_0} = 20$ small support

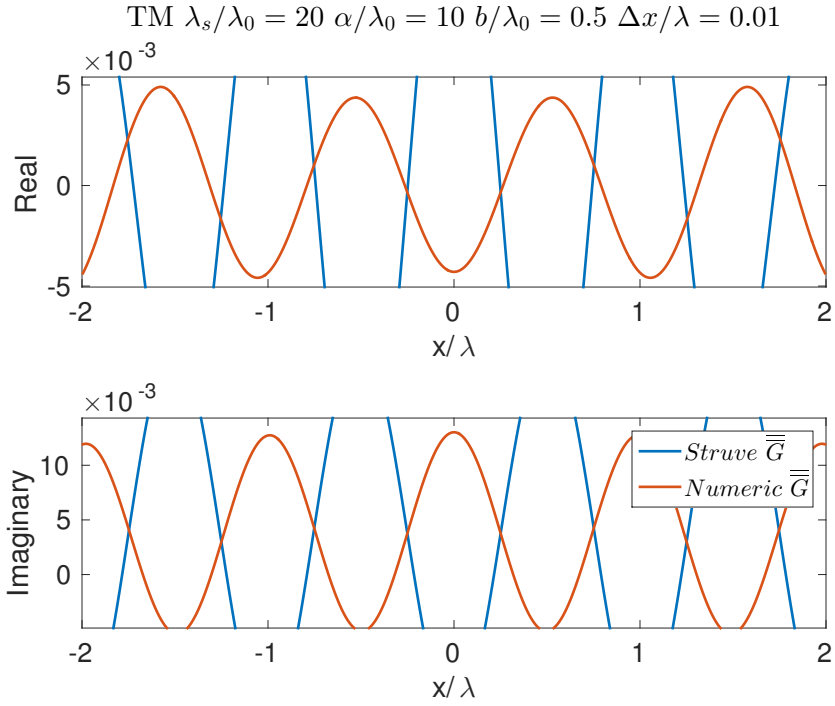


Figure 4.49: Struve Approximation of $\overline{\overline{G}}$ $\frac{\lambda_s}{\lambda_0} = 20$ slightly larger support

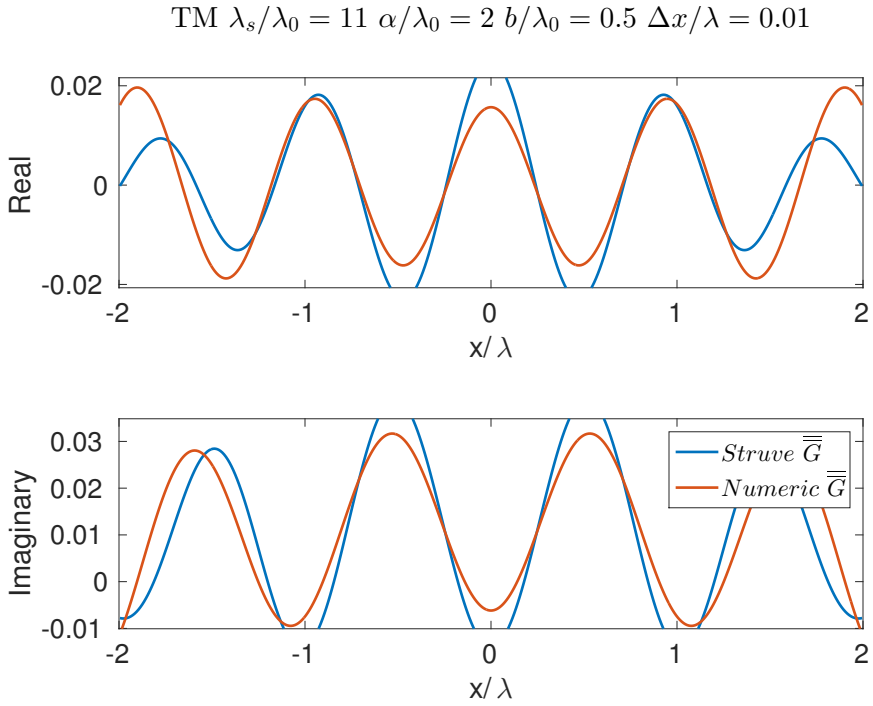


Figure 4.50: Struve Approximation of $\overline{\overline{G}}$ $\frac{\lambda_s}{\lambda_0} = 11$ small support

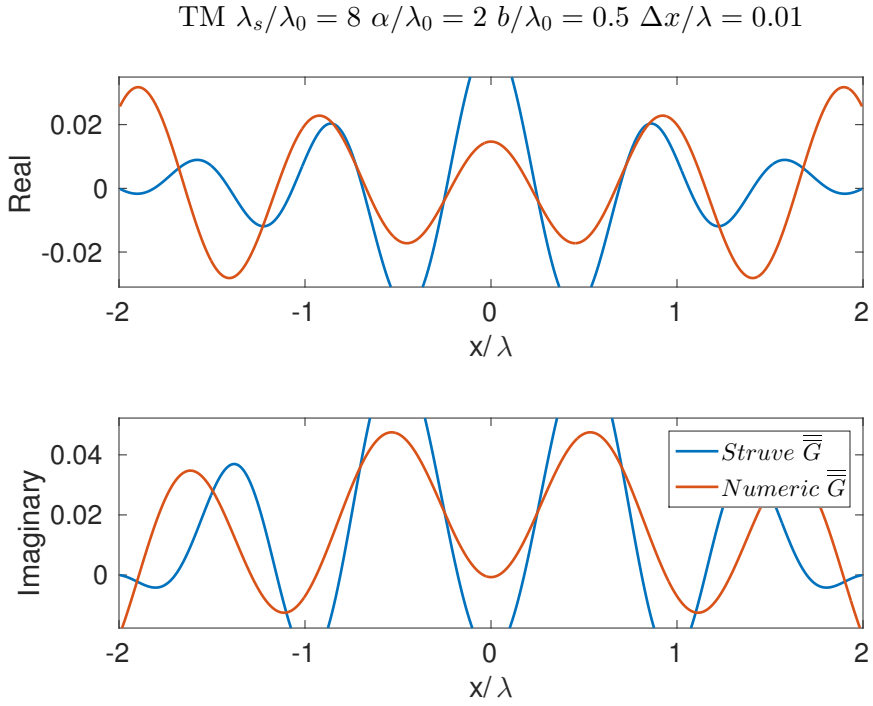


Figure 4.51: Struve Approximation of $\overline{\overline{G}}$ $\frac{\lambda_s}{\lambda_0} = 8$ small support

ization with two main effects. First, the maximum amplitude of $\overline{\overline{G}}_{TM}$ oscillates by increasing as $\frac{\alpha}{\lambda_0}$ was increased from 100 to 101 and to 108 before finally decreasing below the initial value (of $\frac{\alpha}{\lambda_0} = 100$) at 150 where a strictly decaying amplitude was expected. Secondly, there is a 180° phase shift back and forth as the integration support is increased. Neither of these are present for TE polarization, but some subtle phase shifting in the wavelength-order oscillation does appear. The present work hopes to use the Fresnel Function approximations to explain these phenomena as it must be the tail integrations causing this effect since the only parameter varied is the integration support $\alpha$.

The finite $\overline{\overline{G}}(x, \alpha)$ integral was previously split in the following manner to allow the analytical handling of the tail integrations:

$$\begin{aligned}\overline{\overline{G}}(x, \alpha) &= \int_{\alpha}^{\alpha} G(x, x')\, dx' \\ &= \int_{\alpha}^{c} G(x, x')\, dx' + \int_{c}^{d} G(x, x')\, dx' + \int_{d}^{\alpha} G(x, x')\, dx' \\ &= \overline{\overline{G}}(x, \alpha, c, d) + \int_{c}^{d} G(x, x')\, dx'\end{aligned}$$

Where we will be interested in the integrals:

$$\overline{\overline{G}}(x, \alpha, c, d) = \int_{\alpha}^{c} G(x, x')\, dx' + \int_{d}^{\alpha} G(x, x')\, dx' = A_l^{FF_{pol}}(x, \alpha, c) + A_u^{FF_{pol}}(x, \alpha, d)$$

The Fresnel Function Approximation for each polarization will be collected below and the terms which vary with increased integration support highlighted as the function $V_{is}^{POL}$. These terms will then be compared against the anomalous results as a possible explanation.

**TM** For TM polarization the Fresnel function approximation of the tail integrals is given by Equations 4.4.7, 4.4.8 and 4.4.9:

As the integration support is expanded only terms involving $\alpha$ will vary.

$$V_{is}^{TM}(x,\alpha) = \frac{bk_s}{2}\frac{(-1+j)}{\sqrt{2}}\left\{e^{jk_sx}\left[\frac{F\left(\left(k_0-k_s\right)(\alpha-x)\right)}{\sqrt{(1-K_s)}} - \frac{F\left(\left(k_0+k_s\right)(x+\alpha)\right)}{\sqrt{1+K_s}}\right]\right.$$
$$\left. + e^{-jk_sx}\left[\frac{F\left(\left(k_0-k_s\right)(x+\alpha)\right)}{\sqrt{1-K_s}} - \frac{F\left(\left(k_0+k_s\right)(\alpha-x)\right)}{\sqrt{(1+K_s)}}\right]\right\}$$

For simplicity we will examine the observation point $x = 0$, creating a symmetric integration support leading to

$$V_{is}^{TM}(0,\alpha) = bk_s\frac{(-1+j)}{\sqrt{2}}\left\{\frac{F\left(\left(k_0-k_s\right)\alpha\right)}{\sqrt{(1-K_s)}} - \frac{F\left(\left(k_0+k_s\right)\alpha\right)}{\sqrt{1+K_s}}\right\} \quad (4.4.16)$$

In the results presented below, a symmetric integration support (about $x = 0$) is plotted for Equation 4.4.16 for increasing $\frac{\alpha}{\lambda_0}$. Note that $\frac{-j\zeta_{xx}}{2k_0} \times \frac{1}{2}$ has been biased as guided from the empiric formula for the infinite case with additional scaling[5] to account for the finite truncation in order bring the imaginary component to the proper amplitude to match the numeric. Figure 4.52 show that the Fresnel function does explain the oscillation in amplitude observed on TM for a range of integration supports, but begins to have increasing error as the support is increased from $\frac{\alpha}{\lambda_0} = 106$ to 110. Figure 4.53 shows that this error is oscillatory on the order of the surface wavelength, changing between excellent agreement, then increasing error before returning to excellent agreement. This trend is expected to continue and suggests an improvement is necessary to the approximations of the integral tails.

**TE** For TE polarization the Fresnel function approximation of the tail integrals is given by Equation 4.4.6:

[5] Empirically derived.

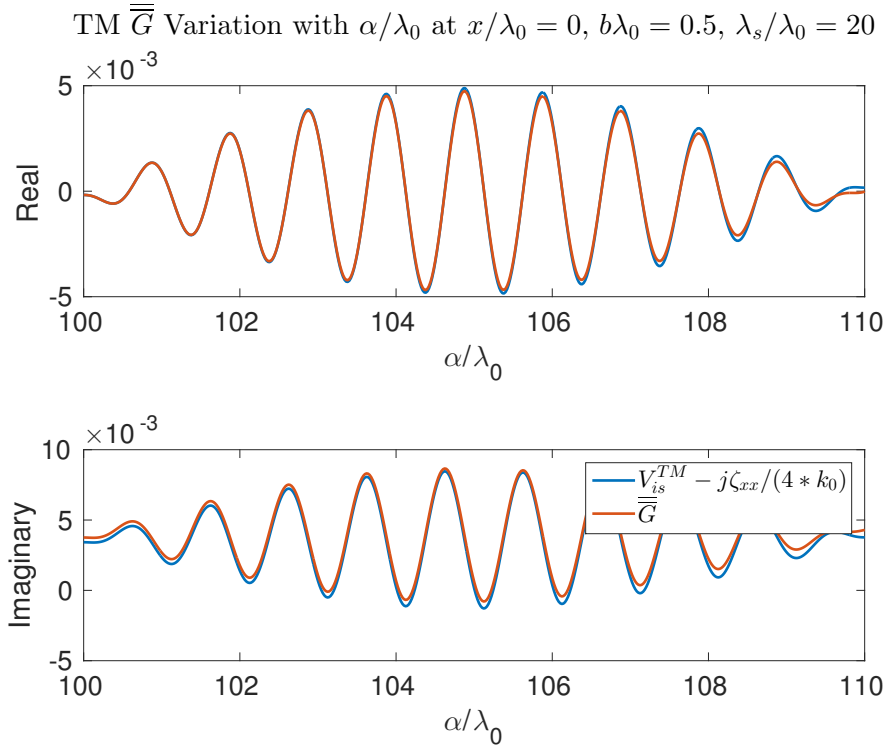


Figure 4.52: TM $\overline{\overline{G}}$ Variation with $\frac{\alpha}{\lambda_0}$ Explained by Fresnel Approximation -$\frac{j\zeta_{xx}}{2k_0}$

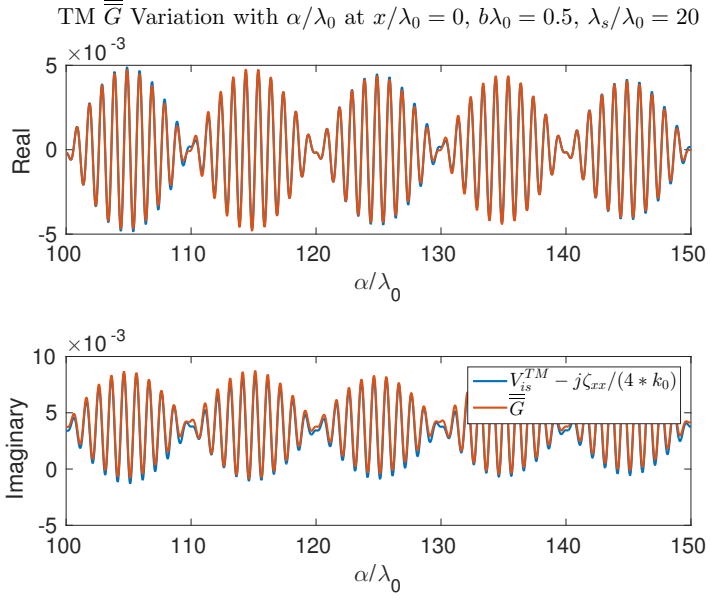


Figure 4.53: TM $\overline{\overline{G}}$ Variation with $\frac{\alpha}{\lambda_0}$ Explained by Fresnel Approximation -$\frac{j\zeta_{xx}}{2k_0}$

As the integration support is expanded only terms involving $\alpha$ will vary.

$$V_{is}^{TE}(x,\alpha) = \frac{\zeta_x(x)(-1+j)}{j\sqrt{1+\zeta_x^2}\sqrt{2}}\left\{\left(1+\frac{b^2k_s^2}{4}\right)\left[F\left(\left(x+\alpha\right)k_0\right)-F\left(\left(\alpha-x\right)k_0\right)\right]\right.$$
$$+\frac{b^2k_s^2}{8}\left[\exp\left(j2k_sx\right)\left(\frac{F\left(\left(\alpha-x\right)\left(k_0-2k_s\right)\right)}{\sqrt{\left(1-2K_s\right)}}-\frac{F\left(\left(x+\alpha\right)\left(k_0+2k_s\right)\right)}{\sqrt{\left(1+2K_s\right)}}\right)\right.$$
$$\left.\left.+\exp\left(-j2k_sx\right)\left(\frac{F\left(\left(\alpha-x\right)\left(k_0+2k_s\right)\right)}{\sqrt{\left(1+2K_s\right)}}-\frac{F\left(\left(x+\alpha\right)\left(k_0-2k_s\right)\right)}{\sqrt{\left(1-2K_s\right)}}\right)\right]\right\} \quad (4.4.17)$$

For simplicity we will once again examine the observation point $x = 0$, giving a symmetric integration support and leading to

$$V_{is}^{TE}(0,\alpha) = 0$$

Which explains why the phase reversal and amplitude modulation is not present for TE. However, $V_{is}^{TE}(x,\alpha)$ can be explored for some x where the small phase shift was observed, although this is not pursued here.

Thus, TM polarization will be chosen first to explore the possibility of a higher-order approximation.

**TM Higher Order Hankel Approximation** As demonstrated above, there is some behavior not explained by the Fresnel function TM integral tail approximation so a more accurate approximation is necessary. Since results for TE polarization appear well-behaved, Eq. 4.4.6 is sufficient. There are three approximations taken in the derivation that may be improved, the small height $\frac{\Delta\zeta}{\Delta x} \ll 1$, the small slope $\zeta_x^2 \ll 1$ and the Hankel function approximation which has terms that goes as $\Delta x^{-\frac{n}{2}}$. Since the surfaces thus far analyzed have had $\frac{b}{\lambda_0} \ll 1$ and $\frac{k_s}{k_0} > 1$, even for moderate $\Delta x$, both the height and slope approximations

will be better than that of the Hankel function. Appendix A.4 gives a derivation of the analytic tail integration using an arbitrary order Hankel function approximation, as well as a form in which most of the infinite sum has been calculated analytically and given below:

$$A_l^{FF_{tm}^h}(x,\alpha,c) = -\frac{bk_s}{2}e^{j\frac{3\pi}{4}}\left(F_l+E_l+G_l\right) \quad (4.4.18)$$

with

$$F_l=\sqrt{2}\left[\frac{e^{jk_sx}}{\sqrt{1+K_s}}\frac{(2+K_s)}{\sqrt{3+K_s}}\left[F\left(k_+r_\alpha\right)-F\left(k_+r_c\right)\right]-\frac{e^{-jk_sx}}{\sqrt{(1-K_s)}}\frac{(2-K_s)}{\sqrt{3-K_s}}\left[F\left(k_-r_\alpha\right)-F\left(k_-r_c\right)\right]\right]$$

$$E_l=\frac{(-1)^{\frac{3}{4}}\sqrt{\pi}}{\sqrt{k_0}\sqrt{(1-K_s^2)}} \left[e^{jk_sx}\left(\operatorname{erf}\left(\sqrt{jk_+r_\alpha}\right)-\operatorname{erf}\left(\sqrt{jk_+r_c}\right)\right)\left(\sqrt{2}K_s+\sqrt{1-K_s}\right) -e^{-jk_sx}\left(\operatorname{erf}\left(\sqrt{jk_-r_\alpha}\right)-\operatorname{erf}\left(\sqrt{jk_-r_C}\right)\right)\left(-\sqrt{2}K_s+\sqrt{1+K_s}\right)\right]$$

$$G_l=\frac{1}{\sqrt{\pi}}\sum_{m=1}^{\infty}\frac{\Gamma\left(m-\frac{1}{2}\right)\left(m+\frac{1}{2}\right)(2m-1)!}{m!\left(2k_0\right)^m2^m}(-1)^m\times \left[\frac{k_+^m}{\sqrt{1+K_s}}\left(\Gamma\left(\frac{1}{2}-m,jk_+r_\alpha\right)-\Gamma\left(\frac{1}{2}-m,jk_+r_c\right)\right) -\frac{k_-^m}{\sqrt{1-K_s}}\left(\Gamma\left(\frac{1}{2}-m,jk_-r_\alpha\right)-\Gamma\left(\frac{1}{2}-m,jk_-r_c\right)\right)\right]$$

and

$$A_u^{FF_{tm}}(x,\alpha,d) = \frac{bk_s}{2} e^{j\frac{3\pi}{4}} (F_u + E_u + G_u) \tag{4.4.19}$$

with

$$F_u = \sqrt{2}\left[\frac{e^{-jk_s x}}{\sqrt{1+K_s}}\frac{(2+K_s)}{\sqrt{3+K_s}}\left[F(k_+ r_{\alpha u}) - F(k_+ r_d)\right] - \frac{e^{jk_s x}}{\sqrt{(1-K_s)}}\frac{(2-K_s)}{\sqrt{3-K_s}}\left[F(k_- r_{\alpha u}) - F(k_- r_d)\right]\right]$$

$$E_u = \frac{(-1)^{\frac{3}{4}}\sqrt{\pi}}{\sqrt{k_0}\sqrt{(1-K_s^2)}} \left[e^{-jk_s x}\left(\operatorname{erf}\left(\sqrt{jk_+ r_{\alpha u}}\right) - \operatorname{erf}\left(\sqrt{jk_+ r_d}\right)\right)\left(\sqrt{2}K_s + \sqrt{1-K_s}\right) - e^{jk_s x}\left(\operatorname{erf}\left(\sqrt{jk_- r_{\alpha u}}\right) - \operatorname{erf}\left(\sqrt{jk_- r_d}\right)\right)\left(-\sqrt{2}K_s + \sqrt{1+K_s}\right)\right]$$

$$G = \frac{(-1)^{\frac{3}{4}}}{\sqrt{\pi}} \sum_{m=1}^{\infty} \frac{\Gamma\left(m-\frac{1}{2}\right)\left(m+\frac{1}{2}\right)(2m-1)!}{m!\,(2k_0)^m\,2^m} (-1)^m \times \left[\frac{e^{-jk_s x}k_+^m}{\sqrt{1+K_s}}\left(\Gamma\left(\frac{1}{2}-m, jk_+ r_{\alpha u}\right) - \Gamma\left(\frac{1}{2}-m, jk_+ r_d\right)\right) - \frac{e^{jk_s x}k_-^m}{\sqrt{1-K_s}}\left(\Gamma\left(\frac{1}{2}-m, jk_- r_{\alpha u}\right) - \Gamma\left(\frac{1}{2}-m, jk_- r_d\right)\right)\right]$$

Although there is a minimum of 24 special function evaluations required for this computation, this approximation may still be a significant improvement over the thousands of evaluations of the Hankel function required by numerical integration.

#### 4.4.3.5 TE Polarization Empiric formula

While a near-region analytic integral, and a higher-order analytic tail integral were derived for TM, both and their combination failed to provide the entire integral and match the numeric results. In contrast, for TE an empiric formula which has good agreement was found:

$$\mathrm{Re}\left\{\overline{\overline{G}}_{te}^{emp}(x)\right\} = \frac{-\zeta_x(x)}{\sqrt{\pi k_0 \alpha}}\sin(k_0 x)$$

$$\mathrm{Im}\left[\overline{\overline{G}}_{te}^{emp}(x)\right] = \mathrm{Re}\left[\overline{\overline{G}}_{te}^{emp}(x)\right] + \frac{1}{k_0}\left(\frac{\zeta_{xx}(x)}{2}\right)$$

Figures 4.54 and 4.55 show good agreement over a bulk of a surface period for a $\frac{\lambda_s}{\lambda_0} = 20$ surface for amplitudes less than an electromagnetic wavelength. Not shown is an enhanced effect at the edges of the integration support not modeled by the empiric formula given above. Though the value of $\overline{\overline{G}}(x)$ becomes large here, the current will be zero in these regions due to the beam illumination so it will have no effect.

It is interesting to examine the physics represented in this equation. Examining more closely the real component:

$$\mathrm{Re}\left\{\overline{\overline{G}}_{te}^{emp}(x)\right\} = \frac{-\zeta_x(x)}{\sqrt{\pi k_0 \alpha}}\sin(k_0 x)$$

The $\sin(k_0 x)$ portion is a standing wave between the two edges of the surface imposed by finite illumination as uncanceled multiple scattering builds up at the edges. It appears the sharp cutoff imposed by finite truncation has been forced upon the smooth roll off of the Green function creating two inward traveling waves, violating the definition of single scattering. This suggests $\mathrm{Re}\left\{\overline{\overline{G}}_{te}^{emp}(x)\right\}$ is an error term from truncation and should be minimized by selecting $\alpha$ large. Work must be performed to determine if this is an artifact

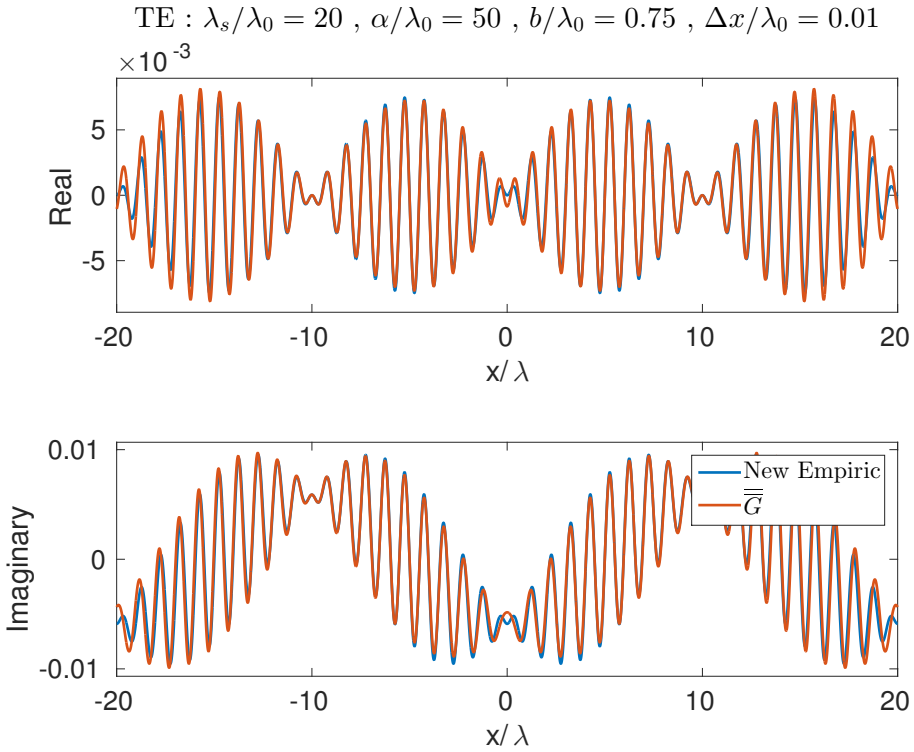


Figure 4.54: Simplified New Empiric $\frac{b}{\lambda_0} = 0.75$

produced by the $S^3$ method, or has larger implications for the understanding of the use of truncated versions of MFIE.

#### 4.4.3.6 Empiric Analytic Formula

**TM** As shown in Section 4.4.3.4, the behavior of the finite $\overline{\overline{G}}$ for TM polarization is more complicated than that for TE. Thus a simple empiric formula directly from simulation results has not been found. Instead a combination empiric and analytic formula is suggested based on the empiric formula of Eq. 4.4.1 and the analytic tail integral approximation of Eqs. 4.4.8 and 4.4.9. A more detailed account of this derivation is given in Appendix B.1.

Begin by noting

$$\int_{-\infty}^{\infty} G\left(x, x'\right) dx' - \int_{-\infty}^{\infty} G\left(x, x'\right) dx' = 0$$

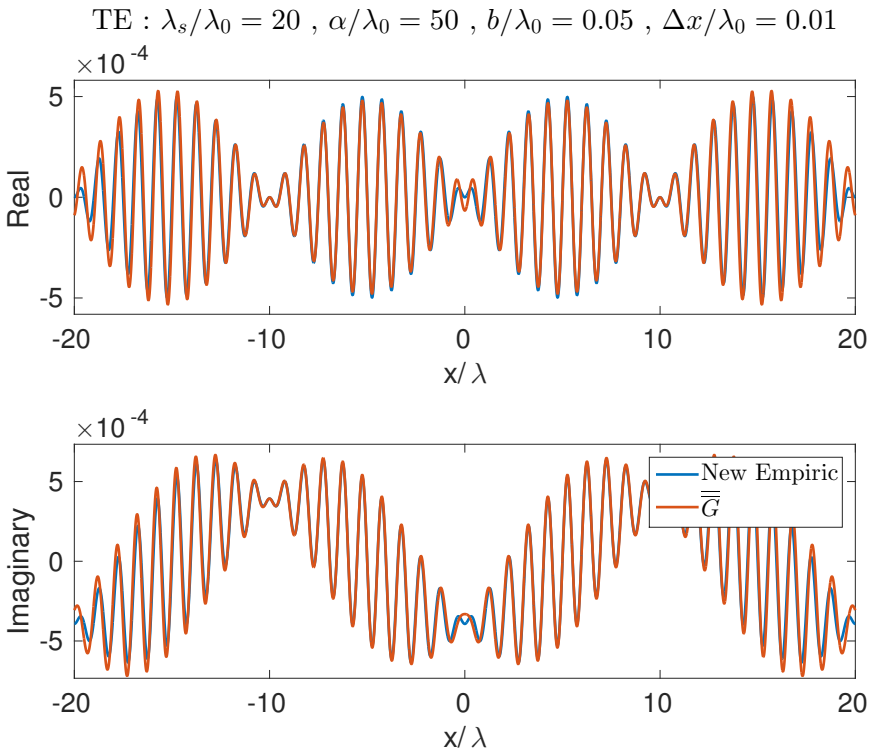


Figure 4.55: Simplified New Empiric $\frac{b}{\lambda_0} = 0.05$

$$\int_{-\infty}^{\infty} G\left(x,x'\right)dx' - \left(\int_{-\infty}^{-\alpha} G\left(x,x'\right)dx' + \int_{-\alpha}^{\alpha} G\left(x,x'\right)dx' + \int_{\alpha}^{\infty} G\left(x,x'\right)dx'\right) = 0$$

Now using the infinite case empiric formula of Equation 4.4.1, this is equivalent to

$$\overline{G}\left(x\right) - \left(\overline{\overline{G}}\left(x\right) + A^{FF_{tm}}\left(x,\infty,-\alpha,\alpha\right)\right) = 0$$

or

$$\overline{\overline{G}}\left(x\right) = \overline{G}\left(x\right) - A^{FF_{tm}}\left(x,\infty,-\alpha,\alpha\right)$$

which with the expressions for $F\left(x\right)|x \to \infty$ and the large argument expression:

$$F\left(x\right) = \frac{1}{2} + \frac{1}{\sqrt{2\pi x}}\sin\left(x\right) - j\left(\frac{1}{2} - \frac{1}{\sqrt{2\pi x}}\cos\left(x\right)\right)$$

Gives after algebraic manipulations:

$$\overline{\overline{G}}(x) = j\frac{\zeta_{xx}(x)}{2k_0} - \frac{bk_s}{2}\frac{(-1+j)}{\sqrt{2}}\left\{2\cos(k_s x)(1-j)\left(\frac{1}{\sqrt{1+K_s}} - \frac{1}{\sqrt{1-K_s}}\right)\right.$$
$$\left. + \frac{je^{-jk_0\alpha}}{(1+K_s^2)\sqrt{(\alpha^2-x^2)}\sqrt{2\pi}}\left[\left(\sqrt{(\alpha-x)}e^{-jk_0x} + \sqrt{(x+\alpha)}e^{jk_0x}\right)\left((1-K_s)e^{-jk_s\alpha} - (1+K_s)e^{jk_s\alpha}\right)\right]\right\}$$

Note the similarity between the first term and the first term in the curly braces. It was found that using both of these terms lead to an over estimation of the imaginary component by exactly a factor or two, so dropping the first term in the curly braces gives the following expression for the finite kernel integral for TM polarization:

$$\overline{\overline{G}}_{TM}(x) = -j\frac{\zeta_{xx}(x)}{2k_0} - \frac{bk_s}{2}\frac{(-1+j)}{\sqrt{2}}\left\{\frac{je^{-jk_0\alpha}}{(1-K_s^2)\sqrt{(\alpha^2-x^2)}\sqrt{2\pi k_0}}\right.$$
$$\left. * \left[\left(\sqrt{(\alpha-x)}e^{-jk_0x} + \sqrt{(x+\alpha)}e^{jk_0x}\right)\left((1-K_s)e^{-jk_s\alpha} - (1+K_s)e^{jk_s\alpha}\right)\right]\right\} \quad (4.4.20)$$

It is important to note that only the first-order integral approximation has been used here, in order to keep the resultant expression as simple as possible. Despite work in section 4.4.3.4 suggesting that the higher-order approximation was necessary to fully describe the behavior of the kernel integral, it will be shown that this relatively simple expression is a powerful approximation, with a range of validity extending very near to the special surface wavelengths of $\frac{\lambda_s}{\lambda_0} = 1$ and 2 which are singular for the infinite support case.

**Range of Validity** Figures 4.56 through 4.57 show the empiric analytic formula for an amplitude of $\frac{b}{\lambda_0} = 0.05$ is valid to surface wavelength $\frac{\lambda_s}{\lambda_0} \geq 2$ while Figures 4.58 through

4.70 show $\frac{b}{\lambda_0} = 0.1$ is for $\frac{\lambda_s}{\lambda_0} \geq 3$. Good agreement for $\frac{b}{\lambda_0} = 0.5$ and 1.0 is found down to $\frac{\lambda_s}{\lambda_0} \geq 5$ and $\frac{\lambda_s}{\lambda_0} \geq 7$ respectively as shown in the Figures 4.71 through4.85. Figures 4.59, 4.62, 4.67 and 4.78 show the difference between the numeric and empiric analytic formula with a worst-case error of 10%.

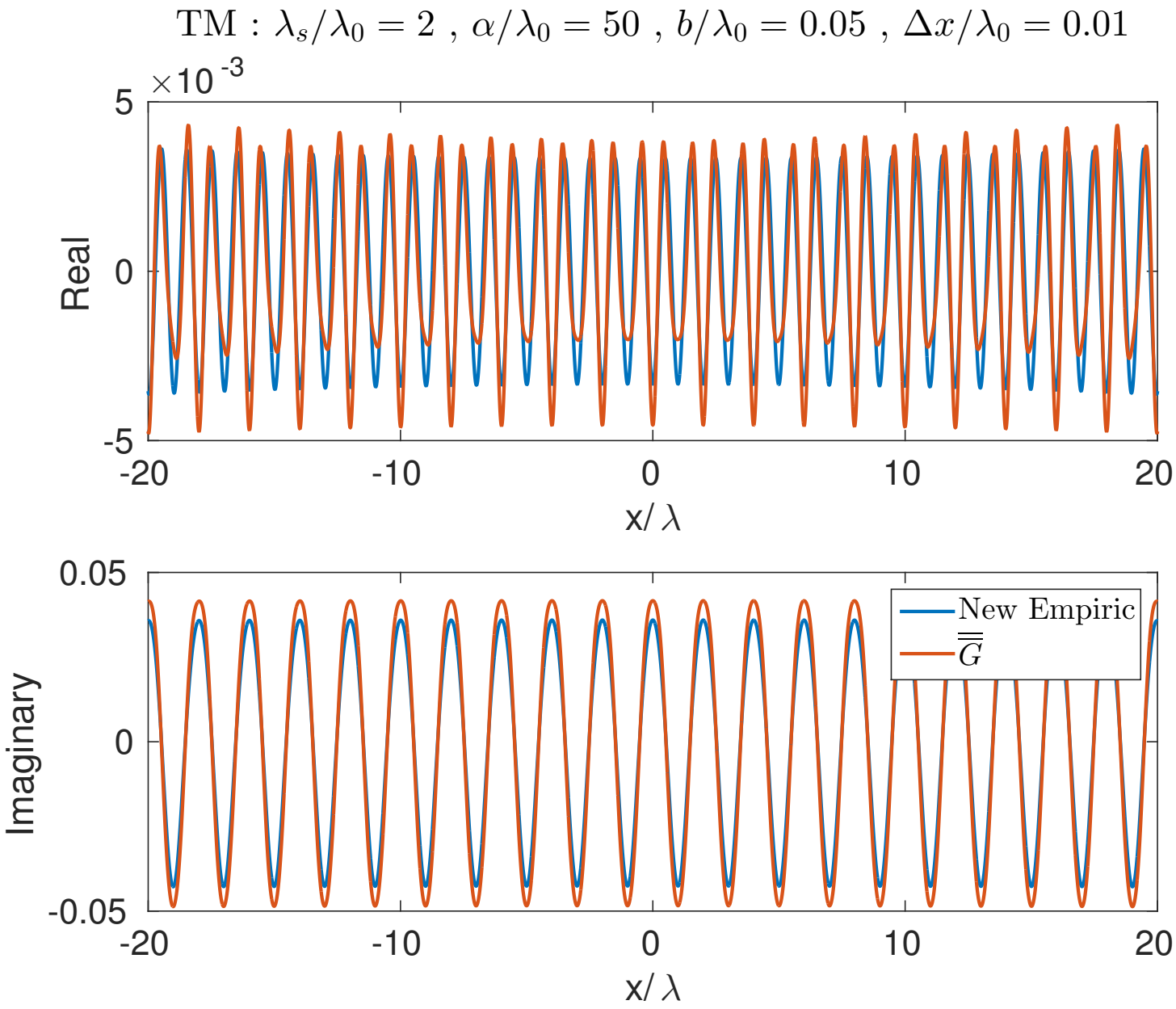


Figure 4.56: TM Empiric Analytic

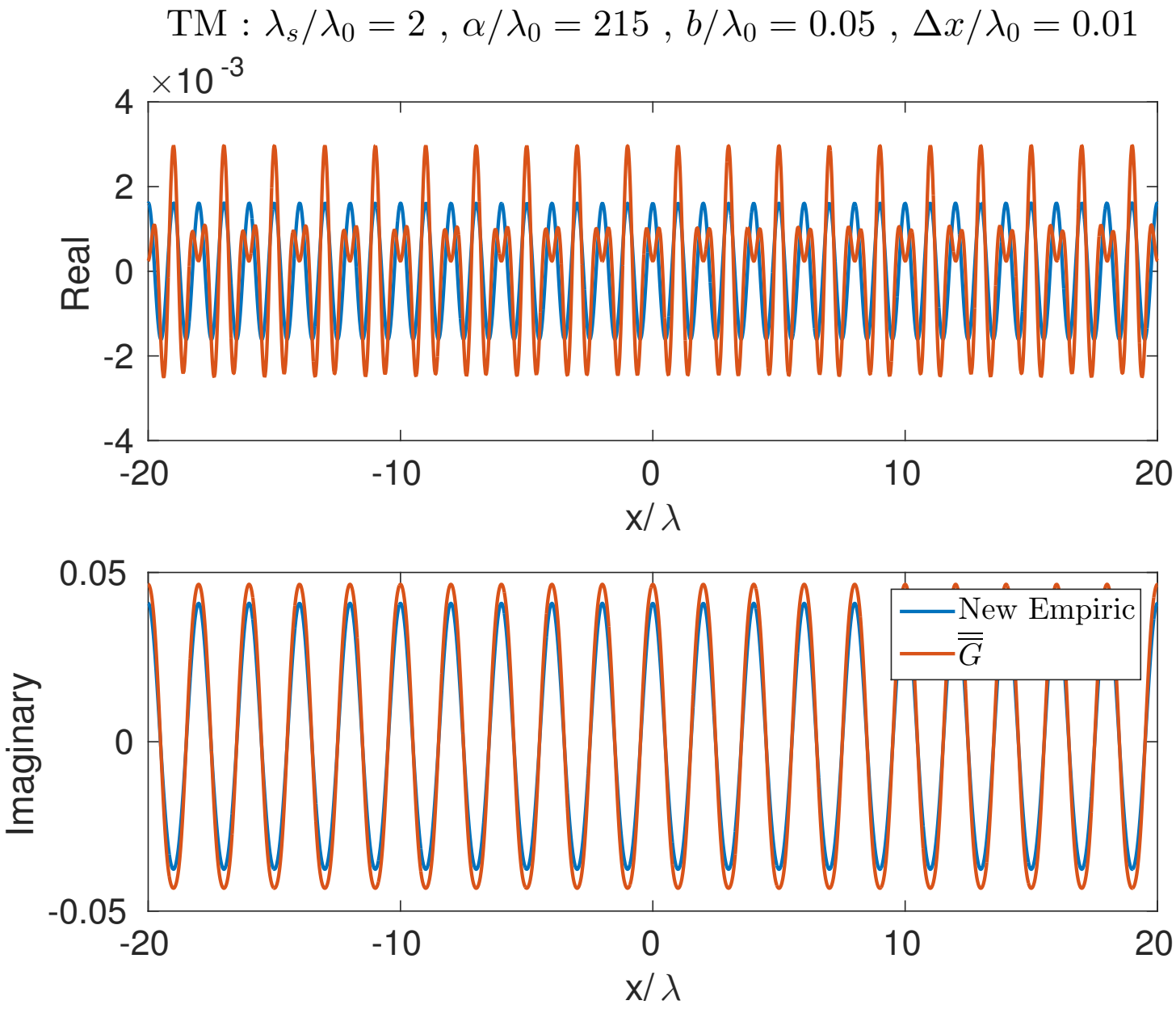


Figure 4.57: TM Empiric Analytic

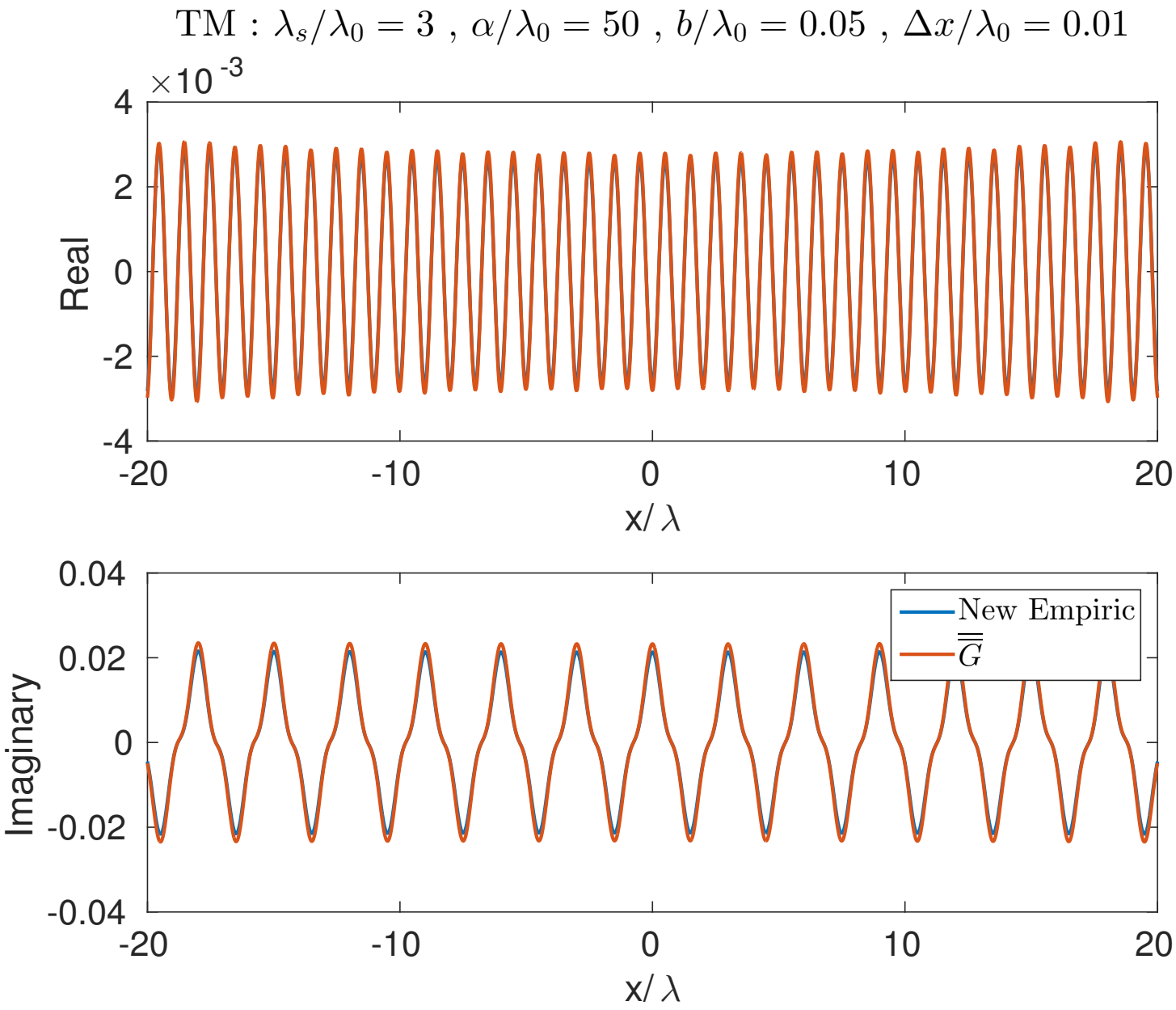


Figure 4.58: TM Empiric Analytic

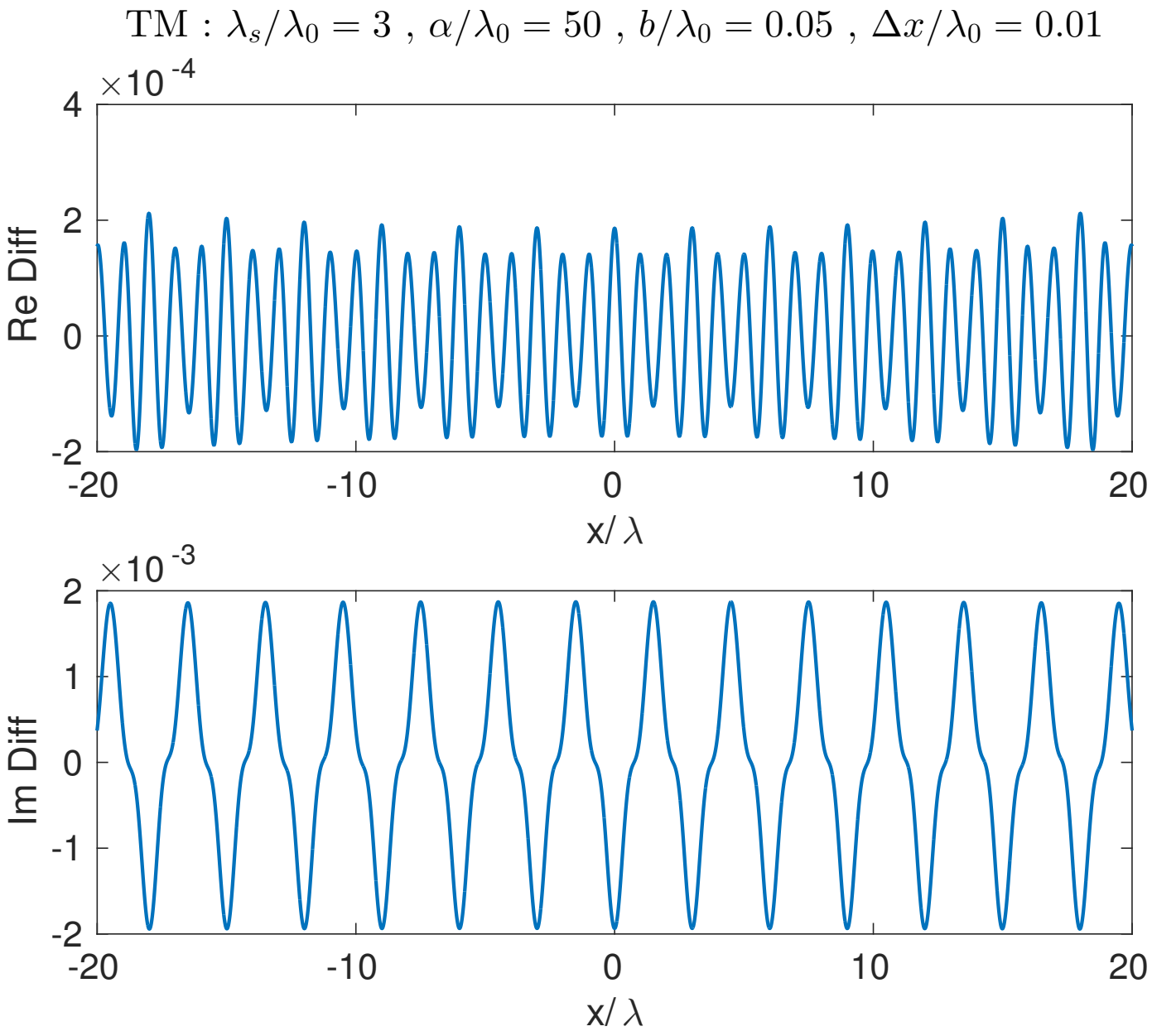


Figure 4.59: TM Empiric Analytic

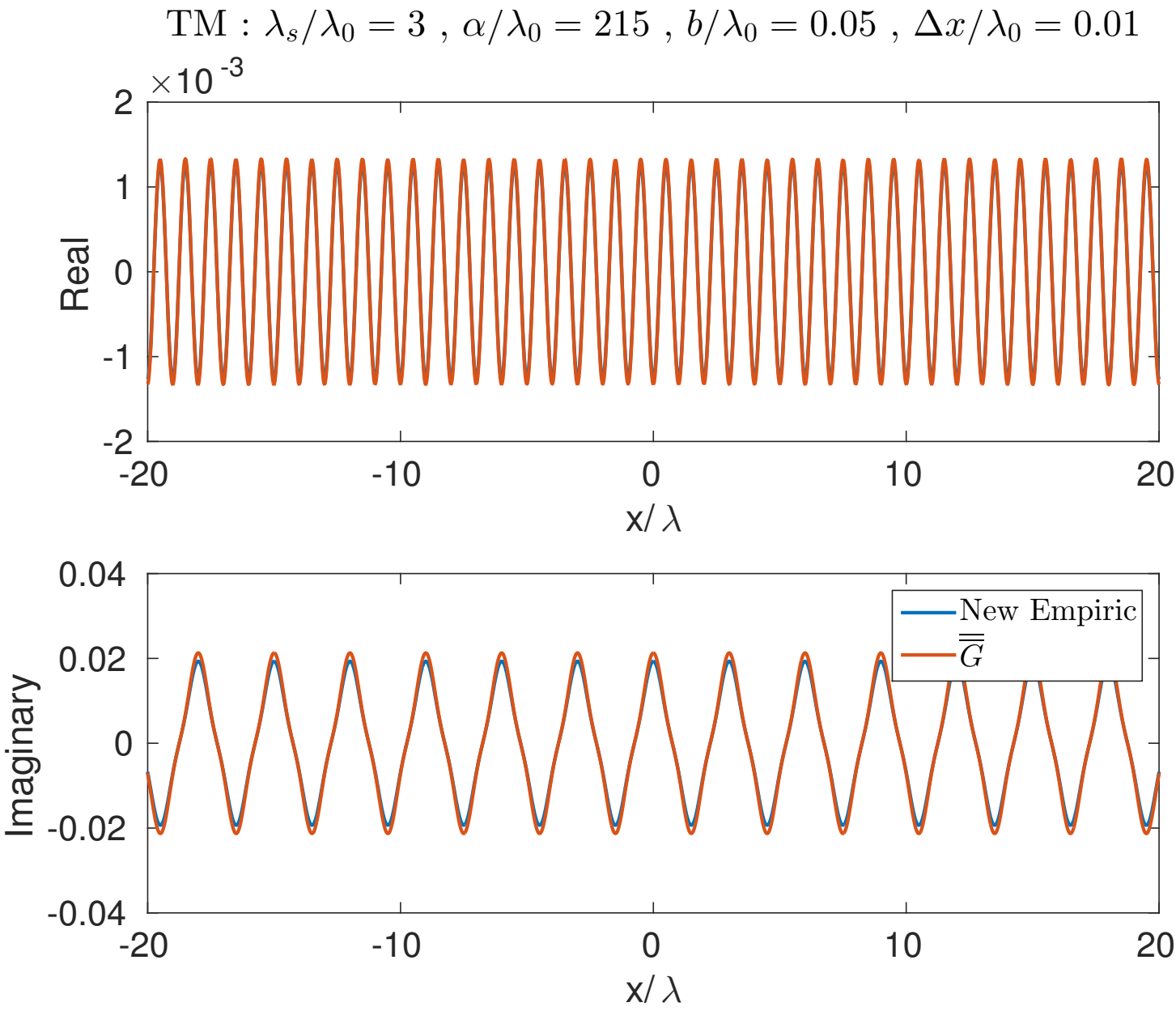


Figure 4.60: TM Empiric Analytic

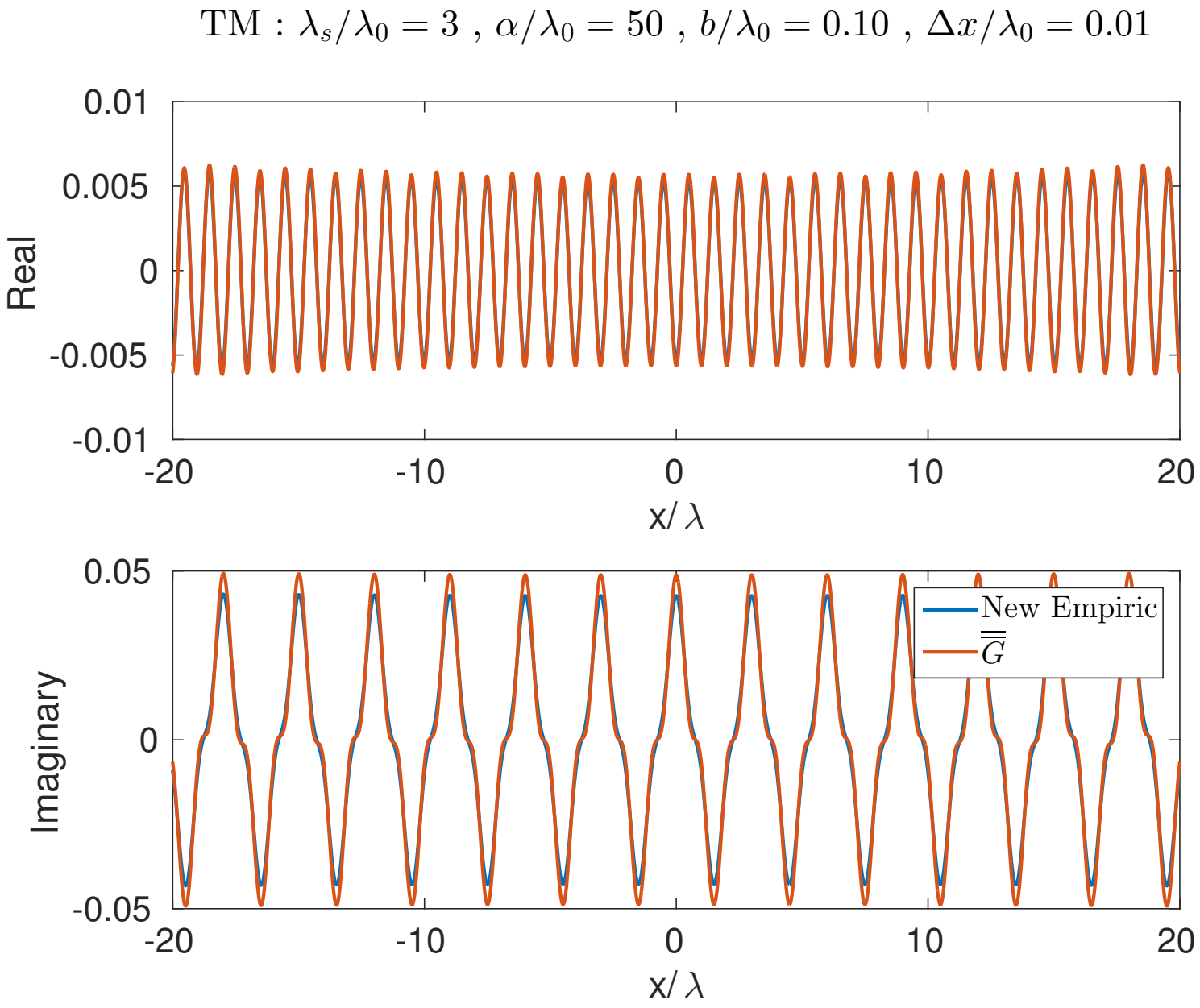


Figure 4.61: TM Empiric Analytic

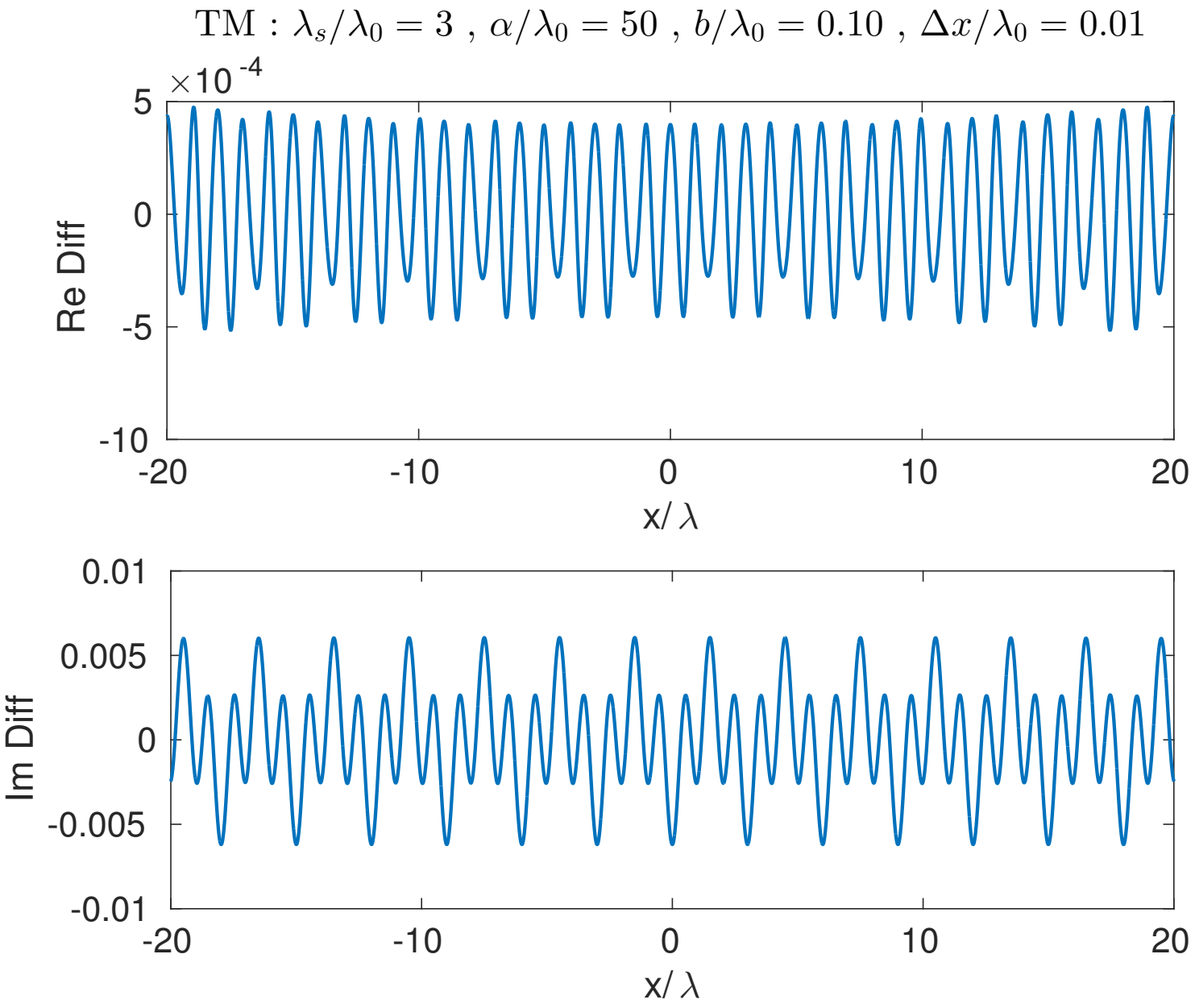


Figure 4.62: TM Empiric Analytic

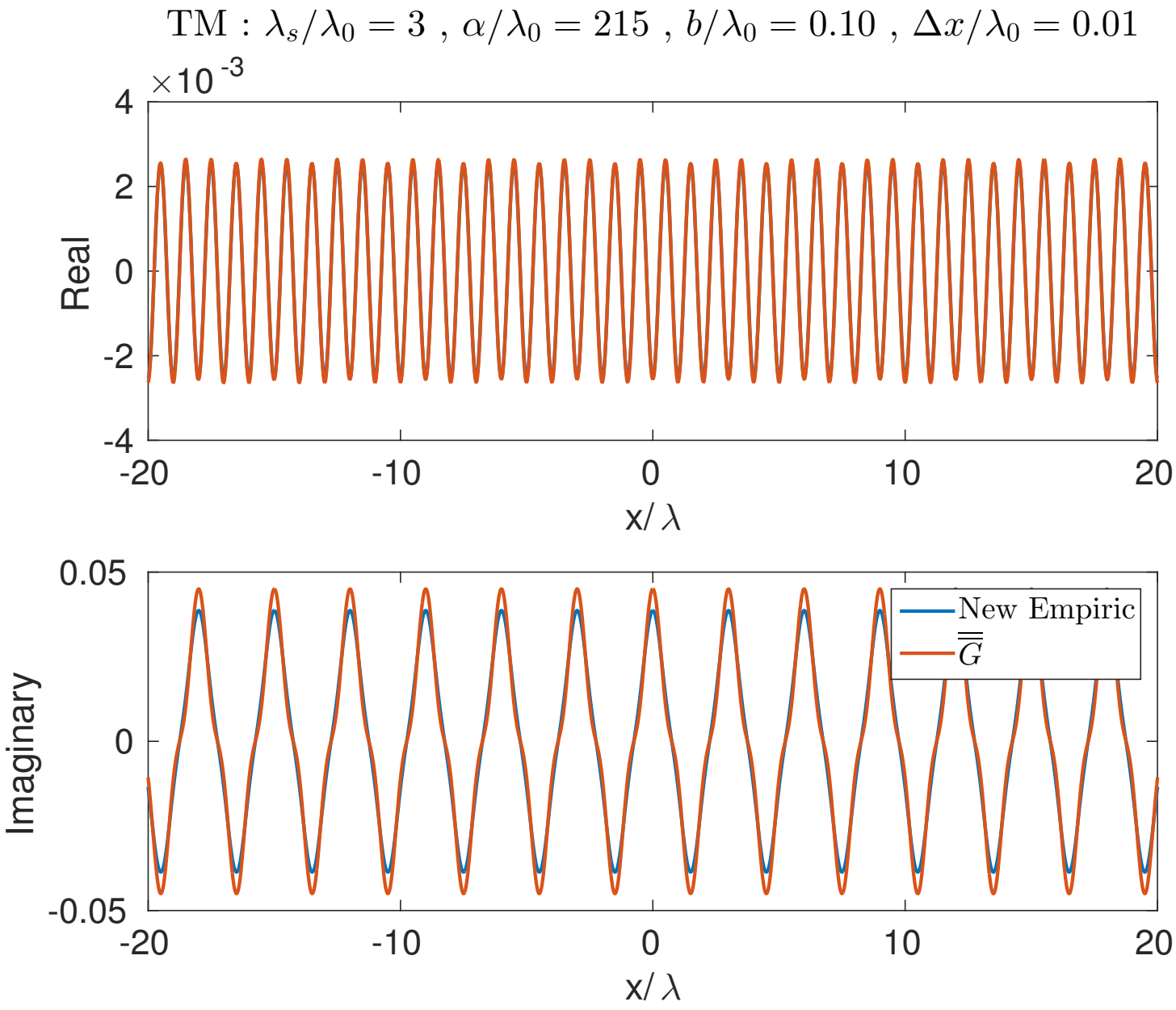


Figure 4.63: TM Empiric Analytic

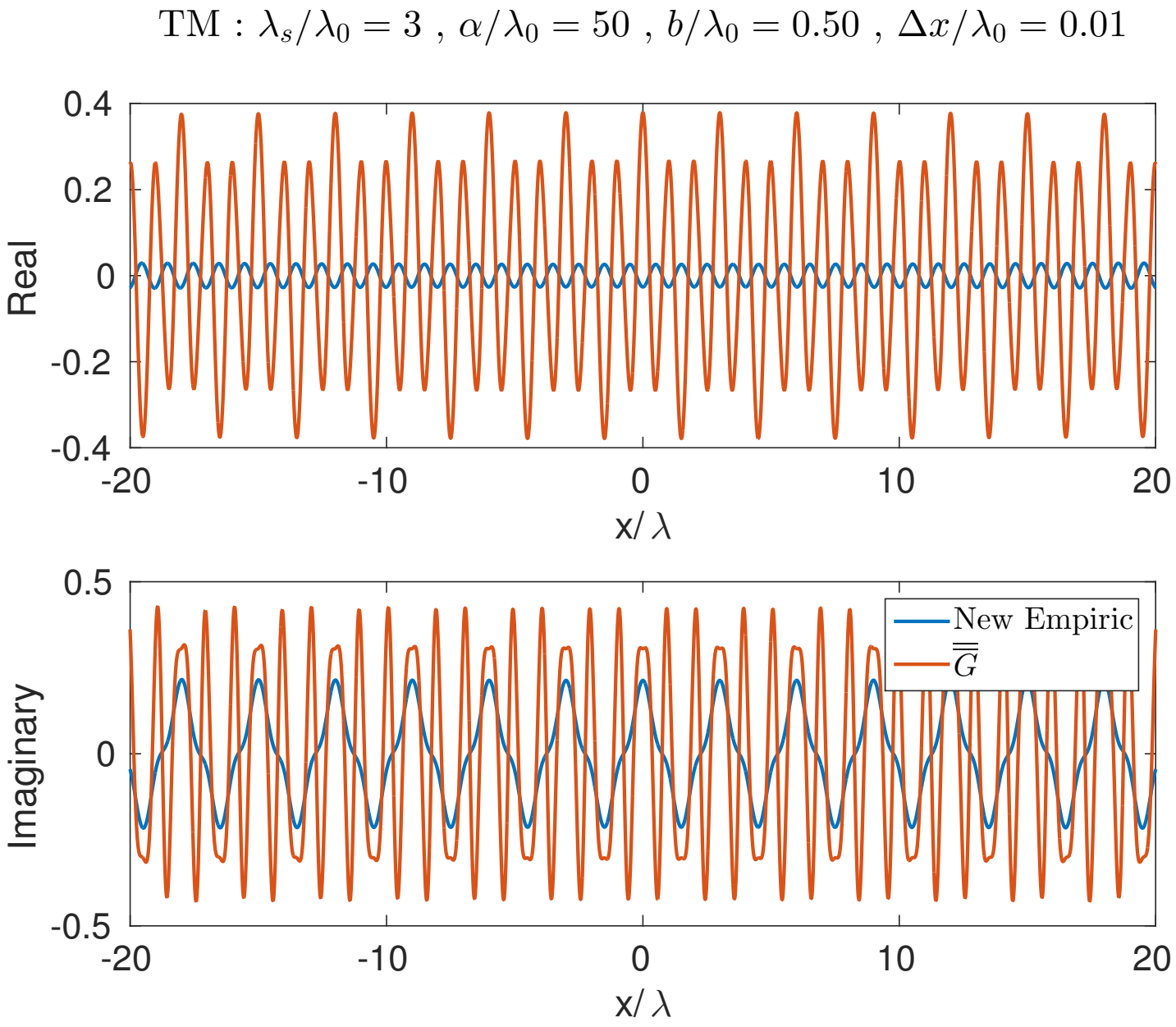


Figure 4.64: TM Empiric Analytic

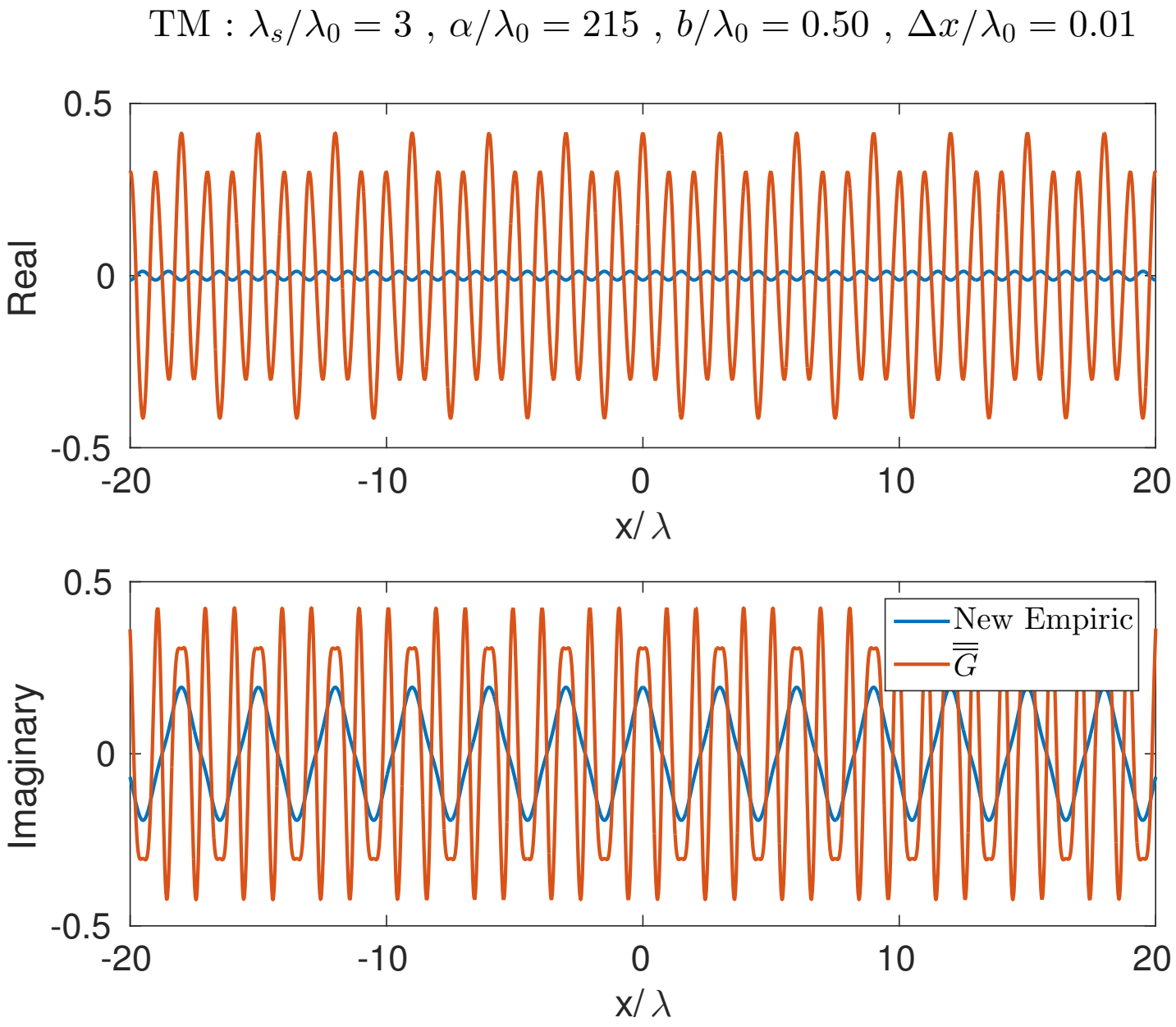


Figure 4.65: TM Empiric Analytic

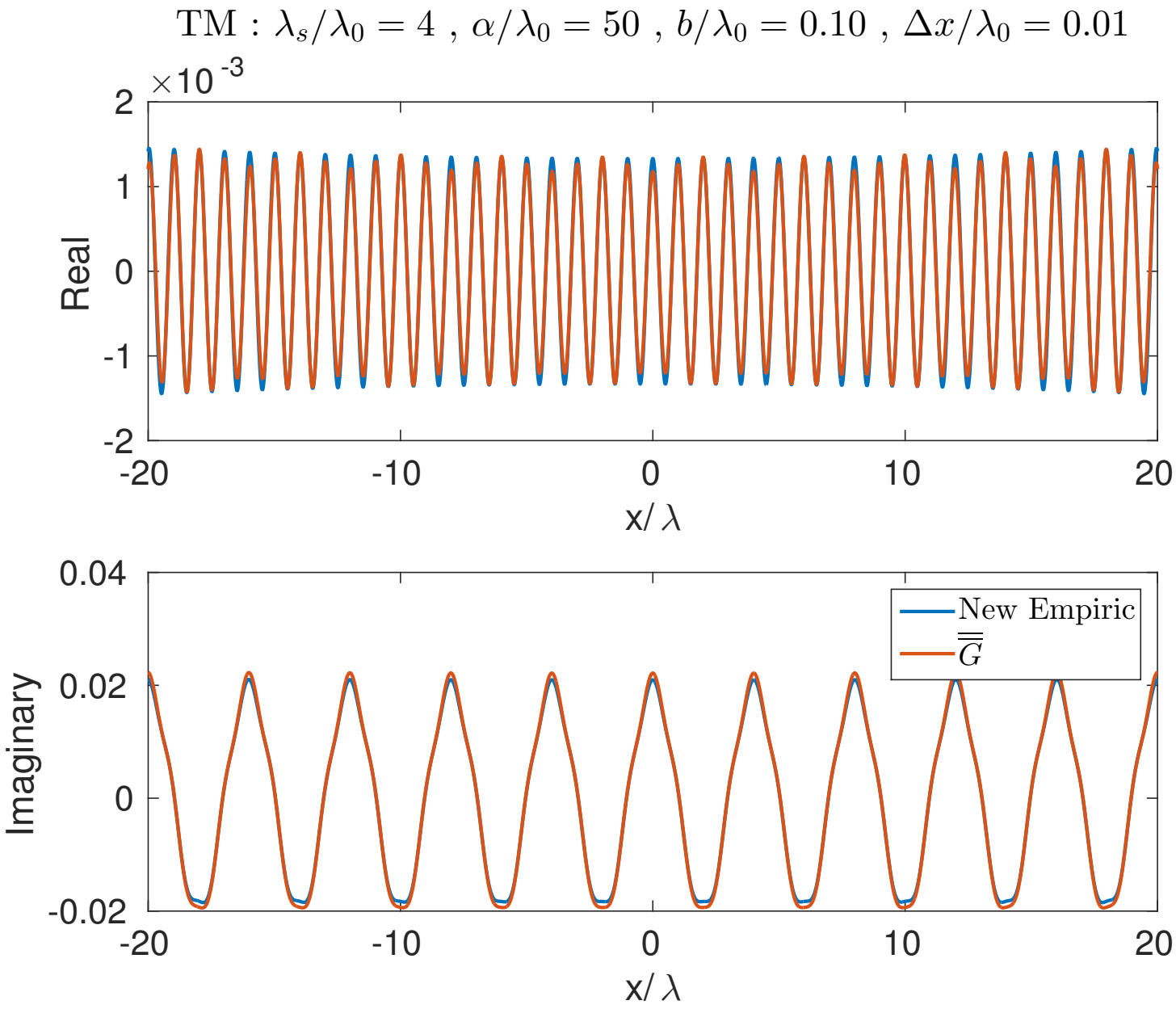


Figure 4.66: TM Empiric Analytic

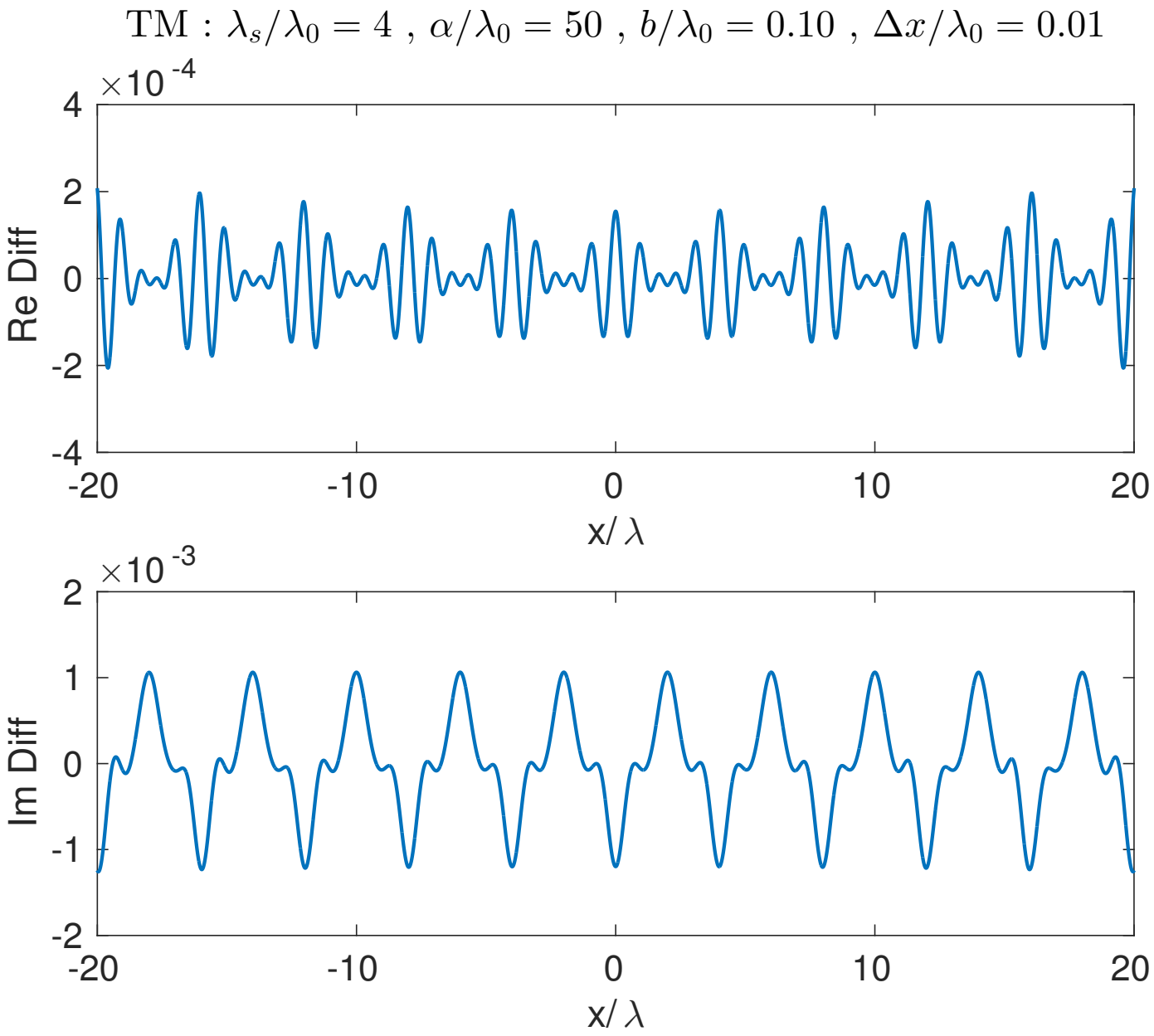


Figure 4.67: TM Empiric Analytic

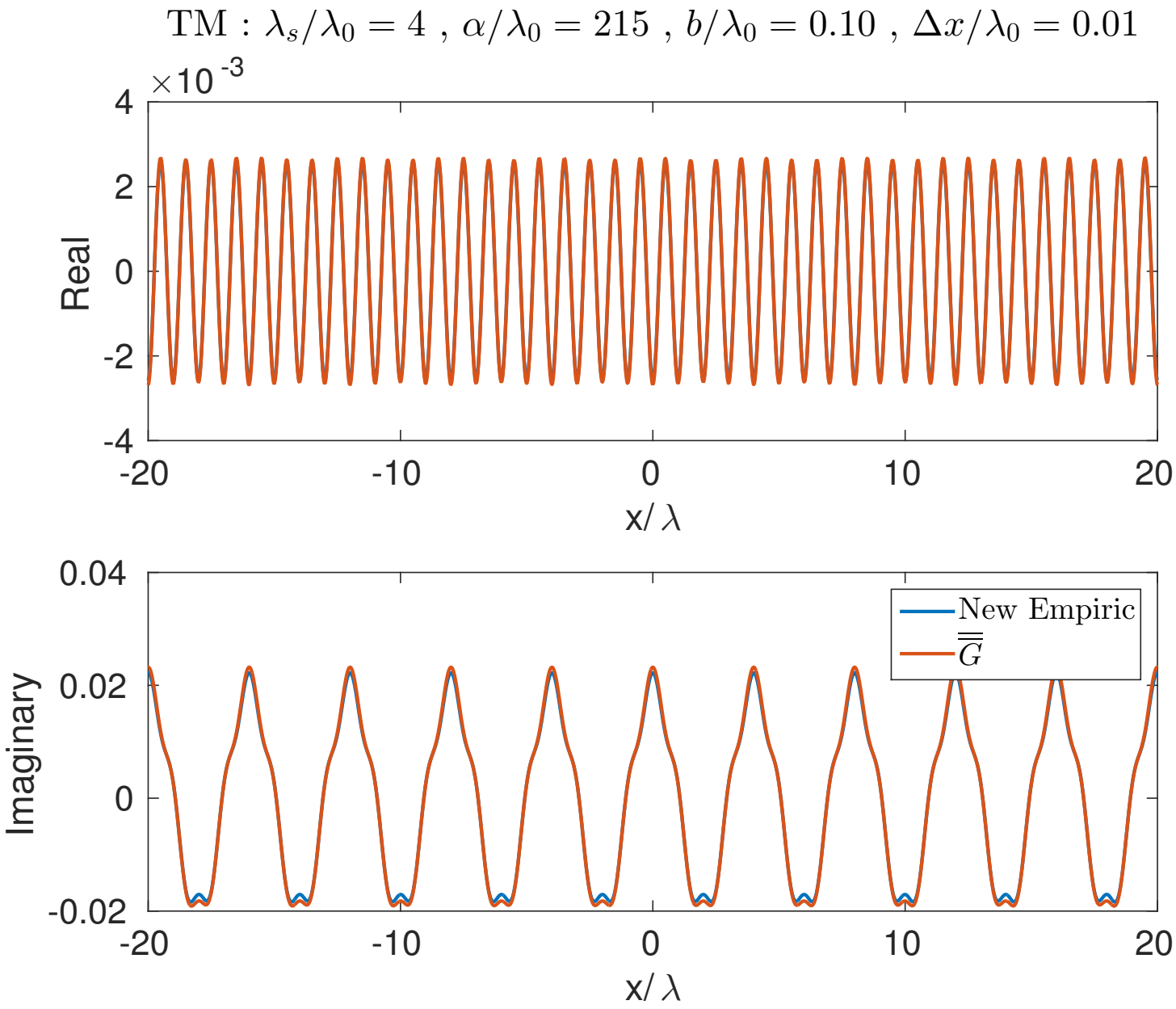


Figure 4.68: TM Empiric Analytic

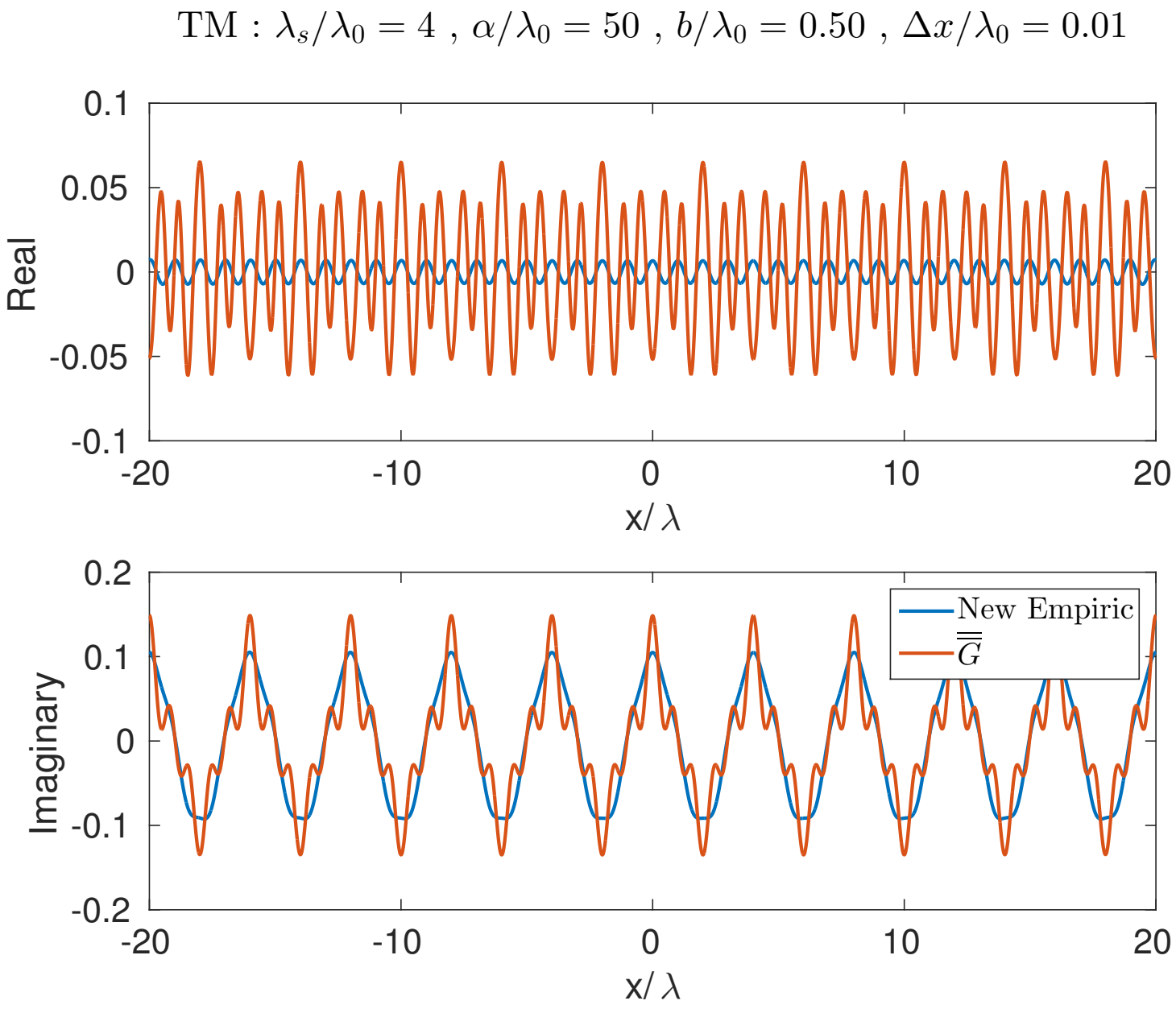


Figure 4.69: TM Empiric Analytic

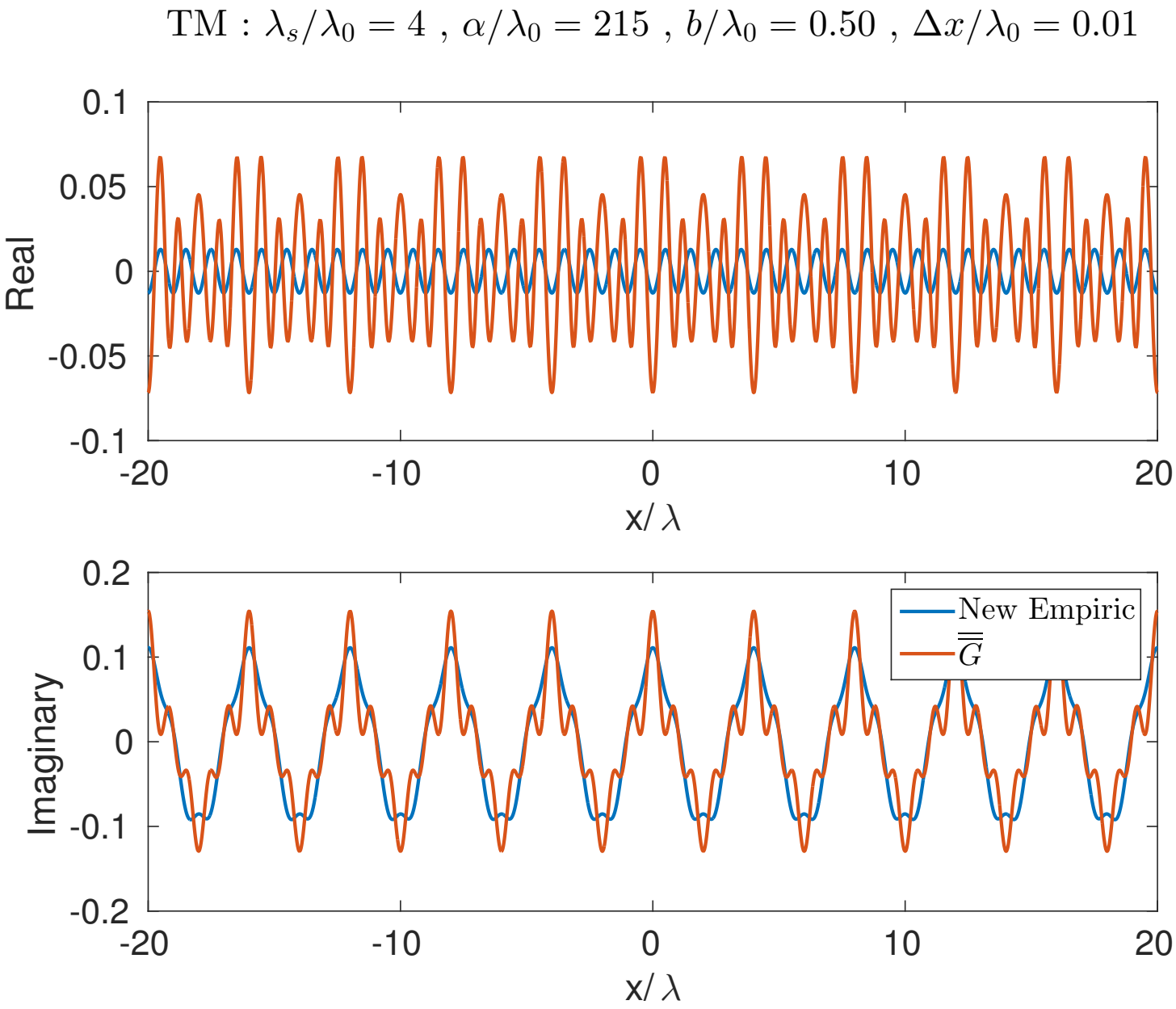


Figure 4.70: TM Empiric Analytic

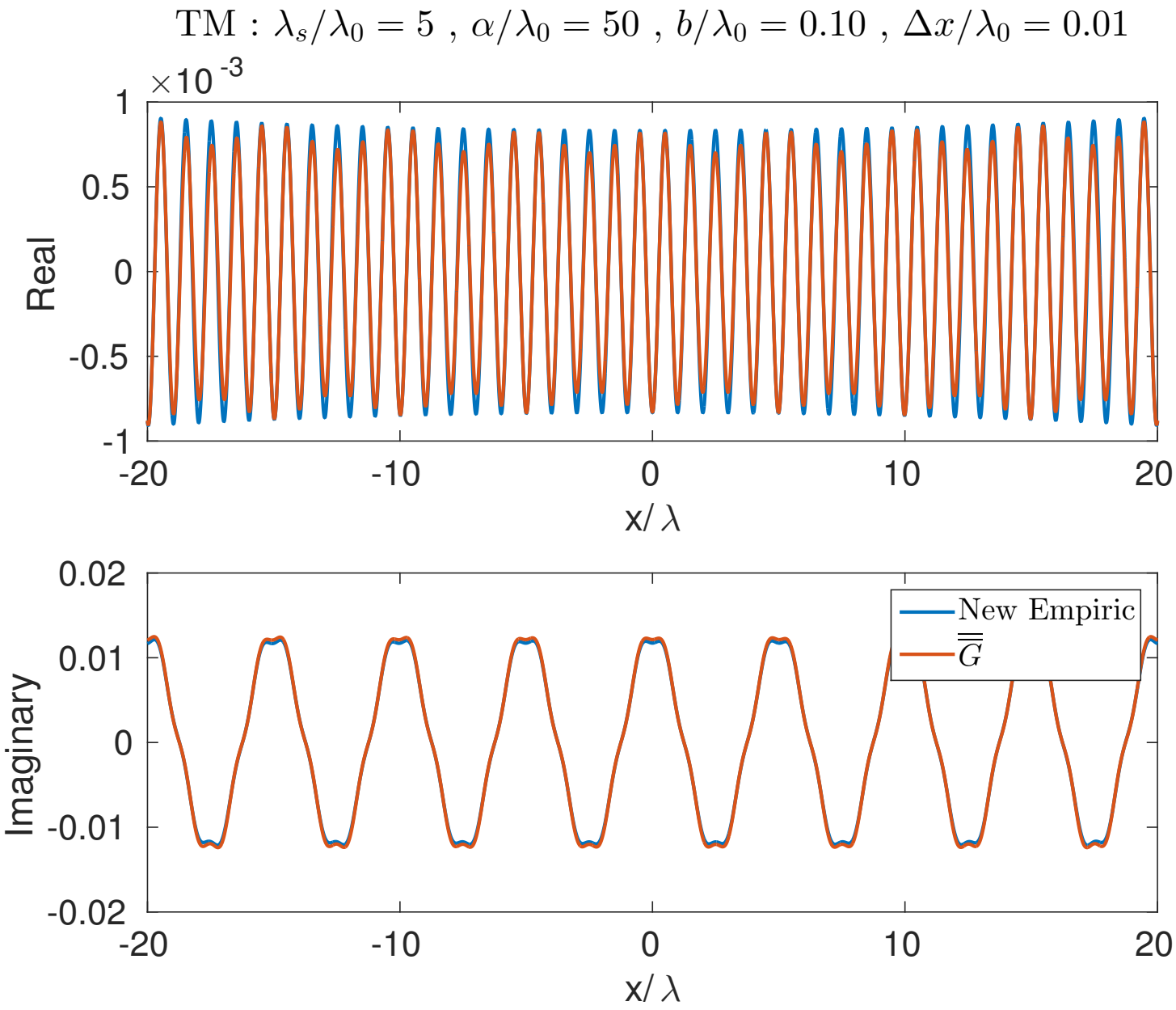


Figure 4.71: TM Empiric Analytic

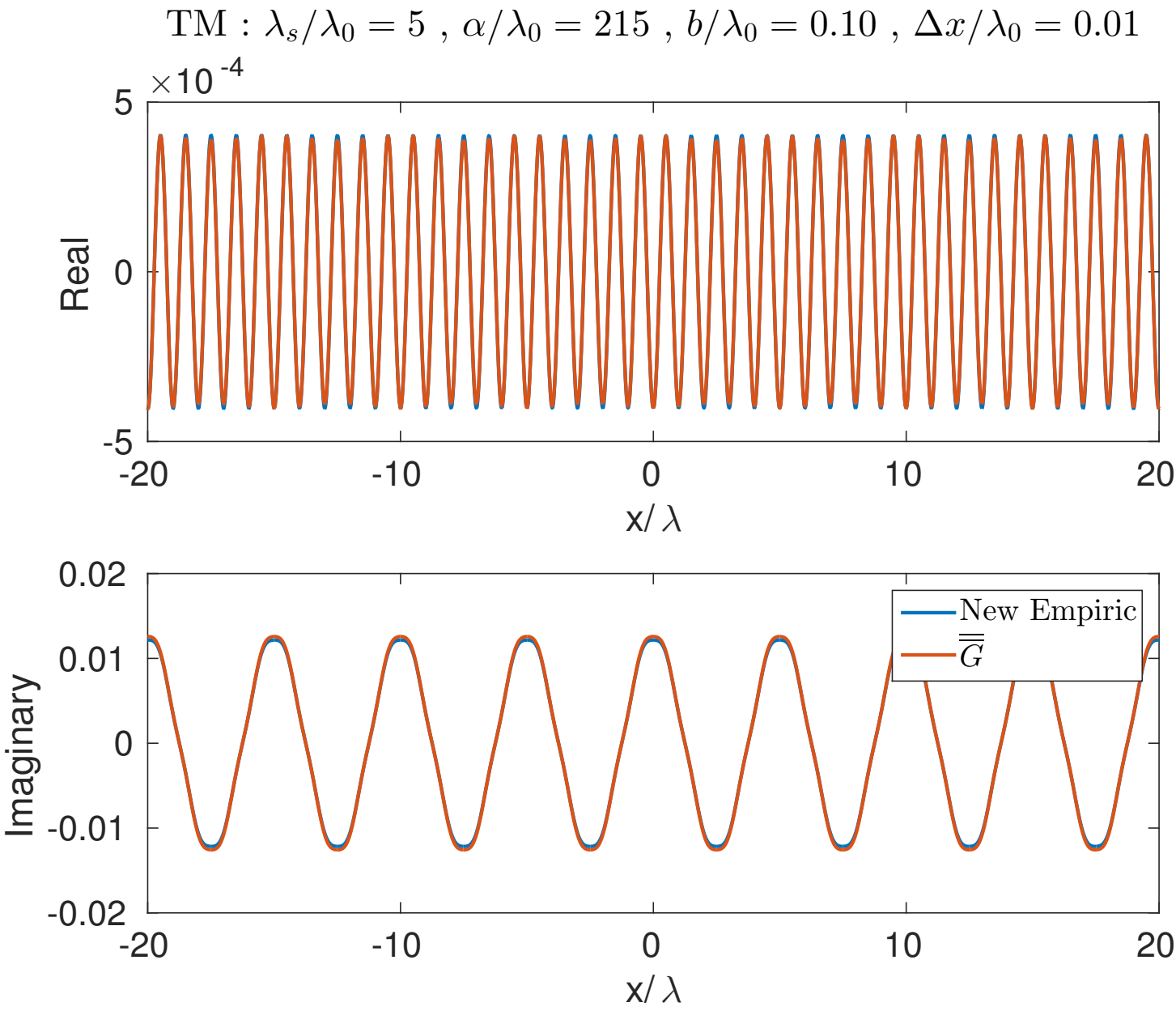


Figure 4.72: TM Empiric Analytic

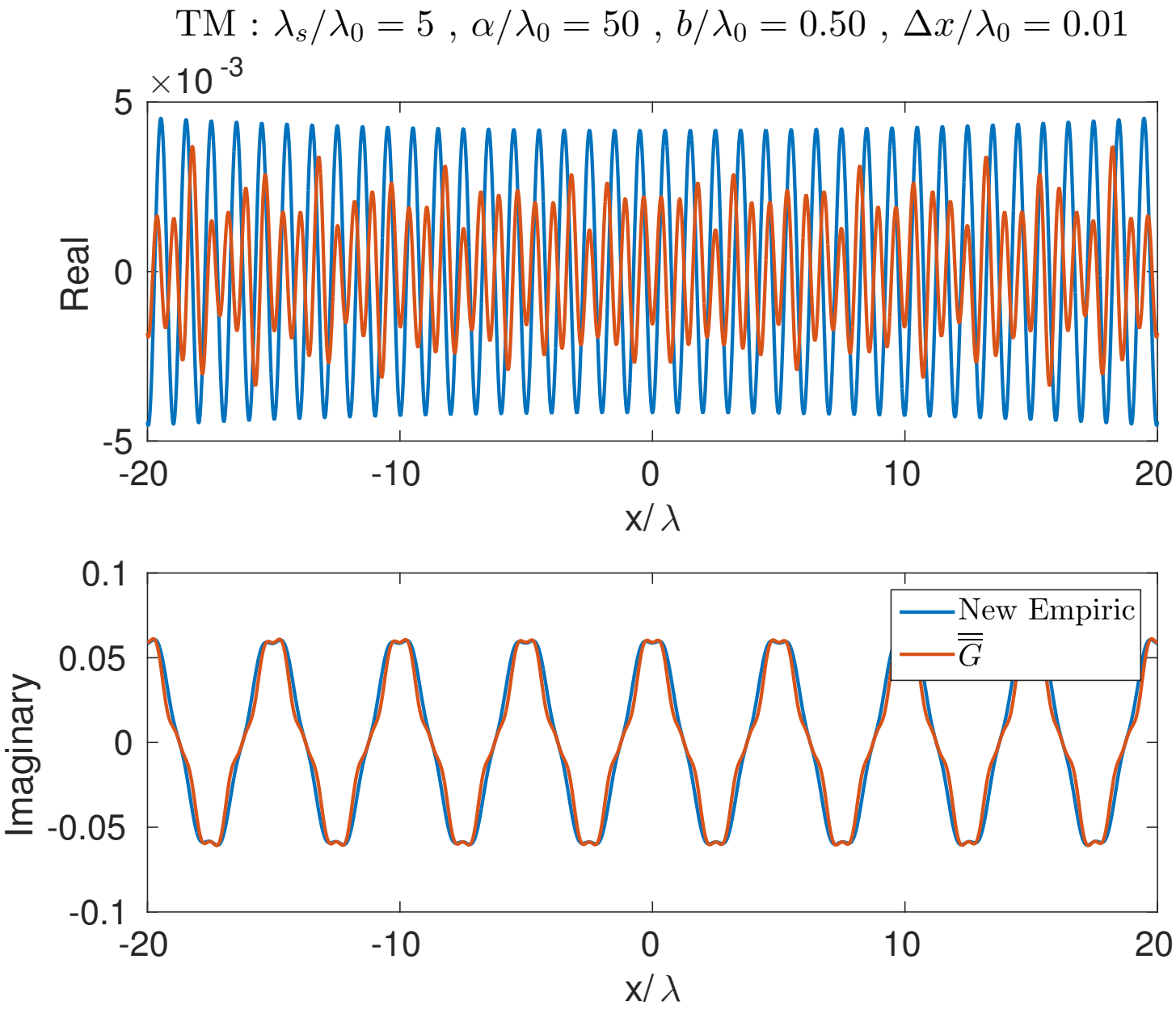


Figure 4.73: TM Empiric Analytic

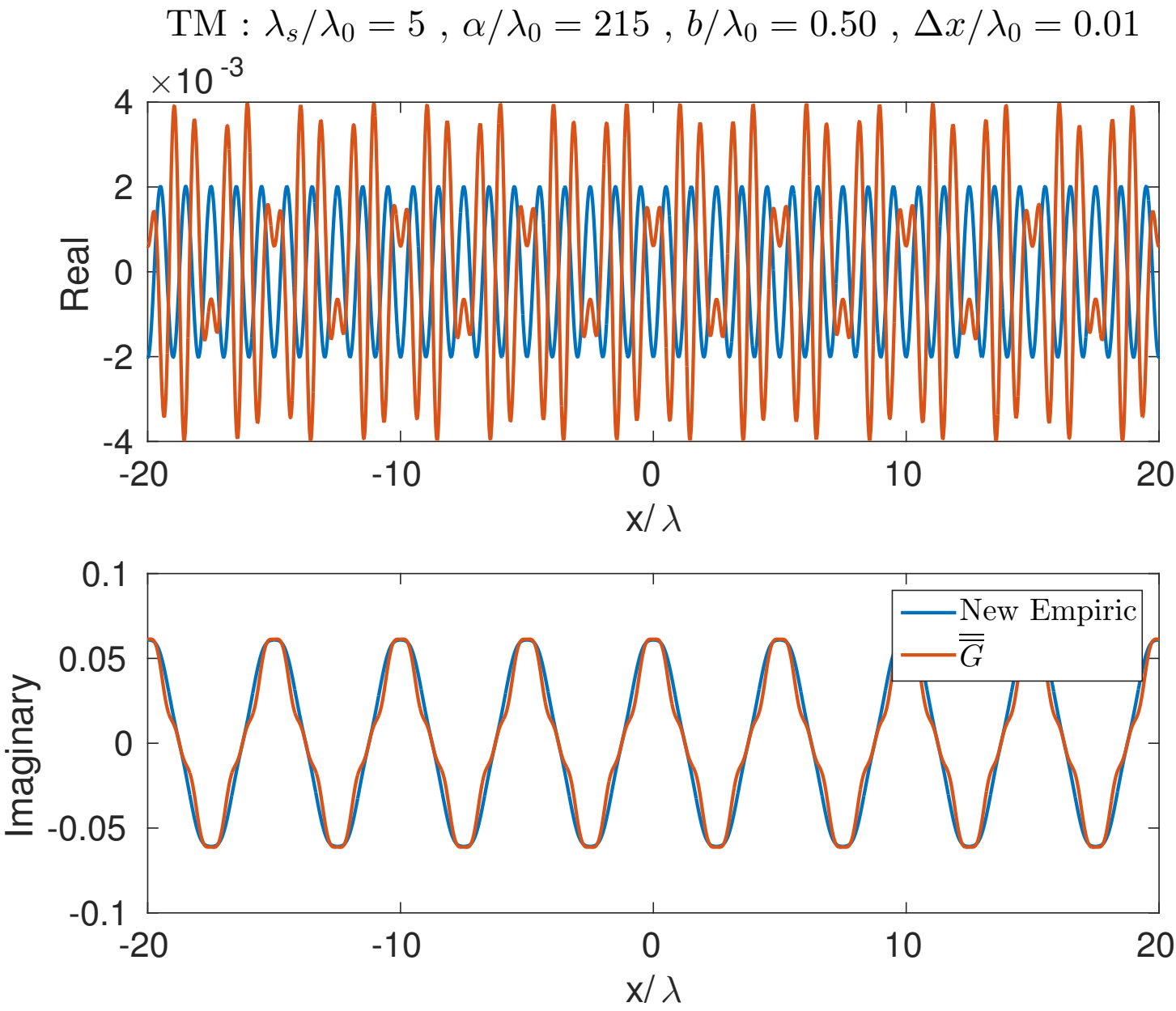


Figure 4.74: TM Empiric Analytic

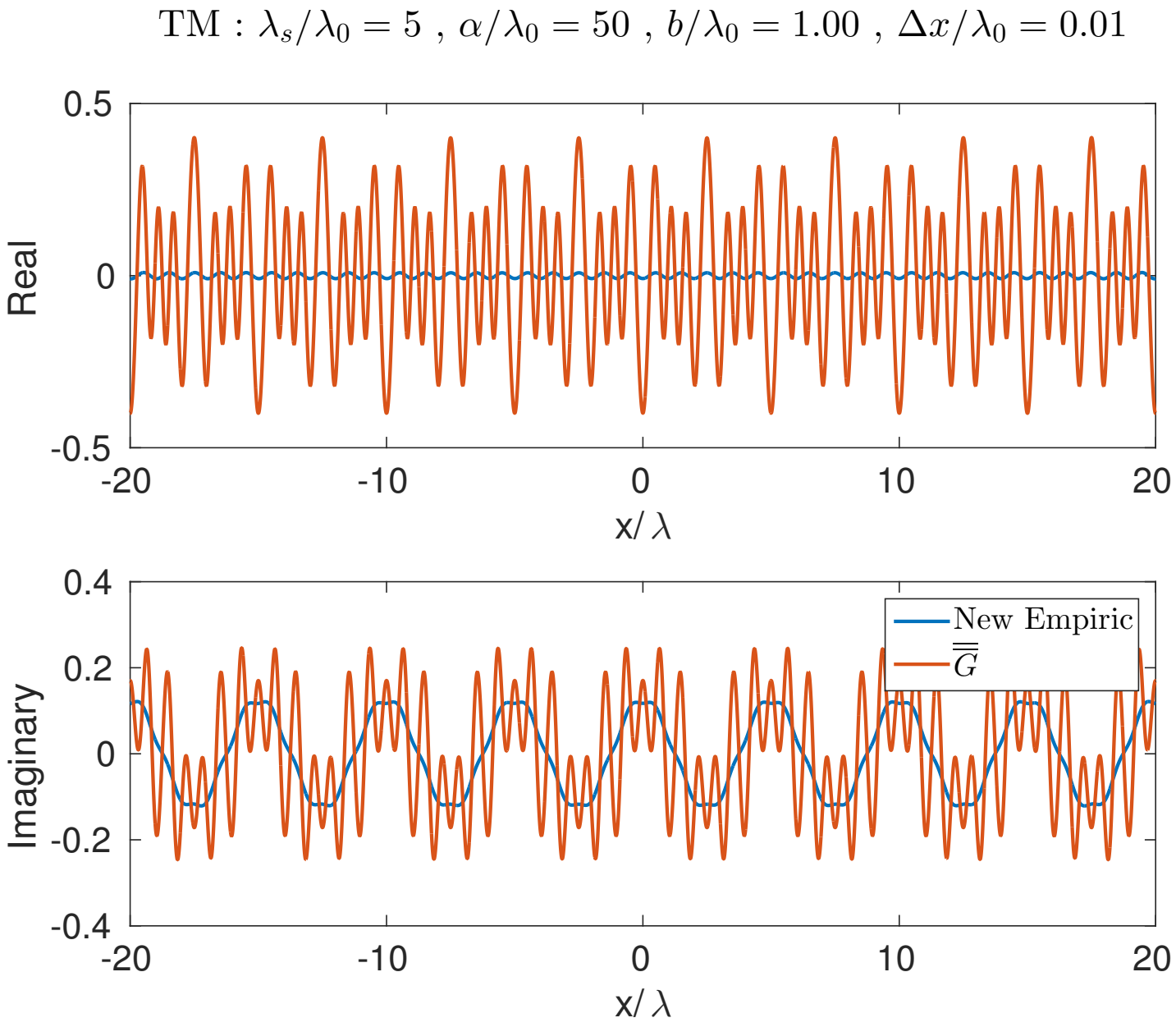


Figure 4.75: TM Empiric Analytic

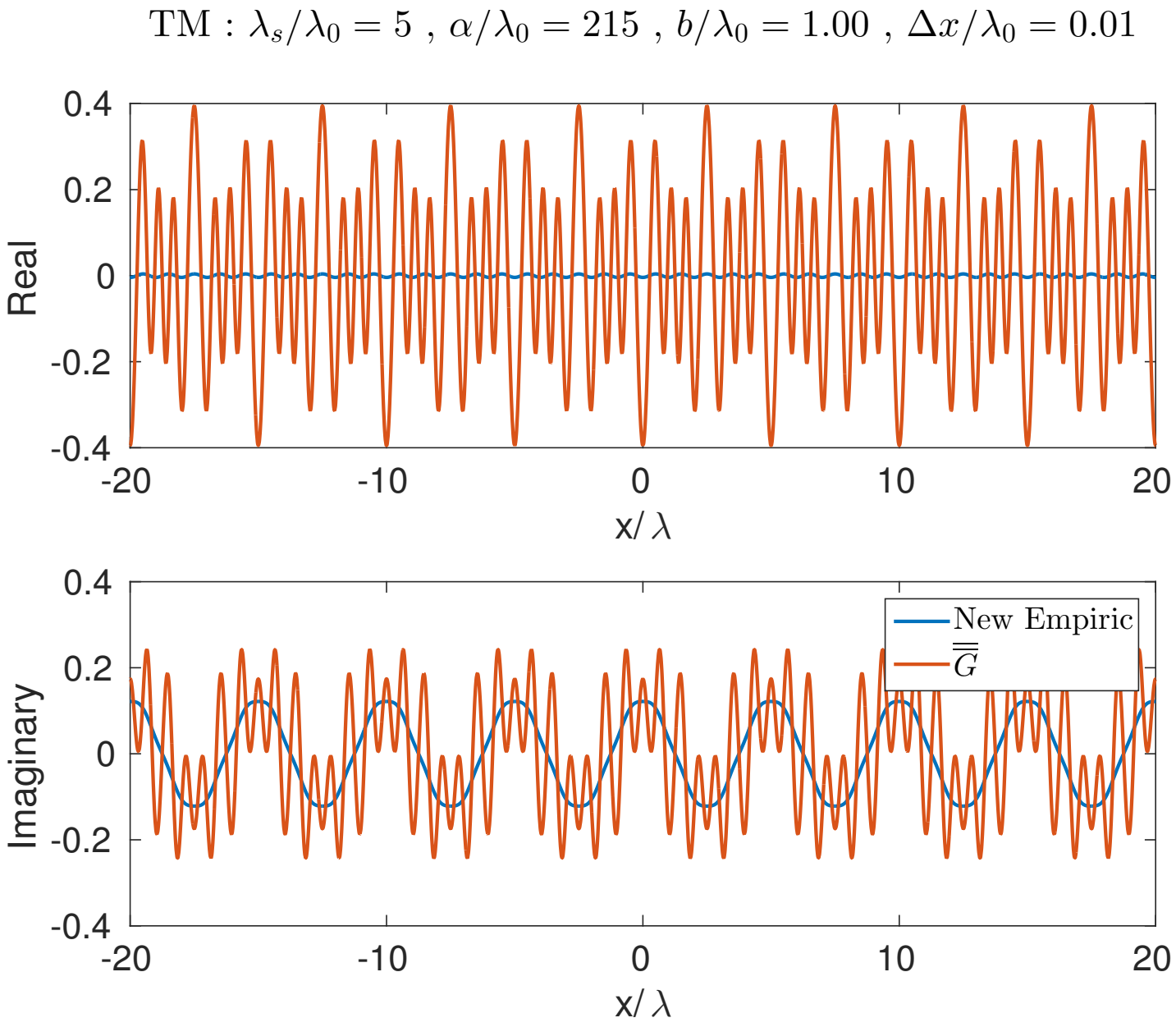


Figure 4.76: TM Empiric Analytic

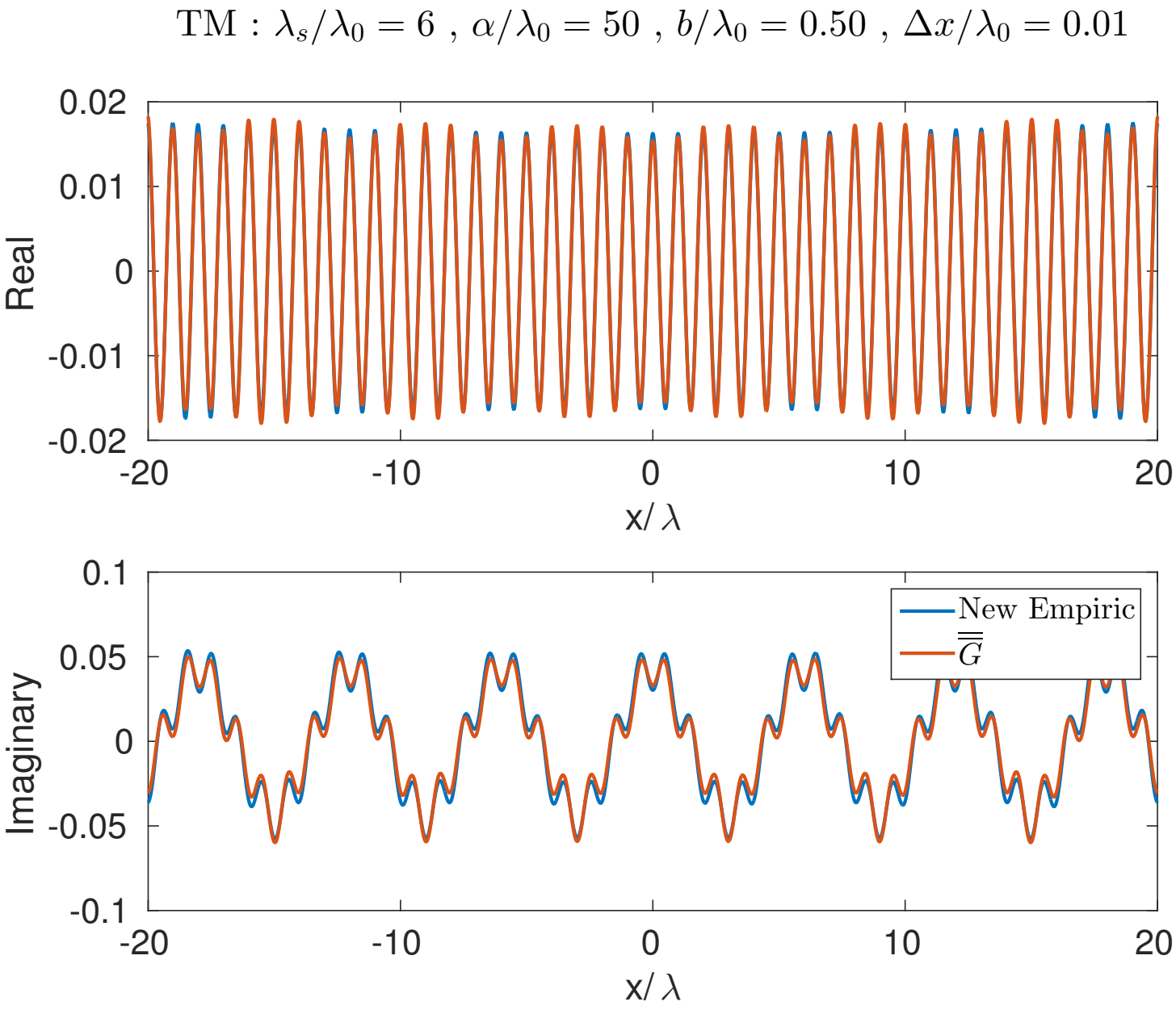


Figure 4.77: TM Empiric Analytic

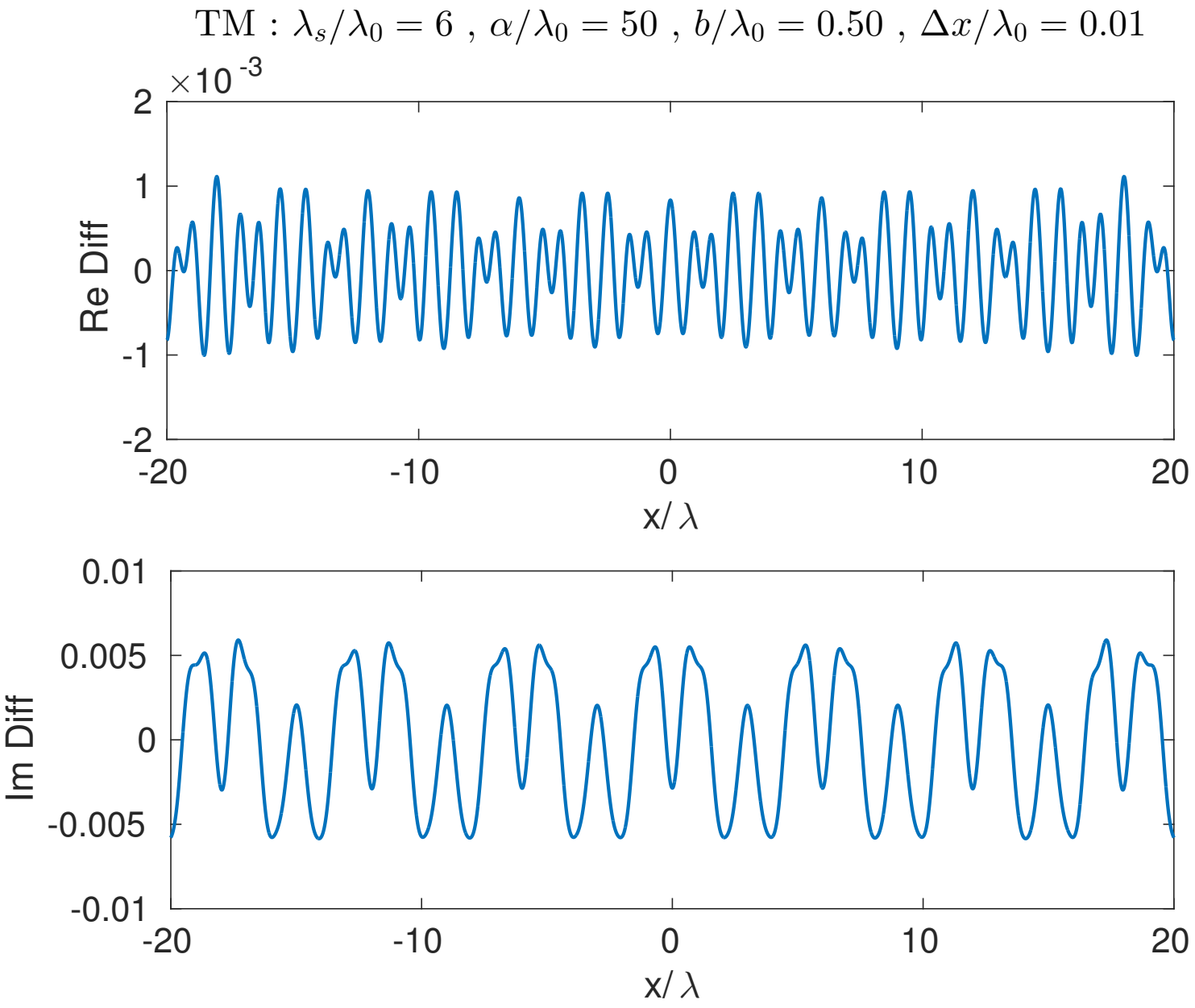


Figure 4.78: TM Empiric Analytic

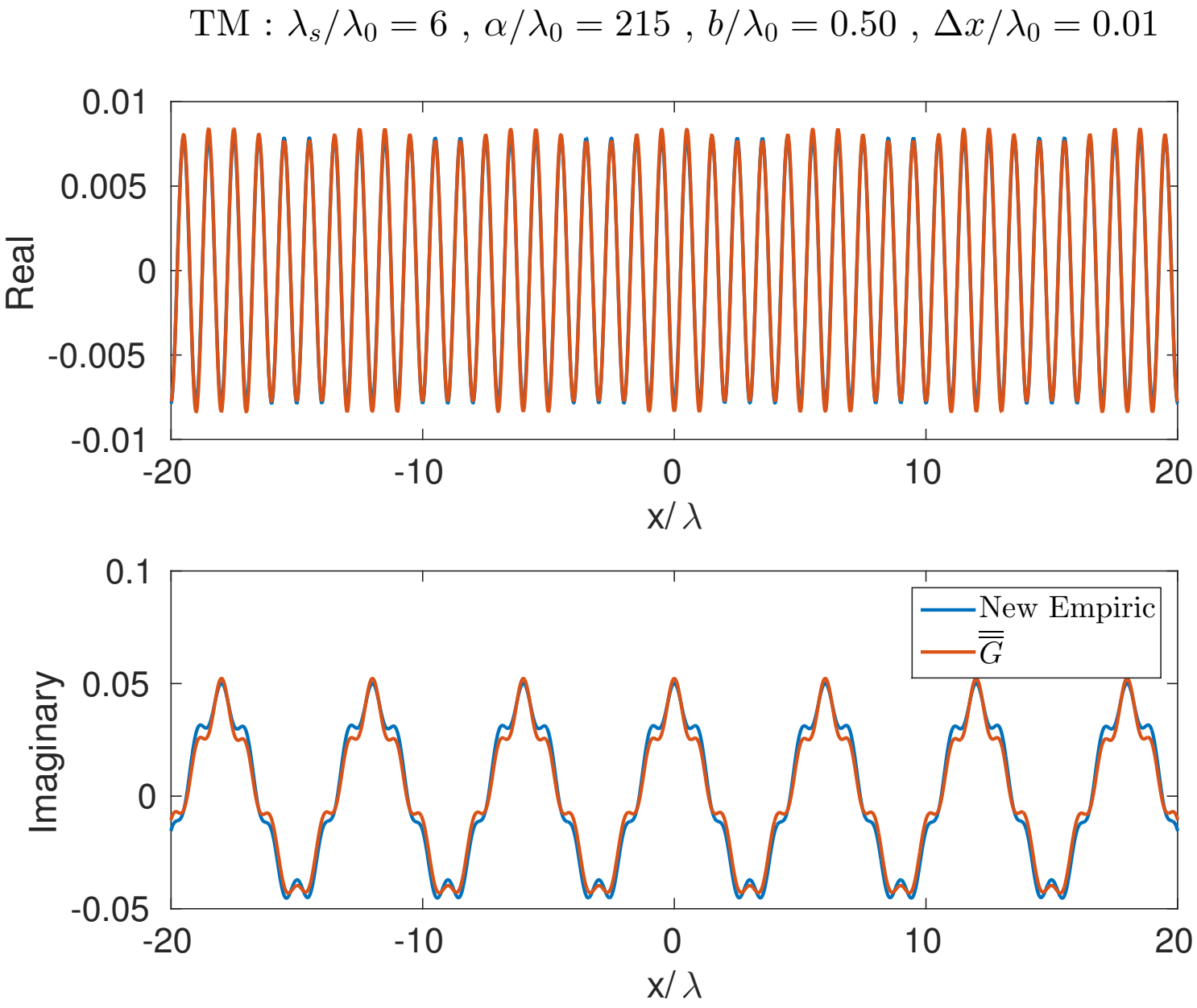


Figure 4.79: TM Empiric Analytic

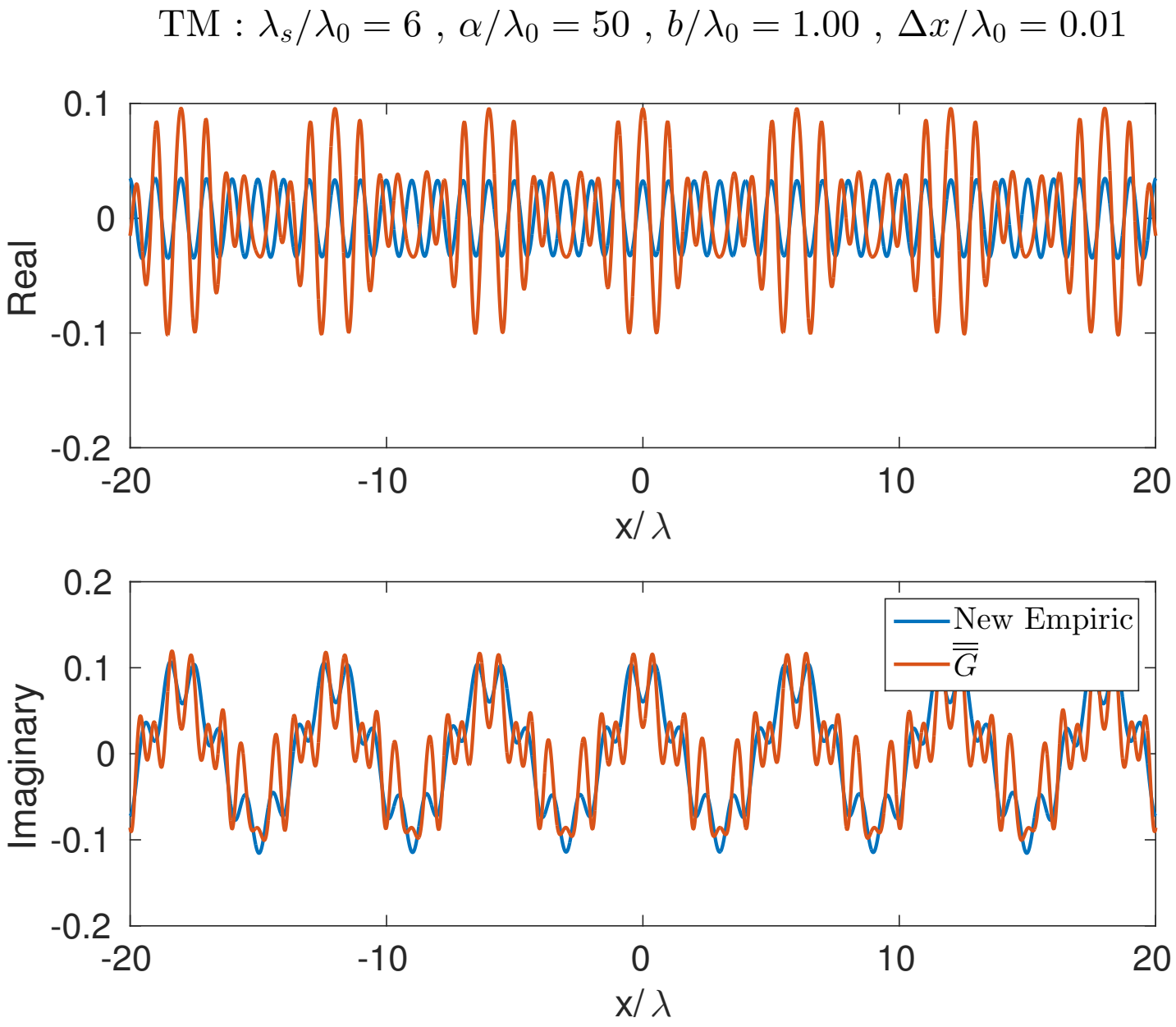


Figure 4.80: TM Empiric Analytic

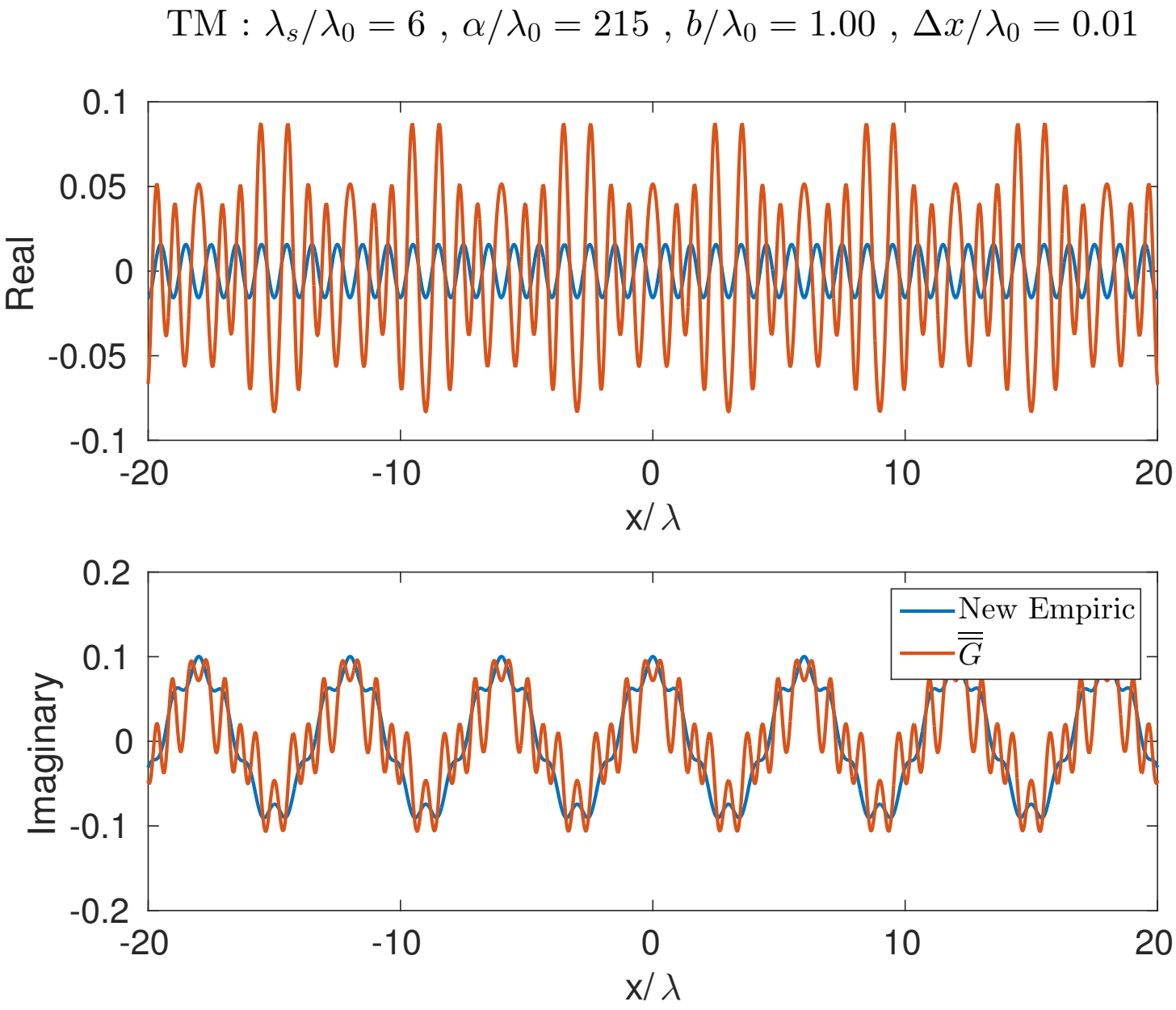


Figure 4.81: TM Empiric Analytic

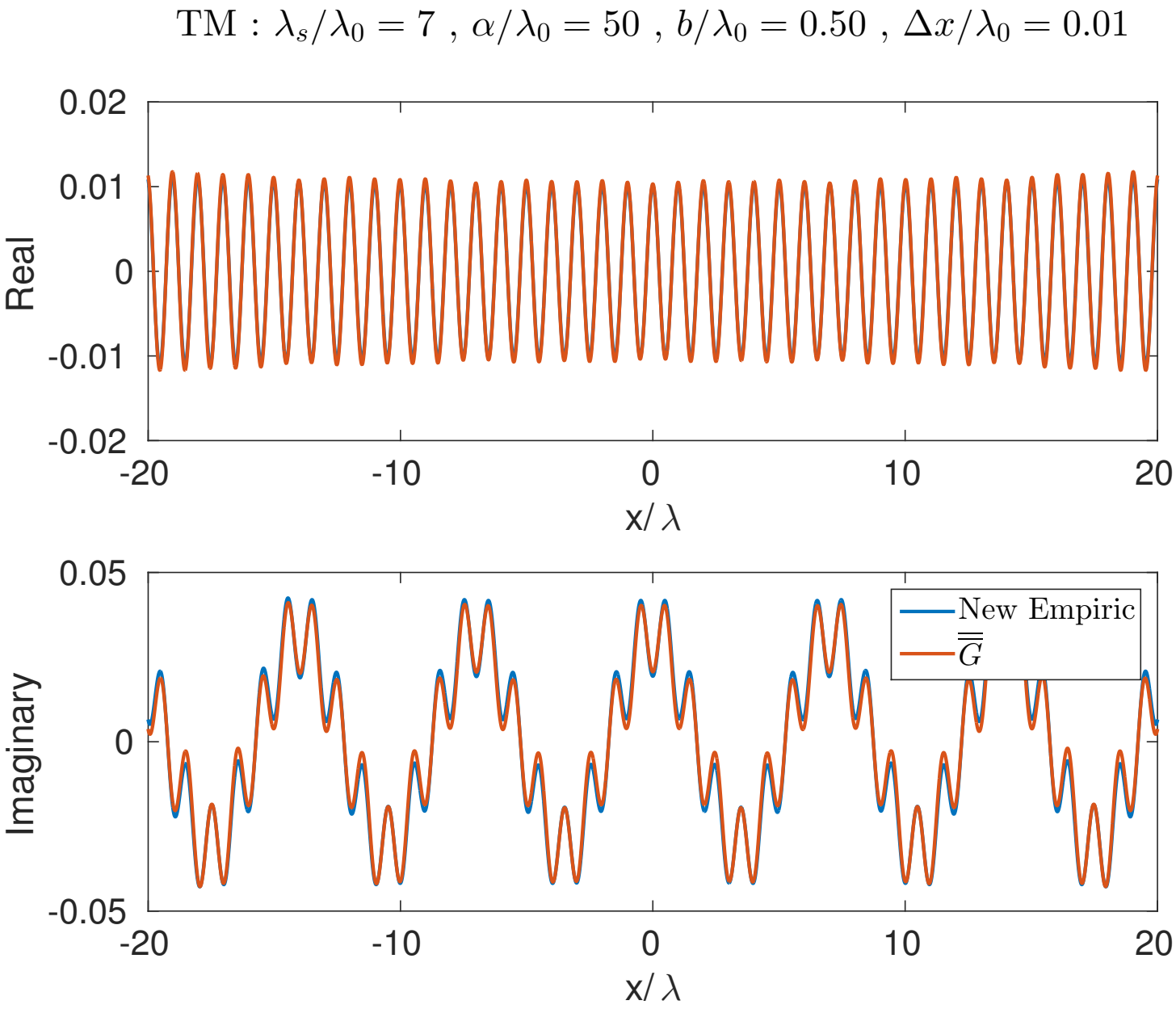


Figure 4.82: TM Empiric Analytic

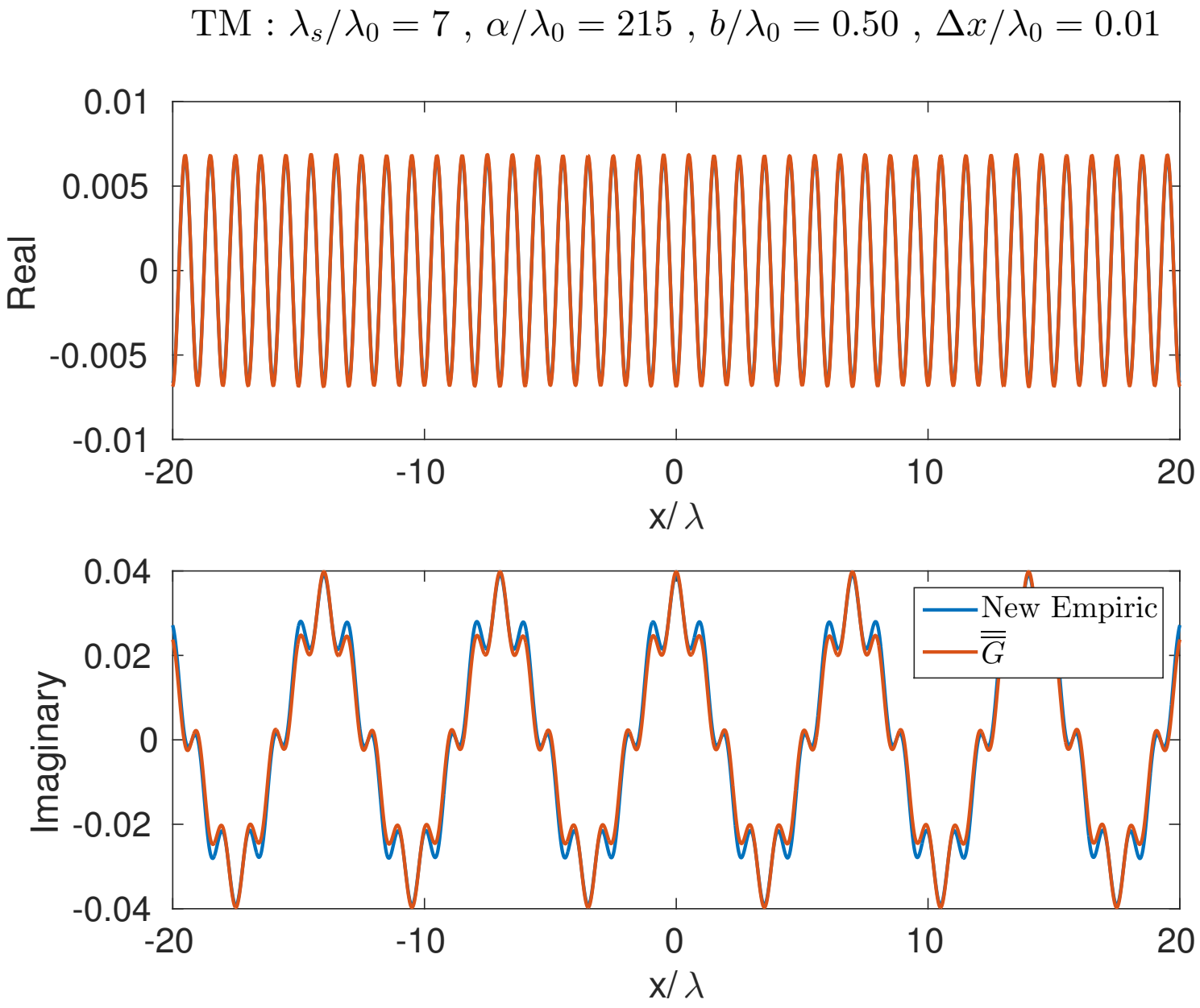


Figure 4.83: TM Empiric Analytic

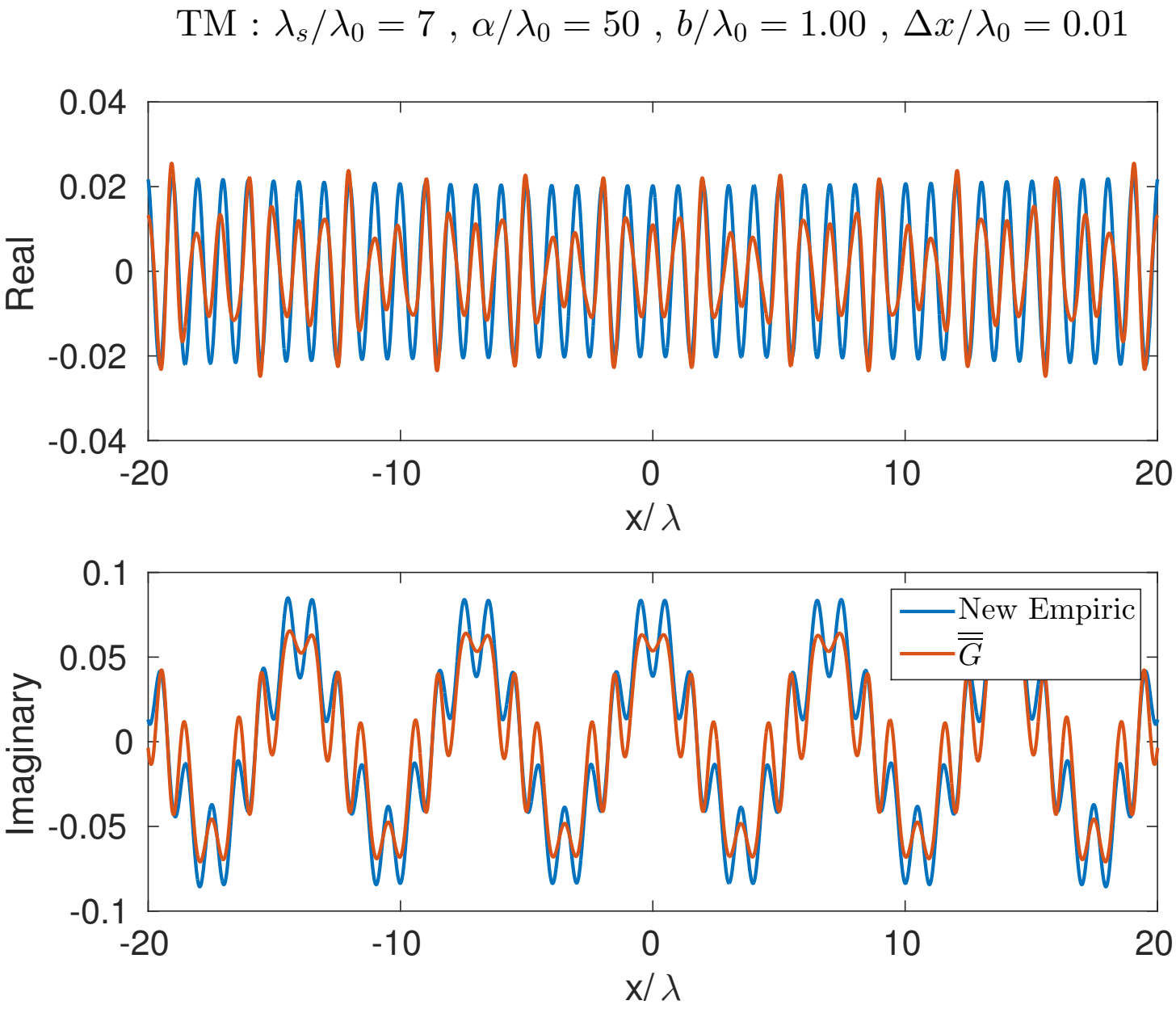


Figure 4.84: TM Empiric Analytic

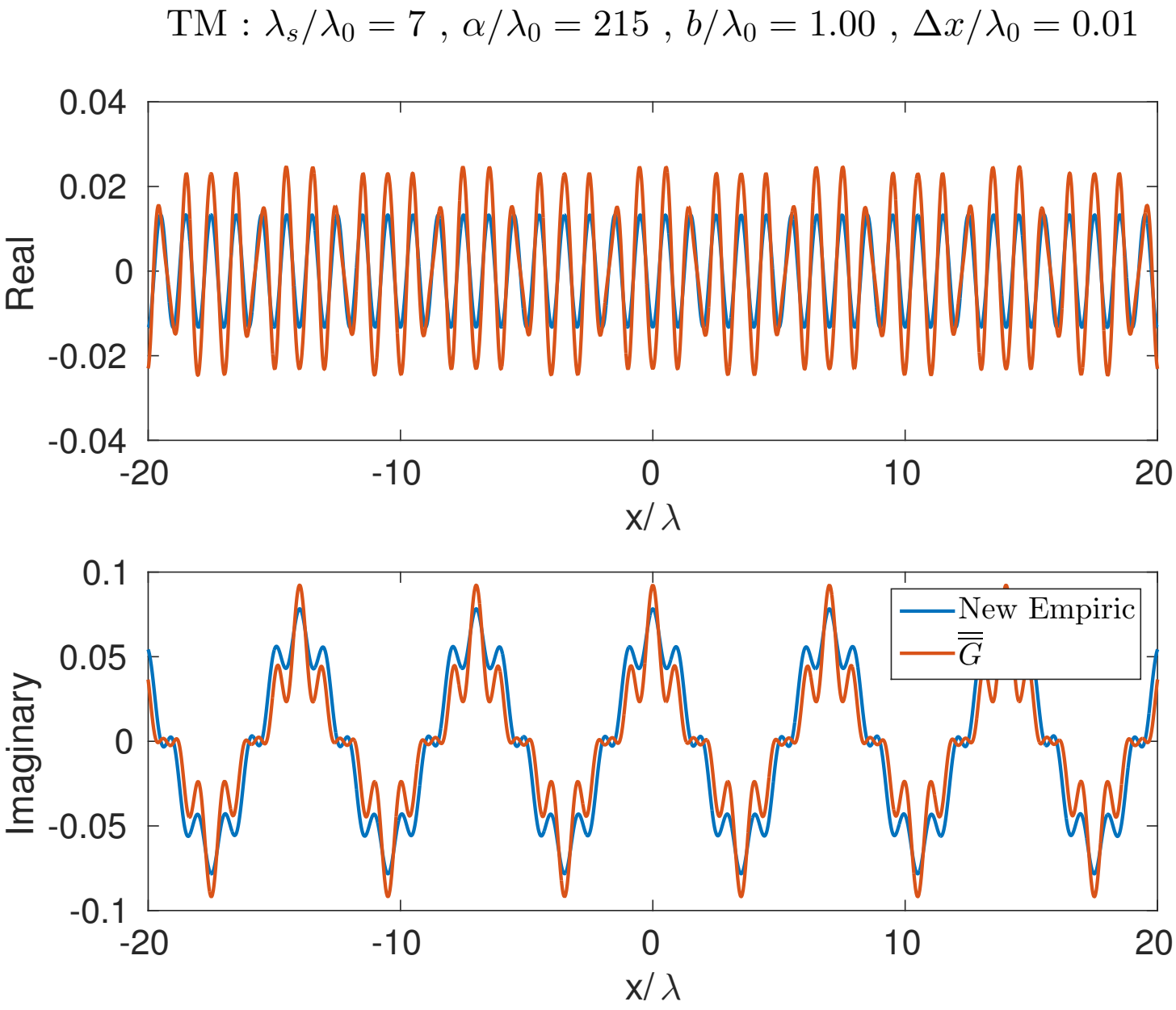


Figure 4.85: TM Empiric Analytic

**TE** Using the same type of approximations used to produce Equation4.4.20, a detailed derivation given in Appendix B.2 produces the following equation for TE polarization:

$$\overline{\overline{G}}(x) = j\frac{\zeta_{xx}(x)}{2k_0} - \frac{\zeta_x(x)(-1+j)}{\sqrt{1+\zeta_x^2}\sqrt{2}} \frac{\left[\left(\sqrt{(x+\alpha)}\exp\left(-j(\alpha-x)k_0\right) - \sqrt{(\alpha-x)}\exp\left(-j(x+\alpha)k_0\right)\right)\right]}{\sqrt{2\pi k_0(\alpha^2-x^2)}} \left(1+\frac{b^2k_s^2}{4}\left(1-\frac{1}{2}\left(\frac{\exp(j2\alpha k_s)}{(1-2K_s)}+\frac{\exp(-j2\alpha k_s)}{(1+2K_s)}\right)\right)\right) \quad (4.4.21)$$

Unlike TM, no terms of this expression are required to be dropped but like TM this expression proves to be a powerful approximation to the kernel integral for TE polarization. The additional complexity of this equation results from the $\sqrt{1+\zeta_{x'}^2(x')}$ factor of TE while TM is only linearly dependent on the surface slope.

**Range of Validity** Figures 4.86 through 4.100 show good agreement for surface amplitudes $\frac{b}{\lambda_0} \leq 0.1$ for surface wavelengths $\frac{\lambda_s}{\lambda_0} \geq 3$. Similarly, Figures 4.101 through 4.115 show good agreement for $\frac{b}{\lambda_0} = 0.5$ and 1.0 is found down to $\frac{\lambda_s}{\lambda_0} \geq 5$ and $\frac{\lambda_s}{\lambda_0} \geq 7$ respectively. Figures 4.89, 4.92, 4.97, and 4.108 show the difference between the numeric and empiric formula showing about a 10% magnitude difference in the worst case.

The range of validity for both polarizations is shown in Figure 4.116, where the formula is valid for all combinations of surface wavelengths and amplitudes above the curve, inclusive, in the region labeled "Valid" while below the curve in the region labeled "Not Valid" it finds poor agreement.

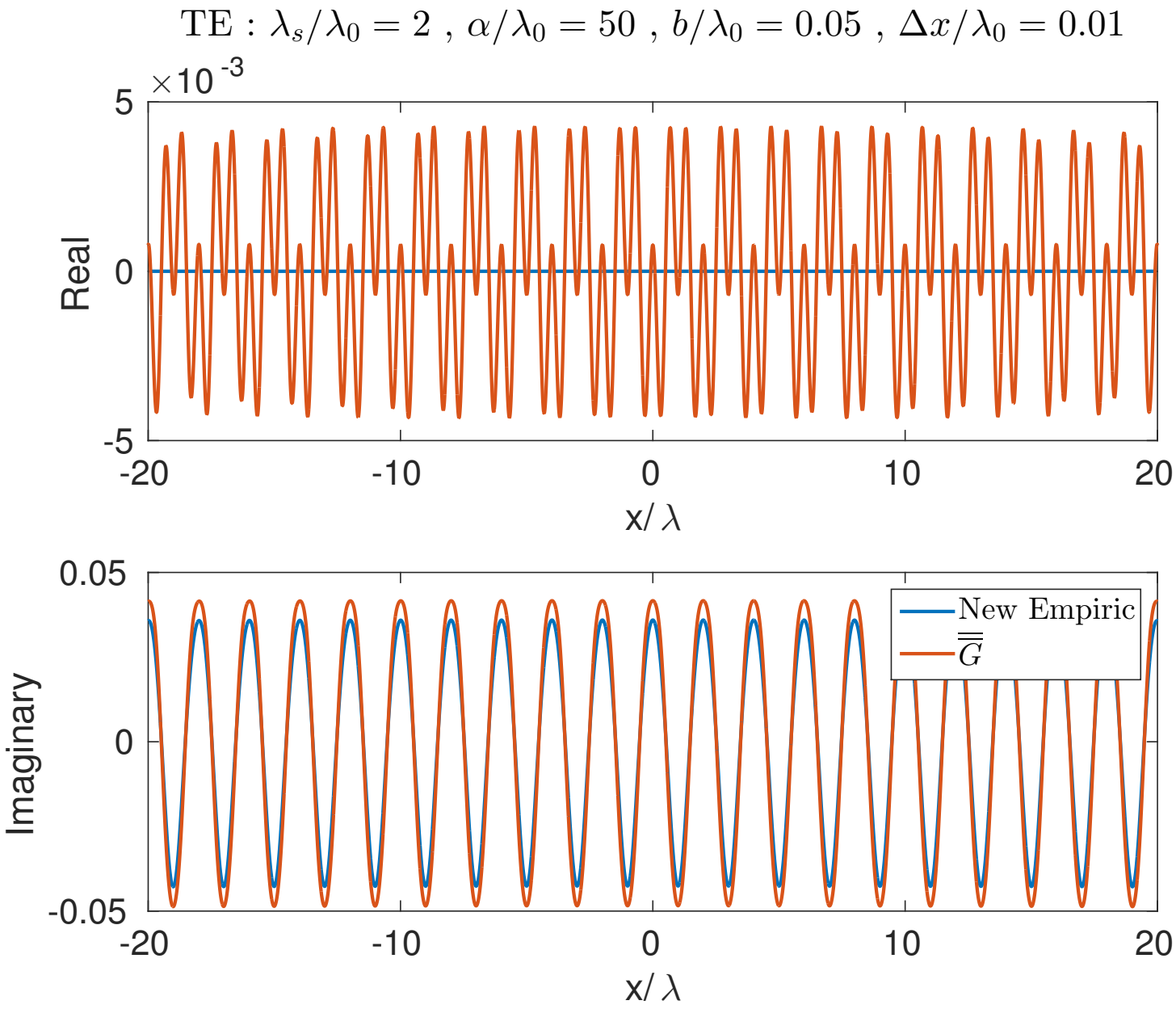


Figure 4.86: TE Empiric Analytic

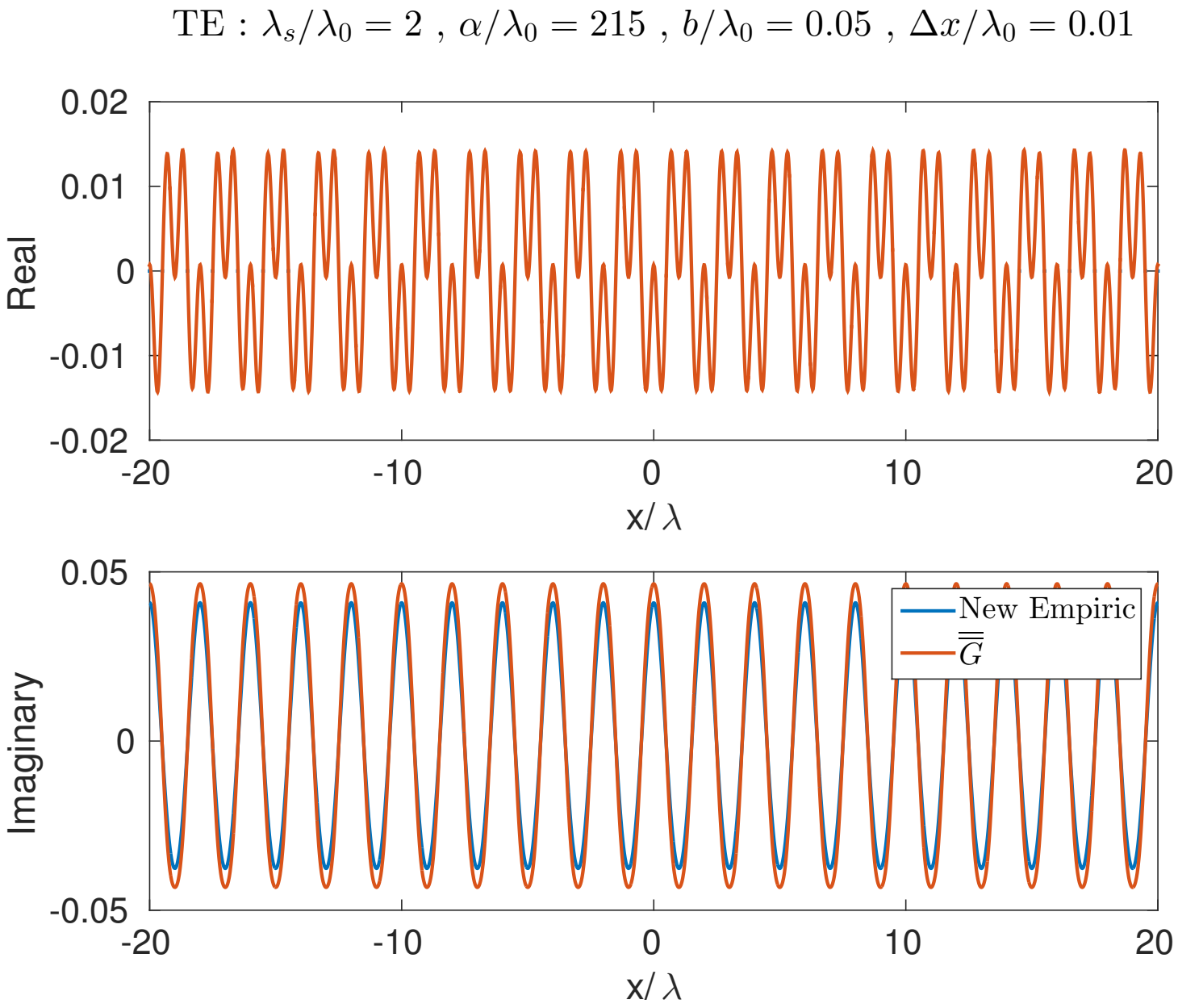


Figure 4.87: TE Empiric Analytic

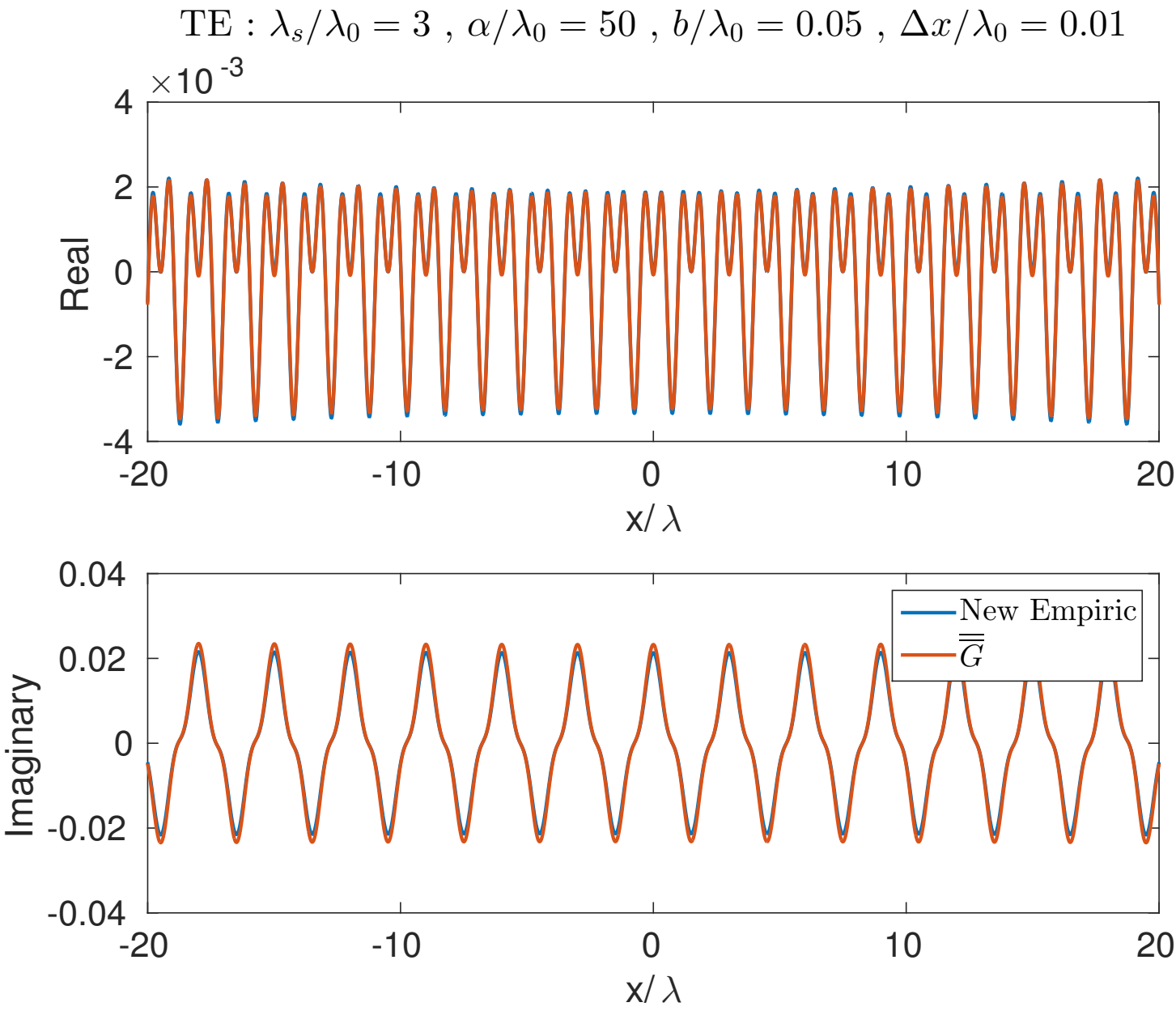


Figure 4.88: TE Empiric Analytic

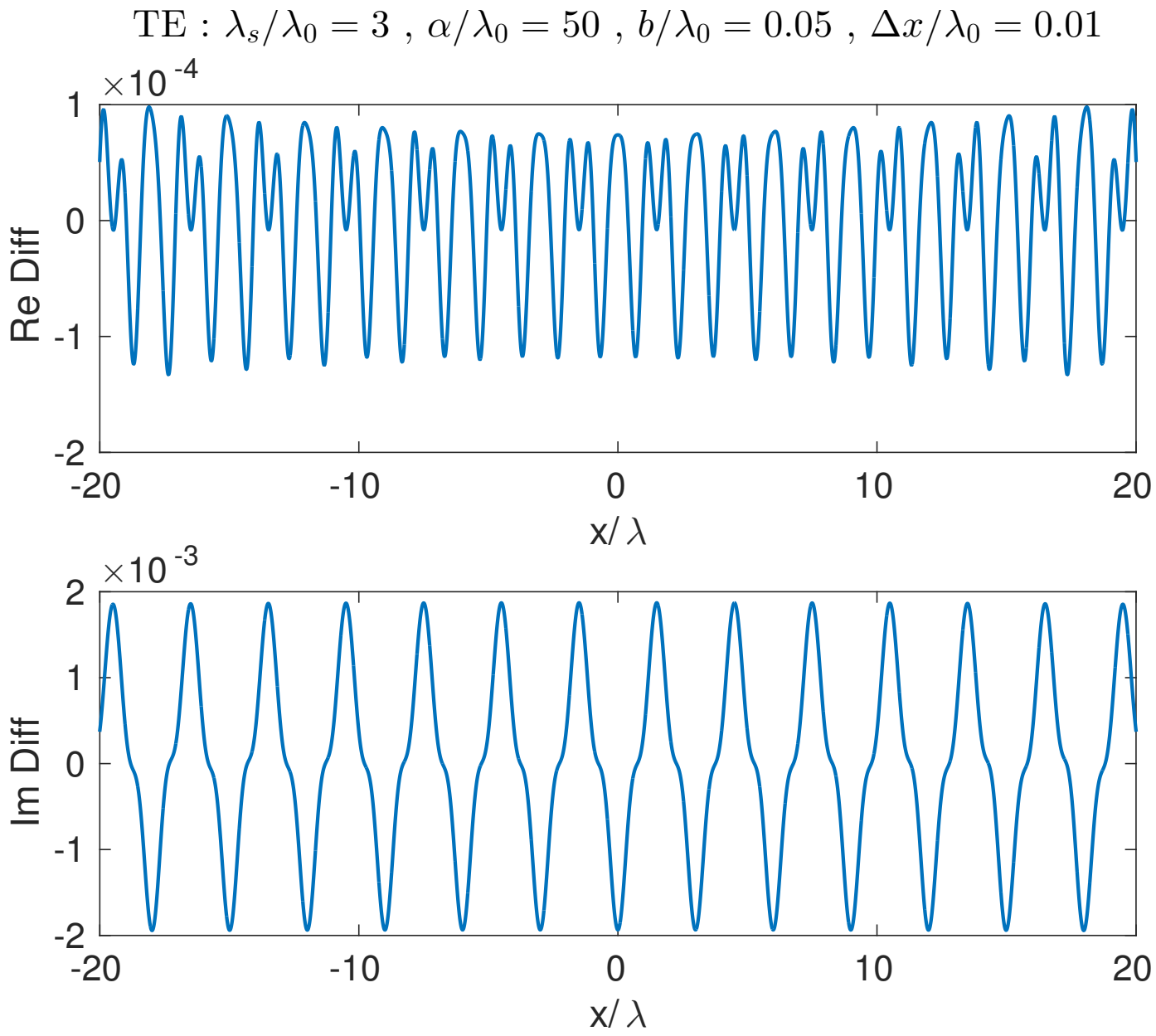


Figure 4.89: TE Empiric Analytic

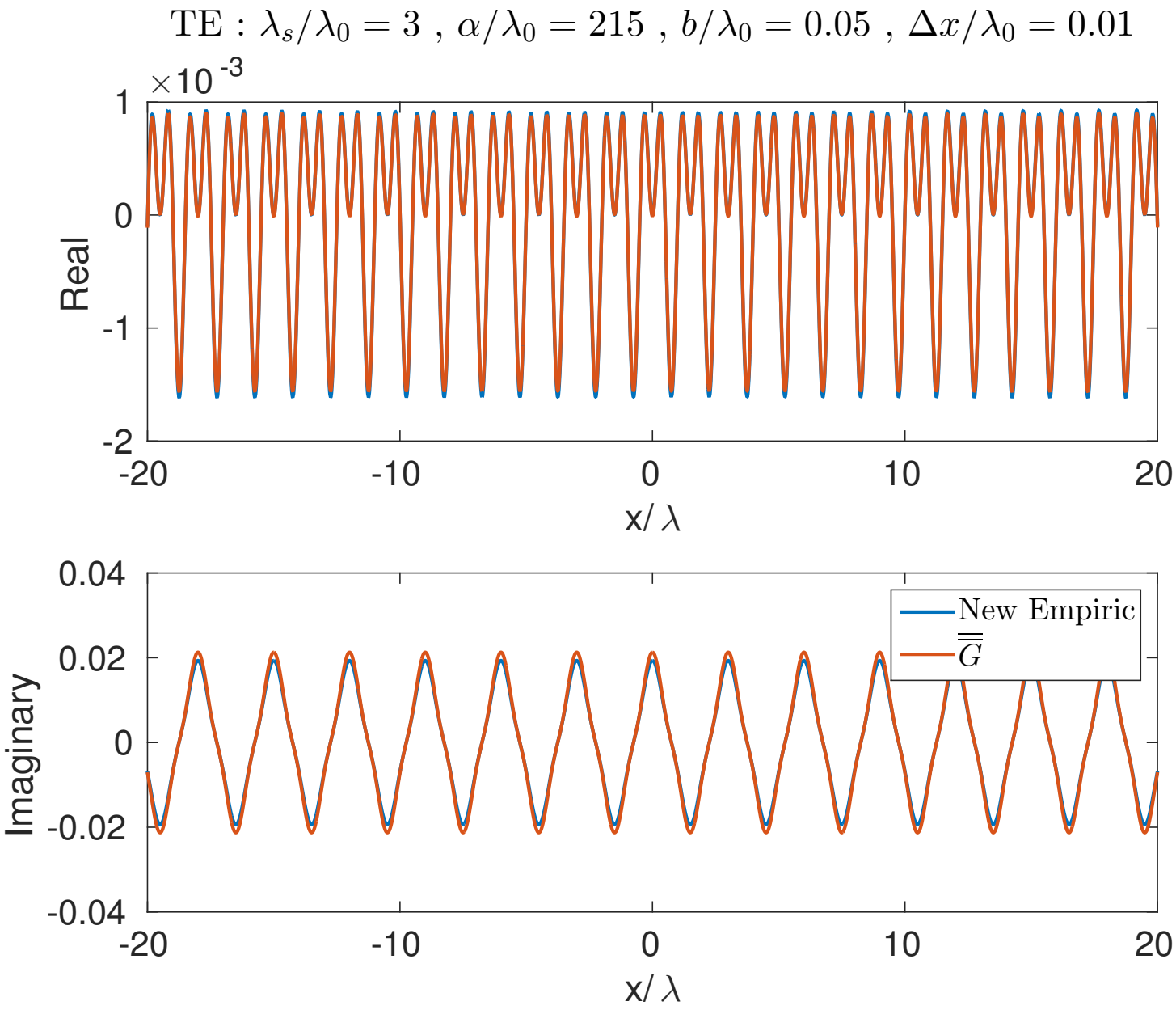


Figure 4.90: TE Empiric Analytic

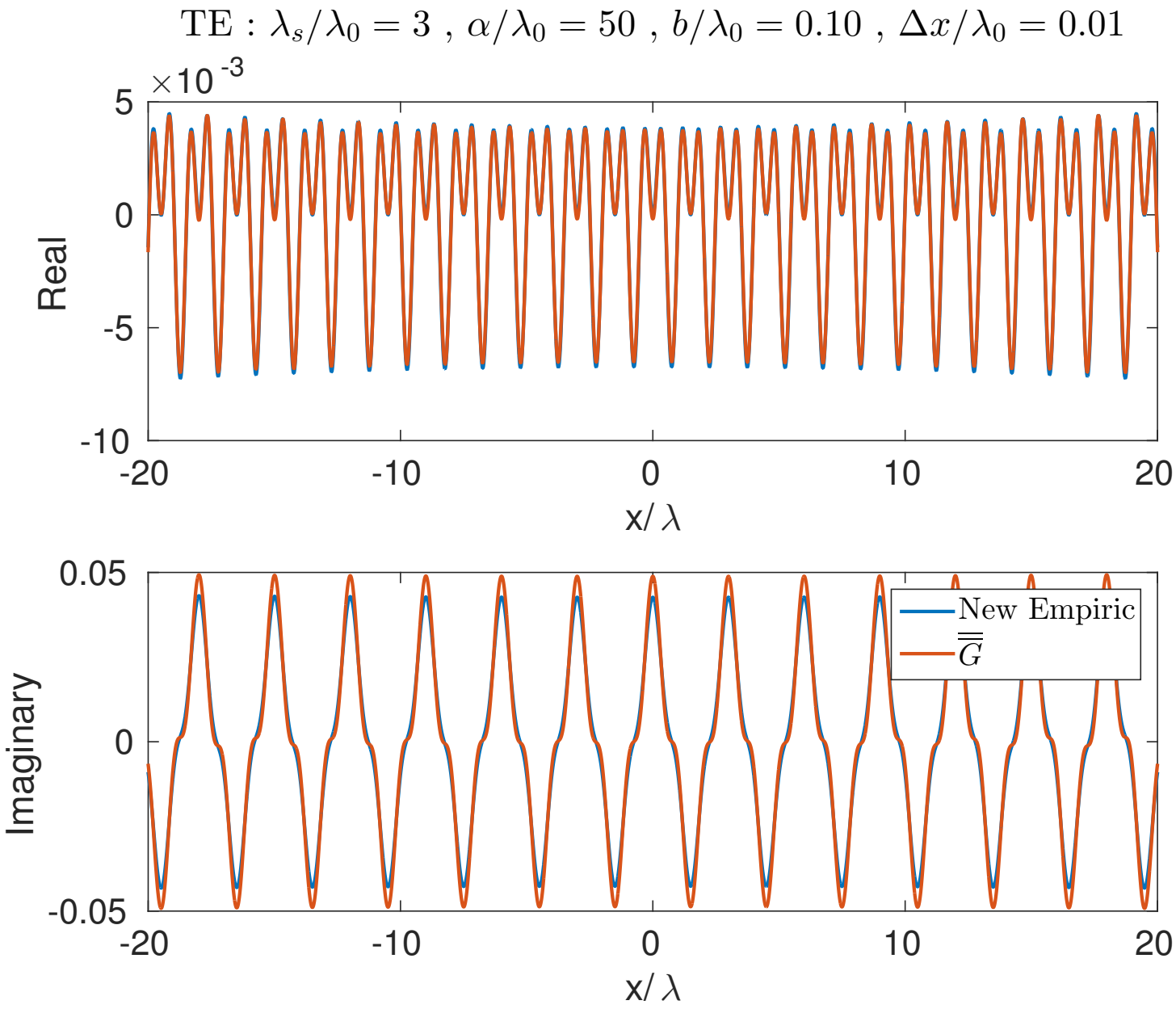


Figure 4.91: TE Empiric Analytic

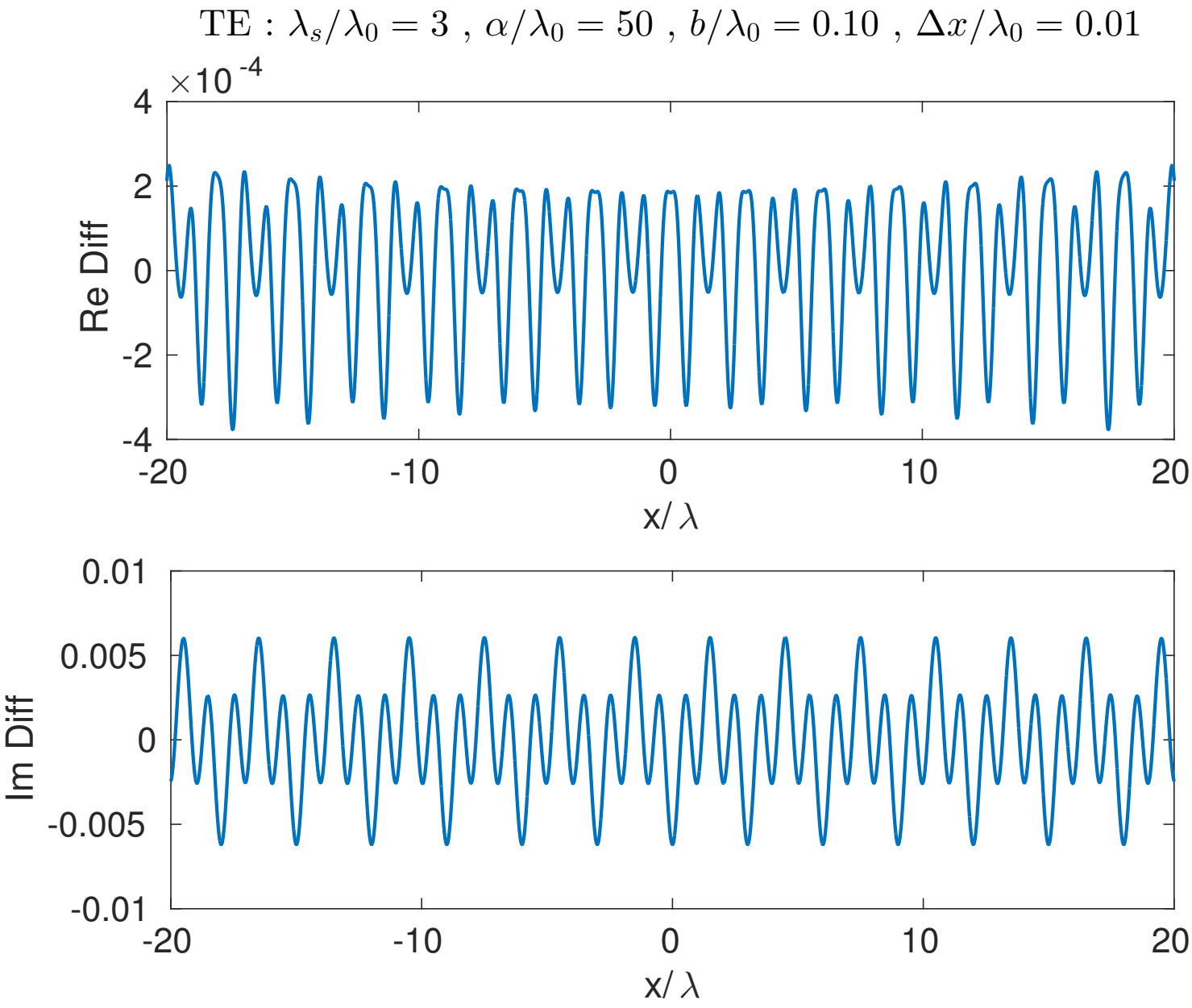


Figure 4.92: TE Empiric Analytic

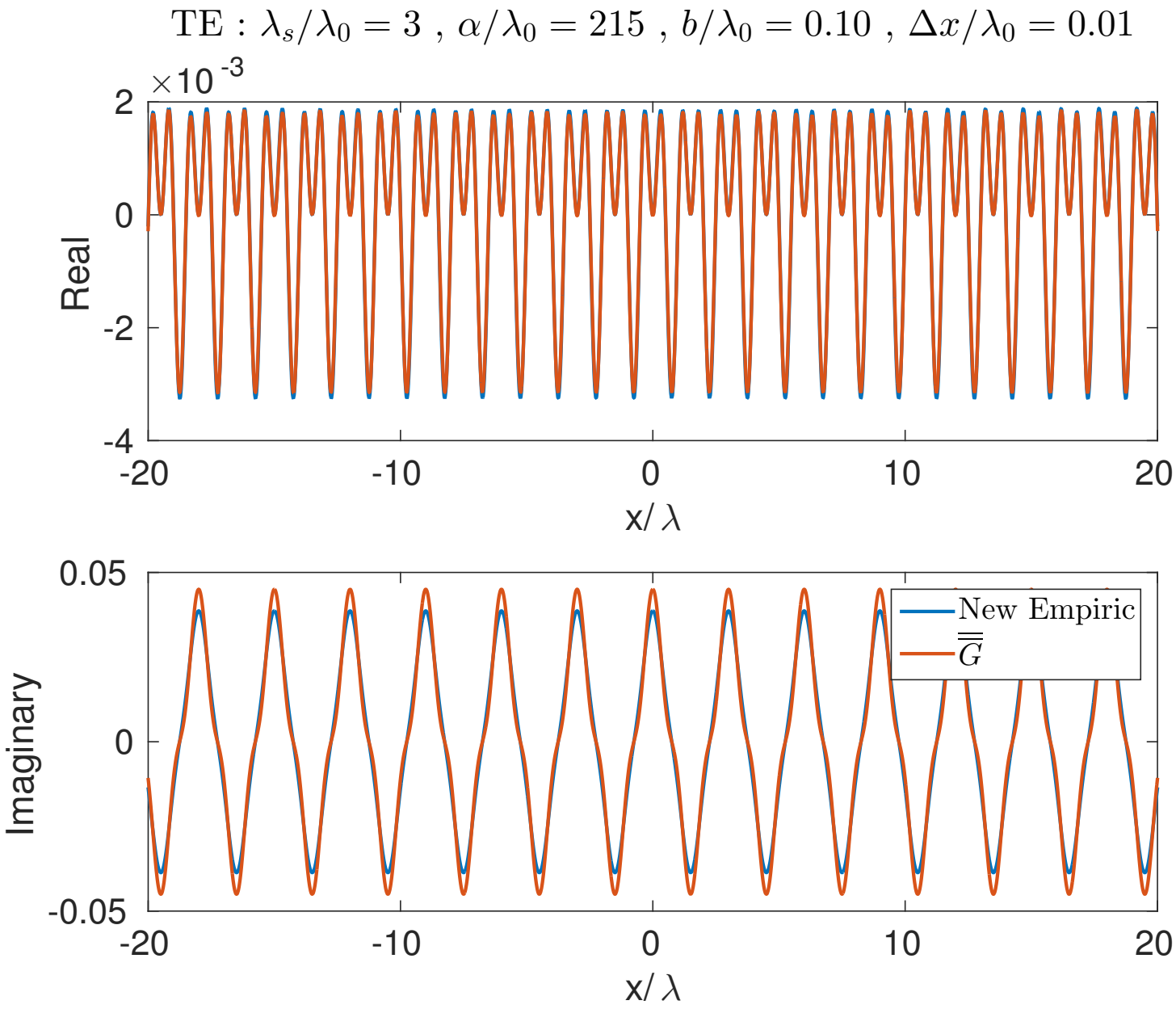


Figure 4.93: TE Empiric Analytic

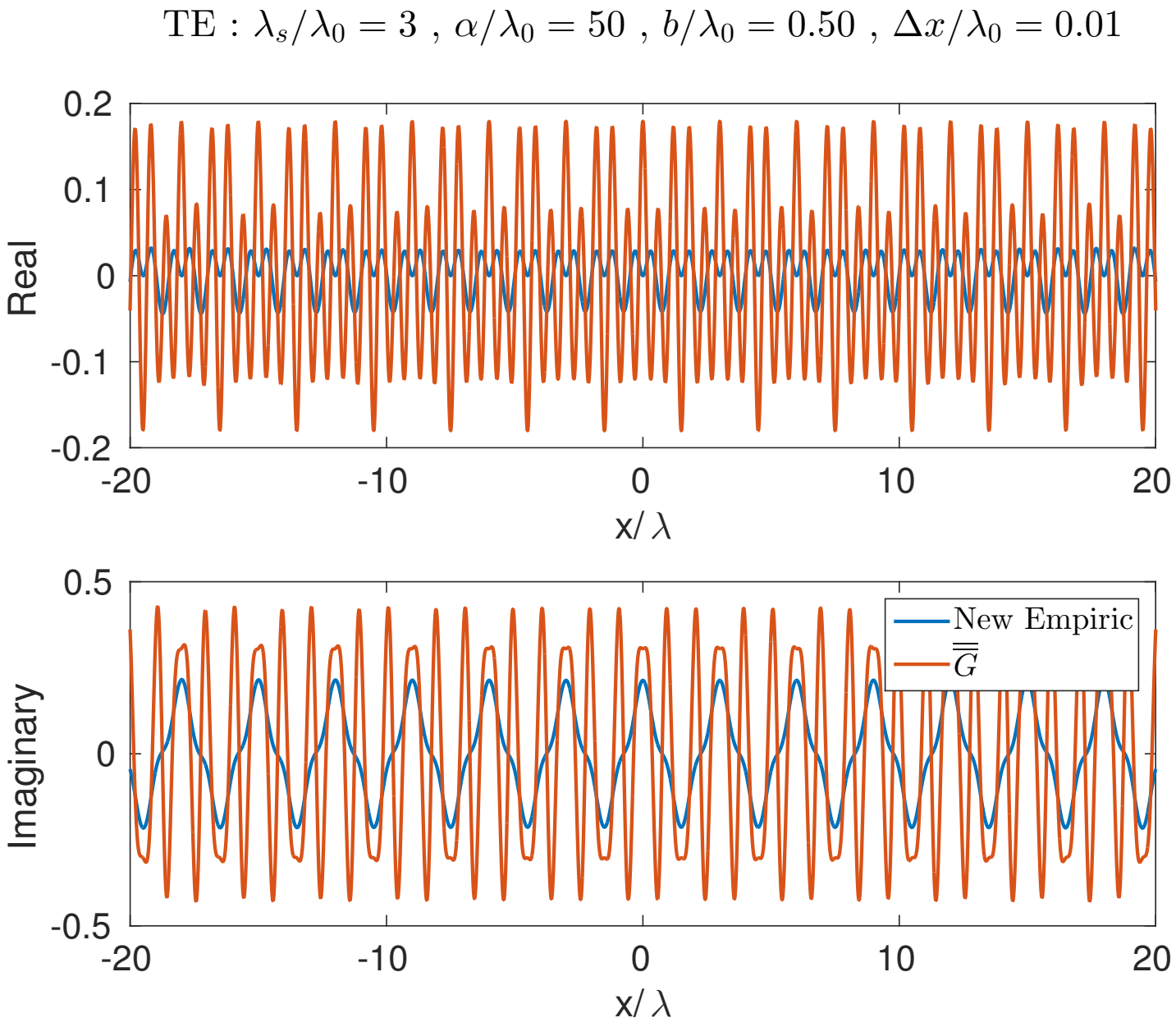


Figure 4.94: TE Empiric Analytic

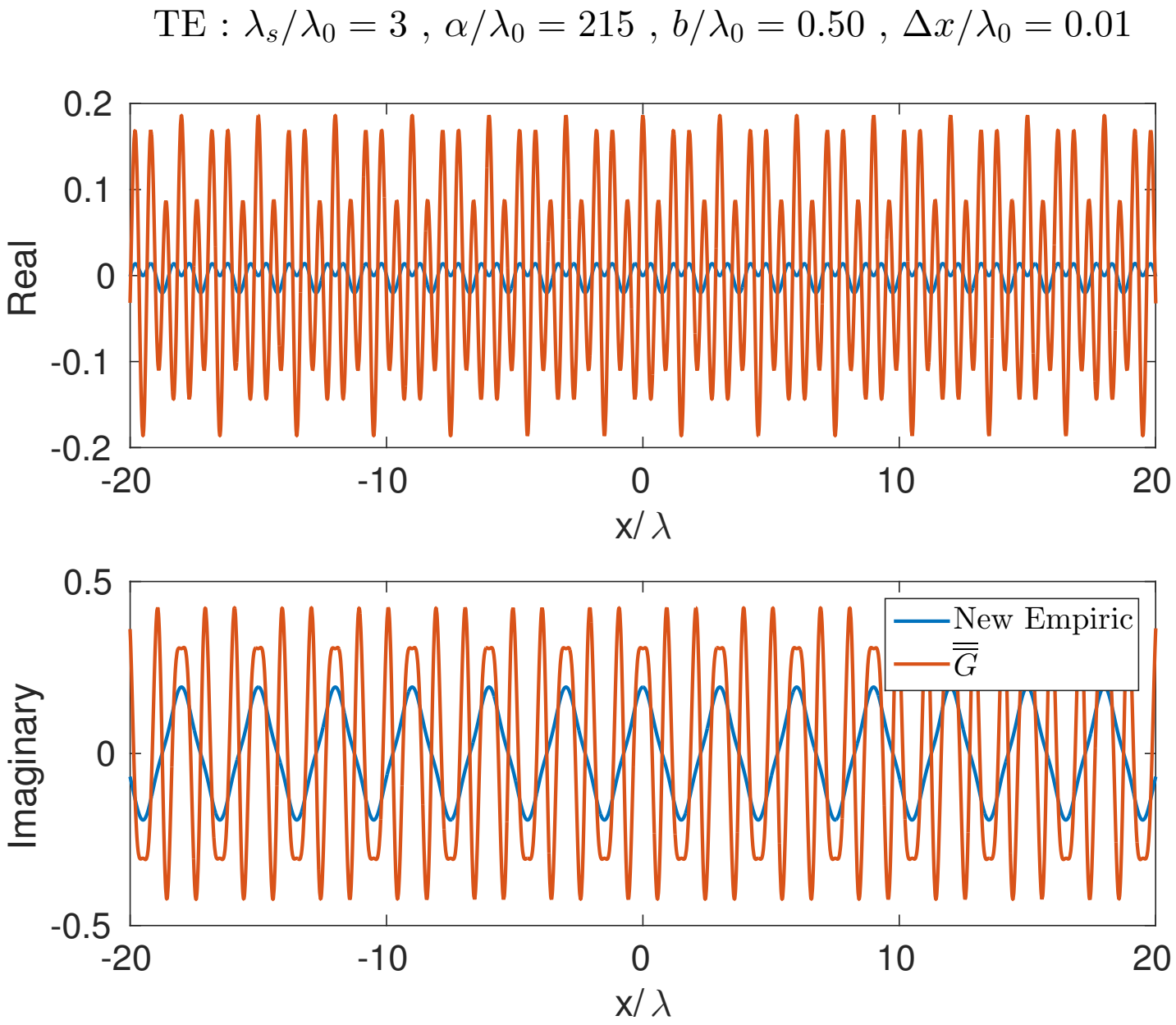


Figure 4.95: TE Empiric Analytic

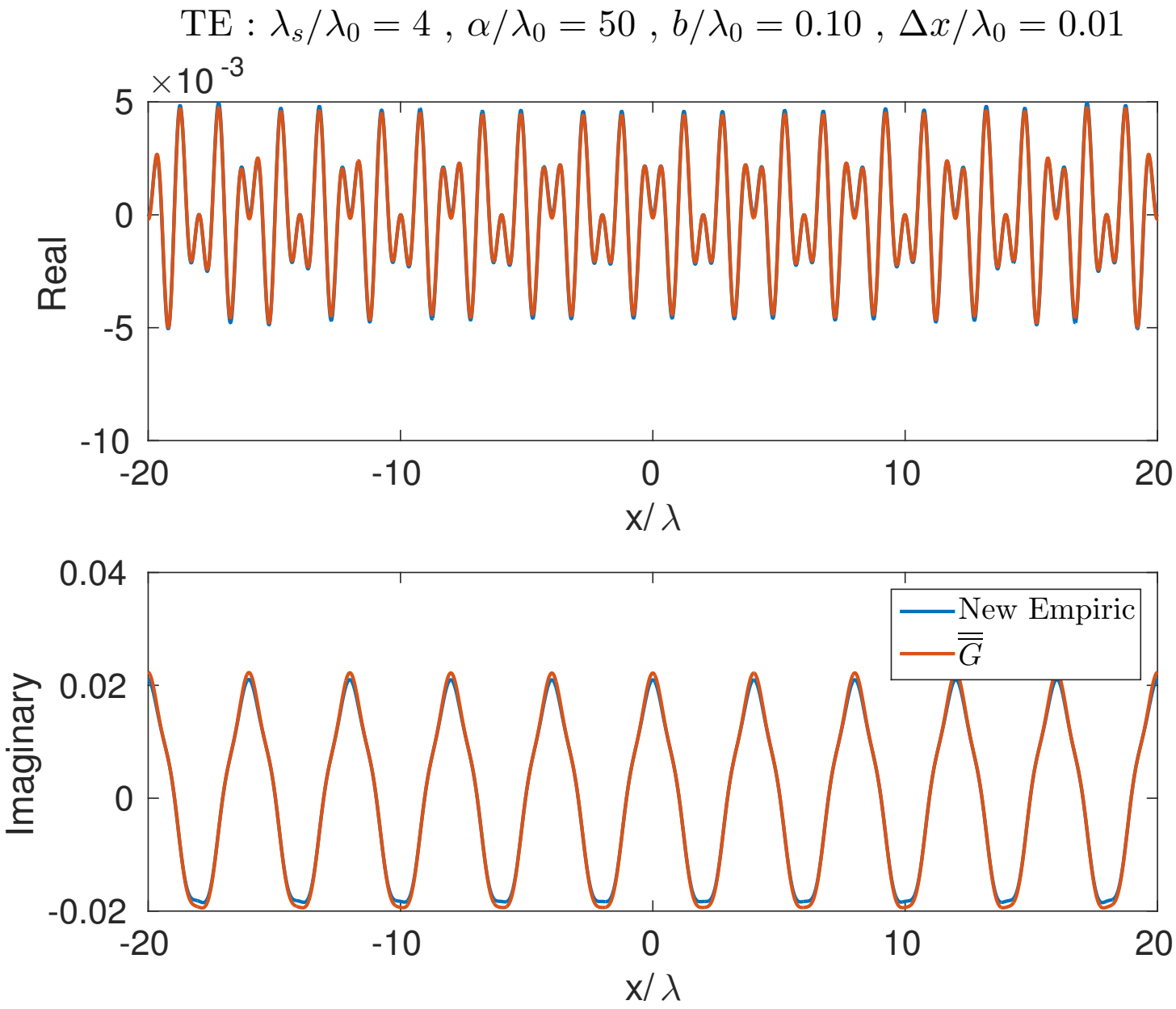


Figure 4.96: TE Empiric Analytic

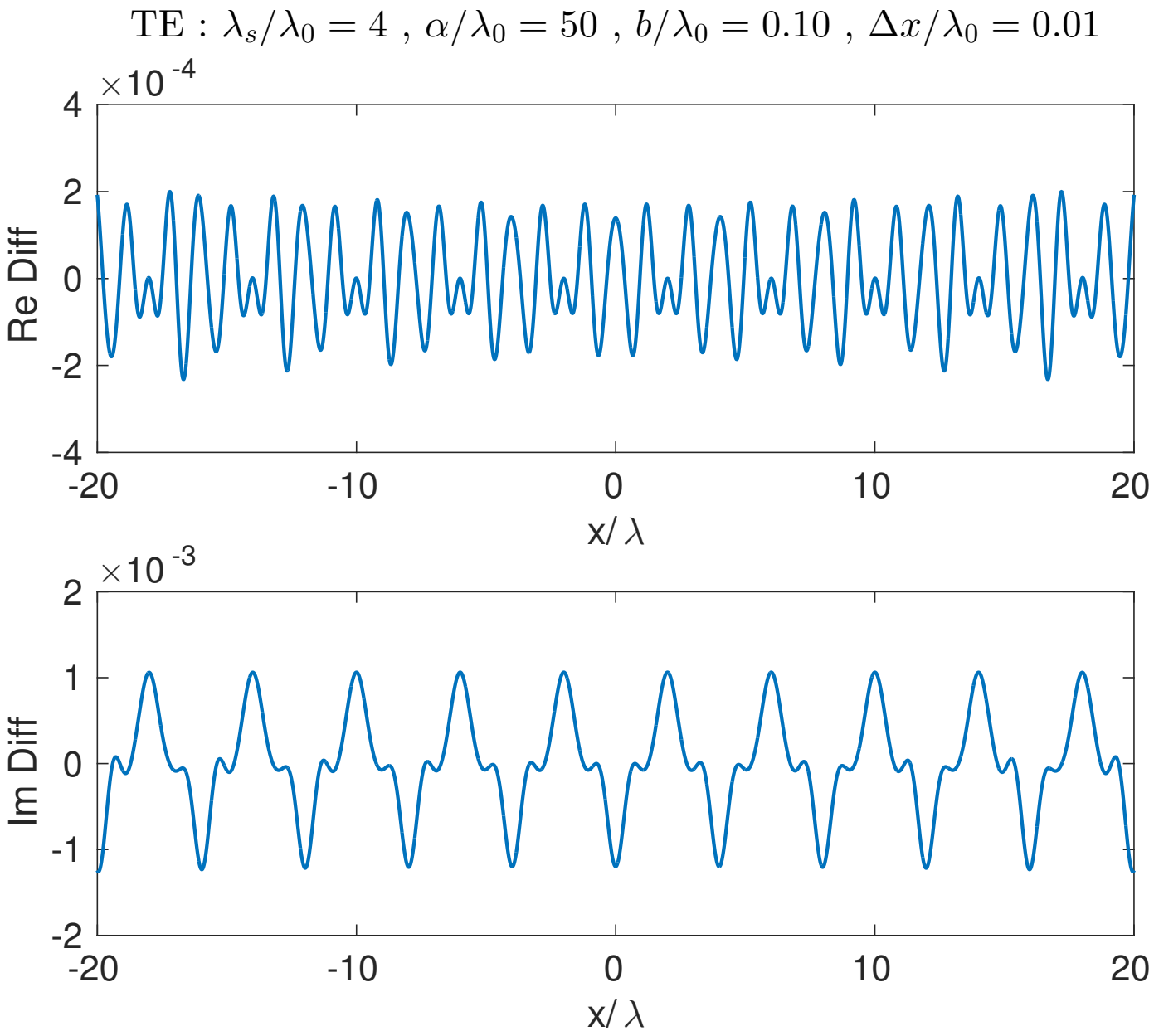


Figure 4.97: TE Empiric Analytic

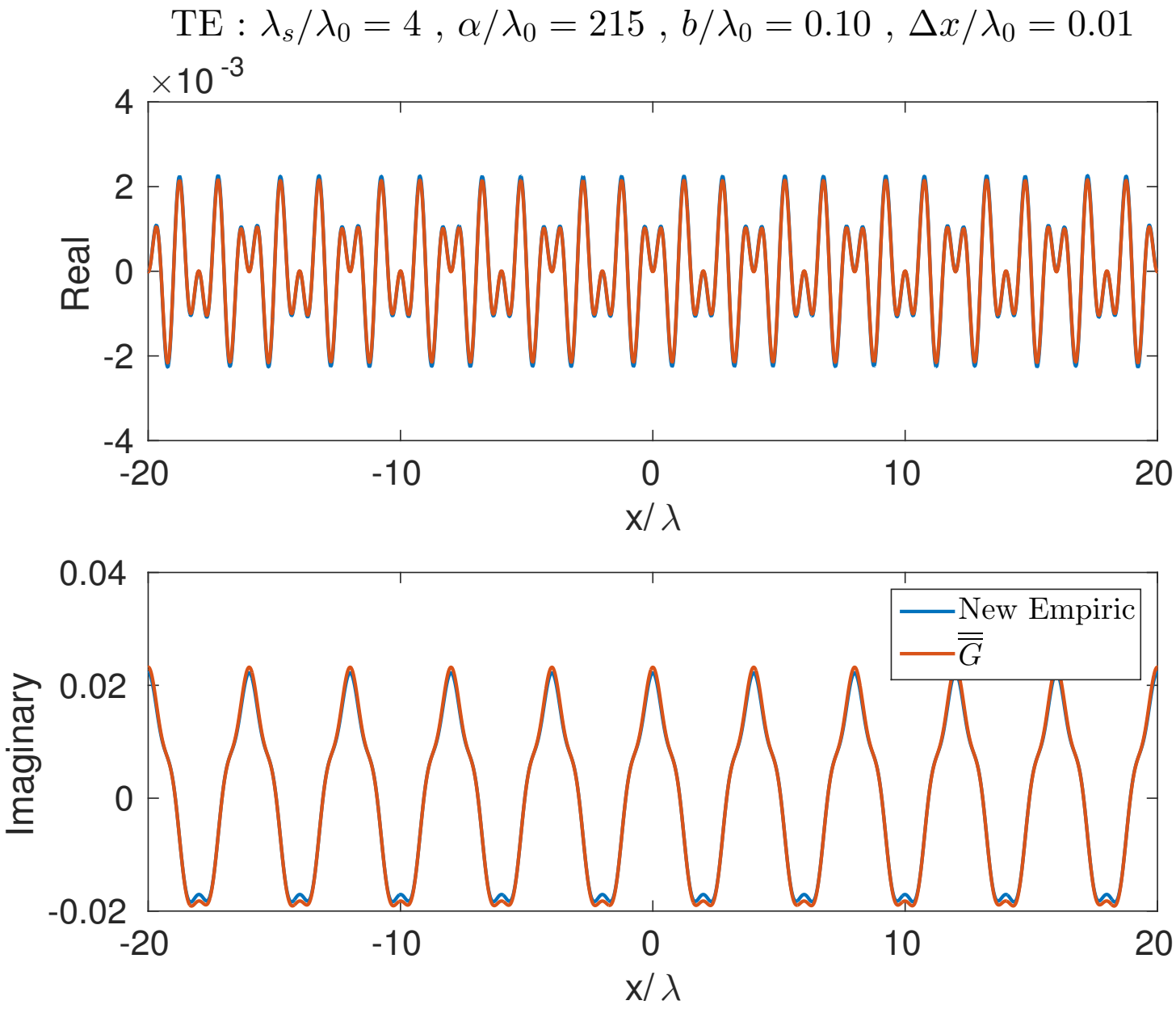


Figure 4.98: TE Empiric Analytic

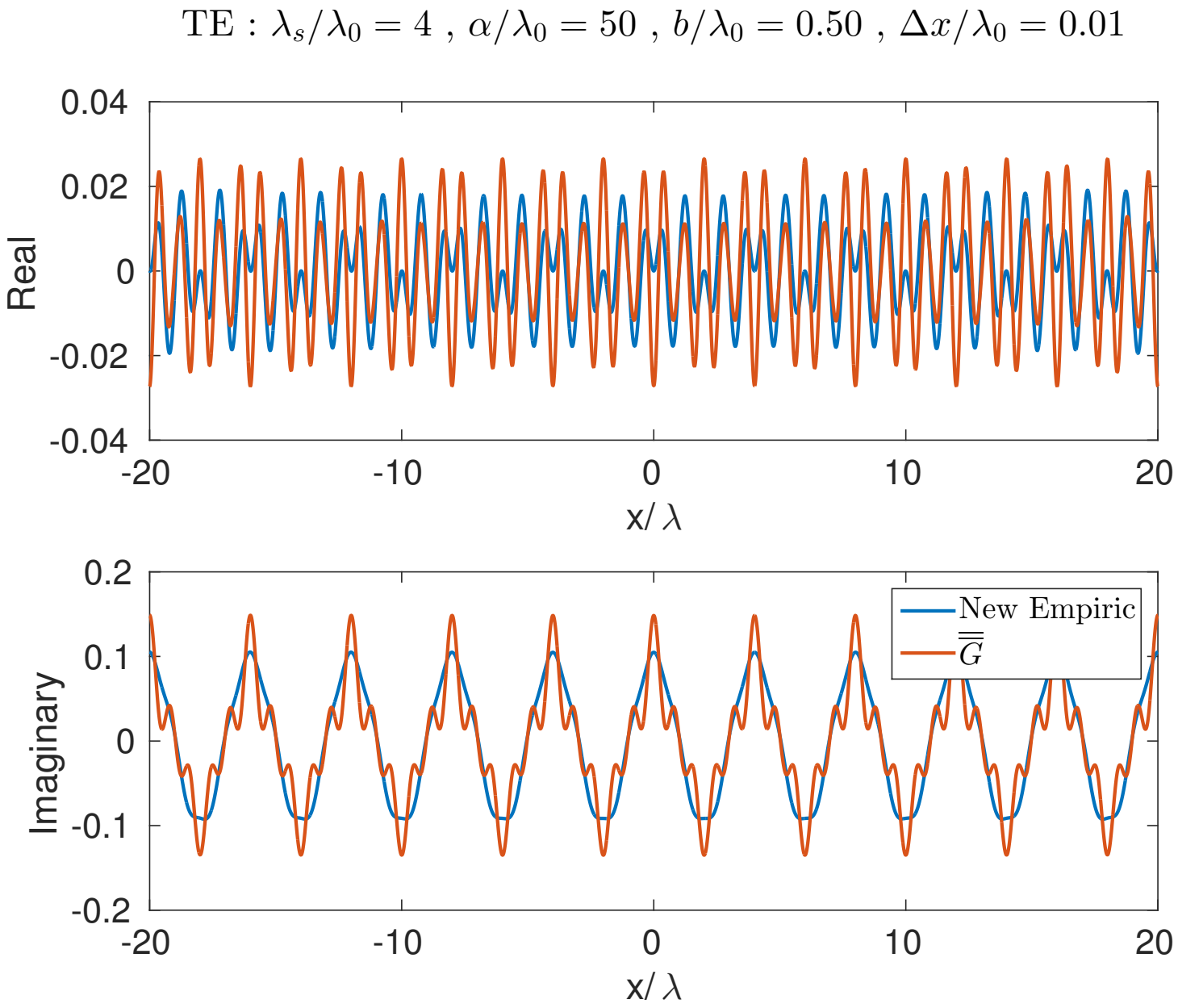


Figure 4.99: TE Empiric Analytic

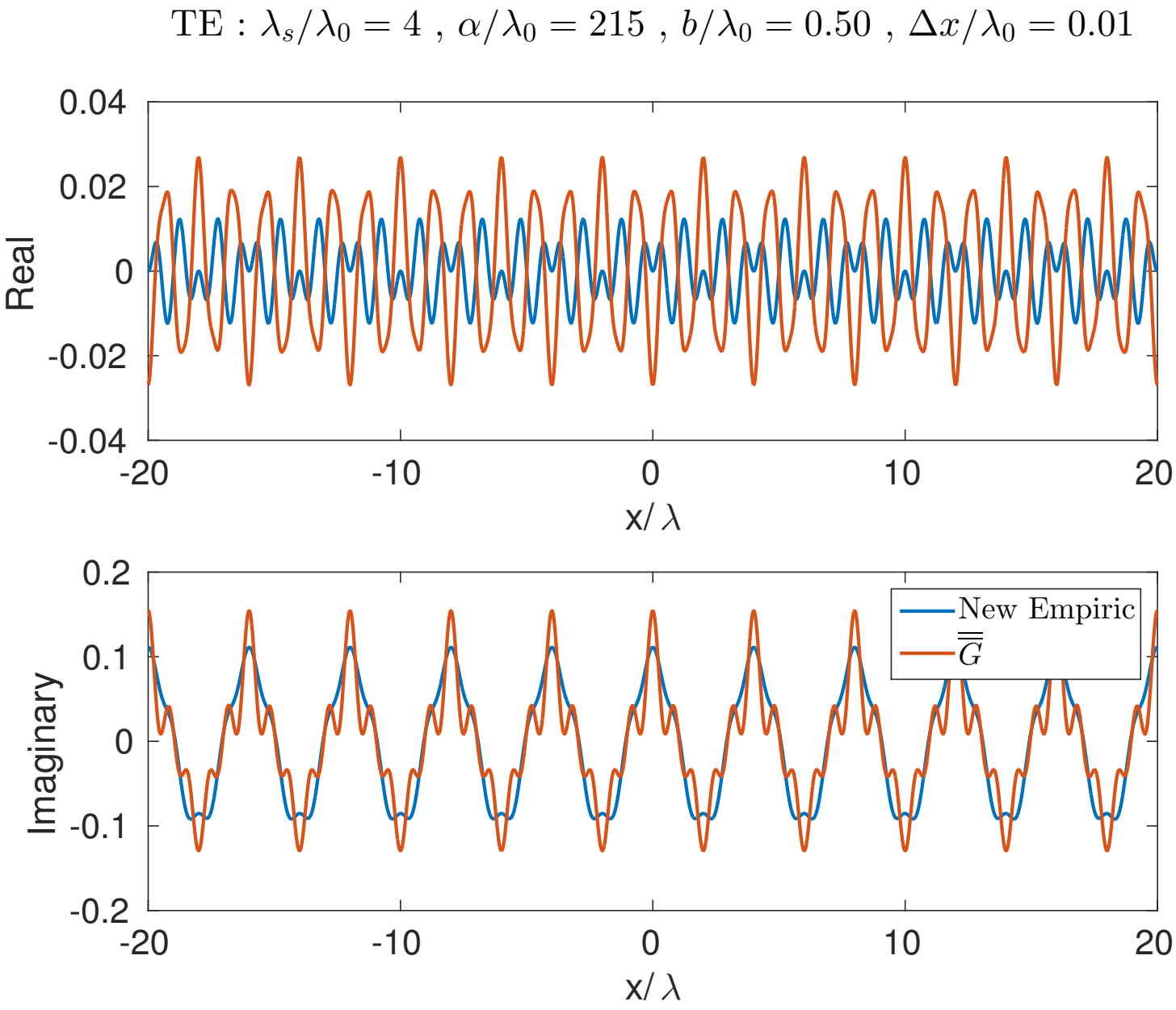


Figure 4.100: TE Empiric Analytic

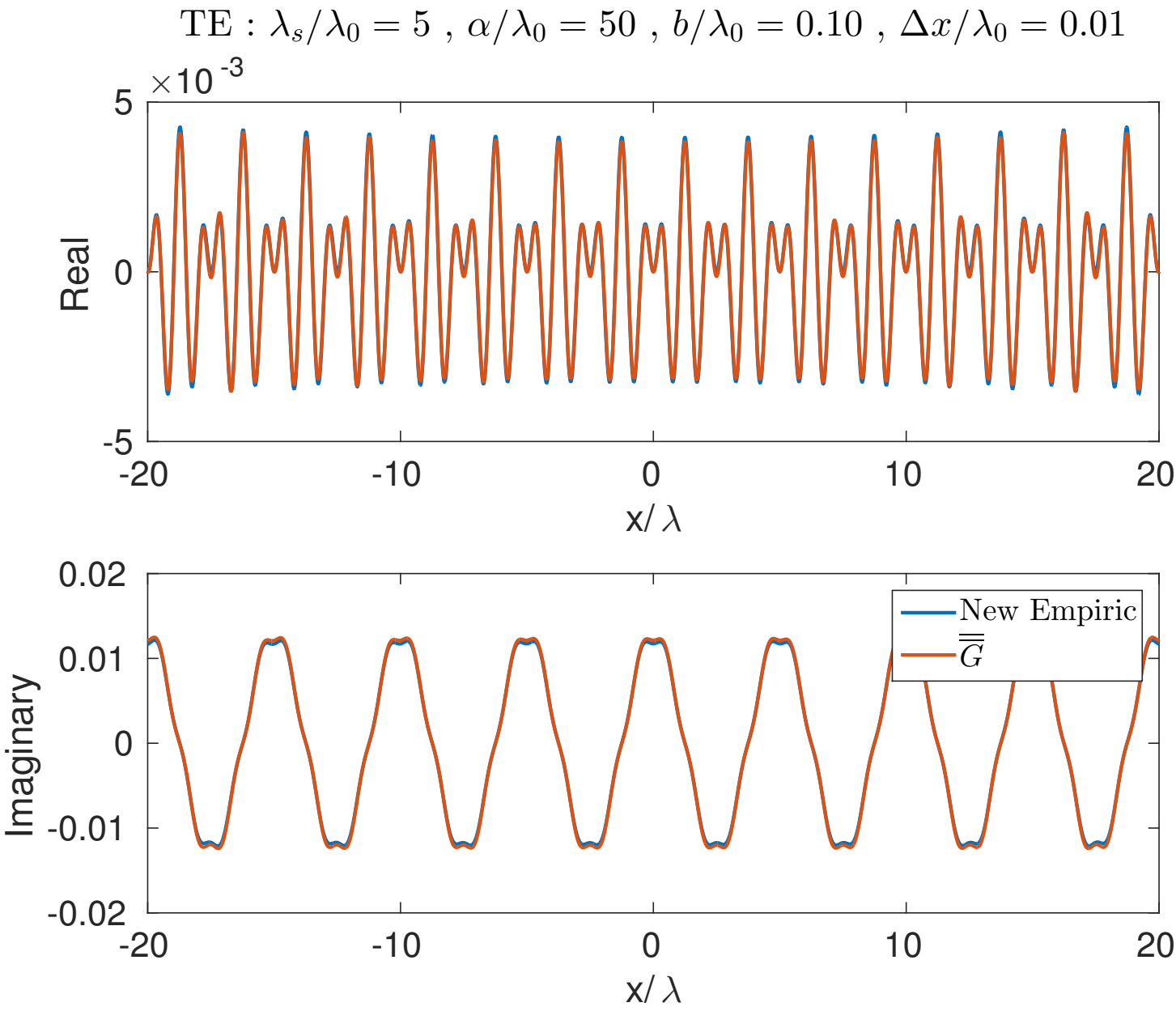


Figure 4.101: TE Empiric Analytic

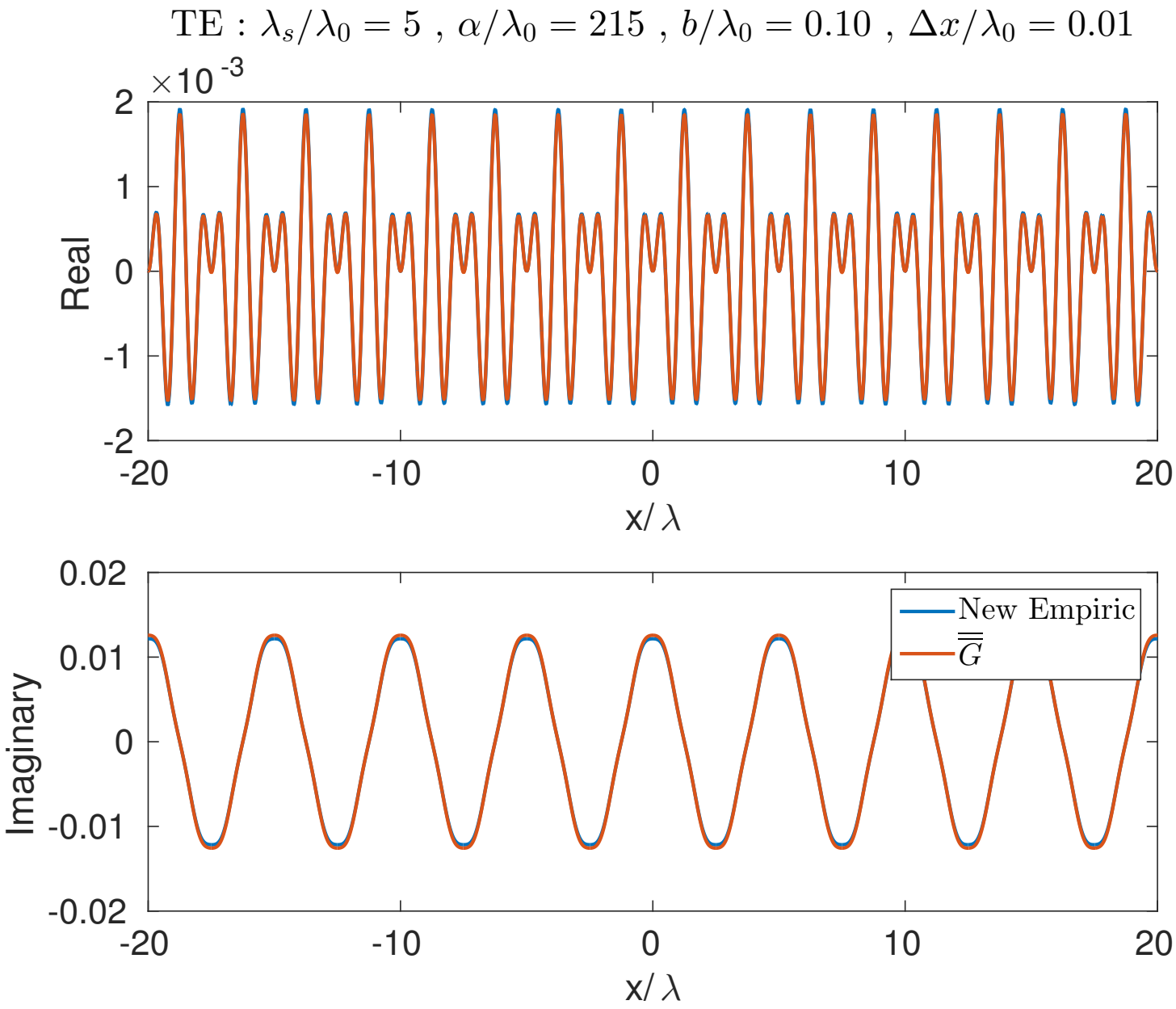


Figure 4.102: TE Empiric Analytic

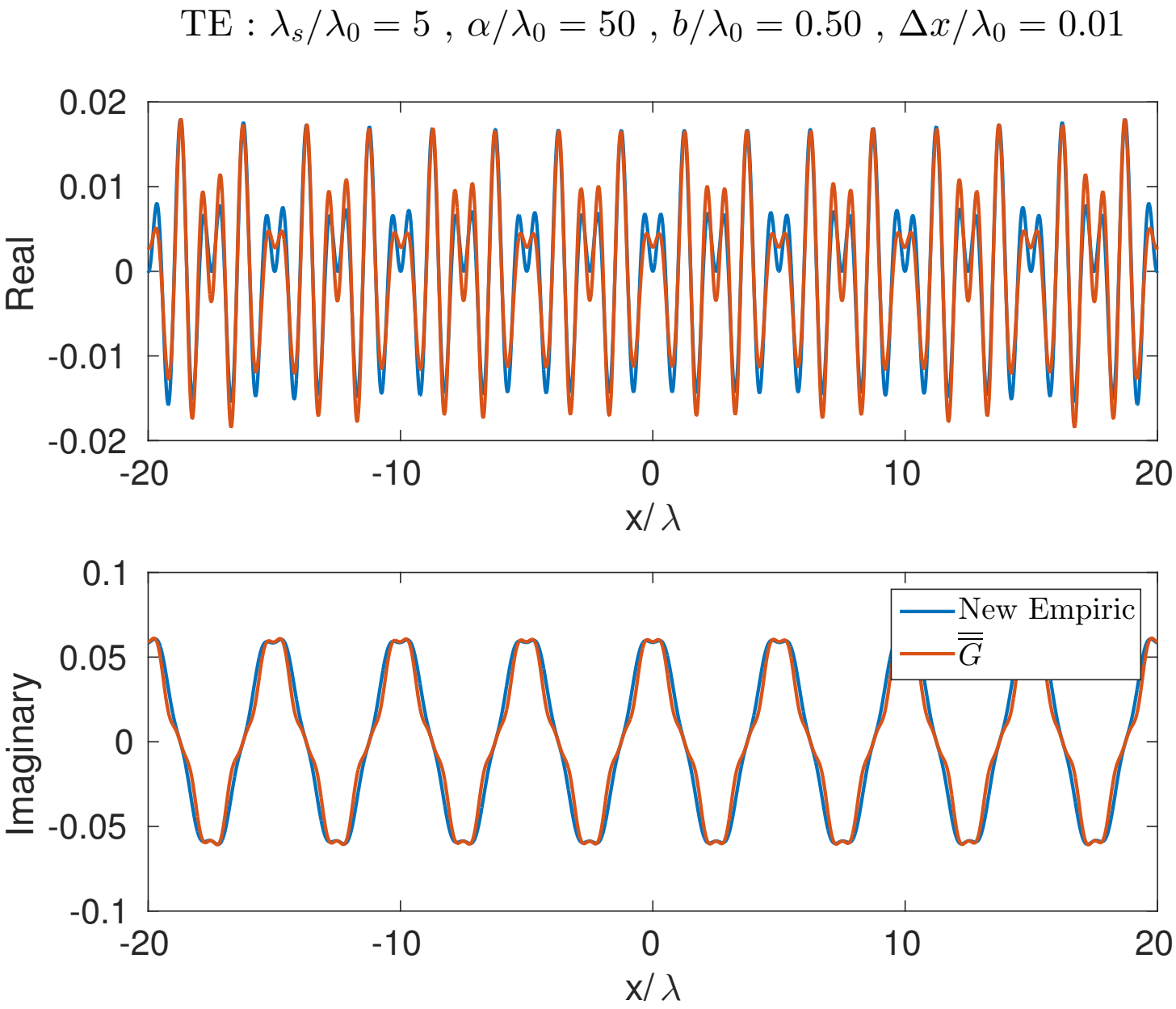


Figure 4.103: TE Empiric Analytic

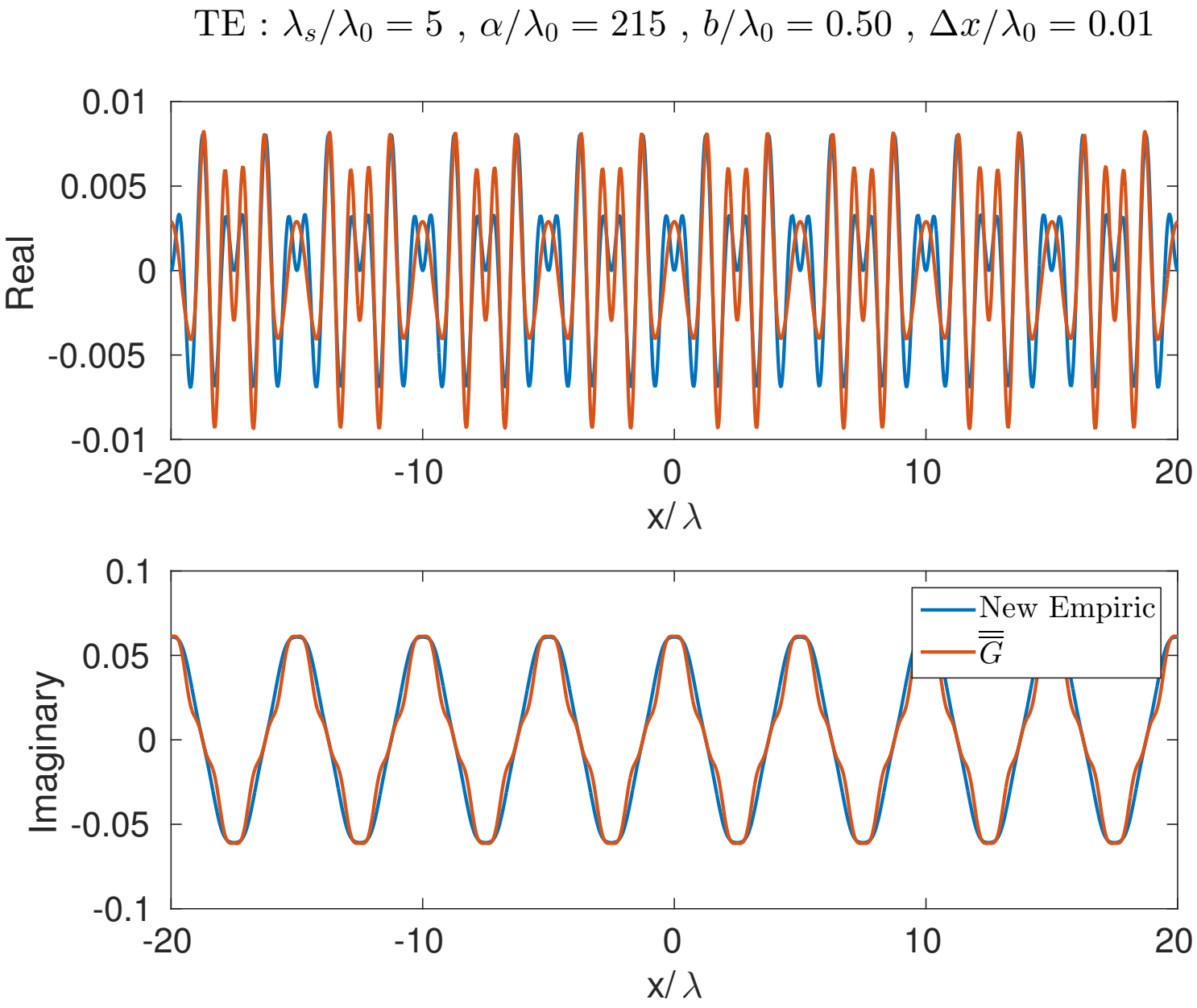


Figure 4.104: TE Empiric Analytic

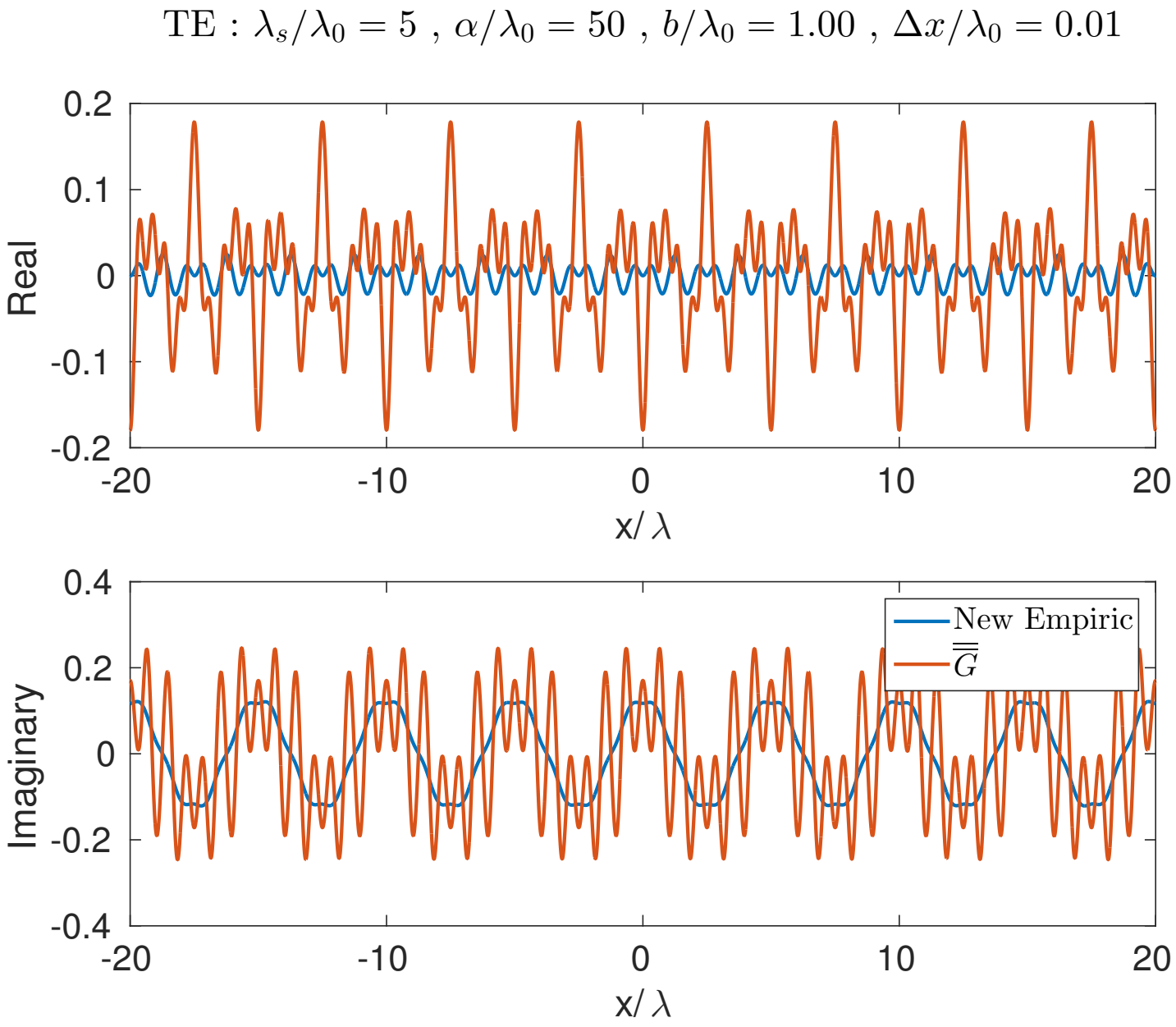


Figure 4.105: TE Empiric Analytic

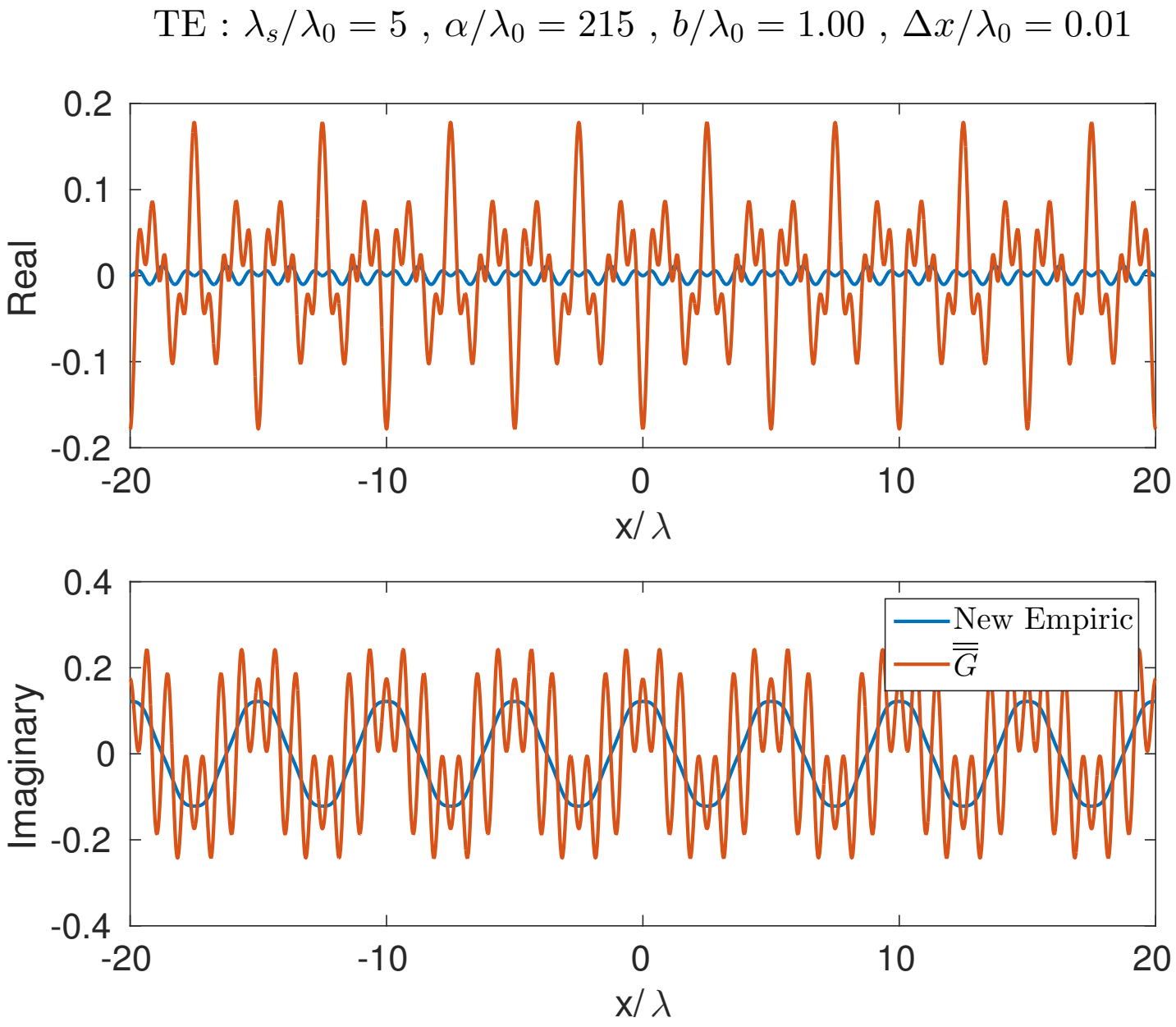


Figure 4.106: TE Empiric Analytic

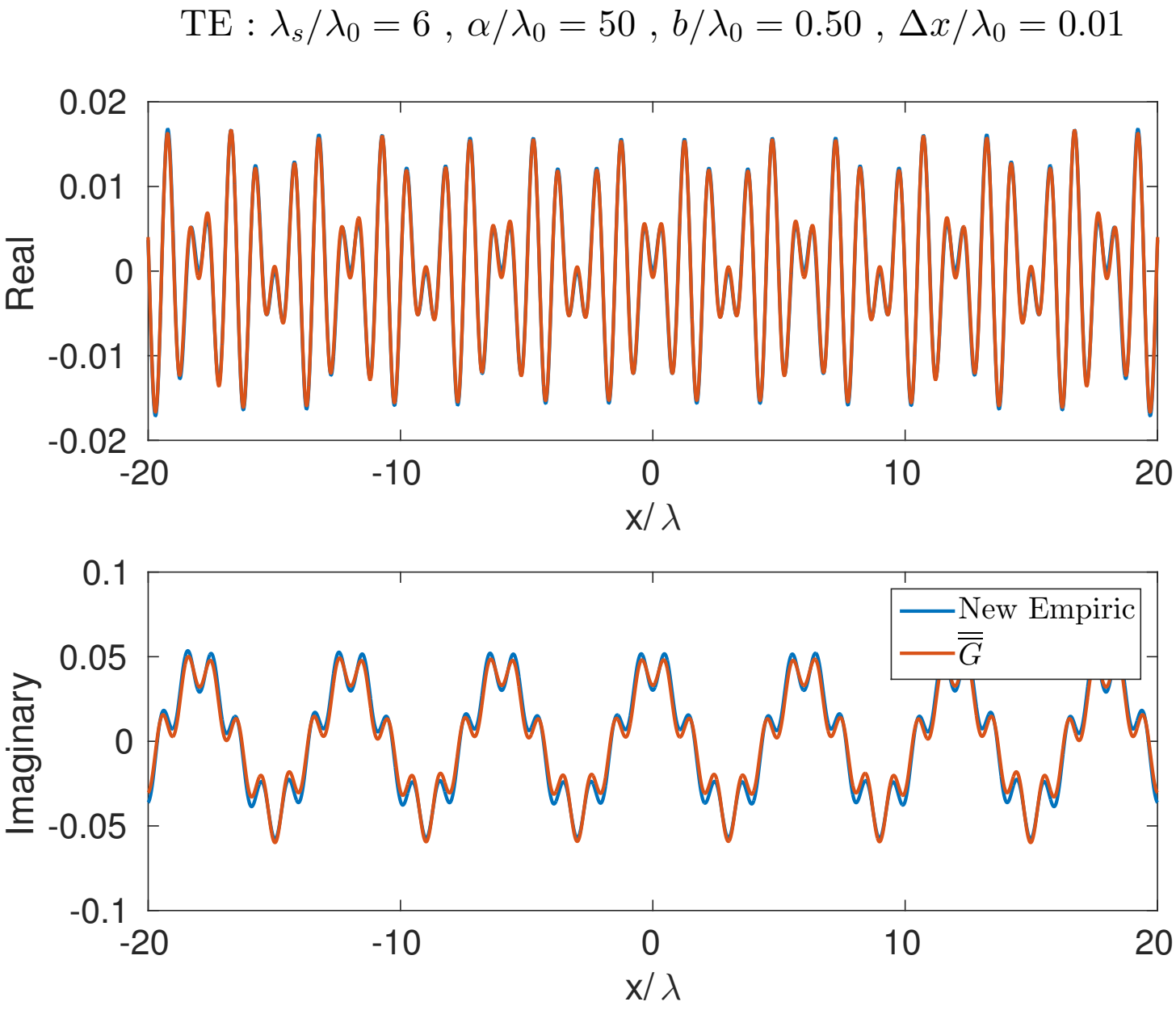


Figure 4.107: TE Empiric Analytic

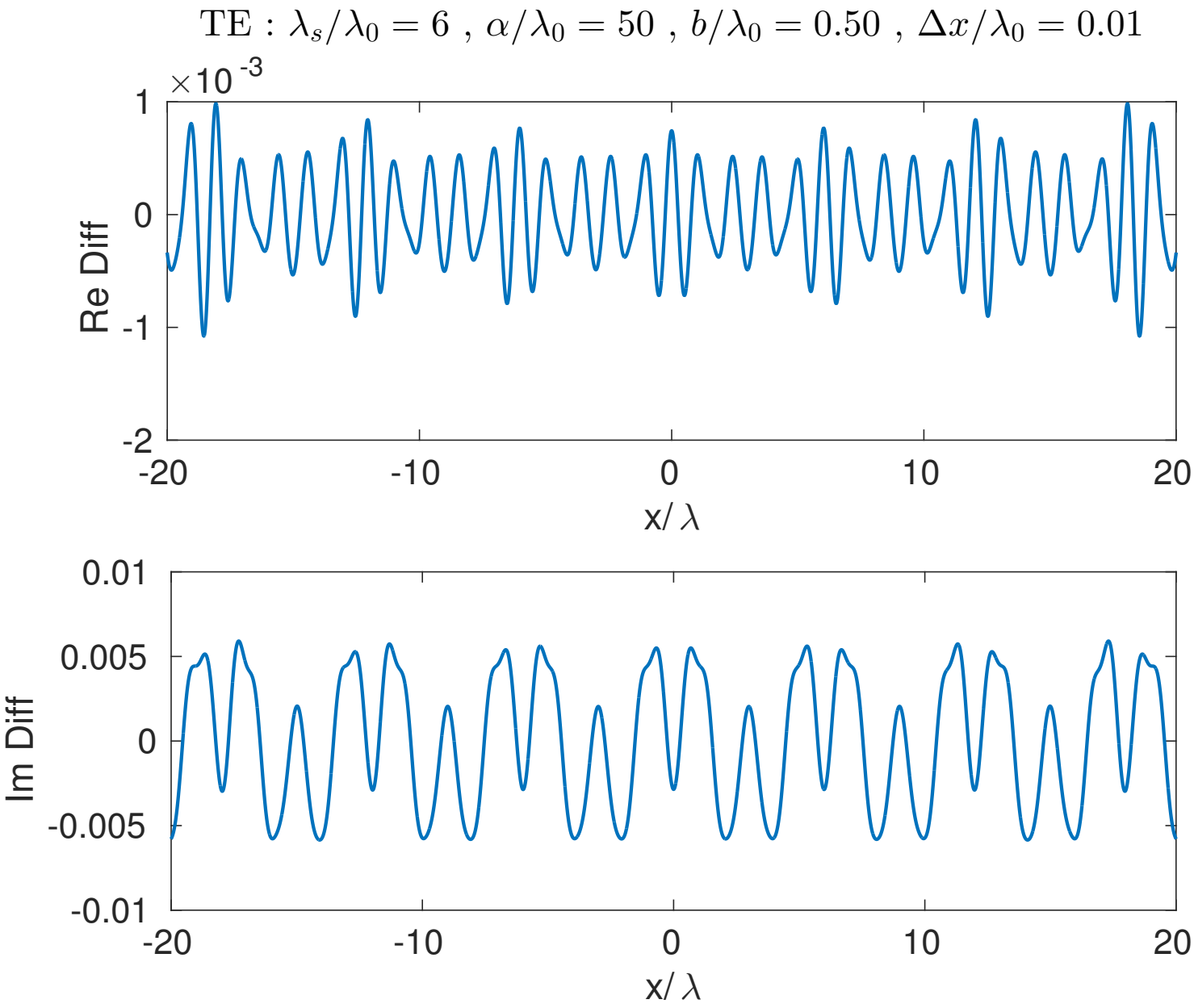


Figure 4.108: TE Empiric Analytic

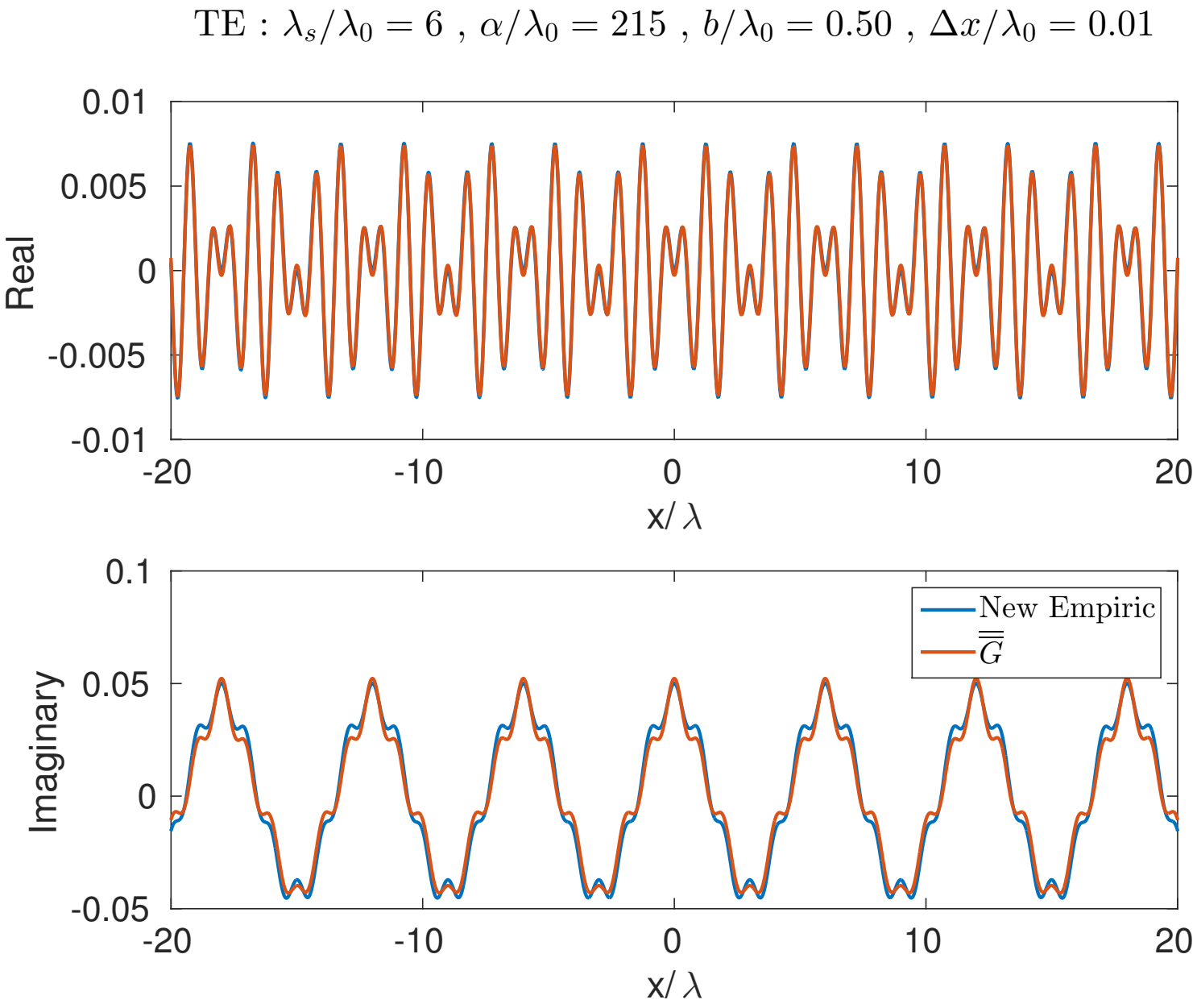


Figure 4.109: TE Empiric Analytic

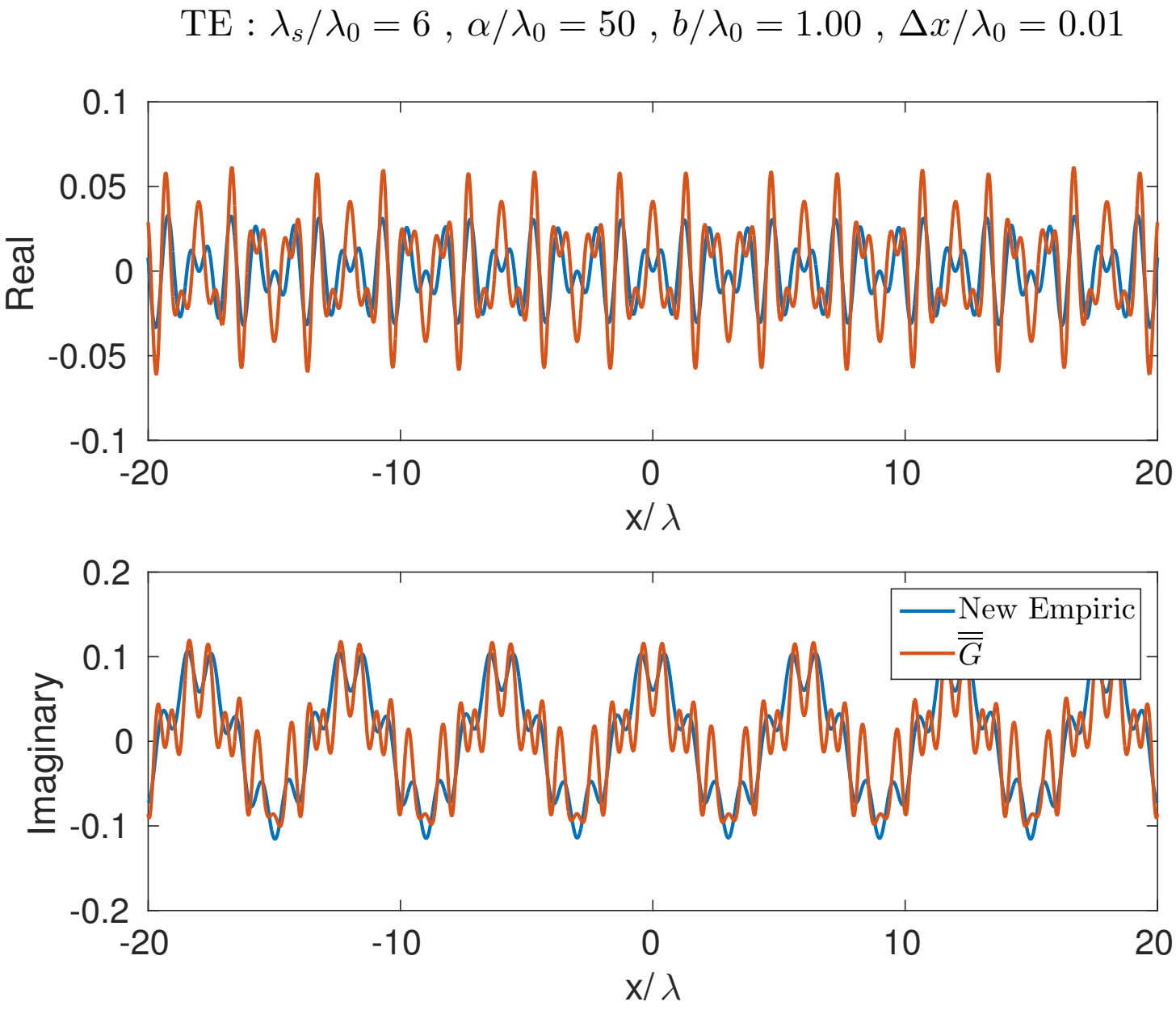


Figure 4.110: TE Empiric Analytic

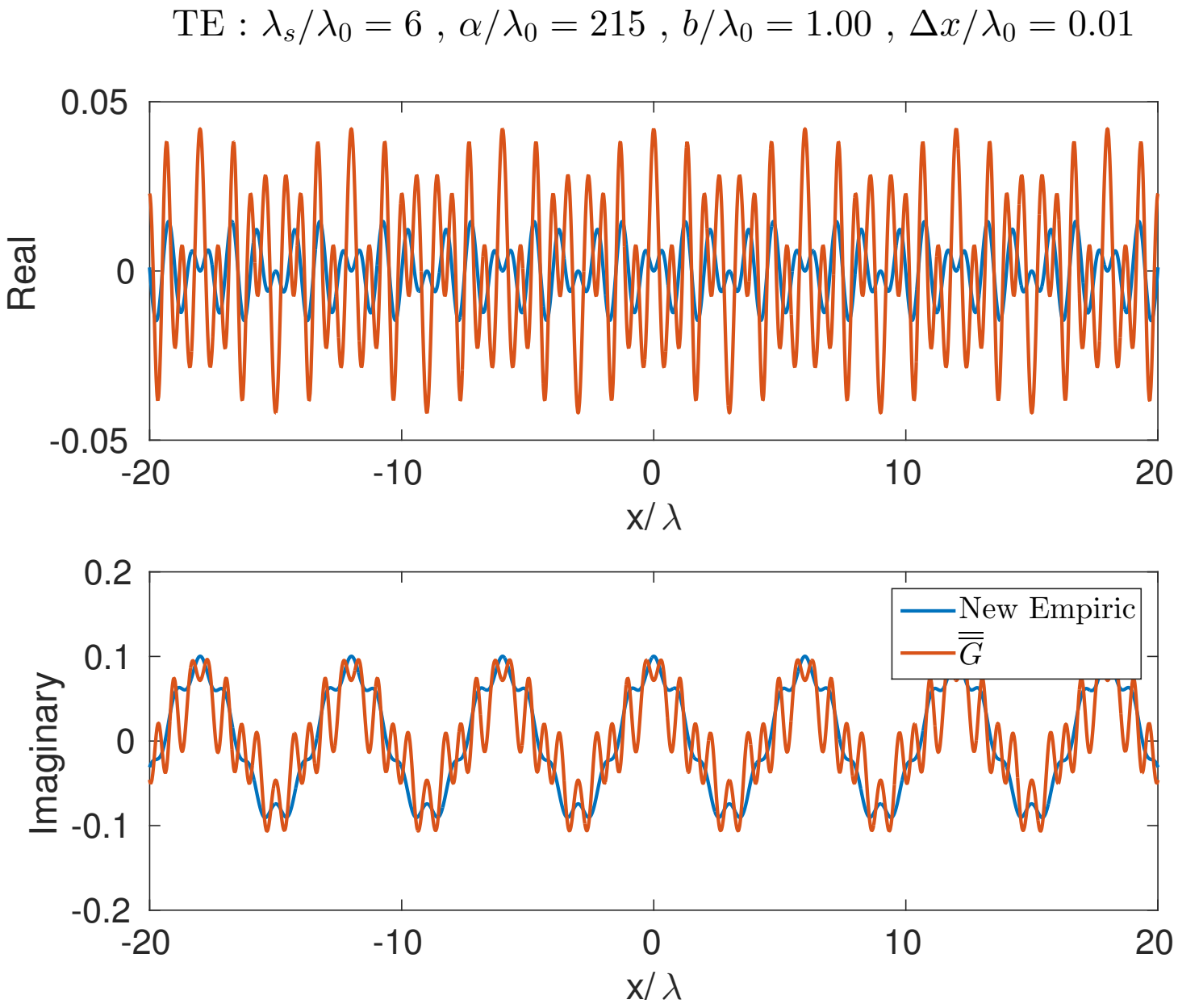


Figure 4.111: TE Empiric Analytic

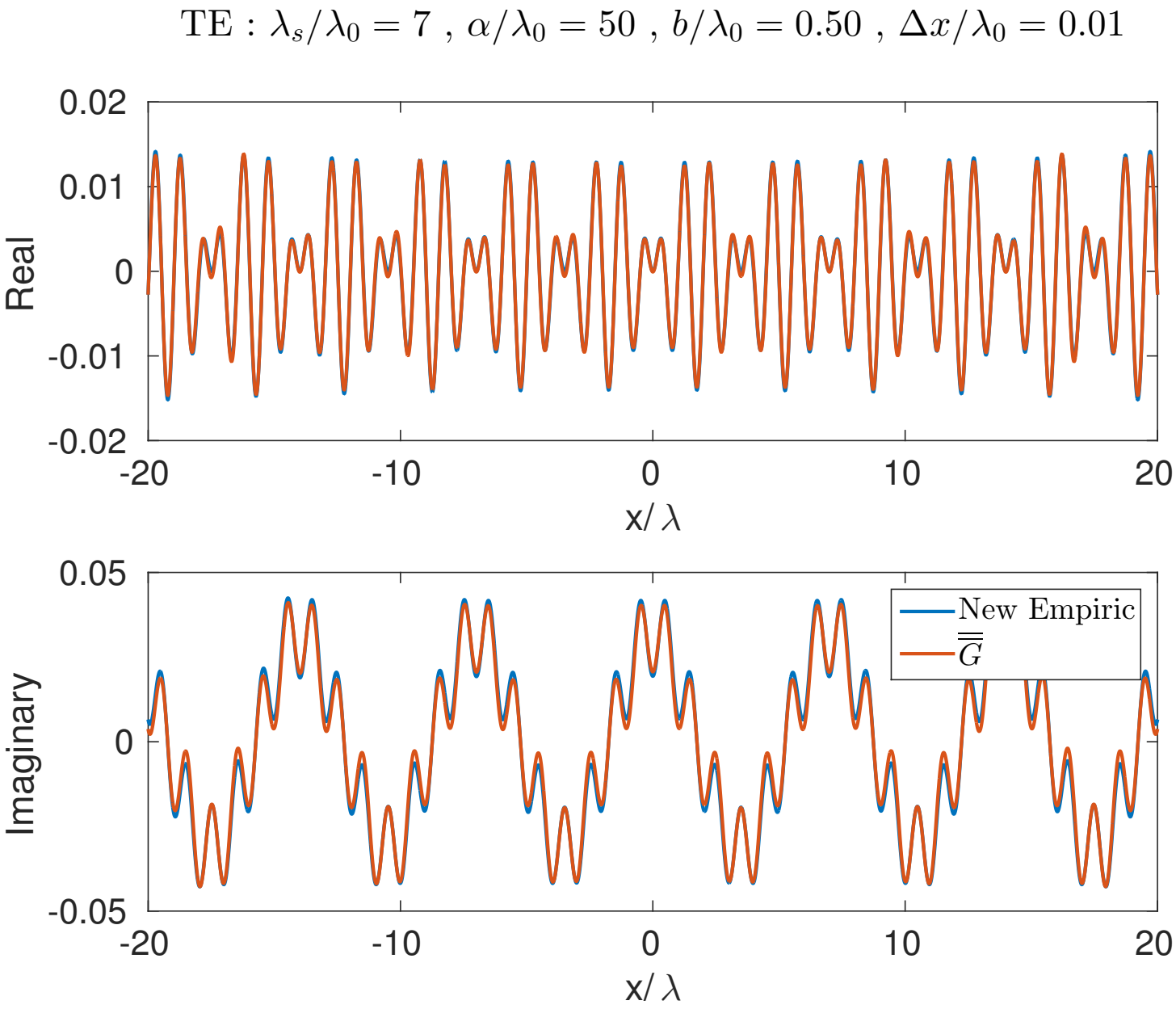


Figure 4.112: TE Empiric Analytic

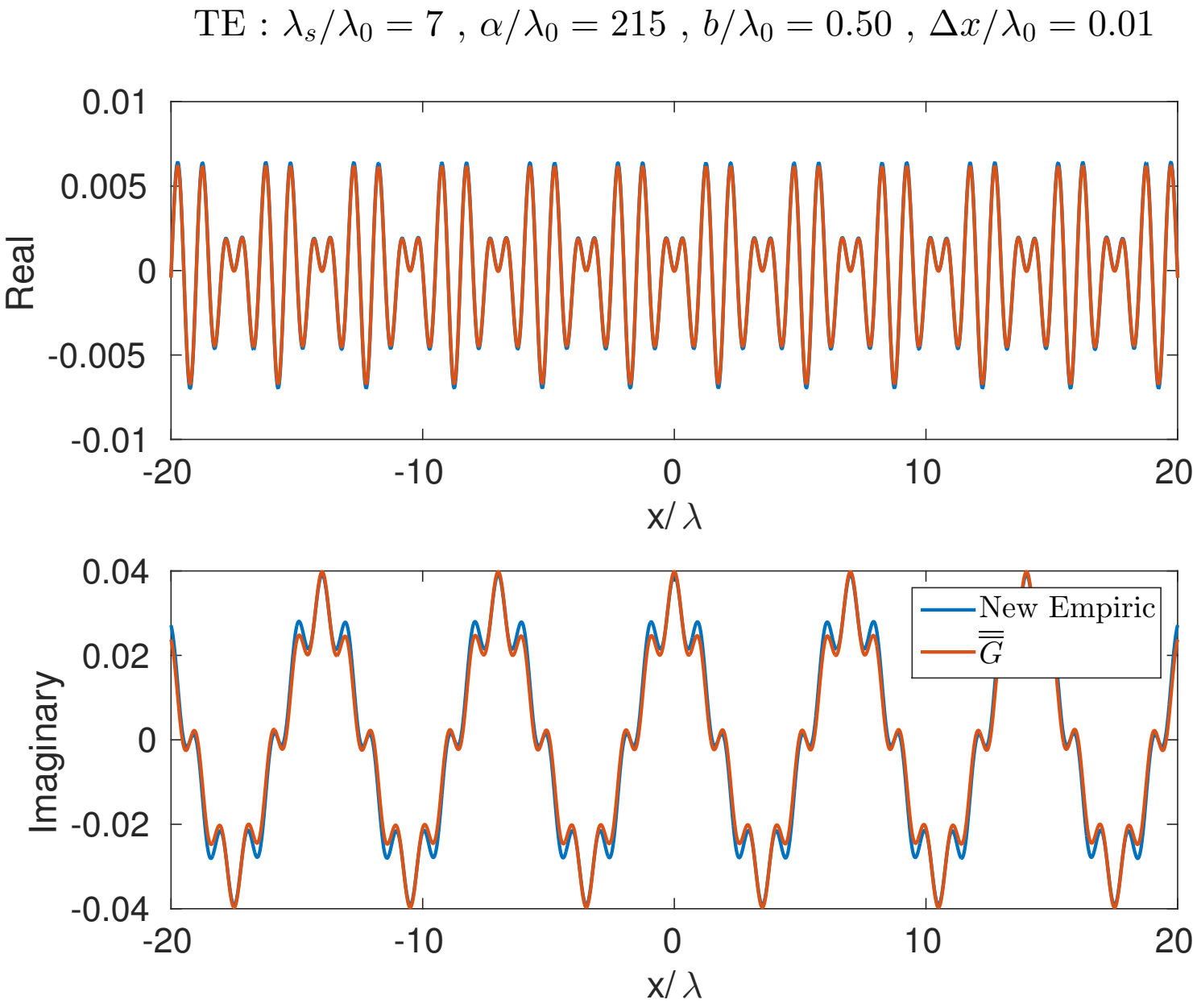


Figure 4.113: TE Empiric Analytic

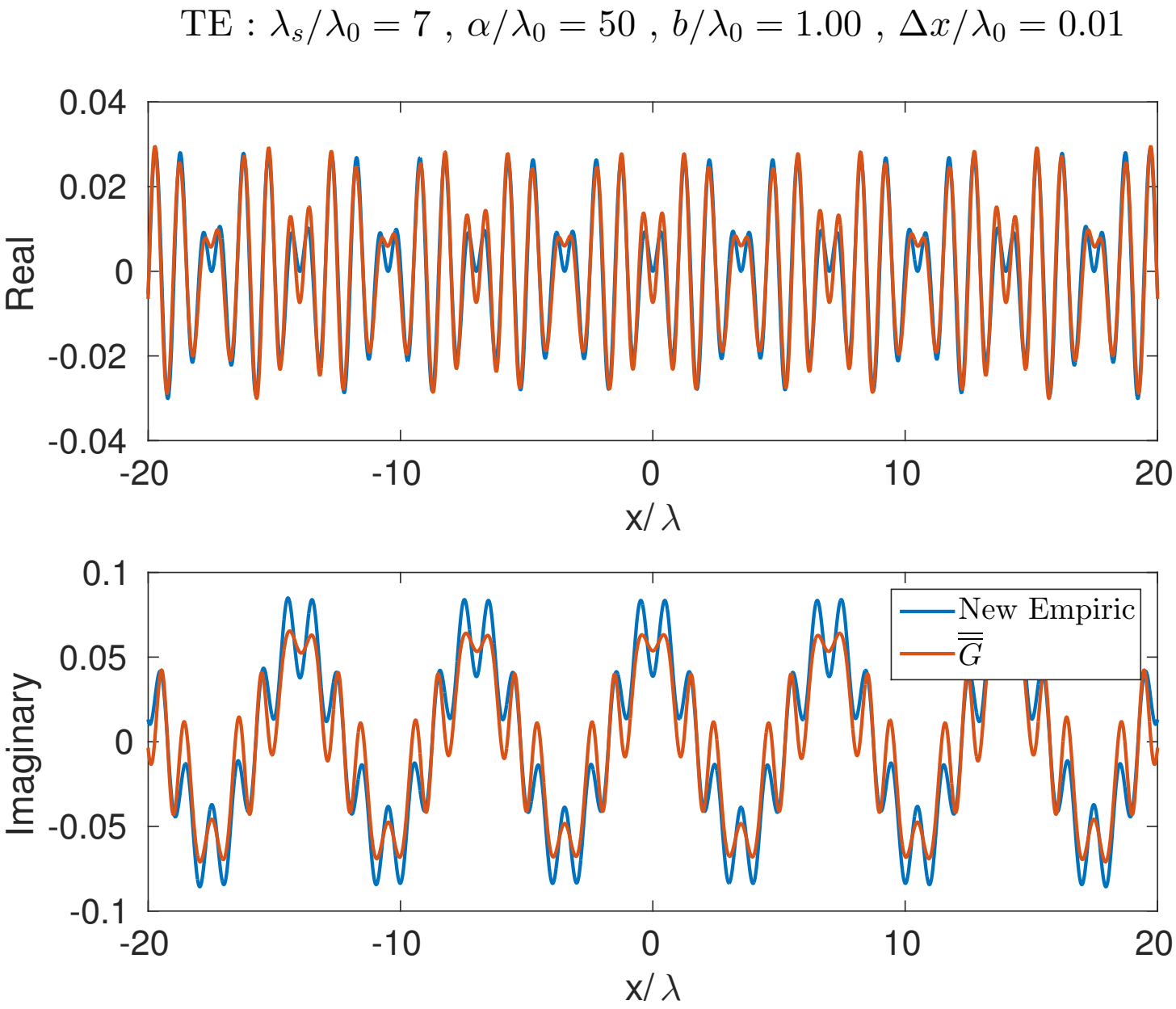


Figure 4.114: TE Empiric Analytic

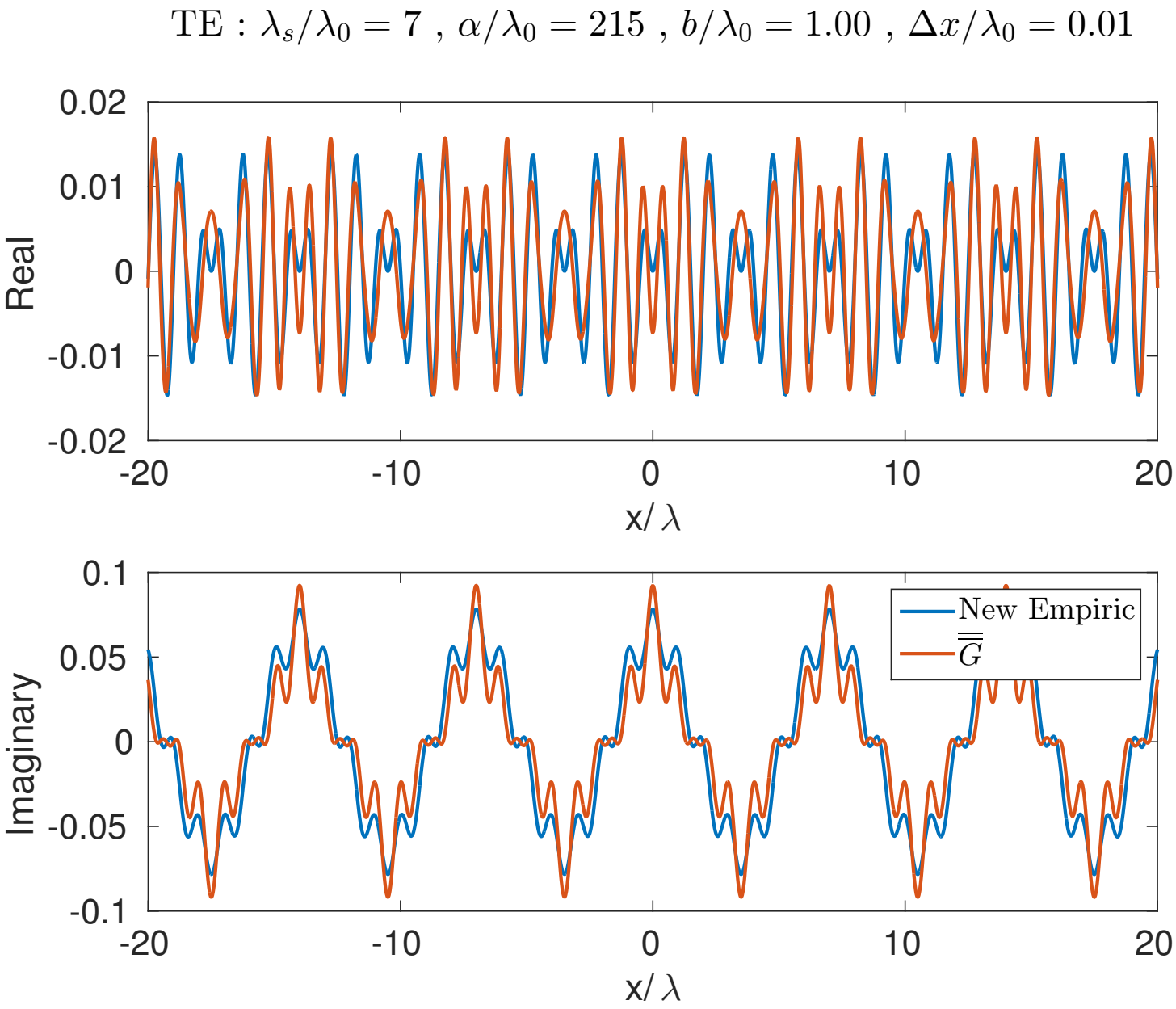


Figure 4.115: TE Empiric Analytic

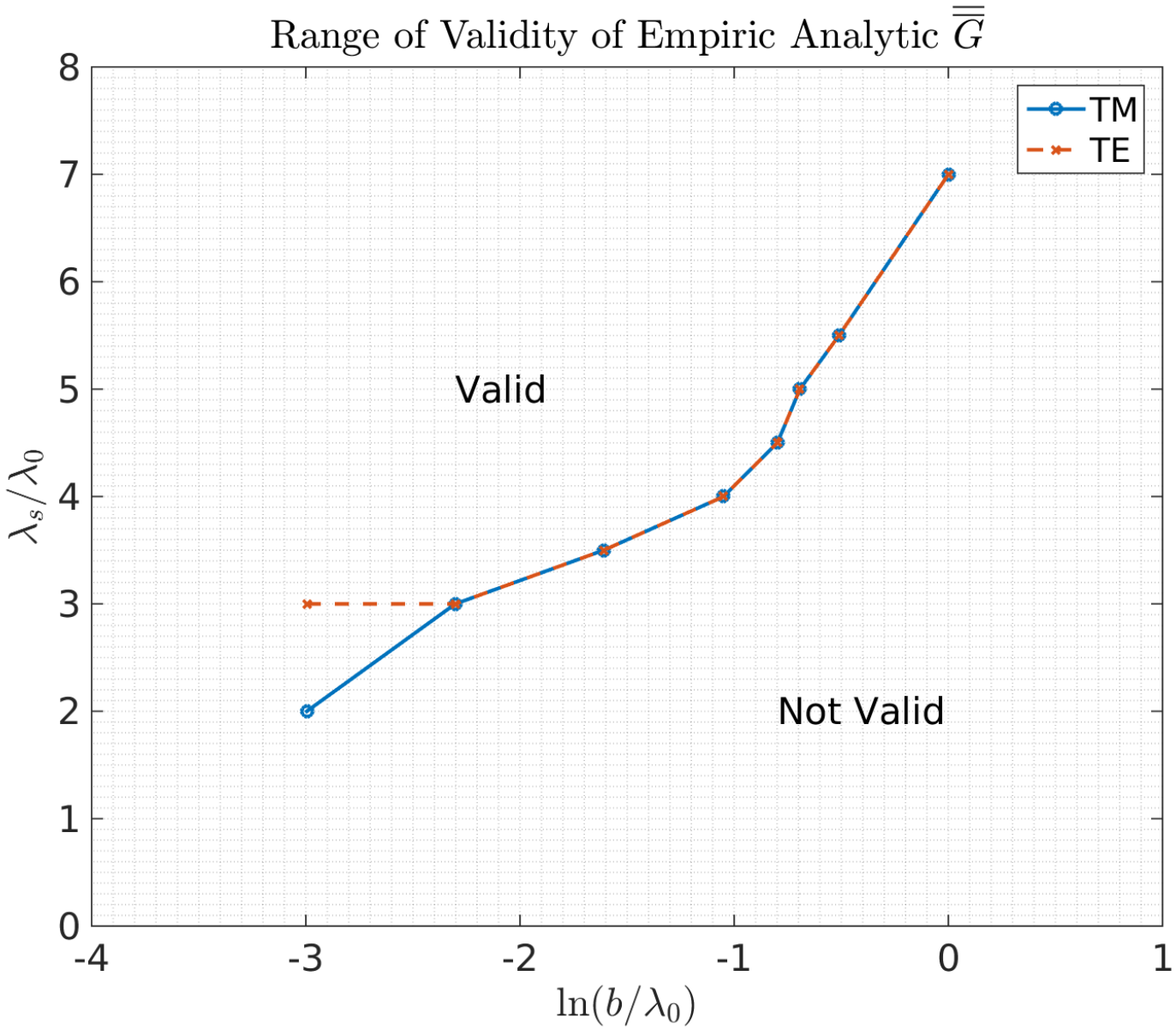


Figure 4.116: Range of Validity of Analytic Formula

### 4.4.4 Spectral Surfaces

The realistic surfaces will be composed of the superposition of sinusoids. Since the approximations found for the tails of the kernel integral were for a single frequency, they must be extended to spectral surfaces. A more detailed exposition is given in Appendix A.3, with the summary of results here. After deriving the extension of these analytic approximations to multi-frequency surfaces, the predictions that they make will be tested against numeric computation.

For TM polarization, the tail integrals can be found by simply adding the empiric analytic formula of Eq. 4.4.20 for each surface period present on the surface.

On the other hand, TE polarization contains a $\zeta_x^2(x)$ term so it will not be a direct linear superposition. Instead, it can be found by a scaled linear addition of the approximations for the single surface plus an additional term consisting of pairs of surface frequencies as shown below:

$$A^{FF_{te}}(x,\alpha,c,d) = A_p^{FF_{te}}(x,\alpha,c,d) + \frac{1}{\sqrt{1+\left(\zeta_x^c(x)\right)^2}} \sum_n \sqrt{1+\left(\zeta_{xn}(x)\right)^2} A_{s_n}^{FF_{te}}(x,\alpha,c,d) \tag{4.4.22}$$

where $A_{s_n}^{FF_{te}}$ is that given by Equation 4.4.6 or the empiric analytic formula of Eq. 4.4.21 for each individual surface frequency and

$$A_p^{FF_{te}}(x,\alpha,c,d) = \frac{\zeta_x^c(x)}{j4\sqrt{1+\left(\zeta_x^c\right)^2}} e^{j\frac{3\pi}{4}} \sum_{n=0}^{N-2} \sum_{m=n+1}^{N-1} b_n k_{sn} b_m k_{sm} \left(S_1+S_2+S_3+S_4\right) \tag{4.4.23}$$

$$S_1 = \exp\left(j\left(k_{sn} - k_{sm}\right)x\right)\left\{\frac{\left[F\left(\left(k_0 + k_{sn} - k_{sm}\right)\left(x+\alpha\right)\right) - F\left(\left(k_0 + k_{sn} - k_{sm}\right)\left(x-c\right)\right)\right]}{\sqrt{\left(1 + K_{sn} - K_{sm}\right)}}\right.$$
$$\left. - \frac{\left[F\left(\left(k_0 - k_{sn} + k_{sm}\right)\left(\alpha - x\right)\right) - F\left(\left(k_0 - k_{sn} + k_{sm}\right)\left(d-x\right)\right)\right]}{\sqrt{1 - K_{sn} + K_{sm}}}\right\}$$

$$S_2 = \exp\left(-j\left(k_{sn} - k_{sm}\right)x\right)\left\{\frac{\left[F\left(\left(k_0 - k_{sn} + k_{sm}\right)\left(x+\alpha\right)\right) - F\left(\left(k_0 - k_{sn} + k_{sm}\right)\left(x-c\right)\right)\right]}{\sqrt{\left(1 - K_{sn} + K_{sm}\right)}}\right.$$
$$\left. - \frac{\left[F\left(\left(k_0 + k_{sn} - k_{sm}\right)\left(\alpha - x\right)\right) - F\left(\left(k_0 + k_{sn} - k_{sm}\right)\left(d-x\right)\right)\right]}{\sqrt{1 + K_{sn} - K_{sm}}}\right\}$$

$$S_3 = \exp\left(j\left(k_{sn} + k_{sm}\right)x\right)\left\{\frac{\left[F\left(\left(k_0 + k_{sn} + k_{sm}\right)\left(x+\alpha\right)\right) - F\left(\left(k_0 + k_{sn} + k_{sm}\right)\left(x-c\right)\right)\right]}{\sqrt{\left(1 + K_{sn} + K_{sm}\right)}}\right.$$
$$\left. - \frac{\left[F\left(\left(k_0 - k_{sn} - k_{sm}\right)\left(\alpha - x\right)\right) - F\left(\left(k_0 - k_{sn} - k_{sm}\right)\left(d-x\right)\right)\right]}{\sqrt{1 - K_{sn} - K_{sm}}}\right\}$$

$$S_4 = \exp\left(-j\left(k_{sn} + k_{sm}\right)x\right)\left\{\frac{\left[F\left(\left(k_0 - k_{sn} - k_{sm}\right)\left(x+\alpha\right)\right) - F\left(\left(k_0 - k_{sn} - k_{sm}\right)\left(x-c\right)\right)\right]}{\sqrt{\left(1 - K_{sn} - K_{sm}\right)}}\right.$$
$$\left. - \frac{\left[F\left(\left(k_0 + k_{sn} + k_{sm}\right)\left(\alpha - x\right)\right) - F\left(\left(k_0 + k_{sn} + k_{sm}\right)\left(d-x\right)\right)\right]}{\sqrt{1 + K_{sn} + K_{sm}}}\right\}$$

Where each of the Fresnel functions may be approximated with:

$$F\left(x\right) = \frac{1}{2} + \frac{1}{\sqrt{2\pi x}}\sin\left(x\right) - j\left(\frac{1}{2} - \frac{1}{\sqrt{2\pi x}}\cos\left(x\right)\right)$$

when using the empiric analytic formula of Eq. 4.4.21.

Numeric calculations with two surface frequencies, shown in Figures 4.117 through 4.130 starting with TE and moving to TM, where the first $\frac{\lambda_{s1}}{\lambda_0} = 20$ and $\frac{b_1}{\lambda_0} = 0.5$ are fixed and the second frequency is varied between $\frac{\lambda_{s2}}{\lambda_0} = \{8, 10, 15\}$ with amplitudes $\frac{b_2}{\lambda_0} = \{0.05, 0.1, 0.5\}$ show that for this range of parameters, both polarizations are in fact linear, in contrast to the prediction of Eq. 4.4.22. This equation examined only the integral tails after a number of approximations so it is not surprising that it fails to adequately describe the behavior of the kernel integral and the behavior is better than hoped for.

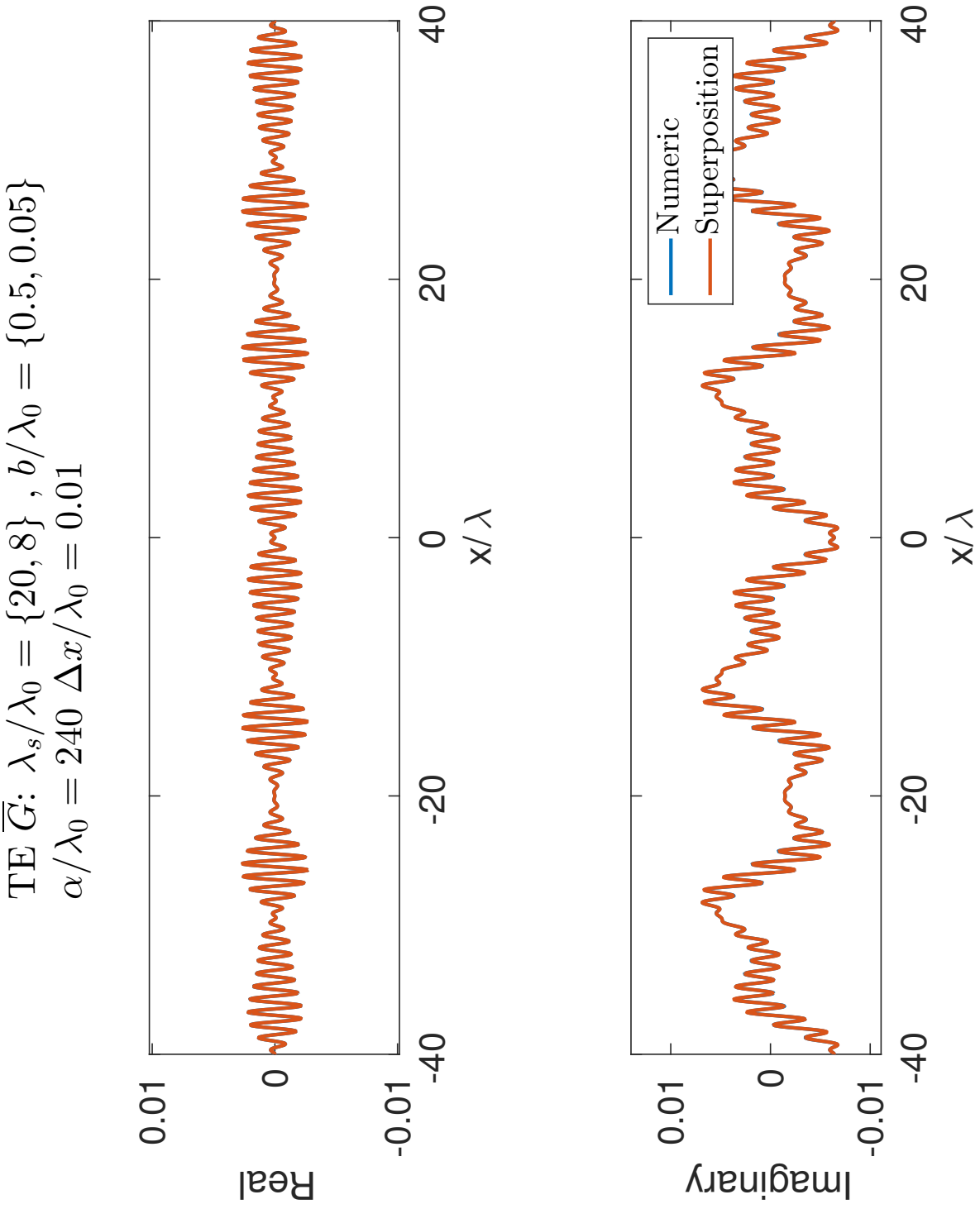


Figure 4.117: TE $\frac{\lambda_s}{\lambda_0} = \{20, 8\}$ $\frac{b}{\lambda_0} = \{0.5, 0.05\}$ All Numeric Calculations

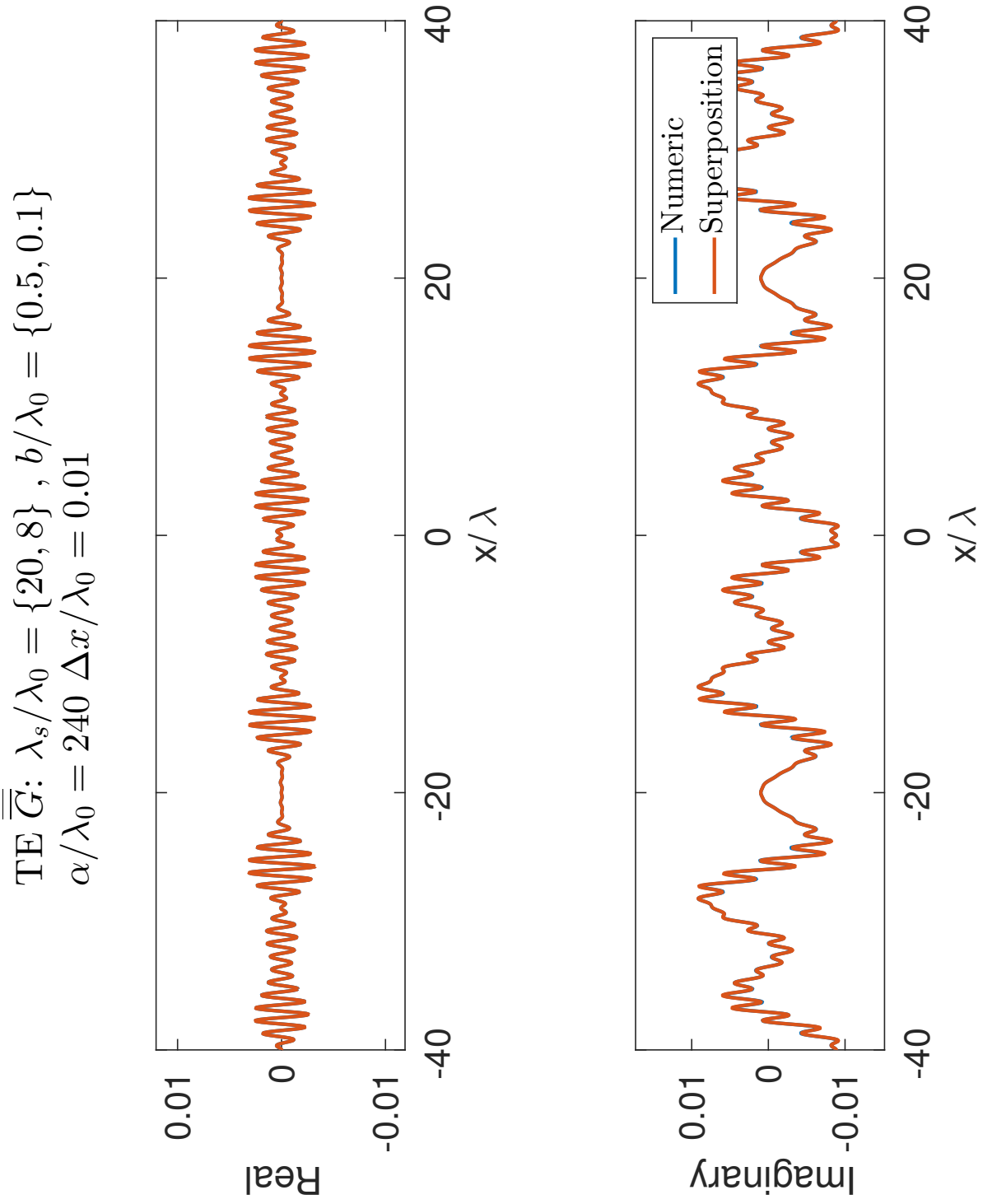


Figure 4.118: TE $\frac{\lambda_s}{\lambda_0} = \{20, 8\}$ $\frac{b}{\lambda_0} = \{0.5, 0.1\}$ All Numeric Calculations

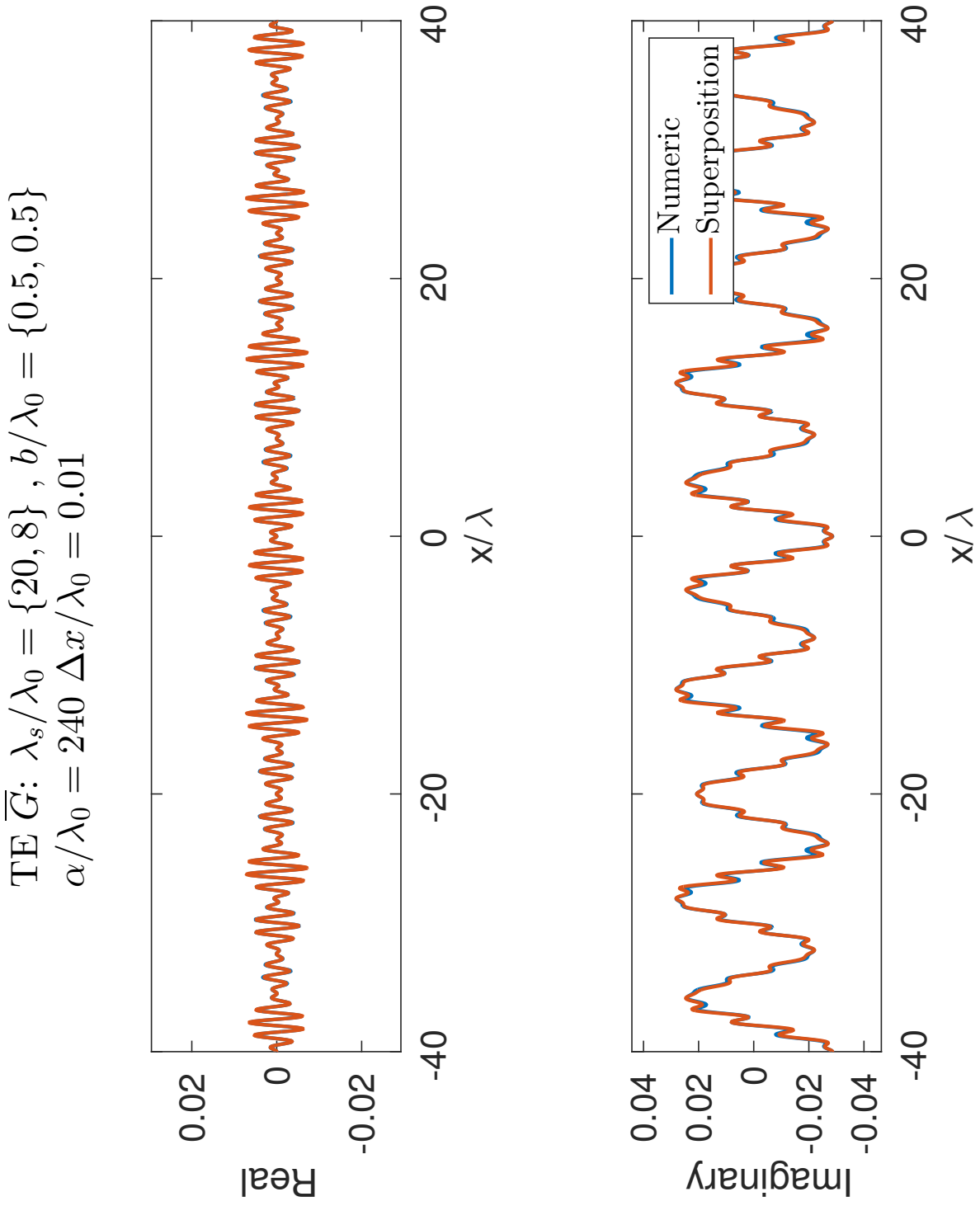


Figure 4.119: TE $\frac{\lambda_s}{\lambda_0} = \{20, 8\}$ $\frac{b}{\lambda_0} = \{0.5, 0.5\}$ All Numeric Calculations

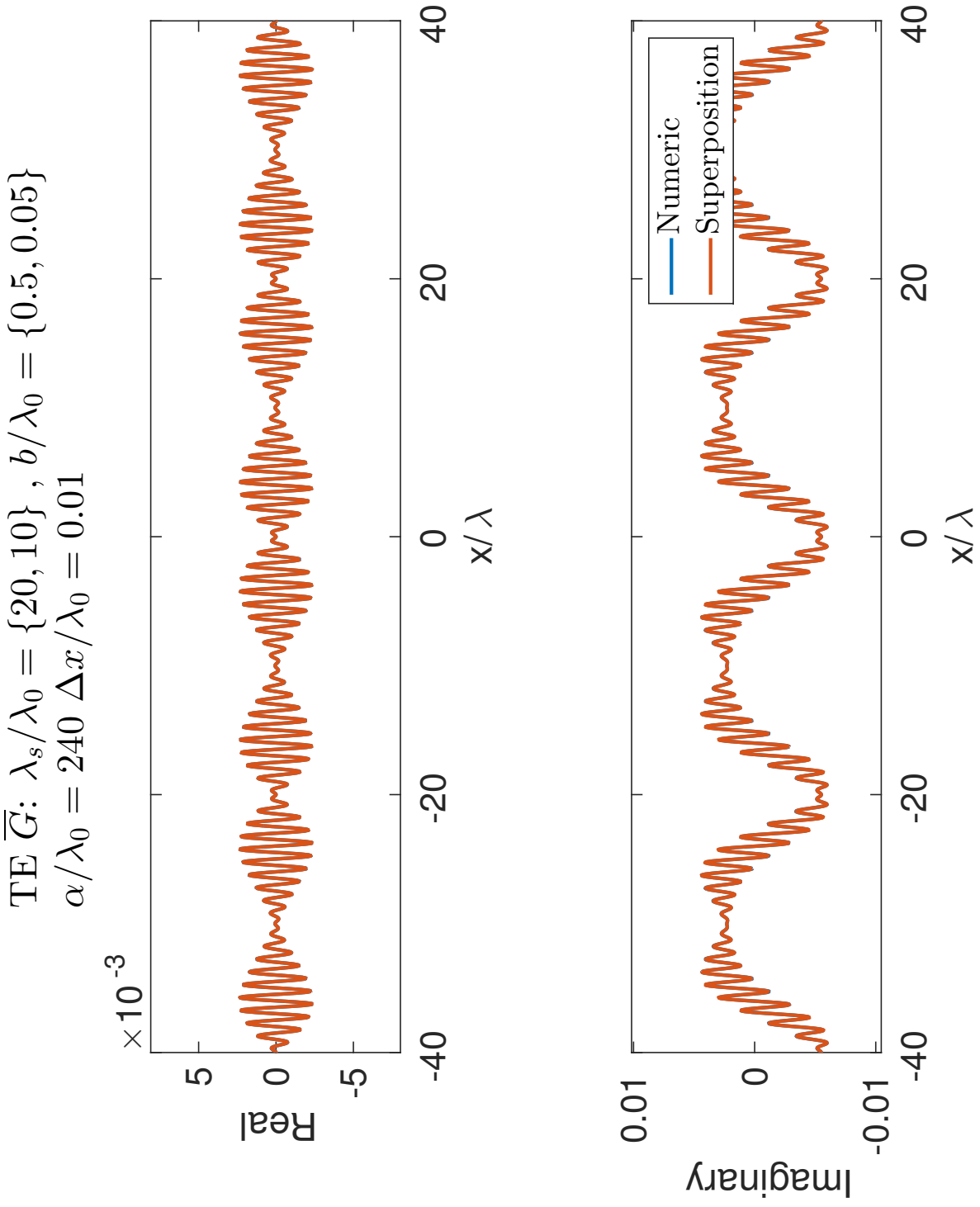


Figure 4.120: TE $\frac{\lambda_s}{\lambda_0} = \{20, 10\}$ $\frac{b}{\lambda_0} = \{0.5, 0.05\}$ All Numeric Calculations

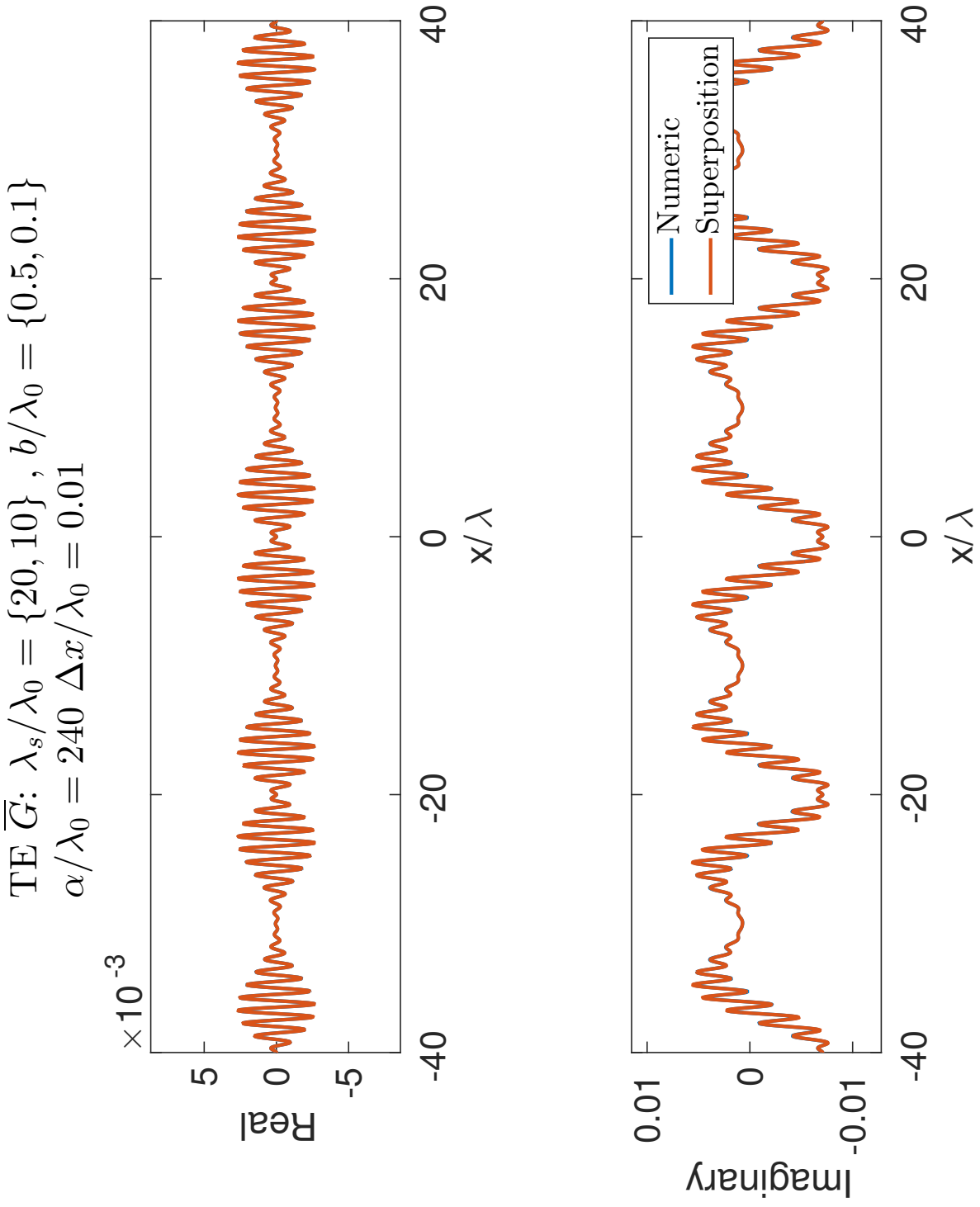


Figure 4.121: TE $\frac{\lambda_s}{\lambda_0} = \{20, 10\}$ $\frac{b}{\lambda_0} = \{0.5, 0.1\}$ All Numeric Calculations

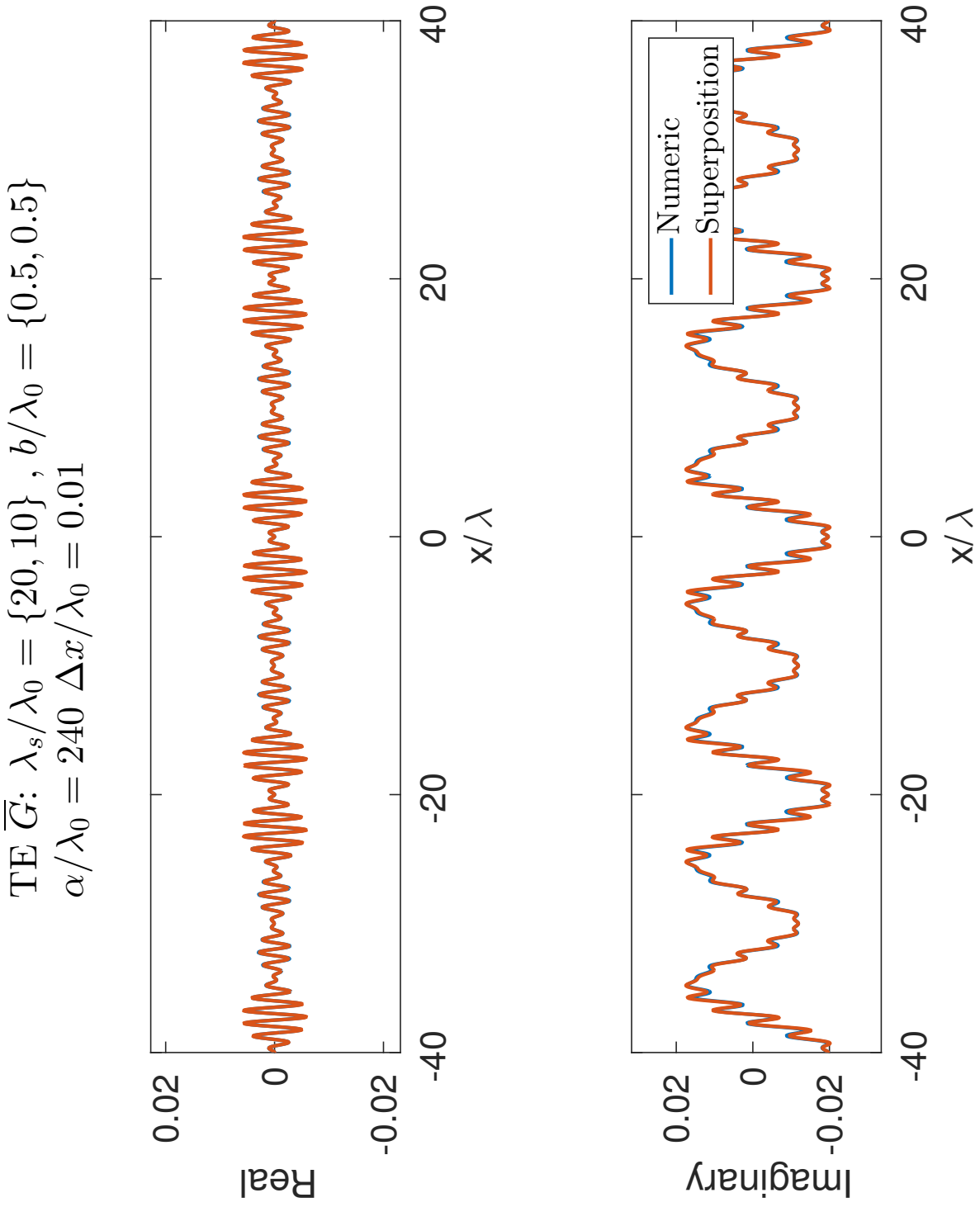


Figure 4.122: TE $\frac{\lambda_s}{\lambda_0} = \{20, 10\}$ $\frac{b}{\lambda_0} = \{0.5, 0.5\}$ All Numeric Calculations

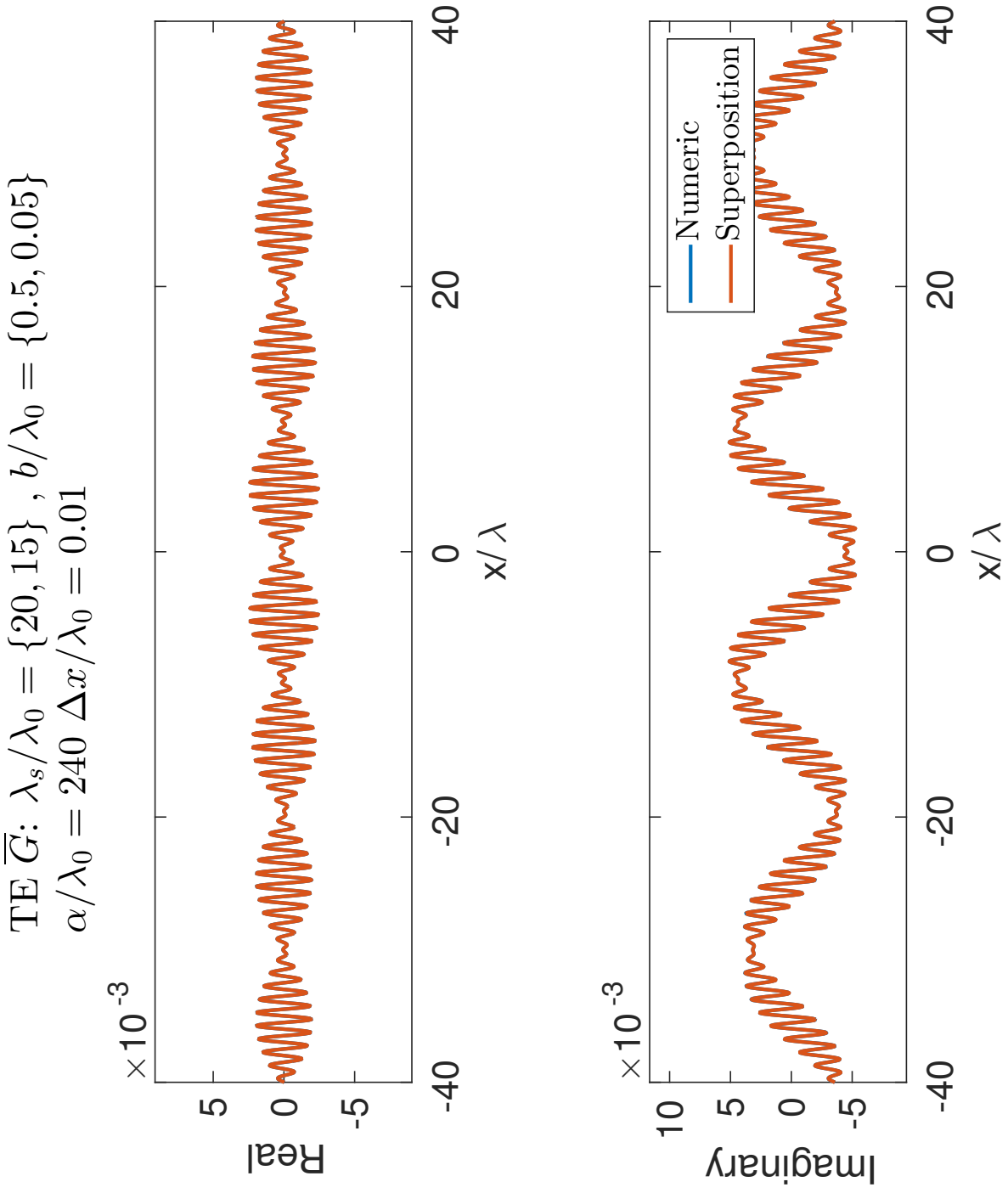


Figure 4.123: TE $\frac{\lambda_s}{\lambda_0} = \{20, 15\}$ $\frac{b}{\lambda_0} = \{0.5, 0.05\}$ All Numeric Calculations

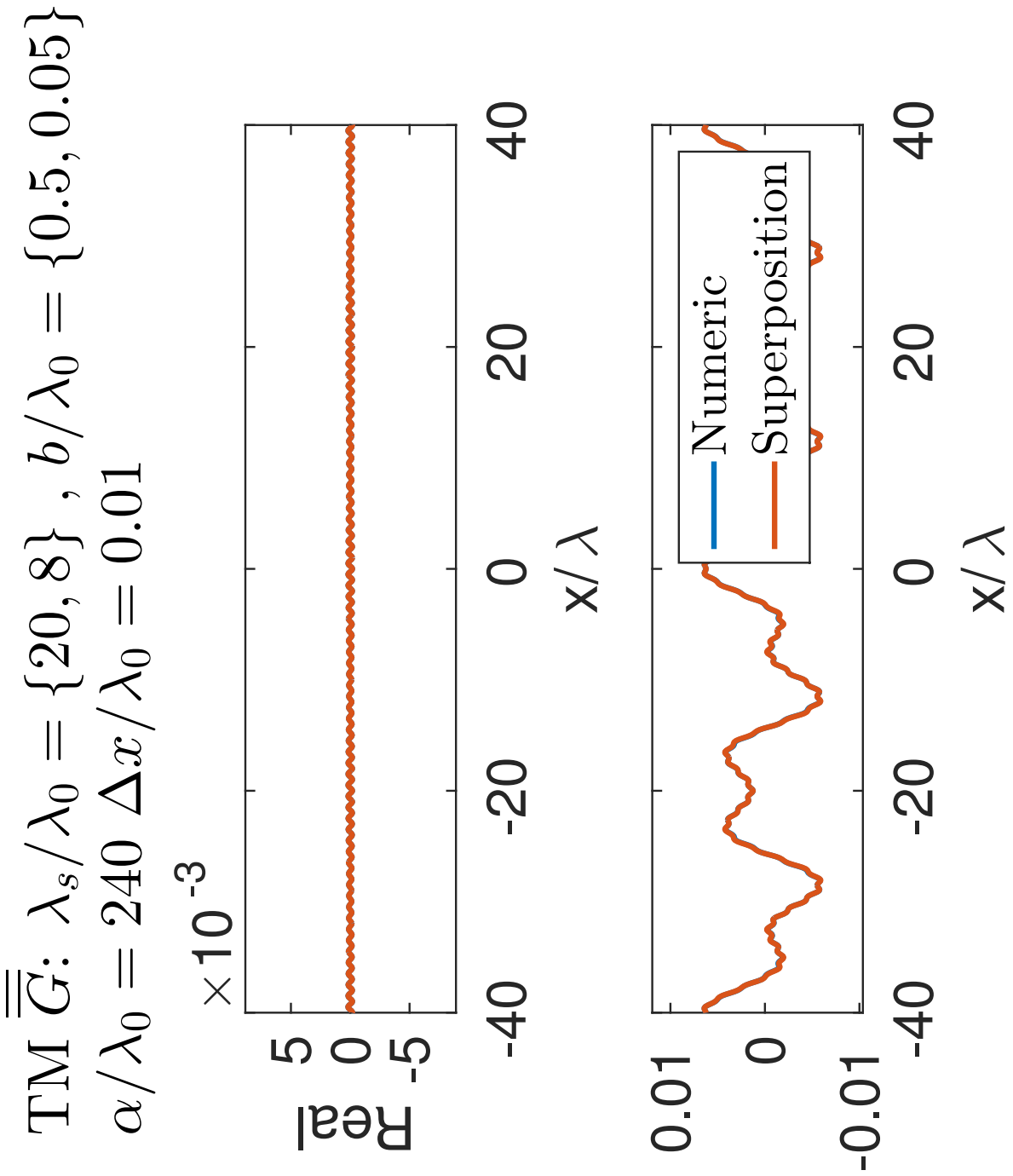


Figure 4.124: TM $\frac{\lambda_s}{\lambda_0} = \{20, 8\}$ $\frac{b}{\lambda_0} = \{0.5, 0.05\}$ All Numeric Calculations

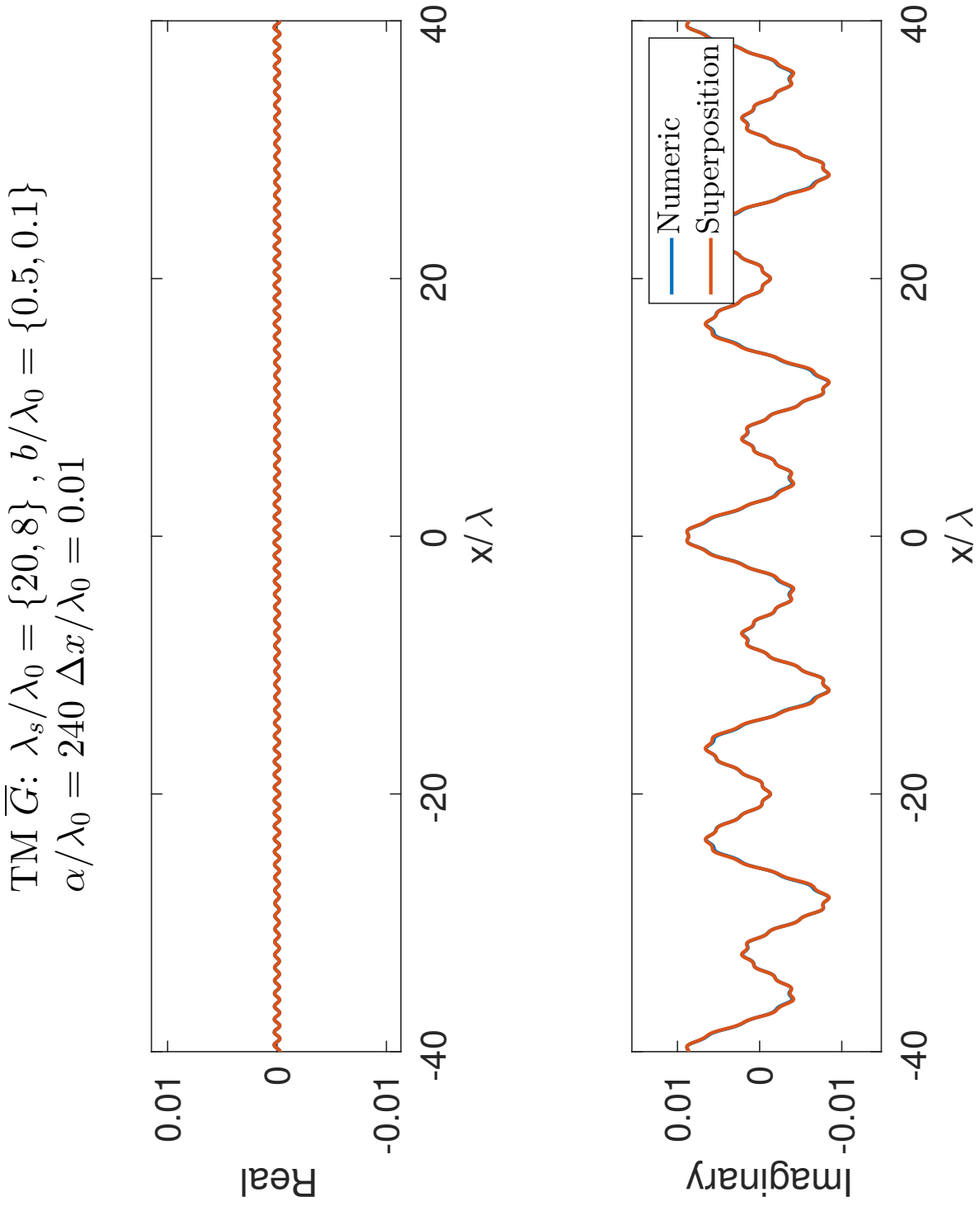


Figure 4.125: TM $\frac{\lambda_s}{\lambda_0} = \{20, 8\}$ $\frac{b}{\lambda_0} = \{0.5, 0.1\}$ All Numeric Calculations

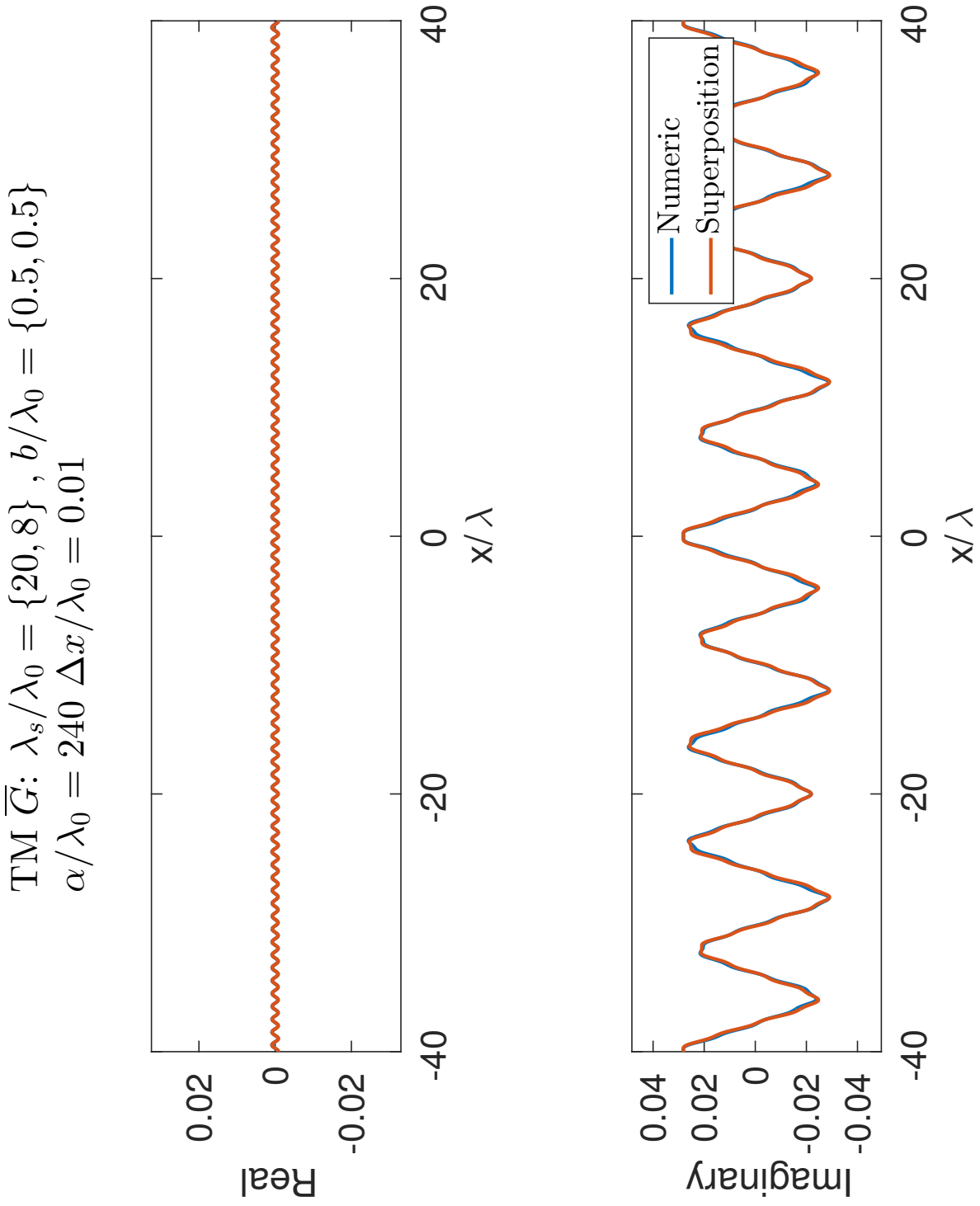


Figure 4.126: TM $\frac{\lambda_s}{\lambda_0} = \{20, 8\}$ $\frac{b}{\lambda_0} = \{0.5, 0.5\}$ All Numeric Calculations

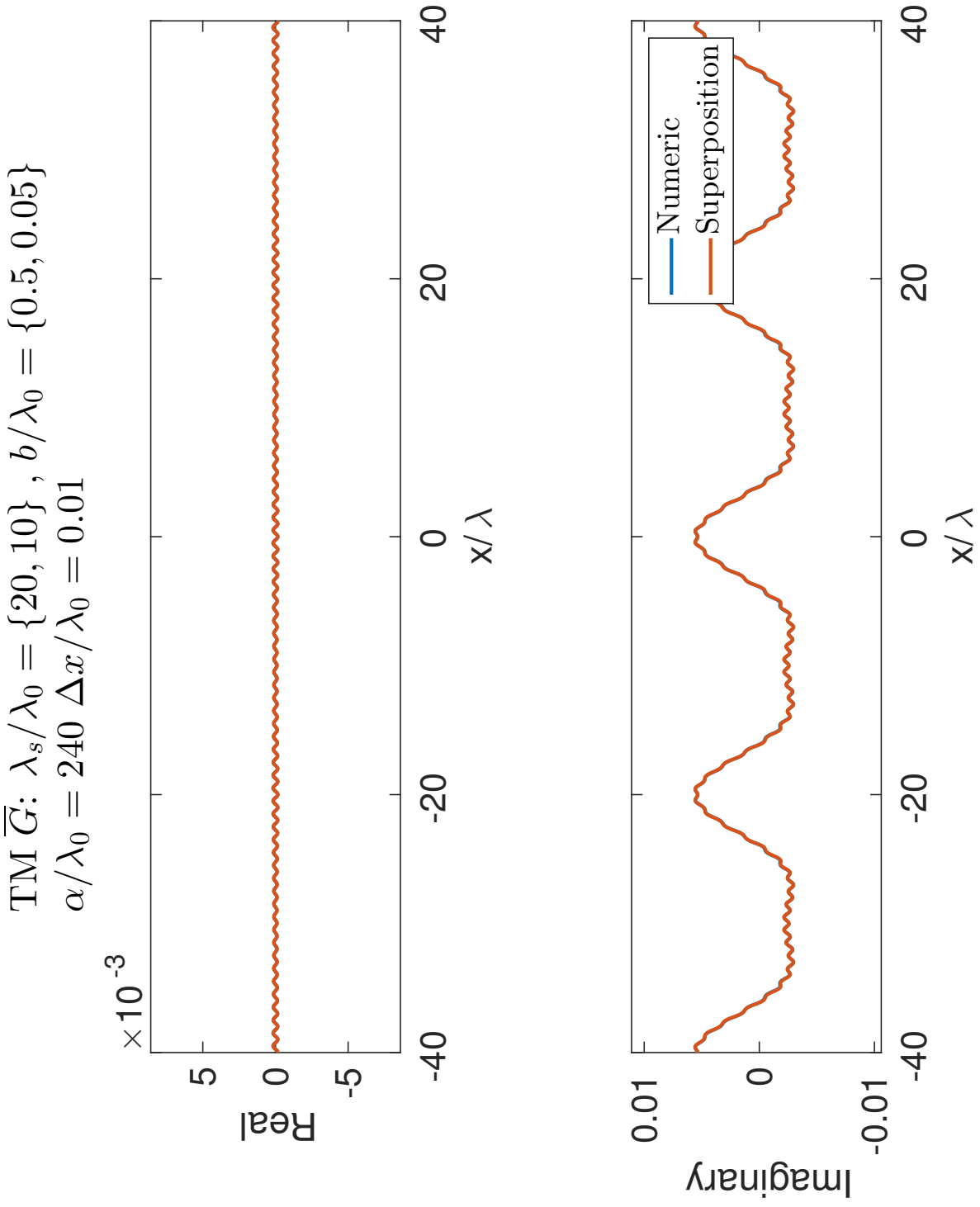


Figure 4.127: TM $\frac{\lambda_s}{\lambda_0} = \{20, 10\}$ $\frac{b}{\lambda_0} = \{0.5, 0.05\}$ All Numeric Calculations

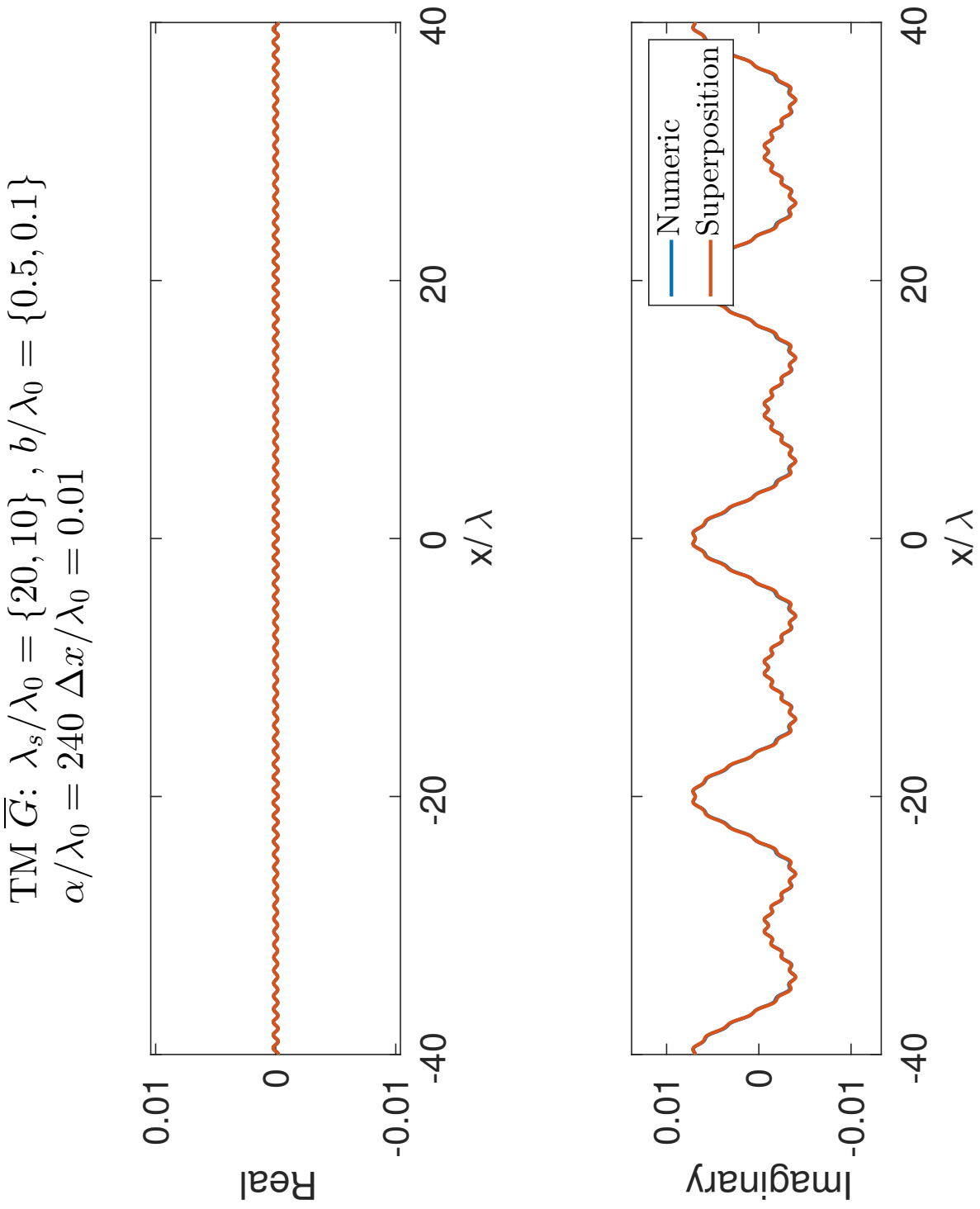


Figure 4.128: TM $\frac{\lambda_s}{\lambda_0} = \{20, 10\}$ $\frac{b}{\lambda_0} = \{0.5, 0.1\}$ All Numeric Calculations

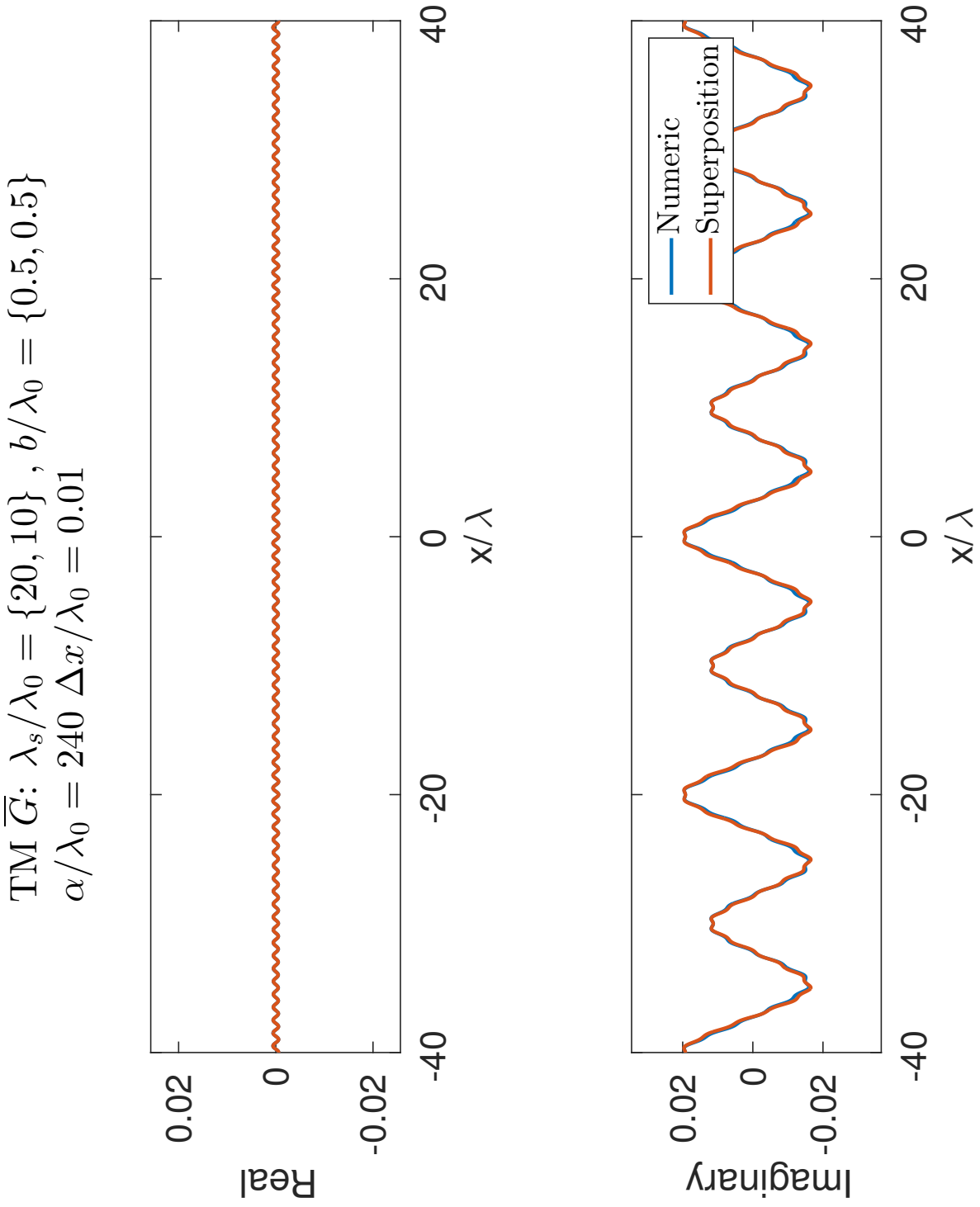


Figure 4.129: TM $\frac{\lambda_s}{\lambda_0} = \{20, 10\}$ $\frac{b}{\lambda_0} = \{0.5, 0.5\}$ All Numeric Calculations

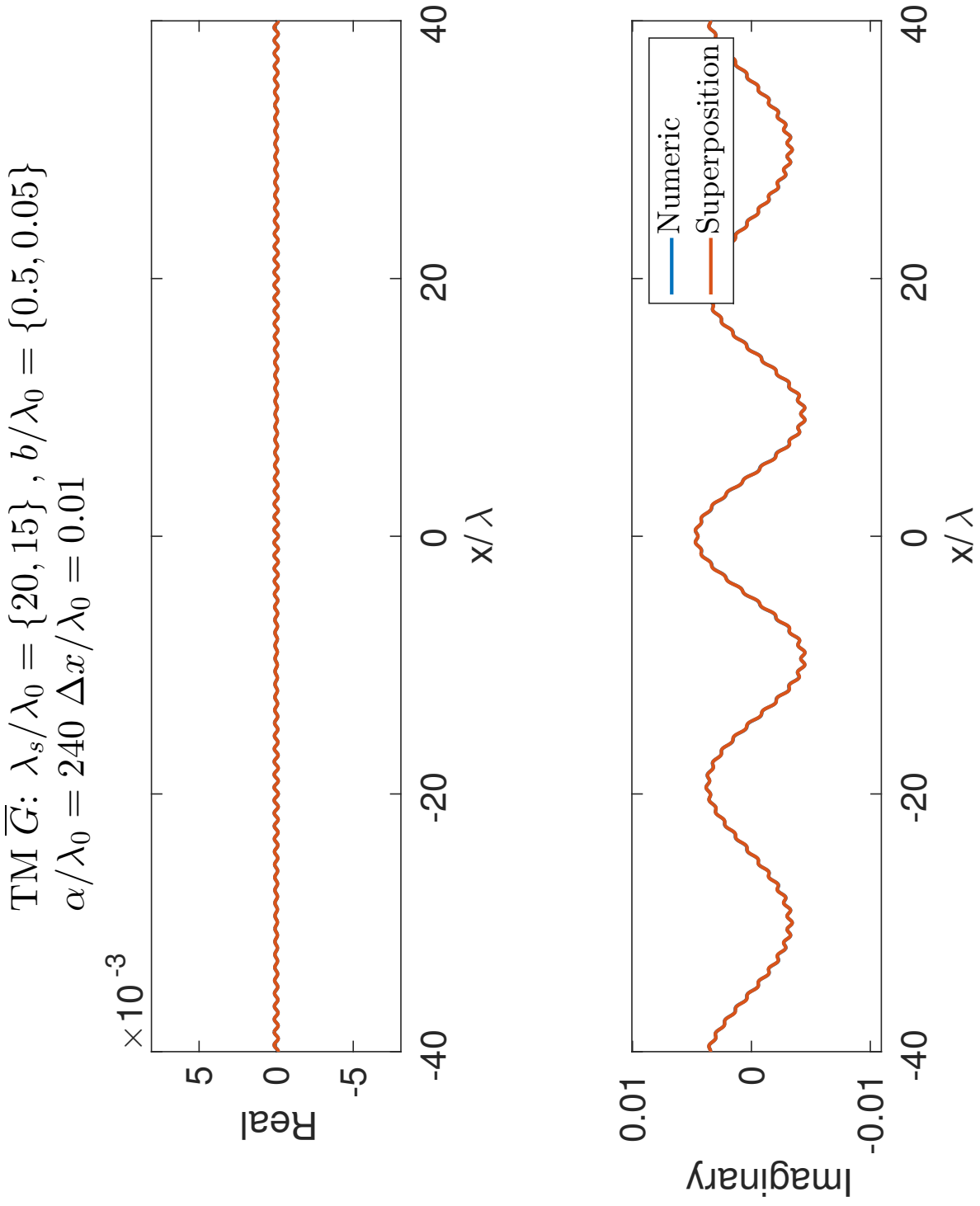


Figure 4.130: TM $\frac{\lambda_s}{\lambda_0} = \{20, 15\}$ $\frac{b}{\lambda_0} = \{0.5, 0.05\}$ All Numeric Calculations

#### 4.4.4.1 Predicted Singularities

Equation 4.4.23 contains terms with the following proportionalities:

$$S_1 \propto \frac{f}{\sqrt{(1+K_{sn}-K_{sm})}} - \frac{g}{\sqrt{1-K_{sn}+K_{sm}}} \quad S_2 \propto \frac{f}{\sqrt{(1-K_{sn}+K_{sm})}} - \frac{g}{\sqrt{1+K_{sn}-K_{sm}}}$$
$$S_3 \propto \frac{f}{\sqrt{(1+K_{sn}+K_{sm})}} - \frac{g}{\sqrt{1-K_{sn}-K_{sm}}} \quad S_4 \propto \frac{f}{\sqrt{(1-K_{sn}-K_{sm})}} - \frac{g}{\sqrt{1+K_{sn}+K_{sm}}}$$

where f and g are functions, different for each $S$, which are finite when $|K_{sn} - K_{sm}| = 1$ . Thus it appears to contain "singularities" like the single frequency case when the surface wavelengths are separated by an electromagnetic wavelength. For an infinite surface this formula suggests the result is infinite, while for finite surfaces it suggests they will become progressively larger with surface integration support. To test this prediction, results of numeric calculations with $\frac{\lambda_{s1}}{\lambda_0} = 20$ and $\frac{\lambda_{s2}}{\lambda_0} = 19$ with equal amplitudes $\frac{b}{\lambda_0} = \{0.05, 0.5, 1.0\}$ are shown below for varied integration supports $\frac{\alpha}{\lambda_0} = \{50, 400\}$. Figures 4.131 through 4.134 show the $\frac{b}{\lambda_0} = 0.05$ amplitude surface alternating between a small region around the center and the whole surface, while Figures 4.135 through 4.138 show the same for $\frac{b}{\lambda_0} = 0.5$ and results for $\frac{b}{\lambda_0} = 1.0$ are shown in Figures 4.139 through 4.142.

It appears that spectral surfaces containing surface wavelengths separated by an electromagnetic wavelength are not singular across the range of surface amplitudes. So there must be some cancellation between terms leading to a more docile character of the kernel integral.

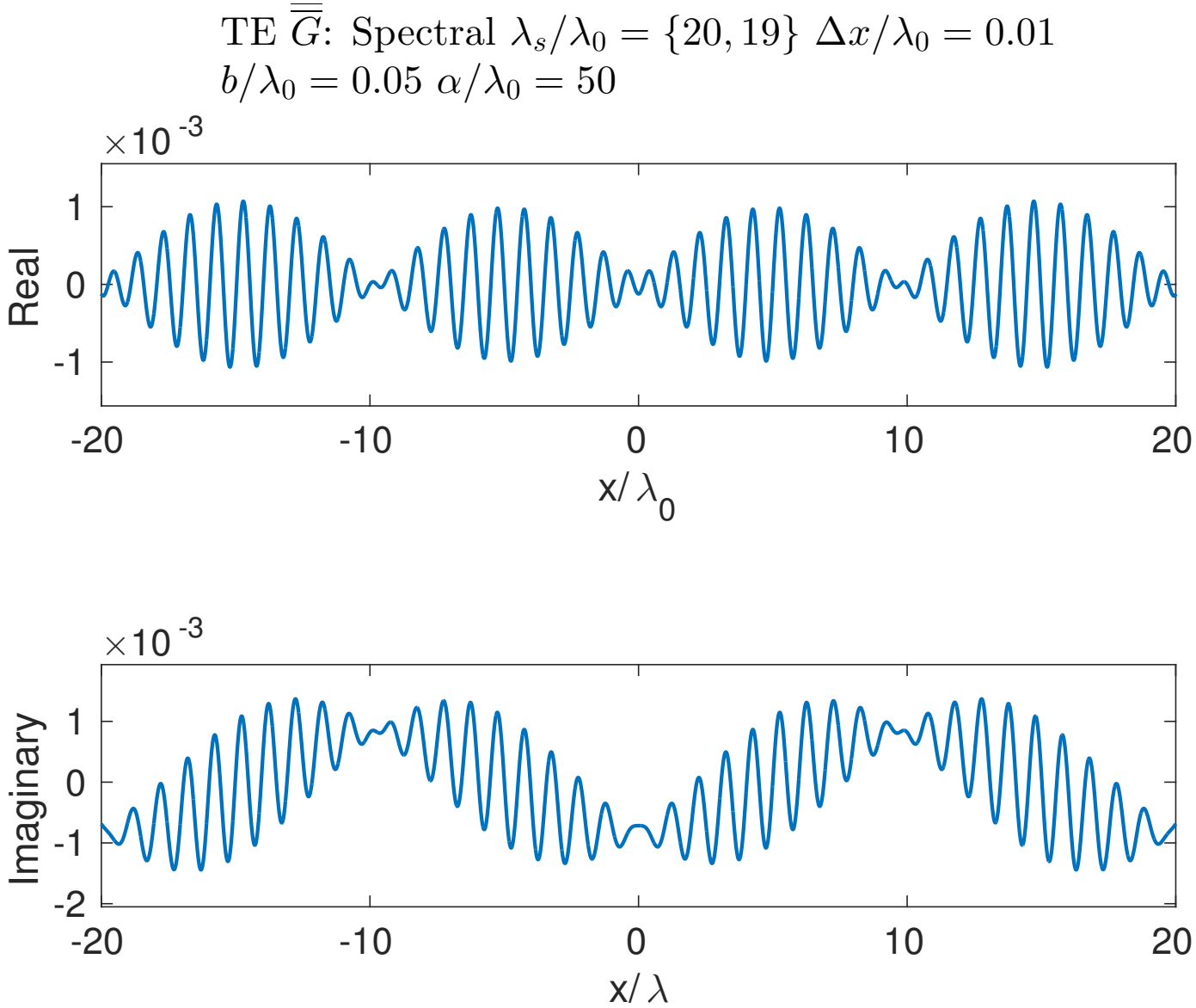


Figure 4.131: TE $\frac{b}{\lambda_0} = 0.05$ $\frac{\alpha}{\lambda_0} = 50$

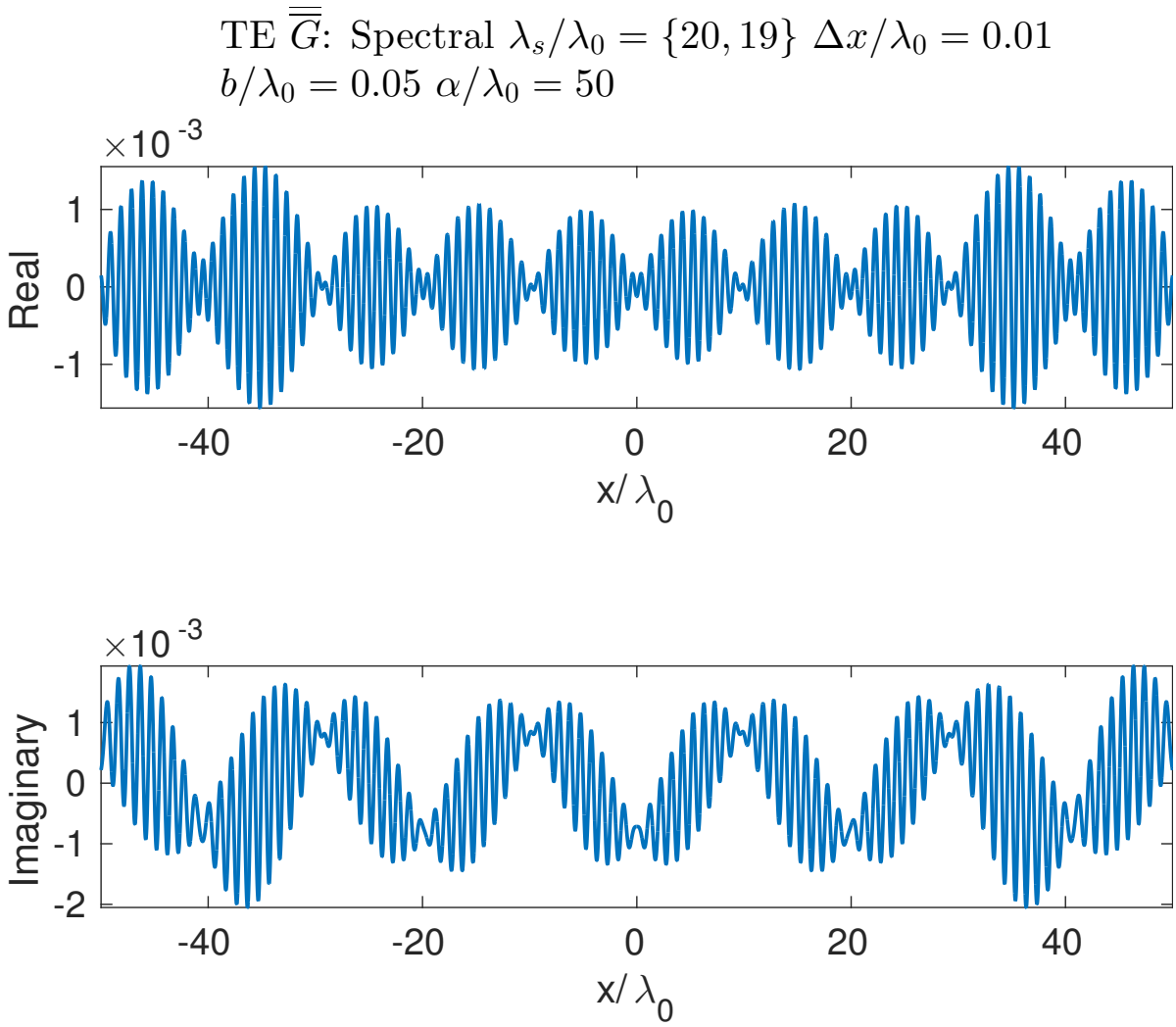


Figure 4.132: TE $\frac{b}{\lambda_0} = 0.05$ $\frac{\alpha}{\lambda_0} = 50$

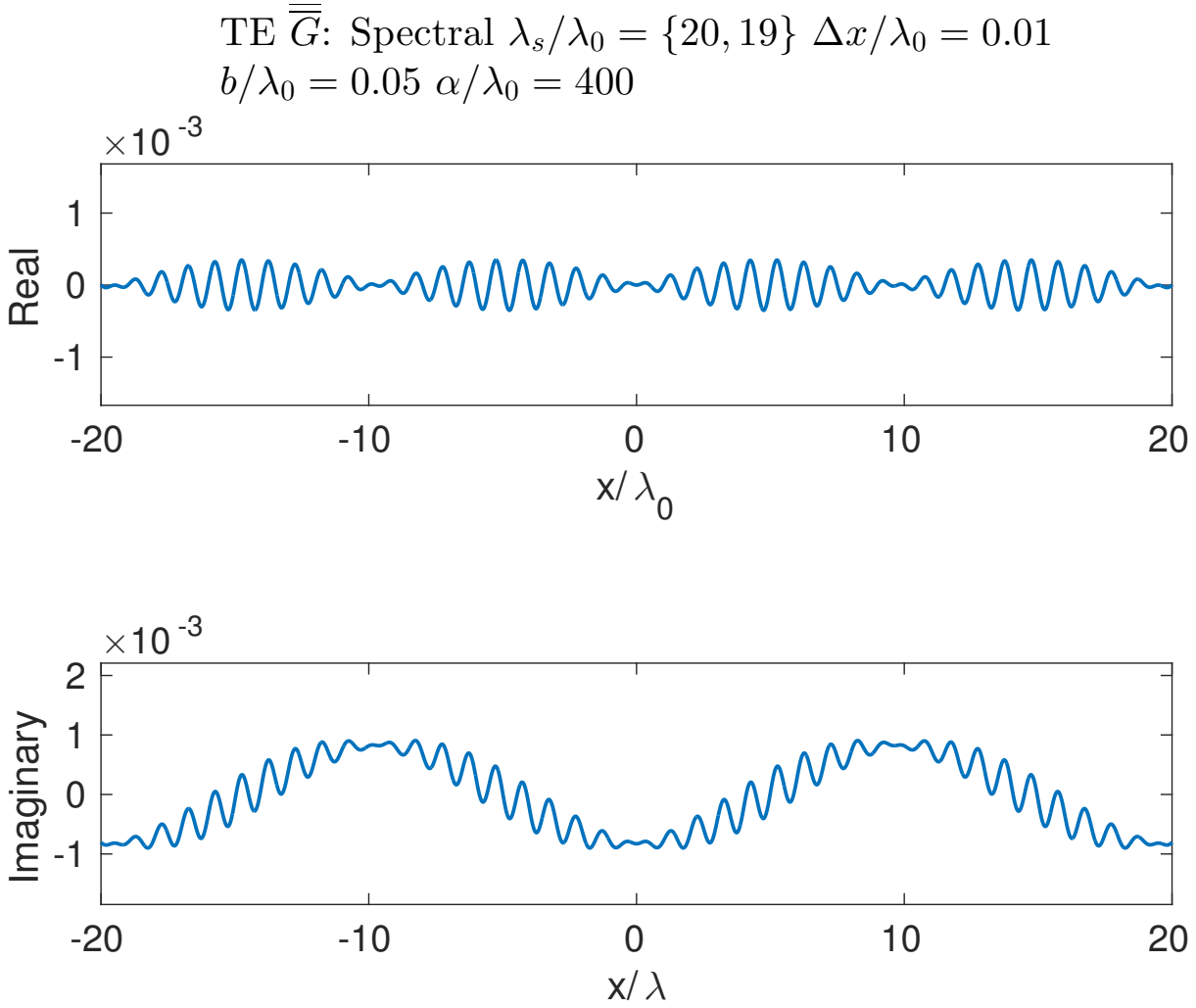


Figure 4.133: TE $\frac{b}{\lambda_0} = 0.05$ $\frac{\alpha}{\lambda_0} = 400$

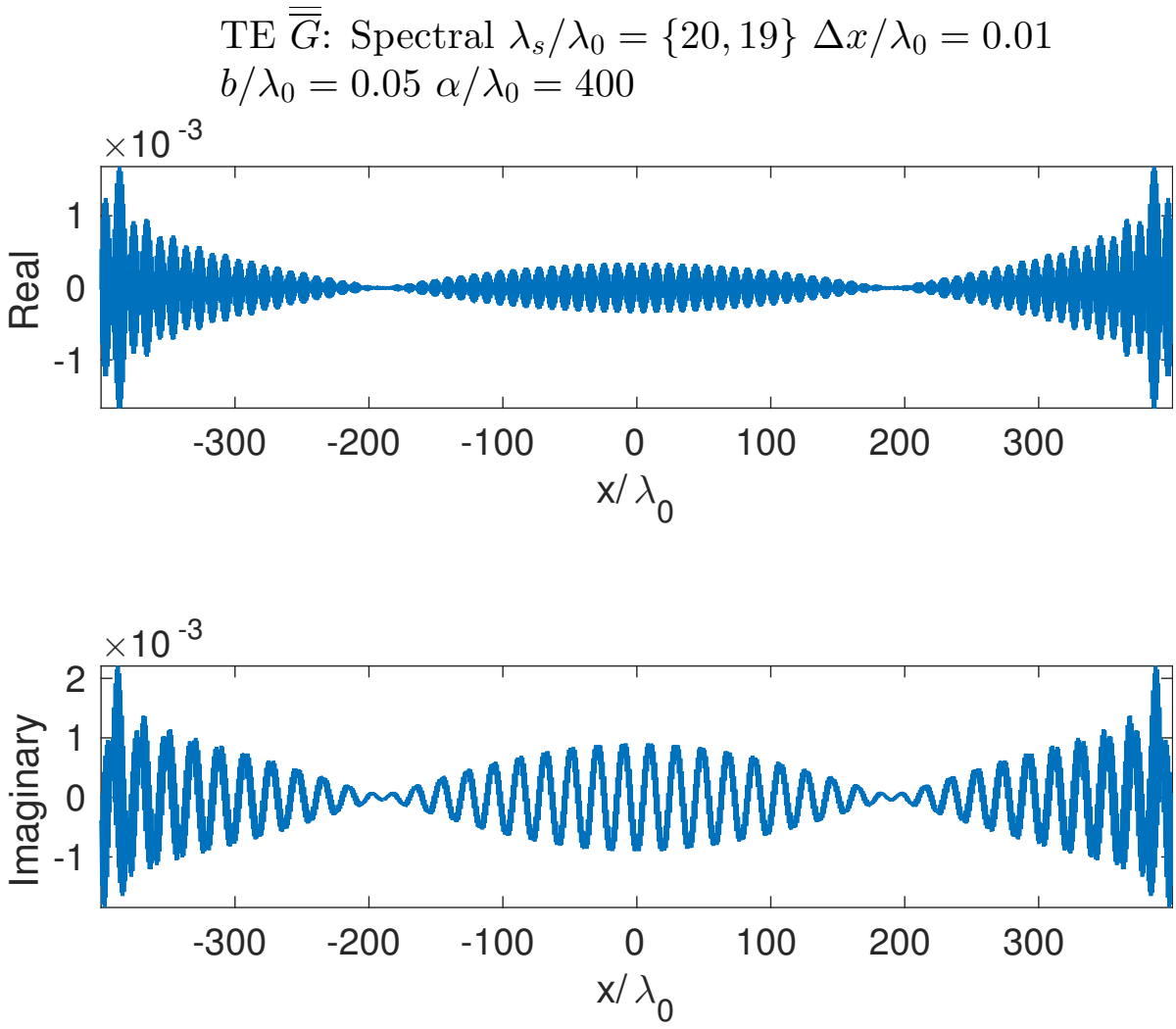


Figure 4.134: TE $\frac{b}{\lambda_0} = 0.05$ $\frac{\alpha}{\lambda_0} = 400$

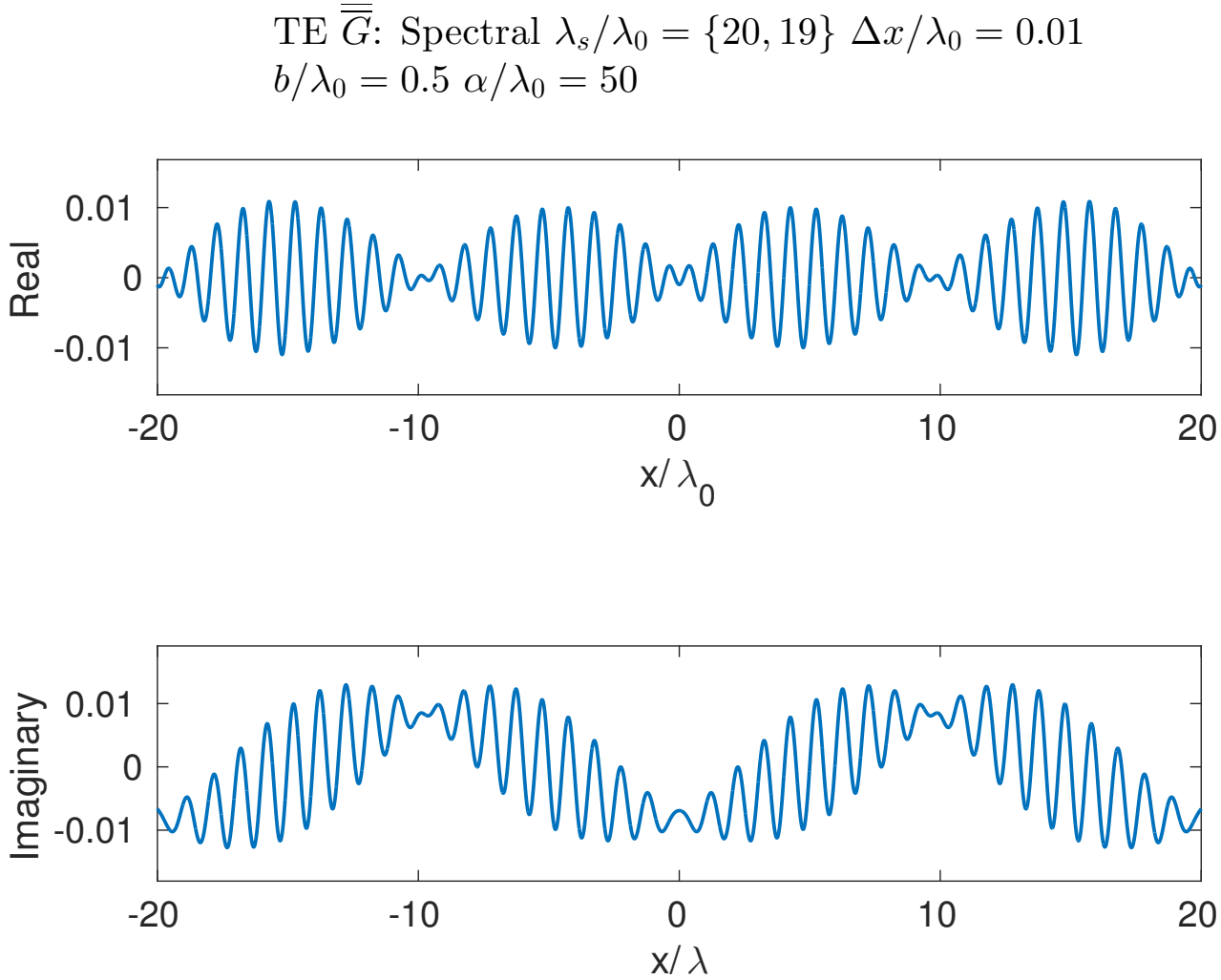


Figure 4.135: TE $\frac{b}{\lambda_0} = 0.5$ $\frac{\alpha}{\lambda_0} = 50$

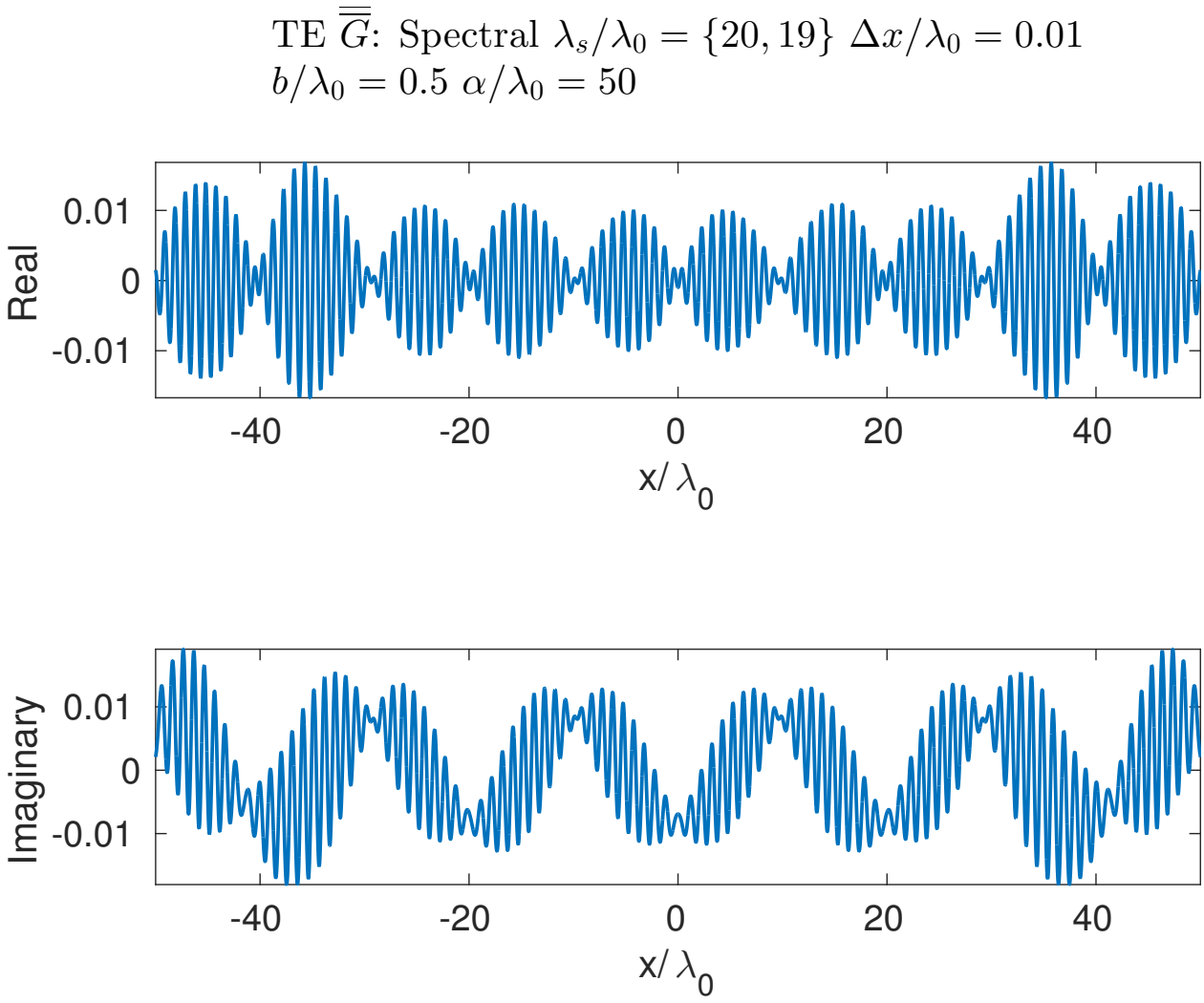


Figure 4.136: TE $\frac{b}{\lambda_0} = 0.5$ $\frac{\alpha}{\lambda_0} = 50$

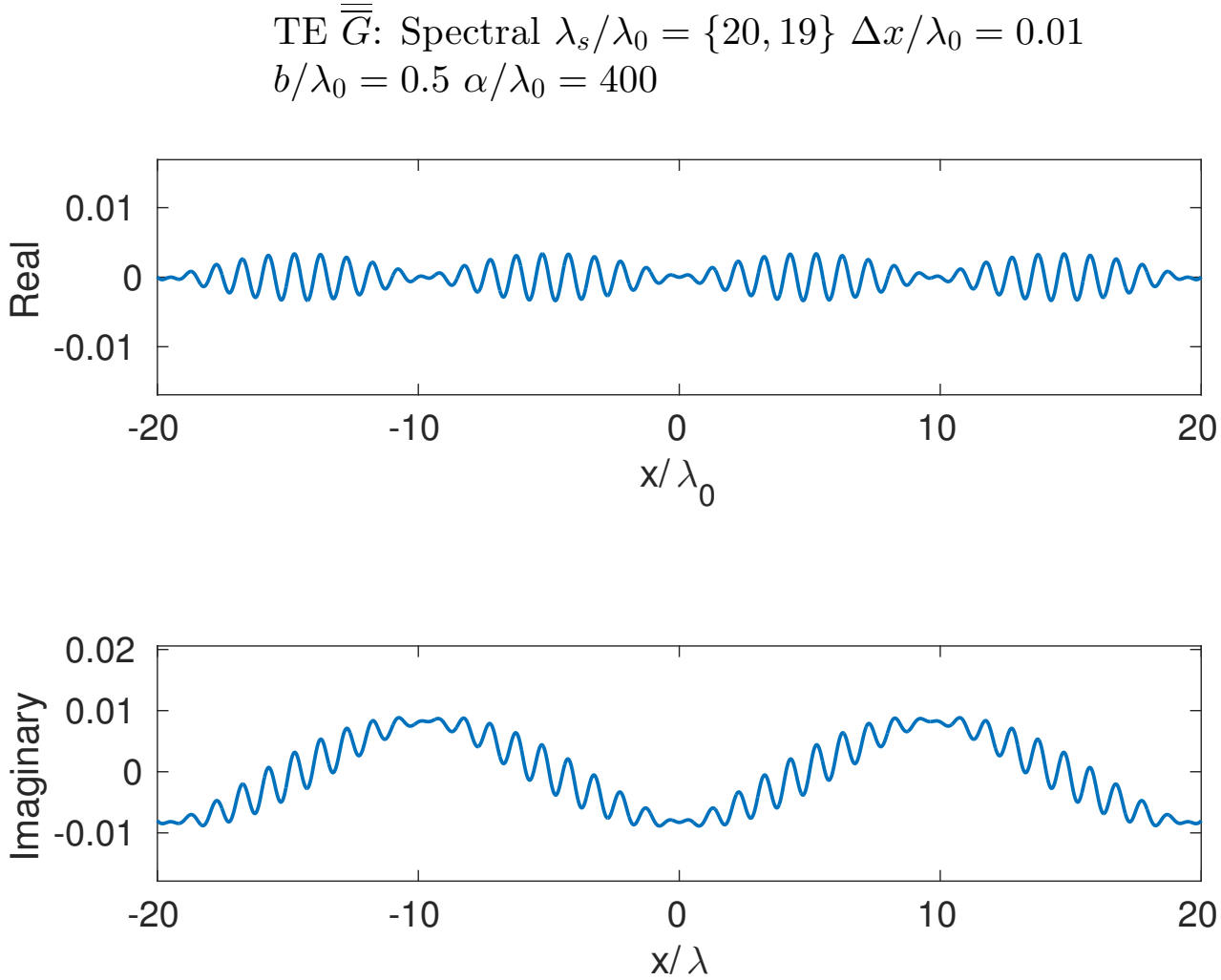


Figure 4.137: TE $\frac{b}{\lambda_0} = 0.5$ $\frac{\alpha}{\lambda_0} = 400$

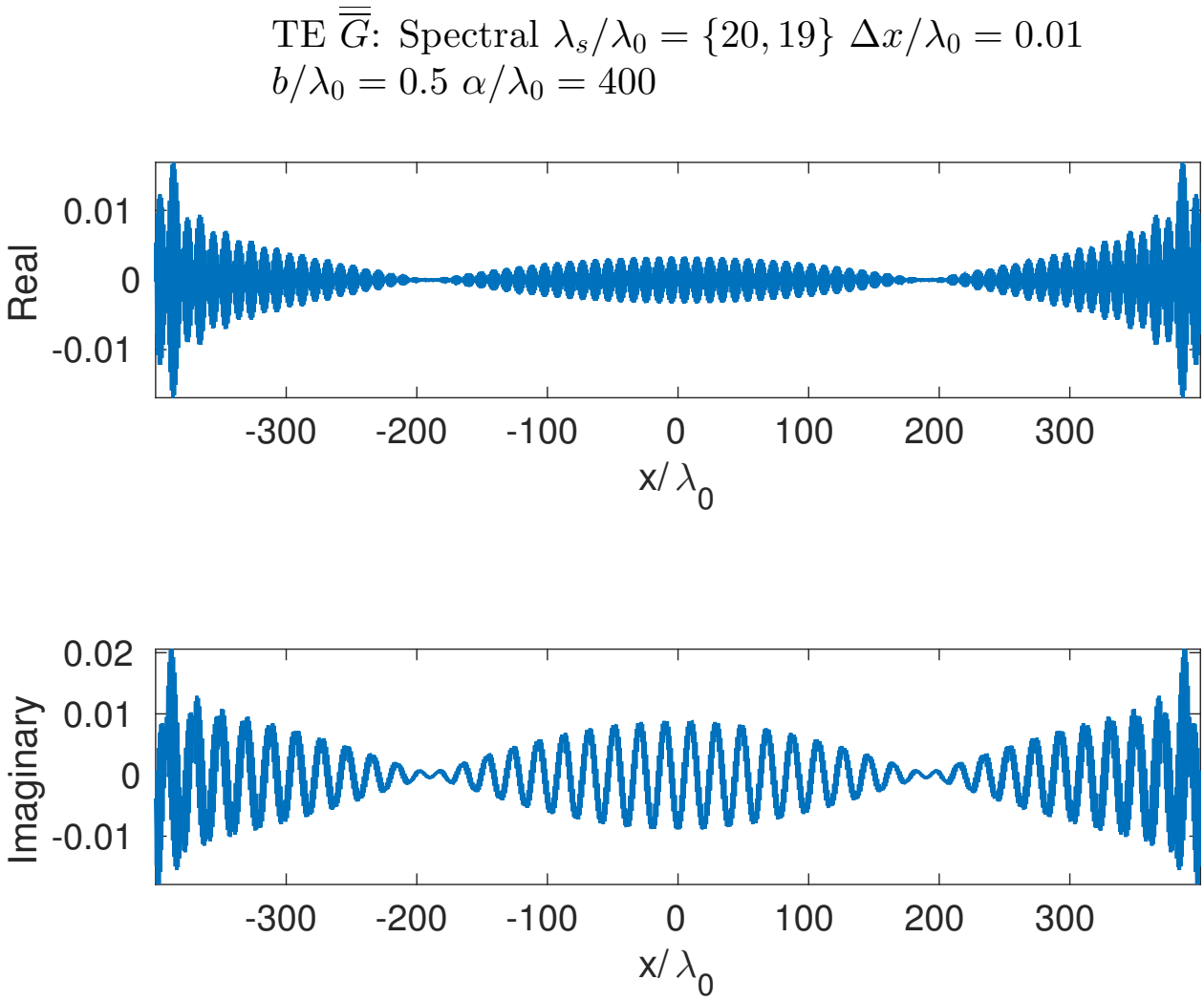


Figure 4.138: TE $\frac{b}{\lambda_0} = 0.5$ $\frac{\alpha}{\lambda_0} = 400$

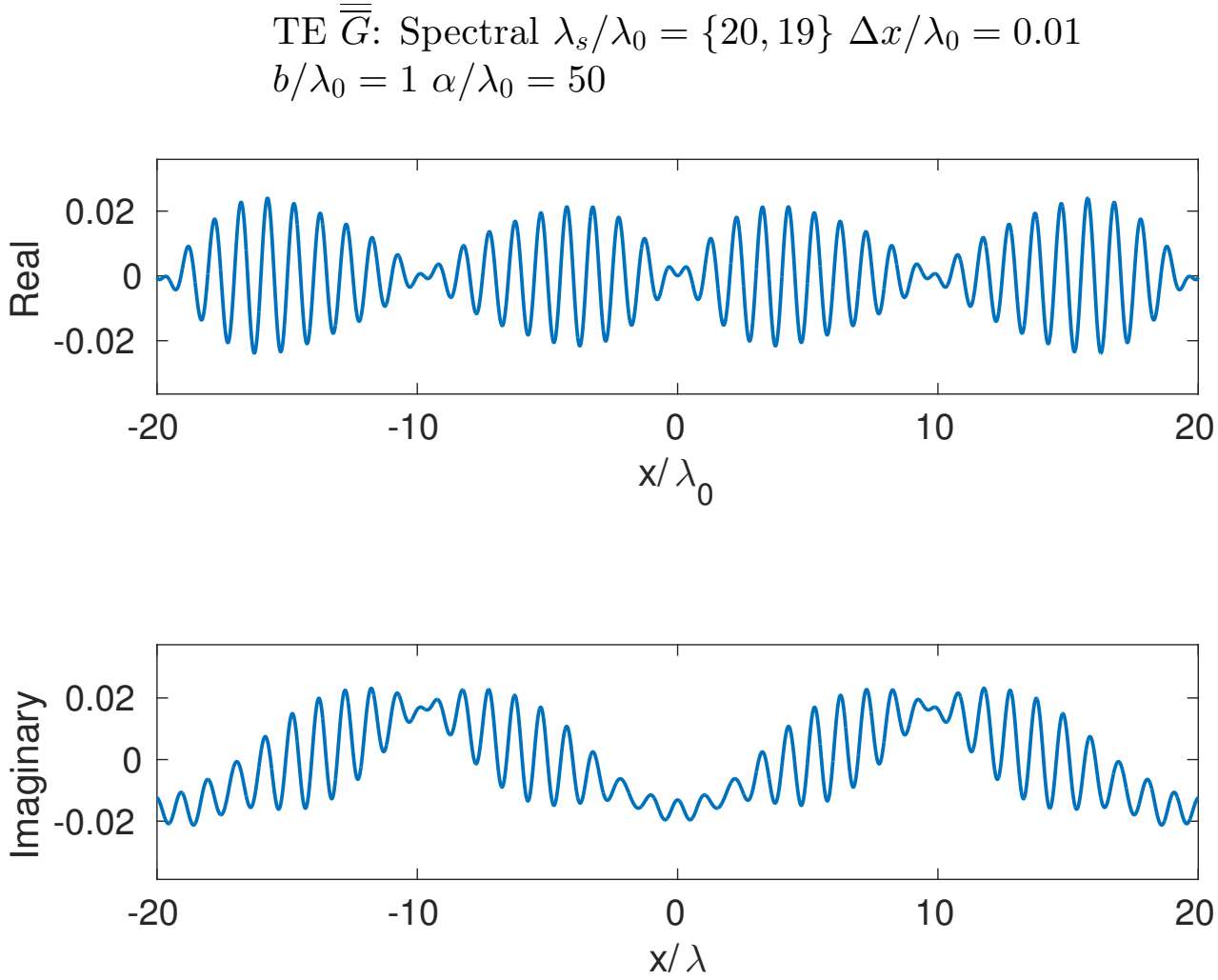


Figure 4.139: TE $\frac{b}{\lambda_0} = 1.0$ $\frac{\alpha}{\lambda_0} = 50$

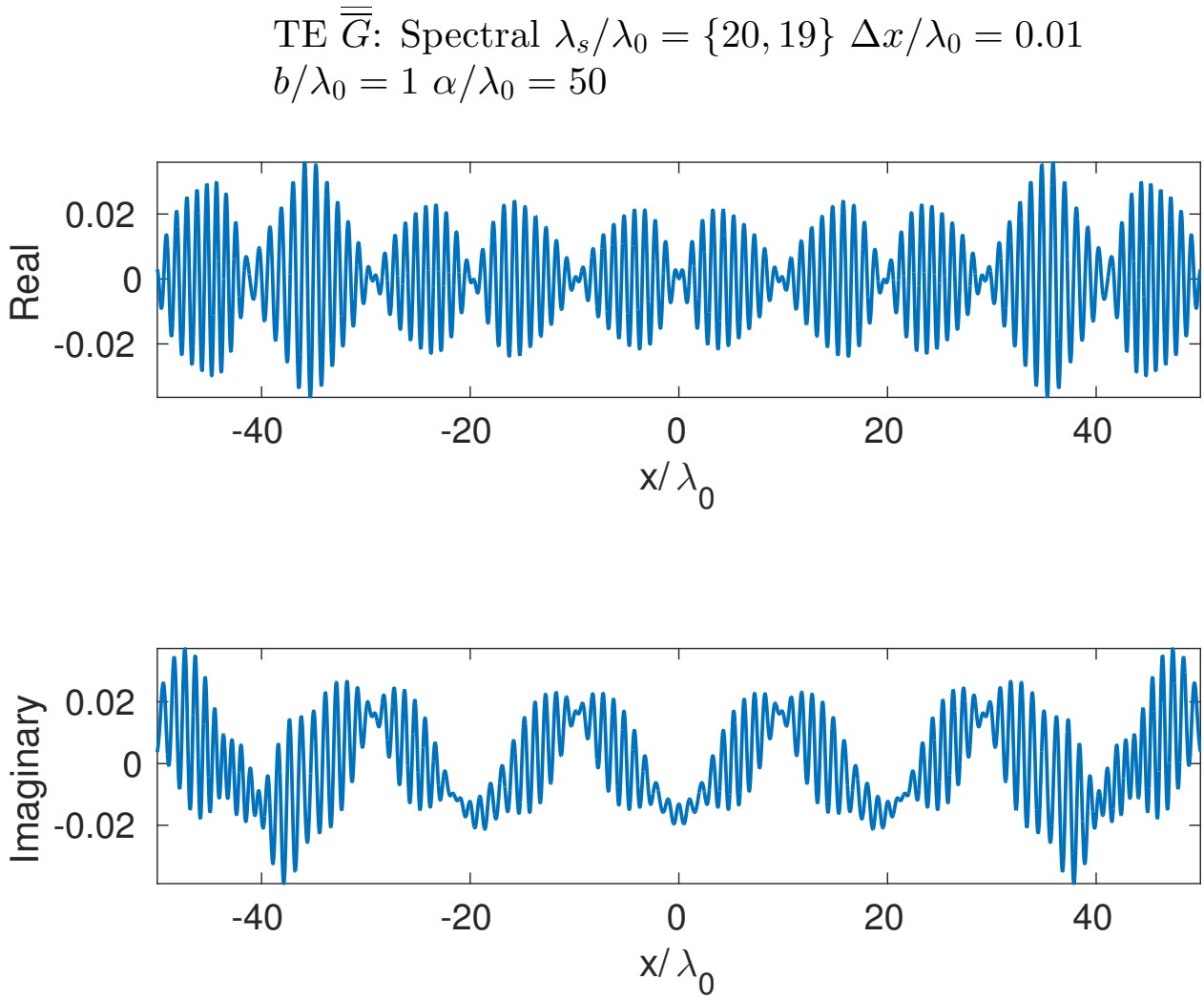


Figure 4.140: TE $\frac{b}{\lambda_0} = 1.0$ $\frac{\alpha}{\lambda_0} = 50$

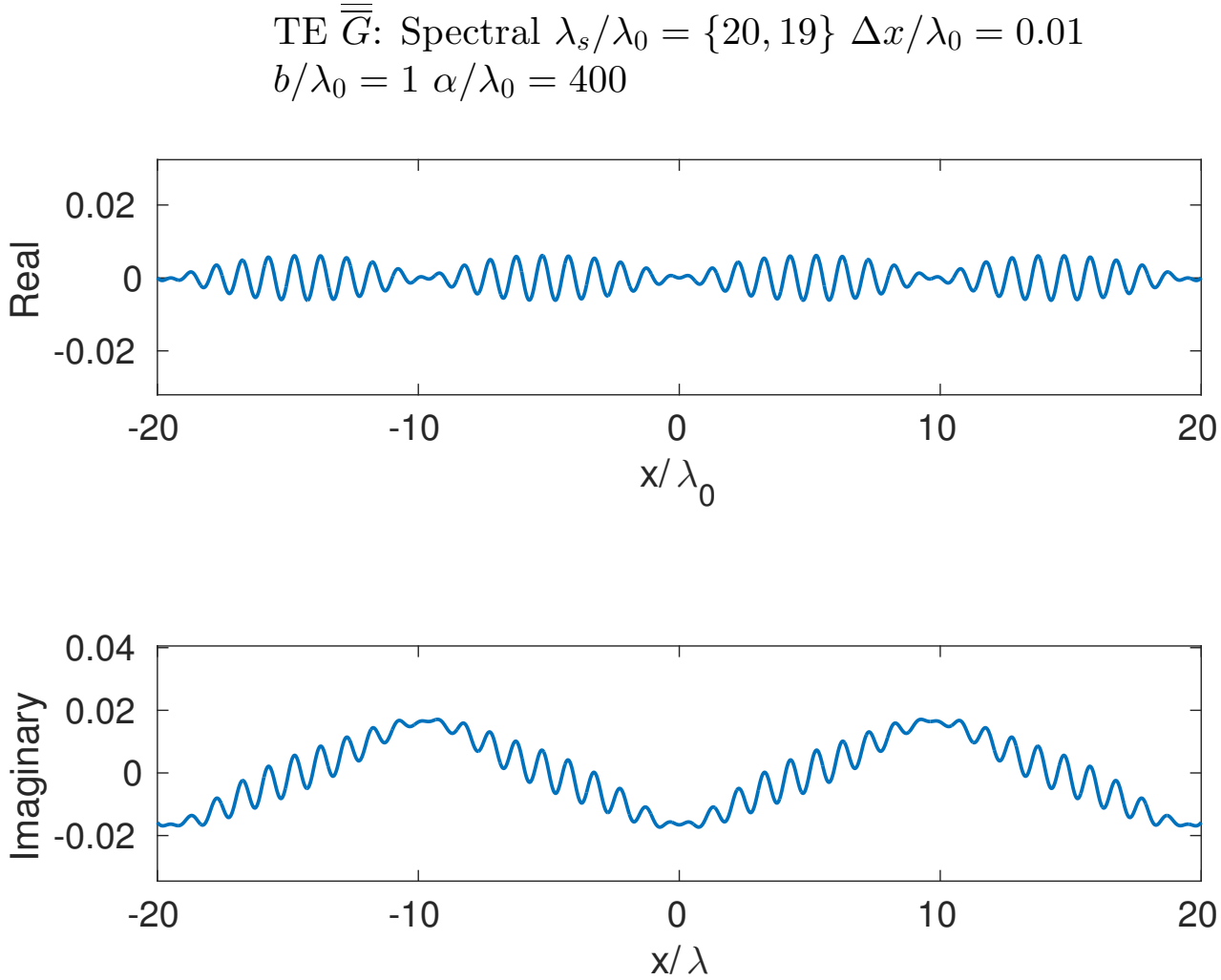


Figure 4.141: TE $\frac{b}{\lambda_0} = 1.0$ $\frac{\alpha}{\lambda_0} = 400$

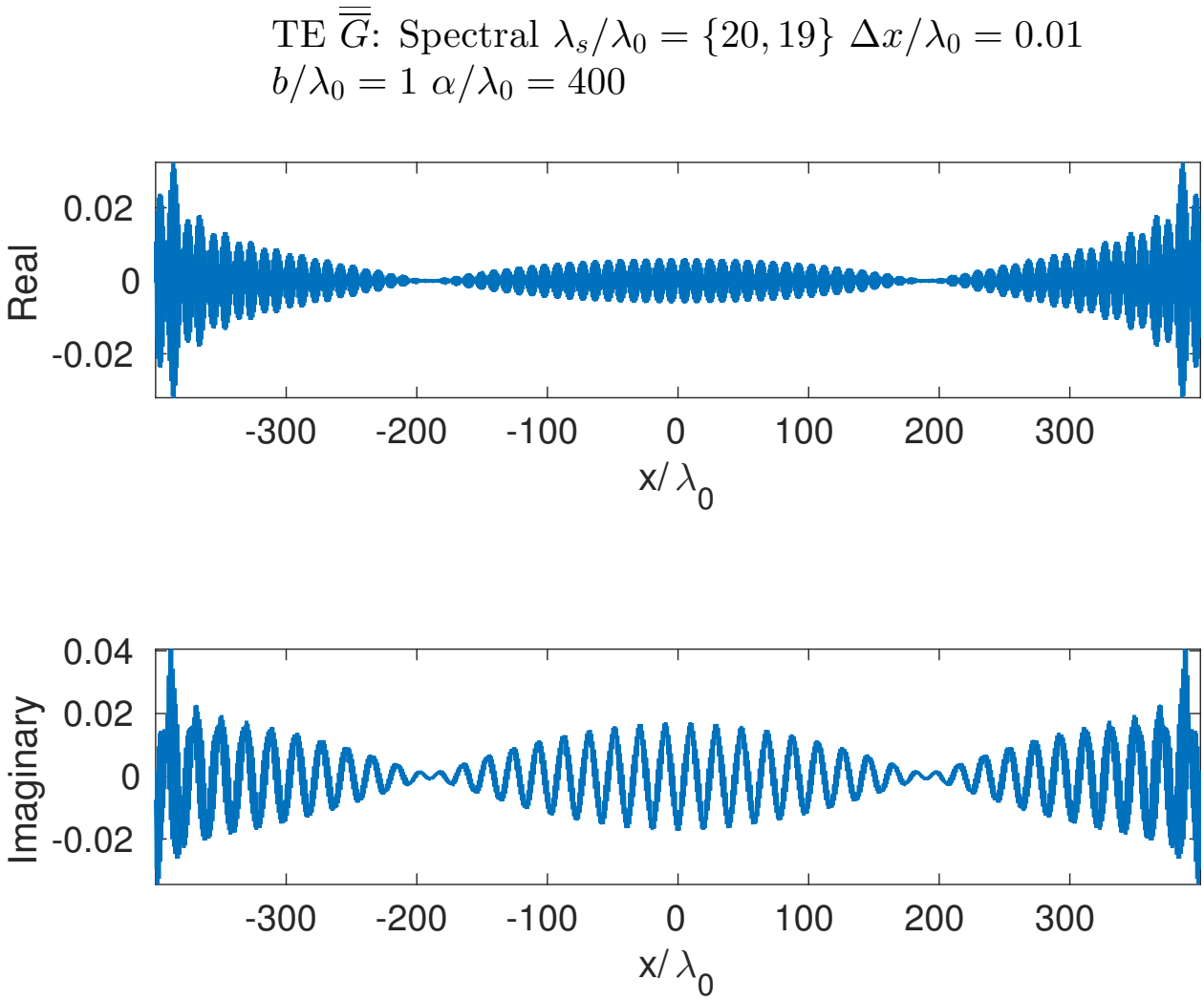


Figure 4.142: TE $\frac{b}{\lambda_0} = 1.0$ $\frac{\alpha}{\lambda_0} = 400$

#### 4.4.4.2 Singular Single Frequency

For TM polarization $\frac{\lambda_s}{\lambda_0} = 1$ gives singular values for a planewave illumination, and very large values for beam illumination. The numeric results in Figures 4.143 through 4.145 show that this is still the case when this frequency is included in a spectral surface as $\overline{\overline{G}}$ is very large and increases with $\frac{\alpha}{\lambda_0}$.

#### 4.4.4.3 TM Linearity

A further failure of the analysis performed in Section 4.4.4 is shown in Figures 4.146 and 4.147 where a two frequency surface with large maximum slope is not a simple linear combination of the two independently numerically calculated surface frequencies. It appears that both TM and TE obey a restriction on slope or higher order surface derivatives for linearity.

#### 4.4.4.4 Characterization vs RMS slope

Previous results found spectral surfaces for both TE and TM to be linear within most of the region of validity for the single frequency empiric analytic formulas of Eqs. 4.4.21 and 4.4.20. It is suspected that this region of validity was limited by the maximum slope or higher order derivative of the surface, but these maximums are only obtained infrequently at discrete points on the surface so are not a good measure. Further, such a metric does not generalize well to random surfaces. To overcome this, the limits on validity of the linear approximation will be recast in terms of the RMS values.

In determining the limit in terms of maximum slope, a spectral surfaces with periods $\frac{\lambda_s}{\lambda_0} = \{20, 8\}$ with respective amplitudes $\frac{b}{\lambda_0} = \{0.5, 0.5\}$ was found to have excellent agreement which corresponds to an RMS slope of about 0.3, this does not appear to be a limit though. The limit of validity was found for $\frac{\lambda_s}{\lambda_0} = \{7, 8\}$ with respective amplitudes $\frac{b}{\lambda_0} = \{0.5, 0.5\}$

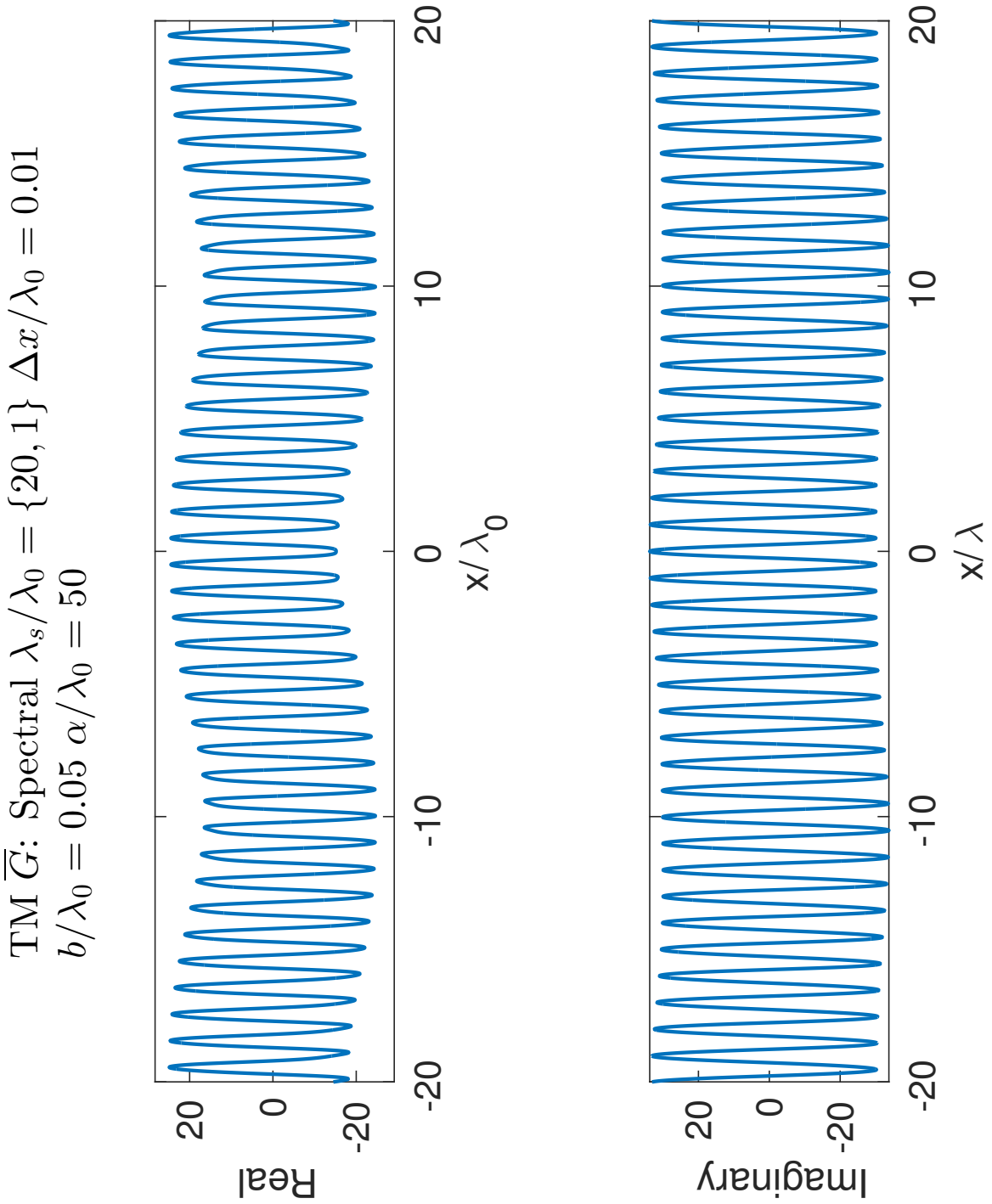


Figure 4.143: TM $\frac{\lambda_s}{\lambda_0} = \{20, 1\}$ $\frac{\alpha}{\lambda_0} = 50$

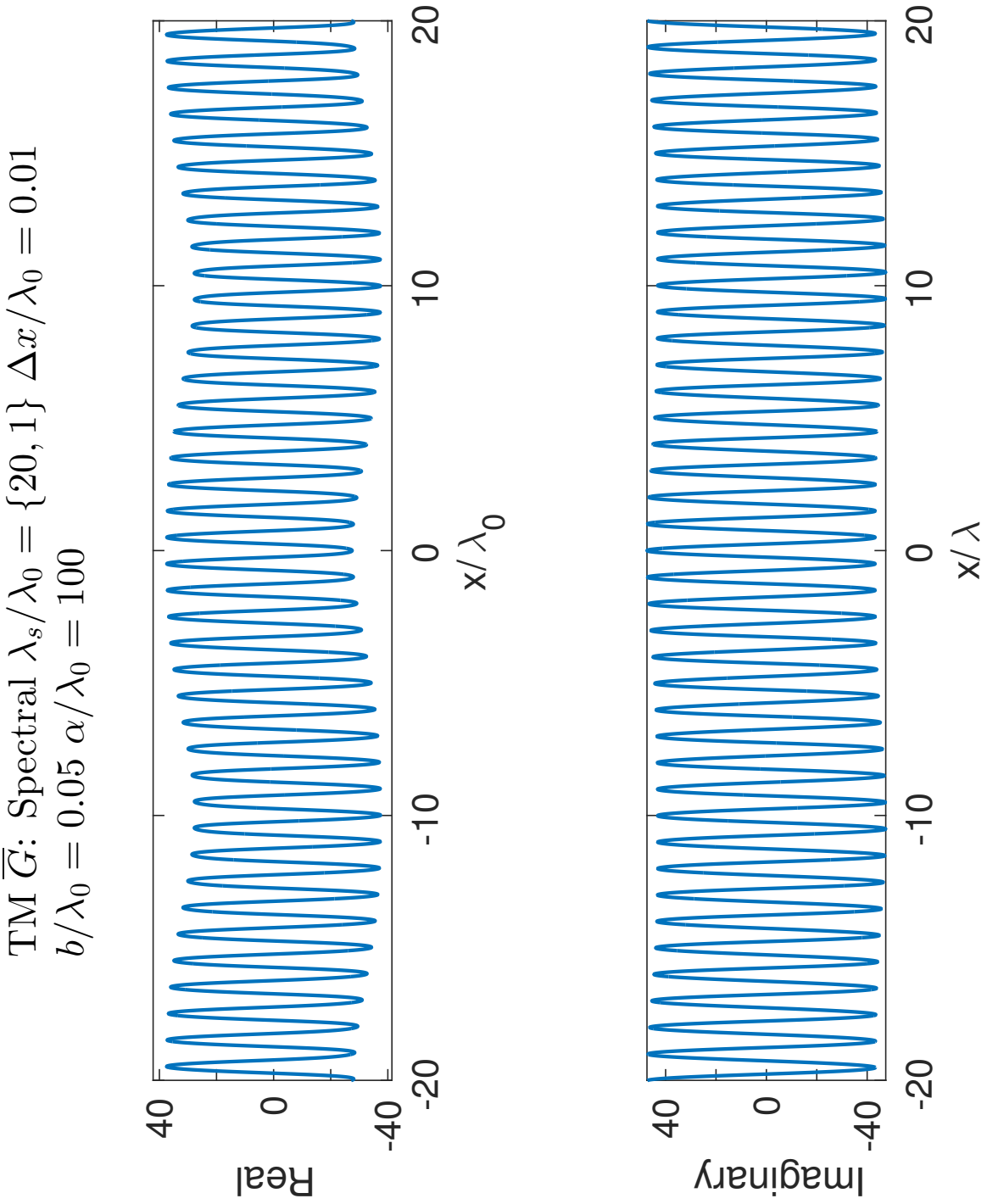


Figure 4.144: TM $\frac{\lambda_s}{\lambda_0} = \{20, 1\}$ $\frac{\alpha}{\lambda_0} = 100$

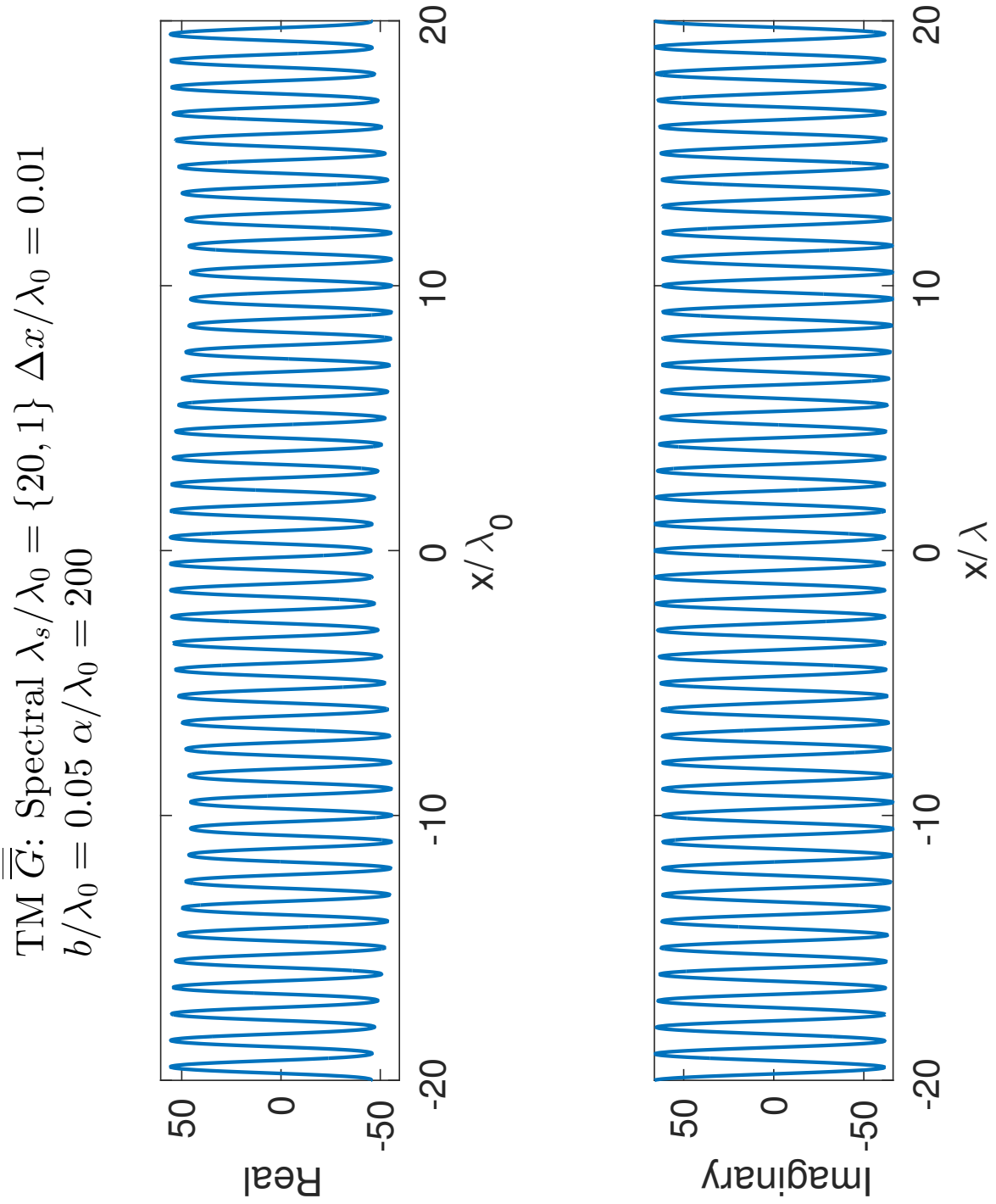


Figure 4.145: TM $\frac{\lambda_s}{\lambda_0} = \{20, 1\}$ $\frac{\alpha}{\lambda_0} = 200$

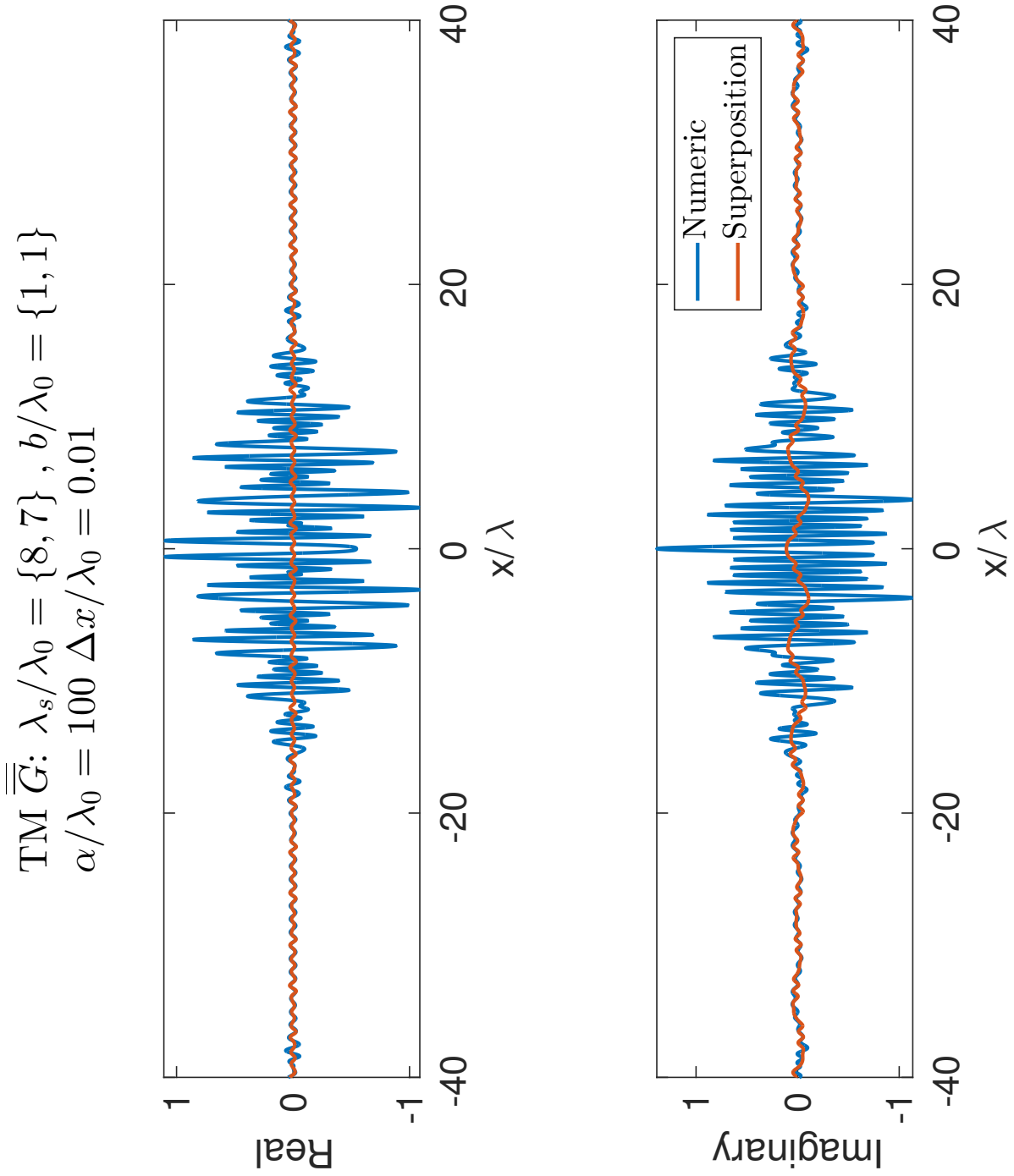


Figure 4.146: TM $\overline{\overline{G}}$ $\frac{\lambda_s}{\lambda_0} = \{8, 7\}$ $\frac{b}{\lambda_0} = \{1, 1\}$

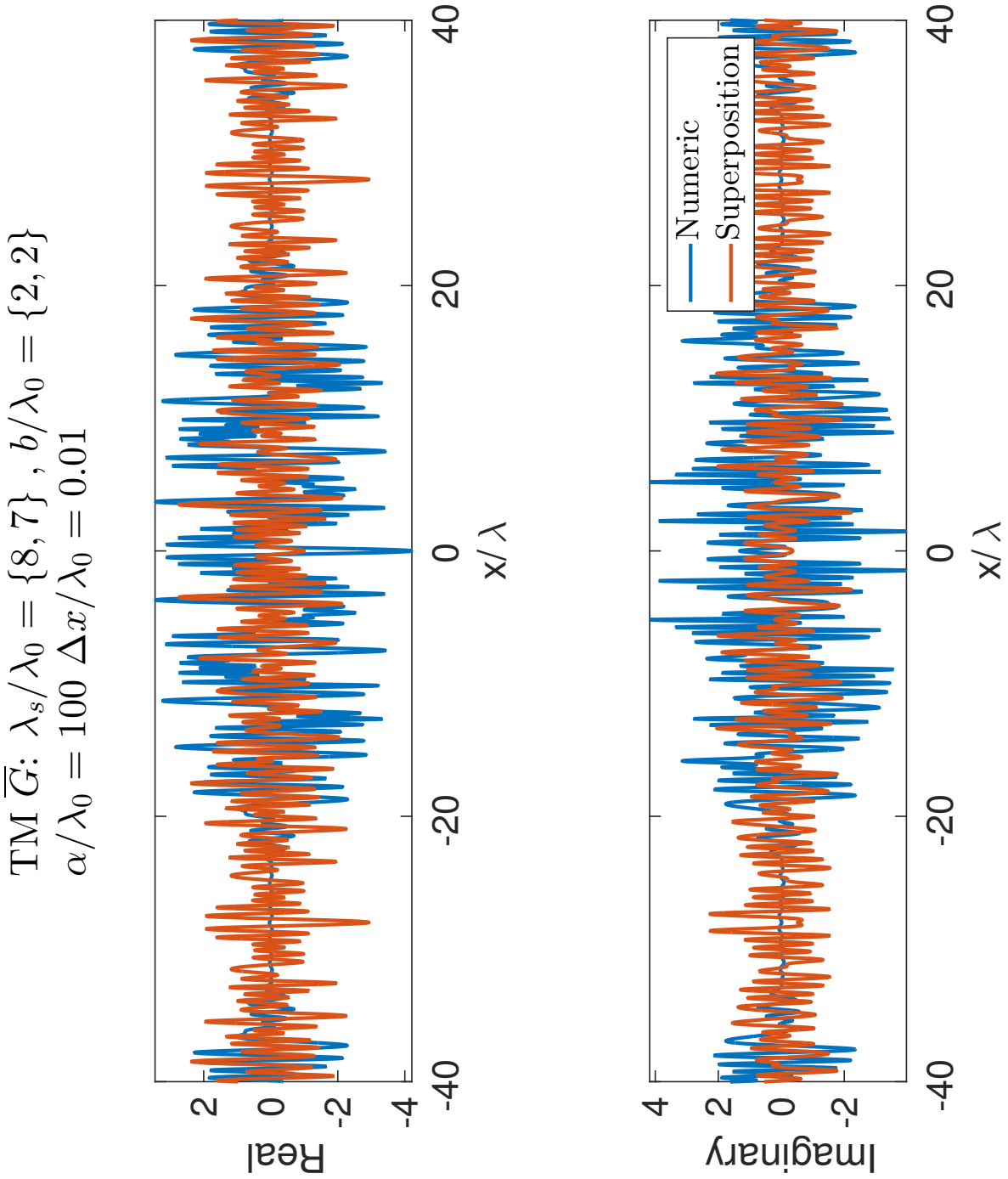


Figure 4.147: TM $\overline{\overline{G}}$ $\frac{\lambda_s}{\lambda_0} = \{8,7\}$ $\frac{b}{\lambda_0} = \{2,2\}$

| $\frac{\lambda_s}{\lambda_0}$ | $\zeta_{x_{rms}} \approx 0.30$ | $\zeta_{x_{rms}} \approx 0.35$ | $\zeta_{x_{rms}} \approx 0.40$ | $\zeta_{x_{rms}} \approx 0.45$ |
|---|---|---|---|---|
| $\{7, 8\}$ | $\frac{b}{\lambda_0} = 0.35$ | $\frac{b}{\lambda_0} = 0.42$ | $\frac{b}{\lambda_0} = 0.47$ | $\frac{b}{\lambda_0} = 0.53$ |
| $\{7, 20\}$ | $\frac{b}{\lambda_0} = 0.45$ | $\frac{b}{\lambda_0} = 0.52$ | $\frac{b}{\lambda_0} = 0.59$ | $\frac{b}{\lambda_0} = 0.67$ |
| $\{19, 20\}$ | $\frac{b}{\lambda_0} = 0.93$ | $\frac{b}{\lambda_0} = 1.09$ | $\frac{b}{\lambda_0} = 1.24$ | $\frac{b}{\lambda_0} = 1.40$ |
| $\{20, 40\}$ | $\frac{b}{\lambda_0} = 1.21$ | $\frac{b}{\lambda_0} = 1.41$ | $\frac{b}{\lambda_0} = 1.61$ | $\frac{b}{\lambda_0} = 1.81$ |
| $\{10, 15, 20\}$ | $\frac{b}{\lambda_0} = 0.52$ | $\frac{b}{\lambda_0} = 0.61$ | $\frac{b}{\lambda_0} = 0.69$ | $\frac{b}{\lambda_0} = 0.78$ |
| $\{7, 8, 9\}$ | $\frac{b}{\lambda_0} = 0.31$ | $\frac{b}{\lambda_0} = 0.36$ | $\frac{b}{\lambda_0} = 0.41$ | $\frac{b}{\lambda_0} = 0.46$ |

Table 4.4.2: Surface Parameters for Simulation

which gives an RMS slope of about 0.42.

This bound of about $\zeta_{x_{rms}} \approx 0.4$ was tested by calculating $\overline{\overline{G}}$ for different combinations of surface periods with corresponding amplitudes to give RMS slopes of $\{0.30, 0.35, 0.40, 0.45\}$. By selecting the surface periods and a desired RMS slope for each two frequency surface, a discrete set of the peak amplitudes of the individual frequency components can be found to give the desired RMS slope. For the results to follow, the peak amplitudes of the frequency components will be equivalent for simplicity. Additionally, a few three and four frequency surfaces will be run with the same RMS slopes. The surface parameters which were simulated are given in Table 4.4.2 . Note that surface periods have been chosen to include shorter, longer and combinations of both.

The result for two frequency surfaces show that in general the real component has smaller relative errors than the imaginary and the error increases as the slope is increased. In the charts that follow, the term *Numeric* means "exactly" calculated through numeric integration of $\overline{\overline{G}}$ of the full spectral surface and *Superposition* is found by numerically calculating $\overline{\overline{G}}$ and adding each of the individual surface frequency components. Figures 4.148 through 4.151 show TM and TE for $\frac{\lambda_s}{\lambda_0} = \{20, 40\}$ with RMS slopes of $\zeta_{x_{rms}} \approx 0.30$ and $\zeta_{x_{rms}} \approx 0.45$, 4.152 through 4.155 for $\frac{\lambda_s}{\lambda_0} = \{19, 20\}$, 4.156 through 4.159 for $\frac{\lambda_s}{\lambda_0} = \{7, 20\}$ and 4.160 through 4.163 for $\frac{\lambda_s}{\lambda_0} = \{7, 8\}$.

TM appears to fare worse than TE but both look acceptable on all surfaces up to $\zeta_{x_{rms}} = 0.4$. Only on the surface with short periods $\frac{\lambda_s}{\lambda_0} = \{7, 8\}$ does the $\zeta_{x_{rms}} = 0.45$ really become questionable for TM only with significant errors in magnitude (half) and phase. The error here is most prominent when the phases of surface components begin to line up and the maximum surface slopes are obtained and seems to be true for all surfaces for which the period of the spectral surface falls in the support of $\overline{\overline{G}}$.

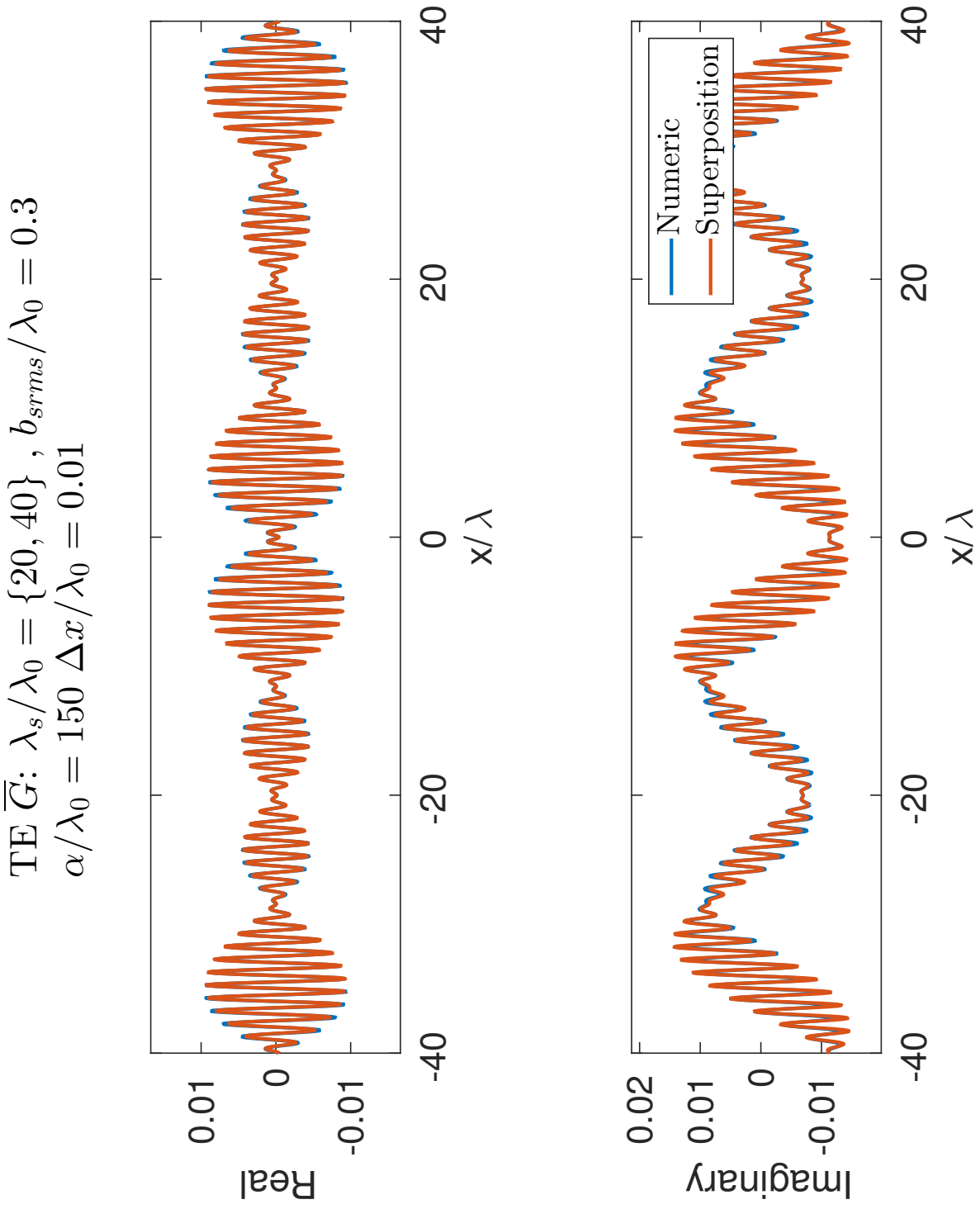


Figure 4.148: TE $\overline{\overline{G}}$ $\frac{\lambda_s}{\lambda_0} = \{20, 40\}$ $\frac{b_{rms}}{\lambda_0} = 30$ (Enlarged)

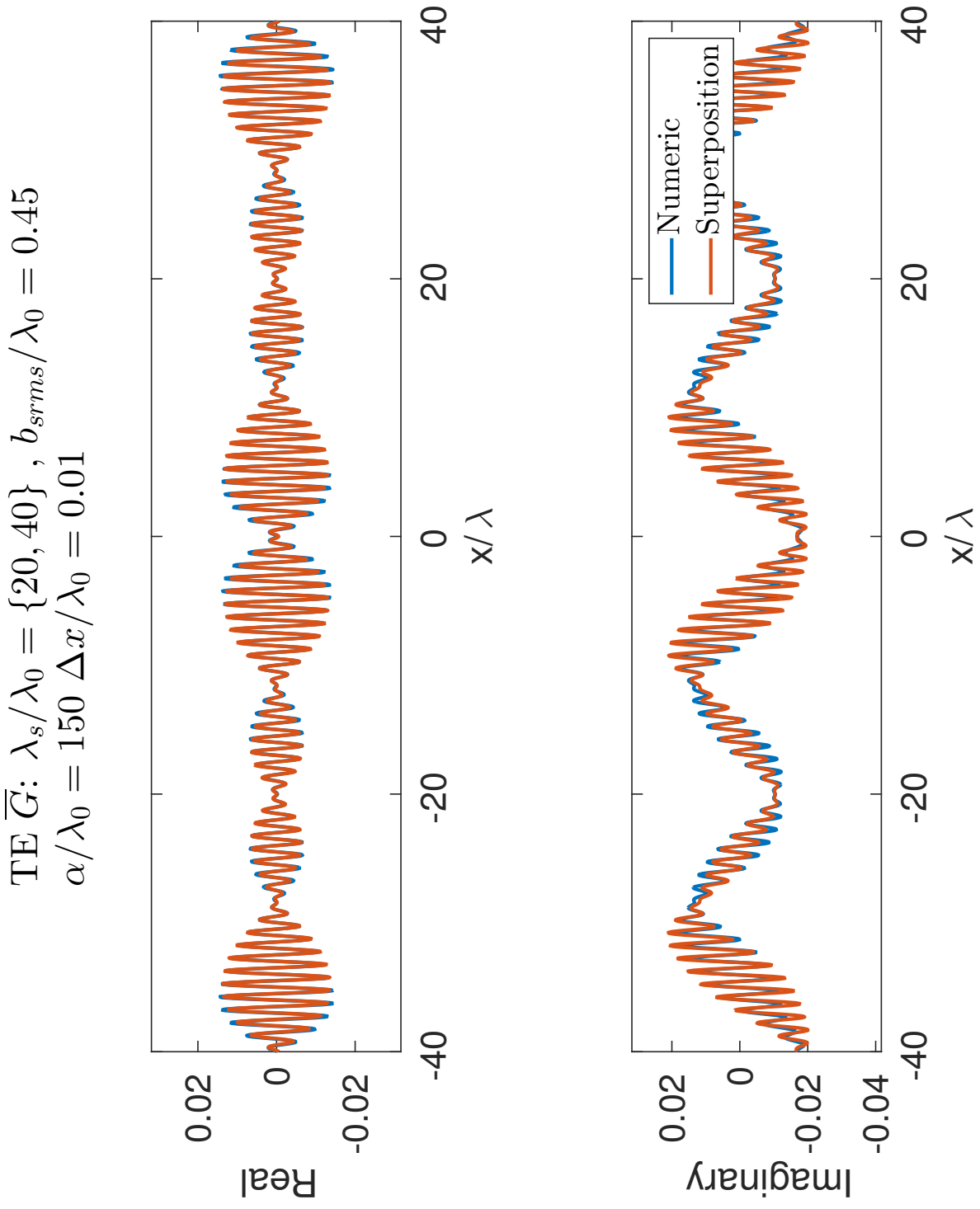


Figure 4.149: TE $\overline{\overline{G}}$ $\frac{\lambda_s}{\lambda_0} = \{20, 40\}$ $\frac{b_{rms}}{\lambda_0} = 45$ (Enlarged)

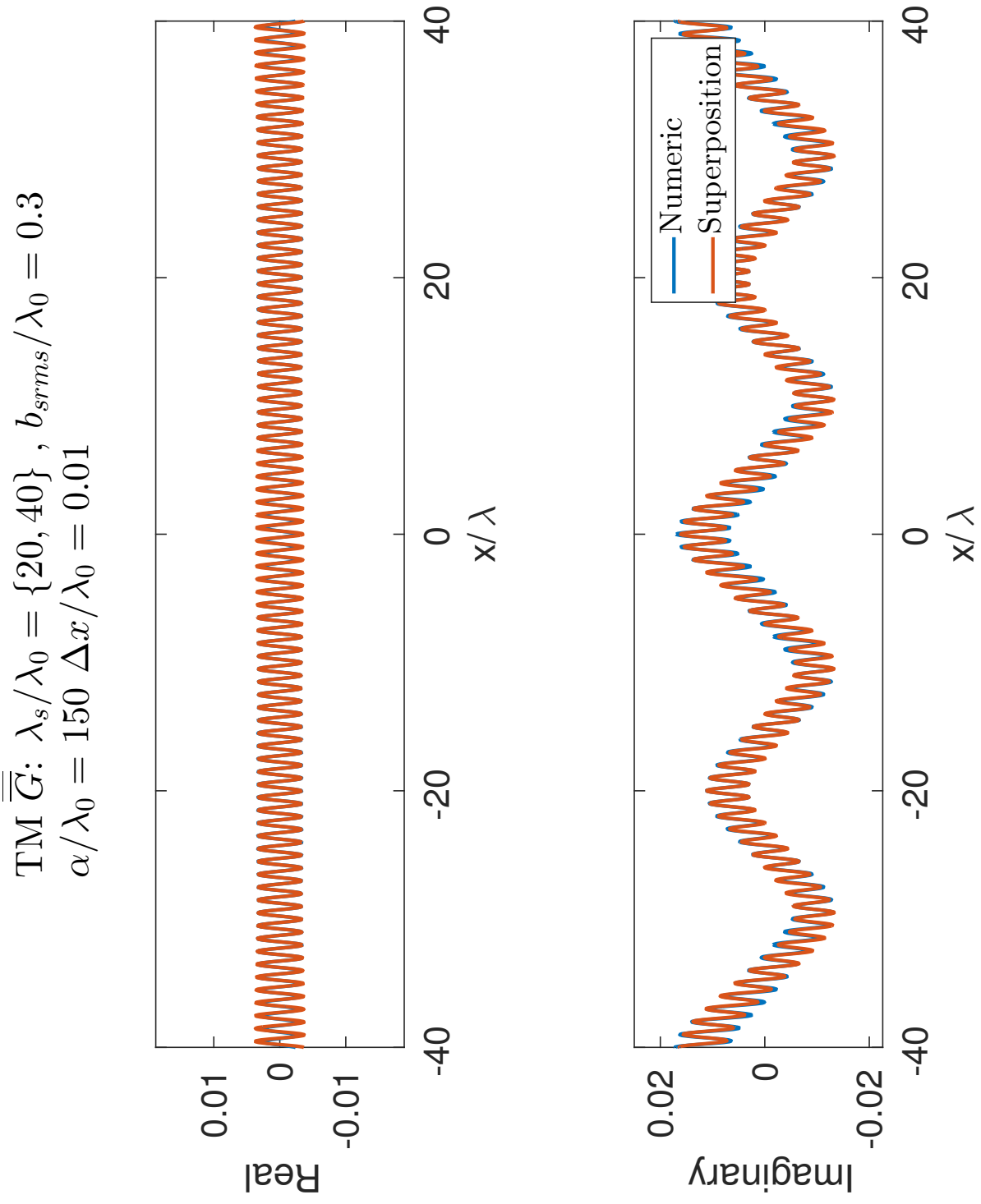


Figure 4.150: TM $\overline{\overline{G}}$ $\frac{\lambda_s}{\lambda_0} = \{20, 40\}$ $\frac{b_{rms}}{\lambda_0} = 30$ (Enlarged)

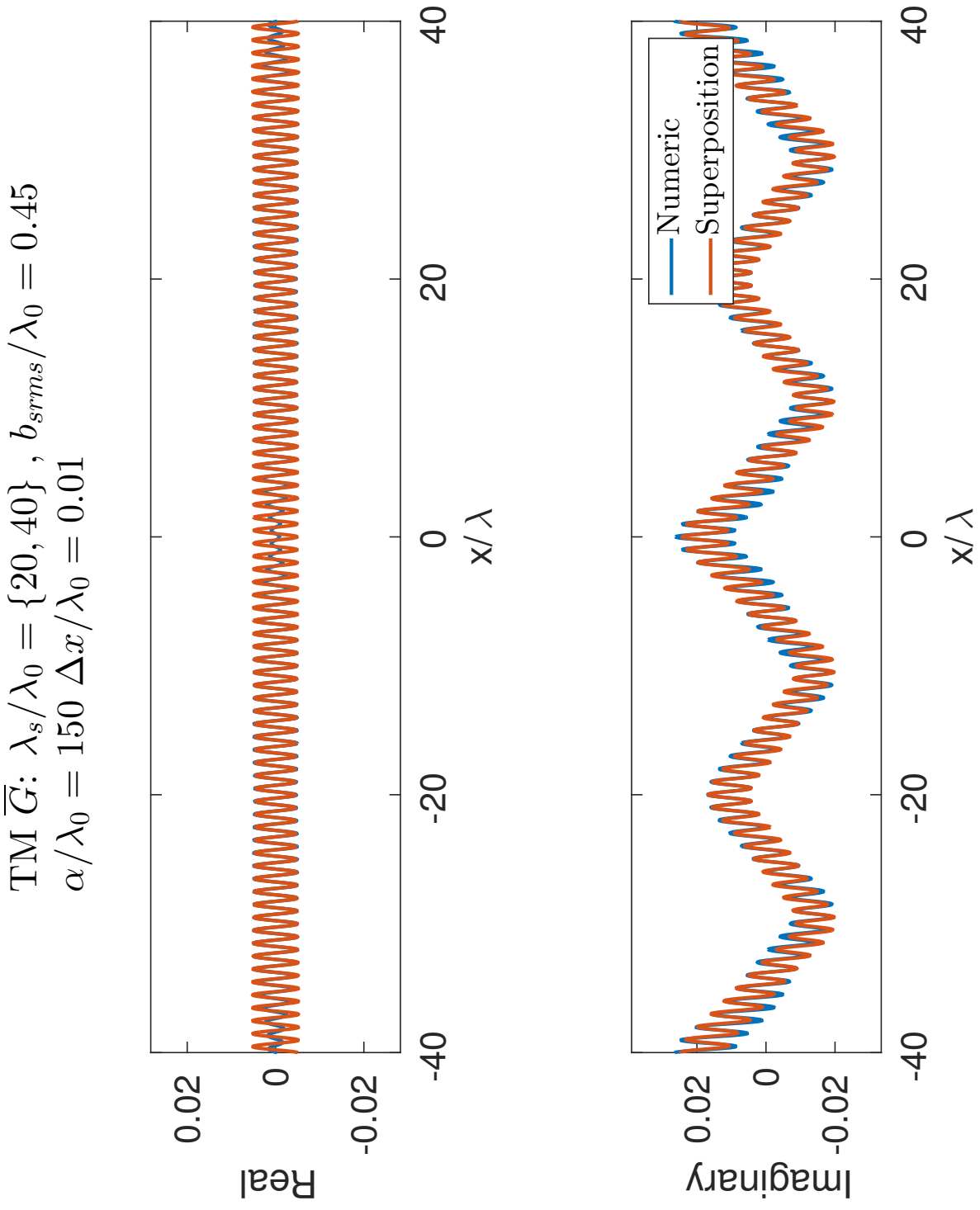


Figure 4.151: TM $\overline{\overline{G}}$ $\frac{\lambda_s}{\lambda_0} = \{20, 40\}$ $\frac{b_{rms}}{\lambda_0} = 45$ (Enlarged)

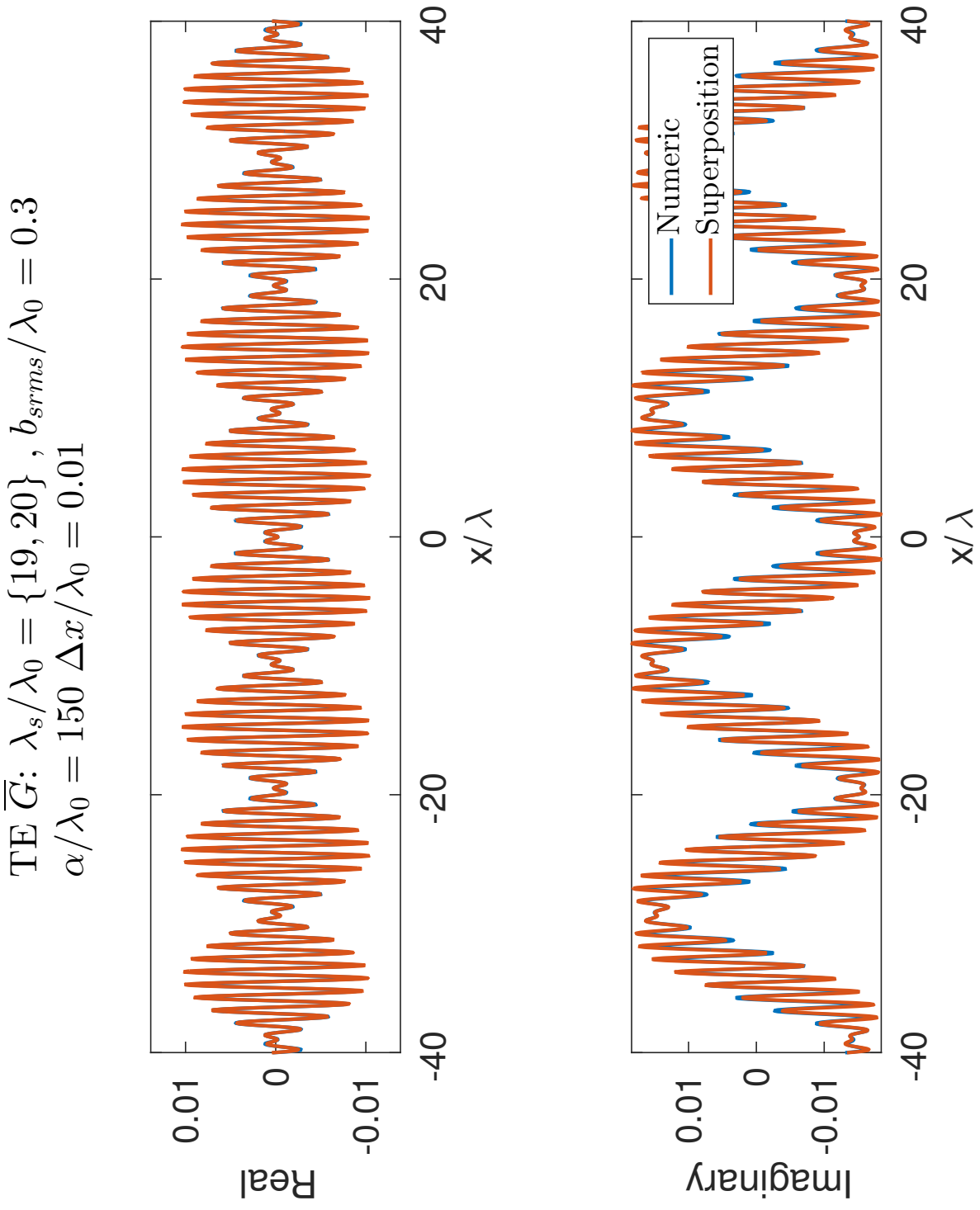


Figure 4.152: TE $\overline{\overline{G}}$ $\frac{\lambda_s}{\lambda_0} = \{19, 20\}$ $\frac{b_{rms}}{\lambda_0} = 30$ (Enlarged)

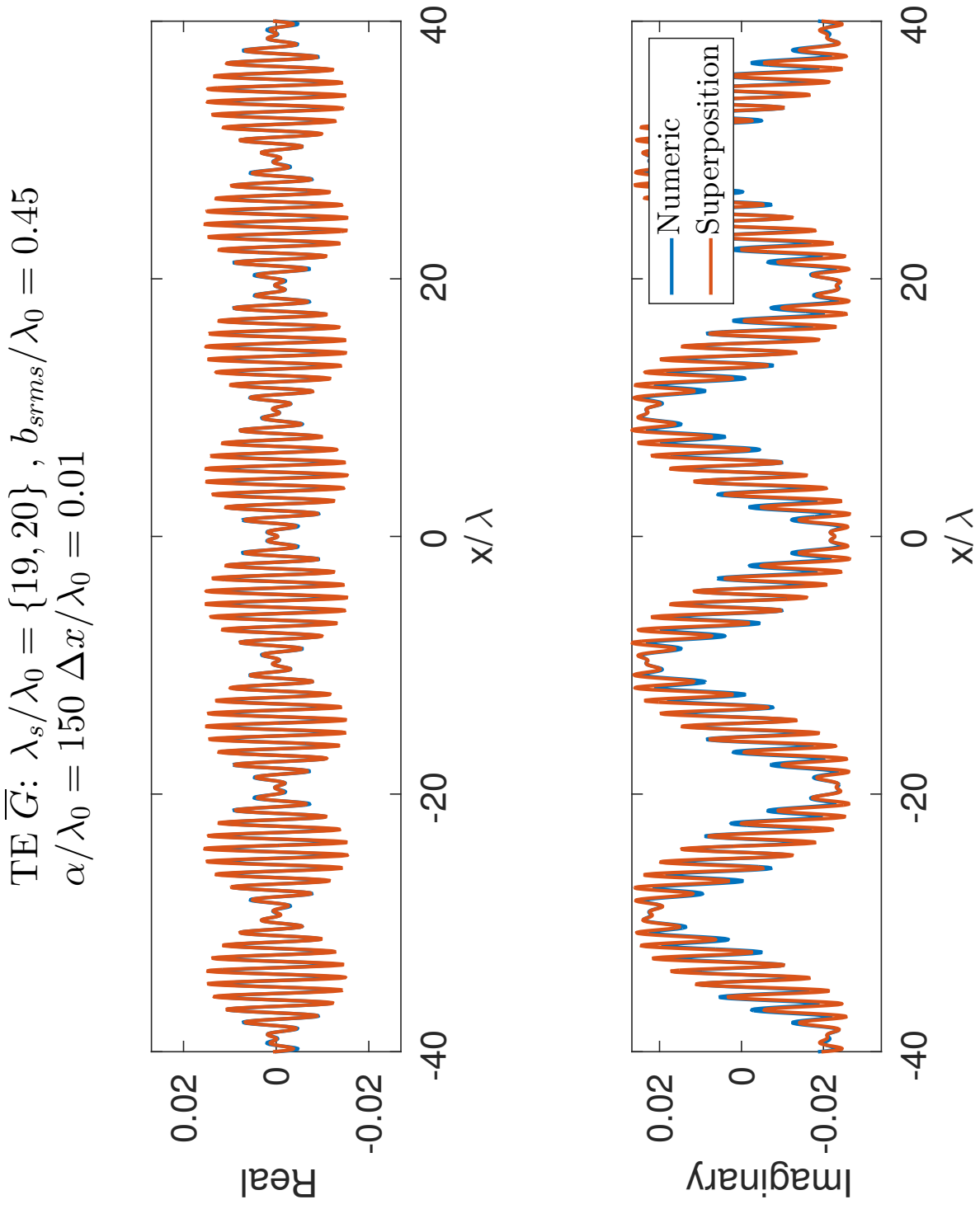


Figure 4.153: TE $\overline{\overline{G}}$ $\frac{\lambda_s}{\lambda_0} = \{19, 20\}$ $\frac{b_{rms}}{\lambda_0} = 45$ (Enlarged)

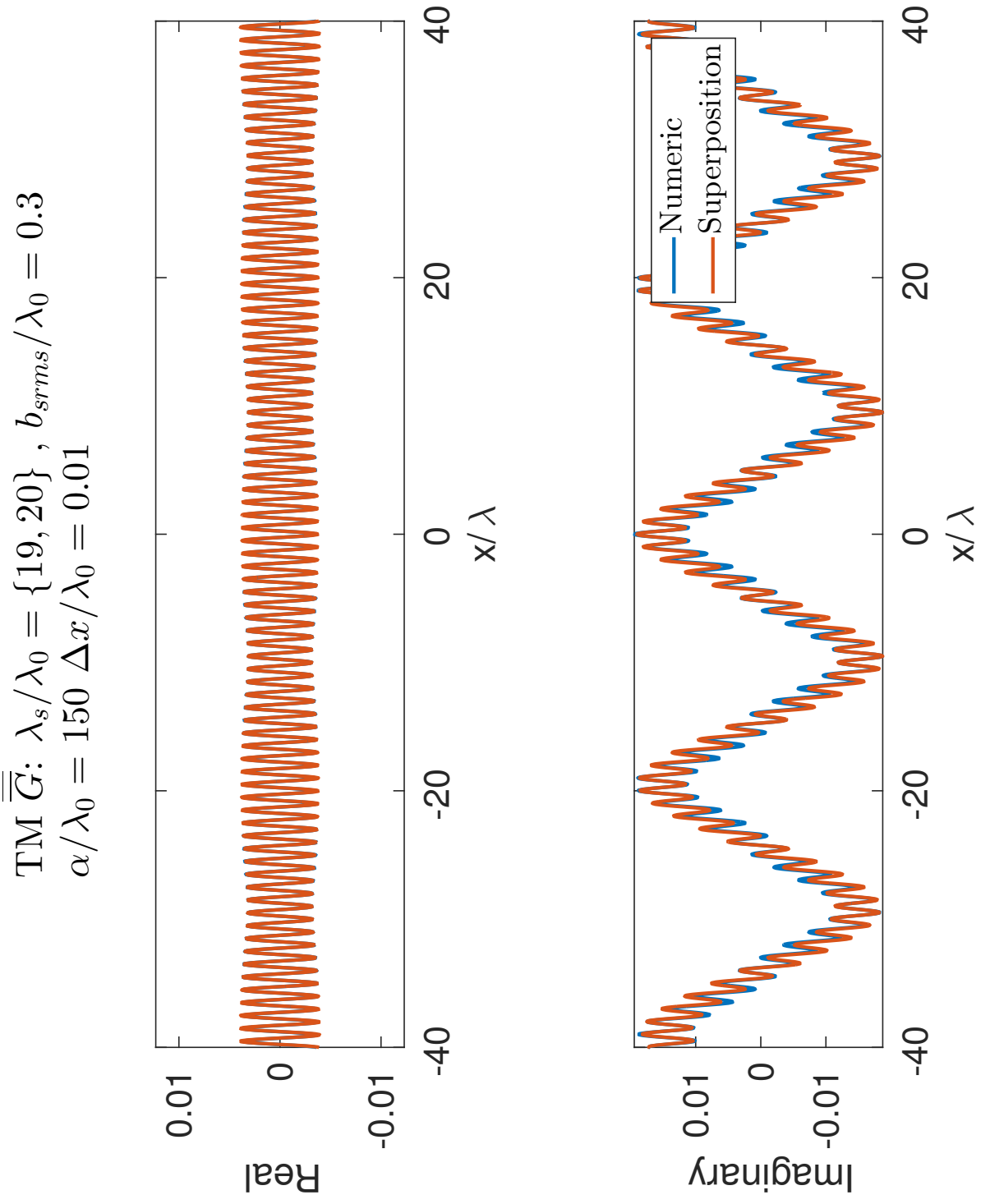


Figure 4.154: TM $\overline{\overline{G}}$ $\frac{\lambda_s}{\lambda_0} = \{19, 20\}$ $\frac{b_{rms}}{\lambda_0} = 30$ (Enlarged)

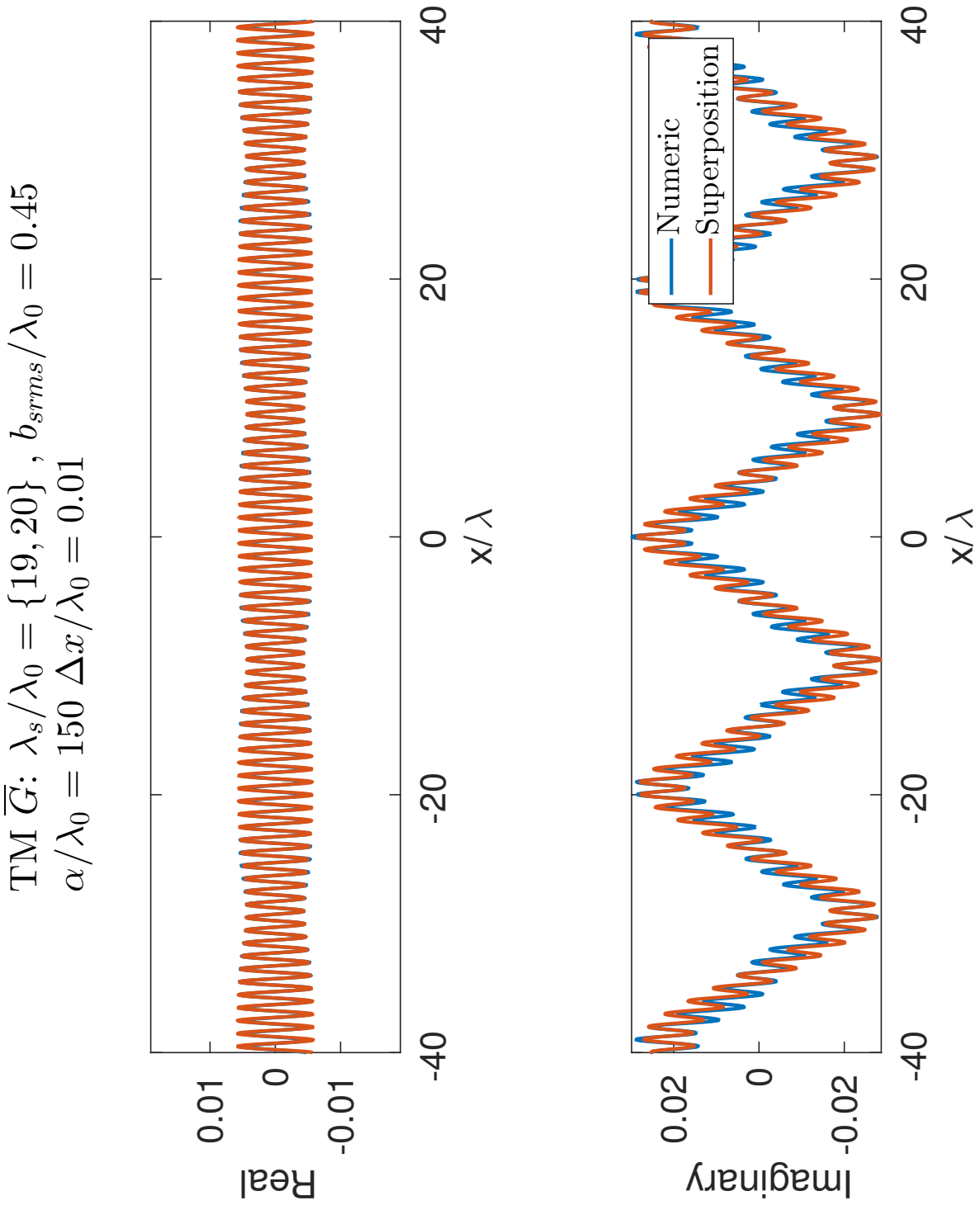


Figure 4.155: TM $\overline{\overline{G}}$ $\frac{\lambda_s}{\lambda_0} = \{19, 20\}$ $\frac{b_{rms}}{\lambda_0} = 45$ (Enlarged)

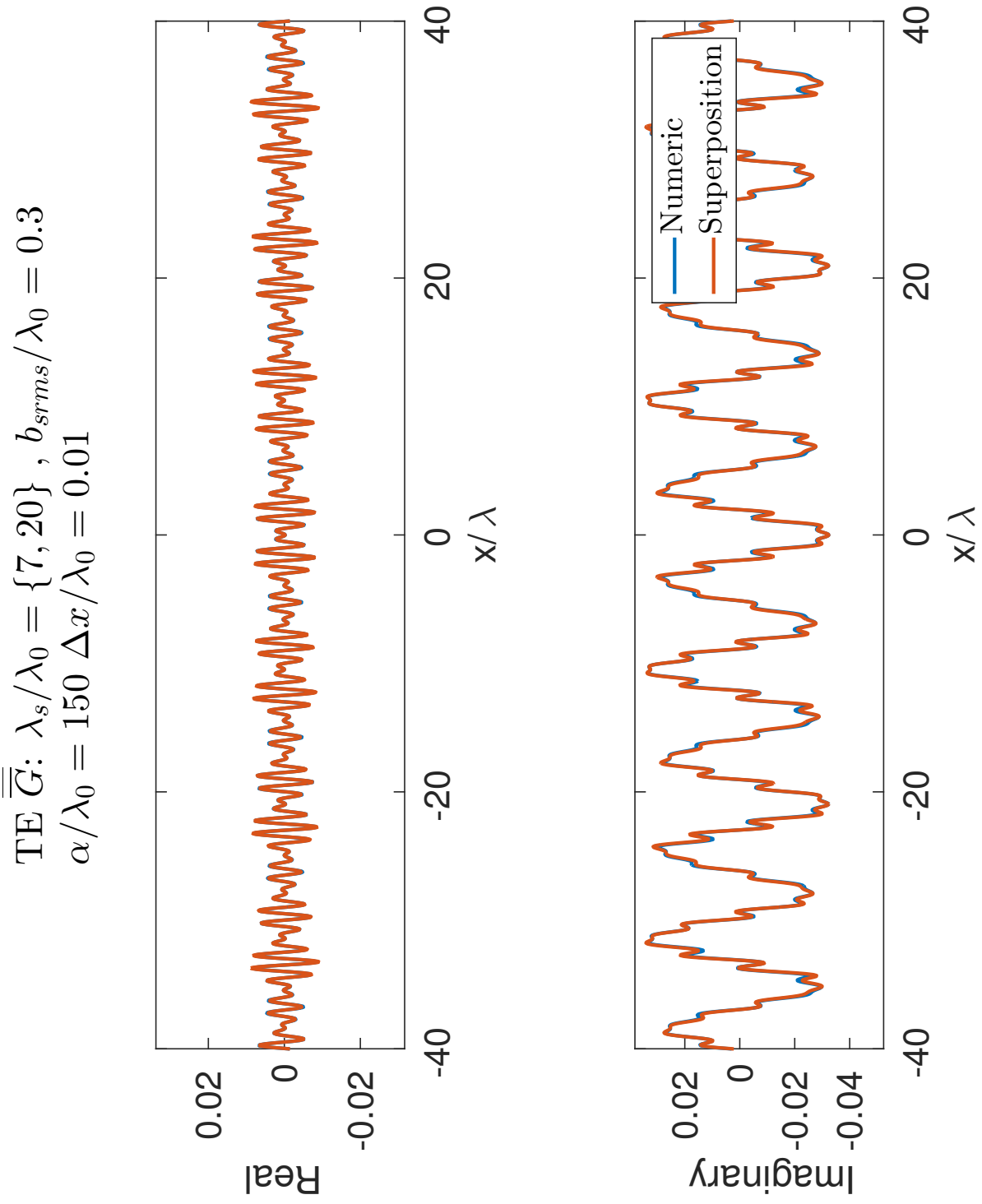


Figure 4.156: TE $\overline{\overline{G}}$ $\frac{\lambda_s}{\lambda_0} = \{7, 20\}$ $\frac{b_{rms}}{\lambda_0} = 30$ (Enlarged)

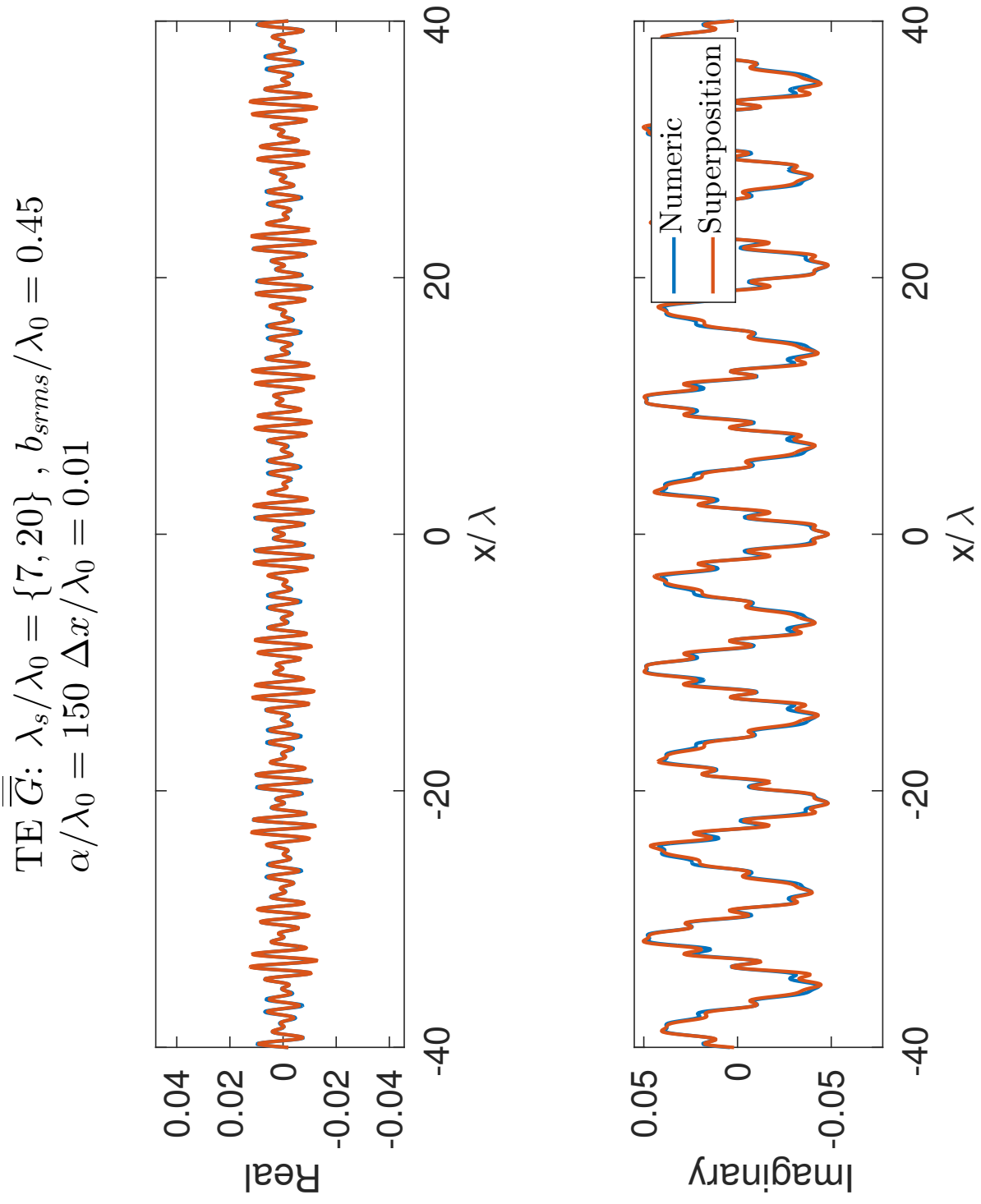


Figure 4.157: TE $\overline{\overline{G}}$ $\frac{\lambda_s}{\lambda_0} = \{7, 20\}$ $\frac{b_{rms}}{\lambda_0} = 45$ (Enlarged)

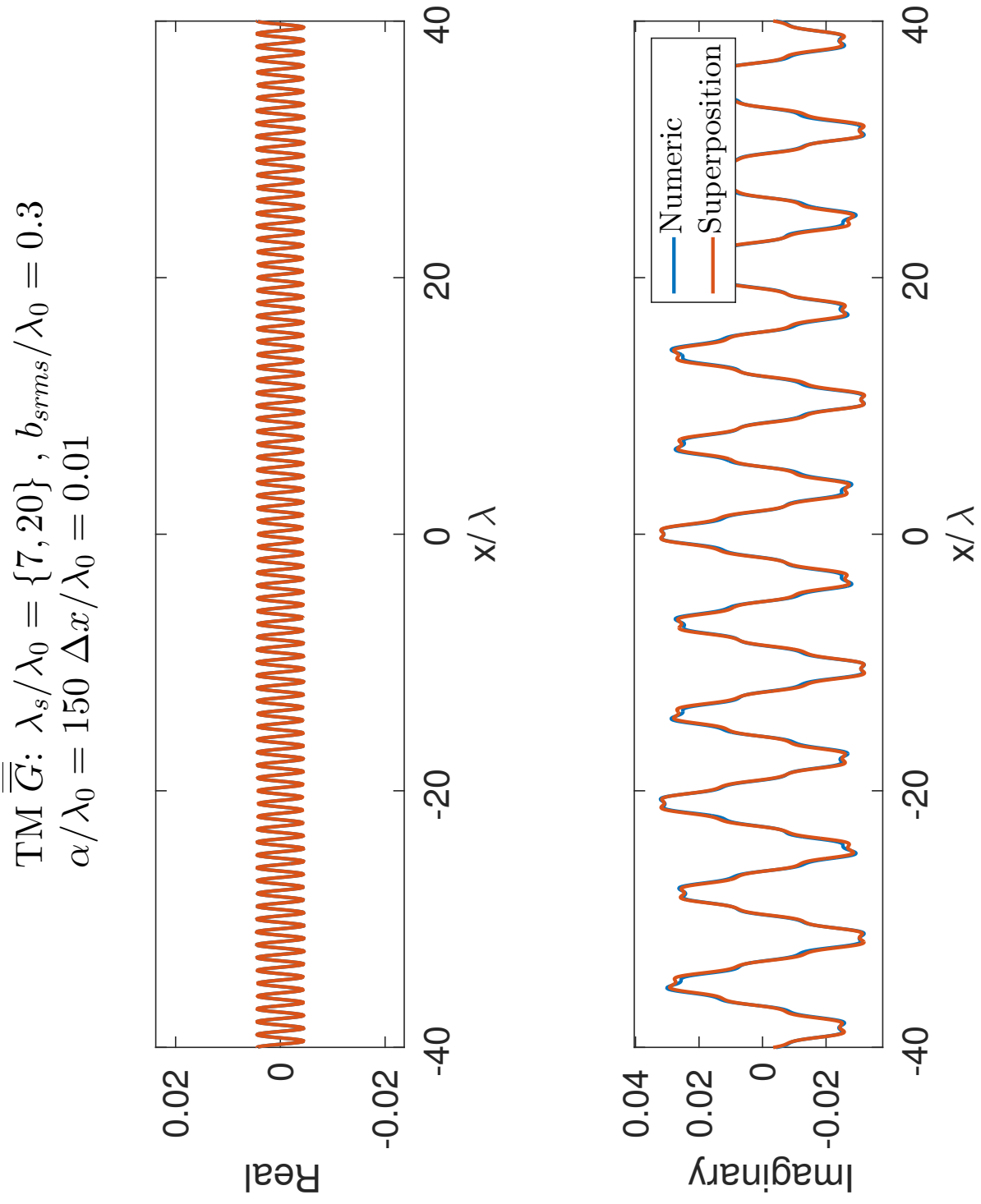


Figure 4.158: TM $\overline{\overline{G}}$ $\frac{\lambda_s}{\lambda_0} = \{7, 20\}$ $\frac{b_{rms}}{\lambda_0} = 30$ (Enlarged)

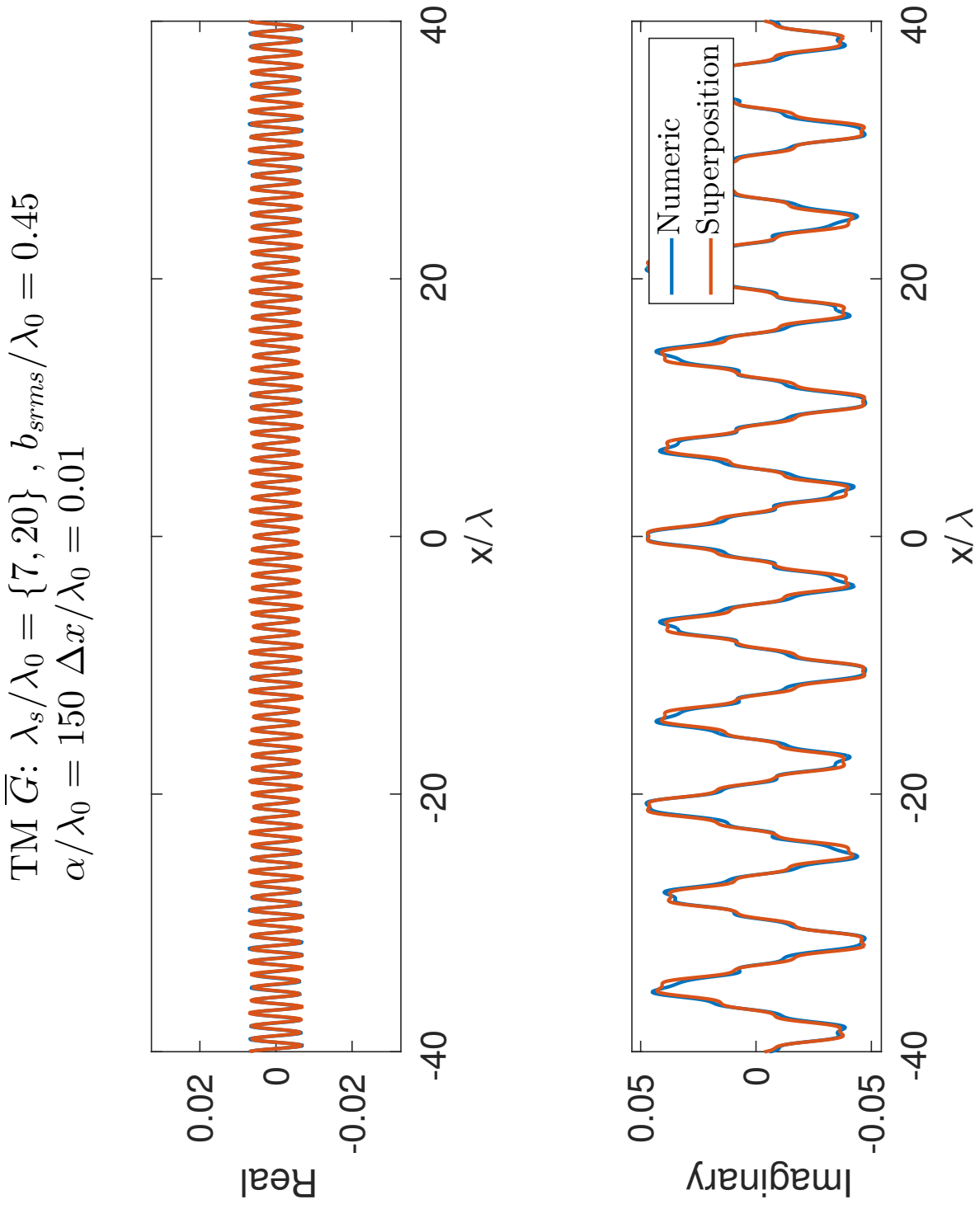


Figure 4.159: TM $\overline{\overline{G}}$ $\frac{\lambda_s}{\lambda_0} = \{7, 20\}$ $\frac{b_{rms}}{\lambda_0} = 45$ (Enlarged)

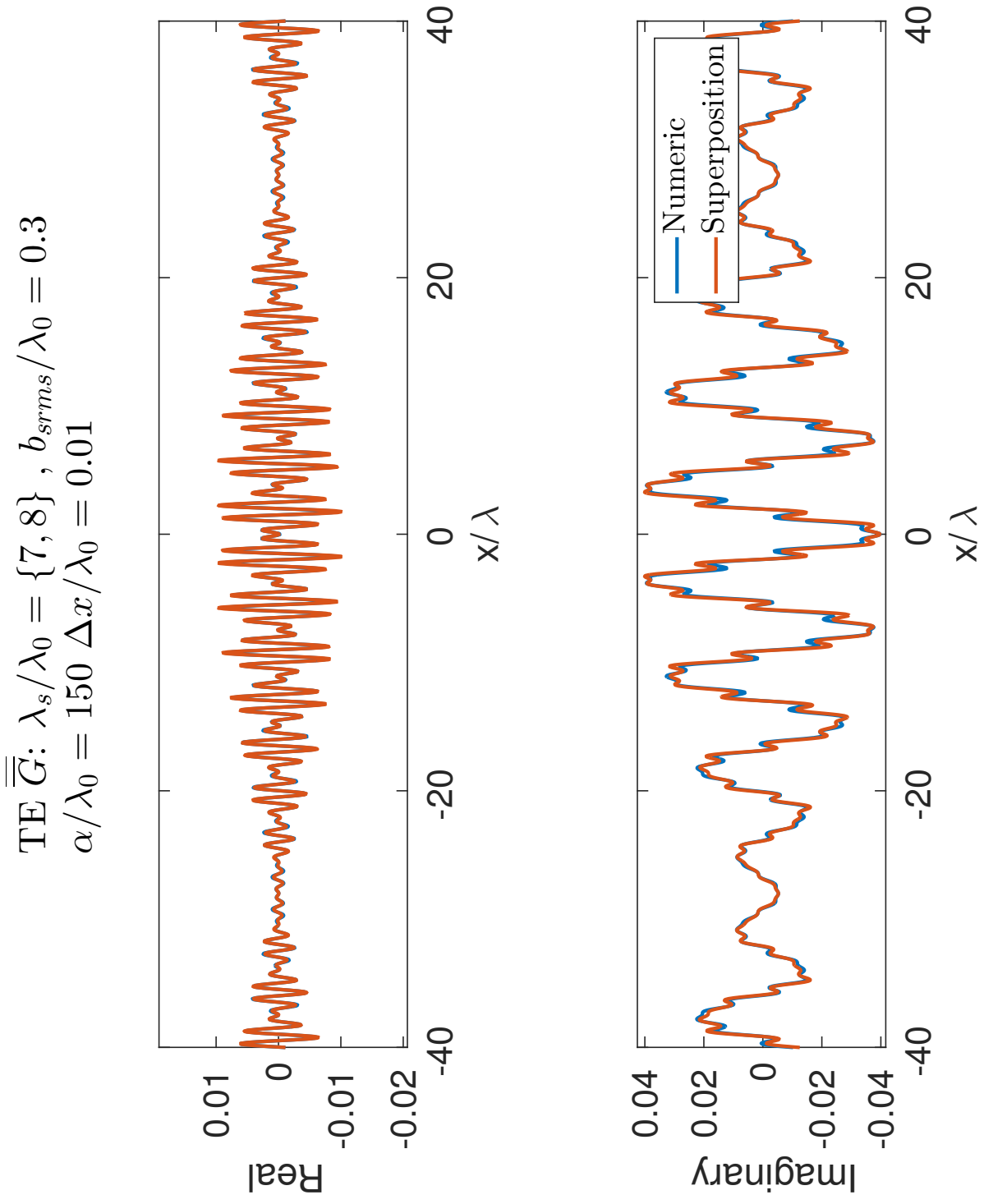


Figure 4.160: TE $\overline{\overline{G}}$ $\frac{\lambda_s}{\lambda_0} = \{7, 8\}$ $\frac{b_{rms}}{\lambda_0} = 30$ (Enlarged)

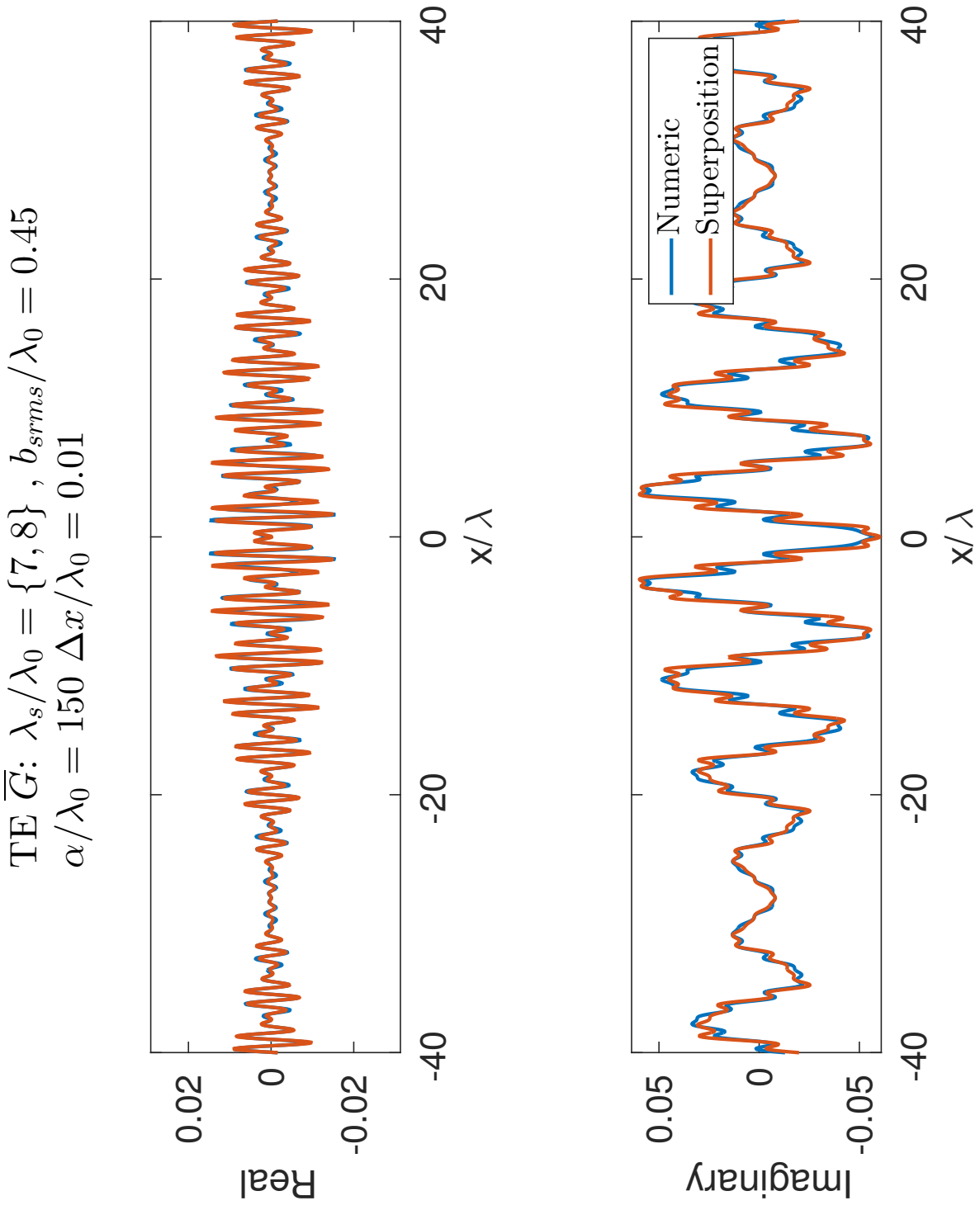


Figure 4.161: TE $\overline{\overline{G}}$ $\frac{\lambda_s}{\lambda_0} = \{7, 8\}$ $\frac{b_{rms}}{\lambda_0} = 45$ (Enlarged)

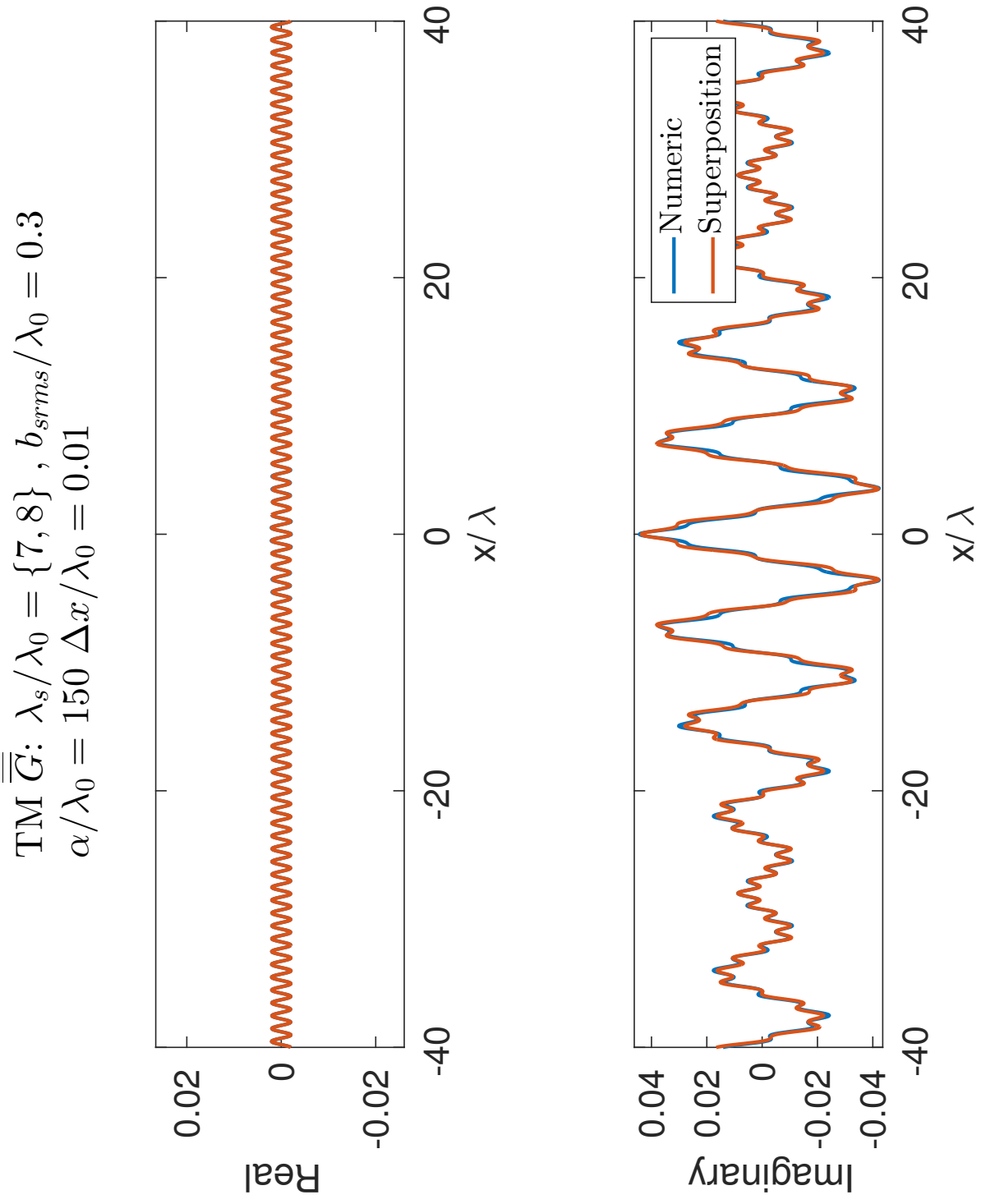


Figure 4.162: TM $\overline{\overline{G}}$ $\frac{\lambda_s}{\lambda_0} = \{7, 8\}$ $\frac{b_{rms}}{\lambda_0} = 30$ (Enlarged)

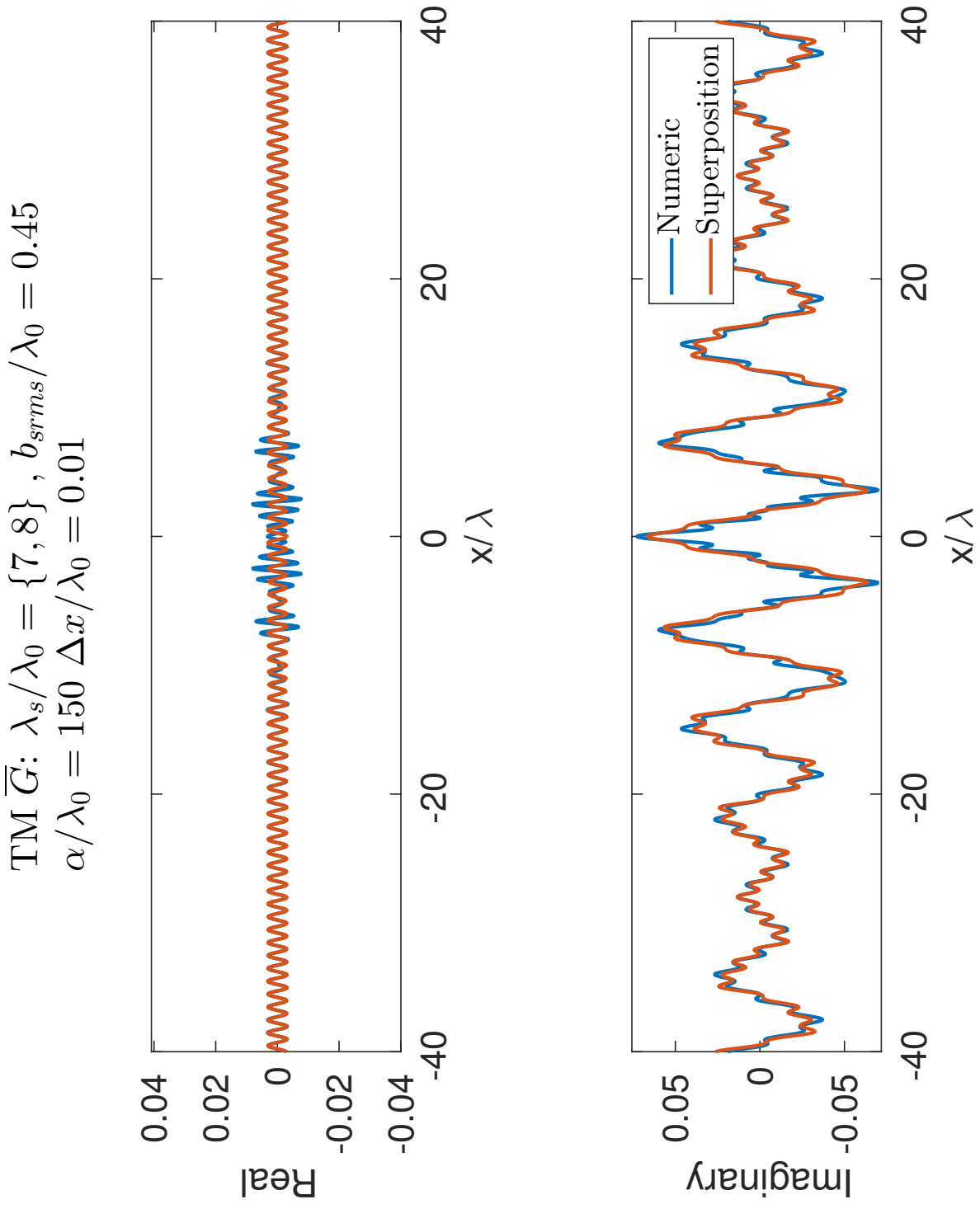


Figure 4.163: TM $\overline{\overline{G}}$ $\frac{\lambda_s}{\lambda_0} = \{7, 8\}$ $\frac{b_{rms}}{\lambda_0} = 45$ (Enlarged)

While some of the surface component amplitudes here are much larger than previously investigated, the fact that they are mostly linear is encouraging that the empiric analytic single frequency results could be valid in this region and applied to spectral surfaces.

The three frequency surfaces do not obey the proposed limit on surface slope. While the longer period surface $\frac{\lambda_s}{\lambda_0} = \{10, 15, 20\}$ (Figs. 4.164 through 4.167) behaves like the two frequency surfaces with good agreement even up to $\zeta_{x_{rms}} = 0.45$, $\frac{\lambda_s}{\lambda_0} = \{7, 8, 9\}$ (Figs. 4.168 through 4.171) has significant errors for this RMS slope, instead only finding good agreement up to $\zeta_{x_{rms}} = 0.35$. Examining the RMS curvature (Table 4.4.3) shows that the latter surface is significantly higher than the former, but not more than the two frequency surfaces which had acceptable agreement. These results were run with relatively short integration supports $\frac{\alpha}{\lambda_0} = 100$, since the error seems to be largely from the real component, may be absolved for integration supports of interest due to the $\frac{1}{\sqrt{\alpha}}$ decay.

#### 4.4.4.5 RMS curvatures

Note the 0.35 and 0.40 RMS slope cases were not run for the three frequency surfaces. These values were computed by considering the square root of the sum of the squares of the RMS values of the second derivative of the individual surface components:

$$\zeta_{xx_{rms}} = \sqrt{\sum \left( \frac{b}{\sqrt{2}} \left( \frac{2\pi}{\frac{\lambda_s}{\lambda_0}} \right)^2 \right)^2} = \sqrt{\left( \frac{b}{\sqrt{2}} \right)^2 \sum \left( \frac{2\pi}{\frac{\lambda_s}{\lambda_0}} \right)^4}$$

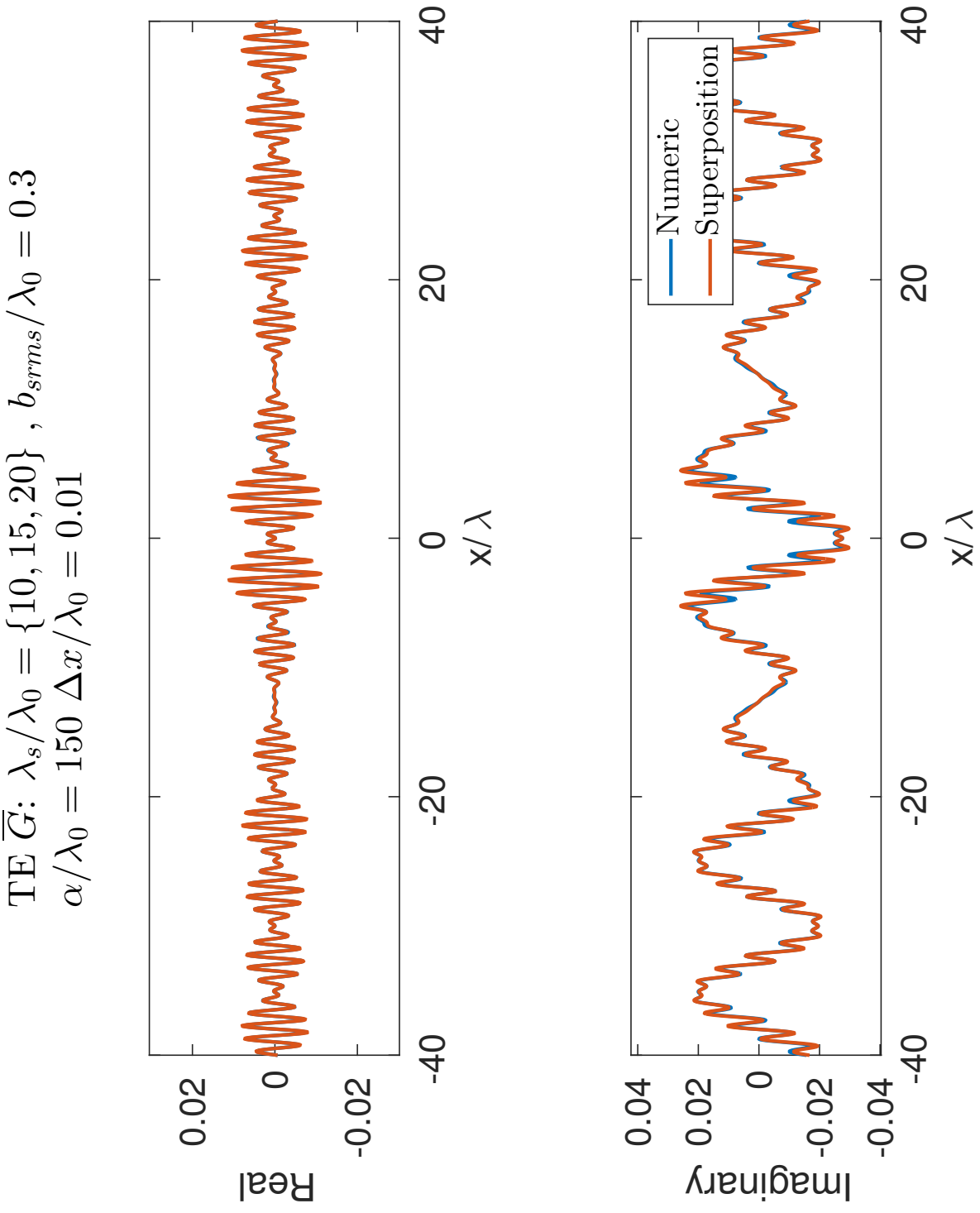


Figure 4.164: TE $\overline{\overline{G}}$ $\frac{\lambda_s}{\lambda_0} = \{10, 15, 20\}$ $\frac{b_{rms}}{\lambda_0} = 30$ (Enlarged)

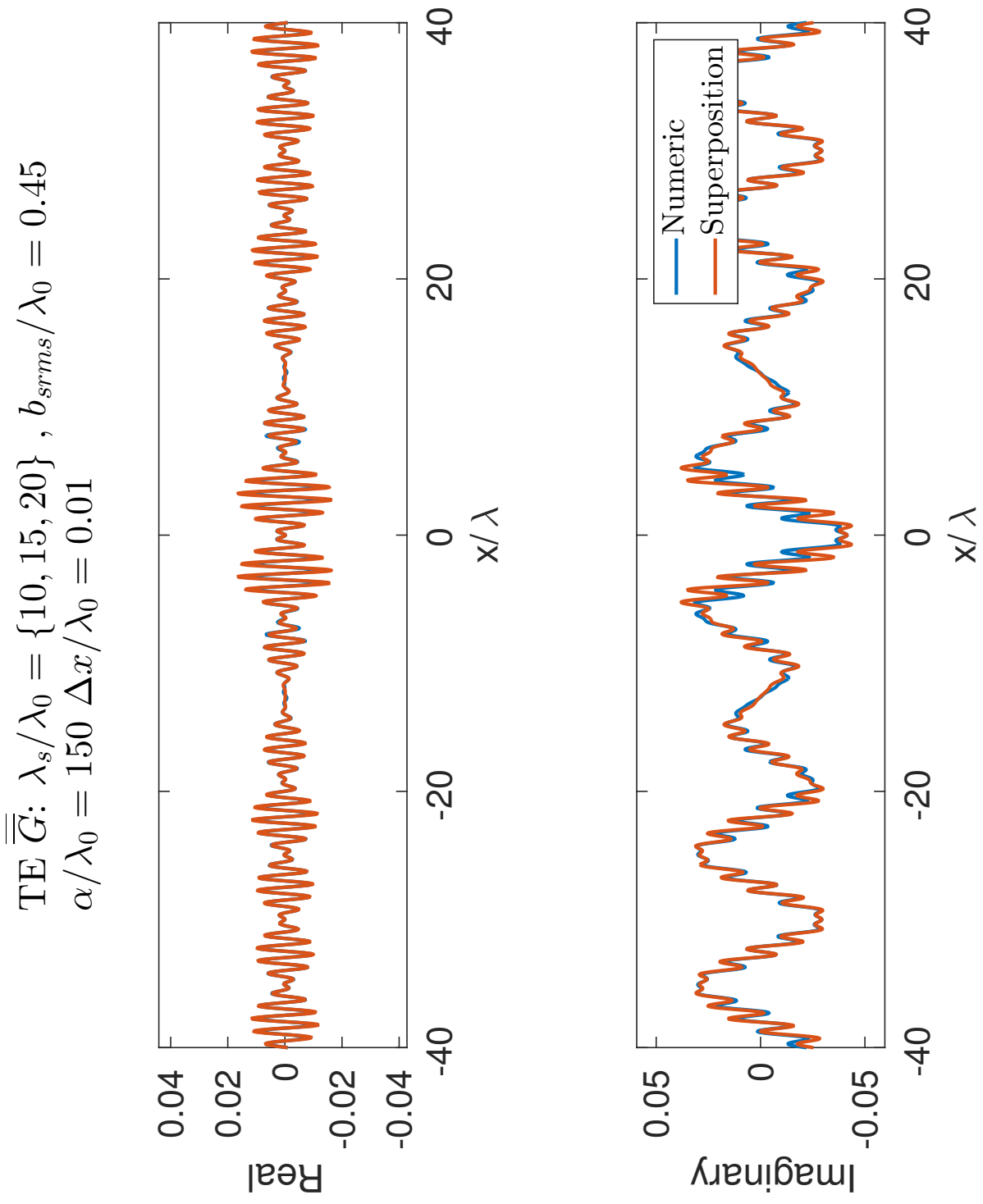


Figure 4.165: TE $\overline{\overline{G}}$ $\frac{\lambda_s}{\lambda_0} = \{10, 15, 20\}$ $\frac{b_{rms}}{\lambda_0} = 45$ (Enlarged)

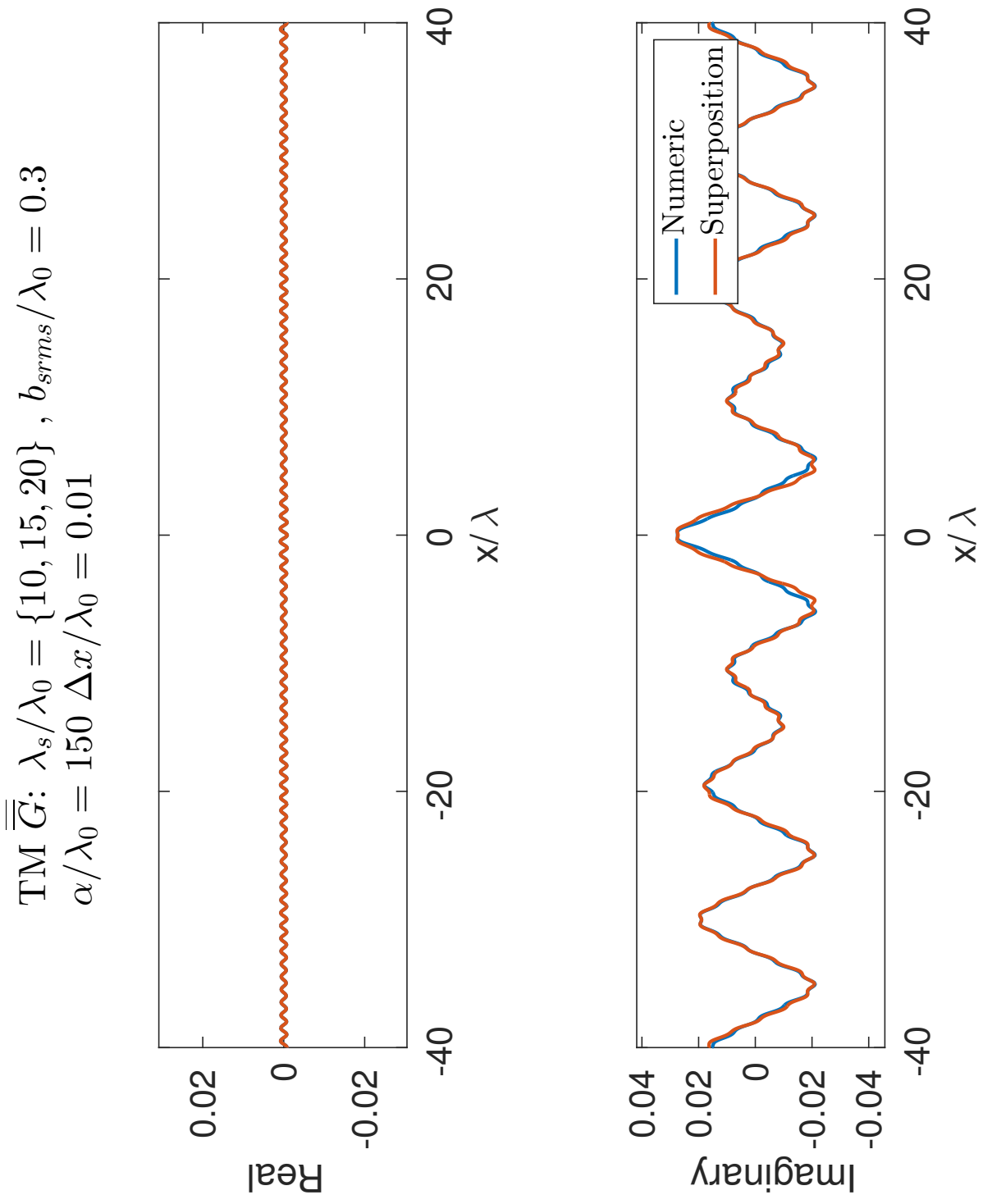


Figure 4.166: TM $\overline{\overline{G}}$ $\frac{\lambda_s}{\lambda_0} = \{10, 15, 20\}$ $\frac{b_{rms}}{\lambda_0} = 30$ (Enlarged)

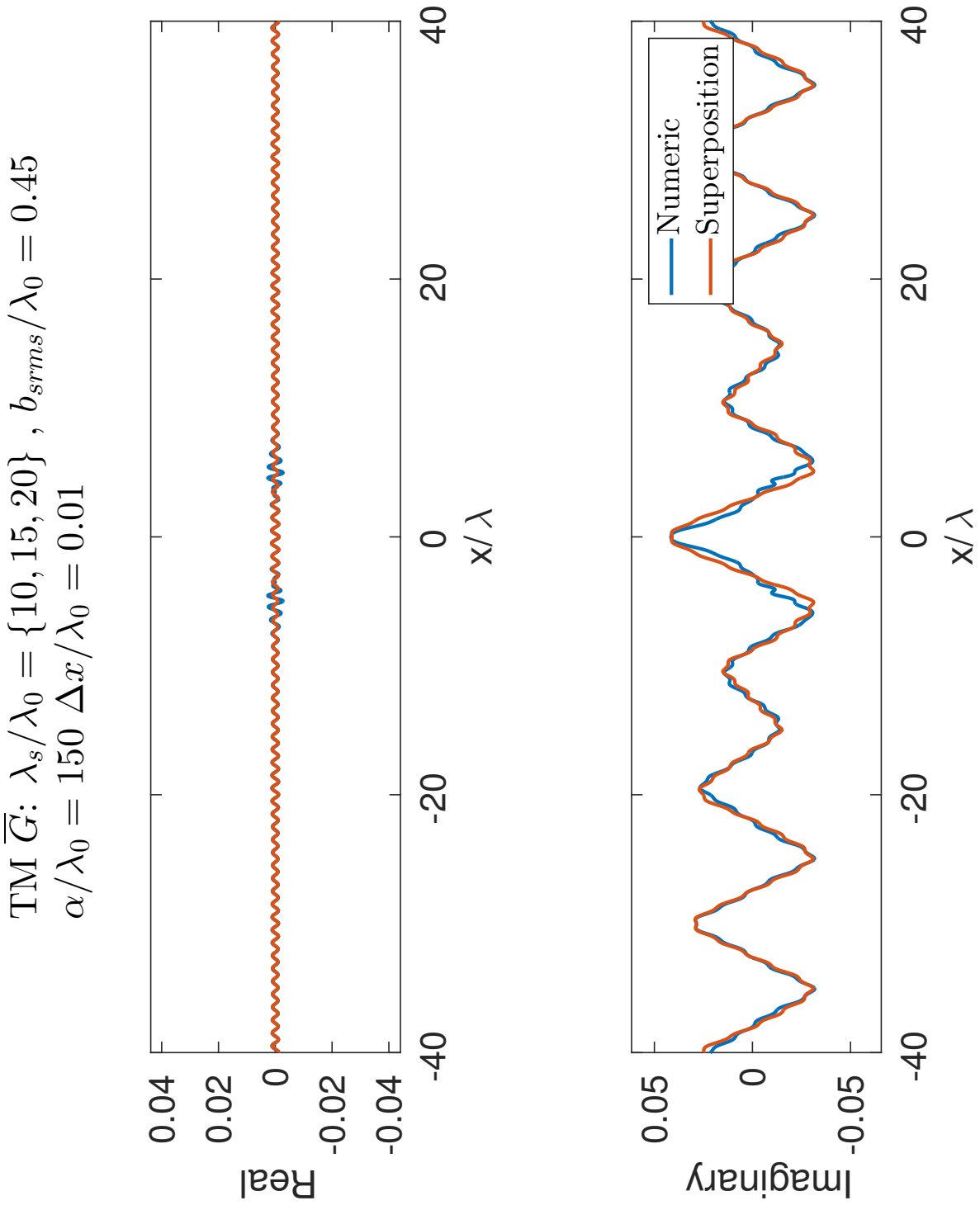


Figure 4.167: TM $\overline{\overline{G}}$ $\frac{\lambda_s}{\lambda_0} = \{10, 15, 20\}$ $\frac{b_{rms}}{\lambda_0} = 45$ (Enlarged)

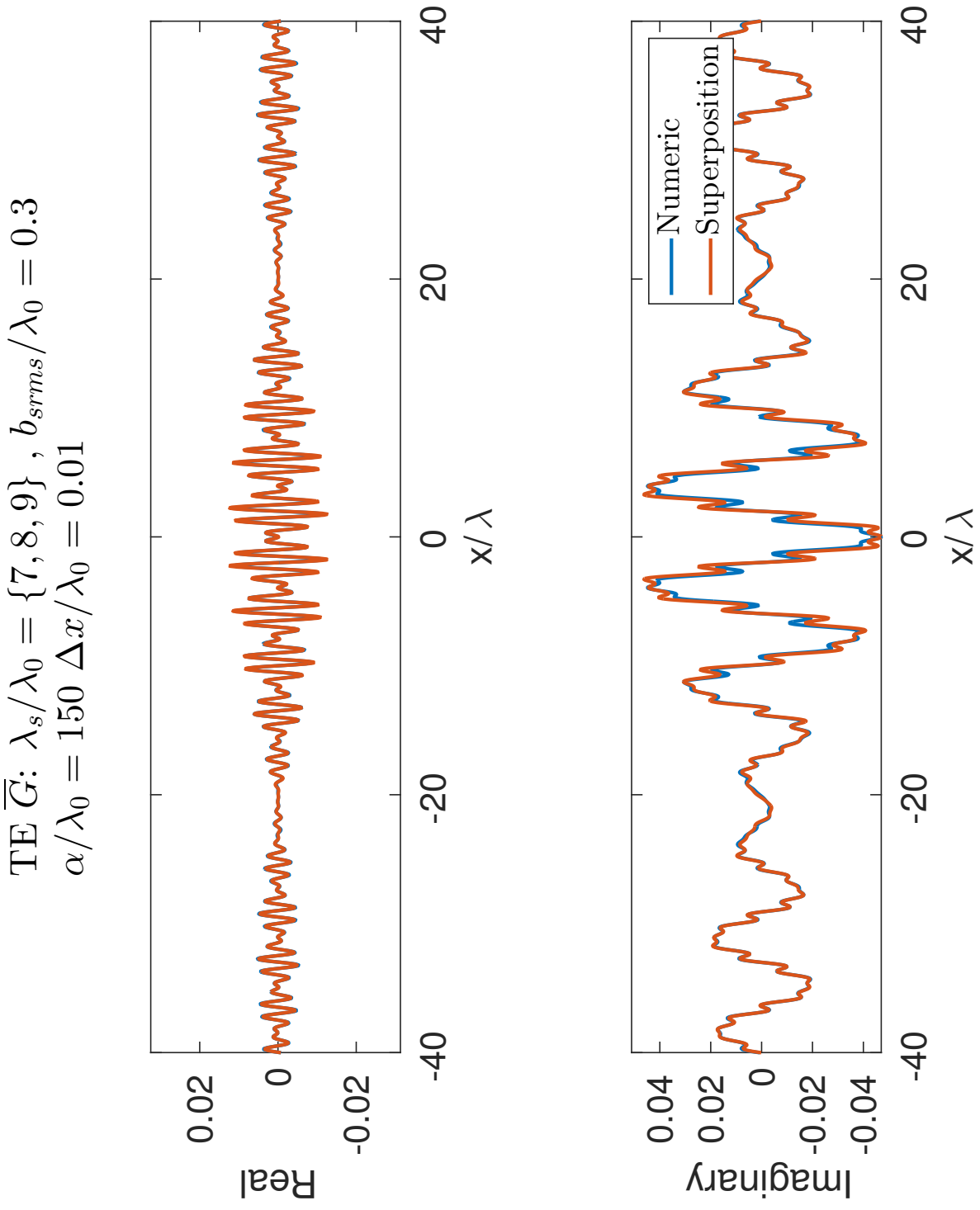


Figure 4.168: TE $\overline{\overline{G}}$ $\frac{\lambda_s}{\lambda_0} = \{7, 8, 9\}$ $\frac{b_{rms}}{\lambda_0} = 30$ (Enlarged)

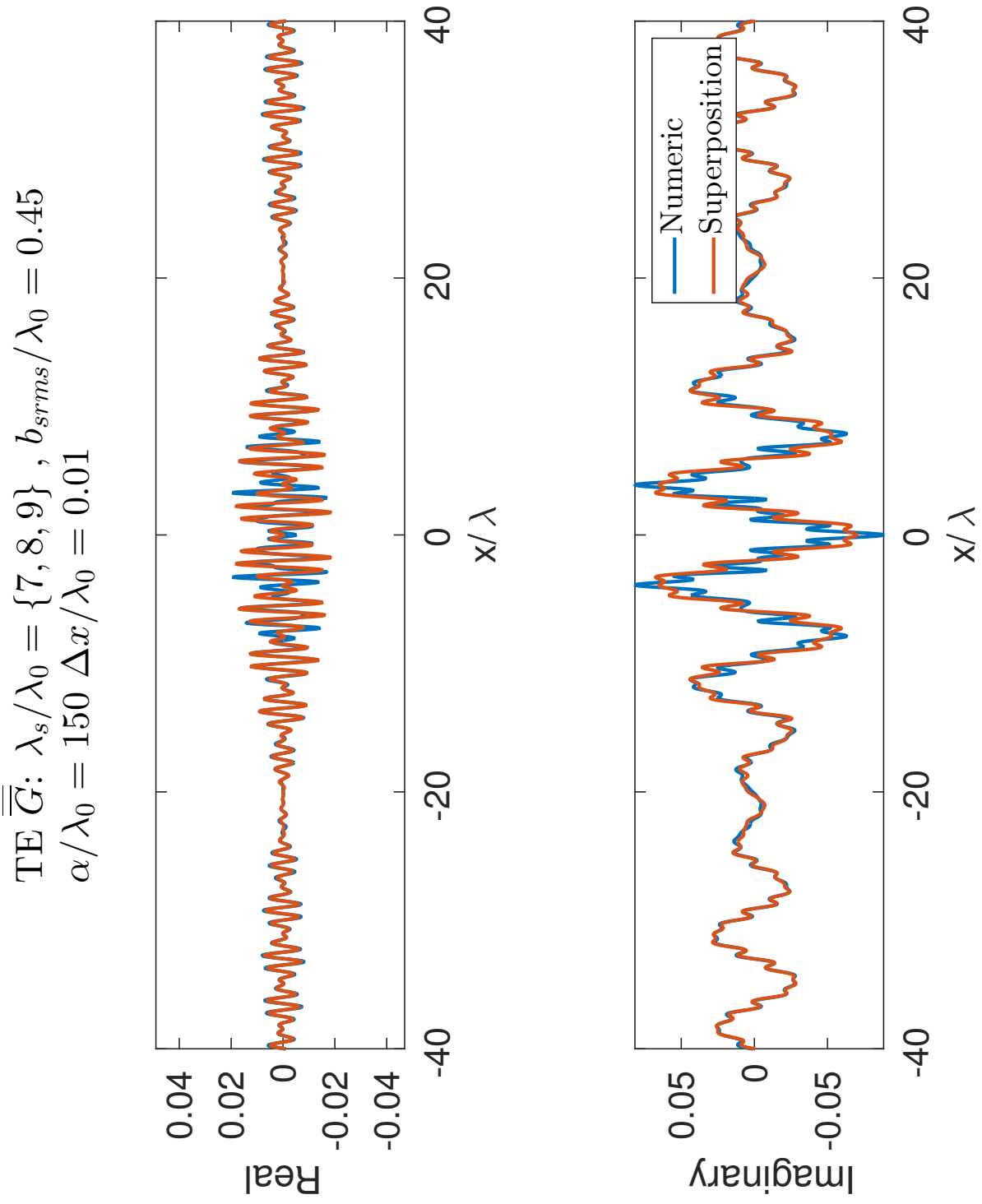


Figure 4.169: TE $\overline{\overline{G}}$ $\frac{\lambda_s}{\lambda_0} = \{7, 8, 9\}$ $\frac{b_{rms}}{\lambda_0} = 45$ (Enlarged)

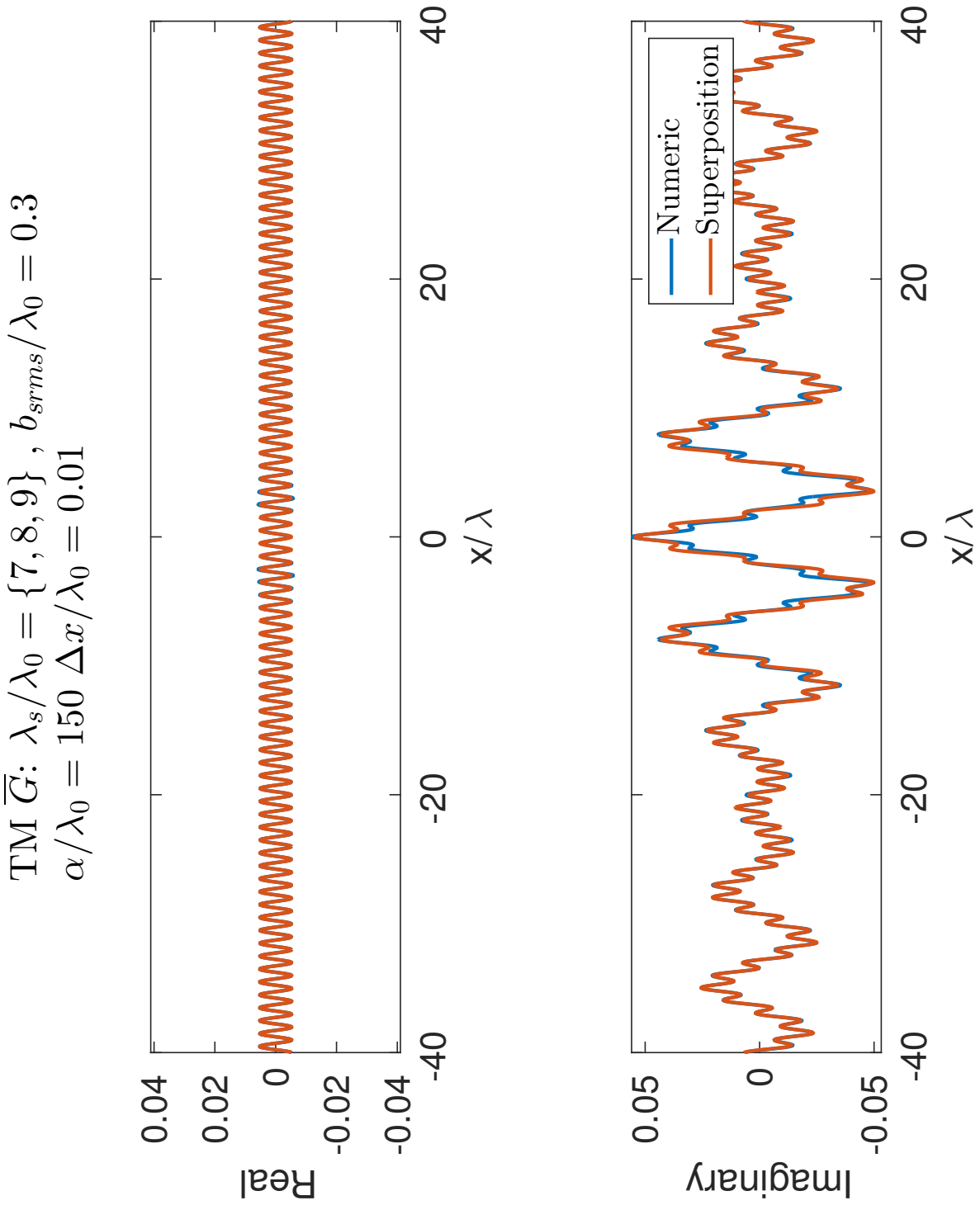


Figure 4.170: TM $\overline{\overline{G}}$ $\frac{\lambda_s}{\lambda_0} = \{7, 8, 9\}$ $\frac{b_{rms}}{\lambda_0} = 30$ (Enlarged)

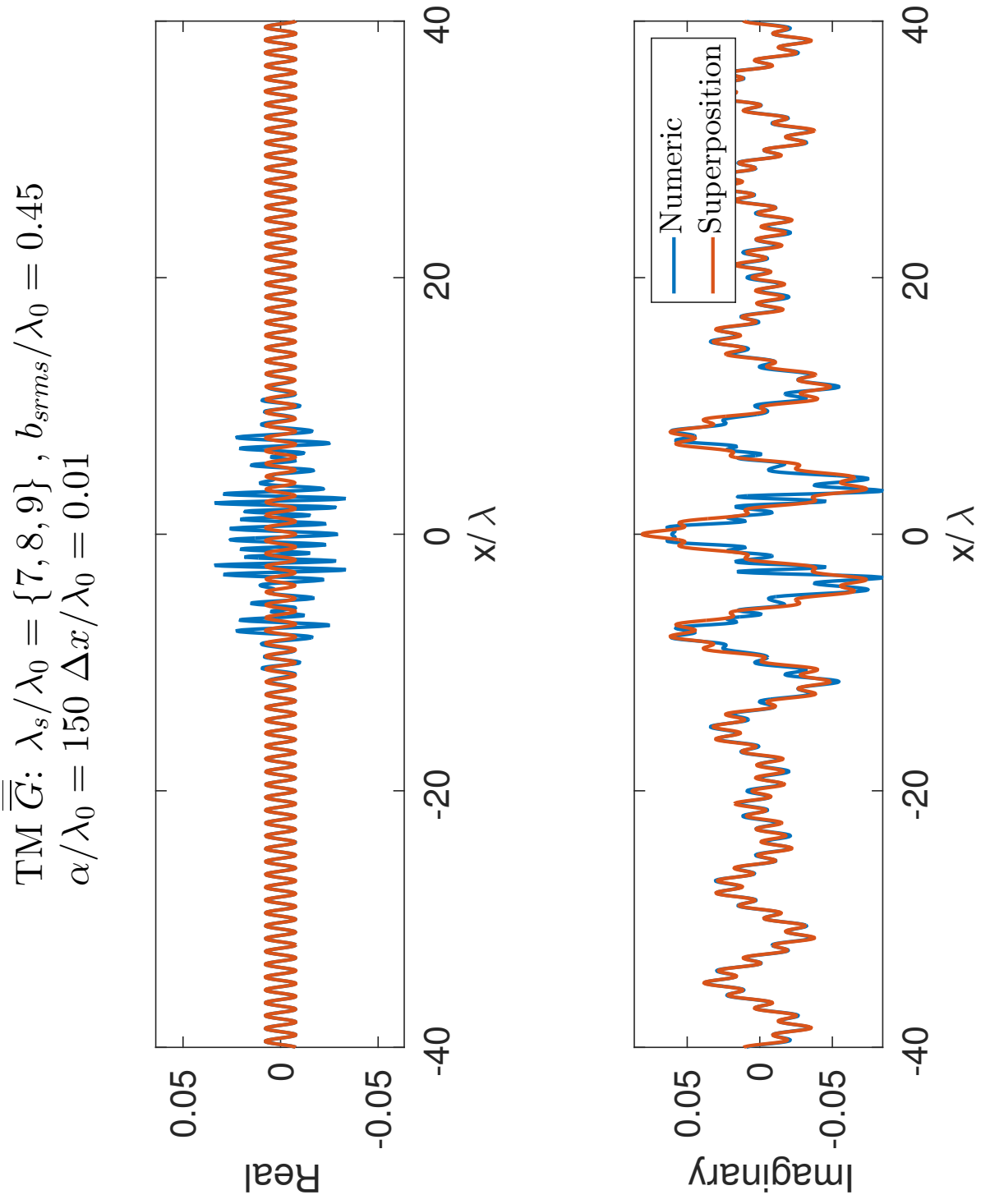


Figure 4.171: TM $\overline{\overline{G}}$ $\frac{\lambda_s}{\lambda_0} = \{7, 8, 9\}$ $\frac{b_{rms}}{\lambda_0} = 45$ (Enlarged)

| $\frac{\lambda_s}{\lambda_0}$ | $\zeta_{x_{rms}} \approx 0.30$ | $\zeta_{x_{rms}} \approx 0.35$ | $\zeta_{x_{rms}} \approx 0.40$ | $\zeta_{x_{rms}} \approx 0.45$ |
|---|---|---|---|---|
| $\{7, 8\}$ | $\zeta_{xx_{rms}} \approx 0.25$ | $\zeta_{xx_{rms}} \approx 0.30$ | $\zeta_{xx_{rms}} \approx 0.34$ | $\zeta_{xx_{rms}} \approx 0.38$ |
| $\{7, 20\}$ | $\zeta_{xx_{rms}} \approx 0.26$ | $\zeta_{xx_{rms}} \approx 0.30$ | $\zeta_{xx_{rms}} \approx 0.34$ | $\zeta_{xx_{rms}} \approx 0.38$ |
| $\{19, 20\}$ | $\zeta_{xx_{rms}} \approx 0.097$ | $\zeta_{xx_{rms}} \approx 0.11$ | $\zeta_{xx_{rms}} \approx 0.13$ | $\zeta_{xx_{rms}} \approx 0.15$ |
| $\{20, 40\}$ | $\zeta_{xx_{rms}} \approx 0.087$ | $\zeta_{xx_{rms}} \approx 0.10$ | $\zeta_{xx_{rms}} \approx 0.12$ | $\zeta_{xx_{rms}} \approx 0.13$ |
| $\{10, 15, 20\}$ | $\zeta_{xx_{rms}} \approx 0.16$ | - | - | $\zeta_{xx_{rms}} \approx 0.244$ |
| $\{7, 8, 9\}$ | $\zeta_{xx_{rms}} \approx 0.25$ | - | - | $\zeta_{xx_{rms}} \approx 0.36$ |

Table 4.4.3: RMS surface curvatures

## 4.5 Summary

This chapter provided a characterization of the integrand as well as numeric results of the MFIE kernel integral necessary for the application of the $S^3$ method. Then an empiric formula was found for the infinite support integral which was later used in combination with analytically derived approximations to portions of the finite kernel integral to produce an accurate and powerful closed-form empiric analytic expression for the finite case of both polarizations. Finally, the behavior of the kernel integral on spectral surfaces was considered first by examining the analytic integral tails expression previously derived, which made restrictive predictions on the superposition of surface wavelengths that were found to not hold true in the numeric results which instead showed simple linear combination of the single frequency results was valid on a wide range of surface parameters.

The most accurate approximate formulas for $\overline{\overline{G}}$ are given below

**TM**

$$\overline{\overline{G}}_{TM}(x) = -j\frac{\zeta_{xx}(x)}{2k_0} - \frac{bk_s}{2}\frac{(-1+j)}{\sqrt{2}}\left\{\frac{je^{-jk_0\alpha}}{(1-K_s^2)\sqrt{(\alpha^2-x^2)}\sqrt{2\pi k_0}}\right.$$
$$\left. * \left[\left(\sqrt{(\alpha-x)}e^{-jk_0x} + \sqrt{(x+\alpha)}e^{jk_0x}\right)\left((1-K_s)e^{-jk_s\alpha} - (1+K_s)e^{jk_s\alpha}\right)\right]\right\}$$

Recall for this we had dropped a term to achieve the excellent agreement found.

**TE**

$$\overline{\overline{G}}_{TE}(x) = j\frac{\zeta_{xx}(x)}{2k_0} - \frac{\zeta_x(x)(-1+j)}{\sqrt{1+\zeta_x^2}\sqrt{2}} \frac{\left[\left(\sqrt{(x+\alpha)}\exp\left(-j(\alpha-x)k_0\right) - \sqrt{(\alpha-x)}\exp\left(-j(x+\alpha)k_0\right)\right)\right]}{\sqrt{2\pi k_0(\alpha^2-x^2)}} * \left(1+\frac{b^2k_s^2}{4}\left(1-\frac{1}{2}\left(\frac{\exp(j2\alpha k_s)}{(1-2K_s)}+\frac{\exp(-j2\alpha k_s)}{(1+2K_s)}\right)\right)\right)$$

Note for TE we did NOT drop any terms.

The range of validity for both polarizations is shown in Figure 4.116.

# Chapter 5

# Physical Significance and Scattering Results

## 5.1 Introduction

When the principles are understood then the applications are many. Unfortunately, numerical methods do not provide the same level of physical understanding as analytic methods. The goal of this work is to deepen the understanding of rough surface scattering physics through the novel Single Scatter Subtraction Method.

Building on the physical-based approximations derived in Chapter 4, this chapter opens with a discussion of the interpretation and implications of the single-scatter subtraction method. Beginning with a discussion of the single scattering current as a bent plan approximation, the chapter proceeds to a classification of the physical process of Bragg scattering and the implication of the non-zero real component of the finite $\overline{\overline{G}}$. Following this, scattering results from the derived approximations are presented and compared against the Kirchhoff approximation. First, attention is turned to low grazing backscattering from single sinusoidal surfaces with surface wavelengths approaching the electromagnetic wavelength. Finally, electromagnetic scattering from a selection of spectral surfaces of two and three surface frequencies are studied.

## 5.2 Physical Based Approximations

From the above empiric and analytic approximations an extended approximation to the surface currents from the Kirchhoff current $J_0$ can be made by using the equations developed in Section 3.3.

Ultimately, the interest of the proposed research lies in the scattered fields and cross-sections. The same methodology of analytic and empiric approximations will be applied to the scattering currents to provide extended approximate theories for rough surface scattering.

### 5.2.1 Interpretation of $\overline{G}$ results

#### 5.2.1.1 Bent Tangent Plane Approximation

The single scattering current for the infinite, plane wave case is given by Equations 3.3.4 and 4.4.1:

$$J_{ss}^{pp'}(x) = \frac{J_0(x)}{1-\overline{G}_{pp'}(x)} = \frac{J_0(x)}{1+\tau_{pp'}\frac{\zeta_{xx}(x)}{2k_0}}$$

which when $\frac{\zeta_{xx}(x)}{2k_0} \ll 1$ becomes the first two terms of the Luneburg-Kline high frequency approximation of the surface current. Brown previously showed this series does not contain multiple scattering [13], thus it should be contained within $J_{ss}$.

$$J_{ss}^{pp'} \approx J_0(x)\left[1-\tau_{pp'}\frac{\zeta_{xx}(x)}{2k_0}\right] \tag{5.2.1}$$

Further, $1 \pm j\frac{\zeta_{xx}(x)}{2k_0} \approx \exp\left(\pm j\frac{\zeta_{xx}(x)}{2k_0}\right)$ so this method produces a curvature dependent phase shift improvement to the Kirchhoff solution, so can be seen to be the next step in the physical optics approximation. At the first level, a flat plane through the point $(x, \zeta(x))$ on

the scattering surface is used as $2\hat{z} \times \overrightarrow{H_i}$. Next, the plane is tilted to give the well known tangent plane approximation $2\hat{n} \times \overrightarrow{H_i}$ of the Kirchhoff method. Finally, this tangent plane is bent to account for local surface curvature with $2\hat{n} \times \overrightarrow{H_i}\left[1 \pm j\frac{\zeta_{xx}(x)}{2k_0}\right]$ as given by the $S^3$ method when examining the single scattering current in isolation.

While this result casts $J_{ss}$ as a high-frequency approach, this is due strictly to the high frequency approximation of $\overline{G}$ as no explicit high frequency assumptions were invoked in the derivation of $S^3$. It is unknown at this time if $S^3$ is valid as the frequency is decreased such that the surface wavelength is lower than the electromagnetic wavelength, here multiple scattering will increase and single scattering as a concept may cease to exist. In this case it does not appear that there is mathematically an issue - provided $\overline{G}$ exists - but multiple scattering may so dominate that the Kirchhoff current $J_0$ , the single scattering current $J_{ss}$ and/or even the multiple scattering source term current $J_{00}$ may fail to be a useful approximation or hold any physical significance. If $\overline{G}$ does exist in the small-scale roughness regime, this may represent an opportunity to provide a theory which reduces to Kirchhoff theory in one limit and the perturbation theories in another, an uncommon but desirable quality in an analytic theory of rough surface scattering according to Elfouhaily and Guèrin[20].

#### 5.2.1.2 Bragg Scattering

Equation 5.2.1 is also interesting in that it does not contain terms varying linearly with $k_0$ which lead to Bragg scattering. This seems like a surprising result since Bragg scattering currents can be mathematically described at a point x by terms dependent only on x. Physically, Bragg scattering arises from the constructive interference of two or more separated scattering points and is thus a non-local phenomenon as found by Holliday [27]. This highlights the importance of physical understanding of the mathematics and an advantage of the Single-Scatter Subtraction method.

### 5.2.2 Affect of finite truncation

A close examination of the final empiric analytic formulas of Equations 4.4.20 and 4.4.21 show they contain first the infinite kernel integral result $\overline{\overline{G}}$ and then $\alpha$-dependent error terms since they result from the finite truncation. Physically, the error terms of both polarizations decay to zero with increasing $\alpha$ as $\frac{1}{\sqrt{4\pi k_0 \alpha}}$ due to the one-dimensional surface roughness, but also display the square root singularity of the kernel as $x \to \pm\alpha$ that is also present in the numeric computations. When $x \ll \alpha$, they both can be seen to contain a cylindrical standing wave from the truncation edges. Thus truncation has affected the physical problem, even when far outside the region of illumination, hence afflicts all approaches to the extended rough surface scattering problem. Future work will be to us these error terms to better understand and refine the heuristic for setting the integration bounds when numerically solving the Magnetic Field Integral Equation. As will be shown in Section 5.3, these error terms lead to dramatic anomalous enhancement of backscattering predicted by the single-scatter currents.

## 5.3 Scattering Results

Now that empiric-analytic approximations have been derived and analyzed for their physical significance, they will be used to numerically compute the scattered fields to determine what if any improvement over the Kirchhoff solution they represent. In this section, the empiric-analytic formulas of section 4.4.3.6 will be used to determine the single scattering current for incident angles $\theta_i$ of 0°, 15°, and 45° which will be radiated numerically for the scattered fields and denoted "SS" in the accompanying figures and compared against the incident field or Kirchhoff solution denoted "Kirch". The full wave solution obtained by the the Method of Moments is also plotted with the label "MOM".

### 5.3.1 Short Surface Wavelengths

First, attention is turned to the shortest surface wavelengths for which the empiric analytic formula was found to be valid. Surface wavelengths of $\frac{\lambda_s}{\lambda_0} = 2$ through 4 with an amplitude of $\frac{b}{\lambda_0} = 0.1$ and and $\lambda_s = 5\lambda_0$ with $\frac{b}{\lambda_0} = 0.5$ amplitude are investigated. All surfaces are truncated at $\alpha = \pm 200\lambda_0$ and illuminated with a $g = 20\lambda_0$ projected spot half-width. The figures in this section have dramatic dynamic range, so for some a difference plot from the full-wave solution is also presented and the scale is fixed to highlight the areas of interest which are the peaks in the scattering. Large and highly oscillatory differences are observed in other regions and clipped, but the results in this region are down below -200dB and at the numerical noise floor for the decomposition solution technique used. Large differences in the scattered results are observed when using the error terms present in the $\overline{\overline{G}}$ empiric-analytic formulas so additionally the $\overline{G}$ infinite case is used. These are differentiated in the figures by $SS_{fin}$ and $SS_{inf}$ respectively.

Since a formula for $\lambda_s = 2\lambda_0$ is not available for TE, only TM is presented in Figures 5.1 through 5.3. The single scattered fields are a slight perturbation of the Kirchhoff scattered fields that shifts the scattering from one peak direction and distributes it among the others. For normal incidence, the center peak at $\theta_s = 0°$ is 0.6dB less, while the endfire peaks are 1dB greater. This is expected given the bent tangent plan approximation which takes energy that would have been directed forward specularly and instead distributes it to the sides. In agreement with this for the $\theta_i = 15°$ illumination, there are four peak scattering directions and the $\theta_s = 15°$ peak has been reduced by 0.6dB, while the others are enhanced by 0.2 to 1dB. Likewise for the $\theta_i = 45°$ case, the specular peak has been reduced by 0.3 dB while the other peaks are enhanced by 0.5, 1 and 2dB in order moving away from the peak at $\theta_s = 45°$. Note that the Kirchhoff current is more accurate here in the specular direction. This can be explained by the fact that the bent-tangent plane is shifting single-scattering away from

this direction and there is multiple scattering which increases the scattering specularly. The accuracy of Kirchhoff is purely incidental here as the single-scattering current is accurate to the physics of single-scattering but not to the full physics.

For normal incidence on the $\frac{\lambda_s}{\lambda_0} = 3$ and 4 surfaces there is about a 1dB difference between the Kirchhoff and Single Scatter fields at endfire for both polarizations, but the former is larger for TE while the latter is larger for TM (Figures 5.4 and 5.7). A dramatic difference for TE polarization is observed as the incident angle is increased to 15°, with a 6 dB enhancement in the $SS_{fin}$ backscattering shown in Figure 5.5 for the $\lambda_s = 3\lambda_0$ surface and 30 dB increase in Figure 5.8 for $\lambda_s = 4$. In contrast, the TM results show only minor differences of 0.5 dB or less. Increasing the incident angle further towards grazing the backscattering enhancement increases further for $SS_{fin}$ TE with a 16dB difference in Figure 5.6 and a 65 dB in 5.9. At this incident angle, the TM polarization also shows a difference of 10dB and 40dB respectively. Again, scattered power has been shifted away from the specular direction due to the bent tangent plane approximation.

Normal and 15 degree incidence (Figures 5.10 and 5.11) on the $\lambda_s = 5\lambda_0$ surface follow the same trend as the shorter wavelength surfaces, with smaller differences between the Kirchhoff and single scattered fields as expected due to the smaller surface curvature. For $\theta_i = 45°$, there is a notch in the scattered fields around $\theta_s = 19°$ for both polarizations in the Kirchhoff fields. Figure 5.12 shows that this notch is shifted towards broadside by a degree for TE, and endfire for TM.

This section demonstrated the effect of the bent tangent plane approximation on the scattered fields. As expected for normal incidence on all surfaces, the scattering results are symmetric about broadside as a result of the symmetric surface and symmetric illumination. The most dramatic changes in the scattered fields are shown on TE and in general the difference increases as we approach grazing. The effect of the bent plane is to shift scattering away

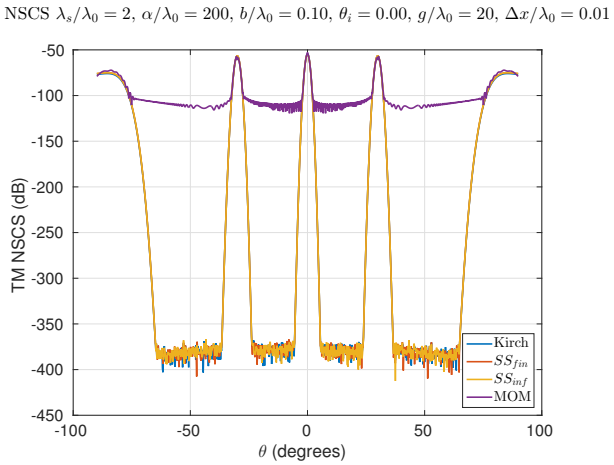


Figure 5.1: TM Scattered Fields from $\lambda_s = 2\lambda_0$ Surface Normal Incidence

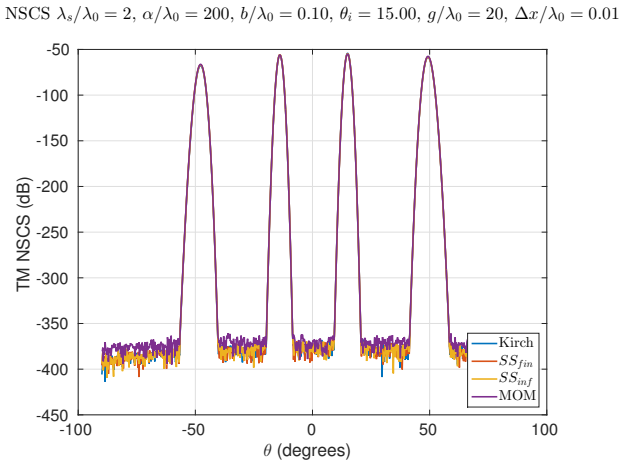


Figure 5.2: TM Scattered Fields from $\lambda_s = 2\lambda_0$ Surface $\theta_i = 15°$ Incidence

from specular for TM and towards specular for TE, but both have enhanced backscattering from the single scattering fields versus the Kirchhoff fields when the error terms are included.

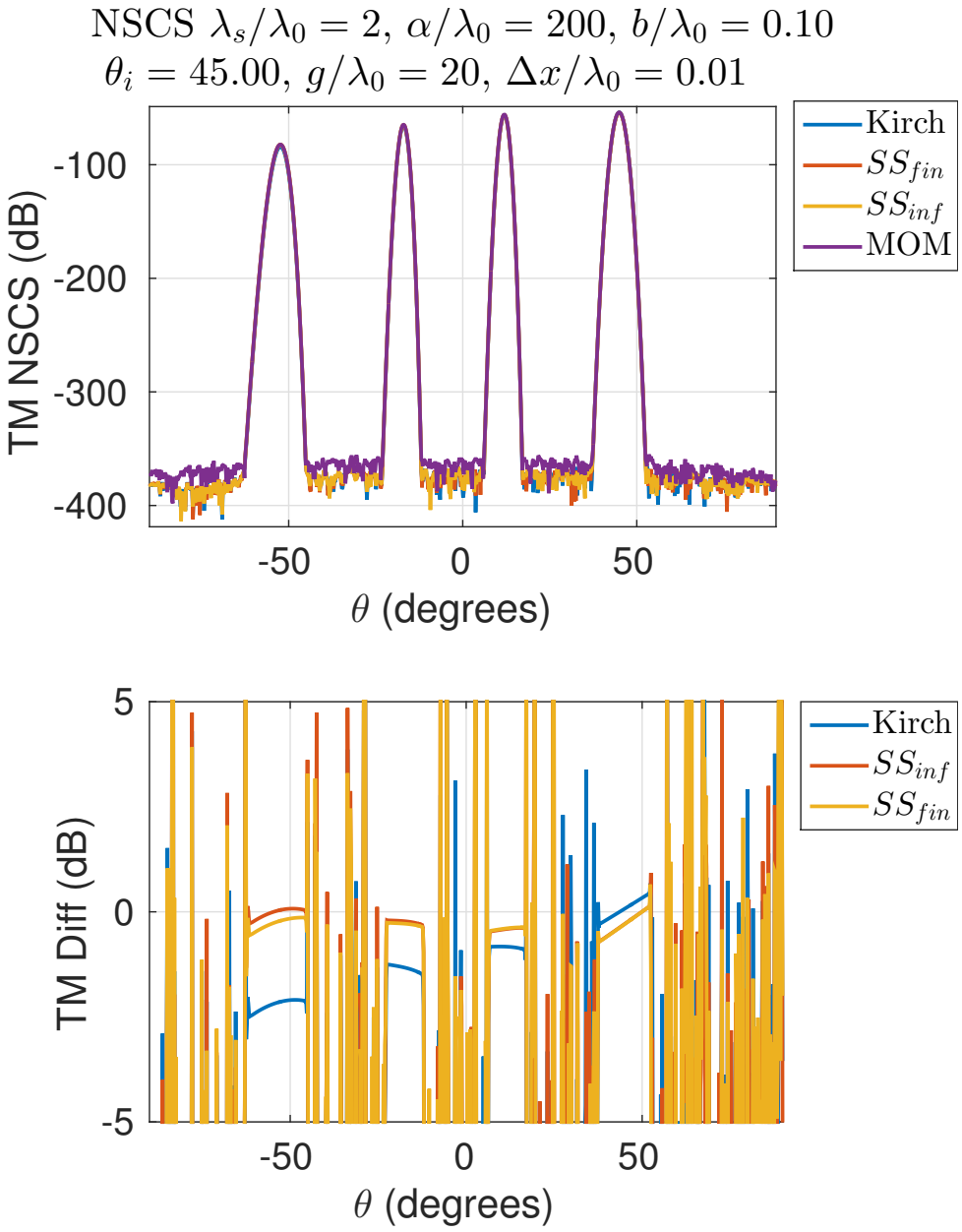


Figure 5.3: TM Scattered Fields from $\lambda_s = 2\lambda_0$ Surface $\theta_i = 15°$ Incidence

NSCS $\lambda_s/\lambda_0 = 3$, $\alpha/\lambda_0 = 200$, $b/\lambda_0 = 0.10$, $\theta_i = 0.00$, $g/\lambda_0 = 20$, $\Delta x/\lambda_0 = 0.01$

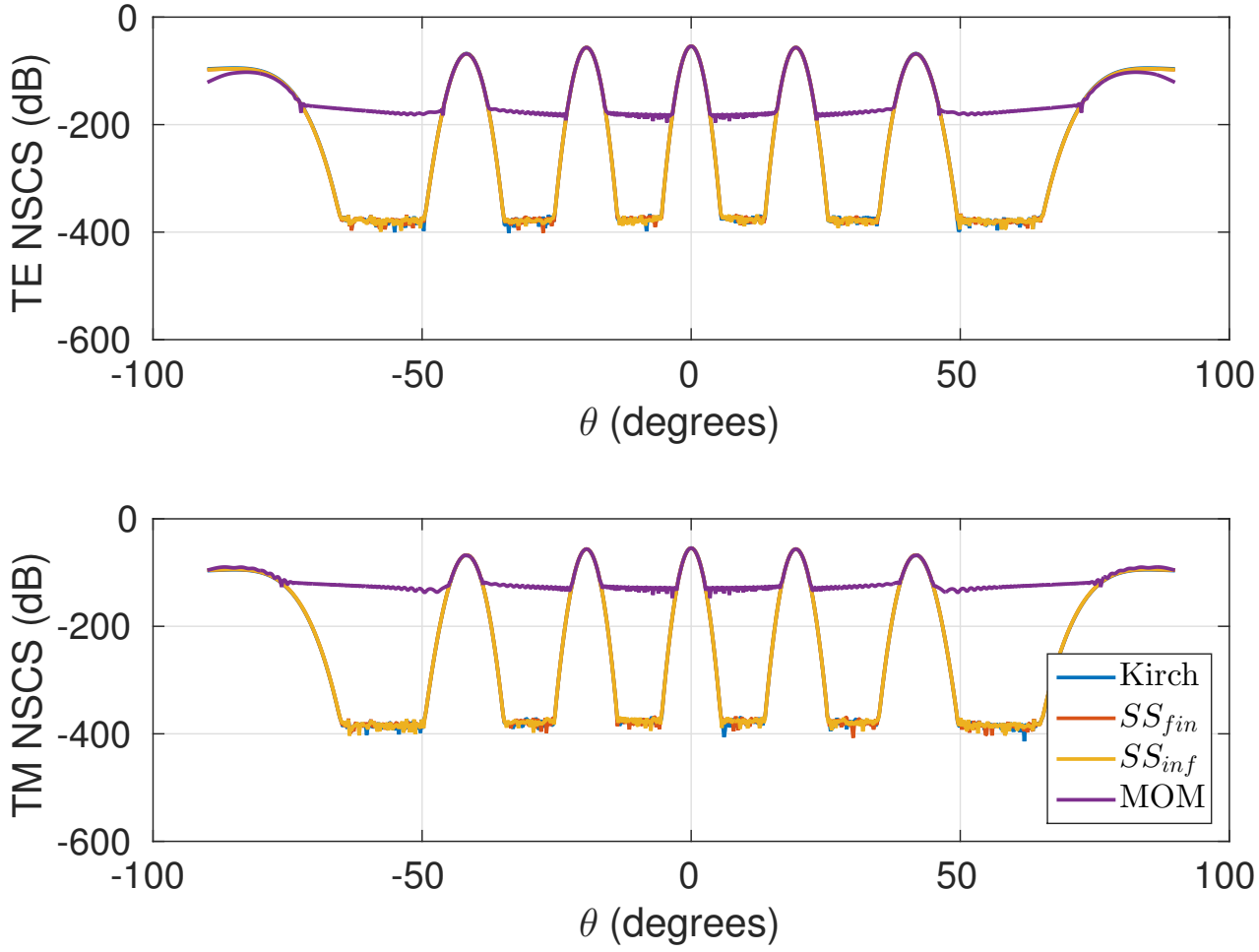


Figure 5.4: Scattered Fields from $\lambda_s = 3\lambda_0$ Surface Normal Incidence

NSCS $\lambda_s/\lambda_0 = 3$, $\alpha/\lambda_0 = 200$, $b/\lambda_0 = 0.10$, $\theta_i = 15.00$, $g/\lambda_0 = 20$, $\Delta x/\lambda_0 = 0.01$

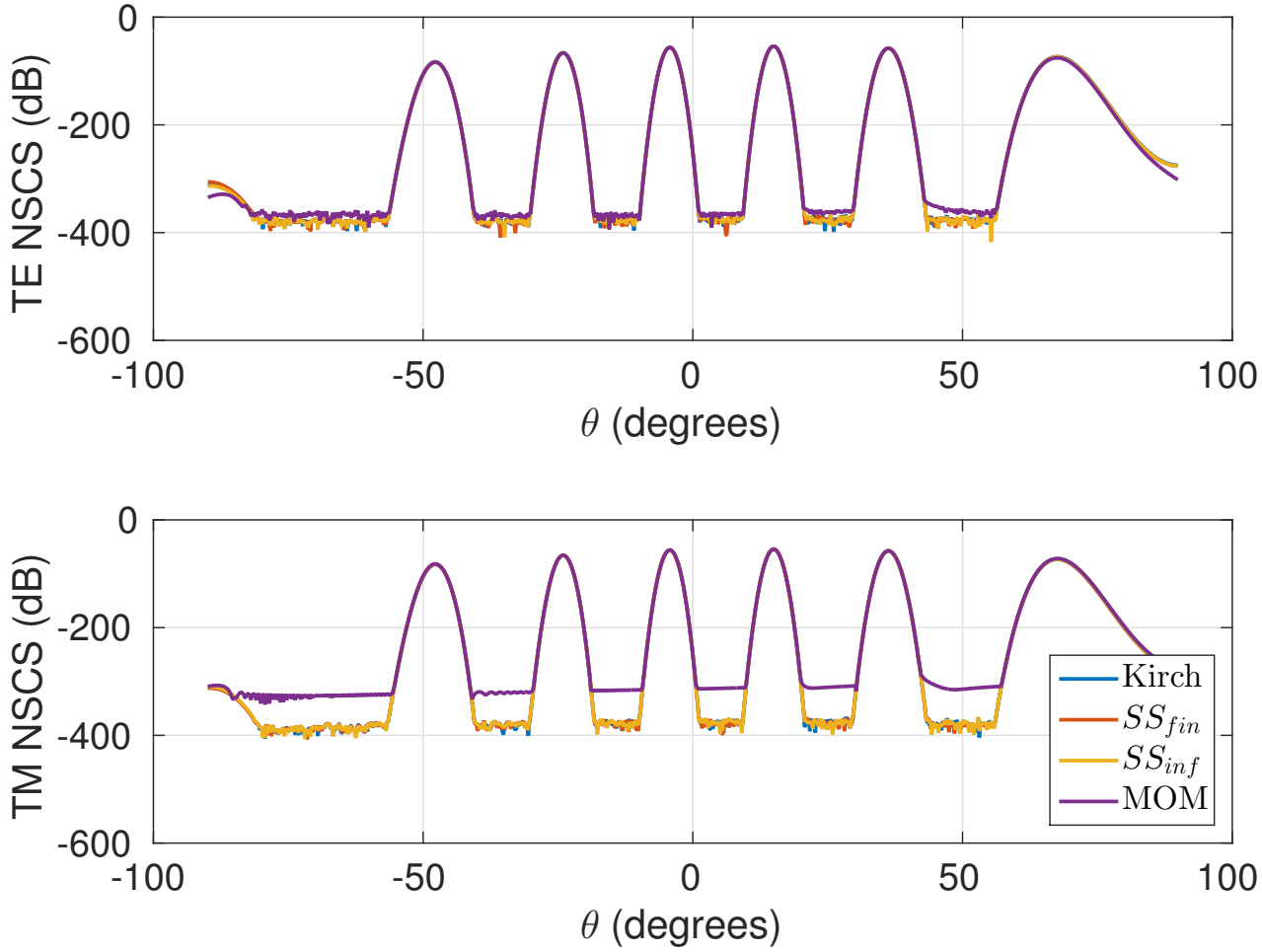


Figure 5.5: Scattered Fields from $\lambda_s = 3\lambda_0$ Surface $\theta_0 = 15°$ Incidence

NSCS $\lambda_s/\lambda_0 = 3$, $\alpha/\lambda_0 = 200$, $b/\lambda_0 = 0.10$, $\theta_i = 45.00$, $g/\lambda_0 = 20$, $\Delta x/\lambda_0 = 0.01$

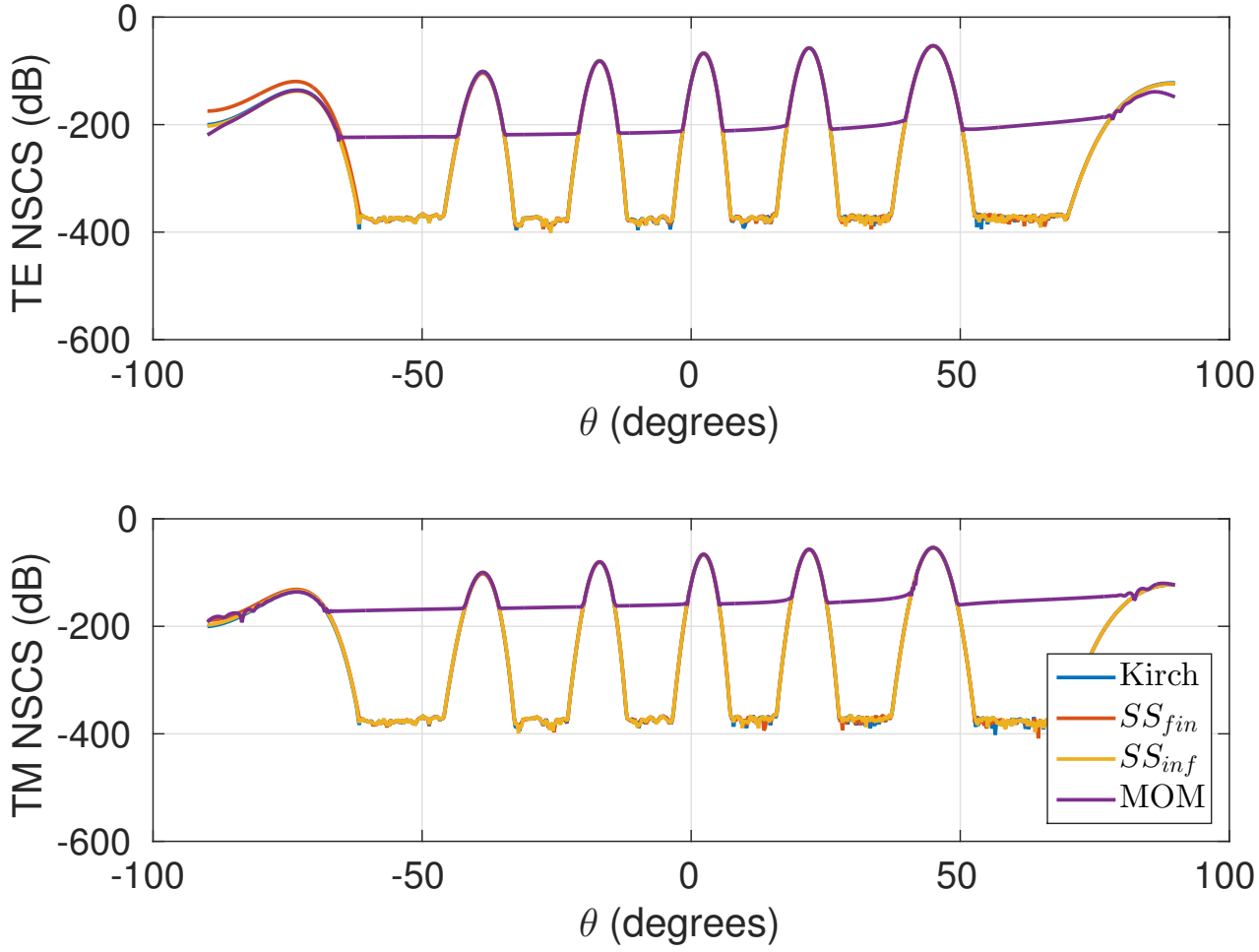


Figure 5.6: Scattered Fields from $\lambda_s = 3\lambda_0$ Surface $\theta_0 = 45°$ Incidence

NSCS $\lambda_s/\lambda_0 = 4$, $\alpha/\lambda_0 = 200$, $b/\lambda_0 = 0.10$, $\theta_i = 0.00$, $g/\lambda_0 = 20$, $\Delta x/\lambda_0 = 0.01$

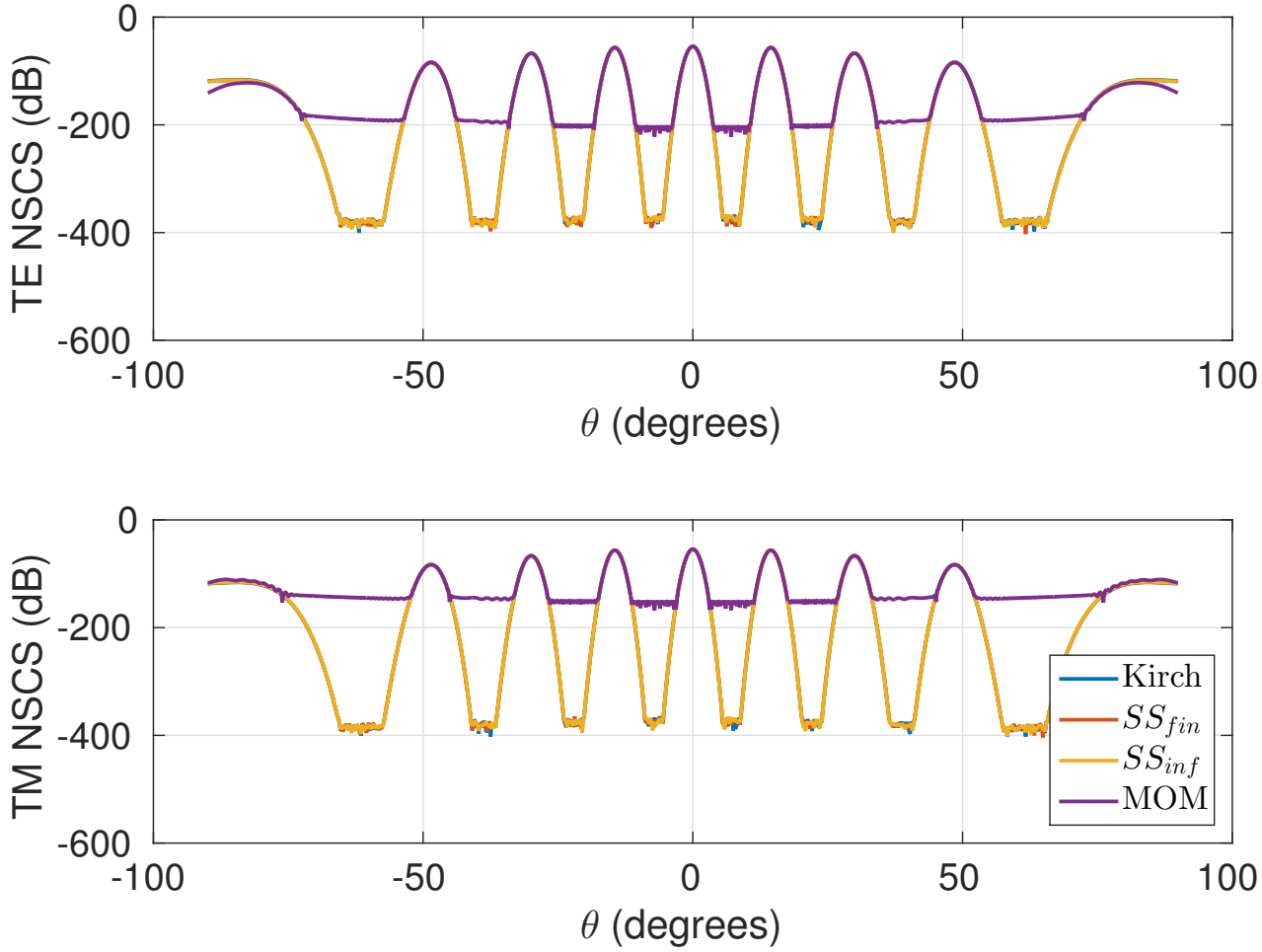


Figure 5.7: Scattered Fields from $\lambda_s = 4\lambda_0$ Surface Normal Incidence

NSCS $\lambda_s/\lambda_0 = 4$, $\alpha/\lambda_0 = 200$, $b/\lambda_0 = 0.10$, $\theta_i = 15.00$, $g/\lambda_0 = 20$, $\Delta x/\lambda_0 = 0.01$

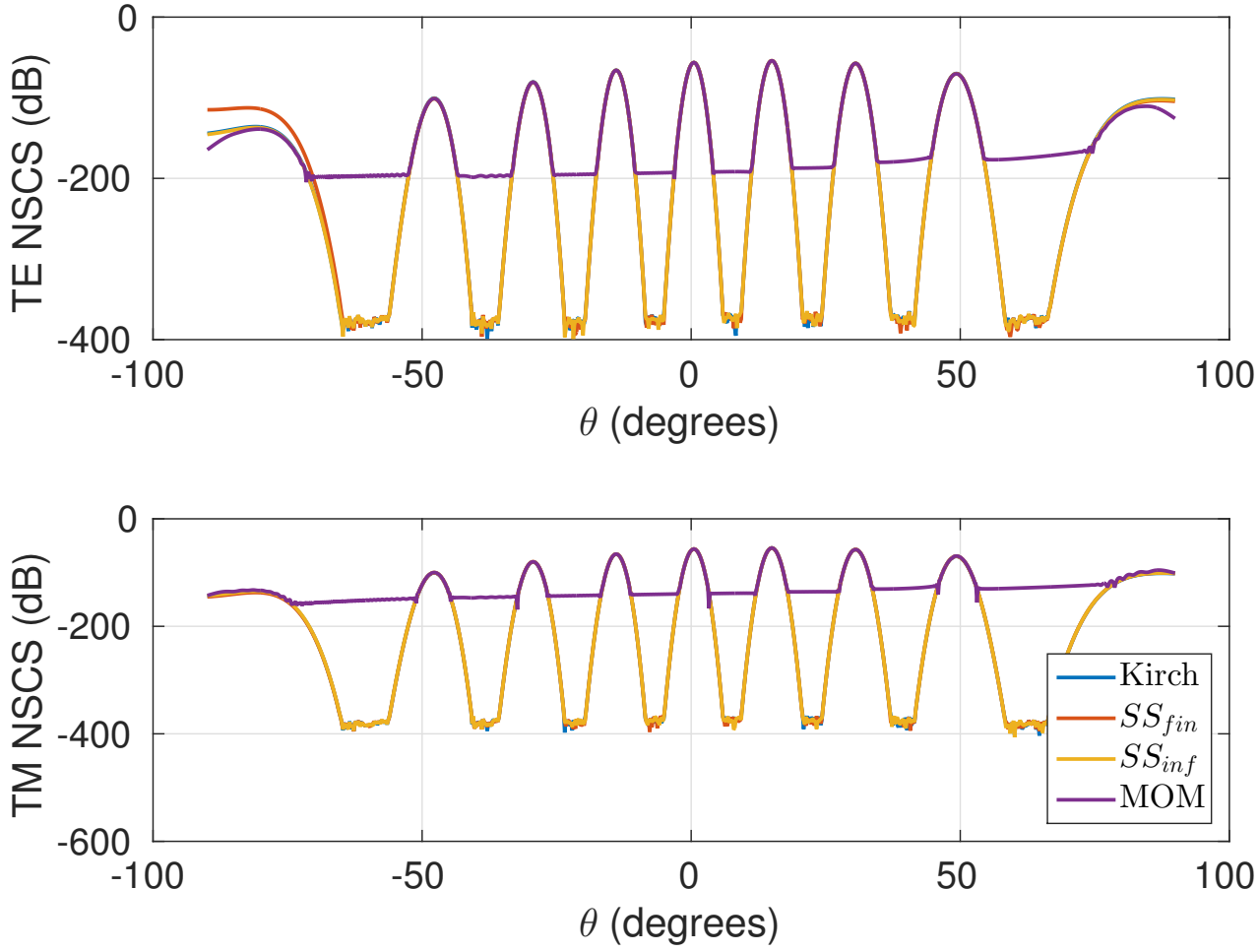


Figure 5.8: Scattered Fields from $\lambda_s = 4\lambda_0$ Surface $\theta_0 = 15°$ Incidence

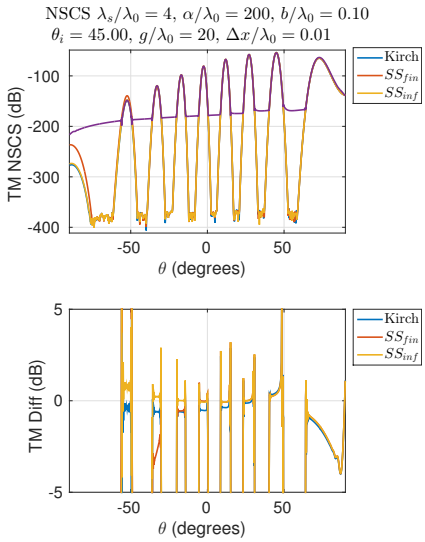


Figure 5.9: TM Scattered Fields from $\lambda_s = 4\lambda_0$ Surface $\theta_0 = 45$ Incidence

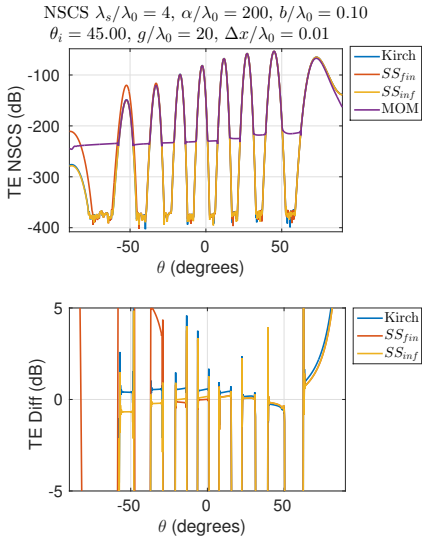


(a) TE Scattered Fields from $\lambda_s = 4\lambda_0$ Surface $\theta_0 = 45$ Incidence

NSCS $\lambda_s/\lambda_0 = 5$, $\alpha/\lambda_0 = 200$, $b/\lambda_0 = 0.50$, $\theta_i = 0.00$, $g/\lambda_0 = 20$, $\Delta x/\lambda_0 = 0.01$

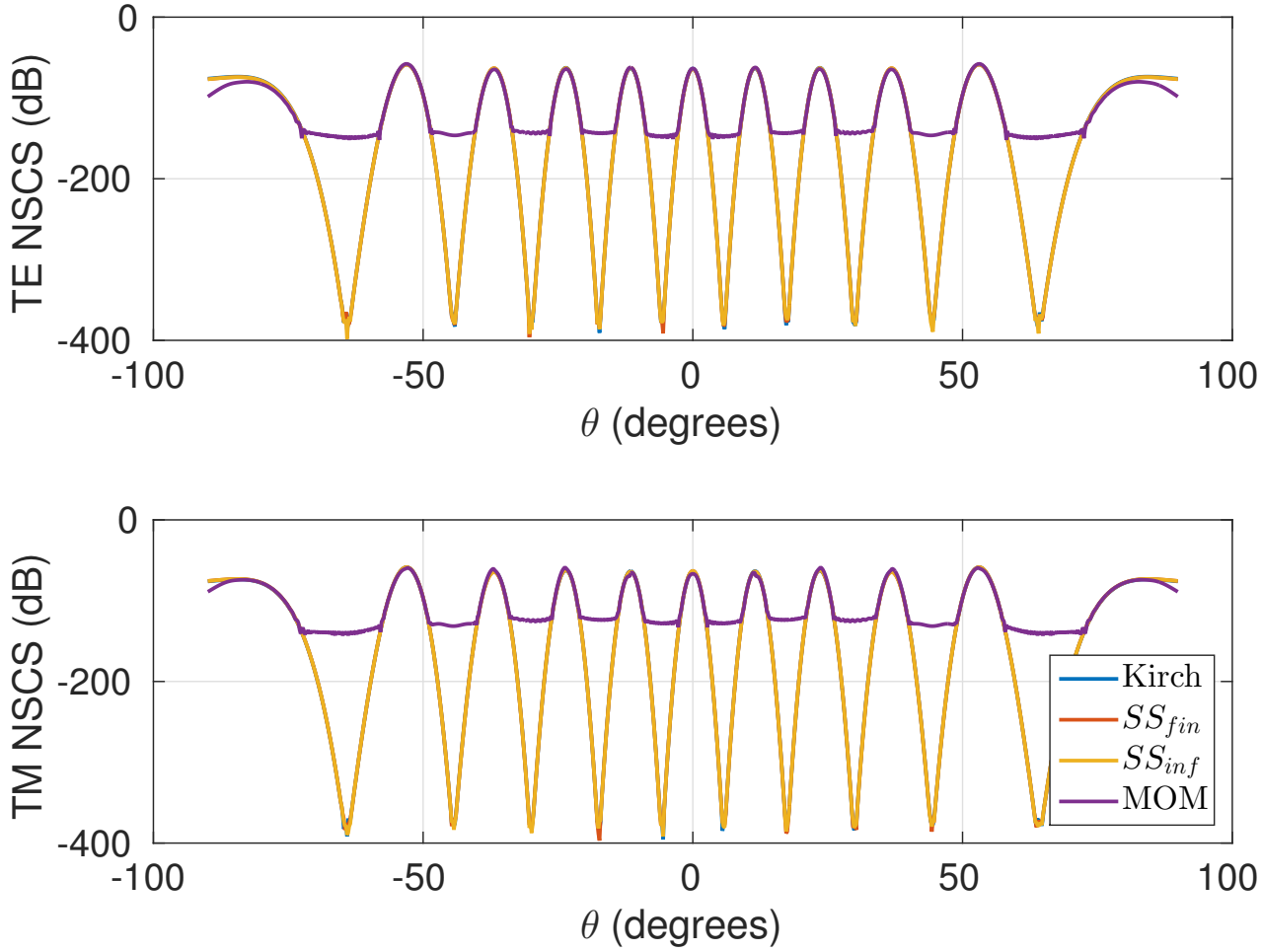


Figure 5.10: Scattered Fields from $\lambda_s = 5\lambda_0$ Surface Normal Incidence

NSCS $\lambda_s/\lambda_0 = 5$, $\alpha/\lambda_0 = 200$, $b/\lambda_0 = 0.50$, $\theta_i = 15.00$, $g/\lambda_0 = 20$, $\Delta x/\lambda_0 = 0.01$

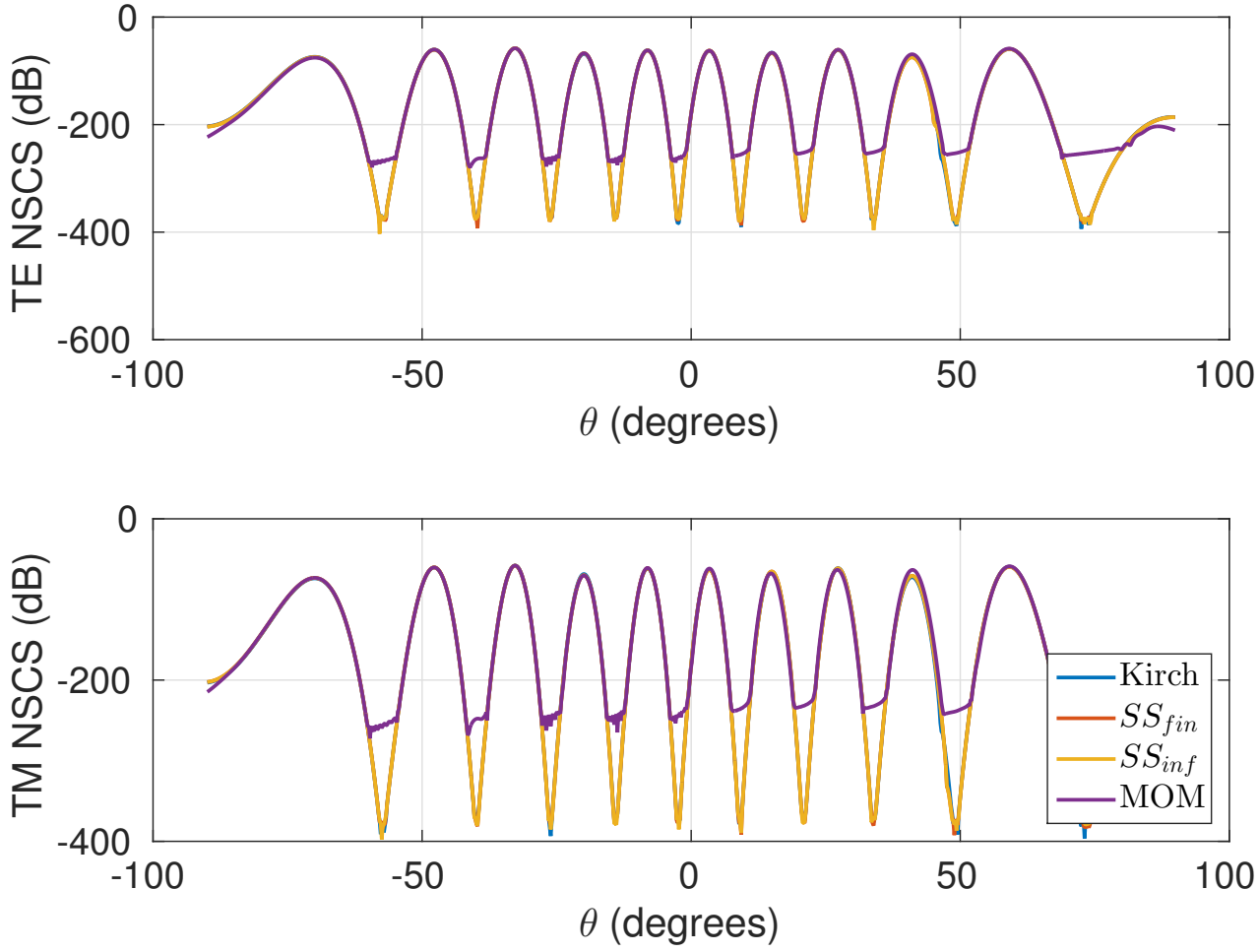


Figure 5.11: Scattered Fields from $\lambda_s = 5\lambda_0$ Surface $\theta_0 = 15°$ Incidence

NSCS $\lambda_s/\lambda_0 = 5$, $\alpha/\lambda_0 = 200$, $b/\lambda_0 = 0.50$, $\theta_i = 45.00$, $g/\lambda_0 = 20$, $\Delta x/\lambda_0 = 0.01$

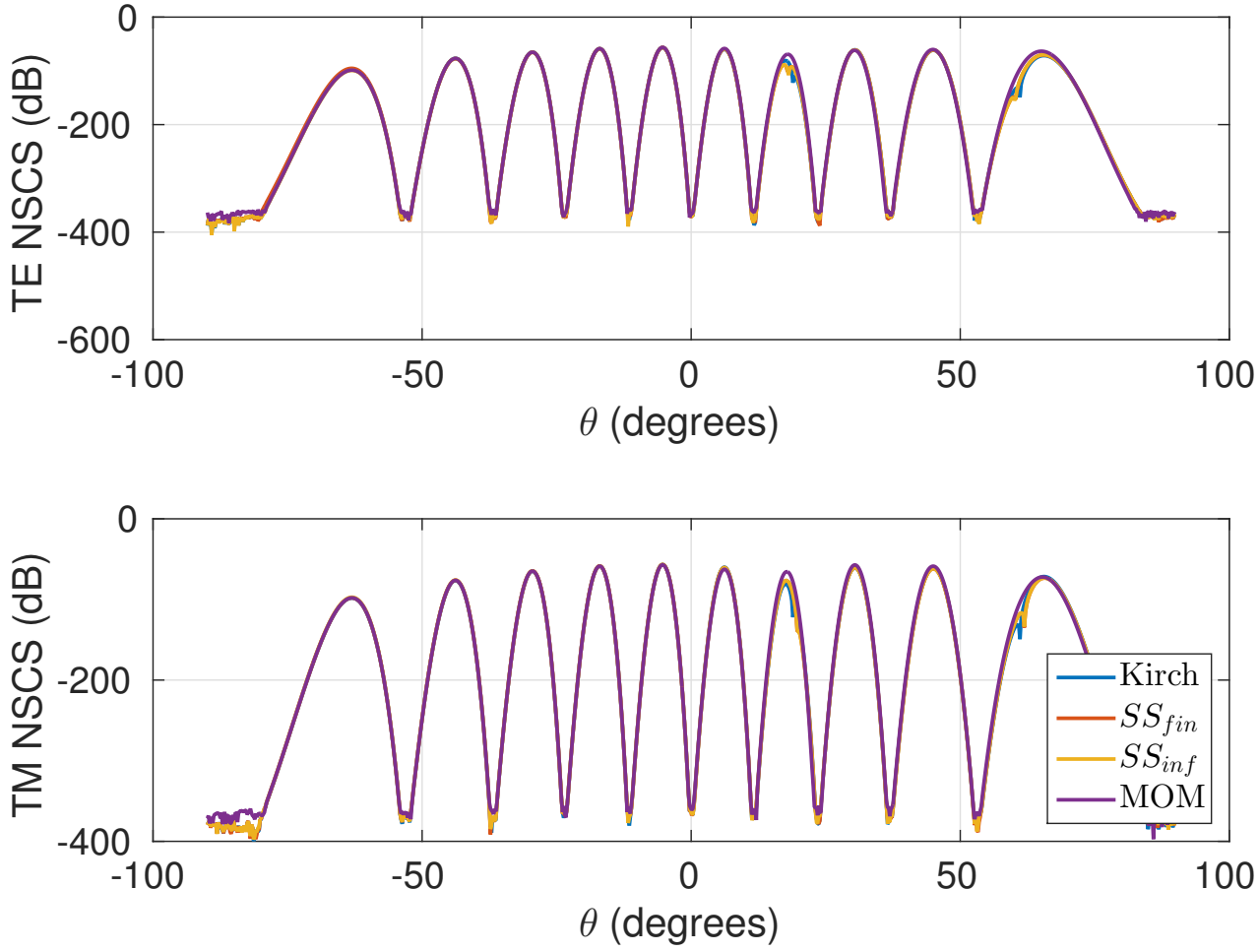


Figure 5.12: Scattered Fields from $\lambda_s = 5\lambda_0$ Surface $\theta_0 = 45°$ Incidence

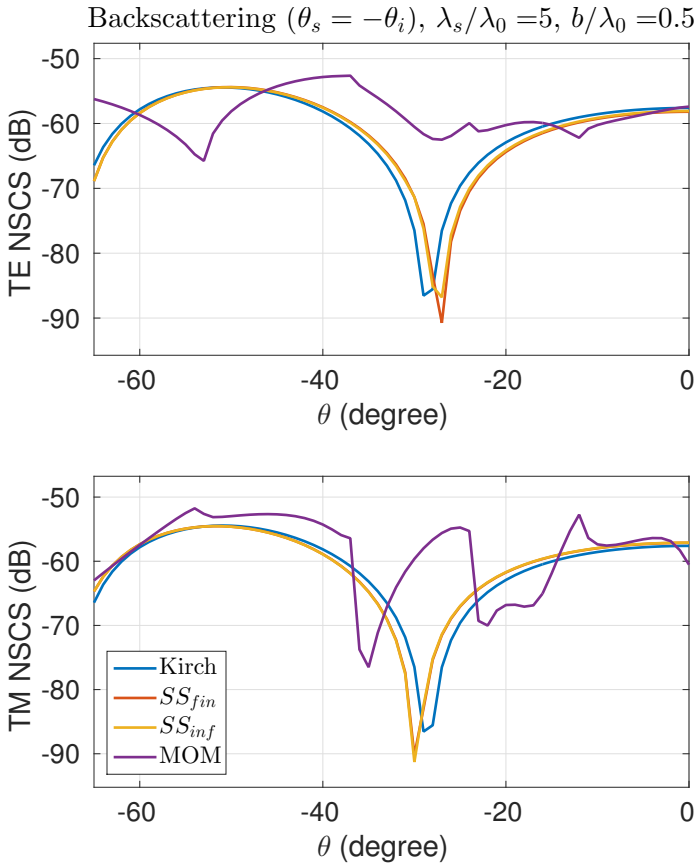


Figure 5.13: $\frac{\lambda_s}{\lambda_0} = 5$ Backscatter $\theta_i = -\theta_s$

Figures 5.13 and 5.14 show backscatter results as would be observed by a monostatic radar with $\theta_s = -\theta_i$. These results clearly demonstrate a polarization sensitivity that has never before been shown in a single-scattering result. The null observed in the Kirchhoff scattered fields has been shifted $+2^\circ$ for TE and $-2^\circ$ for TM, leading to a total of 4 degree difference between the respective nulls. Additionally, it is clear that multiple-scattering is an important effect here. Also of interest in Fig. 5.14 is the TE polarization for which $\overline{G}$ diverges. Here the $J_{ss_{inf}}$ radiated fields are essentially zero, but the formulas from the finite case provides improved agreement with the full-wave solution for the entire range of interest, and is nearly exact for $\theta_i > 50^\circ$ and $\theta_i < 15^\circ$.

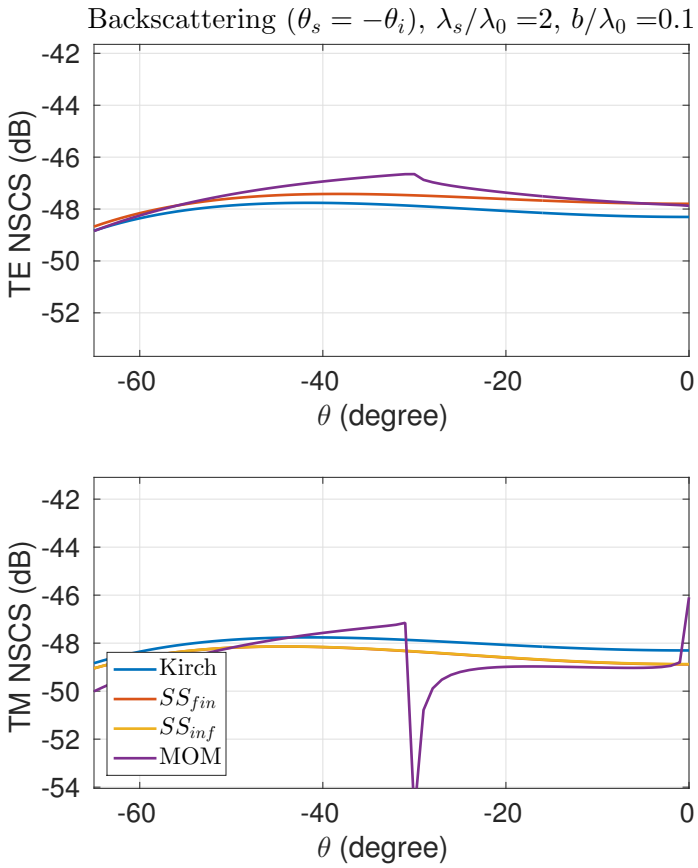


Figure 5.14: $\frac{\lambda_s}{\lambda_0} = 2$ Backscatter $\theta_i = -\theta_s$

### 5.3.2 Multiple frequency surfaces

Three cases of multiple frequency surfaces are examined in this section. Surface parameters are taken from the analysis of spectral surfaces in Section 4.4.4 such that the empiric-analytic formula is valid for $\overline{\overline{G}}$. Figures 5.15 through 5.17 show a gentle surface with two normalized surface wavelengths of 19 and 20 , while Figures 5.18 through 5.20 show a moderate surface with two normalized surface wavelengths of 7 and 8. A three frequency surface with normalized wavelengths of 7,8 and 9 are shown in Figures 5.21 through 5.23.

For all three cases, there are only only very localized differences between the Kirchhoff and Single Scatter fields with normal incidence and like the single surface frequency results of Section 5.3.1 the Single Scatter fields are decreased for TE and enhanced for TM near endfire and at broadside on the order of 1-2dB. As the incident angle is increased on the gentle $\frac{\lambda_s}{\lambda_0} = \{19, 20\}$ surface, dramatic enhancement of backscattering is observed for both polarizations. Figure 5.16 shows a 23dB and 17dB increase for TE and TM respectively, while Figure 5.17 shows a nearly 150 dB increase for both polarizations from $-70 \leq \theta_s \leq -90$.

For the rougher multi-frequency surfaces, the $\theta_i = 15^\circ$ results behave similarly to the normal incident results but with 2dB differences in Figure 5.19 and 4dB differences in Figure 5.22. When the incident angle is increased to 45° a difference of 44dB and 36dB for TE and TM respectively is observed for negative scattering angles near grazing and additionally a 54dB enhancement in the Single Scattered fields for positive angles near grazing as shown in Figure 5.20. For the three frequency surface with 45 degree incident illumination of Figure 5.23, the enhanced backscattering is observed with a 44dB difference for TE and a 13.3dB for TM.

NCSC $\lambda_s/\lambda_0 = 19, 20$, $\alpha/\lambda_0 = 300$, $b/\lambda_0 = 1.40$, $\theta_i = 0.00$, $g/\lambda_0 = 30$, $\Delta x/\lambda_0 = 0.01$

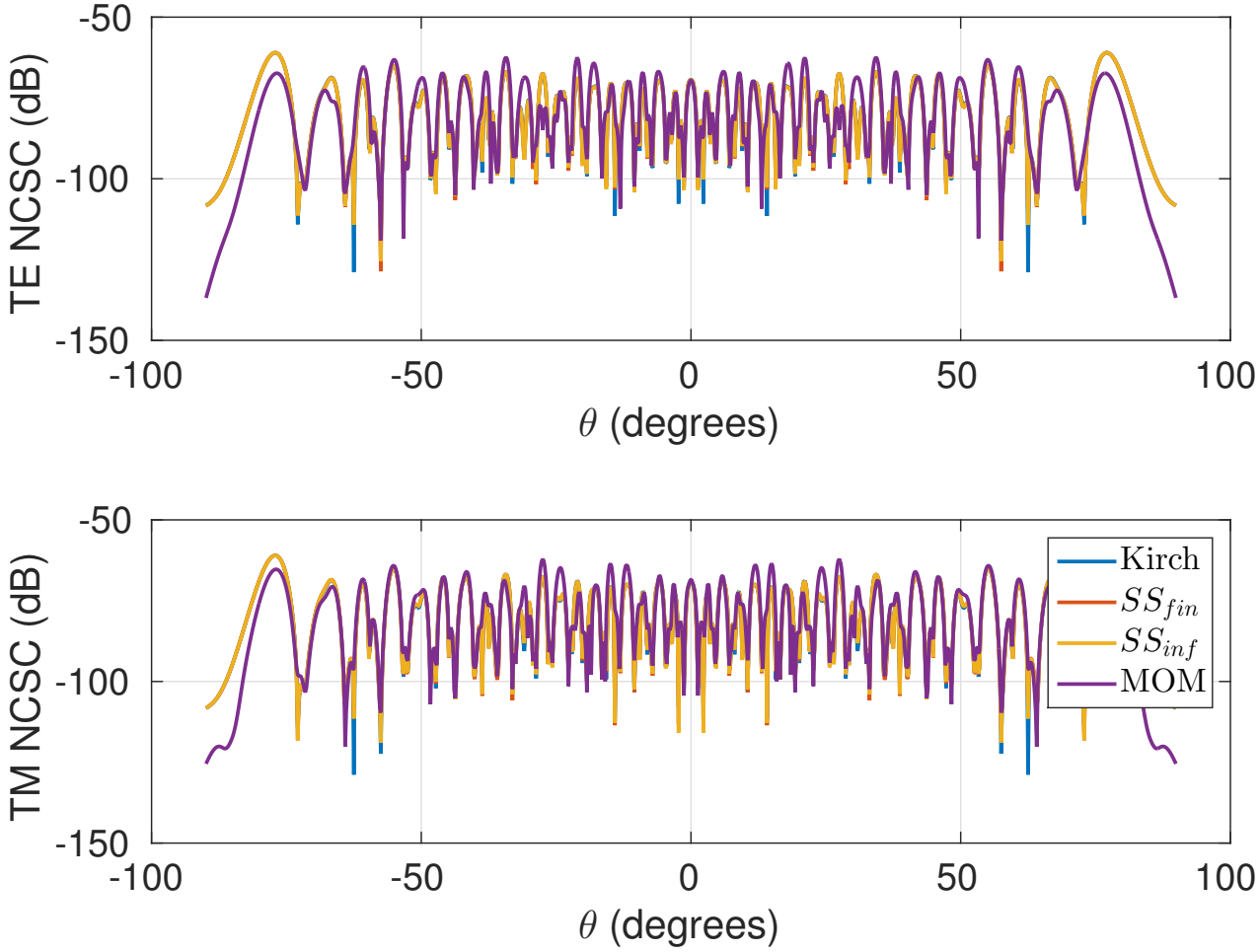


Figure 5.15: Gentle Two Frequency Surface Normal Incidence

NCSC $\lambda_s/\lambda_0 = 19, 20$, $\alpha/\lambda_0 = 300$, $b/\lambda_0 = 1.40$, $\theta_i = 15.00$, $g/\lambda_0 = 30$, $\Delta x/\lambda_0 = 0.01$

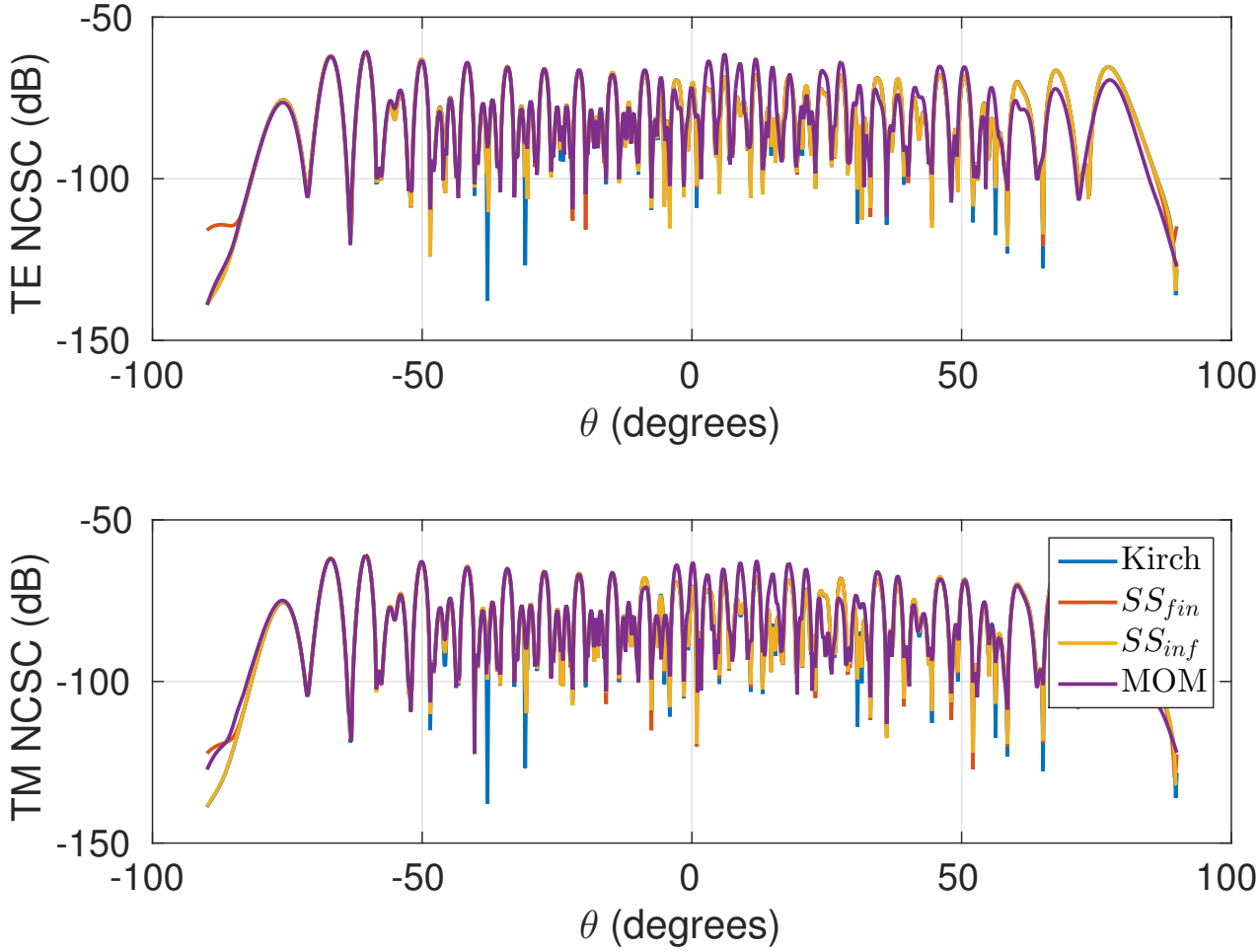


Figure 5.16: Gentle Two Frequency Surface Mild Incident Angle

NCSC $\lambda_s/\lambda_0 = 19, 20,\ \alpha/\lambda_0 = 300,\ b/\lambda_0 = 1.40,\ \theta_i = 45.00,\ g/\lambda_0 = 30,\ \Delta x/\lambda_0 = 0.01$

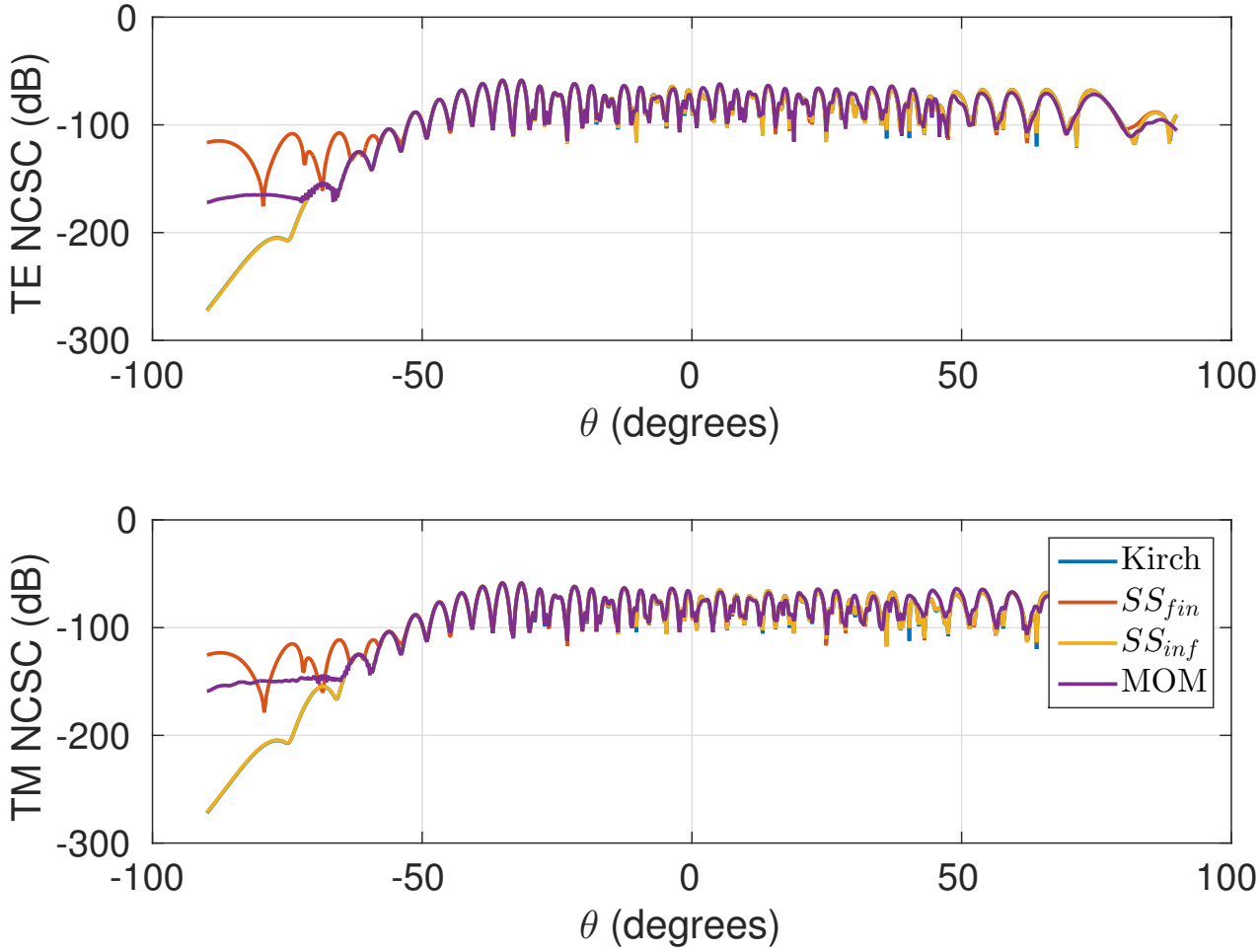


Figure 5.17: Gentle Two Frequency Surface Moderate Incident Angle

NCSC $\lambda_s/\lambda_0 = 7, 8,\ \alpha/\lambda_0 = 300,\ b/\lambda_0 = 0.47,\ \theta_i = 0.00,\ g/\lambda_0 = 30,\ \Delta x/\lambda_0 = 0.01$

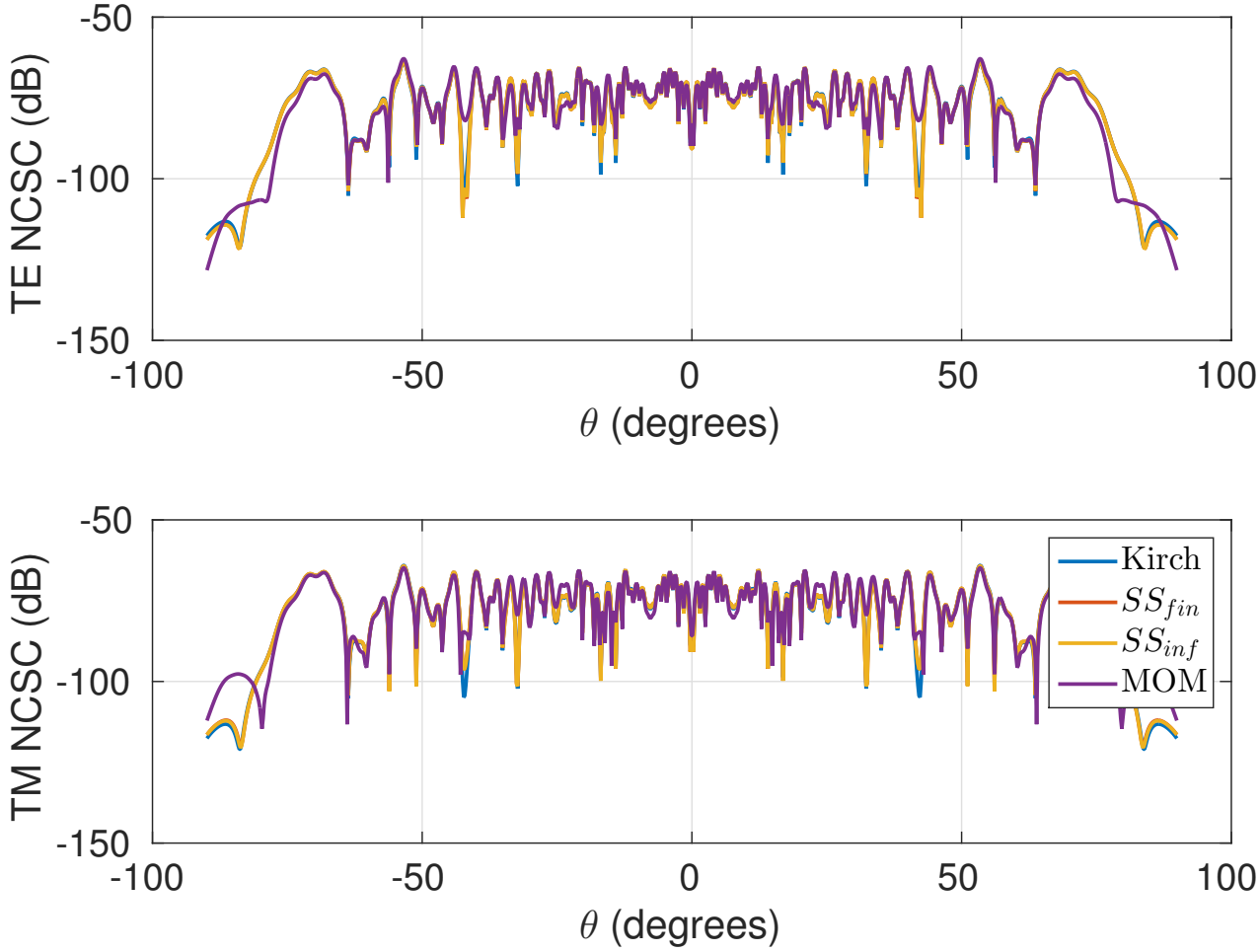


Figure 5.18: Moderate Two Frequency Surface Normal Incidence

NCSC $\lambda_s/\lambda_0 = 7,8,\ \alpha/\lambda_0 = 300,\ b/\lambda_0 = 0.47,\ \theta_i = 15.00,\ g/\lambda_0 = 30,\ \Delta x/\lambda_0 = 0.01$

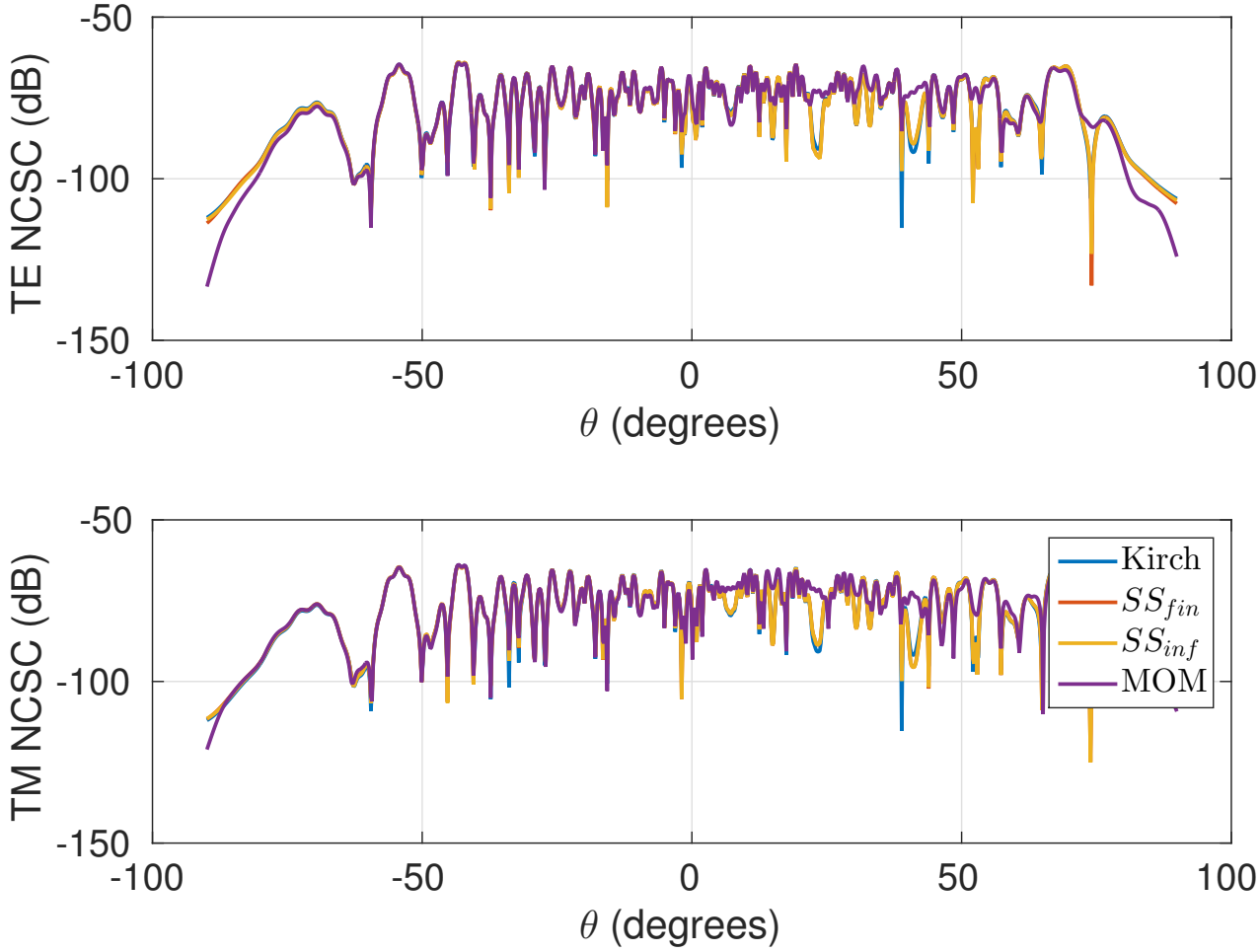


Figure 5.19: Moderate Two Frequency Surface Mild Incident Angle

NCSC $\lambda_s/\lambda_0 = 7, 8$, $\alpha/\lambda_0 = 300$, $b/\lambda_0 = 0.47$, $\theta_i = 45.00$, $g/\lambda_0 = 30$, $\Delta x/\lambda_0 = 0.01$

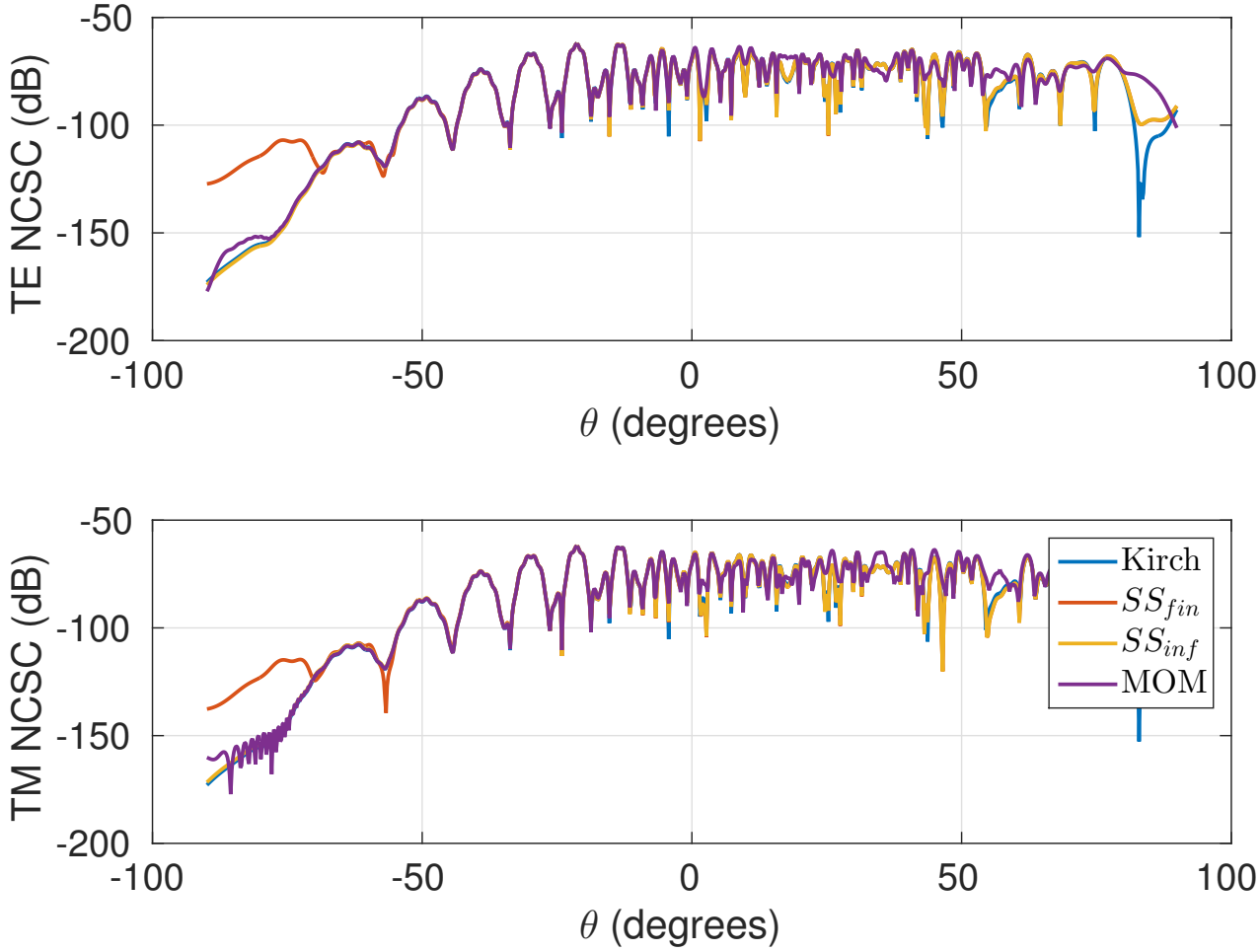


Figure 5.20: Moderate Two Frequency Surface Moderate Incident Angle

## 5.4 Summary

Numeric computations fail to provide the physical insight offered by analytic results, continue to be computationally expensive and are difficult to validate. Candidate analytic diffraction theories applicable to scattering from finite and deterministic objects cannot be applied to extended statistically rough surfaces. The physical insight garnered by analytical methods is required to drive novel applications, validate numeric computations and interpret existing results. In this chapter, analytical results from the Single Scatter Subtraction method were

NCSC $\lambda_s/\lambda_0 = 7, 8, 9$, $\alpha/\lambda_0 = 300$, $b/\lambda_0 = 0.31$, $\theta_i = 0.00$, $g/\lambda_0 = 30$, $\Delta x/\lambda_0 = 0.01$

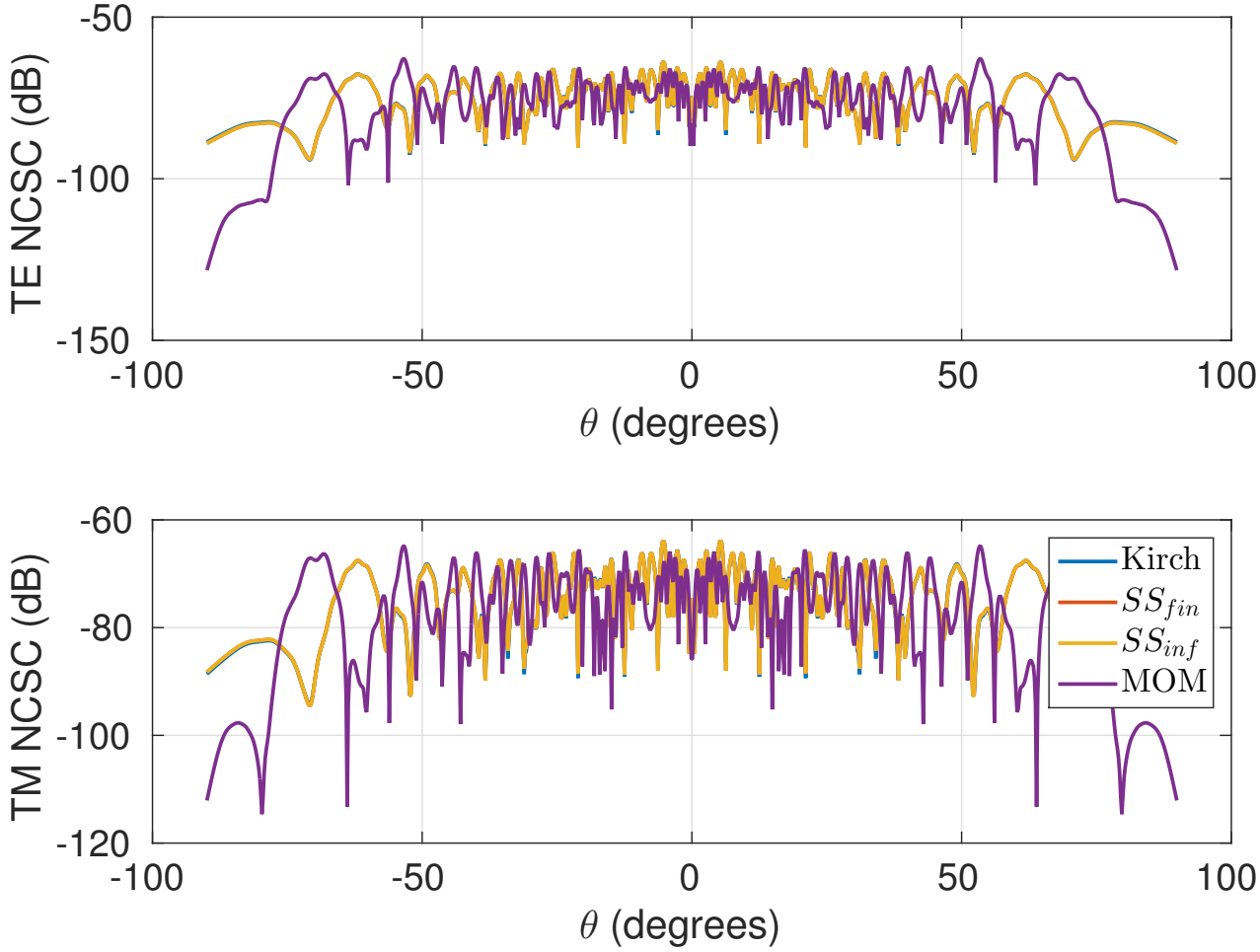


Figure 5.21: Three Frequency Surface Normal Incidence

NCSC $\lambda_s/\lambda_0 = 7, 8, 9$, $\alpha/\lambda_0 = 300$, $b/\lambda_0 = 0.31$, $\theta_i = 15.00$, $g/\lambda_0 = 30$, $\Delta x/\lambda_0 = 0.01$

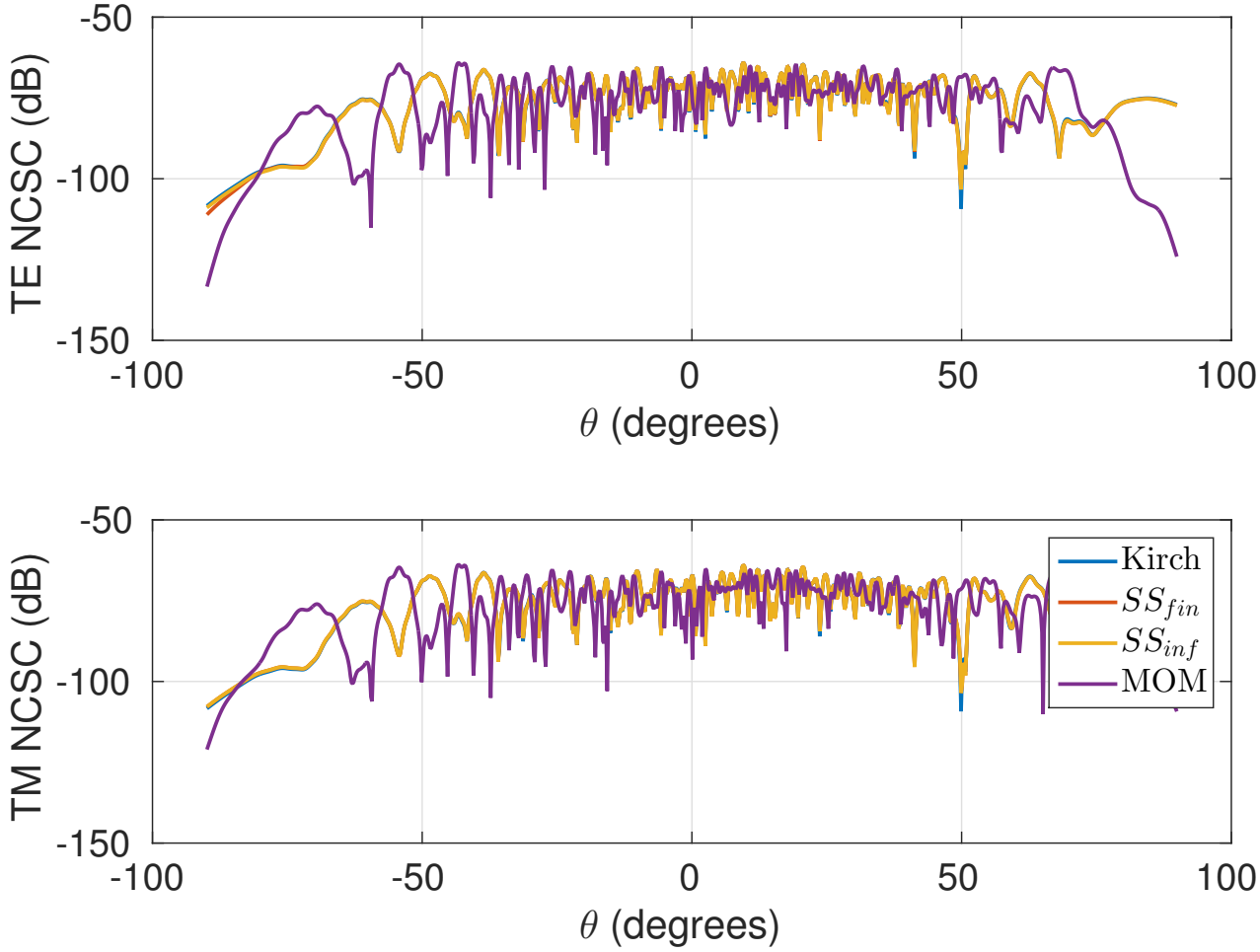


Figure 5.22: Three frequency Surface Mild Incident Angle

NCSC $\lambda_s/\lambda_0 = 7, 8, 9,\ \alpha/\lambda_0 = 300,\ b/\lambda_0 = 0.31,\ \theta_i = 45.00,\ g/\lambda_0 = 30,\ \Delta x/\lambda_0 = 0.01$

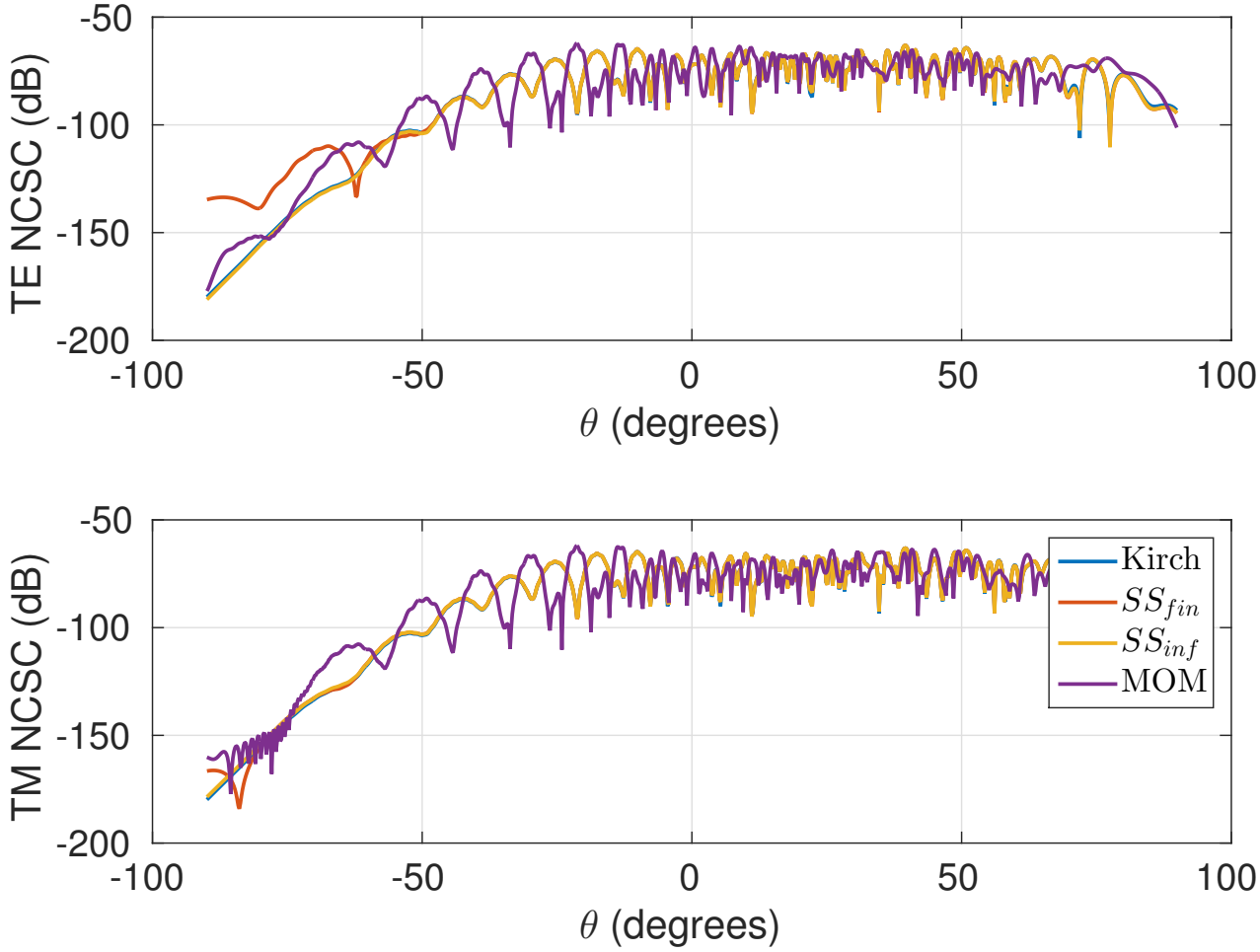


Figure 5.23: Three Frequency Surface Moderate Incident Angle

used to produce an extension to the tangent plane Kirchhoff approximation that resembles a curved tangent plane. Additionally, a long-standing dispute on the physical nature of Bragg scatter was settled as multiple-scattering phenomenon. It was also demonstrated that the finite $\overline{\overline{G}}$ real component appears to contain a standing wave, resulting from the edge effect of a finite truncation imposed by beam illumination which has implications for all practical numerical solutions to the MFIE.

From these analytic expressions for the currents on both single and multi-sinusoidal surfaces, the scattered fields were calculated numerically and demonstrated the effect of the bent plane as shifting the scattered power from some peaks to others. In these results, polarization sensitivity was demonstrated for the first time in a single-scattering result.

# Chapter 6

# Conclusion

## 6.1 Summary

This work has advanced the study of electromagnetic rough surface scattering by introducing a novel theoretical approach to solving the Magnetic Field Integral Equation. By separating the single scattering portion of the current from the integral term of the MFIE and decomposing the total current into single-scattering and multiple-scattering while making no assumptions on surface parameters, dimensionality or illumination the Single Scatter Subtraction method was defined. A new quantity, the kernel integral, never before studied plays a crucial role in this method. After restricting the study to a 1D perfect electrically conducting surface and beginning with numerical simulations, the quantity was characterized first for approximately infinite surfaces 2 million electromagnetic wavelengths long as essentially pure imaginary, then on a series of finite surfaces representative of those of interest in beam-illuminated scattering problems. The finite case was found to resemble the infinite with additional small-scale oscillations in the real and imaginary components. A number of features of the kernel integral were noted, including the highly oscillatory and slow $\frac{1}{\sqrt{|d|}}$ decay as well as singularities when the surface oscillations approach the electromagnetic wavelength. Pure analytical approaches such as the calculus of residues found little traction, and even advanced numerical integration techniques proved difficult for solution so instead a simple, highly discretized numerical technique was used and validated with approximate,

truncated analytic techniques. By study, experience and intuition an "empiric" formula was produced by comparison with numeric computations and validated over a large range of surface parameters.

Following this, a catalog of approximations to the finite support kernel integral were derived. First, analytic approximations for the integral tails were produced and used to validate the numeric solutions. Then a small argument form was found but unfortunately with bounds too restrictive to allow it to be combined with the integral tails to form a full solution. Finally, combining the integral tails with the infinite empiric formula and applying an additional series of approximations produced an "empiric analytic" formula that was found to have excellent agreement over an even wider range of surface parameters even approaching the singular wavelengths. A thorough characterization of the range of validity was found by examining a wide swath of surface parameters. Following this, multi-frequency surfaces were studied and found to be linear for TM and, surprisingly, also for TE polarization for a range of parameters with a bound that seems to depend on surface curvatures.

The empiric analytic formulas for the kernel integral were then analyzed for their physical significance which showed that the single scatter current is a bent-tangent plane approximation, the next step augmentation to the Kirchhoff tangent-plane approximation. A connection to the Luneburg-Kline series approximation was noted and represents the first time it was applied to the surface currents instead of the scattered fields hence may be combined with previous research to given an even better approximation. A long-standing controversy on the nature of Bragg scattering was also resolved, as the single scattering current did not contain Bragg scatter terms which must thus be multiple-scatter. The finite support formulas also shed light on the altered physics of the scattering problem when the MFIE is solved numerically by truncation - even when beam-limited illumination is used.

Finally, numeric computations of the scattered fields from the analytic single scatter cur-

rents showed the effect of the bent-tangent plane approximation is to shift scattered power, modulating some lobes higher and other lower. TM shifted power away from the specular direction, while TE shifted it towards the specular direction. As the incident angle was increased towards grazing, enhanced backscatter was also observed when the error terms of the finite $\overline{\overline{G}}$ were include. In some cases the enhancement was dramatic, with up to a 150dB increase in scattered power. For the first time, polarization sensitivity was demonstrated for single-scattering and a 4 degree difference in the nulls was observed between polarizations with the single scattering shifting it 2 degrees in the positive direction for TE and 2 degrees in the negative for TM.

## 6.2 Accomplishments

- Introduced novel method of solution of the MFIE based on a physics-based decomposition called the Single-Scatter Subtraction method.
  - Separated single and multiple scattering currents from integral equation without assumptions on dimensionality, surface or illumination.
  - Identified new quantity which is the kernel integral, denoted $\overline{G}$ for the infinite case and $\overline{\overline{G}}$ for the finite.
  - Found that finite beam illumination leads to truncated kernel integral $\overline{\overline{G}}$.
- Discovered $\overline{G}$ highly integration support dependent, even for large values and required integration support up to $\pm$1million wavelengths to converge[1] to a stable value.
- Successful calculation of $\overline{G}$ for the plane wave case.

[1] Not to be confused with iterative convergence.

- Discovered empiric formula for $\overline{G}$ based on numeric calculations, experience and intuition which found excellent agreement for a clearly defined, and wide range of surface parameters.

  - Empiric formula agrees with expected from literature suggesting improvement to tangent plane approximation as primarily coming from local surface curvature.

- Catalog of Analytic approximations for the finite kernel integral $\overline{\overline{G}}$

  - Analytic approximations to the tail integrals of both the finite and infinite kernel integrals were found and proven to be accurate for singly sinusoid surfaces. Allowing extension of finite numerical integration to infinite case, as well as speeding up calculation of finite case by reducing required numeric computation. Additionally, they were used to validate numeric computations.
  - An approximation for the small argument ($|x'| \to |x|$) region of the kernel integral for TM which may possibly be combined with the higher order tail approximation to provide a complete analytical expression for the TM kernel integral.
  - A higher order approximation to the tail integral was found for the TM case to arbitrary order in the Hankel function approximation, with an almost complete sum of the infinite series found. This allows both increased accuracy and a shorter interval for which numeric integration is necessary.
  - An understanding of and approach to extend these analytic approximation to the general case of a spectral surface.

- Simple empiric formulas found for the infinite case (both polarizations) and a combination empiric analytic formula for finite case.

  - Powerful empiric analytic formula for both polarizations with large and well-defined region of validity.

- Physical interpretation of single scattering result to increase intuition and understanding of physics and numerical solution.

  - Interpreted the $J_{ss}$ result using previously found expressions for $\overline{G}$ and $\overline{\overline{G}}$ for the high frequency limit as providing a bent-plane or curvature approximation as expected as the next step improvement to the Kirchhoff current.

  - Resolution of controversy involving Bragg scattering which was determined to be a multiple scattering phenomenon supporting results found by Holliday [27].

  - Finite $\overline{\overline{G}}$ real component appears to contain a standing wave, resulting from the edge effect of a finite truncation imposed by beam illumination which has implications for all such approaches.

- Numeric calculation of scattered fields from empiric analytic currents

  - Modulation of scattered fields found congruent with the bent-tangent plane approximation intuition.

  - Anomalous enhanced backscatter observed as incident angle increases towards grazing due to error terms.

  - Polarization sensitivity demonstrated for the first time.

  - 4° shift in the null between TE and TM polarization

- Single-Scatter approximation often better then Kirchhof by up to 2.5dB

  - The fact that this is “often” not “always” is incidental.

  - Kirchhoff is often better in specular direction as a result of the bent-tangent plane.

- Approximation accurate to physical single-scattering.
- Multiple-scattering contributes here.

## 6.3 Future Research

The Single-Scatter Subtraction method provides the solid foundation of a robust research program as there are myriad avenues to pursue. Suggestions for further research include:

- Investigate single and multi-sinusoid surface at sub-EM wavelength surface frequencies to answer the physical questions: "does single scatter cease to exist as meaningful concept?" and "how and when does multiple scatter arise as the dominant factor?" and hopefully produce an analytic theory of wave scattering which apply in both the high frequency Kirchhoff and small scale perturbation regimes.

- Combine the Luneburg-Kline series current approximation of the single-scattering as the source for the Luneburg-Kline series for scattered fields.

- $S^3$ has multiple new terms, including the multiple scattering source current $J_{00}$ or pieces thereof, some of which have a closed form from empiric analytic form which may produce more powerful approximations and lead to increased understanding of the physical processes of rough surface scattering. Also, investigate the multiple scatter iteration which in addition to the single-scatter and multiple-scatter source term, may be akin to examining a Taylor series expansion, except each term has a true physical meaning.

- Analyze of eigenvalues of S3 integral equation to determine iterative convergence properties to determine if they have improved over the standard MFIE.

- Extend the analysis to fully random rough surfaces characterized only by the surface statistics using all the newly produced techniques, of this thesis and suggested above, in the Single-Scatter subtraction toolbox.

- In depth study of the physical scattering mechanisms of simplified geometries, such as a single sinusoid hump or small-scale sinusoids riding on the back of larger ones like those investigated in Kapp [30].

- Repeat all the above suggestions with a general lossy dielectric interfaces as opposed to the PEC one investigated here. All new expressions for the kernel integral will be required and new physics discovered.

- Extension to 3D as initially motivated by the difficulty in doing so with MOMI. Again, all the above suggestions may again be repeated for fruitful research.

# Bibliography


[1] Milton Abramowitz and Irene A Stegun. Handbook of mathematical functions, 10th printing, 1964.

[2] R.S. Awadallah. *Rough Surface Scattering and Propagation over Rough Terrain in Ducting Environments*. PhD thesis, Virginia Polytechnic Institute and State University, 1998.

[3] Constantine A Balanis. *Advanced engineering electromagnetics*. John Wiley & Sons, 2012.

[4] D Barrick. Remote sensing of sea state by radar. In *Engineering in the Ocean Environment, Ocean 72-IEEE International Conference on*, pages 186–192. IEEE, 1972.

[5] DE Barrick. Unacceptable height correlation coefficients and the quasi-specular component in rough surface scattering. *Radio Science*, 5(4):647–654, 1970.

[6] Donald E Barrick. Theory of hf and vhf propagation across the rough sea, 1, the effective surface impedance for a slightly rough highly conducting medium at grazing incidence. *Radio Science*, 6(5):517–526, 1971.

[7] Fridrikh Gershonovich Bass and Iosif Moiseevich Fuks. Wave scattering from statistically rough surfaces. *Oxford Pergamon Press International Series on Natural Philosophy*, 93, 1979.

[8] P Beckmann and A Spizzichino. *The scattering of electromagnetic waves from rough surface*. Pergamon, 1963.

[9] Alexandra Bringer, Charles-Antoine Guérin, Bertrand Chapron, and Alexis A Mouche. Peakedness effects in near-nadir radar observations of the sea surface. *IEEE Transactions on Geoscience and Remote Sensing*, 50(9):3293–3301, 2012.

[10] G. S. Brown. Application of the integral equation method of smoothing to random surface scattering. *Antennas and Propagation, IEEE Transactions on*, 32(12):1308–1312, Dec 1984.

[11] G. S. Brown. Backscattering from a gaussian-distributed perfectly conducting rough surface. *Antennas and Propagation, IEEE Transactions on*, 26(3):472–482, May 1978. ISSN 0018-926X.

[12] Gary S. Brown. The validity of shadowing corrections in rough surface scattering. *Radio Science*, 19(6):1461–1468, 1984. ISSN 1944-799X. doi: 10.1029/RS019i006p01461. URL http://dx.doi.org/10.1029/RS019i006p01461.

[13] G.S. Brown. An inherent limitation of the luneburg-kline representation for the current on a conducting body. *Antennas and Propagation, IEEE Transactions on*, 38(11):1889–1892, Nov 1990. ISSN 0018-926X. doi: 10.1109/8.102756.

[14] G.S. Brown. private communication, 2012–2015.

[15] Douglass D Crombie. Doppler spectrum of sea echo at 13.56 mc./s. 1955.

[16] H Davies. The reflection of electromagnetic waves from a rough surface. *Proceedings of the IEE-Part IV: Institution Monographs*, 101(7):209–214, 1954.

[17] D.E. Davis. *A Technique for Evaluating the Uncertainties in Path Loss Predictions Caused by Sparsely Sampled of Terrain Data*. PhD thesis, Virginia Polytechnic Institute and State University, 2013.

[18] Philip J Davis and Philip Rabinowitz. *Numerical integration*. Blaisdell Publishing Company London, 1967.

[19] Tanos M Elfouhaily and Joel T Johnson. The reduced local curvature approximation for rough surface scattering. In *2007 IEEE International Geoscience and Remote Sensing Symposium*, pages 1354–1357. IEEE, 2007.

[20] Tanos Mikhael Elfouhaily, Charles-Antoine Guérin, et al. A critical survey of approximate scattering wave theories from random rough surfaces. *Waves in Random Media*, 14(4):R1–R40, 2004.

[21] Gwynne. Evans. *Practical numerical integration*. Wiley, Chichester; New York, 1993.

[22] Gwynne A Evans and KC Chung. Evaluating infinite range oscillatory integrals using generalised quadrature methods. *Applied numerical mathematics*, 57(1):73–79, 2007.

[23] I Fuks. Diffraction corrections to the kirchhoff approximation in the problem of rough surface scattering. In *Electromagnetics in Advanced Applications, 2009. ICEAA'09. International Conference on*, pages 27–330. IEEE, 2009.

[24] Iosif M Fuks. Backscattering from a statistically rough 2-d surface: Diffraction corrections to geometrical optics cross sections. *Radio Science*, 42(6), 2007.

[25] AK Fung and HJ Eom. Note on the kirchhoff rough surface solution in backscattering. *Radio Science*, 16(3):299–302, 1981.

[26] Roger F Harrington. Field computation by moment methods. 1993.

[27] Dennis Holliday. Backscattering of electromagnetic waves from a perfectly conducting, gently sloping surface of finite amplitude. *IEEE transactions on antennas and propagation*, 39(2):251–252, 1991.

[28] Akira Ishimaru and Jei Shuan Chen. Scattering from very rough metallic and dielectric surfaces: a theory based on the modified kirchhoff approximation. *Waves in Random Media*, 2006.

[29] Jian-Ming Jin. *Theory and computation of electromagnetic fields*. Wiley, Hoboken, N.J., 2010.

[30] D.A. Kapp. *A New Method to Calculate Wave Scattering from Rough Surfaces at Low Grazing Angles*. PhD thesis, Virginia Polytechnic Institute and State University, 1995.

[31] D.A. Kapp and G.S. Brown. A new numerical method for rough-surface scattering calculations. *Antennas and Propagation, IEEE Transactions on*, 44(5):711–, May 1996. ISSN 0018-926X. doi: 10.1109/8.496258.

[32] Joseph B Keller. Geometrical theory of diffraction. *JOSA*, 52(2):116–130, 1962.

[33] Rafaat Khan, Desmond Power, and John Walsh. Ocean clutter suppression for an hf ground wave radar. In *Electrical and Computer Engineering, 1997. Engineering Innovation: Voyage of Discovery. IEEE 1997 Canadian Conference on*, volume 2, pages 512–515. IEEE, 1997.

[34] Rafaat H Khan. Ocean-clutter model for high-frequency radar. *IEEE journal of oceanic engineering*, 16(2):181–188, 1991.

[35] Robert G Kouyoumjian and Prabhakar H Pathak. A uniform geometrical theory of diffraction for an edge in a perfectly conducting surface. *Proceedings of the IEEE*, 62 (11):1448–1461, 1974.

[36] EG Liszka and JJ McCoy. Scattering at a rough boundary-extensions of the kirchhoff approximation. *The Journal of the Acoustical Society of America*, 71(5):1093–1100, 1982.

[37] SK Lucas. Evaluating infinite integrals involving products of bessel functions of arbitrary order. *Journal of computational and applied mathematics*, 64(3):269–282, 1995.

[38] SK Lucas and HA Stone. Evaluating infinite integrals involving bessel functions of arbitrary order. *Journal of Computational and Applied Mathematics*, 64(3):217–231, 1995.

[39] PJ Lynch. Curvature corrections to rough-surface scattering at high frequencies. *The Journal of the Acoustical Society of America*, 47(3B):804–815, 1970.

[40] Diana F McCammon and Suzanne T McDaniel. Surface reflection: On the convergence of a series solution to a modified helmholtz integral equation and the validity of the kirchhoff approximation. *The Journal of the Acoustical Society of America*, 79(1):64–70, 1986.

[41] William C Meecham. On the use of the kirchhoff approximation for the solution of reflection problems. Technical report, DTIC Document, 1955.

[42] Theodore J Myers, Wayne A Scales, and Robert E Marshall. Determination of aircraft wake vortex radar cross section due to coherent bragg scatter from mixed atmospheric water vapor. *Radio Science*, 34(1):103–111, 1999.

[43] Michael H Newkirk and Gary S Brown. A waveform model for surface and volume scattering from ice and snow. *IEEE transactions on geoscience and remote sensing*, 34 (2):444–456, 1996.

[44] J. A. Ogilvy. *Theory of wave scattering from random rough surfaces.* A. Hilger, Bristol, England; Philadelphia, 1991.

[45] JA Ogilvy. Wave scattering from rough surfaces. *Reports on Progress in Physics*, 50 (12):1553, 1987.

[46] John William Strutt Baron Rayleigh. *The theory of sound*, volume 2. Macmillan, 1896.

[47] Stephen O Rice. Reflection of electromagnetic waves from slightly rough surfaces. *Communications on pure and applied mathematics*, 4(2-3):351–378, 1951.

[48] Ernesto Rodriguez. Beyond the kirchhoff approximation. *Radio Science*, 24(5):681–693, 1989.

[49] Ernesto Rodríguez. Beyond the kirchhoff approximation ii electromagnetic scattering. *Radio science*, 26(1):121–132, 1991.

[50] M Saillard and A Sentenac. Rigorous solutions for electromagnetic scattering from rough surfaces. *Waves in Random Media*, 11(3):103–137, 2001.

[51] Avram Sidi. A user-friendly extrapolation method for oscillatory infinite integrals. *Mathematics of Computation*, 51(183):249–266, 1988.

[52] Bruce G Smith. Lunar surface roughness: Shadowing and thermal emission. *Journal of Geophysical Research*, 72(16):4059–4067, 1967.

[53] Robert H Stewart. *Introduction to physical oceanography*. 2008.

[54] Eric I Thorsos. Acoustic scattering from a pierson-moskowitz sea surface. *The Journal of the Acoustical Society of America*, 88(1):335–349, 1990.

[55] J.V. Toporkov. *Study of Electromagnetic Scattering from Randomly Rough Ocean- Like Surfaces Using Integral-Equation-Based Numerical Technique*. PhD thesis, Virginia Polytechnic Institute and State University, 1998.

[56] P Ya Ufimtsev. Method of edge waves in the physical theory of diffraction. Technical report, FOREIGN TECHNOLOGY DIV WRIGHT-PATTERSONAFB OH, 1971.

[57] Pyotr Ya Ufimtsev. *Fundamentals of the physical theory of diffraction*. John Wiley & Sons, 2007.

[58] G Valenzuela. Depolarization of em waves by slightly rough surfaces. *IEEE Transactions on Antennas and Propagation*, 15(4):552–557, 1967.

[59] Gaspar R Valenzuela. Theories for the interaction of electromagnetic and oceanic waves-a review. *Boundary-Layer Meteorology*, 13(1-4):61–85, 1978.

[60] John F Vesecky. A short bibliography of russian literature in radio oceanography. *Boundary-Layer Meteorology*, 13(1):427–429, 1978.

[61] AG Voronovich and YU Zavorotny. Curvature effects in the composite model for low-grazing-angle rough-surface scatter. *waves in random media*, 8(1):41–52, 1998.

[62] George Neville Watson. *A treatise on the theory of Bessel functions*. Cambridge university press, 1995.

[63] B.A. Westin. *Applications in Remote Sensing Using the Method of Ordered Multiple Interactions*. PhD thesis, Virginia Polytechnic Institute and State University, 2013.

# Appendices

# Appendix A

# Fresnel-Based Finite Analytic Tail Approximations

## A.1 TE Finite Analytic Tail Integration

Below an analytical approximation for the tails of the $\overline{\overline{G}}$ integral for TE polarization is derived, as discussed in Section 4.4.3.1.

From above we have for TE polarization:

$$\overline{\overline{G}}_{TE} = -\frac{2k_0}{j4}\int_{-\alpha}^{\alpha} \frac{\sqrt{1+\zeta_{x'}^2\left(x'\right)}\left[-\zeta_x\left(x\right)\Delta x+\zeta\left(x\right)-\zeta\left(x'\right)\right]}{\sqrt{1+\zeta_x^2\left(x\right)}\sqrt{\Delta x^2+\left(\zeta\left(x\right)-\zeta\left(x'\right)\right)^2}} H_1^{(2)}\left(k_0\sqrt{\Delta x^2+\left(\zeta\left(x\right)-\zeta\left(x'\right)\right)^2}\right)dx'$$

Let $\Delta x = x - x'$ so that $x' = x - \Delta x$ and $-d\Delta x = dx'$ and $\zeta_{x'} = \frac{d\zeta(x')}{dx'} = \frac{d\zeta(x-\Delta x)}{d\Delta x}\frac{d\Delta x}{dx'} =$

$-\frac{d\zeta(x-\Delta x)}{d\Delta x} = -\zeta_{\Delta x}$

$$\overline{\overline{G}}_{TE} = \frac{k_0}{j2}\int_{-\alpha}^{\alpha} \frac{\sqrt{1+\zeta_{\Delta x}^2(x-\Delta x)}\left[-\zeta_x(x)\operatorname{sgn}(\Delta x) + \frac{\zeta(x)-\zeta(x-\Delta x)}{|\Delta x|}\right]}{\sqrt{1+\zeta_x^2(x)}\sqrt{1+\left(\frac{\zeta(x)-\zeta(x-\Delta x)}{\Delta x}\right)^2}} H_1^{(2)}\left(k_0|\Delta x|\sqrt{1+\left(\frac{\zeta(x)-\zeta(x-\Delta x)}{\Delta x}\right)^2}\right) d\Delta x$$

Rewrite using the following function to provide clarity in the integral manipulations

$$F(x,\Delta x) = \frac{\sqrt{1+\zeta_{\Delta x}^2(x-\Delta x)}\left[-\zeta_x(x) + \frac{\zeta(x)-\zeta(x-\Delta x)}{\operatorname{sgn}(\Delta x)|\Delta x|}\right]}{\sqrt{1+\left(\frac{\zeta(x)-\zeta(x-\Delta x)}{\Delta x}\right)^2}} H_1^{(2)}\left(k_0|\Delta x|\sqrt{1+\left(\frac{\zeta(x)-\zeta(x-\Delta x)}{\Delta x}\right)^2}\right)$$

Then

$$\overline{\overline{G}}_{TE} = \frac{k_0}{j2\sqrt{1+\zeta_x^2(x)}}\left\{\int_{x+\alpha}^{0} F(x,\Delta x)\operatorname{sgn}(\Delta x)\,d\Delta x + \int_{0}^{x-\alpha} F(x,\Delta x)\operatorname{sgn}(\Delta x)\,d\Delta x\right\}$$

Here we must be careful to note that $\Delta x$ is positive over the whole left integral. Likewise with $\alpha \geq x$,$\Delta x$ is negative for the right integral

$$\overline{\overline{G}}_{TE} = \frac{k_0}{j2\sqrt{1+\zeta_x^2(x)}}\left\{\int_{x-\alpha}^{0} F(x,\Delta x)\,d\Delta x - \int_{0}^{x-\alpha} F(x,\Delta x)\,d\Delta x\right\}$$

Later we will require both of these integrals to be taken in the positive direction over a positive interval. Flipping the limits in the first integral, and making the substitution $-\Delta x' = \Delta x$ in the second:

$$\overline{\overline{G}}_{TE} = \frac{k_0}{j2\sqrt{1+\zeta_x^2(x)}}\left\{-\int_{0}^{x-\alpha} F(x,\Delta x)\,d\Delta x + \int_{0}^{\alpha-x} F(x,-\Delta x')\,d\Delta x'\right\}$$

Now we will truncate the integration so the following approximations hold. First, take $|\Delta x| \gg |\Delta\zeta|$ so we have $\left|\frac{\Delta\zeta}{\Delta x}\right| \ll 1$, and thus $\sqrt{1+\left(\frac{\Delta\zeta}{\Delta x}\right)^2} \approx 1$. Concurrent with this, approximate the Hankel function by

$$H_1^{(2)}(k_0 a) \approx \sqrt{\frac{2}{\pi k_0 a}} \exp\left(-jk_0 a + j\frac{3\pi}{4}\right)$$

giving

$$F(x,\Delta x) \approx \sqrt{1+\zeta_{\Delta x}^2(x-\Delta x)}\left[-\zeta_x(x)\right]\sqrt{\frac{2}{\pi k_0|\Delta x|}} \exp\left(-jk_0|\Delta x| + j\frac{3\pi}{4}\right)$$

Restricting the integration to a region in which this is valid:

$$A^{FF_{te}}(x,\alpha,c,d) = \frac{k_0}{j2\sqrt{1+\zeta_x^2(x)}}\left\{-\int_{x-c}^{x-\alpha} F(x,\Delta x)\,d\Delta x + \int_{d-x}^{\alpha-x} F(x,-\Delta x')\,d\Delta x'\right\}$$

with $-\alpha < c < x < d < \alpha$ making $\Delta x$ and $\Delta x'$ positive on these intervals so taking the absolute value:

$$A^{FF_{te}} = \frac{-\zeta_x(x)\sqrt{k_0}}{j\sqrt{1+\zeta_x^2(x)}} e^{j\frac{3\pi}{4}}\left\{-\int_{x-c}^{x-\alpha}\sqrt{1+\zeta_{\Delta x}^2(x-\Delta x)}\sqrt{\frac{1}{2\pi\Delta x}}\exp(-jk_0\Delta x)\,d\Delta x\right.$$
$$\left.+\int_{d-x}^{\alpha-x}\sqrt{1+\zeta_{\Delta x}^2(x+\Delta x')}\sqrt{\frac{1}{2\pi\Delta x'}}\exp(-jk_0\Delta x')\,d\Delta x'\right\}$$

If $\zeta_{\Delta x}(x \pm \Delta x) \ll 1$, Taylor expanding gives the following:

$$A^{FF_{te}} = \frac{-\zeta_x(x)\sqrt{k_0}}{j\sqrt{1+\zeta_x^2(x)}} e^{j\frac{3\pi}{4}} \left\{ -\int_{x-c}^{x-\alpha} \left(1 + \frac{1}{2}\zeta_{\Delta x}^2(x-\Delta x) - O\left(\zeta_{\Delta x}^4\right)\right) \sqrt{\frac{1}{2\pi\Delta x}} \exp\left(-jk_0\Delta x\right) d\Delta x \right.$$
$$\left. + \int_{d-x}^{\alpha-x} \left(1 + \frac{1}{2}\zeta_{\Delta x}^2(x+\Delta x') - O\left(\zeta_{\Delta x}^4\right)\right) \sqrt{\frac{1}{2\pi\Delta x'}} \exp\left(-jk_0\Delta x'\right) d\Delta x' \right\}$$

It will help to split the integral $A^{FF_{te}}$ into the upper and lower parts:

$$A^{FF_{te}}(x,\alpha,c,d) = A_l^{FF_{te}}(x,\alpha,c) + A_u^{FF_{te}}(x,\alpha,d)$$

$$A_l^{FF_{te}}(x,\alpha,c) = \frac{\zeta_x(x)\sqrt{k_0}}{j\sqrt{1+\zeta_x^2(x)}} e^{j\frac{3\pi}{4}} \int_{x-c}^{x-\alpha} \left(1 + \frac{1}{2}\zeta_{\Delta x}^2(x-\Delta x)\right) \sqrt{\frac{1}{2\pi\Delta x}} \exp\left(-jk_0\Delta x\right) d\Delta x \tag{A.1.1}$$

$$A_u^{FF_{te}}(x,\alpha,d) = \frac{-\zeta_x(x)\sqrt{k_0}}{j\sqrt{1+\zeta_x^2(x)}} e^{j\frac{3\pi}{4}} \int_{d-x}^{\alpha-x} \left(1 + \frac{1}{2}\zeta_{\Delta x}^2(x+\Delta x')\right) \sqrt{\frac{1}{2\pi\Delta x'}} \exp\left(-jk_0\Delta x'\right) d\Delta x' \tag{A.1.2}$$

### A.1.1 Squared Slope Terms

Before finishing the integration for the upper and lower parts, examine$\zeta_{\Delta x}$ more closely:

The surface height is a singly sinusoid surface, $\zeta(x-\Delta x) = b\cos(k_s(x-\Delta x))$. Thus

$$\zeta_{\Delta x}(x-\Delta x) = \frac{d\zeta(x-\Delta x)}{d\Delta x} = bk_s \sin(k_s(x-\Delta x)) = bk_s \frac{e^{j(k_s(x-\Delta x))} - e^{-j(k_s(x-\Delta x))}}{2j}$$

so that the squared slope term becomes:

$$\zeta_{\Delta x}^{2}\left(x-\Delta x\right)=\left[bk_{s}\frac{e^{j(k_{s}(x-\Delta x))}-e^{-j(k_{s}(x-\Delta x))}}{2j}\right]^{2}$$

$$=-\frac{b^{2}k_{s}^{2}}{4}\left[\left(e^{j(k_{s}(x-\Delta x))}e^{j(k_{s}(x-\Delta x))}-e^{j(k_{s}(x-\Delta x))}e^{-j(k_{s}(x-\Delta x))}\right)\right.$$
$$\left.-\left(e^{-j(k_{s}(x-\Delta x))}e^{j(k_{s}(x-\Delta x))}-e^{-j(k_{s}(x-\Delta x))}e^{-j(k_{s}(x-\Delta x))}\right)\right]$$

$$\zeta_{\Delta x}^{2}\left(x-\Delta x\right)=-\frac{b^{2}k_{s}^{2}}{4}\left[\exp\left(j2k_{s}x\right)\exp\left(-j2k_{s}\Delta x\right)+\exp\left(-j2k_{s}x\right)\exp\left(j2k_{s}\Delta x\right)-2\right] \tag{A.1.3}$$

While, $\zeta_{\Delta x}\left(x+\Delta x'\right)=\frac{d\zeta(x+\Delta x')}{d\Delta x}=-bk_{s}\sin\left(k_{s}\left(x+\Delta x'\right)\right)\frac{d\Delta x'}{d\Delta x}=bk_{s}\frac{e^{j(k_{s}(x+\Delta x'))}-e^{-j(k_{s}(x+\Delta x'))}}{2j}$ which means the squared slope term is

$$\zeta_{\Delta x}^{2}\left(x+\Delta x\right)=\left[bk_{s}\frac{e^{j(k_{s}(x+\Delta x'))}-e^{-j(k_{s}(x+\Delta x'))}}{2j}\right]^{2}$$

$$\zeta_{\Delta x}^{2}\left(x+\Delta x'\right)=-\frac{b^{2}k_{s}^{2}}{4}\left[\exp\left(j2k_{s}x\right)\exp\left(j2k_{s}\Delta x'\right)+\exp\left(-j2k_{s}x\right)\exp\left(-j2k_{s}\Delta x'\right)-2\right] \tag{A.1.4}$$

### A.1.2 Lower Tail Integral

Since the expression for $\zeta_{\Delta x}^2(x-\Delta x)$ is somewhat complicated, split the lower integral (Eq. A.1.1) further into two integrals:

$$A_l^{FF_{te}}(x,\alpha,c) = A_{l_1}^{FF_{te}}(x,\alpha,c) + A_{l_2}^{FF_{te}}(x,\alpha,c)$$

$$A_{l_1}^{FF_{te}}(x,\alpha,c) = \frac{\zeta_x(x)\sqrt{k_0}}{j\sqrt{1+\zeta_x^2(x)}} e^{j\frac{3\pi}{4}} \int_{x-c}^{x-\alpha} \sqrt{\frac{1}{2\pi\Delta x}} \exp(-jk_0\Delta x)\, d\Delta x \tag{A.1.5}$$

$$A_{l_2}^{FF_{te}}(x,\alpha,c) = \frac{\zeta_x(x)\sqrt{k_0}}{j2\sqrt{1+\zeta_x^2(x)}} e^{j\frac{3\pi}{4}} \int_{x-c}^{x-\alpha} \zeta_{\Delta x}^2(x-\Delta x) \sqrt{\frac{1}{2\pi\Delta x}} \exp(-jk_0\Delta x)\, d\Delta x \tag{A.1.6}$$

#### A.1.2.1 Unity Term of Lower Integral

Begin solving the lower integral by integrating Equation A.1.5.

$$A_{l_1}^{FF_{te}}(x,\alpha,c) = \frac{\zeta_x(x)\sqrt{k_0}}{j\sqrt{1+\zeta_x^2(x)}} e^{j\frac{3\pi}{4}} \int_{x-c}^{x-\alpha} \sqrt{\frac{1}{2\pi\Delta x}} \exp(-jk_0\Delta x)\, d\Delta x$$

Defining the following for substitution, $\tau = k_0\Delta x$ and $d\tau = k_0 d(\Delta x)$.

$$A_{l_1}^{FF_{te}} = \frac{\zeta_x(x)}{j\sqrt{1+\zeta_x^2(x)}} e^{j\frac{3\pi}{4}} \int_{(x-c)k_0}^{(x-\alpha)k_0} \frac{1}{\sqrt{2\pi\tau}} \exp(-j\tau)\, d\tau$$

Since $\int_e^g d(\Delta x) = \int_0^g d(\Delta x) - \int_0^e d(\Delta x)$ and $\int_0^g \frac{e^{-jt}}{\sqrt{2\pi t}} dt = F(g)$ with $F(g)$ the Fresnel Integral,

$$A_{l_1}^{FF_{te}}(x,\alpha,c)=\frac{\zeta_x(x)}{j\sqrt{1+\zeta_x^2(x)}}\frac{(-1+j)}{\sqrt{2}}\left[F\left(\left(x-\alpha\right)k_0\right)-F\left(\left(x-c\right)k_0\right)\right] \tag{A.1.7}$$

#### A.1.2.2 Squared Slope Term of Lower Integral

Turning our attention to Equation A.1.6

$$A_{l_2}^{FF_{te}}(x,\alpha,c)=\frac{\zeta_x(x)\sqrt{k_0}}{j2\sqrt{1+\zeta_x^2(x)}}e^{j\frac{3\pi}{4}}\int_{x-c}^{x-\alpha}\zeta_{\Delta x}^2(x-\Delta x)\sqrt{\frac{1}{2\pi\Delta x}}\exp\left(-jk_0\Delta x\right)d\Delta x$$

Substituting the expression for $\zeta_{\Delta x}^2(x-\Delta x)$ in equation A.1.4 for this surface.

$$\begin{aligned}A_{l_2}^{FF_{te}}=-\frac{b^2k_s^2}{4}\frac{\zeta_x(x)\sqrt{k_0}}{j2\sqrt{1+\zeta_x^2(x)}}e^{j\frac{3\pi}{4}}\Bigg\{&\int_{x-c}^{x-\alpha}\frac{\exp\left(j2k_sx\right)\exp\left(-j2k_s\Delta x\right)}{\sqrt{2\pi\Delta x}}\exp\left(-jk_0\Delta x\right)d\Delta x\\&+\int_{x-c}^{x-\alpha}\frac{\exp\left(-j2k_sx\right)\exp\left(j2k_s\Delta x\right)}{\sqrt{2\pi\Delta x}}\exp\left(-jk_0\Delta x\right)d\Delta x\\&-\int_{x-c}^{x-\alpha}\frac{2}{\sqrt{2\pi\Delta x}}\exp\left(-jk_0\Delta x\right)d\Delta x\Bigg\}\end{aligned}$$

Combining exponential terms,

$$\begin{aligned}A_{l_2}^{FF_{te}}=-\frac{b^2k_s^2}{4}\frac{\zeta_x(x)\sqrt{k_0}}{j2\sqrt{1+\zeta_x^2(x)}}e^{j\frac{3\pi}{4}}\Bigg\{&\exp\left(j2k_sx\right)\int_{x-c}^{x-\alpha}\frac{\exp\left(-j\left(k_0+2k_s\right)\Delta x\right)}{\sqrt{2\pi\Delta x}}d\Delta x\\&+\exp\left(-j2k_sx\right)\int_{x-c}^{x-\alpha}\frac{\exp\left(-j\left(k_0-2k_s\right)\Delta x\right)}{\sqrt{2\pi\Delta x}}d\Delta x-2\int_{x-c}^{x-\alpha}\frac{\exp\left(-jk_0\Delta x\right)}{\sqrt{2\pi\Delta x}}d\Delta x\Bigg\}\end{aligned}$$

Defining the following variables for substitution

$t=\left(k_0+2k_s\right)\Delta x$, so that $dt=\left(k_0+2k_s\right)d\left(\Delta x\right)$ and $\Delta x=\frac{t}{\left(k_0+2k_s\right)}$

$\tau = (k_0 - 2k_s)\,\Delta x$, so that $d\tau = (k_0 - 2k_s)\,d(\Delta x)$ and $\Delta x = \frac{\tau}{(k_0 - 2k_s)}$

$\varsigma = k_0 \Delta x$, so that $d\varsigma = k_0 d(\Delta x)$ and $\Delta x = \frac{\varsigma}{k_0}$

$K_s = \frac{k_s}{k_0}$

$$A_{l_2}^{FF_{te}} = -\frac{b^2 k_s^2 \zeta_x(x)}{j8\sqrt{1+\zeta_x^2(x)}} e^{j\frac{3\pi}{4}} \left\{ \frac{\exp(j2k_s x)}{\sqrt{(1+2K_s)}} \int_{(x-c)(k_0+2k_s)}^{(x-\alpha)(k_0+2k_s)} \frac{\exp(-jt)}{\sqrt{2\pi t}} dt \right.$$
$$\left. + \frac{\exp(-j2k_s x)}{\sqrt{(1-2K_s)}} \int_{(x-c)(k_0-2k_s)}^{(x-\alpha)(k_0-2k_s)} \frac{\exp(-j\tau)}{\sqrt{2\pi\tau}} d\tau - 2\int_{(x-c)k_0}^{(x-\alpha)k_0} \frac{\exp(-j\varsigma)}{\sqrt{2\pi\varsigma}} d\varsigma \right\}$$

Since $\int_e^g d(\Delta x) = \int_0^g d(\Delta x) - \int_0^e d(\Delta x)$ and $\int_0^e \frac{e^{-jt}}{\sqrt{2\pi t}} dt = F(e)$ with $F(e)$ the Fresnel Integral,

$$A_{l_2}^{FF_{te}} = -\frac{b^2 k_s^2 \zeta_x(x)}{j8\sqrt{1+\zeta_x^2(x)}} \frac{(-1+j)}{\sqrt{2}} \left\{ \frac{\exp(j2k_s x)}{\sqrt{(1+2K_s)}} \left[F((x-\alpha)(k_0+2k_s)) - F((x-c)(k_0+2k_s))\right] \right.$$
$$+ \frac{\exp(-j2k_s x)}{\sqrt{(1-2K_s)}} \left[F((x-\alpha)(k_0-2k_s)) - F((x-c)(k_0-2k_s))\right]$$
$$\left. -2\left[F((x-\alpha)k_0) - F((x-c)k_0)\right] \right\} \quad \text{(A.1.8)}$$

### A.1.3 Upper Tail Integral

As was done for the lower integral, the upper integral of Eq. A.1.2 will be split into two integrals

$$A_u^{FF_{te}}(x,\alpha,d) = A_{u_1}^{FF_{te}}(x,\alpha,d) + A_{u_2}^{FF_{te}}(x,\alpha,d)$$

$$A_{u_1}^{FF_{te}}(x,\alpha,d) = \frac{-\zeta_x(x)\sqrt{k_0}}{j\sqrt{1+\zeta_x^2(x)}} e^{j\frac{3\pi}{4}} \int_{d-x}^{\alpha-x} \frac{\exp(-jk_0\Delta x')}{\sqrt{2\pi\Delta x'}} d\Delta x' \tag{A.1.9}$$

$$A_{u_2}^{FF_{te}}(x,\alpha,d) = \frac{-\zeta_x(x)\sqrt{k_0}}{j2\sqrt{1+\zeta_x^2(x)}} e^{j\frac{3\pi}{4}} \int_{d-x}^{\alpha-x} \frac{\zeta_{\Delta x}^2(x+\Delta x')}{\sqrt{2\pi\Delta x'}} \exp(-jk_0\Delta x')\, d\Delta x' \tag{A.1.10}$$

#### A.1.3.1 Unity term of Upper Integral

Begin solving the upper integral by integrating Equation A.1.9.

$$A_{u_1}^{FF_{te}}(x,\alpha,d) = \frac{-\zeta_x(x)\sqrt{k_0}}{j\sqrt{1+\zeta_x^2(x)}} e^{j\frac{3\pi}{4}} \int_{d-x}^{\alpha-x} \frac{\exp(-jk_0\Delta x')}{\sqrt{2\pi\Delta x'}} d\Delta x'$$

Defining the following for substitution, $\tau = k_0\Delta x$ and $d\tau = k_0 d(\Delta x)$.

$$A_{u_1}^{FF_{te}} = \frac{-\zeta_x(x)\exp\left(j\frac{3\pi}{4}\right)}{j\sqrt{1+\zeta_x^2(x)}} \int_{(d-x)k_0}^{(\alpha-x)k_0} \frac{\exp(-j\tau)}{\sqrt{2\pi\tau}} d\tau$$

Since $\int_e^g d(\Delta x) = \int_0^g d(\Delta x) - \int_0^e d(\Delta x)$ and $\int_0^g \frac{e^{-jt}}{\sqrt{2\pi t}} dt = F(g)$ with $F(g)$ the Fresnel Integral,

$$A_{u_1}^{FF_{te}}(x,\alpha,d) = \frac{-\zeta_x(x)}{j\sqrt{1+\zeta_x^2(x)}} \frac{(-1+j)}{\sqrt{2}} \left[F((\alpha-x)k_0) - F((d-x)k_0)\right] \tag{A.1.11}$$

### A.1.3.2 Squared Slope Term of Upper Integral

Turning our attention to Equation A.1.10

$$A_{u_2}^{FF_{te}}(x,\alpha,d) = \frac{-\zeta_x(x)\sqrt{k_0}}{j2\sqrt{1+\zeta_x^2(x)}} e^{j\frac{3\pi}{4}} \int_{d-x}^{\alpha-x} \frac{\zeta_{\Delta x}^2(x+\Delta x')}{\sqrt{2\pi\Delta x'}} \exp(-jk_0\Delta x')\, d\Delta x'$$

Substituting the expression for $\zeta_{\Delta x}^2(x+\Delta x')$ in equation A.1.3 for this surface.

$$\begin{aligned} A_{u_2}^{FF_{te}} = -\frac{b^2k_s^2}{4}\frac{-\zeta_x(x)}{j2\sqrt{1+\zeta_x^2(x)}}\sqrt{k_0}e^{j\frac{3\pi}{4}} \Bigg\{ & \int_{d-x}^{\alpha-x} \frac{\exp(j2k_sx)\exp(j2k_s\Delta x')}{\sqrt{2\pi\Delta x'}} \exp(-jk_0\Delta x')\, d\Delta x' \\ & + \int_{d-x}^{\alpha-x} \frac{\exp(-j2k_sx)\exp(-j2k_s\Delta x')}{\sqrt{2\pi\Delta x'}} \exp(-jk_0\Delta x')\, d\Delta x' \\ & - \int_{d-x}^{\alpha-x} \frac{2\exp(-jk_0\Delta x')}{\sqrt{2\pi\Delta x'}} d\Delta x' \Bigg\} \end{aligned}$$

Combining exponential terms,

$$\begin{aligned} A_{u_2}^{FF_{te}} = \frac{b^2k_s^2}{4}\frac{\zeta_x(x)}{j2\sqrt{1+\zeta_x^2(x)}}\sqrt{k_0}e^{j\frac{3\pi}{4}} \Bigg\{ & \exp(j2k_sx) \int_{d-x}^{\alpha-x} \frac{\exp(-j(k_0-2k_s)\Delta x)}{\sqrt{2\pi\Delta x}} d\Delta x \\ & + \exp(-j2k_sx) \int_{d-x}^{\alpha-x} \frac{\exp(-j(k_0+2k_s)\Delta x)}{\sqrt{2\pi\Delta x}} d\Delta x - 2\int_{d-x}^{\alpha-x} \frac{\exp(-jk_0\Delta x)}{\sqrt{2\pi\Delta x}} d\Delta x \Bigg\} \end{aligned}$$

Defining the following variables for substitution

$t = (k_0 - 2k_s)\Delta x$, so that $dt = (k_0 - 2k_s)\, d(\Delta x)$ and $\Delta x = \frac{t}{(k_0-2k_s)}$

$\tau = (k_0 + 2k_s)\Delta x$, so that $d\tau = (k_0 + 2k_s)\, d(\Delta x)$ and $\Delta x = \frac{\tau}{(k_0+2k_s)}$

$\varsigma = k_0\Delta x$, so that $d\varsigma = k_0 d(\Delta x)$ and $\Delta x = \frac{\varsigma}{k_0}$

$K_s = \frac{k_s}{k_0}$

$$A_{u_2}^{FF_{te}} = \frac{b^2 k_s^2}{j8} \frac{\zeta_x(x)}{\sqrt{1+\zeta_x^2(x)}} e^{j\frac{3\pi}{4}} \left\{ \frac{\exp(j2k_s x)}{\sqrt{(1-2K_s)}} \int_{(d-x)(k_0-2k_s)}^{(\alpha-x)(k_0-2k_s)} \frac{\exp(-jt)}{\sqrt{2\pi t}} dt \right.$$
$$\left. + \frac{\exp(-j2k_s x)}{\sqrt{(1+2K_s)}} \int_{(d-x)(k_0+2k_s)}^{(\alpha-x)(k_0+2k_s)} \frac{\exp(-j\tau)}{\sqrt{2\pi\tau}} d\tau - 2\int_{(d-x)k_0}^{(\alpha-x)k_0} \frac{\exp(-j\varsigma)}{\sqrt{2\pi\varsigma}} d\varsigma \right\}$$

Since $\int_e^g d(\Delta x) = \int_0^g d(\Delta x) - \int_0^e d(\Delta x)$ and $\int_0^g \frac{e^{-jt}}{\sqrt{2\pi t}} dt = F(g)$ with $F(g)$ the Fresnel Integral,

$$A_{u_2}^{FF_{te}} = \frac{b^2 k_s^2}{j8} \frac{\zeta_x(x)}{\sqrt{1+\zeta_x^2(x)}} \frac{(-1+j)}{\sqrt{2}} \left\{ \frac{\exp(j2k_s x)}{\sqrt{(1-2K_s)}} \left[F((\alpha-x)(k_0-2k_s)) - F((d-x)(k_0-2k_s))\right] \right.$$
$$+ \frac{\exp(-j2k_s x)}{\sqrt{(1+2K_s)}} \left[F((\alpha-x)(k_0+2k_s)) - F((d-x)(k_0+2k_s))\right]$$
$$\left. -2\left[F((\alpha-x)k_0) - F((d-x)k_0)\right] \right\} \quad \text{(A.1.12)}$$

### A.1.4 Conclusion

By taking a small slope approximation and restricting the region of integration to allow the large argument form of the Hankel function to be used an analytical expression was successfully found for a portion of the integral $\overline{G}$.

These two integrals represent the upper and lower tails of the infinite integration of $\overline{G}$ and will be reproduced here for clarity:

$$\overline{\overline{G}} = A_l^{FF_{te}}(x,\alpha,c) + \int_c^d G(x,x')\,dx' + A_u^{TE_{ff}}(x,\alpha,d)$$

And the entire analytical integration of the tails is given by in simplified form:

$$A^{FF_{te}}(x,\alpha,c,d) = A_l^{FF_{te}}(x,\alpha,c) + A_u^{FF_{te}}(x,\alpha,d)$$

$$\begin{aligned}
A^{TE_{ff}}(x,\alpha,c,d) = {} & \frac{\zeta_x(x)(-1+j)}{j\sqrt{1+\zeta_x^2}\sqrt{2}} \\
& \left\{\left(1+\frac{b^2k_s^2}{4}\right)\left[\{F((x+\alpha)k_0) - F((x-c)k_0)\} - \{F((\alpha-x)k_0) - F((d-x)k_0)\}\right]\right. \\
& + \frac{b^2k_s^2}{8}\left[\exp(j2k_sx)\right. \\
& \left(\frac{\{F((\alpha-x)(k_0-2k_s)) - F((d-x)(k_0-2k_s))\}}{\sqrt{(1-2K_s)}}\right. \\
& \left.\left. - \frac{\{F((x+\alpha)(k_0+2k_s)) - F((x-c)(k_0+2k_s))\}}{\sqrt{(1+2K_s)}}\right) \\
& + \exp(-j2k_sx) \\
& \left(\frac{\{F((\alpha-x)(k_0+2k_s)) - F((d-x)(k_0+2k_s))\}}{\sqrt{(1+2K_s)}}\right. \\
& \left.\left.\left. - \frac{\{F((x+\alpha)(k_0-2k_s)) - F((x-c)(k_0-2k_s))\}}{\sqrt{(1-2K_s)}}\right)\right]\right\}
\end{aligned} \tag{A.1.13}$$

## A.2 TM Finite Analytic Tail Integration

Below an analytical approximation for the tails of the $\overline{\overline{G}}$ integral for TM polarization is derived, as discussed in Section 4.4.3.2.

Beginning with Equation 4.4.2:

$$\overline{\overline{G}}(x,\alpha)=\int_{-\alpha}^{\alpha}G(x,x')\,dx'$$

Which for TM polarization:

$$\overline{\overline{G}}(x,\alpha)=\frac{2k_0}{4j}\int_{-\alpha}^{\alpha}\frac{\{-\zeta_{x'}(x')\,\Delta x+\zeta(x)-\zeta(x')\}}{\sqrt{(\Delta x)^2+(\zeta(x)-\zeta(x'))^2}}H_1^{(2)}\left(k_0|\Delta x|\sqrt{1+\frac{(\zeta(x)-\zeta(x'))^2}{(\Delta x)^2}}\right)dx'$$

$$=\frac{k_0}{2j}\int_{-\alpha}^{\alpha}\frac{\left\{-\zeta_{x'}(x')\operatorname{sgn}(\Delta x)+\frac{\zeta(x)-\zeta(x')}{|\Delta x|}\right\}}{\sqrt{1+\left(\frac{\zeta(x)-\zeta(x')}{\Delta x}\right)^2}}H_1^{(2)}\left(k_0|\Delta x|\sqrt{1+\frac{(\zeta(x)-\zeta(x'))^2}{(\Delta x)^2}}\right)dx'$$

With $\Delta x=x-x'$ so that $x'=x-\Delta x$ and $dx'=-d\Delta x$ and $\zeta_{x'}(x')=\frac{d\zeta(x')}{dx'}=\frac{d\zeta(x-\Delta x)}{d\Delta x}\frac{d\Delta x}{dx'}=-\frac{d\zeta(x-\Delta x)}{d\Delta x}=-\zeta_{\Delta x}$ and $\Delta\zeta=\zeta(x)-\zeta(x-\Delta x)$

$$=\frac{k_0}{2j}\int_{x+\alpha}^{x-\alpha}\frac{\left\{\zeta_{\Delta x}(x-\Delta x)\operatorname{sgn}(\Delta x)+\frac{\Delta\zeta}{|\Delta x|}\right\}}{\sqrt{1+\left(\frac{\Delta\zeta}{\Delta x}\right)^2}}H_1^{(2)}\left(k_0|\Delta x|\sqrt{1+\left(\frac{\Delta\zeta}{\Delta x}\right)^2}\right)(-d\Delta x)$$

Defining

$$F(x,\Delta x)=-\frac{\left\{\zeta_{\Delta x}(x-\Delta x)+\frac{\Delta\zeta}{\operatorname{sgn}(\Delta x)|\Delta x|}\right\}}{\sqrt{1+\left(\frac{\Delta\zeta}{\Delta x}\right)^2}}H_1^{(2)}\left(k_0|\Delta x|\sqrt{1+\left(\frac{\Delta\zeta}{\Delta x}\right)^2}\right)$$

Gives

$$\overline{\overline{G}}(x)=\frac{k_0}{2j}\int_{x+\alpha}^{x-\alpha}\operatorname{sgn}(\Delta x)\,F(x,\Delta x)\,d\Delta x$$

$$=\frac{k_0}{2j}\left[\int_{x+\alpha}^{0}\operatorname{sgn}(\Delta x)\,F(x,\Delta x)\,d\Delta x+\int_{0}^{x-\alpha}\operatorname{sgn}(\Delta x)\,F(x,\Delta x)\,d\Delta x\right]$$

Here we must be careful to note that $\Delta x$ is positive over the whole left integral. Likewise with $\alpha \geq x$,$\Delta x$ is negative for the right integral

$$= \frac{k_0}{2j}\left[\int_{x+\alpha}^{0} F\left(x,\Delta x\right) d\Delta x - \int_{0}^{x-\alpha} F\left(x,\Delta x\right) d\Delta x\right]$$

Later we will require both of these integrals to be taken in the positive direction over a positive interval. Flipping the limits in the first integral, and making the substitution $-\Delta x' = \Delta x$ in the second:

$$= \frac{k_0}{2j}\left[-\int_{0}^{x+\alpha} F\left(x,\Delta x\right) d\Delta x + \int_{0}^{\alpha-x} F\left(x,-\Delta x'\right) d\Delta x'\right] \tag{A.2.1}$$

Now we will truncate the integration so the following approximations hold. First, take $|\Delta x| \gg |\Delta\zeta|$ so we have $\left|\frac{\Delta\zeta}{\Delta x}\right| \ll 1$, and thus $\sqrt{1+\left(\frac{\Delta\zeta}{\Delta x}\right)^2} \approx 1$. Concurrent with this, approximate the Hankel function by [1]

$$H_1^{(2)}\left(k_0 a\right) \approx \sqrt{\frac{2}{\pi k_0 a}} \exp\left(-jk_0 a + j\frac{3\pi}{4}\right)$$

This gives:

$$F\left(x,\Delta x\right) \approx -\left\{\zeta_{\Delta x}\left(x-\Delta x\right)\right\}\sqrt{\frac{2}{\pi k_0\left|\Delta x\right|}} \exp\left(-jk_0\left|\Delta x\right| + j\frac{3\pi}{4}\right)$$

Restricting the integration to a region in which this is valid:

$$A^{FF_{tm}}\left(x,\alpha,c,d\right) = \frac{k_0}{2j}\left[\int_{x-a}^{x+\alpha} F\left(x,\Delta x\right) d\Delta x - \int_{b-x}^{\alpha-x} F\left(x,-\Delta x'\right) d\Delta x'\right]$$

with $x > c > -\alpha$ and $x < d < \alpha$ making $\Delta x$ and $\Delta x'$ positive on these intervals so taking

the absolute value:

$$A^{FF_{tm}} = \frac{1}{j}\sqrt{\frac{k_0}{2\pi}}e^{j\frac{3\pi}{4}}\left[\int_{x-c}^{x+\alpha}\zeta_{\Delta x}\left(x-\Delta x\right)\frac{1}{\sqrt{\Delta x}}\exp\left(-jk_0\Delta x\right)d\Delta x - \int_{d-x}^{\alpha-x}\zeta_{\Delta x}\left(x+\Delta x'\right)\frac{1}{\sqrt{\Delta x'}}\exp\left(-jk_0\Delta x'\right)d\Delta x'\right]$$

Let's now examine the slope terms for a single sinusoid surface:

$\zeta\left(x-\Delta x\right) = b\cos\left(k_s\left(x-\Delta x\right)\right)$, thus $\zeta_{\Delta x}\left(x-\Delta x\right) = \frac{d\zeta(x-\Delta x)}{d\Delta x} = bk_s\sin\left(k_s\left(x-\Delta x\right)\right) = bk_s\frac{e^{j(k_s(x-\Delta x))}-e^{-j(k_s(x-\Delta x))}}{2j}$

While, $\zeta_{\Delta x}\left(x+\Delta x'\right) = \frac{d\zeta(x+\Delta x')}{d\Delta x} = -bk_s\sin\left(k_s\left(x+\Delta x'\right)\right)\frac{d\Delta x'}{d\Delta x} = bk_s\frac{e^{j(k_s(x+\Delta x'))}-e^{-j(k_s(x+\Delta x'))}}{2j}$

Splitting the $A^{FF_{tm}}\left(x,\alpha,c,d\right)$ into the negative and positive $\Delta x$ parts:

$$A^{FF_{tm}}\left(x,\alpha,c,d\right) = A_l^{FF_{tm}}\left(x,\alpha,c\right) + A_u^{FF_{tm}}\left(x,\alpha,d\right)$$

Considering the two components of the integral separately:

$$A_l^{FF_{tm}}\left(x,\alpha,c\right) = \frac{1}{j}\sqrt{\frac{k_0}{2\pi}}e^{j\frac{3\pi}{4}}\int_{x-c}^{x+\alpha}\zeta_{\Delta x}\left(x-\Delta x\right)\frac{1}{\sqrt{\Delta x}}\exp\left(-jk_0\Delta x\right)d\Delta x$$

$$A_u^{FF_{tm}}\left(x,\alpha,d\right) = -\frac{1}{j}\sqrt{\frac{k_0}{2\pi}}e^{j\frac{3\pi}{4}}\int_{d-x}^{\alpha-x}\zeta_{\Delta x}\left(x+\Delta x'\right)\frac{1}{\sqrt{\Delta x'}}\exp\left(-jk_0\Delta x'\right)d\Delta x'$$

### A.2.1 Starting with the lower Integral

By substituting the expression for $\zeta_{\Delta x}(x-\Delta x)$:

$$A_l^{FF_{tm}}(x,\alpha,a)=\frac{1}{j}\sqrt{\frac{k_0}{2\pi}}e^{j\frac{3\pi}{4}}\int_{x-c}^{x+\alpha}\left[bk_s\frac{e^{j(k_s(x-\Delta x))}-e^{-j(k_s(x-\Delta x))}}{2j}\right]\frac{1}{\sqrt{\Delta x}}\exp\left(-jk_0\Delta x\right)d\Delta x$$

$$A_l^{FF_{tm}}=-\frac{bk_s}{2}\sqrt{\frac{k_0}{2\pi}}e^{j\frac{3\pi}{4}}\int_{x-c}^{x+\alpha}\left[e^{jk_sx}e^{-j(k_0+k_s)\Delta x}-e^{-jk_sx}e^{-j(k_0-k_s)\Delta x}\right]\frac{1}{\sqrt{\Delta x}}d\Delta x$$

$$A_l^{FF_{tm}}=-\frac{bk_s}{2}\sqrt{\frac{k_0}{2\pi}}e^{j\frac{3\pi}{4}}\left[e^{jk_sx}\int_{x-c}^{x+\alpha}\frac{e^{-j(k_0+k_s)\Delta x}}{\sqrt{\Delta x}}d\Delta x-e^{-jk_sx}\int_{x-c}^{x+\alpha}\frac{e^{-j(k_0-k_s)\Delta x}}{\sqrt{\Delta x}}d\Delta x\right]$$

With the following definitions:

$\tau=(k_0+k_s)\Delta x$ and $d\tau=(k_0+k_s)\,d(\Delta x)$. Note this means $\Delta x=\frac{\tau}{(k_0+k_s)}$

$t=(k_0-k_s)\Delta x$ and $dt=(k_0-k_s)\,d(\Delta x)$. Note this means $\Delta x=\frac{t}{(k_0-k_s)}$

$$A_l^{FF_{tm}}=-\frac{bk_s}{2}\sqrt{k_0}e^{j\frac{3\pi}{4}}\left[\frac{e^{jk_sx}}{\sqrt{k_0+k_s}}\int_{(k_0+k_s)(x-c)}^{(k_0+k_s)(x+\alpha)}\frac{e^{-j\tau}}{\sqrt{2\pi\tau}}d\tau-\frac{e^{-jk_sx}}{\sqrt{k_0-k_s}}\int_{(k_0-k_s)(x-c)}^{(k_0-k_s)(x+\alpha)}\frac{e^{-jt}}{\sqrt{2\pi t}}dt\right]$$

Defining $K_s=\frac{k_s}{k_0}$

$$A_l^{FF_{tm}}=-\frac{bk_s}{2}e^{j\frac{3\pi}{4}}\left[\frac{e^{jk_sx}}{\sqrt{1+K_s}}\int_{(k_0+k_s)(x-c)}^{(k_0+k_s)(x+\alpha)}\frac{e^{-j\tau}}{\sqrt{2\pi\tau}}d\tau-\frac{e^{-jk_sx}}{\sqrt{1-K_s}}\int_{(k_0-k_s)(x-c)}^{(k_0-k_s)(x+\alpha)}\frac{e^{-jt}}{\sqrt{2\pi t}}dt\right]$$

Since $\int_e^g d(\Delta x)=\int_0^g d(\Delta x)-\int_0^e d(\Delta x)$ and $\int_0^g\frac{e^{-jt}}{\sqrt{2\pi t}}dt=F(g)$ with $F(g)$ the Fresnel Integral [1]

$$A_l^{FF_{tm}}(x,\alpha,c) = -\frac{bk_s}{2}\frac{(-1+j)}{\sqrt{2}}\left\{\frac{e^{jk_sx}}{\sqrt{1+K_s}}\left[F\left((k_0+k_s)(x+\alpha)\right)-F\left((k_0+k_s)(x-c)\right)\right]\right.$$
$$\left.-\frac{e^{-jk_sx}}{\sqrt{1-K_s}}\left[F\left((k_0-k_s)(x+\alpha)\right)-F\left((k_0-k_s)(x-c)\right)\right]\right\}$$

### A.2.2 Now for the upper integral:

$$A_u^{FF_{tm}}(x,\alpha,d) = -\frac{1}{j}\sqrt{\frac{k_0}{2\pi}}e^{j\frac{3\pi}{4}}\int_{d-x}^{\alpha-x}\left[bk_s\frac{e^{j(k_s(x+\Delta x'))}-e^{-j(k_s(x+\Delta x'))}}{2j}\right]\frac{1}{\sqrt{\Delta x'}}\exp\left(-jk_0\Delta x'\right)d\Delta x'$$

$$A_u^{FF_{tm}}(x,\alpha,d) = \frac{bk_s}{2}\sqrt{\frac{k_0}{2\pi}}e^{j\frac{3\pi}{4}}\left\{e^{jk_sx}\int_{d-x}^{\alpha-x}\frac{e^{-j(k_0-k_s)\Delta x'}}{\sqrt{\Delta x'}}d\Delta x' - e^{-jk_sx}\int_{d-x}^{\alpha-x}\frac{e^{-j(k_0+k_s)\Delta x'}}{\sqrt{\Delta x'}}d\Delta x'\right\}$$

With the following definitions:

$\tau = (k_0-k_s)\Delta x'$ and $d\tau = (k_0-k_s)\,d(\Delta x')$. Note this means $\Delta x' = \frac{\tau}{(k_0-k_s)}$ .

$t = (k_0+k_s)\Delta x'$ and $dt = (k_0+k_s)\,d(\Delta x')$. Note this means $\Delta x' = \frac{t}{(k_0+k_s)}$ . Giving:

$$A_u^{FF_{tm}} = \frac{bk_s}{2}\frac{(-1+j)}{\sqrt{2}}\left\{\frac{e^{jk_sx}}{\sqrt{(1-K_s)}}\int_{(k_0-k_s)(d-x)}^{(k_0-k_s)(\alpha-x)}\frac{e^{-j\tau}}{\sqrt{2\pi\tau}}d\tau - \frac{e^{-jk_sx}}{\sqrt{(1+K_s)}}\int_{(k_0+k_s)(d-x)}^{(k_0+k_s)(\alpha-x)}\frac{e^{-jt}}{\sqrt{2\pi t}}dt\right\}$$

Once again with $\int_c^d d(\Delta x) = \int_0^d d(\Delta x) - \int_0^c d(\Delta x)$ and $\int_0^d \frac{e^{-jt}}{\sqrt{2\pi t}}dt = F(d)$ with $F(d)$ the Fresnel Integral

$$A_u^{FF_{tm}}(x,\alpha,d) = \frac{bk_s}{2}\frac{(-1+j)}{\sqrt{2}}\left\{\frac{e^{jk_sx}}{\sqrt{(1-K_s)}}\left[F\left(\left(k_0-k_s\right)(\alpha-x)\right)-F\left(\left(k_0-k_s\right)(d-x)\right)\right]\right.$$
$$\left.-\frac{e^{-jk_sx}}{\sqrt{(1+K_s)}}\left[F\left(\left(k_0+k_s\right)(\alpha-x)\right)-F\left(\left(k_0+k_s\right)(d-x)\right)\right]\right\}$$

## A.3 Analytic Tail Integrals Extension to Spectral Surfaces

A composite surface consists of multiple sinusoid components, while a rough surface contains a spectrum of sinusoid frequencies and amplitudes. The surface height and the first and second derivative (slope and curvature) are required to calculate the electromagnetic scattering from a 1-D surface which will be denoted $\zeta(x)$, $\zeta_x(x)$ and $\zeta_{xx}(x)$. Recall that for singly sinusoid surfaces these are given by:

$$\zeta(x) = b\cos(k_sx)$$

$$\zeta_x(x) = -bk_s\sin(k_sx)$$

$$\zeta_{xx}(x) = -bk_s^2\cos(k_sx)$$

For a general composite or rough surface with N frequency components, these become

$$\zeta^c(x) = \sum_n \zeta_n(x) = \sum_n b_n\cos(k_{sn}x)$$

$$\zeta_x^c(x) = \sum_n \zeta_{xn}(x) = -\sum_n b_nk_{sn}\sin(k_{sn}x)$$

$$\zeta_{xx}^{c}(x) = \sum_{n} \zeta_{xxn}(x) = -\sum_{n} b_n k_{sn}^2 \cos(k_{sn} x)$$

### A.3.1 Squared Slope

$\overline{\overline{G}}$ for TE polarization requires further analysis as it contains a squared slope term.

$$\left(\zeta_{x}^{c}(x)\right)^2 = \left(\sum_{n} \zeta_{xn}(x)\right)^2$$

$$= \left(\sum_{n} \zeta_{xn}(x)\right)\left(\sum_{m} \zeta_{xm}(x)\right)$$

$$= \left(\sum_{n} \zeta_{xn}(x)\right)\left(\zeta_{xn}(x) + \sum_{m\neq n} \zeta_{xm}(x)\right)$$

$$= \left(\sum_{n} \zeta_{xn}^2(x)\right) + \sum_{n}\sum_{m\neq n} \zeta_{xn}(x)\,\zeta_{xm}(x)$$

Which can be simplified further:

$$\left(\zeta_{x}^{c}(x)\right)^2 = \sum_{n} \zeta_{xn}^2(x) + 2\sum_{n=0}^{N-2}\sum_{m=n+1}^{N-1} \zeta_{xn}(x)\,\zeta_{xm}(x) \quad N \geq 2 \tag{A.3.1}$$

To complete the derivation, conversion from the trigonometric to exponential form is required. All terms in equation A.3.1 are a product of two sine functions, so in general each term will be

$$\zeta_{xn}(x)\,\zeta_{xm}(x) = \left(-b_n k_{sn} \sin(k_{sn} x)\right)\left(-b_m k_{sm} \sin(k_{sm} x)\right)$$

$$= \frac{b_n k_{sn} b_m k_{sm}}{2}\left\{\cos\left(\left(k_{sn} - k_{sm}\right)x\right) - \cos\left(\left(k_{sn} + k_{sm}\right)x\right)\right\}$$

$$= \frac{b_n k_{sn} b_m k_{sm}}{4} \{[\exp(-j((-k_{sn}+k_{sm})x)) + \exp(-j((k_{sn}-k_{sm})x))] - [\exp(-j(-k_{sn}-k_{sm})x) + \exp(-j(k_{sn}+k_{sm})x)]\} \quad \text{(A.3.2)}$$

$\pm\Delta x$

The derivation of both polarizations uses a transformation on the integration variable from $x'$ to $\Delta x = (x - x')$ and to $\Delta x' = -\Delta x$.

A single height component of the surface becomes for both sides of the integration:

$$\zeta_n(x - \Delta x) = b_n \cos(k_{sn}(x - \Delta x))$$

$$\zeta_n(x + \Delta x') = b_n \cos(k_{sn}(x + \Delta x'))$$

Taking the derivative leads to the slope component of each:

$$\zeta_{\Delta xn}(x - \Delta x) = \frac{d\zeta_n(x - \Delta x)}{d\Delta x} = b_n k_{sn} \sin(k_{sn}(x - \Delta x)) \quad \text{(A.3.3)}$$

$$\zeta_{\Delta x}(x + \Delta x') = \frac{d\zeta(x + \Delta x')}{d\Delta x} = -b_n k_{sn} \sin(k_{sn}(x + \Delta x'))\frac{d\Delta x'}{d\Delta x} = b_n k_{sn} \sin(k_{sn}(x + \Delta x')) \quad \text{(A.3.4)}$$

While equation A.3.2 becomes for the $(x - \Delta x)$ case

$$\zeta_{\Delta xn}(x - \Delta x)\,\zeta_{\Delta xm}(x - \Delta x) = (b_n k_{sn} \sin(k_{sn}(x - \Delta x)))(b_m k_{sm} \sin(k_{sm}(x - \Delta x)))$$

$$= \frac{b_n k_{sn} b_m k_{sm}}{2} \{\cos(k_{sn}(x - \Delta x) - k_{sm}(x - \Delta x)) - \cos(k_{sn}(x - \Delta x) + k_{sm}(x - \Delta x))\}$$

$$= \frac{b_n k_{sn} b_m k_{sm}}{2} \{\cos((k_{sn} - k_{sm})x - (k_{sn} - k_{sm})\Delta x) - \cos((k_{sn} + k_{sm})x - (k_{sn} + k_{sm})\Delta x)\}$$

$$= \frac{b_n k_{sn} b_m k_{sm}}{4} \{[\exp(j((k_{sn} - k_{sm})x - (k_{sn} - k_{sm})\Delta x)) + \exp(-j((k_{sn} - k_{sm})x - (k_{sn} - k_{sm})\Delta x))]$$

$$- [\exp(j((k_{sn} + k_{sm})x - (k_{sn} + k_{sm})\Delta x)) + \exp(-j((k_{sn} + k_{sm})x - (k_{sn} + k_{sm})\Delta x))]\}$$

$$\zeta_{\Delta xn}(x - \Delta x)\,\zeta_{\Delta xm}(x - \Delta x) = \frac{b_n k_{sn} b_m k_{sm}}{4}$$
$$\times\{[\exp(j(k_{sn} - k_{sm})x)\exp(-j(k_{sn} - k_{sm})\Delta x) + \exp(-j(k_{sn} - k_{sm})x)\exp(-j(-k_{sn} + k_{sm})\Delta x)]$$
$$- [\exp(j(k_{sn} + k_{sm})x)\exp(-j(k_{sn} + k_{sm})\Delta x) + \exp(-j(k_{sn} + k_{sm})x)\exp(-j(-k_{sn} - k_{sm})\Delta x)]\} \tag{A.3.5}$$

and for the $(x + \Delta x')$ case

$$\zeta_{\Delta xn}(x + \Delta x')\,\zeta_{\Delta xm}(x + \Delta x') = \frac{b_n k_{sn} b_m k_{sm}}{4}$$
$$\times\{[\exp(j(k_{sn} - k_{sm})x)\exp(-j(-k_{sn} + k_{sm})\Delta x') + \exp(-j(k_{sn} - k_{sm})x)\exp(-j(k_{sn} - k_{sm})\Delta x')]$$
$$- [\exp(j(k_{sn} + k_{sm})x)\exp(-j(-k_{sn} - k_{sm})\Delta x') + \exp(-j(k_{sn} + k_{sm})x)\exp(-j(k_{sn} + k_{sm})\Delta x')]\} \tag{A.3.6}$$

If $n = m$, these expressions become:

$$\left(\zeta_{\Delta xn}\left(x-\Delta x\right)\right)^2 = \frac{\left(b_n k_{sn}\right)^2}{4}\left[2-\left[\exp\left(j2k_{sn}x\right)\exp\left(-j2k_{sn}\Delta x\right)+\exp\left(-j2k_{sn}x\right)\exp\left(j2k_{sn}\Delta x\right)\right]\right] \tag{A.3.7}$$

and

$$\left(\zeta_{\Delta xn}\left(x+\Delta x'\right)\right)^2 = \frac{\left(b_n k_{sn}\right)^2}{4}\left\{2-\left[\exp\left(j2k_{sn}x\right)\exp\left(j2k_{sn}\Delta x'\right)+\exp\left(-j2k_{sn}x\right)\exp\left(-j2k_{sn}\Delta x'\right)\right]\right\} \tag{A.3.8}$$

### A.3.2 TM Polarization

Previous results manipulated the upper and lower tail integrals of $\overline{\overline{G}}$ to the following result:

$$A^{FF_{tm}}\left(x,\alpha,c,d\right) = A_l^{FF_{tm}}\left(x,\alpha,c\right) + A_u^{FF_{tm}}\left(x,\alpha,d\right)$$

Considering the two components of the integral separately:

$$A_l^{FF_{tm}}\left(x,\alpha,c\right) = \frac{1}{j}\sqrt{\frac{k_0}{2\pi}}e^{j\frac{3\pi}{4}}\int_{x-c}^{x+\alpha}\zeta_{\Delta x}^{c}\left(x-\Delta x\right)\frac{1}{\sqrt{\Delta x}}\exp\left(-jk_0\Delta x\right)d\Delta x$$

$$A_u^{FF_{tm}}\left(x,\alpha,d\right) = -\frac{1}{j}\sqrt{\frac{k_0}{2\pi}}e^{j\frac{3\pi}{4}}\int_{d-x}^{\alpha-x}\zeta_{\Delta x}^{c}\left(x+\Delta x'\right)\frac{1}{\sqrt{\Delta x'}}\exp\left(-jk_0\Delta x'\right)d\Delta x'$$

where we require $\alpha \leq x \leq \alpha$ and $x-c$ and $d-x$ be chosen to provide $\Delta x \gg \Delta\zeta'$ and ensure the large argument approximation of the Hankel function is valid over the integrals. Then substituting for $\zeta_{\Delta x}^{c}\left(x \pm \Delta x\right)$:

$$A_l^{FF_{tm}}\left(x,\alpha,c\right) = \frac{1}{j}\sqrt{\frac{k_0}{2\pi}}e^{j\frac{3\pi}{4}}\int_{x-c}^{x+\alpha}\sum_n \zeta_{\Delta xn}\left(x-\Delta x\right)\frac{\exp\left(-jk_0\Delta x\right)}{\sqrt{\Delta x}}d\Delta x$$

$$A_u^{FF_{tm}}(x,\alpha,d) = -\frac{1}{j}\sqrt{\frac{k_0}{2\pi}}e^{j\frac{3\pi}{4}}\int_{d-x}^{\alpha-x}\sum_n \zeta_{\Delta xn}(x+\Delta x')\frac{\exp(-jk_0\Delta x')}{\sqrt{\Delta x'}}d\Delta x' x$$

But the sum and integral can be exchanged:

$$A_l^{FF_{tm}}(x,\alpha,c) = \sum_n \frac{1}{j}\sqrt{\frac{k_0}{2\pi}}e^{j\frac{3\pi}{4}}\int_{x-c}^{x+\alpha}\zeta_{\Delta xn}(x+\Delta x)(x-\Delta x)\frac{\exp(-jk_0\Delta x)}{\sqrt{\Delta x}}d\Delta x$$

$$A_u^{FF_{tm}}(x,\alpha,d) = \sum_n \frac{(-1)}{j}\sqrt{\frac{k_0}{2\pi}}e^{j\frac{3\pi}{4}}\int_{d-x}^{\alpha-x}\zeta_{\Delta xn}(x+\Delta x')\frac{\exp(-jk_0\Delta x')}{\sqrt{\Delta x'}}d\Delta x'$$

Thus for TM polarization, the tail integrals can be found by simply adding Equations 4.4.8 and 4.4.9 for each surface period present on the surface.

### A.3.3 TE Polarization

As with TM Polarization, previous results for TE manipulated the upper and lower tail integrals of $\overline{G}$ to the following result:

$$A^{FF_{te}}(x,\alpha,c,d) = A_l^{FF_{te}}(x,\alpha,c) + A_u^{FF_{te}}(x,\alpha,d)$$

Which were further split into the following for the lower tail:

$$A_l^{FF_{te}}(x,\alpha,c) = A_{l_1}^{FF_{te}}(x,\alpha,c) + A_{l_2}^{FF_{te}}(x,\alpha,c)$$

$$A_{l_1}^{FF_{te}}(x,\alpha,c) = \frac{\zeta_x^c(x)\sqrt{k_0}}{j\sqrt{1+(\zeta_x^c)^2}}e^{j\frac{3\pi}{4}}\int_{x-c}^{x+\alpha}\sqrt{\frac{1}{2\pi\Delta x}}\exp(-jk_0\Delta x)\,d\Delta x \tag{A.3.9}$$

$$A_{l_2}^{FF_{te}}(x,\alpha,c) = \frac{\zeta_x^c(x)\sqrt{k_0}}{j2\sqrt{1+(\zeta_x^c)^2}} e^{j\frac{3\pi}{4}} \int_{x-c}^{x+\alpha} \left(\zeta_{\Delta x}^c(x-\Delta x)\right)^2 \sqrt{\frac{1}{2\pi\Delta x}} \exp(-jk_0\Delta x)\, d\Delta x \tag{A.3.10}$$

and for the upper tail:

$$A_u^{FF_{te}}(x,\alpha,d) = A_{u_1}^{FF_{te}}(x,\alpha,d) + A_{u_2}^{FF_{te}}(x,\alpha,d)$$

$$A_{u_1}^{FF_{te}}(x,\alpha,d) = \frac{-\zeta_x^c(x)\sqrt{k_0}}{j\sqrt{1+(\zeta_x^c)^2}} e^{j\frac{3\pi}{4}} \int_{d-x}^{\alpha-x} \frac{\exp(-jk_0\Delta x')}{\sqrt{2\pi\Delta x'}} d\Delta x' \tag{A.3.11}$$

$$A_{u_2}^{FF_{te}}(x,\alpha,d) = \frac{-\zeta_x^c(x)\sqrt{k_0}}{j2\sqrt{1+(\zeta_x^c)^2}} e^{j\frac{3\pi}{4}} \int_{d-x}^{\alpha-x} \frac{\left(\zeta_{\Delta x}^c(x+\Delta x')\right)^2}{\sqrt{2\pi\Delta x'}} \exp(-jk_0\Delta x')\, d\Delta \tag{A.3.12}$$

Equations A.3.9 and A.3.11 are of the same form as the single sinusoid case so the previous results can be used. While the slope term in the numerator is linear, care must be taken with the square root in the denominator is which not. It is a simple matter to multiply the single frequency term by the square root of the sum of the slope squared with unity[1] and divide the ensemble sum by the square root containing the composite surface slope squared. See Equation A.3.17 below for details.

On the other hand, equations A.3.10 and A.3.12 must be re-derived.

[1] $\left(\sqrt{1+(\zeta_x(x))^2}\right)$

#### A.3.3.1 Lower Squared Slope Term

Beginning with equations A.3.10 and A.3.1

$$A_{l_2}^{FF_{te}}(x,\alpha,c) = \frac{\zeta_x^c(x)\sqrt{k_0}}{j2\sqrt{1+(\zeta_x^c)^2}} e^{j\frac{3\pi}{4}} \left\{ \int_{x-c}^{x-\alpha} \left[ \sum_{n=0}^{N-1} \zeta_{\Delta xn}^2(x-\Delta x) + 2\sum_{n=0}^{N-2}\sum_{m=n+1}^{N-1} \zeta_{\Delta xn}(x-\Delta x)\,\zeta_{\Delta xm}(x-\Delta x) \right] \frac{\exp(-jk_0\Delta x)}{\sqrt{2\pi\Delta x}} d\Delta x \right\}$$

Then

$$= \frac{\zeta_x^c(x)\sqrt{k_0}}{j2\sqrt{1+(\zeta_x^c)^2}} e^{j\frac{3\pi}{4}} \left\{ \sum_{n=0}^{N-1} \int_{x-c}^{x+\alpha} \zeta_{\Delta xn}^2(x-\Delta x) \frac{\exp(-jk_0\Delta x)}{\sqrt{2\pi\Delta x}} d\Delta x + 2\sum_{n=0}^{N-2}\sum_{m=n+1}^{N-1} \int_{x-c}^{x+\alpha} \zeta_{\Delta xn}(x-\Delta x)\,\zeta_{\Delta xm}(x-\Delta x) \frac{\exp(-jk_0\Delta x)}{\sqrt{2\pi\Delta x}} d\Delta x \right\}$$

The first integral is the same as found previously for the singly sinusoid surface.

$$A_{l_2}^{FF_{te}}(x,\alpha,c) = A_{l_{2s}}^{FF_{te}}(x,\alpha,c) + A_{l_{2p}}^{FF_{te}}(x,\alpha,c)$$

$$A_{l_{2s}}^{FF_{te}}(x,\alpha,c) = \sum_{n=0}^{N-1} \frac{\zeta_x^c(x)\sqrt{k_0}}{j2\sqrt{1+(\zeta_x^c)^2}} e^{j\frac{3\pi}{4}} \int_{x-c}^{x+\alpha} \zeta_{\Delta xn}^2(x-\Delta x) \frac{\exp(-jk_0\Delta x)}{\sqrt{2\pi\Delta x}} d\Delta x$$

$$A_{l_{2s}}^{FF_{te}}(x,\alpha,c) = -\frac{\zeta_x^c(x)}{j8\sqrt{1+(\zeta_x^c)^2}}\frac{(-1+j)}{\sqrt{2}}\sum_{n=0}^{N-1} b_n^2 k_{sn}^2$$
$$\times\left\{\frac{\exp(j2k_{sn}x)}{\sqrt{(1+2K_{sn})}}\left[F\left((x+\alpha)(k_0+2k_{sn})\right)-F\left((x-c)(k_0+2k_{sn})\right)\right]\right.$$
$$-2\left[F\left((x+\alpha)k_0\right)-F\left((x-c)k_0\right)\right]$$
$$\left.+\frac{\exp(-j2k_{sn}x)}{\sqrt{(1-2K_{sn})}}\left[F\left((x+\alpha)(k_0-2k_{sn})\right)-F\left((x-c)(k_0-2k_{sn})\right)\right]\right\} \quad \text{(A.3.13)}$$

The other term is

$$A_{l_{2p}}^{FF_{te}}(x,\alpha,c) = \frac{\zeta_x^c(x)\sqrt{k_0}}{j\sqrt{1+(\zeta_x^c)^2}}e^{j\frac{3\pi}{4}}\sum_{n=0}^{N-2}\sum_{m=n+1}^{N-1}\int_{x-c}^{x+\alpha}\zeta_{\Delta xn}(x-\Delta x)\,\zeta_{\Delta xm}(x-\Delta x)\frac{\exp(-jk_0\Delta x)}{\sqrt{2\pi\Delta x}}d\Delta x$$

Using Eq. A.3.5

$$A_{l_{2p}}^{FF_{te}}(x,\alpha,c) = \frac{\zeta_x^c(x)\sqrt{k_0}}{j\sqrt{1+(\zeta_x^c)^2}}e^{j\frac{3\pi}{4}}\sum_{n=0}^{N-2}\sum_{m=n+1}^{N-1}\frac{b_n k_{sn} b_m k_{sm}}{4}$$
$$\times\left\{\exp\left(j\left(k_{sn}-k_{sm}\right)x\right)\int_{x-c}^{x+\alpha}\frac{\exp\left(-j\left(k_0+k_{sn}-k_{sm}\right)\Delta x\right)}{\sqrt{2\pi\Delta x}}d\Delta x\right.$$
$$+\exp\left(-j\left(k_{sn}-k_{sm}\right)x\right)\int_{x-c}^{x+\alpha}\frac{\exp\left(-j\left(k_0-k_{sn}+k_{sm}\right)\Delta x\right)}{\sqrt{2\pi\Delta x}}d\Delta x$$
$$-\exp\left(j\left(k_{sn}+k_{sm}\right)x\right)\int_{x-c}^{x+\alpha}\frac{\exp\left(-j\left(k_0+k_{sn}+k_{sm}\right)\Delta x\right)}{\sqrt{2\pi\Delta x}}d\Delta x$$
$$\left.-\exp\left(-j\left(k_{sn}+k_{sm}\right)x\right)\int_{x-c}^{x+\alpha}\frac{\exp\left(-j\left(k_0-k_{sn}-k_{sm}\right)\Delta x\right)}{\sqrt{2\pi\Delta x}}d\Delta x\right\}$$

The four integrals in this equation are of the same form as handled previously. Substituting a variable for the argument of the complex exponential and then noting $\int_e^g d(\Delta x) = \int_0^g d(\Delta x) - \int_0^e d(\Delta x)$. Finally, with the following integral definition $\int_0^g \frac{\exp(-jt)}{\sqrt{2\pi t}}dt = F(g)$

with $F(g)$ the Fresnel integral, the result becomes:

$$A_{l_{2p}}^{FF_{te}}(x,\alpha,c) = \frac{\zeta_x^c(x)}{j4\sqrt{1+(\zeta_x^c)^2}} e^{j\frac{3\pi}{4}} \sum_{n=0}^{N-2}\sum_{m=n+1}^{N-1} b_n k_{sn} b_m k_{sm}$$
$$\left\{ \exp\left(j\left(k_{sn}-k_{sm}\right)x\right) \frac{\left[F\left(\left(k_0+k_{sn}-k_{sm}\right)(x+\alpha)\right)-F\left(\left(k_0+k_{sn}-k_{sm}\right)(x-c)\right)\right]}{\sqrt{\left(1+K_{sn}-K_{sm}\right)}} \right.$$
$$+\exp\left(-j\left(k_{sn}-k_{sm}\right)x\right) \frac{\left[F\left(\left(k_0-k_{sn}+k_{sm}\right)(x+\alpha)\right)-F\left(\left(k_0-k_{sn}+k_{sm}\right)(x-c)\right)\right]}{\sqrt{\left(1-K_{sn}+K_{sm}\right)}}$$
$$-\exp\left(j\left(k_{sn}+k_{sm}\right)x\right) \frac{\left[F\left(\left(k_0+k_{sn}+k_{sm}\right)(x+\alpha)\right)-F\left(\left(k_0+k_{sn}+k_{sm}\right)(x-c)\right)\right]}{\sqrt{\left(1+K_{sn}+K_{sm}\right)}}$$
$$\left. -\exp\left(-j\left(k_{sn}+k_{sm}\right)x\right) \frac{\left[F\left(\left(k_0-k_{sn}-k_{sm}\right)(x+\alpha)\right)-F\left(\left(k_0-k_{sn}-k_{sm}\right)(x-c)\right)\right]}{\sqrt{\left(1-K_{sn}-K_{sm}\right)}} \right\} \tag{A.3.14}$$

#### A.3.3.2 Upper Squared Slope Term

Now using Equations A.3.12 andA.3.1

$$A_{u_2}^{FF_{te}}(x,\alpha,d) = \frac{-\zeta_x^c(x)\sqrt{k_0}}{j2\sqrt{1+(\zeta_x^c)^2}} e^{j\frac{3\pi}{4}} \left\{ \int_{d-x}^{\alpha-x} \left[ \sum_{n=0}^{N-1} \zeta_{\Delta xn}^2(x+\Delta x') \right.\right.$$
$$\left.\left. +2\sum_{n=0}^{N-2}\sum_{m=n+1}^{N-1} \zeta_{\Delta xn}(x+\Delta x')\,\zeta_{\Delta xm}(x+\Delta x') \right] \frac{\exp\left(-jk_0\Delta x'\right)d\Delta x'}{\sqrt{2\pi\Delta x'}} \right\}$$

Then

$$A_{u_2}^{FF_{te}}(x,\alpha,d)=\frac{-\zeta_x^c(x)\sqrt{k_0}}{j2\sqrt{1+(\zeta_x^c)^2}}e^{j\frac{3\pi}{4}}\left\{\sum_{n=0}^{N-1}\int_{d-x}^{\alpha-x}\zeta_{\Delta xn}^2(x+\Delta x')\frac{\exp(-jk_0\Delta x')\,d\Delta x'}{\sqrt{2\pi\Delta x'}}\right.$$
$$\left.+2\sum_{n=0}^{N-2}\sum_{m=n+1}^{N-1}\int_{\beta-x}^{b-x}\zeta_{\Delta xn}(x+\Delta x')\,\zeta_{\Delta xm}(x+\Delta x')\frac{\exp(-jk_0\Delta x')\,d\Delta x'}{\sqrt{2\pi\Delta x'}}\right\}$$

The first integral is the same as found previously for the singly sinusoid surface.

$$A_{u_2}^{FF_{te}}(x,\alpha,d)=A_{u_{2s}}^{FF_{te}}(x,\alpha,d)+A_{u_{2p}}^{FF_{te}}(x,\alpha,d)$$

$$A_{u_{2s}}^{FF_{te}}(x,a,d)=\frac{-\zeta_x^c(x)\sqrt{k_0}}{j2\sqrt{1+(\zeta_x^c)^2}}e^{j\frac{3\pi}{4}}\sum_{n=0}^{N-1}\int_{d-x}^{\alpha-x}\zeta_{\Delta xn}^2(x+\Delta x')\frac{\exp(-jk_0\Delta x')\,d\Delta x'}{\sqrt{2\pi\Delta x'}}$$

$$A_{u_2}^{TE_{ff}}=\frac{\zeta_x^c(x)}{j8\sqrt{1+(\zeta_x^c)^2}}\frac{(-1+j)}{\sqrt{2}}\sum_{n=0}^{N-1}b_n^2k_{sn}^2$$
$$\left\{\exp(j2k_{sn}x)\frac{[F((\alpha-x)(k_0-2k_{sn}))-F((d-x)(k_0-2k_{sn}))]}{\sqrt{(1-2K_{sn})}}\right.$$
$$-2[F((\alpha-x)k_0)-F((d-x)k_0)]$$
$$\left.+\exp(-j2k_{sn}x)\frac{[F((\alpha-x)(k_0+2k_{sn}))-F((d-x)(k_0+2k_{sn}))]}{\sqrt{(1+2K_{sn})}}\right\}\quad(A.3.15)$$

The final term is

$$A_{u_2}^{FF_{te}}(x,\alpha,d)=\frac{-\zeta_x^c(x)\sqrt{k_0}}{j\sqrt{1+(\zeta_x^c)^2}}e^{j\frac{3\pi}{4}}\sum_{n=0}^{N-2}\sum_{m=n+1}^{N-1}\int_{d-x}^{\alpha-x}\zeta_{\Delta xn}(x+\Delta x')\,\zeta_{\Delta xm}(x+\Delta x')\frac{\exp(-jk_0\Delta x')\,d\Delta x'}{\sqrt{2\pi\Delta x'}}$$

Using Eq. A.3.6

$$A_{u_2}^{FF_{te}}(x,\alpha,d) = \frac{-\zeta_x^c(x)\sqrt{k_0}}{j\sqrt{1+(\zeta_x^c)^2}} e^{j\frac{3\pi}{4}} \sum_{n=0}^{N-2}\sum_{m=n+1}^{N-1} \frac{b_n k_{sn} b_m k_{sm}}{4}$$
$$\times \left\{ \exp(j(k_{sn}-k_{sm})x) \int_{d-x}^{\alpha-x} \frac{\exp(-j(k_0-k_{sn}+k_{sm})\Delta x')\, d\Delta x'}{\sqrt{2\pi\Delta x'}} \right.$$
$$\exp(-j(k_{sn}-k_{sm})x) \int_{d-x}^{\alpha-x} \frac{\exp(-j(k_0+k_{sn}-k_{sm})\Delta x')\, d\Delta x'}{\sqrt{2\pi\Delta x'}}$$
$$-\exp(j(k_{sn}+k_{sm})x) \int_{d-x}^{\alpha-x} \frac{\exp(-j(k_0-k_{sn}-k_{sm})\Delta x')\, d\Delta x'}{\sqrt{2\pi\Delta x'}}$$
$$\left. -\exp(-j(k_{sn}+k_{sm})x) \int_{d-x}^{\alpha-x} \frac{\exp(-j(k_0+k_{sn}+k_{sm})\Delta x')\, d\Delta x'}{\sqrt{2\pi\Delta x'}} \right\}$$

The four integrals in this equation are of the same form as handled previously. Substituting a variable for the argument of the complex exponential and then noting $\int_e^g d(\Delta x) = \int_0^g d(\Delta x) - \int_0^e d(\Delta x)$. Finally, with the following integral definition $\int_0^g \frac{\exp(-jt)}{\sqrt{2\pi t}} dt = F(g)$ with $F(g)$ the Fresnel integral, the result becomes:

$$A_{u_2}^{FF_{te}}(x,\alpha,d) = \frac{-\zeta_x^c(x)}{j\sqrt{1+(\zeta_x^c)^2}} e^{j\frac{3\pi}{4}} \sum_{n=0}^{N-2}\sum_{m=n+1}^{N-1} \frac{b_n k_{sn} b_m k_{sm}}{4}$$
$$\times \left\{ \exp(j(k_{sn}-k_{sm})x) \frac{[F((k_0-k_{sn}+k_{sm})(\alpha-x)) - F((k_0-k_{sn}+k_{sm})(d-x))]}{\sqrt{1-K_{sn}+K_{sm}}} \right.$$
$$\exp(-j(k_{sn}-k_{sm})x) \frac{[F((k_0+k_{sn}-k_{sm})(\alpha-x)) - F((k_0+k_{sn}-k_{sm})(d-x))]}{\sqrt{1+K_{sn}-K_{sm}}}$$
$$-\exp(j(k_{sn}+k_{sm})x) \frac{[F((k_0-k_{sn}-k_{sm})(\alpha-x)) - F((k_0-k_{sn}-k_{sm})(d-x))]}{\sqrt{1-K_{sn}-K_{sm}}}$$
$$\left. -\exp(-j(k_{sn}+k_{sm})x) \frac{[F((k_0+k_{sn}+k_{sm})(\alpha-x)) - F((k_0+k_{sn}+k_{sm})(d-x))]}{\sqrt{1+K_{sn}+K_{sm}}} \right\} \quad \text{(A.3.16)}$$

## A.3.4 Conclusion

### A.3.4.1 TM

The spectral analytical tails solution for TM is a superposition of the single frequency solutions.

### A.3.4.2 TE

The spectral analytical tails solution for TE includes the superposition of single frequency terms with an additional sum of cross products of component frequencies.

$$A^{FF_{te}}(x,\alpha,c,d) = A_p^{FF_{te}}(x,\alpha,c,d) + \frac{1}{\sqrt{1+\left(\zeta_x^c(x)\right)^2}} \sum_n \sqrt{1+\left(\zeta_{xn}(x)\right)^2} A_{s_n}^{FF_{te}}(x,\alpha,c,d) \tag{A.3.17}$$

where $A_{s_n}^{FF_{te}}$ is that given by Equation 4.4.6 for each individual surface frequency and

$$A_p^{FF_{te}}(x,\alpha,c,d) = \frac{\zeta_x^c(x)}{j4\sqrt{1+\left(\zeta_x^c\right)^2}} e^{j\frac{3\pi}{4}} \sum_{n=0}^{N-2} \sum_{m=n+1}^{N-1} b_n k_{sn} b_m k_{sm} \left(S_1+S_2+S_3+S_4\right) \tag{A.3.18}$$

$$S_1 = \exp\left(j\left(k_{sn}-k_{sm}\right)x\right) \left\{ \frac{\left[F\left(\left(k_0+k_{sn}-k_{sm}\right)(x+\alpha)\right) - F\left(\left(k_0+k_{sn}-k_{sm}\right)(x-c)\right)\right]}{\sqrt{\left(1+K_{sn}-K_{sm}\right)}} - \frac{\left[F\left(\left(k_0-k_{sn}+k_{sm}\right)(\alpha-x)\right) - F\left(\left(k_0-k_{sn}+k_{sm}\right)(d-x)\right)\right]}{\sqrt{1-K_{sn}+K_{sm}}} \right\}$$

$$S_2 = \exp\left(-j\left(k_{sn} - k_{sm}\right)x\right)\left\{\frac{\left[F\left(\left(k_0 - k_{sn} + k_{sm}\right)(x+\alpha)\right) - F\left(\left(k_0 - k_{sn} + k_{sm}\right)(x-c)\right)\right]}{\sqrt{\left(1 - K_{sn} + K_{sm}\right)}}\right.$$
$$\left. - \frac{\left[F\left(\left(k_0 + k_{sn} - k_{sm}\right)(\alpha - x)\right) - F\left(\left(k_0 + k_{sn} - k_{sm}\right)(d-x)\right)\right]}{\sqrt{1 + K_{sn} - K_{sm}}}\right\}$$

$$S_3 = \exp\left(j\left(k_{sn} + k_{sm}\right)x\right)\left\{\frac{\left[F\left(\left(k_0 + k_{sn} + k_{sm}\right)(x+\alpha)\right) - F\left(\left(k_0 + k_{sn} + k_{sm}\right)(x-c)\right)\right]}{\sqrt{\left(1 + K_{sn} + K_{sm}\right)}}\right.$$
$$\left. - \frac{\left[F\left(\left(k_0 - k_{sn} - k_{sm}\right)(\alpha - x)\right) - F\left(\left(k_0 - k_{sn} - k_{sm}\right)(d-x)\right)\right]}{\sqrt{1 - K_{sn} - K_{sm}}}\right\}$$

$$S_4 = \exp\left(-j\left(k_{sn} + k_{sm}\right)x\right)\left\{\frac{\left[F\left(\left(k_0 - k_{sn} - k_{sm}\right)(x+\alpha)\right) - F\left(\left(k_0 - k_{sn} - k_{sm}\right)(x-c)\right)\right]}{\sqrt{\left(1 - K_{sn} - K_{sm}\right)}}\right.$$
$$\left. - \frac{\left[F\left(\left(k_0 + k_{sn} + k_{sm}\right)(\alpha - x)\right) - F\left(\left(k_0 + k_{sn} + k_{sm}\right)(d-x)\right)\right]}{\sqrt{1 + K_{sn} + K_{sm}}}\right\}$$

## A.4 TM Higher-Order Integral Tails Approximation

The $\overline{\overline{G}}$ TM numeric results have more complicated behavior than TE which appears to depend on integration support, thus coming from the tail integrations. It seems that only a portion of this behavior is described by the Fresnel function based tail integration approximation which is an integration of the first-order Hankel function large-argument approximation. The present work attempts to add all higher order terms to the tail integration approximation. Closed analytical expressions are found for much of the infinite series, with a infinite summation of upper incomplete gamma functions remaining. Work remains to determine how this last infinite summation converges.

From Eq. A.2.1 we have:

$$\overline{\overline{G}}^{TM} = -\frac{k_0}{2j}\left[\int_0^{x+\alpha} F\left(x,\Delta x\right)d\Delta x - \int_0^{\alpha-x} F\left(x,-\Delta x'\right)d\Delta x'\right]$$

where $\Delta x' = -\Delta x$ and

$$F\left(x,\Delta x\right) = -\frac{\left\{\zeta_{\Delta x}\left(x-\Delta x\right)+\frac{\Delta\zeta}{\Delta x}\right\}}{\sqrt{1+\left(\frac{\Delta\zeta}{\Delta x}\right)^2}} H_1^{(2)}\left(k_0\left|\Delta x\right|\sqrt{1+\left(\frac{\Delta\zeta}{\Delta x}\right)^2}\right)$$

Again we will truncate the integration so the following approximations hold. First, take $|\Delta x| \gg |\Delta\zeta|$ so we have $\left|\frac{\Delta\zeta}{\Delta x}\right| \ll 1$, and thus $\sqrt{1+\left(\frac{\Delta\zeta}{\Delta x}\right)^2} \approx 1$ as previously, but now approximate the Hankel function by truncating the infinite series [62]:

$$H_1^{(2)}\left(x\right) = \sqrt{\frac{2}{\pi x}}e^{-j\left(x-\frac{3}{4}\pi\right)}\sum_{m=0}^{\infty}\frac{(1,m)}{(2jx)^m}$$

with

$$(1,m) = \frac{\left(4-1^2\right)\left(4-3^2\right)\ldots\left(4-(2m-1)^2\right)}{2^{2m}m!}$$

so

$$F\left(x,\Delta x\right) = -\zeta_{\Delta x}\left(x-\Delta x\right)\sqrt{\frac{2}{\pi k_0\left|\Delta x\right|}}e^{-j\left(k_0|\Delta x|-\frac{3}{4}\pi\right)}\sum_{m=0}^{\infty}\frac{(1,m)}{\left(2jk_0\left|\Delta x\right|\right)^m}$$

Restricting the integration to a region in which this is valid, and taking the absolute value gives

$$A^{FF^h_{tm}}(x,\alpha,c,d) = \frac{1}{j}\sqrt{\frac{k_0}{2\pi}}e^{j\frac{3}{4}\pi}\left[\int_{x-c}^{x+\alpha}\frac{\zeta_{\Delta x}(x-\Delta x)}{\sqrt{\Delta x}}e^{-j(k_0\Delta x)}\sum_{m=0}^{\infty}\frac{(1,m)}{(2jk_0\Delta x)^m}d\Delta x - \int_{c-x}^{\alpha-x}\frac{\zeta_{\Delta x}(x+\Delta x)}{\sqrt{\Delta x}}e^{-j(k_0\Delta x)}\sum_{m=0}^{\infty}\frac{(1,m)}{(2jk_0\Delta x)^m}d\Delta x'\right]$$

Following the previous analysis on the first order Hankel approximation, split the $\overline{G}_F^{TM}(x,a,b,\alpha,\beta)$ into the negative and positive $\Delta x$ parts:

$$A^{FF^h_{tm}}(x,\alpha,c,d) = A_l^{FF^h_{tm}}(x,\alpha,c) + A_u^{FF^h_{tm}}(x,\alpha,d)$$

so that

$$A_l^{FF^h_{tm}}(x,\alpha,c) = \frac{1}{j}\sqrt{\frac{k_0}{2\pi}}e^{j\frac{3\pi}{4}}\int_{x-c}^{x+\alpha}\frac{\zeta_{\Delta x}(x-\Delta x)}{\sqrt{\Delta x}}e^{-j(k_0\Delta x)}\sum_{m=0}^{\infty}\frac{(1,m)}{(2jk_0\Delta x)^m}d\Delta x \qquad \text{(A.4.1)}$$

$$A_u^{FF^h_{tm}}(x,\alpha,d) = -\frac{1}{j}\sqrt{\frac{k_0}{2\pi}}e^{j\frac{3\pi}{4}}\int_{d-x}^{\alpha-x}\frac{\zeta_{\Delta x}(x+\Delta x')}{\sqrt{\Delta x'}}e^{-j(k_0\Delta x)}\sum_{m=0}^{\infty}\frac{(1,m)}{(2jk_0\Delta x')^m}d\Delta x' \qquad \text{(A.4.2)}$$

Recall that the slopes are as follows:

$$\zeta_{\Delta x}(x-\Delta x) = \frac{bk_s e^{j(k_s(x-\Delta x))} - e^{-j(k_s(x-\Delta x))}}{2j}$$

$$\zeta_{\Delta x}(x+\Delta x')\, bk_s\frac{e^{j(k_s(x+\Delta x'))} - e^{-j(k_s(x+\Delta x'))}}{2j}$$

Starting with the lower Integral

By substituting the expression for $\zeta_{\Delta x}(x-\Delta x)$ in A.4.1 and simplifying:

$$A_l^{FF_{tm}^h}(x,\alpha,c) = -\frac{bk_s}{2}\sqrt{\frac{k_0}{2\pi}}e^{j\frac{3\pi}{4}}\sum_{m=0}^{\infty}\frac{(1,m)}{(2jk_0)^m}\left[e^{jk_sx}\int_{x-c}^{x+\alpha}\frac{e^{-j(k_0+k_s)\Delta x}}{(\Delta x)^{m+\frac{1}{2}}}d\Delta x\right.$$
$$\left.-e^{-jk_sx}\int_{x-c}^{x+\alpha}\frac{e^{-j(k_0-k_s)\Delta x}}{(\Delta x)^{m+\frac{1}{2}}}d\Delta x\right]$$

With the following definitions:

$\tau = (k_0+k_s)\Delta x$ and $d\tau = (k_0+k_s)\,d(\Delta x)$. Note this means $\Delta x = \frac{\tau}{(k_0+k_s)}$

$t = (k_0-k_s)\Delta x$ and $dt = (k_0-k_s)\,d(\Delta x)$. Note this means $\Delta x = \frac{t}{(k_0-k_s)}$

$$A_l^{FF_{tm}^h}(x,\alpha,c) = -\frac{bk_s}{2}\sqrt{\frac{k_0}{2\pi}}e^{j\frac{3\pi}{4}}\sum_{m=0}^{\infty}\frac{(1,m)}{(2jk_0)^m}\left[e^{jk_sx}(k_0+k_s)^{m-\frac{1}{2}}\int_{(k_0+k_s)(x-c)}^{(k_0+k_s)(x+\alpha)}\frac{e^{-j\tau}}{\tau^{m+\frac{1}{2}}}d\Delta\tau\right.$$
$$\left.-e^{-jk_sx}(k_0-k_s)^{m-\frac{1}{2}}\int_{(k_0-k_s)(x-c)}^{(k_0-k_s)(x+\alpha)}\frac{e^{-jt}}{t^{m+\frac{1}{2}}}dt\right] \quad \text{(A.4.3)}$$

Both of these integrals are of the same form,

$$\int t^{-\left(m+\frac{1}{2}\right)}e^{-jt}dt$$

Performing integration by parts:

$u = e^{-jt}$ $du = -je^{-jt}dt$

$dv = t^{-\left(m+\frac{1}{2}\right)}dt$ $v = \frac{t^{-\left(m-1+\frac{1}{2}\right)}}{-\left(m-1+\frac{1}{2}\right)}$

gives

$$\frac{t^{-\left(m-1+\frac{1}{2}\right)}e^{-jt}}{-\left(m-1+\frac{1}{2}\right)}-\frac{j}{\left(m-1+\frac{1}{2}\right)}\int t^{-\left(m-1+\frac{1}{2}\right)}e^{-jt}dt$$

And again:

$u=e^{-jt}\ du=-je^{-jt}dt$

$dv=t^{-\left(m-1+\frac{1}{2}\right)}dt\ v=\frac{t^{-\left(m-2+\frac{1}{2}\right)}}{-\left(m-2+\frac{1}{2}\right)}$

$$\frac{t^{-\left(m-1+\frac{1}{2}\right)}e^{-jt}}{-\left(m-1+\frac{1}{2}\right)}-\frac{j}{\left(m-1+\frac{1}{2}\right)}\left(\frac{t^{-\left(m-2+\frac{1}{2}\right)}e^{-jt}}{-\left(m-2+\frac{1}{2}\right)}-\frac{j}{\left(m-2+\frac{1}{2}\right)}\int t^{-\left(m-2+\frac{1}{2}\right)}e^{-jt}dt\right)$$

continuing this process a total of m times, gives the following:

$$\int t^{-\left(m+\frac{1}{2}\right)}e^{-jt}dt=\frac{j^m}{\prod_{q=1}^{m}\left(m-q+\frac{1}{2}\right)}\int\frac{e^{-jt}}{\sqrt{t}}dt+\sum_{n=1}^{m}\frac{(-1)^n j^{n-1}t^{-\left(m-n+\frac{1}{2}\right)}e^{-jt}}{\prod_{p=1}^{n}\left(m-p+\frac{1}{2}\right)}\quad,\quad m\geq 1$$

Note that the only remaining integral is $\int\frac{e^{-jt}}{\sqrt{t}}dt$ , and by pulling the $\frac{1}{\sqrt{2\pi}}$ from the coefficient in A.4.3, this is exactly the integral solved in the first-order approximation. Thus the lower term becomes:

$$
\begin{aligned}
&A_l^{FF_{tm}^h}(x,\alpha,c) = -\frac{bk_s}{2}\sqrt{k_0}e^{j\frac{3\pi}{4}} \\
&\times\Bigg[\Bigg\{\frac{e^{jk_sx}}{\sqrt{k_0+k_s}}\left[F\left(\left(k_0+k_s\right)\left(x+\alpha\right)\right)-F\left(\left(k_0+k_s\right)\left(x-c\right)\right)\right]\left(1+\sum_{m=1}^{\infty}\left(\frac{k_0+k_s}{2k_0}\right)^m\frac{(1,m)}{\prod_{q=1}^{m}\left(m-q+\frac{1}{2}\right)}\right) \\
&\quad+e^{jk_sx}\sum_{m=1}^{\infty}\frac{(1,m)}{\left(2jk_0\right)^m}\sum_{n=1}^{m}\frac{\left(-1\right)^n j^{n-1}\left(k_0+k_s\right)^{n-1}}{\prod_{p=1}^{n}\left(m-p+\frac{1}{2}\right)}\left(\frac{e^{-j(k_0+k_s)(x+\alpha)}}{(x+\alpha)^{\left(m-n+\frac{1}{2}\right)}}-\frac{e^{-j(k_0+k_s)(x-c)}}{(x-c)^{\left(m-n+\frac{1}{2}\right)}}\right)\Bigg\} \\
&-\Bigg\{\frac{e^{-jk_sx}}{\sqrt{(k_0-k_s)}}\left[F\left(\left(k_0-k_s\right)\left(x+\alpha\right)\right)-F\left(\left(k_0-k_s\right)\left(x-c\right)\right)\right]\left(1+\sum_{m=1}^{\infty}\left(\frac{k_0-k_s}{2k_0}\right)^m\frac{(1,m)}{\prod_{q=1}^{m}\left(m-q+\frac{1}{2}\right)}\right) \\
&\quad+e^{-jk_sx}\sum_{m=1}^{\infty}\frac{(1,m)}{\left(2jk_0\right)^m}\sum_{n=1}^{m}\frac{\left(-1\right)^n j^{n-1}\left(k_0-k_s\right)^{n-1}}{\prod_{p=1}^{n}\left(m-p+\frac{1}{2}\right)}\left(\frac{e^{-j(k_0-k_s)(x+\alpha)}}{(x+\alpha)^{\left(m-n+\frac{1}{2}\right)}}-\frac{e^{-j(k_0-k_s)(x-c)}}{(x-c)^{\left(m-n+\frac{1}{2}\right)}}\right)\Bigg\}\Bigg]
\end{aligned}
\tag{A.4.4}
$$

Now an attempt to analytically sum the infinite series in this expression will be made. All of these sums can be reduced to two types. The first type are the ones multiplied by the Fresnel function differences:

$\left(1+\sum_{m=1}^{\infty}\left(\frac{k_0+k_s}{2k_0}\right)^m\frac{(1,m)}{\prod_{q=1}^{m}\left(m-q+\frac{1}{2}\right)}\right)$ and $\left(1+\sum_{m=1}^{\infty}\left(\frac{k_0-k_s}{2k_0}\right)^m\frac{(1,m)}{\prod_{q=1}^{m}\left(m-q+\frac{1}{2}\right)}\right)$

Which with $r=\left(\frac{k_0+k_s}{2k_0}\right)$ and $r=\left(\frac{k_0-k_s}{2k_0}\right)$ respectively, become:

$$
\begin{aligned}
\left(1+\sum_{m=1}^{\infty}r^m\frac{(1,m)}{\prod_{q=1}^{m}\left(m-q+\frac{1}{2}\right)}\right) &= 1+\sum_{m=1}^{\infty}r^m\frac{\left(4-1^2\right)\left(4-3^2\right)\ldots\left(4-\left(2m-1\right)^2\right)}{2^{2m}m!\prod_{q=1}^{m}\left(m-q+\frac{1}{2}\right)} \\
&= 1+\sum_{m=1}^{\infty}r^m\frac{\prod_{q=1}^{m}\left(4-\left(2q-1\right)^2\right)}{2^{2m}m!\prod_{q=1}^{m}\left(m-q+\frac{1}{2}\right)} \\
&= 1+2\sum_{m=1}^{\infty}r^m\frac{\prod_{q=1}^{m}\left(4-\left(2q-1\right)^2\right)}{2^{m}m!\prod_{q=1}^{m}\left(2\left(m-q\right)+1\right)}
\end{aligned}
$$

Expanding the bottom product:

$$(2(m-1)+1)(2(m-2)+1)...(2(m-(m-1))+1)(2(m-m)+1)$$

$$=(2m-1)(2(m-1)-1)...(3)(1)$$

$$=\prod_{q=1}^{m}(2q-1)$$

So the sum becomes

$$1+2\sum_{m=1}^{\infty}r^m\frac{\prod_{q=1}^{m}\left(4-(2q-1)^2\right)}{2^m m!\prod_{q=1}^{m}(2q-1)}$$

then

$$=1+2\sum_{m=1}^{\infty}r^m\frac{\prod_{q=1}^{m}\left(4-(2q-1)^2\right)}{2^m m!\prod_{q=1}^{m}(2q-1)}$$

$$=1+2\sum_{m=1}^{\infty}r^m\frac{\prod_{q=1}^{m}\left(4-(2q-1)^2\right)}{2^m m!\prod_{q=1}^{m}(2q-1)}$$

Calculating the finite product:

$$\prod_{q=1}^{m}\frac{\left(4-(2q-1)^2\right)}{(2q-1)}=-\frac{(-1)^m 2^{m-1}(2m+1)\Gamma\left(m-\frac{1}{2}\right)}{\sqrt{\pi}}$$

$$=1-2\sum_{m=1}^{\infty}\frac{r^m}{2^m m!}\frac{(-1)^m 2^{m-1}(2m+1)\Gamma\left(m-\frac{1}{2}\right)}{\sqrt{\pi}}$$

$$=1-\sum_{m=1}^{\infty}\frac{r^m}{m!}\frac{(-1)^m(2m+1)\Gamma\left(m-\frac{1}{2}\right)}{\sqrt{\pi}}$$

When $|r| < 1$ the series converges to the following:

$$\left(1 + \sum_{m=1}^{\infty} r^m \frac{(1,m)}{\prod_{q=1}^{m}\left(m-q+\frac{1}{2}\right)}\right) = 1 - \frac{\left(-2r+\sqrt{r+1}-1\right)}{\sqrt{r+1}}$$

$$= \frac{2r+1}{\sqrt{r+1}} \tag{A.4.5}$$

Looking at the first of the second type of sum:

$$\sum_{m=1}^{\infty} \frac{(1,m)}{(2jk_0)^m} \sum_{n=1}^{m} \frac{(-1)^n j^{n-1} (k_0+k_s)^{n-1}}{\prod_{p=1}^{n}\left(m-p+\frac{1}{2}\right)} \left(\frac{e^{-j(k_0+k_s)(x+\alpha)}}{(x+\alpha)^{\left(m-n+\frac{1}{2}\right)}} - \frac{e^{-j(k_0+k_s)(x-c)}}{(x-c)^{\left(m-n+\frac{1}{2}\right)}}\right)$$

When separated become the following two similar double summations:

$$e^{-j(k_0+k_s)(x+\alpha)} \sum_{m=1}^{\infty} \frac{(1,m)}{(2jk_0)^m} \frac{1}{(x+\alpha)^{\left(m-\frac{1}{2}\right)}} \sum_{n=1}^{m} \frac{(-1)^n j^{n-1} (x+\alpha)^{(n-1)} (k_0+k_s)^{n-1}}{\prod_{p=1}^{n}\left(m-p+\frac{1}{2}\right)}$$
$$- e^{-j(k_0+k_s)(x-c)} \sum_{m=1}^{\infty} \frac{(1,m)}{(2jk_0)^m} \frac{1}{(x-c)^{\left(m-\frac{1}{2}\right)}} \sum_{n=1}^{m} \frac{(-1)^n j^{n-1} (x-c)^{(n-1)} (k_0+k_s)^{n-1}}{\prod_{p=1}^{n}\left(m-p+\frac{1}{2}\right)}$$

First examining the inner sums by taking either $(x+\alpha)^{(n-1)} (k_0+k_s)^{n-1} = r^{n-1}k^{n-1}$ or $(x-c)^{(n-1)} (k_0+k_s)^{n-1} = r^{n-1}k^{n-1}$ these series are of the same form:

$$\sum_{n=1}^{m} \frac{j^{n-1} (-1)^n (rk)^{n-1}}{\prod_{p=1}^{n}\left(m-p+\frac{1}{2}\right)}$$

Substituting $\prod_{p=1}^{n}\left(m-p+\frac{1}{2}\right) = \frac{\Gamma\left(m+\frac{1}{2}\right)}{\Gamma\left(m-n+\frac{1}{2}\right)}$ and noting that $r > 0$,$k > 0$

$$\sum_{n=1}^{m} j^{n-1} (-1)^n (rk)^{n-1} \frac{\Gamma\left(m-n+\frac{1}{2}\right)}{\Gamma\left(m+\frac{1}{2}\right)} = \frac{1}{\Gamma\left(m+\frac{1}{2}\right)} \sum_{n=1}^{m} (-1)^n j^{n-1} (kr)^{n-1} \Gamma\left(m-n+\frac{1}{2}\right)$$

$$= \frac{1}{\Gamma\left(m+\frac{1}{2}\right)}\frac{1}{2}\left(-1\right)^{\frac{3}{4}} j^m \exp\left(jkr\right)\left(kr\right)^{\left(m-\frac{1}{2}\right)}$$
$$\left(2\pi\exp\left(i\pi m\right)\operatorname{erf}\left(\sqrt{jkr}\right) - \left(2m-1\right)\Gamma\left(m-\frac{1}{2}\right)\left(\Gamma\left(\frac{1}{2}-m\right) - \Gamma\left(\frac{1}{2}-m, jkr\right)\right)\right) \tag{A.4.6}$$

Returning to the entirety of the second sum type, which with similar substitutions for $k$ and $r$

$$e^{-jkr}\sum_{m=1}^{\infty}\frac{\left(1,m\right)}{\left(2jk_0\right)^m}\frac{1}{r^{\left(m-\frac{1}{2}\right)}}\sum_{n=1}^{m}\frac{\left(-1\right)^n j^{n-1}r^{(n-1)}k^{n-1}}{\prod_{p=1}^{n}\left(m-p+\frac{1}{2}\right)} \tag{A.4.7}$$

With Equation A.4.6 and $\left(1,m\right) = \frac{\prod_{q=1}^{m}\left(4-(2q-1)^2\right)}{2^{2m}m!} = -\frac{(-4)^m\Gamma\left(m-\frac{1}{2}\right)\Gamma\left(m+\frac{3}{2}\right)}{2^{2m}m!\pi}$ becomes:

Then the total sum becomes:

$$e^{-jkr}\sum_{m=1}^{\infty}\frac{\left(-4\right)^m\Gamma\left(m-\frac{1}{2}\right)\Gamma\left(m+\frac{3}{2}\right)}{2^{2m}m!\pi\left(2jk_0\right)^m}\frac{1}{r^{\left(m-\frac{1}{2}\right)}}\sum_{n=1}^{m}\frac{\left(-1\right)^n j^{n-1}r^{(n-1)}k^{n-1}}{\prod_{p=1}^{n}\left(m-p+\frac{1}{2}\right)}$$

$$= \frac{\left(-1\right)^{\frac{3}{4}}}{\pi}\left[\pi\operatorname{erf}\left(\sqrt{jkr}\right)\sum_{m=1}^{\infty}k^{m-1/2}\frac{\Gamma\left(m-\frac{1}{2}\right)\Gamma\left(m+\frac{3}{2}\right)}{m!\left(2k_0\right)^m\Gamma\left(m+\frac{1}{2}\right)}\right.$$
$$\left. - \sum_{m=1}^{\infty}k^{m-1/2}\frac{\Gamma\left(m-\frac{1}{2}\right)\Gamma\left(m+\frac{3}{2}\right)}{m!\left(2k_0\right)^m}\left(-1\right)^m\gamma\left(\frac{1}{2}-m, jkr\right)\right]$$

Examining these two series separately:

$$\sum_{m=1}^{\infty}k^{m-1/2}\frac{\Gamma\left(m-\frac{1}{2}\right)\Gamma\left(m+\frac{3}{2}\right)}{m!\left(2k_0\right)^m\Gamma\left(m+\frac{1}{2}\right)} = \frac{\sqrt{\pi}\left(\sqrt{2}\left(\frac{k}{k_0}-1\right)+\sqrt{2-\frac{k}{k_0}}\right)}{\sqrt{k}\sqrt{2-\frac{k}{k_0}}}, \left|\frac{k}{k_0}\right| < 2 \tag{A.4.8}$$

and

$$\sum_{m=1}^{\infty} k^{m-1/2} \frac{\Gamma\left(m-\frac{1}{2}\right)\Gamma\left(m+\frac{3}{2}\right)}{m!\left(2k_0\right)^m}(-1)^m \gamma\left(\frac{1}{2}-m, jkr\right)$$

$$\sqrt{\pi}\sum_{m=1}^{\infty} k^{m-1/2} \frac{\Gamma\left(m-\frac{1}{2}\right)\left(m+\frac{1}{2}\right)(2m-1)!}{m!\left(2k_0\right)^m 2^m}(-1)^m \gamma\left(\frac{1}{2}-m, jkr\right)$$

With $\gamma(x,z) = \Gamma(x) - \Gamma(x,z)$, this becomes two sums:

$$\sqrt{\pi}\sum_{m=1}^{\infty} k^{m-1/2} \frac{\Gamma\left(m-\frac{1}{2}\right)\left(m+\frac{1}{2}\right)(2m-1)!}{m!\left(2k_0\right)^m 2^m}(-1)^m \left(\Gamma\left(\frac{1}{2}-m\right) - \Gamma\left(\frac{1}{2}-m, jkr\right)\right)$$

The first of which can be analytically summed:

$$\begin{aligned}\sqrt{\pi}\sum_{m=1}^{\infty} k^{m-1/2} \frac{\Gamma\left(m-\frac{1}{2}\right)\left(m+\frac{1}{2}\right)(2m-1)!}{m!\left(2k_0\right)^m 2^m}(-1)^m \Gamma\left(\frac{1}{2}-m\right) \\ = \pi^{\frac{3}{2}} \frac{\sqrt{2}\left(\frac{k}{k_0}-1\right)+\sqrt{2-\frac{k}{k_0}}}{\sqrt{k}\sqrt{2-\frac{k}{k_0}}}\end{aligned} \tag{A.4.9}$$

While no simple form was found for the second. Combining equationsA.4.8, A.4.9 with the remaining infinite sum gives for A.4.7:

$$e^{-jkr}\sum_{m=1}^{\infty} \frac{(-4)^m \Gamma\left(m-\frac{1}{2}\right)\Gamma\left(m+\frac{3}{2}\right)}{2^{2m} m!\pi\left(2jk_0\right)^m} \frac{1}{r^{\left(m-\frac{1}{2}\right)}} \sum_{n=1}^{m} \frac{(-1)^n j^{n-1} r^{(n-1)} k^{n-1}}{\prod_{p=1}^{n}\left(m-p+\frac{1}{2}\right)}$$

$$= (-1)^{\frac{3}{4}} \left[ \left( \operatorname{erf}\left(\sqrt{jkr}\right) - 1 \right) \frac{\sqrt{\pi}\left(\sqrt{2}\left(\frac{k}{k_0}-1\right) + \sqrt{2-\frac{k}{k_0}}\right)}{\sqrt{k}\sqrt{2-\frac{k}{k_0}}} \right.$$
$$\left. + \frac{1}{\sqrt{\pi}} \sum_{m=1}^{\infty} k^{m-1/2} \frac{\Gamma\left(m-\frac{1}{2}\right)\left(m+\frac{1}{2}\right)(2m-1)!}{m!\,(2k_0)^m\, 2^m} (-1)^m \left( \Gamma\left(\frac{1}{2}-m, jkr\right)\right)\right] \quad \text{(A.4.10)}$$

With these two identities (Eq. A.4.5 and A.4.10), and $k_+ = (k_0 + k_s)$ , $k_- = (k_0 - k_s)$ , $r_\alpha = (x + \alpha)$ and $r_c = (x - c)$. Equation A.4.4 becomes:

$$A_l^{FF_{tm}^h}(x, \alpha, c) = -\frac{bk_s}{2} e^{j\frac{3\pi}{4}} (F_l + E_l + G_l) \quad \text{(A.4.11)}$$

with

$$F_l = \sqrt{2}\left[ \frac{e^{jk_s x}}{\sqrt{1+K_s}} \frac{(2+K_s)}{\sqrt{3+K_s}} \left[F(k_+ r_\alpha) - F(k_+ r_c)\right] - \frac{e^{-jk_s x}}{\sqrt{(1-K_s)}} \frac{(2-K_s)}{\sqrt{3-K_s}} \left[F(k_- r_\alpha) - F(k_- r_c)\right]\right]$$

$$E_l = \frac{(-1)^{\frac{3}{4}}\sqrt{\pi}}{\sqrt{k_0}\sqrt{(1-K_s^2)}}$$
$$\left[ e^{jk_s x} \left( \operatorname{erf}\left(\sqrt{jk_+ r_\alpha}\right) - \operatorname{erf}\left(\sqrt{jk_+ r_c}\right)\right)\left(\sqrt{2}K_s + \sqrt{1-K_s}\right)\right.$$
$$\left. - e^{-jk_s x} \left( \operatorname{erf}\left(\sqrt{jk_- r_\alpha}\right) - \operatorname{erf}\left(\sqrt{jk_- r_C}\right)\right)\left(-\sqrt{2}K_s + \sqrt{1+K_s}\right)\right]$$

$$G_l = \frac{1}{\sqrt{\pi}} \sum_{m=1}^{\infty} \frac{\Gamma\left(m-\frac{1}{2}\right)\left(m+\frac{1}{2}\right)(2m-1)!}{m!\,(2k_0)^m\,2^m} (-1)^m \times \left[\frac{k_+^m}{\sqrt{1+K_s}}\left(\Gamma\left(\frac{1}{2}-m, jk_+r_\alpha\right)-\Gamma\left(\frac{1}{2}-m, jk_+r_c\right)\right) - \frac{k_-^m}{\sqrt{1-K_s}}\left(\Gamma\left(\frac{1}{2}-m, jk_-r_\alpha\right)-\Gamma\left(\frac{1}{2}-m, jk_-r_c\right)\right)\right]$$

The upper integral can be found by taking the same substitutions and the mth order integration by parts with $\zeta_{\Delta x}\left(x+\Delta x'\right)$ in Eq. A.4.2 with $r_{\alpha u}=(\alpha-x)$ and $r_d=(d-x)$

$$A_u^{FF_{tm}}(x,\alpha,d) = \frac{bk_s}{2} e^{j\frac{3\pi}{4}} \left(F_u+E_u+G_u\right) \tag{A.4.12}$$

with

$$F_u = \sqrt{2}\left[\frac{e^{-jk_sx}}{\sqrt{1+K_s}}\frac{(2+K_s)}{\sqrt{3+K_s}}\left[F\left(k_+r_{\alpha u}\right)-F\left(k_+r_d\right)\right] - \frac{e^{jk_sx}}{\sqrt{(1-K_s)}}\frac{(2-K_s)}{\sqrt{3-K_s}}\left[F\left(k_-r_{\alpha u}\right)-F\left(k_-r_d\right)\right]\right]$$

$$E_u = \frac{(-1)^{\frac{3}{4}}\sqrt{\pi}}{\sqrt{k_0}\sqrt{(1-K_s^2)}} \left[e^{-jk_sx}\left(\operatorname{erf}\left(\sqrt{jk_+r_{\alpha u}}\right)-\operatorname{erf}\left(\sqrt{jk_+r_d}\right)\right)\left(\sqrt{2}K_s+\sqrt{1-K_s}\right) - e^{jk_sx}\left(\operatorname{erf}\left(\sqrt{jk_-r_{\alpha u}}\right)-\operatorname{erf}\left(\sqrt{jk_-r_d}\right)\right)\left(-\sqrt{2}K_s+\sqrt{1+K_s}\right)\right]$$

$$G = \frac{(-1)^{\frac{3}{4}}}{\sqrt{\pi}} \sum_{m=1}^{\infty} \frac{\Gamma\left(m-\frac{1}{2}\right)\left(m+\frac{1}{2}\right)(2m-1)!}{m!\,(2k_0)^m\,2^m} (-1)^m \times \left[\frac{e^{-jk_sx}k_+^m}{\sqrt{1+K_s}}\left(\Gamma\left(\frac{1}{2}-m, jk_+r_{\alpha u}\right)-\Gamma\left(\frac{1}{2}-m, jk_+r_d\right)\right) - \frac{e^{jk_sx}k_-^m}{\sqrt{1-K_s}}\left(\Gamma\left(\frac{1}{2}-m, jk_-r_{\alpha u}\right)-\Gamma\left(\frac{1}{2}-m, jk_-r_d\right)\right)\right]$$

### A.4.1 Conclusion

More work must be done to understand the relative contributions of each of the Fresnel, Error function and Incomplete Gamma terms. Since no analytic sum could be found for the Gamma terms, a bound on the number of terms necessary or some other approximation of the series should be found. If nothing else, it should be proven whether the series converges or diverges. Even if it diverges it may still be possible to use it as an asymptotic expansion to desired accuracy. Further, it may be that cancellation within each successive order improves the accuracy of the approximation and it may be beneficial to use Eq. A.4.4 to a few terms instead of Equations A.4.11 and A.4.12.

This work may shed light on a possible empiric formula for TM.

Though there is a minimum of 24 special function evaluations required for this computation (plus those of the near region Struve-based analytic integration expressions). This may still be a significant improvement over the thousands of evaluations of the Hankel function required by numerical integration.

# Appendix B

# $\overline{\overline{G}}$ Empiric Analytic Formula

## B.1 $\overline{\overline{G}}$ TM Derived Formula

Begin by noting

$$\int_{-\infty}^{\infty} G(x,x')\,dx' - \int_{-\infty}^{\infty} G(x,x')\,dx' = 0$$

$$\int_{-\infty}^{\infty} G(x,x')\,dx' - \left(\int_{-\infty}^{-\alpha} G(x,x')\,dx' + \int_{-\alpha}^{\alpha} G(x,x')\,dx' + \int_{\alpha}^{\infty} G(x,x')\,dx'\right) = 0$$

Which is equivalent to

$$\overline{G}(x) - \left(\overline{\overline{G}}(x) + A^{FF_{tm}}(x,\infty,-\alpha,\alpha)\right) = 0$$

or

$$\overline{\overline{G}}(x) = \overline{G}(x) - A^{FF_{tm}}(x,\infty,-\alpha,\alpha) \tag{B.1.1}$$

Using Equations 4.4.8 and 4.4.9 with modifications for the infinite case gives:

$$\begin{aligned} A^{FF_{tm}}(x,\infty,-\alpha,\alpha) = \frac{bk_s}{2}\frac{(-1+j)}{\sqrt{2}}\Bigg\{ & -\cos(k_s x)(1-j)\left(\frac{1}{\sqrt{1-K_s}} - \frac{1}{\sqrt{1+K_s}}\right) \\ & + \frac{1}{\sqrt{(1+K_s)}}\left[e^{-jk_s x}F((k_0+k_s)(\alpha-x)) + e^{jk_s x}F((k_0+k_s)(x+\alpha))\right] \\ & - \frac{1}{\sqrt{(1-K_s)}}\left[e^{jk_s x}F((k_0-k_s)(\alpha-x)) + e^{-jk_s x}F((k_0-k_s)(x+\alpha))\right]\Bigg\} \end{aligned} \tag{B.1.2}$$

Approximating the Fresnel functions for large arguments [1]:

$$F(x) = \frac{1}{2} + \frac{1}{\sqrt{2\pi x}} \sin(x) - j\left(\frac{1}{2} - \frac{1}{\sqrt{2\pi x}} \cos(x)\right)$$

And for clarity define

$$R_1 = \left[e^{-jk_s x} F\left(\left(k_0 + k_s\right)(\alpha - x)\right) + e^{jk_s x} F\left(\left(k_0 + k_s\right)(x + \alpha)\right)\right]$$

$$R_2 = \left[e^{jk_s x} F\left(\left(k_0 - k_s\right)(\alpha - x)\right) + e^{-jk_s x} F\left(\left(k_0 - k_s\right)(x + \alpha)\right)\right]$$

After simplifying, results in

$$R_1 = (1 - j)\cos(k_s x) + \frac{j}{\sqrt{2\pi\left(k_0 + k_s\right)}}\left[e^{jk_s x}\frac{\exp\left(-j\left(k_0 + k_s\right)(x + \alpha)\right)}{\sqrt{(x + \alpha)}} + e^{-jk_s x}\frac{\exp\left(-j\left(k_0 + k_s\right)(\alpha - x)\right)}{\sqrt{(\alpha - x)}}\right]$$

$$R_2 = (1 - j)\cos(k_s x) + j\frac{1}{\sqrt{2\pi\left(k_0 - k_s\right)}}\left[e^{jk_s x}\frac{\exp\left(-j\left(k_0 - k_s\right)(\alpha - x)\right)}{\sqrt{(\alpha - x)}} + e^{-jk_s x}\frac{\exp\left(-j\left(k_0 - k_s\right)(x + \alpha)\right)}{\sqrt{(x + \alpha)}}\right]$$

So that Eq. B.1.2 becomes

$$A^{FF_{tm}}(x,\infty,-\alpha,\alpha) = \frac{bk_s}{2}\frac{(-1+j)}{\sqrt{2}}\left\{-\cos(k_s x)(1-j)\left(\frac{1}{\sqrt{1-K_s}}-\frac{1}{\sqrt{1+K_s}}\right)\right.$$
$$\left.+\frac{R_1}{\sqrt{(1+K_s)}}-\frac{R_2}{\sqrt{(1-K_s)}}\right\}$$

$$A^{FF_{tm}}(x,\infty,-\alpha,\alpha) = \frac{bk_s}{2}\frac{(-1+j)}{\sqrt{2}}\left\{2\cos(k_s x)(1-j)\left(\frac{1}{\sqrt{1+K_s}}-\frac{1}{\sqrt{1-K_s}}\right)\right.$$
$$+\frac{1}{\sqrt{(1+K_s)}}\left[\frac{j}{\sqrt{2\pi(k_0+k_s)}}\left[e^{jk_s x}\frac{\exp(-j(k_0+k_s)(x+\alpha))}{\sqrt{(x+\alpha)}}+e^{-jk_s x}\frac{\exp(-j(k_0+k_s)(\alpha-x))}{\sqrt{(\alpha-x)}}\right]\right]$$
$$\left.-\frac{1}{\sqrt{(1-K_s)}}\left[j\frac{1}{\sqrt{2\pi(k_0-k_s)}}\left[e^{jk_s x}\frac{\exp(-j(k_0-k_s)(\alpha-x))}{\sqrt{(\alpha-x)}}+e^{-jk_s x}\frac{\exp(-j(k_0-k_s)(x+\alpha))}{\sqrt{(x+\alpha)}}\right]\right]\right\}$$

Simplifying:

$$A^{FF_{tm}}(x,\infty,-\alpha,\alpha) = \frac{bk_s}{2}\frac{(-1+j)}{\sqrt{2}}\left\{2\cos(k_s x)(1-j)\left(\frac{1}{\sqrt{1+K_s}}-\frac{1}{\sqrt{1-K_s}}\right)\right.$$
$$+\frac{j\exp(-j(k_0 x+(k_0+k_s)\alpha))}{(1+K_s^2)\sqrt{(\alpha^2-x^2)}\sqrt{2\pi}}$$
$$\left.\left[\left(\sqrt{(\alpha-x)}+\sqrt{(x+\alpha)}\exp(j2k_0 x)\right)((1-K_s)-(1+K_s)\exp(j2k_s\alpha))\right]\right\} \quad \text{(B.1.3)}$$

Thus Equation B.1.1 with 4.4.1 and B.1.3 gives an empiric analytic formula for the finite support integral kernel.

$$\overline{\overline{G}}(x) = j\frac{\zeta_{xx}(x)}{2k_0} - \frac{bk_s}{2}\frac{(-1+j)}{\sqrt{2}}\left\{2\cos(k_s x)(1-j)\left(\frac{1}{\sqrt{1+K_s}} - \frac{1}{\sqrt{1-K_s}}\right)\right.$$
$$+ \frac{j\exp(-j(k_0 x + (k_0+k_s)\alpha))}{(1+K_s^2)\sqrt{(\alpha^2-x^2)}\sqrt{2\pi}}$$
$$\left.\left[\left(\sqrt{(\alpha-x)} + \sqrt{(x+\alpha)}\exp(j2k_0 x)\right)((1-K_s) - (1+K_s)\exp(j2k_s\alpha))\right]\right\}$$

or

$$\overline{\overline{G}}(x) = j\frac{\zeta_{xx}(x)}{2k_0} - \frac{bk_s}{2}\frac{(-1+j)}{\sqrt{2}}\left\{2\cos(k_s x)(1-j)\left(\frac{1}{\sqrt{1+K_s}} - \frac{1}{\sqrt{1-K_s}}\right)\right.$$
$$\left.+\frac{je^{-jk_0\alpha}}{(1+K_s^2)\sqrt{(\alpha^2-x^2)}\sqrt{2\pi}}\left[\left(\sqrt{(\alpha-x)}e^{-jk_0 x} + \sqrt{(x+\alpha)}e^{jk_0 x}\right)\left((1-K_s)e^{-jk_s\alpha} - (1+K_s)e^{jk_s\alpha}\right)\right]\right\}$$

## B.2 $\overline{\overline{G}}$ TE Derived Formula

### B.2.1 Introduction

The goal is to produce a similar formula as found for TM by investigating the analytic tails integration. This will be done in two ways, the first by subtracting the expression from the full empiric formula and the second by looking at only the outer limits of integration of the analytic tails.

The analytic tail integration is given by:

$$A^{TE_{ff}}(x,a,b,\alpha,\beta) = \int_a^{\alpha} G(x,x')\,dx' + \int_{\beta}^{b} G(x,x')\,dx'$$

such that $a > \alpha > \beta > b$ .

$$
\begin{aligned}
A^{TE_{ff}}(x,a,b,\alpha,\beta) &= \frac{\zeta_x(x)(-1+j)}{j\sqrt{1+\zeta_x^2}\sqrt{2}} \\
&\left\{\left(1+\frac{b^2k_s^2}{4}\right)\left[\{F((x-a)k_0)-F((x-\alpha)k_0)\}-\{F((b-x)k_0)-F((\beta-x)k_0)\}\right]\right. \\
&\quad+\frac{b^2k_s^2}{8}\left[\exp(j2k_sx)\left(\frac{\{F((b-x)(k_0-2k_s))-F((\beta-x)(k_0-2k_s))\}}{\sqrt{(1-2K_s)}}\right.\right. \\
&\qquad\left.-\frac{\{F((x-a)(k_0+2k_s))-F((x-\alpha)(k_0+2k_s))\}}{\sqrt{(1+2K_s)}}\right) \\
&\quad+\exp(-j2k_sx)\left(\frac{\{F((b-x)(k_0+2k_s))-F((\beta-x)(k_0+2k_s))\}}{\sqrt{(1+2K_s)}}\right. \\
&\qquad\left.\left.\left.-\frac{\{F((x-a)(k_0-2k_s))-F((x-\alpha)(k_0-2k_s))\}}{\sqrt{(1-2K_s)}}\right)\right]\right\} \qquad \text{(B.2.1)}
\end{aligned}
$$

### B.2.2 Full expression from infinite.

We want to find an approximation for

$$\overline{\overline{G}} \approx \overline{G} - A^{TE_{ff}}$$

Begin by setting limits as follows:

$$A^{TE_{ff}}(x,-\infty,\infty,-\alpha,\alpha)$$

Eq B.2.1 then becomes:

$$A^{TE_{ff}}(x,-\infty,\infty,-\alpha,\alpha)=\frac{\zeta_x(x)(-1+j)}{j\sqrt{1+\zeta_x^2}\sqrt{2}}$$
$$\left\{\left(1+\frac{b^2k_s^2}{4}\right)\left[\{F((x+\infty)k_0)-F((x+\alpha)k_0)\}-\{F((\infty-x)k_0)-F((\alpha-x)k_0)\}\right]\right.$$
$$+\frac{b^2k_s^2}{8}\left[\exp(j2k_sx)\left(\frac{\{F((\infty-x)(k_0-2k_s))-F((\alpha-x)(k_0-2k_s))\}}{\sqrt{(1-2K_s)}}\right.\right.$$
$$\left.-\frac{\{F((x+\infty)(k_0+2k_s))-F((x+\alpha)(k_0+2k_s))\}}{\sqrt{(1+2K_s)}}\right)$$
$$+\exp(-j2k_sx)\left(\frac{\{F((\infty-x)(k_0+2k_s))-F((\alpha-x)(k_0+2k_s))\}}{\sqrt{(1+2K_s)}}\right.$$
$$\left.\left.\left.-\frac{\{F((x+\infty)(k_0-2k_s))-F((x+\alpha)(k_0-2k_s))\}}{\sqrt{(1-2K_s)}}\right)\right]\right\}$$

With $F(\infty)=\frac{1}{2}(1-j)$:

$$A^{TE_{ff}}(x,-\infty,\infty,-\alpha,\alpha)=\frac{\zeta_x(x)(-1+j)}{j\sqrt{1+\zeta_x^2}\sqrt{2}}\left\{\left(1+\frac{b^2k_s^2}{4}\right)\right.$$
$$\left.\left[\left\{\frac{1}{2}(1-j)-F((x+\alpha)k_0)\right\}-\left\{\frac{1}{2}(1-j)-F((\alpha-x)k_0)\right\}\right]\right.$$
$$+\frac{b^2k_s^2}{8}\left[\exp(j2k_sx)\left(\frac{\left\{\frac{1}{2}(1-j)-F((\alpha-x)(k_0-2k_s))\right\}}{\sqrt{(1-2K_s)}}-\frac{\left\{\frac{1}{2}(1-j)-F((x+\alpha)(k_0+2k_s))\right\}}{\sqrt{(1+2K_s)}}\right)\right.$$
$$\left.\left.+\exp(-j2k_sx)\left(\frac{\left\{\frac{1}{2}(1-j)-F((\alpha-x)(k_0+2k_s))\right\}}{\sqrt{(1+2K_s)}}-\frac{\left\{\frac{1}{2}(1-j)-F((x+\alpha)(k_0-2k_s))\right\}}{\sqrt{(1-2K_s)}}\right)\right]\right\}$$

Simplifying gives:

$$A^{TE_{ff}}(x,-\infty,\infty,-\alpha,\alpha)=\frac{\zeta_x(x)(-1+j)}{j\sqrt{1+\zeta_x^2}\sqrt{2}}\left\{\left(1+\frac{b^2k_s^2}{4}\right)\left[-F\left(\left(x+\alpha\right)k_0\right)+F\left(\left(\alpha-x\right)k_0\right)\right]\right.$$
$$+\frac{b^2k_s^2}{8}\left[\frac{1}{2}(1-j)\,2j\sin(2k_sx)\left(\frac{1}{\sqrt{(1-2K_s)}}-\frac{1}{\sqrt{(1+2K_s)}}\right)\right.$$
$$-\frac{1}{\sqrt{(1-2K_s)}}\left(\exp(j2k_sx)F\left(\left(\alpha-x\right)(k_0-2k_s)\right)-\exp(-j2k_sx)F\left(\left(x+\alpha\right)(k_0-2k_s)\right)\right)$$
$$\left.\left.+\frac{1}{\sqrt{(1+2K_s)}}\left(\exp(j2k_sx)F\left(\left(x+\alpha\right)(k_0+2k_s)\right)-\exp(-j2k_sx)F\left(\left(\alpha-x\right)(k_0+2k_s)\right)\right)\right]\right\}$$

Approximating the Fresnel functions for large arguments:

$$F(x)=\frac{1}{2}+\frac{1}{\sqrt{2\pi x}}\sin(x)-j\left(\frac{1}{2}-\frac{1}{\sqrt{2\pi x}}\cos(x)\right)$$

$$=\frac{1}{2}+\frac{1}{\sqrt{2\pi x}}\left(\frac{\exp(jx)-\exp(-jx)}{2j}\right)-j\left(\frac{1}{2}-\frac{1}{\sqrt{2\pi x}}\left(\frac{\exp(jx)+\exp(-jx)}{2}\right)\right)$$

$$=\frac{1}{2}-j\left(\frac{1}{2}-\frac{1}{\sqrt{2\pi x}}\exp(-jx)\right)$$
$$=\frac{1}{2}(1-j)+j\frac{1}{\sqrt{2\pi x}}\exp(-jx)$$

Defining for clarity:

$$R_1=-F\left(\left(x+\alpha\right)k_0\right)+F\left(\left(\alpha-x\right)k_0\right)$$

$$R_2=\exp(j2k_sx)F\left(\left(\alpha-x\right)(k_0-2k_s)\right)-\exp(-j2k_sx)F\left(\left(x+\alpha\right)(k_0-2k_s)\right)$$

$$R_3=\left(\exp(j2k_sx)F\left(\left(x+\alpha\right)(k_0+2k_s)\right)-\exp(-j2k_sx)F\left(\left(\alpha-x\right)(k_0+2k_s)\right)\right)$$

Simplifying:

$$R_1 = j\frac{1}{\sqrt{2\pi k_0\left(\alpha^2 - x^2\right)}}\left(\sqrt{(x+\alpha)}\exp\left(-j\left(\alpha - x\right)k_0\right) - \sqrt{(\alpha - x)}\exp\left(-j\left(x+\alpha\right)k_0\right)\right)$$

$$\begin{aligned} R_2 = {} & (1-j)\left(j\sin\left(2k_s x\right)\right) \\ & + \frac{j}{\sqrt{2\pi k_0\left(\alpha^2 - x^2\right)\left(1 - 2K_s\right)}}\left(\sqrt{(x+\alpha)}\exp\left(-j\left(\alpha\left(k_0 - 2k_s\right) - xk_0\right)\right)\right) \\ & - \sqrt{(\alpha - x)}\exp\left(-j\left(xk_0 + \alpha\left(k_0 - 2k_s\right)\right)\right) \end{aligned}$$

$$\begin{aligned} R_3 = {} & (1-j)\, j\sin\left(2k_s x\right) \\ & + \frac{j}{\sqrt{2\pi k_0\left(a^2 - x^2\right)\left(1 + 2K_s\right)}} \\ & \left[\sqrt{(\alpha - x)}\exp\left(-j\left(xk_0 + \alpha\left(k_0 + 2k_s\right)\right)\right) - \sqrt{(x+\alpha)}\exp\left(-j\left(\alpha\left(k_0 + 2k_s\right) - xk_0\right)\right)\right] \end{aligned}$$

So

$$A^{TE_{ff}}(x,-\infty,\infty,-\alpha,\alpha)=\frac{\zeta_x(x)(-1+j)}{j\sqrt{1+\zeta_x^2}\sqrt{2}}\left\{\left(1+\frac{b^2k_s^2}{4}\right)[R_1]\right.$$
$$+\frac{b^2k_s^2}{8}\left[\frac{1}{2}(1-j)\,2j\sin(2k_sx)\left(\frac{1}{\sqrt{(1-2K_s)}}-\frac{1}{\sqrt{(1+2K_s)}}\right)\right.$$
$$-\frac{1}{\sqrt{(1-2K_s)}}(R_2)$$
$$\left.\left.+\frac{1}{\sqrt{(1+2K_s)}}(R_3)\right]\right\}$$

$$=\frac{\zeta_x(x)(-1+j)}{j\sqrt{1+\zeta_x^2}\sqrt{2}}\left\{\left(1+\frac{b^2k_s^2}{4}\right)\right.$$
$$\left[j\frac{1}{\sqrt{2\pi k_0(\alpha^2-x^2)}}\left(\sqrt{(x+\alpha)}\exp(-j(\alpha-x)k_0)-\sqrt{(\alpha-x)}\exp(-j(x+\alpha)k_0)\right)\right]$$
$$+\frac{b^2k_s^2}{8}\left[\frac{1}{2}(1-j)\,2j\sin(2k_sx)\left(\frac{1}{\sqrt{(1-2K_s)}}-\frac{1}{\sqrt{(1+2K_s)}}\right)\right.$$
$$-\frac{1}{\sqrt{(1-2K_s)}}\left((1-j)(j\sin(j2k_sx))+\frac{j}{\sqrt{2\pi k_0(\alpha^2-x^2)(1-2K_s)}}\right.$$
$$\left.\left(\sqrt{(x+\alpha)}\exp(-j(\alpha(k_0-2k_s)-xk_0))\right)-\sqrt{(\alpha-x)}\exp(-j(xk_0+\alpha(k_0-2k_s)))\right)$$
$$+\frac{1}{\sqrt{(1+2K_s)}}\left((1-j)\,j\sin(2k_sx)+\frac{j}{\sqrt{2\pi k_0(a^2-x^2)(1+2K_s)}}\right.$$
$$\left.\left.\left.\left[\sqrt{(\alpha-x)}\exp(-j(xk_0+\alpha(k_0+2k_s)))-\sqrt{(x+\alpha)}\exp(-j(\alpha(k_0+2k_s)-xk_0))\right]\right)\right]\right\}$$

$$A^{TE_{ff}}(x,a,b,\alpha,\beta) = \frac{\zeta_x(x)(-1+j)}{\sqrt{1+\zeta_x^2}\sqrt{2}} \frac{1}{\sqrt{2\pi k_0(\alpha^2-x^2)}}$$
$$\left\{\left(1+\frac{b^2k_s^2}{4}\right)\left[\left(\sqrt{(x+\alpha)}\exp(-j(\alpha-x)k_0) - \sqrt{(\alpha-x)}\exp(-j(x+\alpha)k_0)\right)\right]\right.$$
$$+\frac{b^2k_s^2}{8}$$
$$\left[-\frac{1}{(1-2K_s)}\left[\left(\sqrt{(x+\alpha)}\exp(-j(\alpha(k_0-2k_s)-xk_0))\right) - \sqrt{(\alpha-x)}\exp(-j(xk_0+\alpha(k_0-2k_s)))\right]\right.$$
$$\left.\left.+\frac{1}{(1+2K_s)}\left(\sqrt{(\alpha-x)}\exp(-j(xk_0+\alpha(k_0+2k_s))) - \sqrt{(x+\alpha)}\exp(-j(\alpha(k_0+2k_s)-xk_0))\right)\right]\right\}$$

And further simplifying gives:

$$A^{TE_{ff}}(x,-\infty,\infty,-\alpha,\alpha) = \frac{\zeta_x(x)(-1+j)}{\sqrt{1+\zeta_x^2}\sqrt{2}}$$
$$\frac{\left[\left(\sqrt{(x+\alpha)}\exp(-j(\alpha-x)k_0) - \sqrt{(\alpha-x)}\exp(-j(x+\alpha)k_0)\right)\right]}{\sqrt{2\pi k_0(\alpha^2-x^2)}}$$
$$\left(1+\frac{b^2k_s^2}{4}\left(1-\frac{1}{2}\left(\frac{\exp(j2\alpha k_s)}{(1-2K_s)}+\frac{\exp(-j2\alpha k_s)}{(1+2K_s)}\right)\right)\right)$$

So an expression for $\overline{\overline{G}}$ may be found as:

$$\overline{\overline{G}}(x) = j\frac{\zeta_{xx}(x)}{2k_0} - \frac{\zeta_x(x)(-1+j)}{\sqrt{1+\zeta_x^2}\sqrt{2}}$$
$$\frac{\left[\left(\sqrt{(x+\alpha)}\exp(-j(\alpha-x)k_0) - \sqrt{(\alpha-x)}\exp(-j(x+\alpha)k_0)\right)\right]}{\sqrt{2\pi k_0(\alpha^2-x^2)}}$$
$$\left(1+\frac{b^2k_s^2}{4}\left(1-\frac{1}{2}\left(\frac{\exp(j2\alpha k_s)}{(1-2K_s)}+\frac{\exp(-j2\alpha k_s)}{(1+2K_s)}\right)\right)\right)$$

# Appendix C

# A Note on Fresnel Integrals

## C.1 Fresnel Integrals

In the derivation for the approximate analytical calculation for $\overline{G}$ we find integrals of the form:

$$A_1 \int_0^{(1-2K_s)k_0a} \frac{e^{-j\tau}}{\sqrt{\tau}} d\tau + A_2 \int_0^{(1+2K_s)k_0a} \frac{e^{-j\tau}}{\sqrt{\tau}} d\tau \tag{C.1.1}$$

for TE and:

$$A_3 \int_0^{(1-K_s)k_0a} \frac{e^{-j\tau}}{\sqrt{2\pi\tau}} d\tau + A_4 \int_0^{(1+K_s)k_0a} \frac{e^{-j\tau}}{\sqrt{2\pi\tau}} d\tau \tag{C.1.2}$$

where $A_{1,2,3,4}$ are constants

[1] the Fresnel Integrals are typically defined by:

$$C(z) = \int_0^z \cos\left(\frac{\pi}{2}t^2\right) dt$$

$$S(z) = \int_0^z \sin\left(\frac{\pi}{2}t^2\right) dt$$

but also lists an alternative definition, which matches the integrals in the approximation given above

$$C_2(x) = \frac{1}{\sqrt{2\pi}} \int_0^x \frac{\cos t}{\sqrt{t}} dt$$

$$S_2(x) = \frac{1}{\sqrt{2\pi}} \int_0^x \frac{\sin t}{\sqrt{t}} dt$$

which are related by

$$C(x) = C_2\left(\frac{\pi}{2}x^2\right) \Rightarrow C_2(x) = C\left(\sqrt{\frac{2}{\pi}}x\right)$$

$$S(x) = S_2\left(\frac{\pi}{2}x^2\right) \Rightarrow S_2(x) = C\left(\sqrt{\frac{2}{\pi}}x\right)$$

Thus we can rewrite C.1.1 and C.1.2 as respectively:

$$A_1\sqrt{2\pi}\left[C_2\left(\left(1-2K_s\right)k_0a\right) - jS_2\left(\left(1-2K_s\right)k_0a\right)\right] + A_2\sqrt{2\pi}\left[C_2\left(\left(1+2K_s\right)k_0a\right) - jS_2\left(\left(1+2K_s\right)k_0a\right)\right]$$

$$A_3\left[C_2\left(\left(1-K_s\right)k_0a\right) - jS_2\left(\left(1-K_s\right)k_0a\right)\right] + A_4\left[C_2\left(\left(1+K_s\right)k_0a\right) - jS_2\left(\left(1+K_s\right)k_0a\right)\right]$$

In terms of the original Fresnel integrals:

$$A_1\sqrt{2\pi}\left[C\left(\sqrt{\frac{2}{\pi}\left(1-2K_s\right)k_0a}\right) - jS\left(\sqrt{\frac{2}{\pi}\left(1-2K_s\right)k_0a}\right)\right]$$

$$+A_2\sqrt{2\pi}\left[C\left(\sqrt{\frac{2}{\pi}\left(1+2K_s\right)k_0a}\right) - jS\left(\sqrt{\frac{2}{\pi}\left(1+2K_s\right)k_0a}\right)\right]$$

$$A_3\left[C\left(\sqrt{\frac{2}{\pi}\left(1-K_s\right)k_0a}\right) - jS\left(\sqrt{\frac{2}{\pi}\left(1-K_s\right)k_0a}\right)\right]$$

$$+A_4\left[C\left(\sqrt{\frac{2}{\pi}\left(1+K_s\right)k_0a}\right) - jS\left(\sqrt{\frac{2}{\pi}\left(1+K_s\right)k_0a}\right)\right]$$

## C.2 Imaginary Argument

When $1-2K_s<0$ for TE and $1-K_s<0$ for TM the argument of the first term of both cases becomes imaginary. Since $K_s$is positive, the second term doesn't change. Considering the first term, for TE:

$$A_1\sqrt{2\pi}\left[C\left(\sqrt{-\frac{2}{\pi}\left|1-2K_s\right|k_0a}\right)-jS\left(\sqrt{-\frac{2}{\pi}\left|1-2K_s\right|k_0a}\right)\right]$$

$$=A_1\sqrt{2\pi}\left[C\left(j\sqrt{\frac{2}{\pi}\left|1-2K_s\right|k_0a}\right)-jS\left(j\sqrt{\frac{2}{\pi}\left|1-2K_s\right|k_0a}\right)\right]$$

$$=A_1\sqrt{2\pi}\left[jC\left(\sqrt{\frac{2}{\pi}\left|1-2K_s\right|k_0a}\right)-S\left(\sqrt{\frac{2}{\pi}\left|1-2K_s\right|k_0a}\right)\right]$$

For TM:

$$A_3\left[C\left(\sqrt{-\frac{2}{\pi}\left|1-K_s\right|k_0a}\right)-jS\left(\sqrt{-\frac{2}{\pi}\left|1-K_s\right|k_0a}\right)\right]$$

$$=A_3\left[C\left(j\sqrt{\frac{2}{\pi}\left|1-K_s\right|k_0a}\right)-jS\left(j\sqrt{\frac{2}{\pi}\left|1-K_s\right|k_0a}\right)\right]$$

$$=A_3\left[jC\left(\sqrt{\frac{2}{\pi}\left|1-K_s\right|k_0a}\right)-S\left(\sqrt{\frac{2}{\pi}\left|1-K_s\right|k_0a}\right)\right]$$

where the following relationships from [1] have been used:

$$C\left(jz\right)=jC\left(z\right)$$

$$S\left(jz\right)=-jS\left(z\right)$$

# Appendix D

# Convergence of $\overline{G}$

## D.1 Introduction

Here the convergence of the kernel integral $\overline{G}$ will be considered. Both polarizations will be considered separately.

Beginning with the kernel integral of Eq. 3.3.3 and noting it is an improper integral:

$$\overline{G}(x) = \lim_{\alpha\to\infty} \int_{-\alpha}^{\alpha} G(x, x')\, dx'$$

Then arbitrarily splitting the integral at points c and d such that $-\alpha < c < d < \alpha$, there by dividing the integration into a middle region and two tail regions as follows:

$$\overline{G}(x) = \lim_{\alpha\to\infty} \left( \int_{-\alpha}^{c} G(x, x')\, dx' + \int_{c}^{d} G(x, x')\, dx' + \int_{d}^{\alpha} G(x, x')\, dx' \right) \tag{D.1.1}$$

For 2D there is an integrable singularity at $x = x'$ in the center integral that has already been handled in the presentation in Sections 3.2.3 and 3.3 by the factor of 2 that has been subsumed into $G(x, x')$ for this discussion. With that handled the center integral is on a finite domain and converges, while the two tails on the intervals $[-\alpha, c]$ and $[d, \alpha]$ remain.

## D.2 TE

### D.2.1 Heuristic argument

It is instructive to first look at the full integrand of $\overline{G}$ for TE and using Eq. 3.2.5

$$\overline{G}(x) = \lim_{\alpha\to\infty}\int_{-\alpha}^{\alpha} 2\left(-\frac{\partial G_0(x,x')}{\partial n}\right)\sqrt{1+\zeta_{x'}^2(x')}dx'$$

$$= \lim_{\alpha\to\infty}\int_{-\alpha}^{\alpha} 2\frac{k_0}{4j}\frac{\{-\zeta_x(x)(x-x')+(\zeta(x)-\zeta(x'))\}}{\sqrt{1+\zeta_x^2(x)}\sqrt{(x-x')^2+(\zeta(x)-\zeta(x'))^2}} \cdot H_1^{(2)}\left(k_0\sqrt{(x-x')^2+\left(\zeta(x)-\zeta(x)'\right)^2}\right)\sqrt{1+\zeta_{x'}^2(x')}dx'$$

When $x'$ gets large, the behavior of the integrand will go as $\frac{1}{\sqrt{|d|}}$ with some oscillation due to the electromagnetics as well as some oscillations from the $\sqrt{1+\zeta_{x'}^2(x)}$ term arising from the surface. While the inverse square root term by itself diverges, the oscillations can be expected to cause a conditional convergence. However, when the electromagnetic oscillations cancel with the surface oscillations, the integral reduces to the inverse square root term and will be expected to be divergent. With this heuristic argument of convergence out of the way, a more rigorous approach follows.

### D.2.2 Rigorous argument

Returning attention to Eq. D.1.1, and recognizing the proper integral on the interval $[c,d]$ converges, only the two tail integrations must be considered. Using the short hand $A^{FF_{te}}$ for

these terms.

$$A^{FF_{te}}(x,\alpha,c,d) = \int_{-\alpha}^{c} G(x,x')\,dx' + \int_{d}^{\alpha} G(x,x')\,dx'$$

And splitting this into the upper and lower tail integrals:

$$A^{FF_{te}}(x,\alpha,c,d) = A_l^{FF_{te}}(x,\alpha,c) + A_u^{FF_{te}}(x,\alpha,d)$$

This is exactly the expression of Section 4.4.3.1 and Appendix A.1 so the final result of these integrals after taking the large argument Hankel and small slope approximation is as follows:

$$\begin{aligned} A^{FF_{te}}(x,\alpha,c,d) = \frac{\zeta_x(x)(-1+j)}{j\sqrt{1+\zeta_x^2}\sqrt{2}} \Bigg\{ \left(1+\frac{b^2k_s^2}{4}\right)\left[\{F(r_{\alpha l}k_0) - F(r_c k_0)\} - \{F(r_{\alpha u}k_0) - F(r_d k_0)\}\right] \\ + \frac{b^2k_s^2}{8}\Bigg[\exp(j2k_s x)\left(\frac{\{F(r_{\alpha u}k_-) - F(r_d k_-)\}}{\sqrt{(1-2K_s)}} - \frac{\{F(r_{\alpha l}k_+) - F(r_c k_+)\}}{\sqrt{(1+2K_s)}}\right) \\ + \exp(-j2k_s x)\left(\frac{\{F(r_{\alpha u}k_+) - F(r_d k_+)\}}{\sqrt{(1+2K_s)}} - \frac{\{F(r_{\alpha l}k_-) - F(r_c k_-)\}}{\sqrt{(1-2K_s)}}\right)\Bigg]\Bigg\} \end{aligned}$$

With $r_{\alpha u} = (\alpha - x)$ , $r_{\alpha l} = (x+\alpha)$ , $r_d = (d-x)$ , $r_c = (x-c)$ , $k_+ = (k_0 + 2k_s)$ and $k_- = (k_0 - 2k_s)$. $F(x) = C(x) + jS(x)$

Taking the limit of $A^{FF_{te}}$ as $\alpha \to \infty$ means that $r_{\alpha u} \to \infty$ and $r_{al} \to \infty$. Thus there are 6 Fresnel integrals with infinite argument, and from [1]

$$\lim_{\alpha\to\infty} F(\alpha) = \frac{1}{2}(1-j)$$

Thus

$$\lim_{\alpha\to\infty} A^{FF_{te}}(x,\alpha,c,d) = \frac{\zeta_x(x)(-1+j)}{j\sqrt{1+\zeta_x^2}\sqrt{2}}\left\{\left(1+\frac{b^2k_s^2}{4}\right)\left[\left\{\frac{1}{2}(1-j)-F(r_ck_0)\right\}-\left\{\frac{1}{2}(1-j)-F(r_dk_0)\right\}\right.\right.$$
$$+\frac{b^2k_s^2}{8}\left[\exp(j2k_sx)\left(\frac{\left\{\frac{1}{2}(1-j)-F(r_dk_-)\right\}}{\sqrt{(1-2K_s)}}-\frac{\left\{\frac{1}{2}(1-j)-F(r_ck_+)\right\}}{\sqrt{(1+2K_s)}}\right)\right.$$
$$\left.\left.\left.+\exp(-j2k_sx)\left(\frac{\left\{\frac{1}{2}(1-j)-F(r_dk_+)\right\}}{\sqrt{(1+2K_s)}}-\frac{\left\{\frac{1}{2}(1-j)-F(r_ck_-)\right\}}{\sqrt{(1-2K_s)}}\right)\right]\right\}$$

Which is finite, hence the integral converges. However,

$$\lim_{\frac{\lambda_s}{\lambda_0}\to 2} A^{FF_{te}}(x,\alpha,c,d) = \infty$$

due to the $\frac{1}{\sqrt{1-2K_s}}$ terms so the integral is singular in this case. This matches the numeric results of Chapter 4 which were convergent except for $\frac{\lambda_s}{\lambda_0}=2$.

## D.3 TM

### D.3.1 Heuristic argument

Just like for TE in Appendix D.2.1, it is instructive to first look at the full integrand of $\overline{G}$ for TM and using Eq. 3.2.6

$$\overline{G}(x) = \lim_{\alpha\to\infty}\int_{-\alpha}^{\alpha} 2\left(\frac{\partial G_0(x,x')}{\partial n'}\right)\sqrt{1+\zeta_{x'}^2(x')}dx'$$

$$= \lim_{\alpha\to\infty} \int_{-\alpha}^{\alpha} 2\frac{k_0}{4j} \frac{\left\{-\zeta_x'\left(x'\right)\left(x-x'\right)+\left(\zeta\left(x\right)-\zeta\left(x'\right)\right)\right\}}{\sqrt{\left(x-x'\right)^2+\left(\zeta\left(x\right)-\zeta\left(x'\right)\right)^2}} \cdot H_1^{(2)}\left(k_0\sqrt{\left(x-x'\right)^2+\left(\zeta\left(x\right)-\zeta\left(x\right)'\right)^2}\right) dx'$$

When $x'$ gets large, the behavior of the integrand will go as $\frac{1}{\sqrt{|d|}}$ with some oscillation due to the electromagnetics as well as some oscillations from the $-\zeta_x\left(x\right)$ term arising from the surface. While the inverse square root term by itself diverges, the oscillations can be expected to cause a conditional convergence. However, when the electromagnetic oscillations cancel with the surface oscillations, the integral reduces to the inverse square root term and will be expected to be divergent. With this heuristic argument of convergence out of the way, a more rigorous approach follows.

### D.3.2 Rigorous argument

The development here closely follows that of Appendix D.2.2. Again returning attention to Eq. D.1.1, and recognizing the proper integral on the interval $[c,d]$ converges, only the two tail integrations must be considered. Using the short hand $A^{FF_{tm}}$ for these terms.

$$A^{FF_{tm}}\left(x,\alpha,c,d\right) = \int_{-\alpha}^{c} G\left(x,x'\right)dx' + \int_{d}^{\alpha} G\left(x,x'\right)dx'$$

And identifying the upper and lower tail integrals:

$$A^{FF_{tm}}\left(x,\alpha,c,d\right) = A_l^{FF_{tm}}\left(x,\alpha,c\right) + A_u^{FF_{tm}}\left(x,\alpha,d\right)$$

It can be shown that

$$A_l^{FF_{tm}}(x,\alpha,c) = -\frac{bk_s}{2}\frac{(-1+j)}{\sqrt{2}}\left\{\frac{e^{jk_sx}}{\sqrt{1+K_s}}\left[F\left(\left(k_0+k_s\right)(x+\alpha)\right)-F\left(\left(k_0+k_s\right)(x-c)\right)\right]\right.$$
$$\left.-\frac{e^{-jk_sx}}{\sqrt{1-K_s}}\left[F\left(\left(k_0-k_s\right)(x+\alpha)\right)-F\left(\left(k_0-k_s\right)(x-c)\right)\right]\right\}$$

and

$$A_u^{FF_{tm}}(x,\alpha,d) = \frac{bk_s}{2}\frac{(-1+j)}{\sqrt{2}}\left\{\frac{e^{jk_sx}}{\sqrt{(1-K_s)}}\left[F\left(\left(k_0-k_s\right)(\alpha-x)\right)-F\left(\left(k_0-k_s\right)(d-x)\right)\right]\right.$$
$$\left.-\frac{e^{-jk_sx}}{\sqrt{(1+K_s)}}\left[F\left(\left(k_0+k_s\right)(\alpha-x)\right)-F\left(\left(k_0+k_s\right)(d-x)\right)\right]\right\}$$

Taking the limit as $\alpha$ approaches infinite for both of these expressions also gives a finite result since the Fresnel function of infinite argument is also finite:

$$\lim_{\alpha\to\infty} F(\alpha) = \frac{1}{2}(1-j)$$

so that

$$\lim_{\alpha\to\infty} A_l^{FF_{tm}}(x,\alpha,c) = -\frac{bk_s}{2}\frac{(-1+j)}{\sqrt{2}}\left\{\frac{e^{jk_sx}}{\sqrt{1+K_s}}\left[\frac{1}{2}(1-j)-F\left(\left(k_0+k_s\right)(x-c)\right)\right]\right.$$
$$\left.-\frac{e^{-jk_sx}}{\sqrt{1-K_s}}\left[\frac{1}{2}(1-j)-F\left(\left(k_0-k_s\right)(x-c)\right)\right]\right\}$$

and

$$\lim_{\alpha\to\infty} A_u^{FF_{tm}}(x,\alpha,d) = \frac{bk_s}{2}\frac{(-1+j)}{\sqrt{2}}\left\{\frac{e^{jk_sx}}{\sqrt{(1-K_s)}}\left[\frac{1}{2}(1-j) - F\left((k_0-k_s)(d-x)\right)\right]\right.$$
$$\left. -\frac{e^{-jk_sx}}{\sqrt{(1+K_s)}}\left[\frac{1}{2}(1-j) - F\left((k_0+k_s)(d-x)\right)\right]\right\}$$

Again like TE, these expressions are finite and hence the integral converges, except when the square-root in the denominator becomes 0 which occurs when $K_s \to 1$ so that:

$$\lim_{\frac{\lambda_s}{\lambda_0}\to 1} A^{FF_{tm}}(x,\alpha,c,d) = \infty$$

This matches the numeric results of Chapter 4 which were convergent except for $\frac{\lambda_s}{\lambda_0} = 1$.